Rahul Sharma
Editor

Deep-Sea Mining

Resource Potential, Technical and Environmental Considerations

Springer

Deep-Sea Mining

Rahul Sharma
Editor

Deep-Sea Mining

Resource Potential, Technical and Environmental Considerations

Springer

Editor
Rahul Sharma
National Institute of Oceanography
Dona Paula, Goa, India

ISBN 978-3-319-52556-3 ISBN 978-3-319-52557-0 (eBook)
DOI 10.1007/978-3-319-52557-0

Library of Congress Control Number: 2017933456

Cover picture: Artist's impression of deep-sea mining system
Images: Research vessel Sindhu Sadhana (National Institute of Oceanography, Goa, India), deep-sea miner (National Institute of Ocean Technology, Chennai, India)
Design: Ms. Sujal Bandodkar

Printed on acid-free paper

This Springer imprint is published by Springer Nature
The registered company is Springer International Publishing AG
The registered company address is: Gewerbestrasse 11, 6330 Cham, Switzerland

Foreword

It is a great pleasure to write this foreword for Dr. Rahul Sharma's book on the resource potential and technical, environmental and management issues associated with deep-sea mining.

After many years 'on hold' the prospects for deep-sea mining have improved significantly in recent years. Better scientific understanding of deep-sea mineral resources as well as the development of new technologies for exploitation and processing of deep-sea minerals has led to renewed commercial interest, particularly in the 'area' beyond national jurisdiction. As a result, the International Seabed Authority has been tasked with the development of a comprehensive code for deep-sea mineral exploitation, consistent with the norms established by the United Nations Convention on the Law of the Sea, under which sustainable harvesting of seabed minerals may be conducted for the benefit of mankind as a whole.

It has taken many years to reach this point. Scientists and engineers from various organizations around the world have for decades been conducting research on developing techniques for mineral prospecting and resource estimation as well as designing efficient and cost-effective systems for mining of these resources. Many of these scientists and engineers are or will be reaching retirement age, and one of the principal aims of Dr. Sharma's book is to bring together in one place the accumulated wisdom and knowledge of several of the world's leading experts on deep-sea mining. Rahul Sharma himself is one of those experts, having spent some 30 years teaching and working in the field conducting research on deep-sea minerals and the environmental issues associated with their exploitation. It has been my pleasure to have worked with him on a number of projects associated with the International Seabed Authority.

I congratulate him and the experts that have contributed to this important book. Whilst many challenges remain, not least the challenge of maintaining environmental balance whilst harvesting marine minerals, I am confident that these challenges can be overcome in order to provide the world with a safe, sustainable and secure supply of critical minerals well into the future. I am confident that this book will serve as an important source of reference for future generations on this topic.

With best wishes.

International Seabed Authority, Kingston, Jamaica Michael Lodge

Preface

Mankind's quest for exploration has led him to traverse from the vast expanse of outer space down to the deepest parts of the oceans. One such discovery in the later part of the nineteenth century was that of minerals on the seafloor, which are now being looked upon as the alternative source of some of the strategic metals that are feared to get exhausted on land in the coming decades.

In the present century, a sudden leap in the number of entities that have filed claims over seabed areas in international waters under the UN Law of the Sea, as well as the growing interest of state sponsored and private entrepreneurs in mining of the seafloor deposits leading to development of guidelines by regulating agencies such as the International Seabed Authority, has necessitated a synthesis of available information related to deep-sea mining.

In spite of several challenges associated with the exploitation of these deposits in terms of operating under extreme conditions in the open seas, the ingenuity of humankind has led not only to the development of technologies to gather information about the environs of where these minerals occur but also to the formulation of techniques to bring them up from the deep-sea floor and extract precious metals. However, the outcomes of research conducted around the world on different aspects of deep-sea mining are only available in scattered sources.

This book attempts to bring together diverse perspectives of authors from around the globe who have been working on various issues related to deep-sea mining for several decades. The first section of the book focuses on the distribution characteristics of deep-sea minerals, their resource potential, and techniques for mapping. The second section is devoted to concepts of deep-sea mining technologies and their utility for other industrial applications.

The book continues with authoritative overviews on metallurgical processing techniques for extraction of metals and sustainable use of mine tailings, as well as the associated environmental concerns for prediction and management of impacts related to deep-sea mining.

I would like to acknowledge the contributions from all authors to make this book a reality. Thanks also to various agencies in funding and supporting the research presented in this volume. My family also deserves a special mention for their love and support throughout my career as well as during the compilation of this work.

Goa, India Rahul Sharma

Contents

Part I
Deep-Sea Minerals: Distribution Characteristics and Their Resource Potential

Chapter 1
Deep-Sea Mining: Current Status and Future Considerations

Rahul Sharma

Abstract Deep-sea minerals such as polymetallic nodule, hydrothermal sulphides, and ferro-manganese crusts have for long attracted attention as an alternative source of metals to terrestrial deposits. The occurrence of many of these deposits in the international waters has necessitated its regulation under the UN Convention on the Law of the Sea through the establishment of International Seabed Authority.

A sudden spurt in the number of 'Contractors' interested in claiming large tracts of seafloor with exclusive rights for exploration from just eight in the first four decades (1970–2010) to 25 in the next 4 years (2011–2015) as well as consistent research and development of technology for prospecting, mining, and processing of these resources, coupled with issuing of licences to private entrepreneurs for deposits within the EEZ of some countries, calls for a re-look at the current status and future prospects of deep-sea mining.

1.1 Historical Perspective

Although the first known discovery of deep-sea minerals (Fig. 1.1) was made during the expedition of H.M.S. Challenger (21 December 1872–24 May 1876) when the expedition leader C.W. Thomson described the dredge haul of polymetallic nodules on 7 March 1873 as 'peculiar black oval bodies about 1 inch long' and the chemist J.Y. Buchanan revealed that they were 'almost pure manganese oxide' (en.wikipedi.org/wiki/HMSChallenger), it was Mero (1965) who unravelled the economic potential of these deposits and predicted that deep-sea mining would commence in 20 years time that steered the world attention towards developing these resources as an alternative source of metals for the future.

A global effort during the conference on 'Ferro-manganese deposits on the ocean floor' at Lamont Doherty Geological Observatory in January 1972 to collate existing data on nodules was followed by studies dealing with distribution, geochemistry, and mineralogy of the deposits in different parts of the Pacific Ocean (Hein et al. 1979; Thijssen et al. 1981; Glasby 1982; Usui and Moritani 1992), as well as Indian

R. Sharma (✉)
CSIR-National Institute of Oceanography, Council of Scientific and Industrial Research, Dona Paula, Goa 403004, India
e-mail: rsharma@nio.org; rsharmagoa@gmail.com

R. Sharma (ed.), *Deep-Sea Mining*, DOI 10.1007/978-3-319-52557-0_1

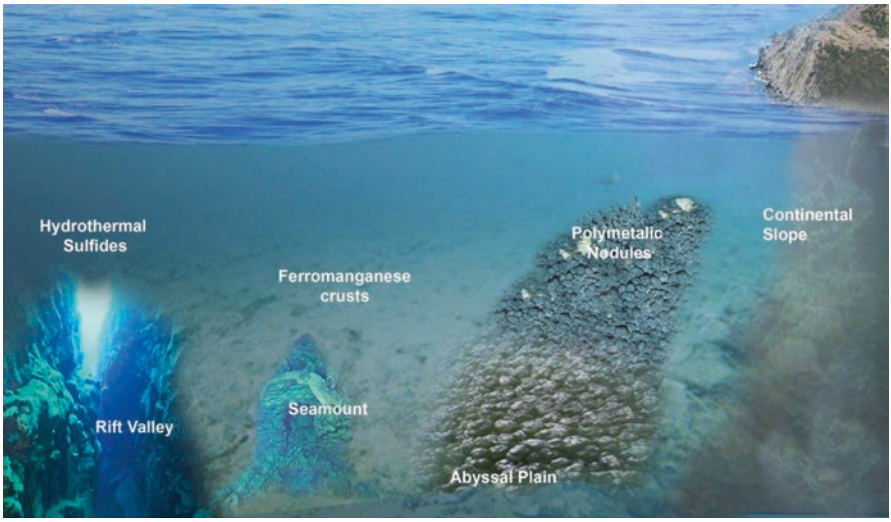

Fig. 1.1 Artist's impression of association of deep-sea minerals with seafloor features

Ocean (Glasby 1972; Siddiquie et al. 1978; Frazer and Wilson 1980; Cronan and Moorby 1981). Many of the studies also deciphered the formation process, geological factors as well as their relationship with sedimentary environment (Cronan 1980; Frazer and Fisk 1981; Glasby et al. 1982; Rao and Nath 1988; Martin-Barajas et al. 1991). Simultaneously, hydrothermal sulphides (Rona 1988; Plueger et al. 1990) and cobalt-rich ferromanganese crusts (Halbach et al. 1989; Hein et al. 1997) were also identified as potential resources.

Following the initial studies, extensive exploration programs ensued leading to several entities laying claims over large tracts of seafloor with potential resources in the international waters for gaining exclusive rights under the United Nations Convention on Law of the Sea, which led to the establishment of International Seabed Authority with its headquarters in Jamaica in 1994 for regulating the activities in the 'Area', i.e. in the international waters beyond the national jurisdiction of any country. Whereas until 2010, there were eight Registered Pioneer Investors subsequently called the 'Contractors' (France, Russia, Japan, China, Korea, Germany and InterOceanMetal Joint Orgnisation—a consortium of East European countries—in the Pacific Ocean and India in the Indian Ocean), all of them for polymetallic nodules only; a sudden spurt of applications was witnessed raising the number to 25 by 2015 for nodules, crusts, and sulfides (Table 1.1, Fig. 1.2a–d) (www.isa.org.jm (2016)).

Persistent interest in exploring these mineral resources, coupled with continued research and development for new technologies for prospecting as well as mining and extracting the metals from these ores, has led to numerous publications in several journals, symposia proceedings, and reports. The objective of this book is to synthesize all the information and make it available in a concise form so as to make it available for future generations. This chapter provides an overview of the

Table 1.1 Contractors for exploration for (a) polymetallic nodules, (b) ferromanganese crusts, (c) hydrothermal sulphides

Contractor	Sponsoring state	General location of the exploration area under contract
Contractors for exploration for polymetallic nodules		
InterOceanMetal Joint Organization	Bulgaria, Cuba, Czech, Poland, Russia, Slovakia	Clarion-Clipperton Fracture Zone (CCFZ), Pacific Ocean
Yuzhmorgeologiya	Russia	CCFZ, Pacific Ocean
Government of the Republic of Korea	Korea	CCFZ, Pacific Ocean
China Ocean Mineral Resources Research and Development Association	China	CCFZ, Pacific Ocean
Deep Ocean Resources Development Co.	Japan	CCFZ, Pacific Ocean
Institut français de recherche pour l'exploitation de lamer	France	CCFZ, Pacific Ocean
Bundesanstalt fur Geowissen Schaften und Rohstoffe	Germany	CCFZ, Pacific Ocean
Nauru Ocean Resources Inc.	Nauru	CCFZ, Pacific Ocean
Tonga Offshore Mining Limited	Tonga	CCFZ, Pacific Ocean
UK Seabed Resources Ltd.—I	UK	CCFZ, Pacific Ocean
G-TEC Mineral Resources NV	Belgium	CCFZ, Pacific Ocean
Marawa Research and Exploration Ltd.	Kiribati	CCFZ, Pacific Ocean
Ocean Mineral Singapore Pte Ltd	Singapore	CCFZ, Pacific Ocean
Cook Islands Investment Corporation	Cook Islands	CCFZ, Pacific Ocean
UK Seabed Resources Ltd.—II	UK	CCFZ, Pacific Ocean
Government of India	India	Indian Ocean
Contractors for exploration for ferromanganese crusts		
Government of the Russia	Russia	Pacific Ocean
China Ocean Mineral Resources Research and Development Association	China	Pacific Ocean
Japan oil, Gas and Metals National Corporation	Japan	Pacific Ocean
Contractors for exploration for hydrothermal sulphides		
Institut français de recherche pour l'exploitation de la mer	France	Mid-Atlantic Ridge
Government of the Russia	Russia	Mid-Atlantic Ridge
Government of the Republic of Korea	Korea	Central Indian Ridge
China Ocean Mineral Resources Research and Development Association	China	Southwest Indian Ridge
Govt of India	India	Southwest Indian Ridge
Bundesanstalt fur Geowissen Schaften und Rohstoffe	Germany	Southeast and Central Indian Ridge

hypothetical estimation of potential of one of the mineral resources in a typical area and introduces economic, technical, environmental, and policy issues related to deep-sea mining. The subsequent chapters deal with each of these issues in detail on the basis of actual experimentation and analysis.

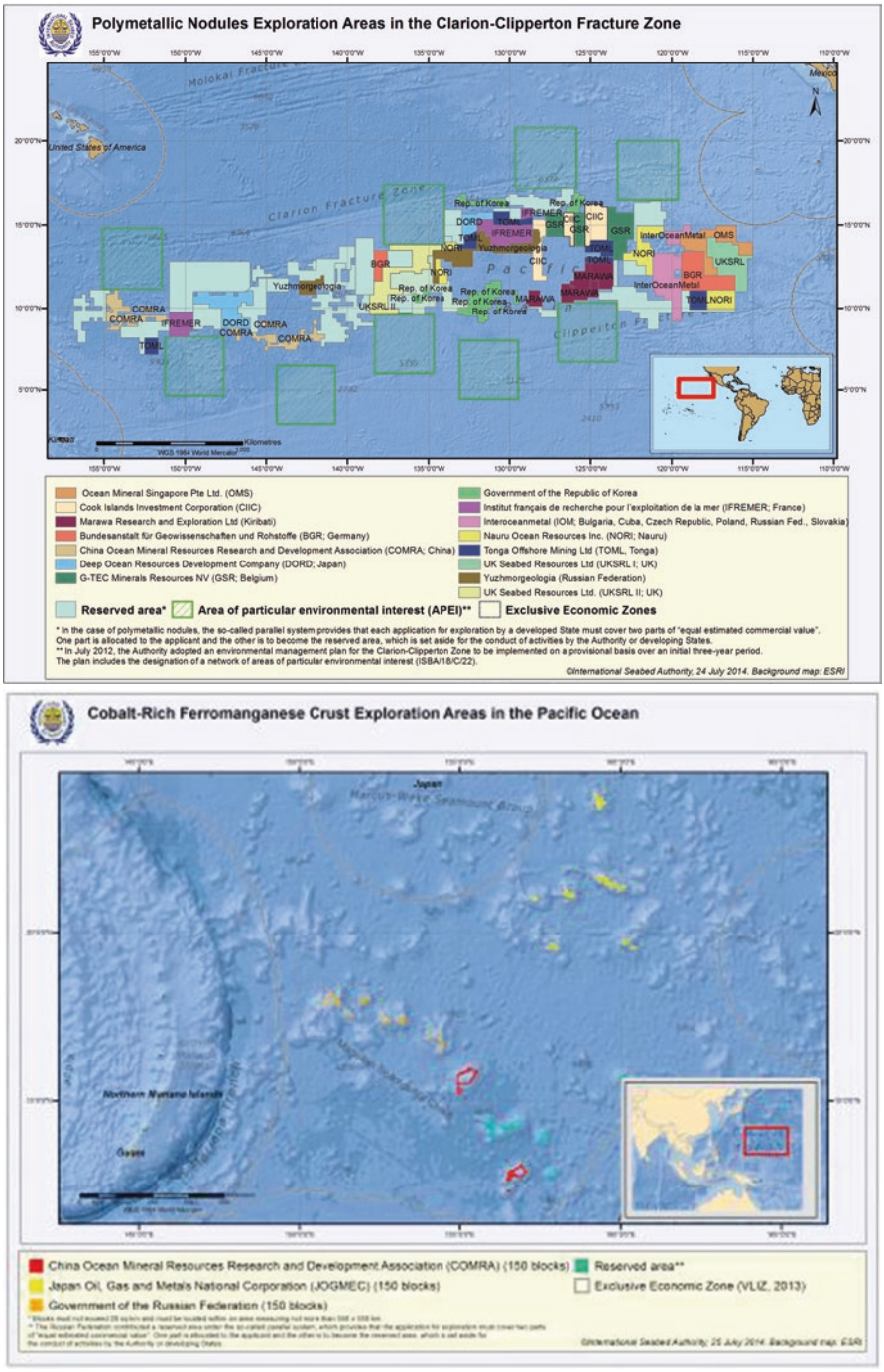

Fig. 1.2 (**a**) Map of exploration areas for polymetallic nodules in Pacific Ocean (www.isa.org.jm). (**b**) Map of exploration areas for ferromanganese crusts in Pacific Ocean (www.isa.org.jm). (**c**) Map of exploration areas for hydrothermal sulphides in Atlantic Ocean (www.isa.org.jm). (**d**) Map of exploration areas for polymetallic nodules and hydrothermal sulphides in Indian Ocean (www.isa.org.jm)

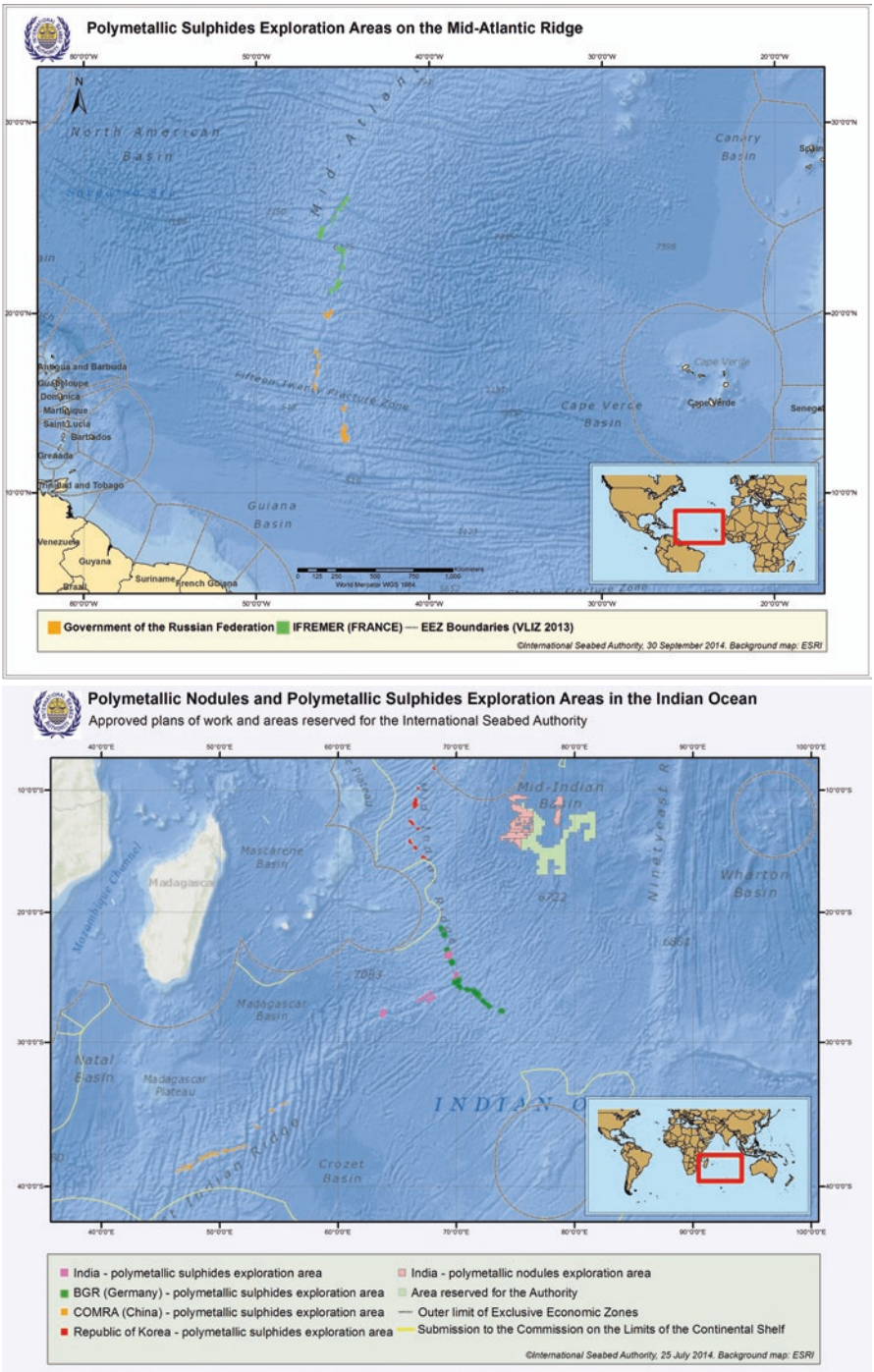

Fig. 1.2 (continued)

1.2 Economic Issues

Periodical evaluation of information on distribution and potential of deep-sea minerals as well as techniques for resource estimation and mining (Pearson 1975; Glasby 1977; Cronan 1980, 2000; UNOET 1982, 1987; Dick 1985; Kunzendorf 1986; Rona 2003) has kept the world's interest in these deposits alive, even leading to the preparation of a geological model for polymetallic nodules in the Clarion-Clipperton Fracture Zone of the Pacific Ocean (ISA 2009). Reports of Fe-Mn deposits from the Christmas island region and Afanasiy-Nikitin seamounts of the Indian Ocean (Exon et al. 2002; Banakar et al. 2007) as well as the Marshall island area of the Pacific Ocean (Usui et al. 2003) and the granting of licences to private entrepreneurs for exploration of seafloor massive sulphides off Papua New Guinea and New Zealand (Gleason 2008) reaffirm the continuing interest of researchers and mining companies in exploring and exploiting the deep sea mineral deposits, indicating the possibility of gradually developing technologies for mining of marine minerals from relatively shallower deposits such as the crusts and sulphides (1000–2500 m) towards the deeper ferro-manganese nodules (4000–6000 m).

Fluctuating metal prices as well as factors such as recycling, new onshore deposits, and technological developments have stalled the commercial exploitation of these deposits, although these are considered important in the overall metal budget of the earth and constitute a substantial resource that would cover the twenty-first century demand for metals such as Mn, Fe, NI, Co, Cu, Mo, and many others including Rare Earth Elements (Kotlinski 2001). According to Lenoble (2000), the commercial viability of deep-sea deposits lies in their concentration compared to the currently mined deposits on land and also in their estimated magnitude. As per one estimate (Glumov et al. 2000), considering the present trends of mining ores with low metal grades, mean metal contents in deep-sea manganese oxide ores will be higher than those in the terrestrial deposits by factors between 1.1 for Ni and >5 for Co in about 2020.

The decision to commence mining of any deep-sea mineral will depend on the availability of metals from terrestrial sources and their price in the world market, as well as the techno-economic analysis based on capital and operating costs of the deep-sea mining system. With each of the Contractors being allotted areas averaging several thousand square kilometers in international waters (ISA 1998), considering the resource potential in a typical area of 75,000 km^2. for polymetallic nodules and their cut off abundance (5 kg/m^2) as specified by UNOET (1987), the total resource available in the area could be 375 Mt (wet) or 281.25 Mt (dry) with a total metal equal to 67.081 Mt (Table 1.2), at a conservative value of concentration of metals (Mn = 22%, Ni = 1.0%, Cu = 0.78%, Co = 0.1%). Out of the 281.25 Mt, only 10.6–21.2% (i.e. 30–60 million tonnes) of the resource will be used at the proposed mining rate of either 1.5 million tonnes/year (ISA 2008a) or 3 million tonnes/year (UNOET 1987) over duration of 20 years, with a large balance (78.8–89.4%) to be mined in future.

The total annual production of metals would range from 0.358 Mt/year (for 1.5 Mt/year) to 0.716 Mt/year (for 3 Mt/year). Considering average metal prices

Table 1.2 Resource potential and metal production estimates—a hypothetical case study

Nodule/ metal	Mean concentr-ation[a]	Resource potential t (Mt)[b]	Metal production per year t (Mt) @ 1.5 Mt/year @ 3 Mt/year		Price of metal ($/Kg)[c]	Gross in-place value of metal $/year @ 1.5 Mt/year @ 3 Mt/year		Gross in-place value of metal $/20 years @ 1.5 Mt/year @ 3 Mt/year	
Wet nodules	–	375,000,000 (375)	–	–	–	–	–	–	–
Dry nodules	25% of wet nodules[d]	281,250,000 (281.25)	–	–	–	–	–	–	–
Manganese	22/24% of dry nodules	61,800,000 (61.8)	330,000 (0.33)	660,000 (0.66)	1.32	435,600,000 (435.6 million)	871,200,000 (871.2 million)	8.712 billion	17.424 billion
Nickel	1.0/1.1% of dry nodules	2,810,750 (2.81)	15,000 (0.015)	30,000 (0.030)	23.00	345,000,000 (345.0 million)	690,000,000 (690 million)	6.90 billion	13.80 billion
Copper	0.78/1.04% of dry nodules	2,190,000 (2.19)	11,700 (0.0117)	23,400 (0.0234)	8.30	97,110,000 (97.11 million)	194,220,000 (194.22 million)	1.9422 billion	3.8844 billion
Cobalt	0.23/0.1% of dry nodules	281,250 (0.281)	1500 (0.0015)	3000 (0.003)	39.20	58,800,000 (58.8 million)	117,600,000 (117.6 million)	1.176 billion	2.352 billion
Total (metals)	24.01/26.24%	67,081,000 (67.081)	358,200 (0.3582)	716,400 (0.7164)	–	936,510,000 (936.51 million)	187,302,000 (1873.02 million)	18.7302 billion	37.460 billion

[a]Source: Morgan (2000) for Clarion-Clipperton Zone in Pacific Ocean/Jauhari and Pattan (2000) for Central Indian Ocean

[b]@5 kg/m^2 for 75,000 km^2 (75×10^9 m^2) considering the lower value of concentration of metals between Pacific and Indian Ocean (in col. 2)

[c]Average metal prices for the period from July 2010 to January 2011 (source: www.metalprices.com)

[d]Mero (1977)

for a given period (www.metalprices.com (2011)), the value of total metals produced annually will be $936.5 million, with a total yield of about $18.73 billion in 20 years from a single mine-site at 1.5 Mt/year mining rate. The same would be double (i.e. $1873 million/year, or ~$37.46 billion in 20 years) for a mining rate of 3 Mt/year (Table 1.2). Here it must be noted that these estimates are based on minimum value of metals and also lowest value of abundance and so the actual returns could be much higher as the in-situ average abundances are normally expected to be higher than the cut off (i.e. 5 kg/m^2) and also the concentrations of metals could be higher in the potential mine-sites than that considered here as have been reported in the Pacific Ocean (Herrouin et al. 1991).

In spite of such a potential, most of the deep-sea mineral deposits can only be termed as 'resources' (and not 'reserves') as they cannot be economically recovered under prevailing economic conditions, but may be exploitable in the foreseeable future and such resources could become economic when price and market conditions or new technologies increase the profit margin to acceptable levels (UNOET 1987). According to estimates, the cost of different types of collectors, power generation, and risers, as proposed by different Contractors that are involved in developing technology for mining at 1.5 Mt of nodules annually, shows a capital expenditure of $372–562 million and an operating cost of $69–96 million/year. Added to this would be the capital expenditure for purchasing three vessels for ore transfer estimated at $495–600 million, with an annual operating cost of $93–132 million and a capital expenditure of $750 million for the processing plant with an annual operating cost of $250 million (ISA 2008a). Even if we consider the highest values (rounded to the nearest 50), the total estimated cost of a single deep-sea mining venture works out to $11.90 billion (Table 1.3), which when compared with the total yield of metals worth $18.73 billion (Table 1.2) may seem promising.

However, in order to 'fix' the timing for commencement of deep-sea mining, a detailed economic study looking at the CAPEX and OPEX with respect to production rates and metal values is required to arrive at an optimum mining rate. Most of the earlier studies conducted in 1970s and 1980s based on conditions existing at that time suggested that processing of 3 Mt/year could be less costly per tonne of nodules (UNOET 1987). Calculations had also shown that mining of 3 Mt/year using a single ship was not viable, except in case of higher nodule abundances, higher ship speed, or larger dredge head (Glasby 1983). Earlier estimates for a 2 Mt/year operation,

Table 1.3 Estimated capital and operating expenditures for polymetallic nodules mining [figures in brackets show the range for different systems as proposed by different Contractors (ISA 2008a)]

Item	Capital expenditures	Operating expenditures	Total
Mining system	$550 mi[a] ($372–562 mi)	$100 mi/year[a] ($69–96 mi) × 20 years = $2.0 billion	$2.55 billion
Ore transfer	$600 mi[a] ($495–600 mi)	$150 mi/year[a] ($93–132 mi/year) × 20 years = $3.0 billion	$3.60 billion
Processing plant	($750 mi)	($250 mi/year) × 20 years = $5.0 billion	$5.75 billion
Total	$1.90 billion	$10.0 billion	$11.90 billion

[a]Rounded off to nearest 50 of the highest value
Source: Sharma (2011)

when the capital investment was estimated at $250 m and metal prices were significantly lower than considered here, showed the expected rate of return at 13% per year (Mero 1977). Alternative scenarios of mining operations from 1.2 to 3 million tonnes per year for a 20 year mine-life produced internal rates of return ranging from 14.9 to 37.8% (ISA 2008a). This scenario could undergo a change taking into consideration the techno-economic feasibility as well as metal markets.

1.3 Technical Issues

1.3.1 Delineation of Mine-Site and Estimation of Area for Mining

A 'mine site' is defined as an ocean bottom area where, under specific geological, technical, and economic conditions, a single mining operation can be carried out for a period of time. For example, the following criteria have been suggested for polymetallic nodules (UNOET 1987):

- Cut off grade = 1.8% Cu + Ni
- Cut off abundance = 5 kg/m^2
- Topography = acceptable
- Duration (D) = 20 years
- Annual recovery (A_r) = 3 million dry tonnes, which has been subsequently proposed as 1.5 million tonnes by ISA (2008a).

Using this information, the total mineable area (M) can be estimated as follows:

$$M = A_t - \left(A_u + A_g + A_a\right) \tag{1.1}$$

where, A_t = total area,

A_u = area un-mineable due to the topography,
A_g = area below cut-off grade;
A_a = area below cut-off abundance.

Furthermore, the size of mine site (A_s) can be calculated as:

$$A_s = \frac{\left(A_r\right)\left(D\right)}{\left(A_n\right)\left(E\right)\left(M\right)} \tag{1.2}$$

where,

A_s = size of mine-site (km^2),
A_r = annual nodule recovery rate (dry tonnes/year),
D = duration of mining operation (years),
A_n = average nodule abundance in the mineable area,
E = overall efficiency of the mining device (%),
M = proportion of mineable area.

Higher the average abundance, smaller would be the size of the mine-site with respect to the allotted area that augers well with the concept of restricting the mining activities to a smaller area, especially from the point of environmental impacts.

1.3.2 Mining System Development

The overall efficiency (E) of a mining system would largely depend upon the collection efficiency of the dredge head that would sweep the seafloor to collect the minerals which is calculated as (UNOET 1987):

$$E = e_{\mathrm{d}} \times e_{\mathrm{s}}, \tag{1.3}$$

where,

e_{d} = dredge efficiency, which is the ratio of minerals effectively gathered by the dredge head, versus the minerals on the seabed before dredging,
e_{s} = sweep efficiency, which is the percentage of the bottom actually swept by the area dredged.

The efficiency of deep-sea mining would also depend on the system for lifting the minerals to the surface, such as, the air-lift, which has 2–5 times higher energy consumption, but is easier to maintain as the compressors are above the water surface as compared to the hydraulic lift, which requires less power, allows higher transport densities, and hence needs smaller pipes for lifting the minerals, but is difficult to maintain due to under water pump system (Amann 1982). Given the high investment–high risk nature of the operations, future technology could consider deployment of a number of autonomous vehicles operating from the mining platform that would provide better operational and maintenance options, even from environmental point of view due to limited area of contact of these devices with the water column and the seafloor; and also in recovery or abandoning them in case of a mishap, as the mining platform and collection devices would be independent of one another (Sharma 2011).

Information available in public domain suggests that development of mining technology has been in different stages, including model studies and a few at-sea tests of crawlers and lifting mechanisms by the Contractors (Table 1.4). However, once these designs and prototypes are tested, the real challenge lies in up-scaling and integrating different subsystems and making them work on a sustained basis continuously for ~300 days/year under variable conditions, including extreme weather (rainfall, winds, and cyclones), hydrographical conditions (high pressure, low temperature, currents, and lack of natural light), and seafloor environment (undulating topography, sediment thickness, and heterogeneous distribution of deposits).

Application of new technology for exploration as well as mining, such as 3D sensing, autonomous navigation, robotic manipulators, and vehicles for the extreme environment adopted from space missions, could provide some of the solutions (Jasiobedzki et al. 2007). Similarly, advances in floating oil platforms, availability of riser hardware for deep-water and harsh environments, sub-sea power systems and pumps required for mining (Halkyard 2008), as well as the advantages of flexible

Table 1.4 Status of mining and processing technologies for deep-sea polymetallic nodules

Sr. no.	Contractor	Mining technology	Processing technology
1	France[a]	Model studies on self-propelled miner with hydraulic recovery system	Tested pyro and hydro-metallurgical processes for Ni, Cu, Co
2	Japan[b]	Passive nodule collector tested At ~2200 m depth	Developed a process to recover Cu, Ni, Co
3	India[c]	(a) Design includes flexible riser and multiple crawlers	(a) Tested 3 possible routes
		(b) Pilot plant set up for 500 kg/day for Cu, Ni, Co	(b) Crawler tested at ~410 m depth in the sea
4	China[c]	(a) Includes rigid riser with self-propelled miner	Developed a process to recover Mn, Ni, Cu, Co, and Mo
		(b) Tried different concepts of collector and lifting mechanisms	
5	Korea[c]	(a) Design includes flexible riser system with self-propelled miner	(Not known)
		(b) Developed 1/20 scale test miner	
6	Russia[c]	Collector and mining subsystems in conceptual stage	Recovered Mn, Ni, Cu, Co from nodules
7	IOM[c]	Conceptual design includes nodule collector, buffer, vertical lift system	Economic assessment of different schemes
8	Germany[c]	Considering innovative concepts for mining	Considering different options for processing

Source:
[a]Herrouin et al. (1991)
[b]Yamada and Yamazaki (1998) (for mining technology)
[c]ISA (2008b)

risers in connecting pumps and power cables, reduced top tension for surface vessel, ability to retrieve and reinstall, and easy handling in severe weather conditions could provide the much required technological support for development of sub-sea mining systems (Hill 2008).

Major research efforts have been concentrated on the development of collector and riser systems (Chung 2003), whereas very few studies have been conducted on the mining platform and ore handling or transfer at sea (Amann 1982; Ford et al. 1987; Herrouin et al. 1991) that have proposed possible designs, dimensions, and infrastructure required to support a deep-sea mining activity. This sector (mining platform and ore transfer) may have to depend on existing infrastructure available for offshore oil and gas production and bulk carriers to be modified into mining platforms and transport vessels.

1.3.3 Processing Technology and Waste Management

Different Contractors are pursuing different approaches or processing routes mainly depending on the number of metals to be extracted (Table 1.4). According to a study 'the incremental capital requirement of manganese recovery (in addition to Cu, Ni, Co)

in a four metal route over a three metal route was small enough to make a 1.5 Mt/year capacity plant economically viable' (ISA 2008b). Further, it has also been suggested that 'a three metal recovery system needed to operate at higher annual capacities, with 3 million dry tonnes per year; whereas, four metal systems with additional costs and revenues from manganese production can operate at half the capacity'. Finally, the decision of extracting three or four metals will depend on the metal prices, available technology, investment potential, and the returns expected from such investments. In terms of post-processing scenario, probably the least attention has been given to the disposal of material that will remain after extraction of metals. In case of polymetallic nodules, it amounts to large quantities of material (as high as 76% in case of four metals and 97.5% in case of three metals) for which due consideration is required for either disposing them or using them for any 'constructive' purpose (see Wiltshire 2000; Wiltshire, this issue).

1.4 Environmental Issues

1.4.1 Impact of Environment on Mining

Generally in case of any developmental activity, the issue of the impact of the activity on the environment occupies higher significance not realising that the component of 'environment' has a two-way implication. As in case of deep-sea mining, the activity in most likelihood would have an impact on the marine environment; the reverse, i.e. impact of environment on mining activity, is equally important because the prevailing conditions such as atmospheric, hydrographic, seafloor topography, mineral characteristics, and associated substrates at the mine-site would play a major role in the design and performance of different sub-systems of the mining system (Table 1.5). Hence, collection of environmental data would not only help in impact assessment after mining activity, but also play a key role in designing of the mining system as well as planning of the mining operation (Sharma 2011).

1.4.2 Impact of Mining on Environment

It is known that the areas likely to be affected by deep-sea mining would range from the surface and water column due to particles discharged (accidently or otherwise) during lifting, at-sea processing, and transportation (Pearson 1975; Amos et al. 1977) to the seafloor where the mineral will be separated from the associated substrate either due to scooping or drilling, leading to resuspension and redistribution of debris in the bottom water along the path of the collector device as well as in the vicinity of the mining tracks (Foell et al. 1990; Trueblood 1993; Fukushima 1995; Tkatchenko et al. 1996; Sharma and Nath 2000; Theil 2001; Sharma 2001, 2005) and the land due to metal extraction and tailing disposal (Fig. 1.3).

Table 1.5 Influence of environmental conditions on mining system design and operation

Sr. no.	Conditions (key parameters)	Influence on mining system
1	Atmospheric (wind, rainfall, cyclone)	Will determine actual fair weather conditions for operating the mining system during different seasons of the year
2	Hydrographic (waves, currents, temperature, pressure)	Will influence operations on the platform including ore-handling and mining system deployment at the surface; and stability of riser system in the water column
3	Topographic (relief, macro and micro-topography, slope angles)	Will have a bearing on the manoeuvrability and stability of the mining device on the seafloor
4	Mineral characteristics (grade, size, abundance, morphology, distribution pattern)	Important for designing the mechanism for collection, crushing as well as screening of mineral at the seafloor from un-wanted material before pumping the nodules to the surface
5	Associated substrates (sediment-size, composition, engineering properties; rock outcrops—extent, elevation)	Will affect the mobility and efficiency of the collector device to be able to operate without sinking (or getting stuck) in the sediment and be able to avoid the rock outcrops for its safety

Source: Sharma (2011)

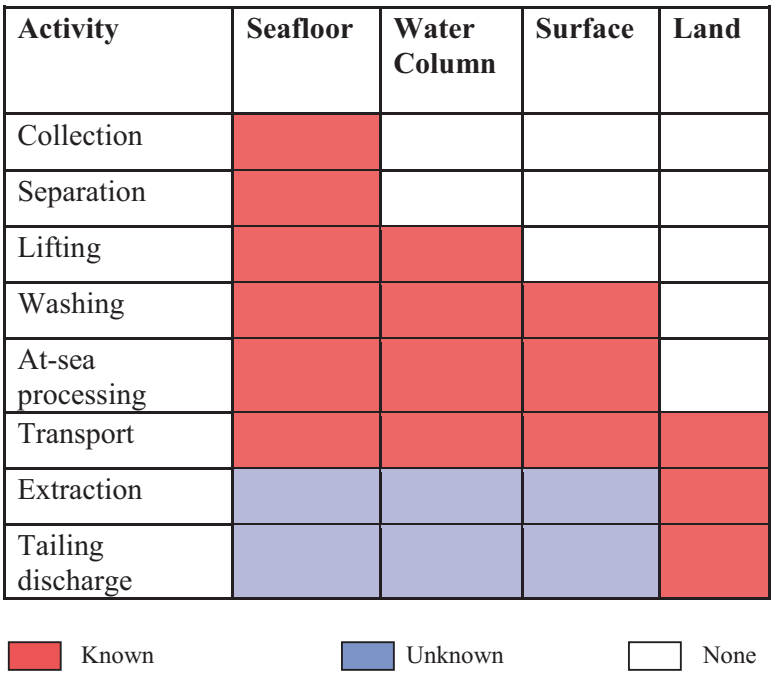

Fig. 1.3 Areas likely to be affected due to different activities of deep-sea mining

The first impact assessment study for deep-sea mining was during two of the pilot mining tests under the Deep Ocean Mining Environment Study (DOMES, 1972–1981) conducted by Ocean mining Inc. (OMI) and Ocean mining Associates (OMA) in the Pacific Ocean (Ozturgut et al. 1980). Subsequently, several experiments have been conducted by Contractors for assessing the potential impacts using devices such as the plough-harrow as well as a hydraulic sediment re-suspension system in the Pacific and Indian Oceans (Table 1.6). Their results have shown that the scale of these experiments was significantly smaller than that expected during commercial mining (Yamazaki and Sharma 2001). Syntheses of the results of these experiments have revealed the need for several improvements for conducting similar experiments in future (Morgan et al. 1999). An engineering and environmental assessment of deep-sea mining has suggested to 'test benthic disturbance in scale and system large enough to represent the commercial mining scale' (Chung et al. 2001).

Table 1.6 Basic data of Benthic Impact Experiments (BIEs) for assessing potential environmental impact of nodule mining

Experiment	Conducted by	Area	Tows	Duration	Area/distance	Discharge[a]
DISCOL[b]	Hamburg University, Germany	Peru Basin	78	~12 days	10.8 km^2	–
NOAA-BIE[c]	National Oceanographic & Atmospheric Administration, USA	Clarion Clipperton Fracture Zone	49	5290 min	141 km	6951 m^3
JET[d]	Metal mining Agency of Japan	Clarion Clipperton Fracture Zone	19	1227 min	33 km	2495 m^3
IOM-BIE[e]	Inter Ocean Metal–consortium of East Europen Countries	Clarion Clipperton Fracture Zone	14	1130 min	35 km	2693 m^3
INDEX[f]	National Institute of Oceanography, Govt. Of India	Central Indian Ocean Basin	26	2534 min	88 km	6015 m^3

Source:
[a]Yamazaki and Sharma (2001)
[b]Foell et al. (1990)
[c]Trueblood (1993)
[d]Fukushima (1995)
[e]Tkatchenko et al. (1996)
[f]Sharma and Nath (2000)

1.5 Policy Issues

A deep-sea mining venture requires the implementation of several components starting with 'Exploration and resource estimation' followed by 'Technology development' for mining and metallurgical processing, and 'Environmental' component so as to establish baseline conditions, undertake impact assessment and monitoring, leading to development of environmental management plan. The final execution of the project would depend on a 'Techno-economic assessment' as well as 'Legal' framework in order to guide the decisions and actions for implementation on the basis of inputs received from other components. Activities under each of these components could initially be independent of each other, but a close networking among these is required to execute the project.

In view of many of the deep-sea mineral deposits occurring in the international waters, any commercial activity related to them could have global implications for which the Preparatory Commission for the International Seabed Authority (ISA) initiated the 'Draft regulations on prospecting, exploration and exploitation of polymetallic nodules in the Area' (UN 1990). With increasing awareness for the need to regulate such activities in the international waters, it was also suggested that the 'UN and ISA should draw up a concrete plan for keeping abreast of scientific progress and at regular intervals assess the need for revising regulations' (Markussen 1994).

Since the formation of the ISA in 1994 (by article 156 of 1982 United Nations Convention on Law of the Sea), it has served as the regulating agency for all activities related to the resources in the Area (i.e. defined as the seabed and subsoil beyond the limits of national jurisdiction); beginning with the notification of the plan of work for exploration of the Pioneer Investors and the area allotted to them (ISA 1998) to the establishment of a comprehensive set of rules, regulations, and procedures for prospecting and exploration for polymetallic nodules in the international seabed Area (ISA 2000). Through a series of international workshops, ISA has also issued the recommendations for assessment of possible environmental impacts from exploration of nodules (ISA 2001) and for establishment of environmental baselines and associated monitoring program for exploration of polymetallic sulphides and cobalt crusts (ISA 2005). The International Marine Minerals Society has also prepared a code for environmental management for marine mining, which provides a framework for development and implementation of an environmental program for a marine exploration and extraction site by marine mining companies and for other stakeholders in evaluating such programs (www.immsoc.org/IMMS_code.htm (2011)).

Deep-sea mining is in an advantageous position due to the substantial lead time available to the regulatory agencies to put in place the policies required for exploration and exploitation of the seabed resources as well as the Contractors to adopt such guidelines and gear themselves up for a sustained development of this common heritage of mankind.

Acknowledgments Author gratefully acknowledges the permission given by Secretary General, International Seabed Authority, Jamaica, for reproducing the maps from website.

References

Amann H (1982) Technological trends in ocean mining. Philos Trans R Soc:377–403
Amos AF, Roels OA, Garside C, Malone TC, Paul AZ (1977) Environmental aspects of nodule mining. In: Glasby GP (ed) Marine manganese deposits. Elsevier, Oxford, pp 391–438
Banakar VK, Hein JR, Rajani RP, Chodankar AR (2007) Platinum group elements and gold in ferromanganese crusts from Afanasiy-Nikitin seamount, equatorial Indian Ocean: sources and fractionation. J Earth Sys Sc 116:3–13
Chung JS (2003) Deep-ocean mining technology: learning curve I. In: Proceedings of ISOPE-ocean mining symposium, International Society for Offshore and Polar Engineers, Tsukuba, Japan, pp 1–16
Chung JS, Schriever G, Sharma R, Yamazaki T (2001) Deep seabed mining environment: engineering and environment assessment. In: Proceedings of ISOPE–ocean mining symposium, International Society for Offshore and Polar Engineers, Szcecin, Poland, pp 8–14
Cronan DS (1980) Underwater minerals. Academic Press, London, p 362
Cronan DS (ed) (2000) Marine mineral deposits handbook. CRC Press, Boca Raton, p 406
Cronan DS, Moorby SA (1981) Manganese nodules and other ferromanganese oxide deposits from the Indian Ocean. J Geol Soc Lond 138:527–539
Dick R (1985) Deep-sea mning versus land mining: a cost comparison. In: Donges JB (ed) The economics of deep-sea mining. Springer-Verlag, Berlin, Germany, pp 2–60
Exon NF, Raven MD, De Carlo EH (2002) Ferromanganese nodules and crusts from the Christmas region, Indian Ocean. Mar Georesour Geotechnol 20:275–297
en.wikipedi.org/wiki/HMSChallenger. Information on HMS Challenger expedition 1873–1876.
Frazer JZ, Fisk MB (1981) Geological factors related to characteristics of seafloor manganese nodule deposits. Deep-Sea Res 28A:1533–1551
Frazer JZ, Wilson LL (1980) Nodule resources in the Indian Ocean. Mar Min 2:257–256
Foell EJ, Thiel H, Schriever G (1990) DISCOL: a long-term, large-scale, disturbance-recolonization experiment in the abyssal eastern tropical South Pacific Ocean. In: Proceedings of offshore technology conference, International Society for Offshore and Polar Engineers, Houston, pp 497–503
Ford G, Niblett C, Walker L (1987) The future for ocean technology. Frances, London, 139 pp
Fukushima T (1995) Overview Japan Deep-Sea impact experiment=JET. In: Proceedings of ISOPE ocean mining symposium. International Society for Offshore and Polar Engineers, Tsukuba, Japan, pp 47–53
Glasby GP (1972) Geochemistry of manganese nodules from the Northwest Indian Ocean. In: Horn DR (ed) Ferromanganese deposits on the ocean floor. National Science Foundation, Washington, pp 93–104
Glasby GP (ed) (1977) Marine manganese deposits. Elsevier, Amsterdam, p 523
Glasby GP (1982) Manganese nodules from the South Pacific: an evaluation. Mar Min 3:231–270
Glasby GP, Stoffers P, Sioulas A, Thijssen T, Friedrich G (1982) Manganese nodules formation in the Pacific Ocean: a general theory. Geo-Mar Lett 2:47–53
Glasby GP (1983) The three-million-tons-per-year manganese nodule "Mine Site": an optimistic assumption? Mar Min 4:73–77
Gleason WM (2008) Companies turning to seafloor in advance of next great metals rush. Min Engg April 2008:14–16
Glumov IF, Kuzneicov KM, Prokazova MS (2000) Ocenka znaczzenija mineralych resursov meidunarod nogo rajona morskogo dna w mineralno syriewom potenciale Rossijskoj Federacii (in Russian). In: Proceedings of geological congress, St. Petersburg, pp 27–29
Halbach P, Sattler CD, Teichmann F, Wahsner M (1989) Cobalt rich and platinum bearing manganese crust deposits on seamounts: nature, formation and metal potential. Mar Min 8:23

Halkyard J (2008) Paper presented in Workshop on polymetallic nodule mining technology: current status and challenges ahead, Chennai, India (Sept. 2008). International Seabed Authority, Jamaica

Hein JR, Yeh H-W, Alexander E (1979) Origin of iron-rich montmorillonite from the manganese nodule belt of the north equatorial Pacific. Clay Clay Miner 27:185–194

Hein JR, Kochinsky A, Halbach P, Manheim FT, Bau M, Kang J-K, Lubick N (1997) Iron and manganese oxide mineralisation in the Pacific. In: Nicholon K, Hein JR, Buhn B, Dasgupta S (eds) Manganese mineralisation: geochemistry and mineralogy of terrestrial and marine deposits. Geological Society Special Publication No. 119, London, p 123

Hill T (2008) Paper presented in workshop on polymetallic nodule mining technology: current status and challenges ahead, Chennai, India, Sept 2008. International Seabed Authority, Jamaica

Herrouin G, Lenoble JP, Charles C, Mauviel F, Bernard J, Taine B (1991) French study indicates profit potential for industrial manganese nodule venture. Trans Soc Min Metall Explor 288:1893–1899

International Marine Minerals Society (2011) Code for environmental management of marine mining. www.immsoc.org/IMMS_code.htm

International Seabed Authority (2016) Areas allotted to Contractors and Reserved areas in the Pacific Ocean, Atlantic Ocean and Indian Ocean. www.isa.org.jm

ISA (1998) Plans of work of exploration of Govt. of India, Inst. Francais de Researche pour L'exploration de la mer, Deep Ocean Resources Development Co. Japan, Yuzhmorgeologiya Russia, China Ocean Mineral Resources R & D Association, Interoceanmetal Joint Organisation, and Govt. of Republic of Korea. Report of the Secretary General, International Seabed Authority, Jamaica. ISBA/4/A/1/Rev.2

ISA (2000) Decision of the assembly relating to the regulations on prospecting and exploration for polymetallic nodules in the Area. ISBA/6/A/18, International Seabed Authority, Jamaica, p 48

ISA (2001) Recommendations for guidance of contractors for the assessment of the possible environmental impacts arising from exploration for polymetallic nodules in the Area. International Seabed Authority, Jamaica. ISBA/7/LTC/1 2001; pp 11.

ISA (2005) Recommendations of the workshop on polymetallic sulphides and cobalt crusts: their environment and considerations for the establishment of environmental baselines and an associated monitoring programme for exploration. ISBA/11/LTC/2 2005, International Seabed Authority, Jamaica, p 26

ISA (2008a) Report on the International Seabed Authority's workshop on Polymetallic nodule mining technology: current status and challenges ahead. ISBA/14/LTC/3, International Seabed Authority, Jamaica, p 4

ISA (2008b) Executive summary of the International Seabed Authority's workshop on Polymetallic nodule mining technology: current status and challenges ahead. International Seabed Authority: Chennai, India, p 20

ISA (2009) A geological model for polymetallic nodules in Clarion-Clipperton Fracture Zone. Technical Report No. 6, International Seabed Authority, Jamaica, p 211

Jasiobedzki P, Corcoran R, Jenkin M, Jakola R (2007) From space robotics to deep seabed mining. In: Proceedings of 37th Underwater Mining Institute. International Marine Minerals Society, Tokyo, Japan, pp J1–11

Jauhari PJ, Pattan JN (2000) Ferromanganese nodules from the Central Indian Ocean Basin. In: Cronan DS (ed) Handbook of marine mineral deposits. CRC Press, Boca Raton, pp 171–195

Kotlinski R (2001) Mineral resources of the world's ocean—their importance for global economy in the 21st century. In: Proceedings of 4th ISOPE ocean mining symposium, International Society for Offshore and Polar Engineers, Szczecin, Poland, pp 1–7

Kunzendorf H (1986) Marine mineral exploration. Elsevier Science Publications, Amsterdam, 300 p

Lenoble JP (2000) A comparison of possible economic returns from mining deep-sea polymetallic nodules, polymetallic massive sulphides and cobalt-rich ferromanganese crusts. In: Proceedings of workshop on mineral resources. International Seabed Authority, Jamaica, pp 1–22

Markussen JM (1994) Deep seabed mining and the environment: consequences, perception and regulations. In: Bergesen H, Parmann G (eds) Green Globe Yearbook of international cooperation on environment and development. Oxford University Press, London, pp 31–39

Martin-Barajas A, Lallier-Verges E, Lecraire L (1991) Characteristics of manganese nodules from the Central Indian Basin: relationship with sedimentary environment. Mar Geol 101:249–265

Metals prices for Cu, Ni, Co, Mn for 5 years (July 2011). www.metalprices.com

Mero JL (1965) The mineral resources of the sea. Elsevier, Amsterdam, The Netherlands, 312 pp

Mero JL (1977) Economic aspects of nodule mining. In: Glasby GP (ed) Marine manganese deposits. Elsevier, Amsterdam, The Netherlands, pp 327–355

Morgan C (2000) Resource estimation of the Clarion-clipperton manganese nodule deposits. In: Cronan DS (ed) Handbook of marine mineral deposits. CRC Press, Boca Raton, pp 145–170

Morgan CL, Odunton N, Jones AT (1999) Synthesis of environmental impacts of deep seabed mining. Mar Georesour Geotechnol 17:307–357

Ozturgut E, Lavelle JW, Steffin O, Swift SA (1980) Environmental investigation during manganese nodule mining tests in the north equatorial pacific, in November 1978. NOAA Tech. Memorandum ERL MESA-48, National Oceanic and Atmospheric Administration, p 50

Pearson JS (1975) Ocean floor mining. Noyes Data Corporation, Park Ridge, NJ, 201 pp

Rao VP, Nath BN (1988) Nature, distribution and origin of clay minerals in grain size fractions of sediments from manganese nodule field, Central Indian Ocean Basin. Ind J Mar Sci 17:202–207

Plueger WL, Herzig PM, Becker K-P, Deissmann G, Schops D, Lange J, Jenisch A, Ladage S, Richnow HH, Schultz T, Michaelis W (1990) Dicovery of the hydrothermal fields at the Central Indian Ridge. Mar Min 9:73

Rona PA (1988) Hydrothermal mineralisation at oceanic ridges. Can Mineral 26:431

Rona PA (2003) Resources of the ocean floor. Science 299:673–674

Sharma R (2011) Deep-sea mining: economic, technical, technological and environmental considerations for sustainable mining. Mar Technol Soc J 45:28–41

Sharma R, Nath BN (eds) (2000) Indian BIE: Indian Deep-sea Environment Experiment (INDEX). Mar Georesour Geotechnol 18:177–294

Sharma R (ed) (2001) Indian deep-sea environment experiment (INDEX): a study for environmental impact of deep seabed mining in Central Indian Ocean. Deep-Sea Res II 48:3295–3426

Sharma R (ed) (2005) Indian deep-sea environment experiment (INDEX): monitoring the restoration of marine environment after artificial disturbance to simulate deep-sea mining in Central Indian Basin. Mar Georesour Geotechnol 23:253–427

Siddiquie HN, Das Gupta DR, Sen Gupta NR, Shrivastava PC, Mallik TK (1978) Manganese-Iron nodules from the Indian Ocean. Ind J Mar Sci 7:239–253

Theil H (ed) (2001) Environmental impact study for mining of polymetallic nodules from the deep sea. Deep-Sea Res II 48:3427–3882

Thijssen T, Glasby GP, Schmitz WA, Friedrich G, Kunzendorf H, Muller D, Richter H (1981) Reconnaissance survey of Manganese Nodules from the Northern Sector of the Peru Basin. Mar Min 2:385–428

Tkatchenko GG, Radziejewska T, Stoyanova V, Modlitba I, Parizek A (1996) Benthic Impact experiment in the IOM pioneer area: testing for effects of deep seabed disturbance. In: Proceedings of International Semimar on deep seabed mining technology. China Ocean Minerals R&D Association, Beijing, China, pp C55–C68

Trueblood DD (1993) US cruise report for BIE II cruise. Techical Memorandum No. OCRS 4, National Oceanic and Atmospheric Administration, Washington, p 51.

UN (1990) Draft regulations on prospecting, exploration and exploitation of polymetallic nodules in the Area. Part VIII. Protection and preservation of the marine environment from activities in the Area. Working paper by Secretariat, UNODC. LOC/PCN/SCN3/WP6/add.5

UNOET (1982) Assessment of manganese nodule resources. UN Ocean Economics and Technology Branch and Graham & Trotman Limited London, 79pp

UNOET (1987) Delineation of mine sites and potential in different sea areas. UN Ocean Economics and Technology Branch and Graham & Trotman Limited, London, 79pp

Usui A, Matsumoto K, Sekimoto M, Okamoto N (2003). Geological study of cobalt-rich ferromanganese crusts using a camera-monitored drill machine in the Marshall Islands Area. In: Proceedings of ISOPE-Ocean Mining symposium, International Society for Offshore and Polar Engineers, Tsukuba, pp 12–15

Usui A, Moritani T (1992) Manganese nodule deposits in the Central Pacific Basin: distribution, geochemistry and genesis. In: Keating BH, Bolton BR (eds) Geology and offshore mineral resources of the Central Pacific Basin, Earth Science series, vol 14. Springer, New York, pp 205–223

Wiltshire JC (2000) Innovation in marine ferromanganese oxide tailings disposal. In: Cronan DS (ed) Handbook of marine mineral deposits. CRC Press, Boca Raton, pp 281–308

Yamada H, Yamazaki T (1998) Japan's ocean test of the nodule mining system. In: Proceedings of international offshore and polar engineering conference. International Society for Offshore and Polar Engineers, Montreal, Canada, pp 13–19

Yamazaki T, Sharma R (2001) Estimation of sediment properties during benthic impact experiments. Mar Georesour Geotechnol 19:269–289

Dr. Rahul Sharma (rsharma@nio.org, rsharma-goa@gmail.com) has been working as a Scientist at the CSIR-National Institute of Oceanography in Goa, India and has led a multidisciplinary group on 'Environmental studies for marine mining'. He has a master's degree in Geology and a doctorate in Marine Science. His professional interests include application of exploration and environmental data to deep-sea mining. He has edited three special issues of scientific journals, one symposium proceeding, published 35 scientific papers, 20 articles, and presented 50 papers at international symposia.

His international assignments include Visiting Scientist to Japan, Visiting Professor to Saudi Arabia, member of the UNIDO mission 'to assess the status of deep-sea mining technologies' in Europe, USA and Japan, invited speaker and consultant for the International Seabed Authority, Jamaica, and has contributed to the 'World Ocean Assessment report I' of the United Nations.

Chapter 2
Composition, Formation, and Occurrence of Polymetallic Nodules

T. Kuhn, A. Wegorzewski, C. Rühlemann, and A. Vink

Abstract Manganese nodules occur as two-dimensional deposits in abyssal plains of all major oceans. In the Clarion-Clipperton Zone of the northeast equatorial Pacific alone, the amount of nodules is estimated to 21 billion tons indicating the huge potential of this deposit type. Apart from manganese, metals of economic interest are nickel, copper, and cobalt, but the nodules also contain interesting amounts of molybdenum, titanium, lithium, and the rare earth elements. Therefore they are also called as polymetallic nodules.

The nodules consist of concentrically banded zones of micro-layers around a nucleus. They form by metal precipitation either from the ambient seawater (hydrogenetic) or from pore water in the sediments (diagenetic). They generally consist of a mixture of both genetic types but in varying proportions. Hydrogenetic precipitation leads to the enrichment of other metals than diagenetic precipitation (cobalt, rare earths versus nickel, copper, etc.), thus controlling the general chemical composition of the nodules. It seems that suboxic conditions (dissolved oxygen content is less than 5% of the saturation concentration) are generally necessary for diagenetic formation and oxic conditions for hydrogenetic formation. The change from oxic to suboxic conditions and vice versa is probably climatically controlled.

Manganese nodules from the sediment surface are mainly composed of phyllomanganates such as vernadite, birnessite, and buserite, whereas amounts of todorokite seem to be negligible. Phyllomanganates contain their metals either as substitutes of manganese in octahedral layers or as hydrated cations in the interlayers.

Well-studied occurrences of manganese nodules are known from the Clarion-Clipperton Zone in the NE equatorial Pacific, the Peru Basin in the SE Pacific, the Cook Island region in the SW Pacific, the central Indian Ocean Basin, and the Baltic Sea.

The original version of this chapter was revised. The correction to this chapter is available at https://doi.org/10.1007/978-3-319-52557-0_19

T. Kuhn (✉) • A. Wegorzewski • C. Rühlemann • A. Vink
Federal Institute for Geosciences and Natural Resources (BGR),
Stilleweg 2, 30655 Hannover, Germany
e-mail: thomas.kuhn@bgr.de

R. Sharma (ed.), *Deep-Sea Mining*, DOI 10.1007/978-3-319-52557-0_2

2.1 Introduction

Manganese nodules occur as potato-shaped concretions on the seafloor of abyssal plains in about 4000–6000 m water depth in all major oceans. They form two-dimensional deposits on top or within the first 10 cm of the deep-sea sediments (Fig. 2.1). Nodules of the eastern tropical Pacific and the central Indian Ocean are of special economic interest due to their high enrichment of metals such as Ni, Cu, Co, Mo, Li, REE, and Ga (e.g., Hein and Koschinsky 2013). Manganese nodules are also known from shallow seas such as the Baltic Sea and from freshwater lakes, but these nodules have considerably lower contents of valuable metals (Glasby et al. 1997; Hlawatsch et al. 2002).

Exploration for and scientific research on manganese nodules have been carried out intensely since the 1970s. Based on the results of these early studies, the environmental conditions and fundamental processes required for nodule formation are well known today. Modern analytical methods have given us new insights into the growth layers and crystal structures of nodules up to an atomic level. Such methods include, among others, high-resolution transmission electron microscopy (HRTEM), X-ray absorption spectroscopy (EXAFS, XANES), and laser-ablation ICP-MS. Advanced knowledge of the crystallographic structure of manganese oxides as well as their oxidation states, structural positions, and coordination environment of metals can be attributed to the utilization of these new methods (Takahashi et al. 2007; Bodeï et al. 2007; Peacock and Sherman 2007a; Manceau

Fig. 2.1 High abundance of large nodules on the seafloor of the Peru Basin (ca. 4000 m water depth; © BGR)

et al. 2014; Wegorzewski et al. 2015). Such knowledge could be fundamental for the development of state-of-the-art tailored metallurgical processing techniques for manganese nodules. Considerable research has also focused on the influence of microbial activity on the formation of Mn oxides (Ehrlich 2000).

In this book section, a review of the current state of knowledge of manganese nodule composition, formation, and occurrence is provided. Firstly, a general description of the macroscopic and microscopic textures of Mn nodules including a review of the various mineralogical nomenclatures of Mn oxides and a suggestion for a general terminology is given. Then, we discuss the chemical composition of nodules with special regard to the metal and trace metal content in nodules of different genesis. The formation of nodules under differing environmental conditions is also discussed. Finally, a brief overview of the main economically interesting occurrences of nodule fields and their characteristics is provided.

2.2 Classification and Description

2.2.1 General Classification

Polymetallic manganese nodules consist of concentrically banded zones of microlayers around a nucleus. The latter can be composed of indurated sediments, rock particles, biogenetic fragments, or micro-nodules (von Stackelberg and Beiersdorf 1987). Individual layers are characterized by different chemical and mineralogical compositions that are determined by two different growth processes: *hydrogenetic* and *diagenetic* growth (Halbach et al. 1988). *Hydrogenetic* layers form as a result of element precipitation from oxygen-rich seawater (Koschinsky and Halbach 1995; Koschinsky and Hein 2003) and *diagenetic* layers form as a result of element precipitation from suboxic pore water (low oxygen content of <5 µmol O_2/l; Burns and Burns 1978; Glasby 2006; Bodeï et al. 2007; Hein and Koschinsky 2013; Wegorzewski and Kuhn 2014). Manganese nodules are usually composed of mixtures of both layer types. In contrast, ferromanganese crusts which usually form on the hard rock of seamounts often consist purely of hydrogenetic layers.

2.2.2 Macroscopic and Microscopic Descriptions

Manganese nodules occur as a monodisperse layer on the sediment-covered seafloor (Fig. 2.1). They can have different size, shape, and surface morphologies (Fig. 2.2) and can reach a size of up to 15 cm in diameter. Some extremely large specimens of 21 cm have been found in the Peru Basin (von Stackelberg 1997). Nodules can have a spheroidal, ellipsoidal, elongated, discoidal, platy, cauliflower, irregular, and polynodule shape. Nodules from the Clarion-Clipperton Zone (CCZ) in the equatorial NE Pacific and from the Central Indian Ocean Basin (CIOB) predominantly have a

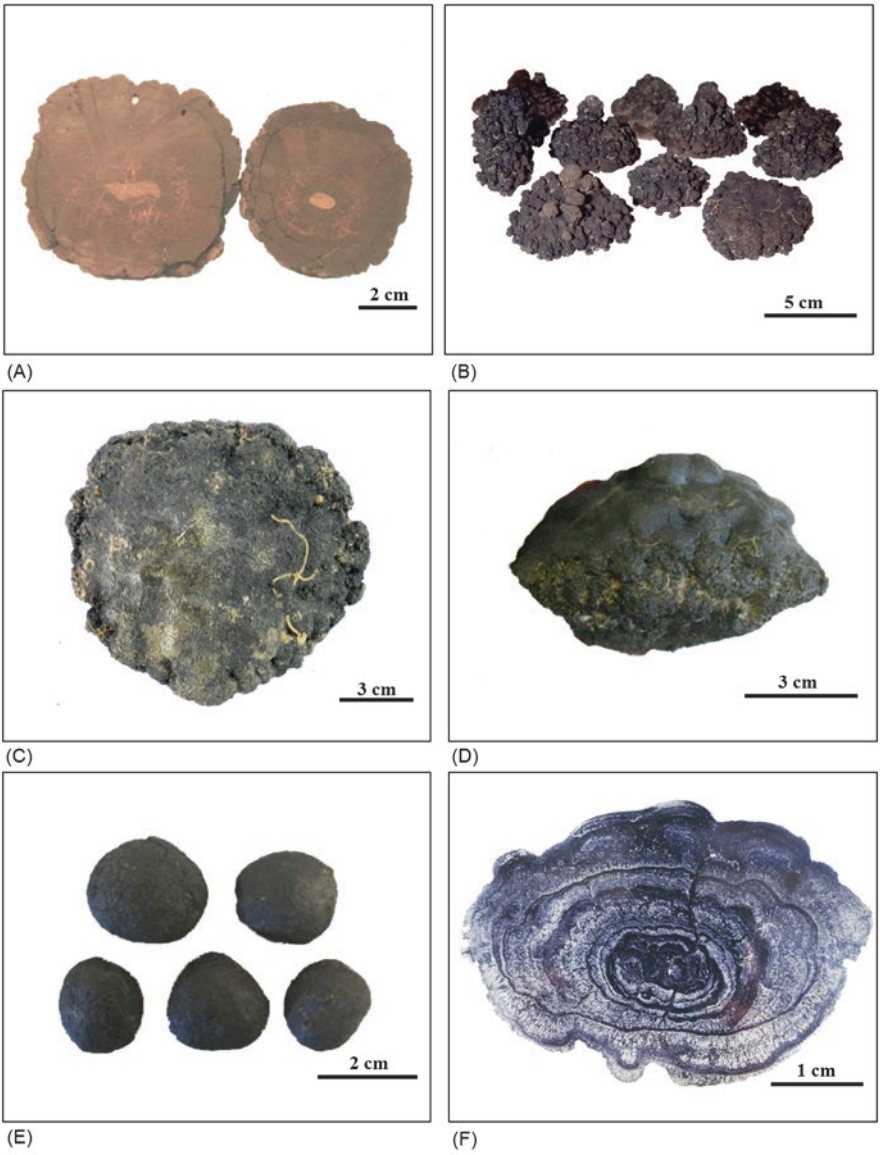

Fig. 2.2 Different sizes and shapes of manganese nodules from different regions. (**a**) Typical hydrogenetic nodule with a spheroidal shape (from Manihiki Plateau, Cook Islands). (**b**) Cauliflower-shaped nodules from the Peru Basin. (**c**) Discoidal-shaped nodule from the Clarion-Clipperton Zone in the equatorial Pacific (CCZ). (**d**) Nodule with an upper smooth and a lower coarse-grained side. (**e**) Small, spheroidal nodules from the CCZ. (**f**) Section through a typical CCZ nodule revealing its layered structure. All figures: © BGR

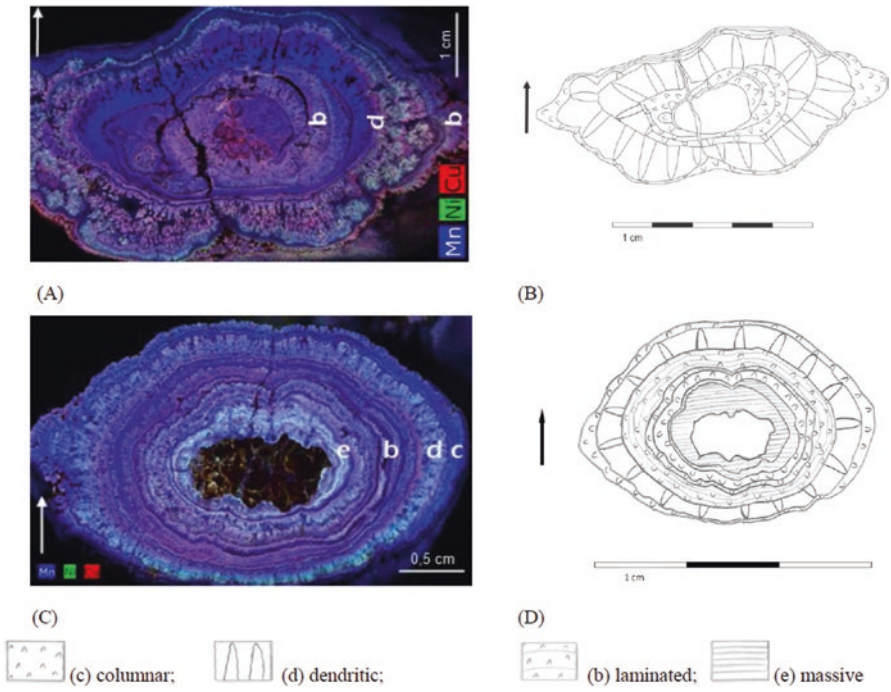

Fig. 2.3 Internal growth structures of manganese nodules. (**a**, **c**) Element distribution based on complete scans of the nodule with the Tornado M4 X-ray scanner. (**b**, **d**) Internal growth structures based on a combination of X-ray scanner, microscopy, and microprobe analyses. The arrows mark the orientation of the nodule during sampling. See text for further explanation. Figures from Krapf (2014)

discoidal shape and a size range of 2–8 cm. Nodules from the Peru Basin (SE Pacific) are often larger and usually display a cauliflower shape. Hydrogenetic nodules such as those from the Exclusive Economic Zone (EEZ) of the Cook Islands have a predominantly spheroidal shape (Fig. 2.2). Surfaces of nodules are either smooth or coarse-grained, with the smooth side being in contact with seawater and the coarse side being surrounded by sediment.

Depending on the environmental conditions that predominate during nodule formation, hydrogenetic or diagenetic layers with different internal growth structures form (Halbach et al. 1988). These internal growth structures are characterized as being finely laminated, columnar, pillar-like, dendritic, and massive (von Stackelberg and Marchig 1987; Figs. 2.3 and 2.4). Hydrogenetic layers are typically composed of finely laminated to columnar structures, whereas diagenetic precipitation mainly leads to the development of dendritic layers and less frequently to dense, massive layers (Figs. 2.3 and 2.4; Wegorzewski and Kuhn 2014; Krapf 2014). Columnar growth during hydrogenetic precipitation is due to the influence of distinct

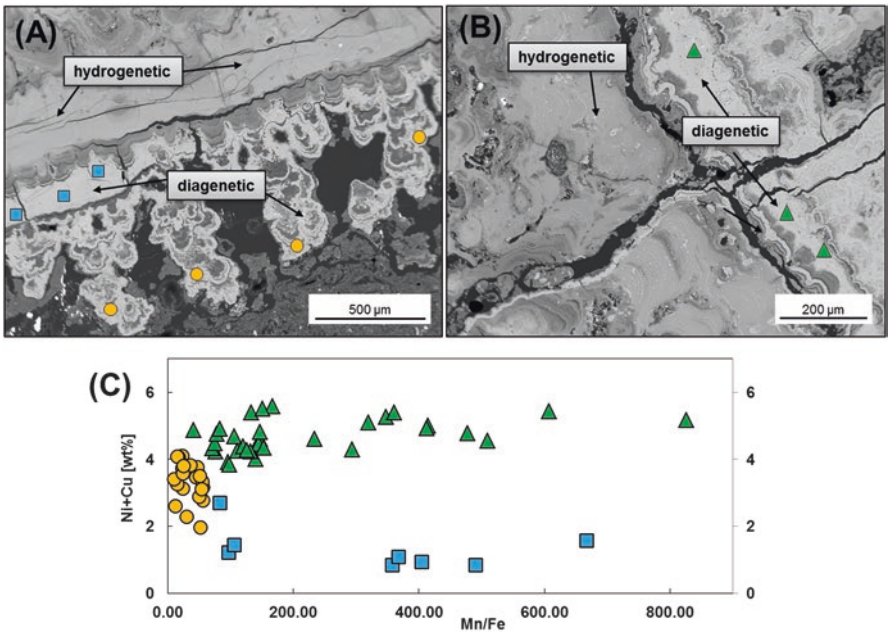

Fig. 2.4 (**a**, **b**) Backscatter electron images of typical hydrogenetic and suboxic-diagenetic layers of a manganese nodule from the CCZ. (**c**) Mn/Fe ratios vs. Ni + Cu contents of individual suboxic-diagenetic layers of the same nodule (Wegorzewski et al. 2015; reproduction with permission of Mineralogical Society of America)

near-bottom currents that not only keep the seafloor sediment-free, but also govern preferential growth on already existing surface areas. In contrast, diagenetic growth takes place within the pore space of the sediments. This often leads to the formation of isolated, rosette-like structures that tend to combine during further growth, thereby encapsulating and incorporating sediment particles.

The growth rate of hydrogenetic layers is typically in the range of 1–5 mm per million years, (Koschinsky and Hein 2003 and references therein, whereas diagenetic layers grow considerably faster (up to 250 mm per million years; von Stackelberg 2000). Altogether, Mn nodules grow with average rates of 10–20 mm per million years and usually have an age of several millions of years.

The dry bulk density of nodules ranges between 1.00 and 2.40 g/cm^3, porosity is in the range of 25–61%, and internal surface area lies in the range of 100–150 m^2/g (Hein et al. 2013; Blöthe et al. 2015).

The high porosity, the large pore size, and the pore connectivity (high permeability) all enable bottom seawater or pore water to enter the nodules constantly during formation. This is very likely the cause for the secondary fillings of pore spaces with either diagenetic or hydrogenetic precipitates (Wegorzewski and Kuhn 2014; Blöthe et al. 2015).

2.3 Chemical and Mineralogical Composition

2.3.1 Chemical Composition

The chemical composition of nodules is controlled by the type of formation (diagenetic versus hydrogenetic), the location (geographic position and water depth), and the growth rate. Hydrogenetic nodules have Mn/Fe ratios ≤5 (Halbach et al. 1988) and high contents of high field strength elements such as Ti, REY, Zr, Nb, Ta, Hf as well as elements that can be oxidized on the surface of Mn oxides such as Co, Ce, and Te (Koschinsky and Hein 2003; Hein et al. 2013). Nodules from the Cook Islands EEZ are mainly of hydrogenetic origin and their element inventory is typical for hydrogenetic nodules (Table 2.1).

Diagenetic nodules are characterized by Mn/Fe ratios >5 (Halbach et al. 1988) and are enriched with elements that either fit into the crystal lattice of these nodules according to their size or stabilize the lattice by balancing ion charge deficits. The latter is caused either by the incorporation of Mn^{3+} instead of Mn^{4+} into the octahedral chains of Mn oxides, or by vacancy sites therein (see below). Typical elements enriched in diagenetic nodules are Ni, Cu, Ba, Zn, Mo, Li, and Ga. Nodules from the Peru Basin are mainly of diagenetic origin (von Stackelberg 1997) and their element inventory is typical for diagenetic nodules (Table 2.1).

Nodules from the CCZ in the NE Pacific generally exhibit a mixture of diagenetic and hydrogenetic origin, with a predominantly diagenetic input (Wegorzewski and Kuhn 2014; Figs. 2.4 and 2.5). Their elemental contents lie between those typical for hydrogenetic nodules (Cook Islands) and those typical for diagenetic nodules (Peru Basin) with the exception of Cu (1.07% in the CCZ nodules), Ba (3500 µg/g), and Mo (590 µg/g). The significantly lower Cu content of Peru Basin nodules may be due to a more efficient Cu recycling in carbonate sediments as compared to the siliceous sediments of the CCZ (Wegorzewski and Kuhn 2014). Indian Ocean nodules are also diagenetic–hydrogenetic mixtures, but CIOB nodules generally exhibit lower metal contents as compared to CCZ nodules (Hein et al. 2013).

In addition to the abovementioned abyssal manganese nodules of the large oceans mentioned above, there are many other locations in the world's oceans that host special Mn-(Fe)-nodules. The formation and composition of such nodules are controlled by local conditions such as hydrothermal (seafloor massive sulfides), hydrocarbon (Gulf of Cadiz), and fault-controlled fluid venting (Galicia Bank) or local rapid exchange between oxic and anoxic conditions (Baltic and Black Sea).

Hydrothermal Mn oxides precipitate from low-temperature fluids at the periphery or during the waning stage of a high-T hydrothermal system (Kuhn et al. 2003). Examples are found in almost every seafloor hydrothermal system along mid-ocean ridges, in back-arc basins, and on seamounts. In many cases, they are enriched in manganese (> 40 wt% Mn) and have very low Fe contents (< 1 wt% Fe) and low trace metal concentrations (<1000 µg/g; Table 2.1). However, there can be local exceptions with increased contents of single metals such as the enrichment of molybdenum in some hydrothermal Mn crusts from the SW Pacific (Rogers et al. 2001; Kuhn et al. 2003) or Cu-rich crusts from the Yap island arc (Hein et al. 1992).

Table 2.1 Compiled chemical composition of nodules from selected areas of the global ocean

	CCZ[a]		Eastern CCZ[b]		Central CCZ[b]		Peru basin[a]	Indian Ocean[a]		Cook Islands[c]		Gulf of Cadiz[d]		Baltic sea[e]	Fiji basin[f]	
Element	Mean	*N*	Mean	*N*	Mean	*N*	Mean	Mean	*N*	Mean	*N*	Mean	*N*	Mean	Mean	*N*
Fe (%)	6.16	66	6.3	575	6.1	39	6.12	7.14	1135	16.1	1158	38.58	36	14.5	0.48	20
Mn	28.4	66	31.4	575	27.56	39	34.2	24.4	1135	16.1	1158	6.03	36	18.1	40.23	20
Si	6.55	12	6.04	523	7.49	17	4.82	10.02	36	7.3	209	3.48	36	–	–	–
Al	2.36	65	2.29	575	2.71	39	1.5	2.92	49	3.01	209	1.38	36	1.02	0.78	20
Mg	1.89	66	1.94	575	2	39	1.71	1.99	53	1.34	204	1.83	36	1.25	1.08	20
Ca	1.7	66	1.68	575	1.68	39	1.82	1.67	53	1.95	209	3.15	36	1.53	1.63	20
Na	1.99	66	2.19	575	2.04	39	2.65	1.86	38	1.84	209	0.26	36	–	–	–
K	0.99	66	0.97	575	1.09	39	0.81	1.14	49	0.89	209	0.34	36	0.86	–	–
Ti	0.32	66	0.26	566	0.33	39	0.16	0.42	53	1.2	74	0.1	36	–	0.04	20
P	0.21	66	0.15	575	0.21	38	0.15	0.17	46	0.34	54	0.19	36	1.48	0.04	20
Cl	0.27	12	0.7	497	0.46	27	>0.50	–	–	0.42	54	–	–	–	–	–
LOI	26.5	12	15.2	497	15.1	27	16.2	–	–	27.7	54	18.05	24	–	–	–
H_2O^-	11.6	12	–	–	–	–	–	–	–	12.7	54	–	–	–	–	–
H_2O^+	8.8	7	–	–	–	–	–	–	–	11.8	54	–	–	–	–	–
CO_2	–	–	–	–	–	–	–	–	–	–	–	–	–	–	–	–
ST	0.17	12	0.16	497	0.1	–	–	–	–	–	–	0.12	24	–	–	–
Ag (ppm)	0.17	12	–	–	–	–	0.05	–	–	0.23	49	–	–	–	–	–
As	67	12	83	497	65	27	65	150	3	147	69	159	34	–	–	–
Au (ppb)	4.5	9	–	–	–	–	–	–	–	6	18	<d/l	10	–	–	–
B (ppm)	–	–	–	–	–	–	–	–	–	–	–	278	10	–	–	–
Ba	3500	66	4304	566	2280	39	3158	1708	42	1160	54	352	34	–	390	20
Be	1.9	12	–	–	1.9	18	1.4	–	–	3.9	54	–	–	–	–	–
Bi	8.8	12	8.4	60	7.25	4	3.3	–	–	11	54	<d/l	34	–	–	–

Br	–	–	–	–	–	–	–	–	–	–	–	10	34	–	–	–
Cd	16	12	–	–	–	–	19	18	3	4.7	54	–	–	b.d.	–	–
Co	2098	66	1738	575	2501	39	475	1111	1124	4113	1158	90	34	60	11	20
Cr	17	12	14	9	18	4	16	18	3	59	54	34	34	70	–	–
Cs	1.5	61	1.34	566	1.51	18	0.78	0.99	3	<0.38	54	–	–	–	–	–
Cu	10,714	66	11,785	575	10,813	39	5988	10,406	1124	2262	1158	39	34	19.1	47	20
Ga	36	12	25.7	45	–	–	32	–	–	<10	54	–	–	–	–	–
Ge	–	–	–	–	–	–	0.6	–	–	–	–	–	–	–	–	–
Hf	4.7	66	4.53	565	4.51	39	4.7	14	3	13	49	–	–	–	–	–
Hg (ppb)	18	3	–	–	–	–	16	–	–	<36	28	–	–	–	–	–
In (ppm)	0.27	12	–	–	–	–	0.08	–	–	–	–	–	–	–	–	–
Li	131	66	133	566	123	39	311	110	38	51	54	17	10	b.d.	459	20
Mo	590	66	622	567	556	39	547	600	38	295	79	47	34	126	958	20
Nb	22	66	18.7	566	21.3	39	13	98	3	90	67	5	34	–	–	–
Ni	13,002	66	14,012	575	13,574	39	13,008	11,010	1124	3805	1145	108	34	67	115	20
Pb	338	66	276	566	358	39	121	731	38	897	202	18	34	–	<10	20
Rb	23	66	20.2	566	25.2	39	12	70	3	15	54	17	34	–	–	–
Sb	41	12	75	90	19	5	61	50	3	36	54	–	–	–	–	–
Sc	11	66	10.1	566	12	39	7.6	25	3	12	54	18	34	–	–	–
Se	0.72	12	–	–	–	–	0.5	–	–	<0.80	54	–	–	–	–	–
Sn	5.3	12	–	–	–	–	0.9	–	–	7.8	54	–	–	–	–	–
Sr	645	66	701	575	592	39	687	709	53	935	54	282	34	–	380	20
Ta	0.33	66	0.27	559	0.33	39	0.23	1.8	3	2.2	54	–	–	–	–	–
Te	3.6	66	3.57	528	3.85	23	1.7	40	3	24	54	–	–	–	–	–
Tl	199	12	–	–	–	–	129	347	3	146	54	–	–	–	–	–
Th	15	66	11.5	566	17.7	39	6.9	76	3	37	67	4	34	–	–	–
U	4.2	66	3.78	566	3.79	39	4.4	16	3	10	67	4	34	–	–	–
V	445	66	617	575	486	39	431	497	16	508	61	339	34	–	88	20

(continued)

Table 2.1 (continued)

	CCZ[a]		Eastern CCZ[b]		Central CCZ[b]		Peru basin[a]	Indian Ocean[a]		Cook Islands[c]		Gulf of Cadiz[d]		Baltic sea[e]	Fiji basin[f]	
Element	Mean	*N*	Mean	*N*	Mean	*N*	Mean	Mean	*N*	Mean	*N*	Mean	*N*	Mean	Mean	*N*
W	62	66	64.3	566	55	39	75	92	3	64	67	–	–	–	–	–
Y	96	66	78.9	566	105	39	69	108	38	141	54	–	–	–	–	–
Zn	1366	66	1544	566	1228	39	1845	1207	692	545	222	62	34	616	158	20
Zr	307	66	302	566	287	39	325	752	3	524	75	63	34	–	–	–
La	114	66	101	566	109	39	68	129	50	173	54	–	–	–	–	–
Ce	284	66	242	566	270	39	110	486	24	991	54	–	–	–	–	–
Pr	33.4	66	29.7	566	33.3	39	14.1	33	37	40.9	54	–	–	–	–	–
Nd	140	66	120	566	137	39	63	146	50	160	54	–	–	–	–	–
Sm	34	66	29.8	566	33.9	39	14	32.4	50	34.7	54	–	–	–	–	–
Eu	8.03	66	7.3	566	8.26	39	3.87	7.83	46	8.53	54	–	–	–	–	–
Gd	31.8	66	29.3	566	32.6	39	15.6	32	24	36.1	54	–	–	–	–	–
Tb	4.98	66	4.45	566	5.05	39	2.52	5	37	6.09	54	–	–	–	–	–
Dy	28.5	66	25.7	566	29.2	39	15.8	26.5	46	34.9	54	–	–	–	–	–
Ho	5.35	66	4.69	566	5.37	39	3.42	4.92	46	7.18	54	–	–	–	–	–
Er	14.6	66	13	566	14.9	39	9.8	12.9	24	19.1	54	–	–	–	–	–
Tm	2.11	66	1.79	566	2.05	39	1.49	2	11	3.02	54	–	–	–	–	–
Yb	13.7	66	12.5	566	13.7	39	10.3	11.8	46	19.8	54	–	–	–	–	–
Lu	2.05	66	1.84	566	2.03	39	1.61	1.93	50	2.98	54	–	–	–	–	–
Ir (ppb)	2	11	–	–	–	–	–	–	–	5	19	–	–	–	–	–
Os	–	–	–	–	–	–	–	–	–	2	11	–	–	–	–	–
Pd	8	12	–	–	–	–	–	–	–	7	19	–	–	–	–	–
Pt	128	12	0.11	7	–	–	40	–	–	210	32	–	–	–	–	–
Rh	9	12	–	–	–	–	–	–	–	17	19	–	–	–	–	–
Ru	12	12	–	–	–	–	–	26	–	18	19	–	–	–	–	–

ΣREY (ppm)	813		701		801	–	403	1039	–	1678	54	78	24	–	–	–
ΣHREY	199	–	172	655	210	–	130	205	–	–	–	10	24	–	–	–
Element ratios																
Mn/Fe	4.61	66	5.15	575	4.52	39	5.59	3.42	1135	1.00	1158	0.16	36	1.23	83.81	20
Co + Cu + Ni (%)	2.58	66	2.75	575	2.69	39	19,471	22,527	1124	3461		237	36	146.1	173	20
Y/Ho	17.94	66	16.9	566	19.54	39	18.13	21.95	38	–	–	–	–	–	–	–
Zr/Hf	65.32	66	67.2	566	63.64	39	69.15	53.71	3	–	–	–	–	–	–	–
Th/U	3.57	66	3.04	566	4.67	39	1.57	4.75	3	3.7	67	1	24	–	–	–
Ce/Ce^*	1.05	–	1.01	–	1.02	–	0.82	1.72	–	2.72	–		–	–	–	–

Units of elements: Fe-ST: %, rest ppm if not otherwise stated

[a]Hein et al. (2013)

[b]BGR data

[c]Hein et al. (2015)

[d]González et al. (2012)

[e]Hlawatsch et al. (2002)

[f]Rogers et al. (2001)

$Ce/Ce^* = Ce_{SN}/(0.5La_{SN}+0.5P_{rSN})$ SN=Shale normalization with data from Lipin & McKay, 1989

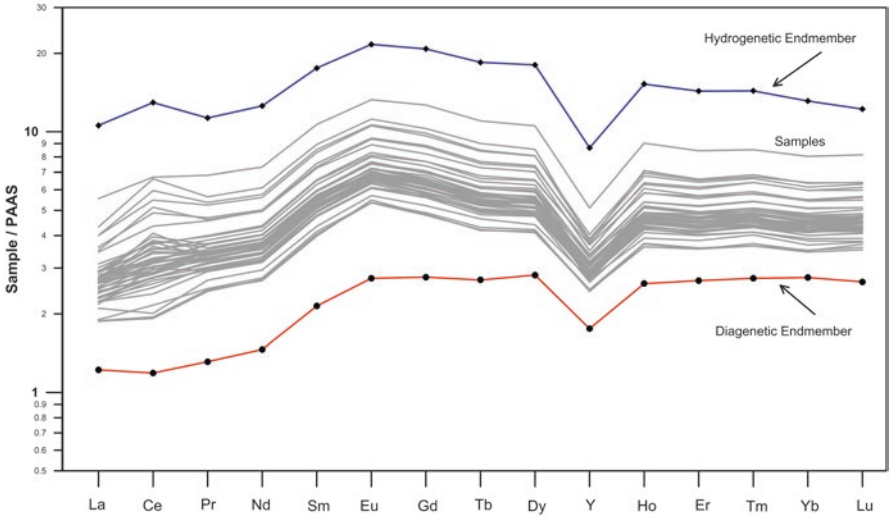

Fig. 2.5 Shale (PAAS) normalized rare earth element and yttrium contents (REY) of manganese nodules from the eastern CCZ (N=47) indicate that the nodules are mixtures of diagenetic and hydrogenetic endmembers (unpublished BGR data; measured with ICP-MS). Diagenetic endmember: nodule from Peru Basin. Hydrogenetic endmember: Fe-Mn crust from CCZ (unpublished BGR data). *PAAS* Post-Archean Australian Shale (McLennan 1989)

Hydrothermal Mn oxide precipitates form by rapid precipitation from low-T hydrothermal fluids at the contact with cold, oxidizing seawater.

Hydrocarbon-related ferromanganese nodule fields occur in the Gulf of Cadiz in 850–1000 m water depth. Their formation is related to hydrocarbon seeps, mud diapirism, and the activity of strong near-bottom currents (González et al. 2012). The nodules grow rapidly (102–124 mm/Ma) and are characterized by a high Fe-Mn fractionation (39 wt% Fe, 6 wt% Mn) and low contents of trace metals (probably due to the high growth rates; Table 2.1).

Cobalt-rich manganese nodules occur together with extensive phosphorite pavements on seamounts and banks on the western Galicia continental margin (NE Atlantic) in ~1200–2000 m water depth (González et al. 2014). These oxidic precipitates are exceptional since they are not only very rich in Co (up to 1.8%) and Mn (up to 45%), but also contain other trace metals such as Ni, Ti, Cu, Mo, REE, Tl, Ga, and Te in high concentrations (González et al. 2014). The formation of these nodules and phosphorites is at least partly related to the activity of deep-reaching faults and the mobilization of metals from a deeper crustal reservoir (J. González, pers. comm.).

In the Baltic Sea, the abundant occurrence of ferromanganese nodules and concretions (up to 40 kg/m^2) is related to the large input of Mn- and Fe-rich suspended matter through rivers in the northeast and east (Gulf of Bothnia, Gulf of Finland) and the formation of an oxidized layer in the upper 2–15 cm of the sediment column (Glasby et al. 1997). Fast-growing Fe-Mn concretions are mainly found in the western Baltic Sea, their formation being related to the development of summer anoxia and the diagenetic mobilization of Mn. The trace metal content of Baltic Sea ferro-

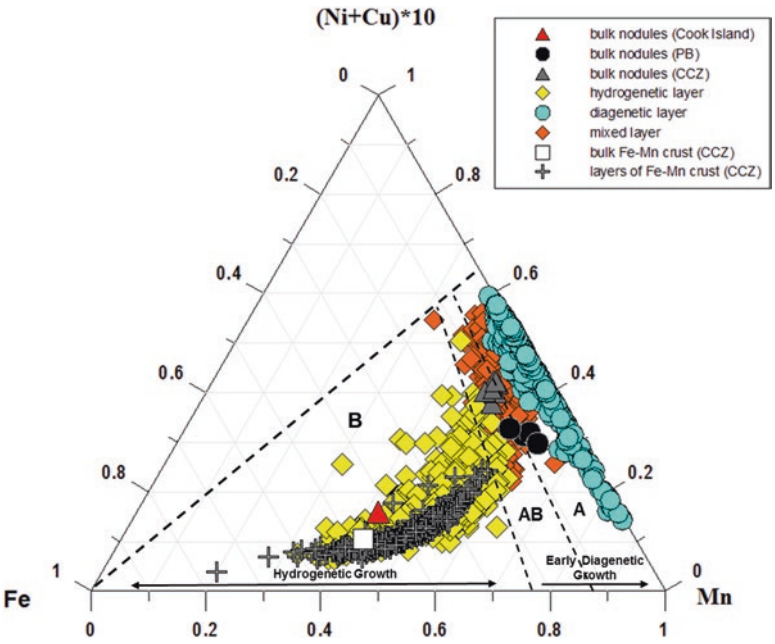

Fig. 2.6 Ternary diagram of Fe-Mn-(Ni + Cu)*10 according to Bonatti et al. (1972) and Halbach et al. (1988) showing the geochemical relationship between different genetic types of nodules and their individual growth layers. *Dashed lines* separate three nodule-type fields: *A* diagenetic nodules, *AB* mixed-type nodules, and *B* hydrogenetic nodules. Bulk analysis of a ferromanganese crust sample lies in field *B* (hydrogenetic growth) but the individual analyses of the crust profile show a high variability in the chemical composition. Analyses of individual hydrogenetic layers within the nodules partly show a diagenetic influence (*AB*). Mixed layers plot into field *AB* and suboxic-diagenetic layers completely into field *A* (suboxic-diagenetic). Bulk nodules from both the CCZ and the PB plot into the mixed-type field (*AB*). Individual layers of nodules, however, show very high scatter as well as much higher Mn/Fe and Ni+Cu concentrations than the bulk nodules. The average bulk nodules from the Cook Islands EEZ show typical hydrogenetic growth and plot into field *B* (data from Hein et al. 2015). Figure from Wegorzewski and Kuhn (2014). Reproduction with permission of Elsevier

manganese oxides is generally low (<0.1%) compared to the nodules from the open oceans (Table 2.1).

Conventionally, a ternary Mn–Fe–Cu+Ni diagram is used to distinguish between the different modes of formation of manganese nodules and ferromanganese crusts (Bonatti et al. 1972; Halbach et al. 1988). In Fig. 2.6, data from seven bulk manganese nodules and one ferromanganese crust from the CCZ and five bulk nodules from the Peru Basin are displayed together with numerous single layer measurements of the same crust and nodules deriving from electron microprobe analyses (EMP; size of measuring points: 1–20 µm; Wegorzewski and Kuhn 2014). It is clear that the single layers of the nodules have a much wider spread within this ternary diagram than the respective bulk nodules (Fig. 2.6), indicating that the bulk nodule content only represents the average concentration of all the single layers (Wegorzewski and Kuhn 2014). Therefore, the chemical composition of bulk nodules must be interpreted with care when inferring the genesis of the nodules.

2.3.2 Mineralogical Composition

As there is no clear terminology with respect to the usage of mineralogical names of Mn oxides at present, we will try to provide a systematic description of their crystallographic structure and suggest a practical terminology in this chapter.

Manganese nodules consist of different Mn oxides and Fe oxyhydroxides. With respect to the Mn oxides, there are two different groups of minerals occurring in natural manganese nodules: phyllomanganates and tectomanganates. They are both built up of [MnO_6] octahedral layers which are separated from each other either by an interlayer containing hydrated cations (phyllomanganates) or they are organized in the form of three-dimensional tunnel structures (tectomanganates, Fig. 2.7; Chukhrov et al. 1979; Turner and Buseck 1979; Bodeï et al. 2007). Phyllomanganates can be subdivided into an ordered (birnessite-buserite) and a disordered group (vernadite). Ordered phyllomanganates with a layer-to-layer distance of ~7Å are named birnessite and contain one plane of water molecules within the interlayer. Ordered phyllomanganates with a layer-to-layer distance of ~10Å are named buserite and contain two planes of water in the interlayer space (Giovanoli et al. 1975; Burns and Burns 1977; Golden et al. 1986; Post and Veblen 1990; Drits et al. 1997; Bodeï et al. 2007; Wegorzewski et al. 2015). The disordered equivalents to these ordered phyllomanganates are termed 7Å vernadite and 10Å vernadite (Manceau et al. 1992a, 2014; Usui and Mita 1995; Drits et al. 1997; Villalobos et al. 2003; Wegorzewski et al. 2015). The crystallographic disorder is termed turbostratic (Warren 1941) because of the random rotation of the [MnO_6] octahedral layers around the c*axis or the translation of the [MnO_6] octahedral layers in the **a–b** plane of the crystallites (Fig. 2.7; Giovanoli 1980; Drits and Tchoubar 1990). Ordered and disordered phyllomanganates can be distinguished by different peaks (reflections) in their diffraction patterns (Fig. 2.8; Drits et al. 2007).

The [MnO_6] octahedral layers of phyllomanganates can contain abundant isomorphic substitution of Mn^{4+} (for example by Mn^{3+}, Ni^{2+}, Cu^{2+}, Co^{3+}) but they can also contain vacancies, i.e., empty octahedrons (cf. Fig. 2.7). In either case, layer charge deficits are induced which can be balanced by incorporation of hydrated interlayer cations either into the middle of the interlayer (e.g., Na^{+}, Li^{+}, Ca^{2+}) or directly above/below layer vacancies (e.g., Mn^{2+}; Mn^{3+}, Ni^{2+}, Cu^{2+}, Zn^{2+}, Cr^{2+}; Post and Bish 1988; Manceau et al. 1997, 2014; Lanson et al. 2000; Peacock and Sherman 2007a, b). Todorokite consists of edge-sharing, 3 × 3 [MnO_6] octahedral chains forming a 3D tunnel structure (Fig. 2.7; Chukhrov et al. 1979; Post et al. 2003; Bodeï et al. 2007). The negative layer charge of todorokite originates from substitution of Mn^{4+} by cations of lower valance (e.g., Mn^{3+}, Ni^{2+}) in the octahedrons. It is balanced by incorporation of mono- and divalent cations into the tunnel structure (e.g., Mg^{2+}, Ba^{2+}; Fig. 2.7). In general, phyllomanganates have a higher layer charge and accordingly a higher potential to sorb metals (e.g., Ni up to 5%) than todorokite (Ni ≤ 2%; Bodeï et al. 2007).

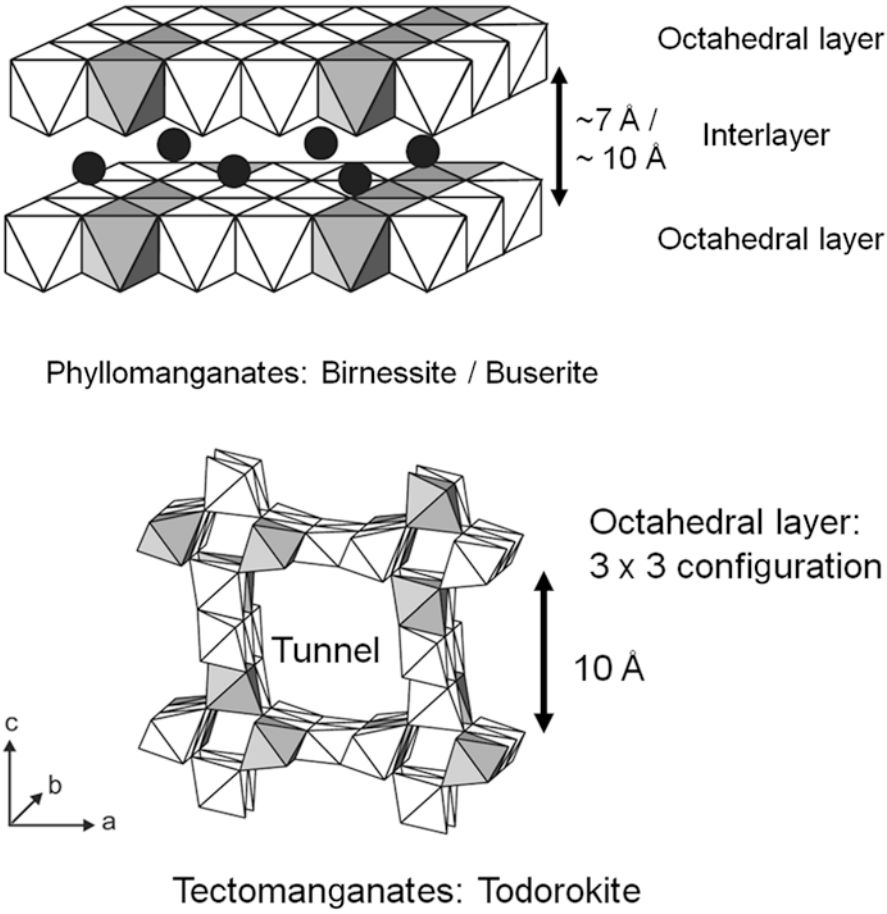

Fig. 2.7 Schematic drawings of the spatial organization of octahedral sheets in different types of manganates. Manganates are built up of [MnO_6] octahedrons (a central Mn^{4+} ion surrounded by 6 oxygen ions in octahedral coordination) which form octahedral layers. In phyllomanganates, these octahedrons form sheets which are stacked in the crystallographic c direction. In tectomanganates, the octahedral sheets form 3D structures such as tunnels. The octahedral sheets contain vacancy sites or Mn^{2+}/Mn^{3+} instead of Mn^{4+}, causing a negative charge deficit. The latter is balanced by cations such as Ni^{2+} and Cu^{2+} (*black dots*) that are located either in the interlayer or the tunnel, or replace Mn ions in the octahedral layer (after Manceau et al. 2012; reproduction with permission of Mineralogical Society of America)

The mineralogical analysis of mainly diagenetic surface nodules from the CCZ and the Peru Basin indicates that nodules from both regions consist of disordered phyllomanganates; todorokite only occurs in minor amounts, if at all (Fig. 2.9; Wegorzewski et al. 2015). This result supports the findings of Usui et al. (1989) and Bodeï et al. (2007) who proposed that marine Mn oxides may consist of two series of manganates: a hydrothermal todorokite-like series and a diagenetic buserite-like series.

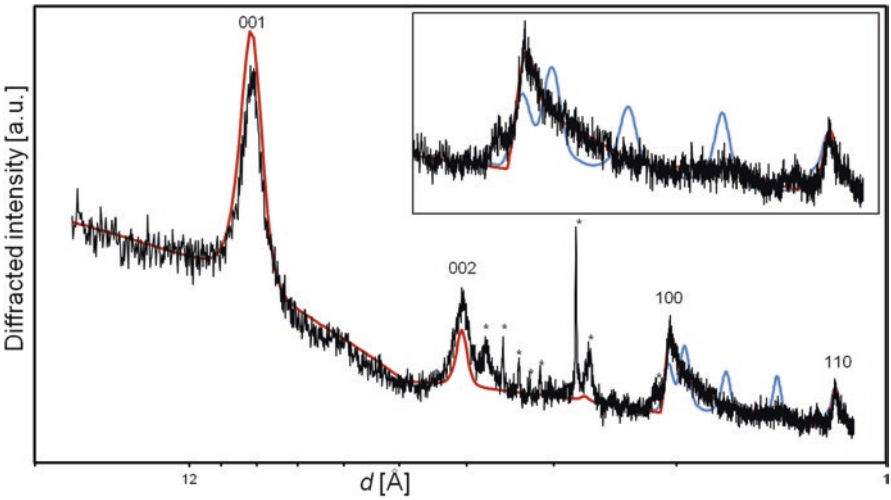

Fig. 2.8 X-ray diffraction pattern of a typical CCZ nodule (*black solid line*) and calculated patterns of a turbostratic (disordered) vernadite (*red line*) and an ordered birnessite (*blue line*). The vernadite and birnessite patterns can be distinguished based on the high angle region (*insert*). The diffractogram of the nodule is similar to the vernadite pattern (*red line*) and different from the birnessite (*blue line*). Several nodules from the CCZ and Peru Basin show similar diffraction patterns, indicating the dominance of disordered phyllomanganates (from Wegorzewski et al. 2015; reproduction with permission of Mineralogical Society of America)

Phyllomanganates can take up many different cations such as alkali, alkali-earth, and transition metals in different amounts and ratios. However, the amount of base metal (Ni, Cu) incorporated into phyllomanganates (Fig. 2.4) does not appear to be dependent on the crystal structure or on the Mn content of the mineral phase, but rather appears to be controlled by the different availability of the respective metal due to varying environmental conditions (Wegorzewski et al. 2015). For instance, nodules from the CCZ and the Peru Basin are composed of the same turbostratic phyllomanganates, yet they have different Cu contents (0.6% versus 1.1%, see above). By taking up the available metals and other cations, the phyllomanganate crystal structure is stabilized or probably can form at all. After formation, different post-depositional exchange processes may lead to the release or uptake of metals and eventually to the stabilization of the phyllomanganate structure. Such post-depositional alteration processes can even lead to the formation of todorokite from a phyllomanganate precursor (Bodeï et al. 2007).

In contrast to abyssal diagenetic manganese nodules, hydrothermal Mn oxides mainly consist of well-crystallized todorokite (Kuhn et al. 2003 and references therein). This is probably due to the higher levels of energy available in a hydrothermal system and the relatively fast growth rates of hydrothermal precipitates. Table 2.2 provides an overview of the mineralogical phases and the crystal characteristics that characterize marine manganese oxide precipitates.

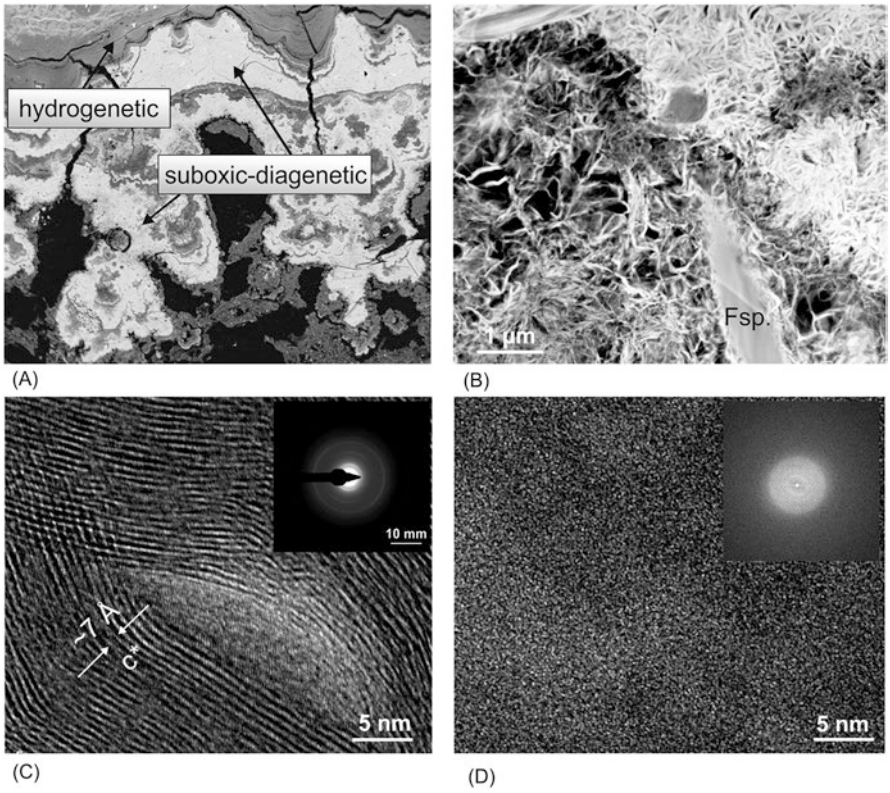

Fig. 2.9 (**a**) Backscatter electron image of two different types of growth layers of a manganese nodule. (**b**) High-resolution image (high-angle annular dark field) of dendritic-diagenetic growth structures (for location, see *rectangle* in **a**). (**c**) HRTEM image of a diagenetic layer (*insert*: corresponding electron diffraction pattern) indicating reflections typical for 10Å and 7Å phyllomanganates. (**d**) HRTEM image of a hydrogenetic layer (*insert*: corresponding SAED pattern) without any lattice fringes or reflections (figures from Wegorzewski et al. 2015; reproduction with permission of Mineralogical Society of America)

2.4 Formation of Manganese Nodules

There are three principal processes leading to the formation of ferromanganese oxides under marine conditions: hydrogenetic precipitation, diagenetic precipitation, and precipitation from hydrothermal fluids.

2.4.1 Hydrogenetic Precipitation

The formation of Mn and Fe oxide colloids in oxic seawater and their precipitation onto hard ground is called hydrogenetic precipitation (Halbach et al. 1988; Koschinsky and Halbach 1995; Koschinsky and Hein 2003 and references therein).

Table 2.2 Characterization of the main different Mn oxide minerals that can occur in manganese nodules

	Mineral name	Basal reflections		Stacking mode	Layer symmetry	Diagnostic reflections (00*l* reflections omitted)	Note
		[001] [002] reflections	Ability to collapse				
Vernadite[a] group/δ-MnO_2[b]	7 Å vernadite[c]	~7 Å; ~3.5 Å	Yes	Turbostratic	Hexagonal	hk bands: 2.40–2.45 and 1.41–1.42 Å	Nanocrystals, the band at ~2.4 Å is asymmetric, one water layer in-between two Mn-O-octahedral sheets, vacancies occur within the Mn-O-octahedral sheets, typical interlayer cation: e.g., K^+
					Orthogonal	hk bands: ~2.4 and ~1.52, 1.4 Å	Nanocrystals, ~2.4 Å band is asymmetrical, the band at ~1.4 Å is split in two, one water layer between two Mn-O-octahedral sheets, Mn^{3+} cations are arranged in rows parallel to the *b* axis, one row of Mn^{3+} cations is followed by two rows of Mn^{4+}, interlayer cation: e.g., K^+
	10 Å vernadite[c]	~10 Å; ~5 Å	Depending on the triple corner (TC) species over layer vacancies, which can stabilize the structure against collapsing	Turbostratic	Hexagonal	hk bands: 2.40–2.45 and 1.41–142 Å	Nanocrystals, ~2.4 Å band is asymmetrical, two water layers between two Mn-O-octahedral sheets, vacancies occur within the Mn-O-octahedral sheets, typical interlayer cation: e.g., Mg^{2+}
					Orthogonal	hk bands: ~2.4 and ~1.52, 1.4 Å	Nanocrystals, ~2.4 Å band is asymmetrical, the band at ~1.4 Å is split in two, two water layers within two Mn-O-octahedral sheets, Mn^{3+} cations are arranged in rows parallel to the *b* axis, one row of Mn^{3+} cations is followed by two rows of Mn^{4+}, typical interlayer cation: e.g., Mg^{2+}
	Fe– vernadite[c,d]	–	Absent	Turbostratic	Hexagonal	hk bands: 2.40–2.45 and 1.41–1.42 Å	Typically single layers (no basal nor *hkl* reflections), vernadite is epitaxially intergrown with amorphous δ-FeOOH

Birnessite group	7 Å birnessite[e,f]	~7 Å; ~3.5 Å	Yes	Ordered	Hexagonal	hkl are variable, depending on the layer stacking	Ordered three-dimensionally, one water layer in-between two Mn-O-octahedral sheets, vacancies occur within the Mn-O-octahedral sheets, typical interlayer cation: e.g., K^+
			Yes	Ordered	Orthogonal	hkl are variable, depending on the layer stacking	Ordered three-dimensionally, one water layer, Mn^{3+} cations arranged in rows parallel to the *b* axis, one row of Mn^{3+} cations is followed by two rows of Mn^{4+}, interlayer cation: e.g., K^+
	10 Å buserite[g,h,i]	~10 Å; ~5 Å	Depending on the TC species, which can inhibit collapsing	Ordered	Hexagonal	hkl are variable, depending on the layer stacking	Ordered three-dimensionally hydrated form of birnessite, two water layers between two Mn-O-octahedral sheets, vacancies occur within the Mn-O-octahedral sheets, typical interlayer cation: e.g., Mg^{2+}
					Orthogonal	hkl are variable, depending on the layer stacking	Ordered three-dimensionally hydrated form of birnessite: two water layers between two Mn-O-octahedral sheets, Mn^{3+} and Mn^{4+} in the octahedra sheets, no significant amounts of vacancies are expected, but the structure has not been refined yet, typical interlayer cation: e.g., Mg^{2+}
	Asbolane[j,k]	~10 Å; ~5 Å	Yes	Turbostratic	Hexagonal	Two incommensurate hexagonal networks of hk bands at positions comparable to vernadite, split of the (100) and (110) reflections	$Ni(OH)_2$, $Cu(OH)_2$, $Co(OH)_2$, $Co(OH)_3$ or CoOOH between interlayer of two Mn-O octahedral sheets

(continued)

Table 2.2 (continued)

	Mineral name	Basal reflections		Stacking mode	Layer symmetry	Diagnostic reflections (00*l* reflections omitted)	Note
		[001] [002] reflections	Ability to collapse				
	Chalcophanite[l]	~6.9 Å; ~3.5 Å	Yes	Ordered	Hexagonal	hkl: 4.07; 3.51; 2.23; 1.59	One out of seven Mn^{4+} is missing and two $Zn^{2+}O_6$ octahedra are below and above vacancies (one on each side)
	Lithiophorite[m]	~9.4 Å; ~4.7 Å	Unknown	Ordered	Hexagonal	hkl: 2.38; 1.88; 1.58; 1.46; 1.39	Alternately stacked layers of Mn-O and (Al, Li)-OH octahedra
	Todorokite[h,k]	No basal reflections but peaks at ~10 Å and ~5 Å (9.7 Å; 4.8 Å)	No (tunnel structure)	Ordered	Layer symmetry is not applicable	hkl: 2.40 (intense and symmetric) and further reflections between 2.2 and 1.7 Å	Tunnel structure with [3 × 3] tunnel size, defective form of todorokite with [3 × *n*] ($n \leq 9$)

[a]Natural mineral
[b]Synthetic form of vernadite
[c]Bodeï et al. (2007)
[d]Burns et al. (1975)
[e]Drits et al. (1997)
[f]Drits et al. (2007)
[g]Giovanoli (1980)
[h]Burns et al. (1983)
[i]Novikov and Bogdanova (2007)
[j]Manceau et al. (1992)
[k]Manceau et al. (2014)
[l]Post and Appleman (1988)
[m]Post and Appleman (1994)

Under normal Eh–pH conditions of seawater (Eh > 0.5 V; pH ~8), manganese tends to oxidize to $Mn^{4+}O_2$ and iron to $Fe^{3+}OOH$. Both phases are not dissolvable under seawater conditions and form colloids. Moreover, both phases tend to hydrolyze and the hydrolyzed, oxidic surface of these oxides contains OH groups with amphoteric character causing a pH-dependent surface charge. At the seawater pH of ~8, MnO_2 has a strong negative surface charge and δ-FeOOH has a slightly positive surface charge. Thus, the negatively charged MnO_2 colloid particles adsorb dissolved cations such as Co^{2+}, Ni^{2+}, Zn^{2+}, Tl^{+} and the slightly positively charged FeOOH particles adsorb all ions that form anionic complexes such as carbonate ($REE(CO_3)_2^-$), hydroxide ($Hf(OH)_5^-$) and/or oxyanion (MoO_4^{2-}) complexes (Koschinsky and Halbach 1995; Koschinsky and Hein 2003; Hein et al. 2013). The enrichment of elements to the Mn oxide surface is the result of strong physical sorption, whereas the enrichment at the FeOOH surface is controlled by chemical bonding such as covalent and coordinative bonds. Both types of colloids eventually combine and precipitate onto sediment-free substrate forming typically hydrogenetic ferromanganese crusts with Mn/Fe ratios around unity. Due to the high internal surface area of hydrogenetic ferromanganese oxides (up to >300 m^2/g; Hein et al. 2013), they can enrich elements up to a factor 10^9 over ambient seawater (e.g., Co, Pb, Mn, Ce, Te; Hein et al. 2010).

Elements having more than one oxidation state in the marine environment, and which are dissolved in the lower oxidation state as positively charged cations, can be oxidized at the surface of MnO_2 after adsorption. In this way, certain elements are especially enriched on the surface of ferromanganese oxides. Typical examples for this oxidative scavenging are cobalt (oxidized from Co^{2+} to Co^{3+}), cerium (Ce^{3+} to Ce^{4+}), lead (Pb^{2+} to Pb^{4+}), thallium (Tl^{+} to Tl^{3+}), and tellurium (Te^{4+} to Te^{6+}). Surface oxidation may be mediated by coordinated surface OH groups which enable the electron transfer from metal ions to the oxygen molecule (Koschinsky and Hein 2003). Oxidative scavenging on Mn oxide surfaces is inversely correlated to the growth rate of these hydrogenetic phases, as illustrated by a Mn/Fe ratio versus element content diagram (Fig. 2.10). Typical hydrogenetic growth rates range between 1 and 5 mm/million years (Halbach et al. 1988).

Hydrogenetic precipitation leads to the formation of hydrogenetic layers in mixed-type manganese nodules from the CCZ and the Central Indian Ocean Basin and may entirely control the formation of nodules within the EEZ of the Cook Islands (Hein et al. 2015). However, the main products of hydrogenetic precipitation are ferromanganese crusts, as they occur on sediment-free seamount slopes, guyots, and other seafloor areas with outcropping bare rocks. A more detailed discussion of hydrogenetic processes and their products can be found in the chapter on ferromanganese crusts in this book (Halbach et al. this edition).

2.4.2 Diagenetic Precipitation

The formation of Mn nodules due to element precipitation from pore water within the sediment or on the sediment surface is called diagenetic precipitation. This form of Mn oxide precipitation is related to the diagenetic sequence of deep-sea

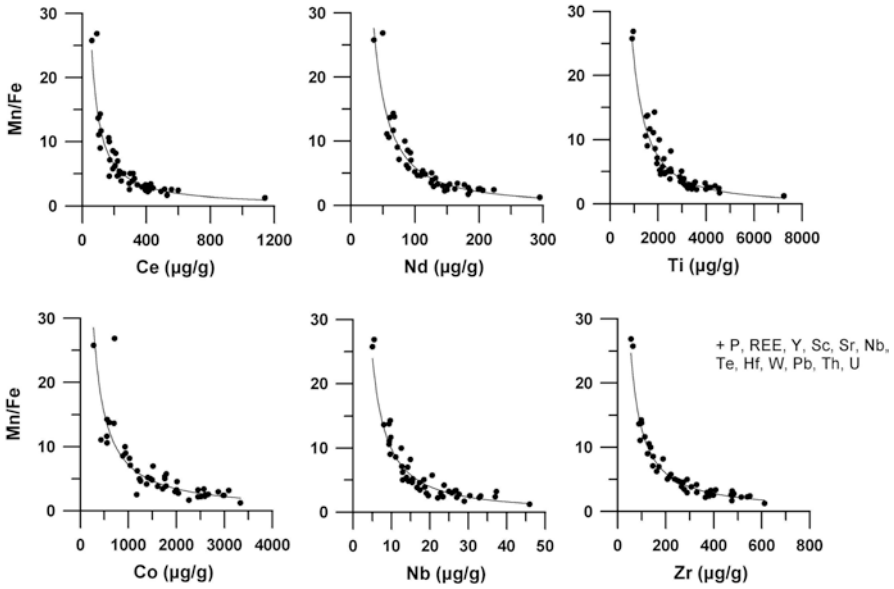

Fig. 2.10 Mn/Fe ratios versus element concentrations of single layers of manganese nodules from the eastern CCZ (BGR data; measured with ICP-OES and -MS). Note the inverse, parabolic curve progression of all elements which is typical for elements enriched by hydrogenetic surface adsorption. The elements listed on the right side exhibit similar geochemical behavior

sediments as described in Froelich et al. (1979). The diagenetic sequence is controlled by the oxidation of organic material through a sequence of redox reactions with different electron acceptors. Although the degradation of organic matter is carried out almost exclusively by bacteria, the microorganisms acquire energy for their metabolism through these reactions and the sequence of reactions is controlled by the redox levels and energy yields, starting with redox reactions yielding the highest energy (Stumm and Morgan 1981; Chester and Jickells 2012).

The sequence starts with the reaction of organic material with dissolved oxygen, i.e., aerobic respiration. Aerobic organisms use dissolved oxygen from overlying or interstitial waters to oxidize organic matter according to the following general equation (Galoway and Bender 1982):

$$\begin{aligned} &5\left(CH_2O\right)_{106}\left(NH_3\right)_{16}\left(H_3PO_4\right)+69O_2 \\ &\rightarrow 530CO_2+80HNO_3+5H_3PO_4+610H_2O \end{aligned} \tag{2.1}$$

The composition of organic material is represented in this and the following equations by the so-called Redfield composition (Chester and Jickells 2012). The reaction according to (2.1) leads to the formation of nitrate and is also termed "nitrification." As >90% of the organic material that reaches the seafloor is degraded through its reaction with O_2, oxygen is regarded as the primary oxidant (Chester and Jickells 2012).

When dissolved oxygen becomes depleted after sufficient consumption, the decomposition of organic matter can continue under anaerobic conditions using secondary oxidants [suboxic diagenesis, (2.2)–(2.4)]. These secondary oxidants are nitrate, MnO_2, Fe_2O_3, and sulfate. However, under the conditions typical for the formation of Mn nodules, only nitrate and MnO_2 play a significant role. If the dissolved oxygen level falls to ~5% of the saturation concentration, nitrate becomes the preferred electron acceptor according to the following reaction ("denitrification"):

$$\begin{aligned} &5\left(CH_2O\right)_{106}\left(NH_3\right)_{16}\left(H_3PO_4\right)+472HNO_3 \\ &\rightarrow 276N_2+520CO_2+5H_3PO_4+886H_20 \end{aligned} \tag{2.2}$$

This denitrification process overlaps with Mn^{4+} as alternative electron acceptor according to:

$$\begin{aligned} &\left(CH_2O\right)_{106}\left(NH_3\right)_{16}\left(H_3PO_4\right)+236MnO_2+472H^+ \\ &\rightarrow 236Mn^{2+}+106CO_2+8N_2+H_3PO_4+336H_2O \end{aligned} \tag{2.3}$$

If Mn^{4+} is consumed, the diagenetic sequence proceeds to Fe^{3+} as electron acceptor according to:

$$\begin{aligned} &\left(CH_2O\right)_{106}\left(NH_3\right)_{16}\left(H_3PO_4\right)+212Fe_2O_3+848H^+ \\ &\rightarrow 424Fe^{2+}+106CO_2+16NH_3+H_3PO_4+530H_2O \end{aligned} \tag{2.4}$$

As the different reactions in this diagenetic sequence follow one another consecutively, a respective series of diagenetic zones in the sediments is formed (Fig. 2.11). Organic carbon is oxidized by manganese oxides in zone 4 and dissolved Mn^{2+} is released into interstitial water. This Mn^{2+} then diffuses upwards and is oxidized back to MnO_2 at the top of zone 3 (Chester and Jickells 2012).

The thickness of the respective diagenetic zones in bottom sediments depends on the supply of organic matter, its accumulation rate, and the rate of supply of oxidizing agents (Chester and Jickells 2012). During phases when the top of zone 3 rises close to the sediment–water interface, diagenetic manganese can significantly contribute to the growth of manganese nodules. Processes of manganese and iron reduction do not occur simultaneously in the diagenetic sequence and the environmental conditions that are typical for diagenetic Mn nodule growth occur in zones 3 and 4 (Fig. 2.11). This is the reason for the strong Mn-Fe fractionation within diagenetic layers of manganese nodules (Mn/Fe ratio up to 800; Wegorzewski and Kuhn 2014).

Diagenetic Mn flux rates are considerably higher than hydrogenetic Mn flux rates, which explains the high diagenetic growth rates of up to 250 mm/Myr (von Stackelberg 2000). Thus, the supply of manganese to the position of the manganese nodule is high enough to form crystallized phyllomanganates, in contrast to hydrogenetic precipitates which are composed of cryptocrystalline vernadite (Wegorzewski et al. 2015). However, especially alkali, alkali-earth, and transition metals are required to stabilize the phyllomanganate lattice (see chapter 3.2). Thus,

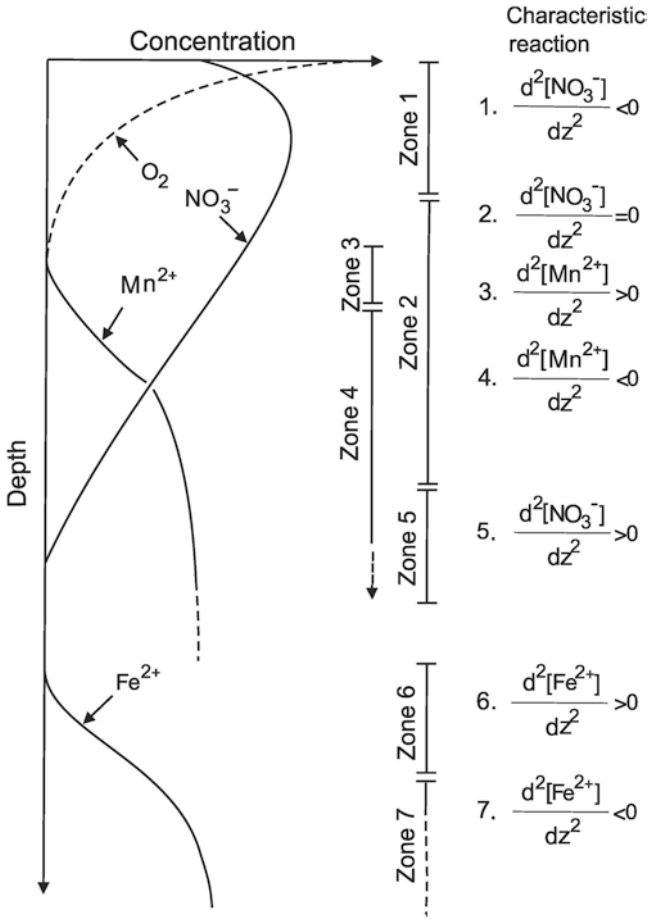

Fig. 2.11 Schematic representation of pore water profiles and different diagenetic zones in deep-sea sediments. In Zone 1 oxygen is the oxidant of organic carbon, in Zones 2–5 nitrate and Mn^{4+} are the oxidants and Mn^{2+} is released into pore water. Dissolved Mn^{2+} diffuses upward until it is reoxidized in Zone 3. In Zones 6 and 7 organic carbon is oxidized by ferric iron and Fe^{2+} is released into pore water (from Froelich et al. 1979; reproduction with permission of Elsevier)

metals such as Ni, Cu, Mo, Zn, Ba, and Li are enriched in diagenetic nodules (Fig. 2.12). The general dominance of Ni in diagenetic nodules of the CCZ is probably a result of the relatively high Ni content in the pore water of siliceous deep-sea sediments (Table. 2.3).

Manganese nodules from the Peru Basin are mainly composed of diagenetic layers. The present-day oxic-suboxic front in this area is located at about 10 cm sediment depth and a strong dissolved Mn^{2+} gradient can be observed in the interstitial waters (Koschinsky 2001). In the sediments of the eastern CCZ, the present-day oxic-suboxic front reaches down to a sediment depth of 2–3 m (Mewes et al. 2014) and in the central CCZ the sediment column even appears to be oxic over tens of meters of depth (Müller et al. 1988). The organic carbon content in the surface sediments

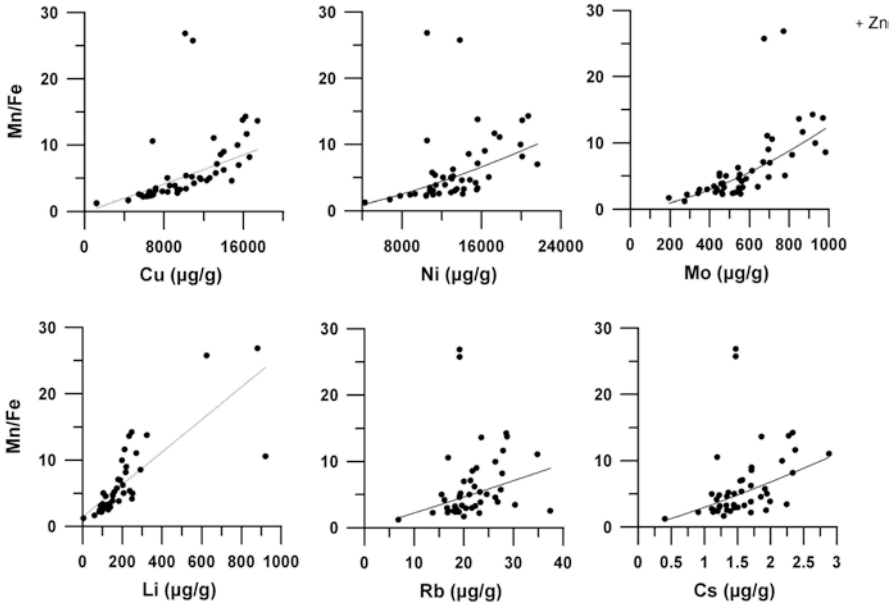

Fig. 2.12 Mn/Fe ratios versus element concentrations of single layers of manganese nodules from the eastern CCZ (BGR data; measured with ICP-OES and -MS). The positive correlation with the Mn/Fe ratio suggests that these elements are incorporated into diagenetic Mn oxides. Note the different curve progression compared to elements enriched by hydrogenetic processes (cf. Fig. 2.10)

Table 2.3 Element contents of interstitial water and seawater of siliceous deep-sea sediments (with up to 14% carbonate content)

	Mn	Fe	Cu	Ni	Co
Oxic pore water[a]	<10	<1	40–80	<50	<5
Suboxic pore water[a]	10,000–100,000	< 1	40–120	200–600	30–60
Near-bottom seawater[b]	0.2–3	0.1–2.5	0.5–6	2–12	0.01–0.1
Principal species in seawater[c]	Mn^{2+} $MnCl^{+}$	$Fe(OH)_2^{+}$ $Fe(OH)_3^{0}$ $Fe(OH)_4^{-}$	Cu^{2+} $CuOH^{+}$ $CuCO_3^{0}$	Ni^{2+} $NiCl^{+}$	Co^{2+} $CoCl^{+}$

[a]Shaw et al. (1990)
[b]Bruland (1983)
[c]Byrne (2002). All concentrations in nmol/l

of the Peru Basin is up to >1% (Haeckel et al. 2001), in the eastern CCZ it is between 0.4 and 0.6% (BGR data), and in the central CCZ it is between 0.2 and 0.4% (Müller et al. 1988). Accordingly, Mn nodules from the Peru Basin are thought to be mainly formed by suboxic diagenesis, whereas CCZ nodules apparently have been formed by oxic diagenesis (von Stackelberg 1997; Chester and Jickells 2012). However, Wegorzewski and Kuhn (2014) have shown that the fabric and the chemical composition of the internal growth structures of nodules from both areas are similar, suggesting that the nodules from both areas have been formed by the same genetic processes over time and consist of a mixture of suboxic-diagenetic and oxic-

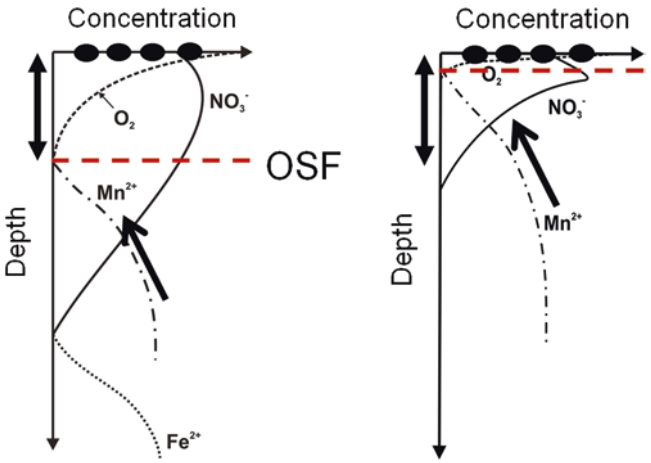

Fig. 2.13 Schematic representation of recent pore water conditions (**a**) and conditions during former suboxic nodule growth in the eastern CCZ (**b**). *Black ellipses* represent Mn nodules at the sediment surface. Under recent conditions, there is no suboxic-diagenetic nodule growth. Temporal fluctuations of the OSF (oxic-suboxic front) may be due to variations in the organic carbon flux, e.g., ultimately controlled by climate change. The arrows on the Mn^{2+} profile indicate the direction of the diffusive Mn-flux. If the OSF is close enough to the seafloor, diffusive diagenetic Mn-flux contributes to Mn nodule growth. Under recent oxic conditions (**a**) Mn nodule growth is only oxic-hydrogenetic (Blöthe et al. 2015). The current OSF reaches down to 2–3 m sediment depth (Mewes et al. 2014)

hydrogenetic layers. Nevertheless, the proportion of hydrogenetic material in CCZ nodules is higher, and hence the metal content of CCZ nodules is in-between that of diagenetic Peru Basin nodules and that of typical hydrogenetic nodules (e.g., from the Cook Islands; Hein et al. 2013, 2015). In order to produce near-surface, suboxic conditions in CCZ sediments (Figs. 2.13 and 2.14) it would be necessary to increase the organic carbon flux to the seafloor by a factor of two, i.e., from a present-day average of 3 µmol cm^{-2} a^{-1} (Mewes et al. 2014) to ~ 6 µmol cm^{-2} a^{-1}, as is the case in the Peru Basin today (Haeckel et al. 2001). Such increases of the organic carbon flux may have occurred during past glacial stages due to enhanced paleoproductivity (Herguera 2000). Moreover, suboxic conditions at the seafloor of the CCZ during glacial stages may also have occurred due to reduced ventilation of the deep ocean as suggested by Bradtmiller et al. (2010).

Irrespective of the absolute oxygen concentrations in bottom and pore waters, oxic diagenesis might only play a minor role in the formation of Mn nodules, as processes of manganese mobilization and transportation in the sediments under oxic conditions are probably limited to the micrometer scale. Diagenetic processes taking place under oxic conditions within the interstitial water seem to be similar to hydrogenetic processes, i.e., enrichment of manganese and other metals is controlled by surface adsorption and oxidation. This assumption is supported by X-ray photoelectron spectroscopy (XPS) measurements of nanometer-thin surface layers of nodules that are in contact with oxic interstitial water (Blöthe et al. 2015). These surface layers have metal contents and elemental ratios that are typical for hydrogenetic precipitation (Wegorzewski and Kuhn 2014).

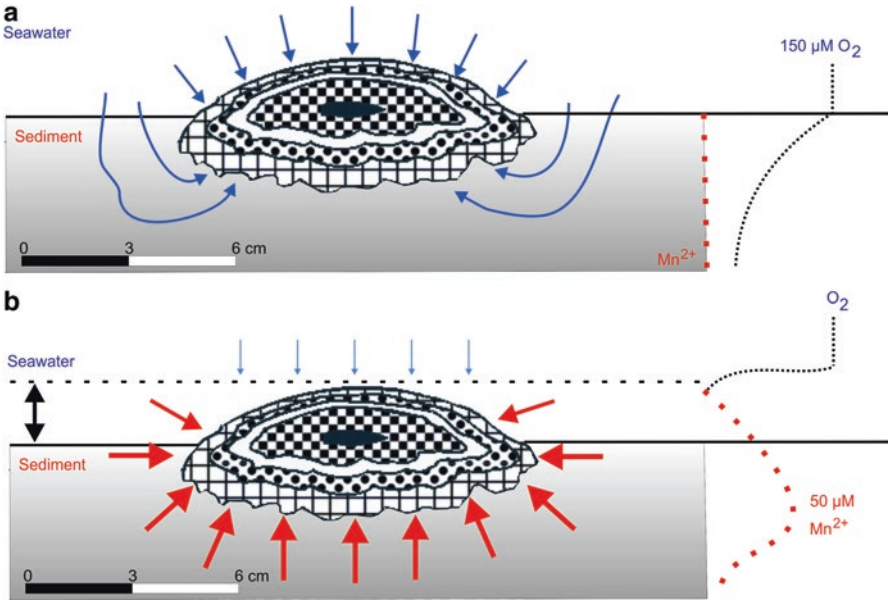

Fig. 2.14 Schematic drawings of recent oxic (**a**) and fossil suboxic (**b**) Mn nodule growth in the CCZ. The *black horizontal line* marks the seafloor; *blue arrows* represent hydrogenetic precipitation under oxic conditions, and *red arrows* represent diagenetic precipitation under suboxic conditions. The thickness of the arrows reflects flux rates. The *dotted lines* represent pore water contents of O_2 and Mn^{2+} (data from Mewes et al. 2014). The *black vertical arrow* on the *left side* (**b**) indicates that the nodules might have been covered by sediments during suboxic growth phases in order to enable diagenetic layer formation all around the nodules

As mentioned above, manganese nodules occur worldwide throughout the abyssal plains, but special conditions in areas such as the CCZ and the CIOB have yielded economically interesting nodule abundances. Interactions between the position of the carbonate compensation depth, water depth, surface bioproductivity, sedimentation rate, sediment type, benthic activity, near-bottom currents, and local micro-topography determine whether nodule abundances reach values that are high enough to become economically interesting. The CCZ area is located just north of the equatorial high bioproductivity zone (Halbach et al. 1988). The combination of water depth and surface bioproductivity in the CCZ leads to its seafloor being near or just below the carbonate compensation depth (CCD). Areas further to the south (close to the equator) are subject to high bioproductivity and high sedimentation rates, leading to a lowering of the CCD. Under such conditions, widespread manganese nodule growth is hampered (Fig. 2.15). The formation of siliceous ooze close to the CCD provides the necessary metal content and the physical properties (such as permeability for the mobility of metals in pore water) for the growth of large diagenetic nodules. The slow subsidence of the seafloor as well as the slow plate motion to the northwest as a consequence of seafloor spreading and oceanic crust alteration together with a constant sedimentation rate provides optimal conditions over a geological time span (a few million years) for Mn nodule growth. Furthermore, numerous seamounts and fault zones provide a high amount of nucleus

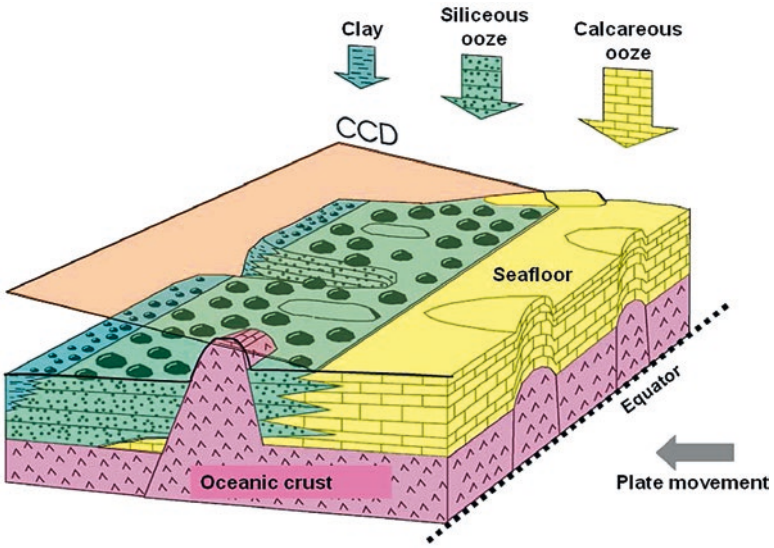

Fig. 2.15 Schematic model of the CCZ area explaining the locations of high and low nodule abundances. Nodules of medium to large size and high abundance occur in areas with medium sedimentation rates at or just below the carbonate compensation depth (CCD) in siliceous ooze. Small-sized nodules of low abundance occur in deep-sea clay with low sedimentation rates and far below the CCD. High bio-productivity at the equator results in high sedimentation rates of predominantly carbonate-rich particles and a deepening of the CCD, thus preventing the formation of manganese nodules. Figure adopted from Beiersdorf (2003); reproduction with permission of International Seabed Authority

material to initiate nodule growth. A flat seafloor over vast areas and moderate near-bottom currents furthermore enable the formation of Mn nodule fields.

Over a period of several million years the CCZ has moved from being an area with optimal conditions for Mn nodule growth to an area with suboptimal conditions, leading to the growth of smaller nodules (Fig. 2.15). This is mainly due to the greater water depths together with lower bioproductivity and particle flux rates, leading to decreasing fluxes of metals and organic material to the seafloor. This leads to a decrease in diagenetic overturn and thus to a smaller diagenetic input to the nodules. These are also the reasons for the lower nodule abundances in the Indian Ocean Basin compared to the CCZ (see above).

2.4.3 Microbial Manganese Mobilization and Deposition

Since several decades, scientists have speculated on the possible influence of microorganisms on the formation of Mn oxides in manganese nodules and ferromanganese crusts. Suggestions have been made that these oxides have not only formed abiotically but that they may form by biologically driven processes due to the activity of microorganisms such as bacteria (Ehrlich 1963; Schweissfurth 1971; Rosson and

Nealson 1982; Villalobos et al. 2003; Webb et al. 2005) and/or fungi (Miyata et al. 2006; Grangeon et al. 2010). Ehrlich (1972) determined three types of bacteria within manganese nodules: Mn^{2+}-oxidizers, Mn^{4+}-reducers, and bacteria which neither oxidize (Mn^{2+}) nor reduce (Mn^{4}) manganese. A recent study of Blöthe et al. (2015) revealed the occurrence of a diverse prokaryotic community dominated by nodule-specific Mn^{4+}-reducing and Mn^{2+}-oxidizing bacteria (*Shewanella* and *Colwellia*) within manganese nodules from the CCZ. The oxidation of cations scavenged onto the nodules may serve as an energy source for the activity of bacteria living on/in them (Tebo et al. 2004; Ehrlich and Newman 2009).

Several studies were conducted in the laboratory to produce synthetic Mn oxides under the influence of bacteria and fungi (e.g., Bargar et al. 2005; Villalobos et al. 2003; Grangeon et al. 2010). Different products were detected after bacterial Mn(II) oxidation. Hastings and Emerson (1986) as well as Mann et al. (1988) revealed hausmannite (Mn_3O_4), which was interpreted to be an intermediate product of marine *Bacillus sp. Strain* SG-1. Mandernack et al. (1995) concluded that Mn(II) is oxidized directly to Mn(IV) without an intermediate phase. Webb et al. (2005) synthesized a Mn-phase primarily as disordered hexagonal birnessite, which transformed after a few days to a pseudo-orthogonal birnessite. These Mn oxides differ slightly from the disordered, hexagonal phyllomanganates of manganese nodules from the CCZ. In contrast, Villalobos et al. (2003) determined a ~ 7Å hexagonal phyllomanganate produced by *Pseudomonas putida*. Furthermore, Hastings and Emerson (1986) and Bargar et al. (2005) showed that bacterial Mn(II) oxidation leads to the production of X-ray amorphous Mn oxides similar to δ-MnO_2 of natural Mn-Fe encrustations. The authors suggest that these Mn oxides are the primary biominerals that are reworked through abiotic processes to become more stable and crystalline Mn oxides such as 10Å phyllomanganates.

Microbially mediated Mn^{2+} oxidation is faster by several orders of magnitude than abiotic oxidation (Villalobos et al. 2003; Morgan 2005; Tebo et al. 2005, 2007). However, the turnover rates of abiotic oxidation correspond much better to the general growth rates of Mn nodules of up to a few tens of mm per million years (Lyle 1982; Halbach et al. 1988; Eisenhauer et al. 1992; Bollhöfer et al. 1996; Han et al. 2003).

Thus, in summary, the occurrence of bacteria in manganese nodules is recognized and there is a general understanding that their activity may influence the formation of manganese oxide minerals. However, whether microbial activity just modifies Mn nodules or whether their activity is essential for nodule formation is still a matter of debate.

2.4.4 Hydrothermal Precipitation

As Mn^{2+} is soluble under reducing and acid conditions, and as its solubility is not temperature-dependent, Mn^{2+} can not only be transported by hydrothermal solutions but also remains dissolved until hydrothermal fluids are oxidized upon contact with oxic seawater. Therefore, Mn^{2+} is enriched in low-temperature hydrothermal

fluids which occur either at the periphery of an active high-temperature hydrothermal vent field or during the waning stage of a hydrothermal system. Manganese will be oxidized and will precipitate as Mn oxide (mainly todorokite) upon mixing of these fluids with cold, oxic seawater, forming manganese crusts or irregularly shaped precipitates within or at the seafloor (Hein et al. 1990; Rogers et al. 2001; Kuhn et al. 2003).

Manganese is also enriched in high-temperature, black smoker fluid emanating from hydrothermal systems into the water column and forming hydrothermal plumes (Lilley et al. 1995). Hydrothermal plumes develop as a layer in the oceanic water column about 100–400 m above the seafloor and drift away from the hydrothermal system due to the activity of near-bottom currents. Manganese (and Fe) is oxidized during the horizontal drift of the hydrothermal plume, forming Mn-Fe-rich plume fallout which can either generate hydrothermal Fe-Mn crusts on rock outcrops or can contribute to a Fe-Mn oxide component of deep-sea sediments (Kuhn et al. 1998, 2000).

Manganese oxide precipitates occur in every marine hydrothermal system worldwide. However, they play no economic role in modern marine systems. In contrast, the largest terrestrial Mn deposit, the giant Proterozoic Kalahari Manganese Field of South Africa containing 77% of all land-based Mn reserves, was formed as fallout from hydrothermal plumes (Cairncross and Beukes 2013).

2.5 Occurrence of Manganese Nodules

Manganese nodules occur in the abyssal plains of all major oceans in ~4000–6000 m water depth. However, Mn nodule fields of economic importance are only known from the Clarion-Clipperton Zone, the Central Indian Ocean Basin, and the Cook Islands area (Fig. 2.16). In these regions and in the Peru Basin, manganese nodule exploration has taken place since more than 30 years.

2.5.1 Clarion-Clipperton Zone

The *Clarion-Clipperton Zone* (CCZ) is the region with the largest contiguous occurrence of Mn nodule fields. It covers an area of about four million square kilometers which almost equals the size of the European Union (ISA 2010). The CCZ is located in the Central Pacific just north of the equator between Hawaii and Mexico (Fig. 2.16). The nodules are mixtures of hydrogenetic and diagenetic endmembers with an average diagenetic proportion of ~80% in the eastern CCZ and a continuously increasing hydrogenetic proportion towards the central and western CCZ. This leads to slightly increased cobalt and rare earth element contents in nodules from the central and western CCZ (Table 2.1). Apart from these slight changes, the chemical composition of the nodules is relatively constant throughout the whole CCZ, especially

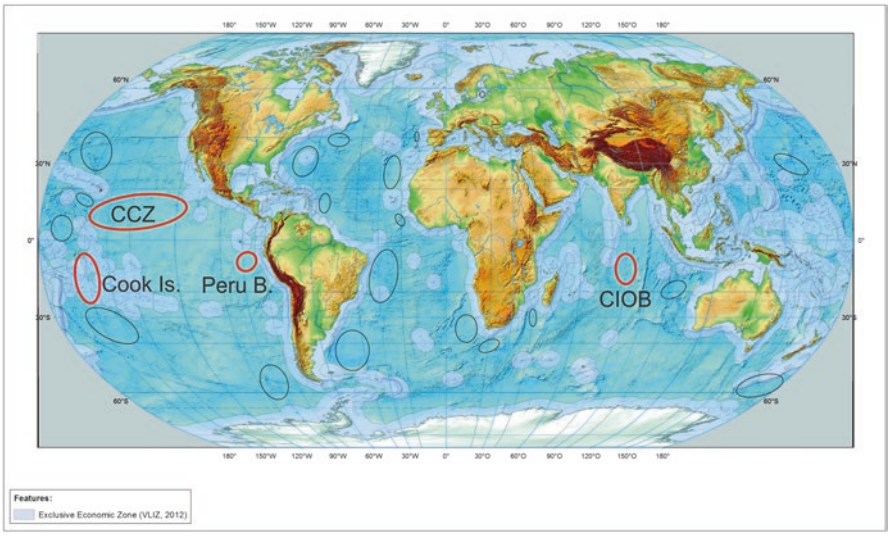

Fig. 2.16 Global occurrence of manganese nodule fields in abyssal plains of the world oceans. Areas marked in *red* are economically important regions and are discussed in the text. Manganese nodules occur in significant abundance in the remaining marked areas. However, they are also found elsewhere in abyssal plains of the world oceans but with lower abundance. *CCZ* Clarion-Clipperton Zone, *Cook Is* Cook Islands (including the Penrhyn Basin and Manihiki Plateau), *Peru B*. Peru Basin, *CIOB* Central Indian Ocean Basin (figure adapted after Hein et al. 2013; background map from ESRI)

when compared to variations in nodule abundance (in kg/m^2). For instance, the coefficient of variation (CoV) of nodule composition in the eastern CCZ is less than 10% whereas that for nodule abundance is >30% (unpublished BGR data). Manganese nodule fields are not equally distributed on the seafloor within the CCZ but occur in patches. Economically interesting "patches" can cover an area of several thousand square kilometers.

Nodule abundance in the CCZ ranges between 0 and ~30 kg/m^2 (based on wet nodule weight) with an average of 15 kg/m^2 (SPC 2013). The total amount of manganese nodules within the CCZ is estimated to be ca. 21 billion tons, which amounts to ca. 6 billion tons of manganese (Table 2.4; Visbeck and Gelpke 2014). The total Mn tonnage of CCZ nodules equals the global Mn reserves on land and total estimated tonnages of Ni, Co, Y, and Tl exceed those of land-based reserves by several factors (Table 2.4). Thus, manganese nodule mining could have a significant effect on the global production of certain metals and hence, on the global prices for those metals. However, one Mn nodule mining project with an annual production of two million tons of dry nodules would have only a small share in the global production of the main metals, except for the rare earth elements (Table 2.5). If five nodule mining projects would run simultaneously, the global share would be medium for cobalt and manganese; low for nickel, molybdenum, and lithium; and insignificant for copper. However, it would be very high for the rare earth elements (Table 2.5).

Table 2.4 Metal contents (in Mio. tons) of manganese nodules from the CCZ compared to land-based reserves and resources[a]

Element	Clarion-Clipperton zone (CCZ)	Global reserves and resources on land[b]	Global reserves on land
Manganese (Mn)	5992	5200	630
Copper (Cu)	226	1000+	690
Titanium (Ti)	67	899	414
Rare earth oxides	15	150	110
Nickel (Ni)	274	150	80
Vanadium (V)	9.4	38	14
Molybdenum (Mo)	12	19	10
Lithium (Li)	2.8	14	13
Cobalt (Co)	44	13	7.5
Tungsten (W)	1.3	6.3	3.1
Niobium (Nb)	0.46	3	3
Arsenic (As)	1.4	1.6	1
Thorium (Th)	0.32	1.2	1.2
Bismuth (Bi)	0.18	0.7	0.3
Yttrium (Y)	2	0.5	0.5
Platinum group metals	0.003	0.08	0.07
Tellurium (Te)	0.08	0.05	0.02
Thallium (TI)	4.2	0.0007	0.0004

[a]Data from Visbeck and Gelpke (2014)
[b]Economically recoverable and sub-economic reserves

Table 2.5 Comparison between annual production of metals from nodule mining in the CCZ and the global annual metal production on land

Metal	Global annual terrestrial production (tons)[a]	Annual production of 1 nodule mining project (tons)[b]	Percentage of global annual production (%)	Annual production of 5 nodule mining projects (tons)[b]	Percentage of global annual production (%)
Cobalt	110,000	3400	3.1	17,000	15
Manganese	17,284,210	600,000	3.5	3,000,000	17
Copper	15,997,172	23,600	0.15	118,000	0.7
Nickel	1,786,300	27,800	1.6	139,000	7.8
Molybdenum	250,314	1200	0.48	6000	2.4
Lithium	62,231	280	0.45	1400	2.2
REO[c]	115,850	12,000	10	60,000	52

[a]EU Report on Critical Raw Materials (2014)
[b]Based on annual production of 2 Mio. tons of dry nodules and the following average metal content of nodules: 0.17% Co, 30% Mn, 1.18% Cu, 1.39% Ni, 0.06% Mo, 0.014% Li, 0.6% REO
[c]Rare earth element oxides

2.5.2 Peru Basin

The *Peru Basin* is located about 3000 km off the coast of Peru and covers about half of the size of the CCZ. A relatively high bioproductivity in the ocean's surface layer and the associated high flux of organic carbon to the seafloor explain the occurrence of an oxic-suboxic front at 10 cm sediment depth in the Peru Basin, this front separating soft oxic surface sediments from stiffer, suboxic sediments (von Stackelberg 1997). The average manganese nodule abundance is 10 kg/m^2 (Visbeck and Gelpke 2014), but maximum abundances of 50 kg/m^2 can be found at locations close to the carbonate compensation depth (CCD) at 4250 m water depth (von Stackelberg 1997). A significant difference to the CCZ is that most parts of the Peru Basin lie close to or above the CCD, leading to a significant carbonate content of up to 50% in the sediments (Koschinsky 2001). In contrast, CCZ surface sediments are almost devoid of carbonate (usually <1%) and consist of a mixture of siliceous ooze and deep-sea clay (ISA 2010).

Manganese nodules of the Peru Basin have similar nickel and molybdenum, distinctly lower copper, cobalt, and REY, but higher lithium contents and higher Mn/Fe ratios than CCZ nodules (Table 2.1). In terms of mineralogy, a recent study has shown that Peru Basin and CCZ surface nodules contain the same types of disordered phyllomanganates, and that todorokite is not a main mineralogical component (Wegorzewski et al. 2015).

The difference in metal content of nodules from the Peru Basin as compared to those of the CCZ can be attributed to a higher contribution of suboxic-diagenetic layers and a distinctly lower percentage of hydrogenetic layers in nodules from the Peru Basin (Wegorzewski and Kuhn 2014).

2.5.3 Cook Islands

The *Cook Islands Exclusive Economic Zone* covers about two million km^2 and includes the Penrhyn and Samoa Basin abyssal plains in the SW Pacific (Fig. 2.16). The seafloor of these plains is usually deeper than 4700 m and the sediments are mainly composed of zeolite-rich, pelagic-brown clays containing minor amounts of volcanic glass, iron and manganese oxides, phosphate debris as well as biogenic carbonate and silica in places (Cronan et al. 2010; Hein et al. 2015). The area is characterized by low sedimentation rates, low fluxes of organic matter, an abundant supply of nucleus material, and strong bottom currents. Evidently, these environmental conditions have remained fairly constant over a long period of time and have caused persistent oxic conditions at the seafloor and within the sediments, leading to the formation of slow-growing (mean 1.9 mm/Myr) hydrogenetic ferromanganese nodules with Mn/Fe ratios around unity (Table 2.1; Hein et al. 2015). Therefore, the nodules contain high amounts of cobalt (0.41%), titanium (1.20%), REY (0.17%),

and zirconium (524 µg/g), but they are low in nickel (0.38%), copper (0.23%), and manganese (16.1%) when compared to CCZ nodules (Table 2.1). Nodule abundances have been investigated in areas of potential exploration and range between 19 and 45 kg/m^2, with a maximum of 58 kg/m^2 in small isolated areas. The relatively high nodule abundance together with elevated contents of high-tech metals (REY, Co, Ti) leads to the value of 1 ton of Cook Islands nodules being similar to the value of 1 ton of CCZ nodules at current metal prices (Hein et al. 2015).

2.5.4 Central Indian Ocean Basin

Within the *Central Indian Ocean Basin* (CIOB), economically interesting contiguous nodule fields occur in an area between 10°S and 16°30′S and 72°E and 80°E, in water depths between 3000 and 6000 m covering about 700,000 km^2. Within this region, a nodule-rich area called the Indian Ocean Nodule Field (IONF) was delineated which covers ca. 300,000 km^2 (Mukhopadhyay et al. 2008; Mukhopadhyay and Ghosh 2010). The total manganese nodules in the IONF amount to about 1400 million tons with an average abundance of 4.5 kg/m^2 and 21.84 million tons of Ni + Cu + Co resources. However, nodule abundance is more variable and inhomogeneous than is the case in other nodule areas. Furthermore, there seems to be a relationship between the number of seamounts and faults and nodule abundance. Seamounts with heights >500 m and fault systems apparently increase the availability of nucleus material and thus the number and mass of nodules (Mukhopadhyay et al. 2008). The IONF consists of different sectors and the mode of nodule formation varies slightly between these sectors, leading to varying Mn/Fe ratios between 1.8 and 4.8, and a Ni + Cu + Co content ranging between 2.48 and 2.53%.

The mineralogical composition ranges from vernadite over birnessite to todorokite (Mukhopadhyay and Ghosh 2010). These results indicate that the nodules are mainly a mixture of variable proportions of diagenetic and hydrogenetic phases. The deep-sea sediments of the different IONF sectors consist of siliceous ooze, terrigeneous material and pelagic red clays in variable amounts. Sedimentation rates decrease from 9 mm/kyr in the northern IONF to 1 mm/kyr in the south (Borole 1993). Apart from the Ni + Cu + Co contents of IONF nodules which are similar to those of CCZ nodules, IONF nodules have higher concentrations of lead and the rare earth elements (Table 2.1). The chemical and mineralogical compositions of nodules as well as the characteristics of the sedimentary environment indicate that IONF nodules are formed by the same hydrogenetic and diagenetic processes as CCZ nodules. The main difference between both areas is the nodule abundance, which is significantly higher in the CCZ. This might be attributed (1) to the lower sedimentation rates in the IONF, which have led to the formation of a higher proportion of hydrogenetic phases in the nodules,

and (2) to a higher input of terrigeneous material, which reduces the supply of metals to the seafloor that can ultimately be mobilized into the nodules during early diagenesis. Nevertheless, given the large area and the available mining technology, a mining operation within the IONF is considered to be economic (Mukhopadhyay et al. 2008).

2.5.5 Other Ocean Areas

Apart from the abovementioned four areas which have been the target of nodule exploration for several decades, there are many other locations in the world oceans where manganese nodules occur (Fig. 2.16). Additional promising areas for investigation could be the abyssal plains in the Atlantic Ocean, which have been omitted from intense exploration so far. Another important but special region in terms of Mn nodule formation is the Baltic Sea with its fast growing (0.013–1 mm $year^{-1}$) diagenetic nodules at several locations. Relatively high nodule abundances between 10 and 40 kg/m^2 occur in the Gulfs of Riga, Finland, and Bothnia in water depths between a few tens of meters and about 150 m, covering areas of a few hundred km^2. In the Russian sector of the Gulf of Finland, the nodule reserves amount to ca. six million tons and despite low trace metal contents (< 0.05% for Co + Cu + Ni + Zn; Glasby et al. 1997), these nodules have already been commercially mined between 2004 and 2007 (Cherkashov et al. 2013).

Manganese nodules and other ferromanganese precipitates of special formation and metal content have been reported from the Gulf of Cadiz and the Galicia Bank offshore Spain (González et al. 2012, 2014). Their unusual metal composition (e.g., up to 1.8% Co and >40% Mn) is probably related to special local conditions, such as the activity of hydrocarbons or fault systems which may tap deeper crustal reservoirs.

References

Bargar JR, Tebo BM, Bergmann U, Webb SM, Glatzel P, Chiu VQ, Villalobos M (2005) Biotic and abiotic products of Mn(II) oxidation by spores of the marine Bacillus sp. strain SG-1. Am Mineral 90:143–154

Beiersdorf H (2003) Scientific challenges related to the development of a geological model for the manganese nodule occurrences in the clarion-clipperton zone (Equatorial North Pacific Ocean). In: Establishment of a geological model of polymetallic deposits in the Clarion-Clipperton Fracture Zone of the equatorial North Pacific Ocean. Intenational Seabed Authority (ISA), Kingston, pp 175–200

Blöthe M, Wegorzewski AV, Müller C, Simon F, Kuhn T, Schippers A (2015) Manganese-cycling microbial communuties inside deep-sea manganese nodules. Environ Sci Technol 49:7692–7700

Bodeï S, Manceau A, Geoffroy N, Baronnet A, Buatier M (2007) Formation of todorokite from vernadite in Ni-rich hemipelagic sediments. Geochim Cosmochim Acta 71:5698–5716

Bollhöfer A, Eisenhauer A, Frank N, Pech D, Mangini A (1996) Thorium and uranium isotopes in a manganese nodule from the Peru basin determined by alpha spectrometry and thermal ionization mass spectrometry (TIMS): are manganese supply and growth related to climate? Geologische Rundschau 85:577–585

Bonatti E, Kraemer T, Rydell H (1972) Classification and genesis of submarine iron-manganese deposits. In: Horn DR (ed) Ferromanganese deposits on the ocean floor. NSF, Washington, pp 149–166

Borole DV (1993) Late Pleistocene sedimentation: a case study in the central Indian Ocean Basin. Deep Sea Res 40:761–775

Bradtmiller LI, Anderson RF, Sachs JP, Fleisher MQ (2010) A deep respired carbon pool in the glacial equatorial Pacific Ocean. Earth Planet Sci Lett 299:417–425

Bruland KW (1983) Trace elements in sea water. In: Riley JP, Chester R (eds) Chemical oceanography, vol 8. Academic Press, London, pp 156–220

Burns RG, Burns VM (1977) Mineralogy. In: Glasby GP (ed) Marine manganese deposits. Elsevier oceanography series, vol 15. Elsevier, Amsterdam, pp 185–248

Burns VM, Burns RG (1978) Authigenic todorokite and phillipsite inside deep sea manganese nodules. Am Mineral 63:827–831

Burns RG, Burns VM, Stockman HW (1983). A review of the todorokite-buserite problem: implications to the mineralogy of marine manganaese nodules. Am Mineral 68:972–980

Byrne RH (2002) Speciation in seawater. In: Ure AM, Davidson CM (eds) Chemical speciation in the environment. Blackwell Publishing Ltd, Oxford, pp 322–357

Cairncross B, Beukes NJ (2013) The Kalahari Manganese Field. Struik Nature Ltd., Cape Town, 383 p

Cherkashov G, Smyslov A, Soreide F (2013) Fe-Mn nodules of the finnish bay (Baltic Sea): exploration and exploitation experience. In: Morgan CL (ed) Recent developments in Atlantic seabed minerals exploration and other topics of timely interest. The Underwater Mining Institute, Rio de Janeiro, 4 p

Chester R, Jickells T (2012) Marine geochemistry, 3rd ed. Wiley-Blackwell, Oxford, 411 p

Chukhrov FV, Gorshkov AI, Beresovskaya VV, Sivtsov AV (1979) Contributions to the mineralogy of authigenic manganese phases from marine manganese deposits. Miner Deposita 14:249–261

Cronan DS, Rothwell G, Croudace I (2010) An ITRAX geochemical study of ferromanganiferous sediments from the Penrhyn Basin, South Pacific Ocean. Mar Georesour Geotechnol 28:207–221

Drits VA, Tchoubar C (1990) X-ray diffraction by disordered lamellar structures: theory and applications to microdivided silicates and carbons. Springer, Berlin, p 371

Drits VA, Silvester E, Gorshkov AI, Manceau A (1997) Structure of synthetic monoclinic Na-rich birnessite and hexagonal birnessite: I. Results from X-ray diffraction and selected-area electron diffraction. Am Mineral 82:946–961

Drits VA, Lanson B, Gaillot AC (2007) Birnessite polytype systematics and identification by powder X-ray diffraction. Am Mineral 92:771–788

Ehrlich HL (1963) Bacteriology of manganese nodules: I. Bacterial action on manganese in nodules enrichments. Appl Microbiol 11:15–19

Ehrlich HL (1972) Response of some activities of ferromanganese nodule bacteria to hydrostatic pressure. In: Cilwell RR, Morita RY (eds) Effect of the ocean environment on microbial activities. University Park Press, Baltimore, pp 208–211

Ehrlich HL (2000) Ocean manganese nodules: biogenesis and bioleaching possibilities. Miner Metall Process 17:121–128

Ehrlich HL, Newman DK (2009) Geomicrobiology, 5th edn. CRC/Taylor & Francis Group, Boca Raton, p 606

Eisenhauer A, Gögen K, Pernicka E, Mangini A (1992) Climatic influences on the growth rates of Mn crusts during the Late Quaternary. Earth Planet Sci Lett 109:25–36

Froelich PN, Klinkhammer GP, Bender ML, Luedtke NA, Cullen D, Dauphin P (1979) Early oxidation of organic matter in pelagic sediments of the eastern equatorial Atlantic: suboxic diagenesis. Geochim Cosmochim Acta 43:1075–1090

Galoway F, Bender M (1982) Diagenetic models of interstitial nitrate profiles in deep-sea suboxic sediments. Limnol Oceanogr 27:624–638

Giovanoli R, Bürki P, Giuffredi M, Stumm W (1975) Layer structured manganese oxide-hydroxides. IV. The buserite group: structure stabilisation by transition elements. Chimia 29:517–520

Giovanoli R (1980) On natural and synthetic manganese nodules. Geol Geochem Manganese 1(65):100–202

Glasby GP (2006) Manganese: predominant role of nodules and crusts. In: Schulz HD, Zabel M (eds) Marine geochemistry. Springer, Heidelberg, pp 371–428

Glasby GP, Emelyanow EM, Zhamoida VA, Baturin GN, Leipe T, Bahlo R and Bonacker P (1997) Environments of formation of ferromanganese concretions in the Baltic Sea: a critical review. In: Nickelson K, Hein JR, Bühn B, Dasgupta S (eds) Manganese mineralization: geochemistry and mineralogy of terrestrial and marine deposits. Geol. Soc. Spec. Publ. No. 119, pp 213–238

Golden DC, Dixon JB, Chen CC (1986) Ion exchange, thermal transformations, and oxidizing properties of birnessite. Clays Clay Miner 34:511–520

González FJ, Somoza L, Leon R, Medialdea T, de Torres T, Ortiz JE, Lunar R, Martinez-Frias J, Merinero R (2012) Ferromanganese nodules and micro-hardgrounds associated with the Cadiz Contourite Channel (NE Atlantic): palaeoenvironmental records of fluid venting and bottom currents. Chem Geol 310–311:56–78

González J, Somoza L, Lunar R, Martínez-Frías J, Medialdea T, León R, Martín-Rubí JA, Torres T, Ortiz JE, Marino E (2014) Polymetallic ferromanganese deposits research on the Atlantic Spanish continental margin. In: Hein JR, Barriga FJAS, Morgan, CL (eds) Harvesting seabed minerals resources in harmony with nature. UMI, Lisbon, Portugal

Grangeon S, Lanson B, Miyata N, Tani Y, Manceau A (2010) Structure of nanocrystalline phyllomanganates produced by freshwater fungi. Am Mineral 95:1608–1616

Haeckel M, König I, Riech V, Weber ME, Suess E (2001) Pore water profiles and numerical modelling of biogeochemical processes in Peru Basin deep-sea sediments. Deep Sea Res II 48:3713–3736

Halbach P, Friedrich G, von Stackelberg U (1988) The manganese nodule belt of the Pacific Ocean. Enke, Stuttgart, p 254

Han X, Jin X, Yang S, Fietzke J, Eisenhauer A (2003) Rhythic growth of Pacific ferromanganese nodules and their Milankovitch climattic origin. Earth Planet Sci Lett 211:143–157

Hastings D, Emerson S (1986) Oxidation of manganese by spores of a marine Bacillus: kinetic and thermodynamic considerations. Geochim Cosmochim Acta 50(8):1819–1824

Hein JR, Koschinsky A (2013) Deep-ocean ferromanganese crust and nodules. In: Holland H, Turekian K (eds) Earth systems and environmental sciences, treatise on geochemistry, 2nd edn. Elsevier, Amsterdam, pp 273–291

Hein JR, Schulz MS, Kang J-K (1990) Insular and submarine ferromanganese mineralization of the Tonga-Lau region. Mar Mining 9:305–354

Hein JR, Conrad TA, Staudigel H (2010) Seamount mineral deposits. A source of rare metals for high-technology industries. Oceanography 23(1):184–189

Hein JR, Mizell K, Koschinsky A, Conrad TA (2013) Deep-ocean mineral deposits as a source of critical metals for high- and green-technology applications: comparison with land-based resources. Ore Geol Rev 51:1–14

Hein JR, Spinardi F, Okamoto N, Mizell K, Thorburn D, Tawake A (2015) Critical metals in manganese nodules from the Cook Islands EEZ, abundances and distributions. Ore Geol Rev 68:97–116

Herguera JC (2000) Last glacial paleoproductivity patterns in the eastern equatorial Pacific: benthic foraminifera records. Mar Micropaleontol 40:259–275

Hlawatsch S, Garbe-Schönberg CD, Lechtenberg F, Manceau A, Tamura N, Kulik DA, Kersten M (2002) Trace metal fluxes to ferromanganese nodules from the western Baltic Sea as a record for long-term environmental changes. Chem Geol 181:697–709

ISA (2010) A geological model of polymetallic nodules in the Clarion-Clipperton Fracture Zone. International Seabed Authority Technical Study No. 6. Kingston, Jamaica, p 75

Koschinsky A (2001) Heavy metal distributions in Peru Basin surface sediments in relation to historic, present and disturbed redox environments. Deep Sea Res II 48:3757–3777

Koschinsky A, Halbach P (1995) Sequential leaching of marine ferromanganese precipitates: genetic implications. Geochim Cosmochim Acta 59:5113–5132

Koschinsky A, Hein JR (2003) Uptake of elements from seawater by ferromanganese crusts: solid-phase associations and seawater speciation. Mar Geol 198:331–351

Krapf E (2014) Investigations of growth structures of manganese nodules from the East Pacific using micro-analytical approaches. Master thesis (in German), University of Clausthal, Clausthal-Zellerfeld, p 62

Kuhn T, Bau M, Blum N, Halbach P (1998) Origin of negative Ce anomalies in mixed hydrothermal-hydrogenetic Fe–Mn crusts from the Central Indian Ridge. Earth Planet Sci Lett 163:207–220

Kuhn T, Burger H, Castradori D, Halbach P (2000) Tectonic and hydrothermal evolution of ridge segments near the Rodrigues Triple Junction (Central Indian Ocean) deduced from sediment geochemistry. Mar Geol 169:391–409

Kuhn T, Bostick BC, Koschinsky A, Halbach P, Fendorf S (2003) Enrichment of Mo in hydrothermal Mn precipitates: possible Mo sources, formation process and phase associations. Chem Geol 199:29–43

Lilley MD, Feely RA, Trefry JH (1995) Chemical and biochemical transformations in hydrothermal plumes. In: Humphris SE, Zierenberg RA, Mullineaux LS, Thomson RE (eds) Seafloor hydrothermal systems. Geophys. Monogr. 91, Am. Geophys. Union, Washington, pp 369–391

Lyle M (1982) Estimating growth rates of ferromanganese nodules from chemical compositions: implications for nodule formation processes. Geochim Cosmochim Acta 46(11):2301–2306

Manceau A, Gorshkov AI, Drits VA (1992a) Structural chemistry of Mn, Fe, Co, and Ni in manganese hydrous oxides: Part II. Infromation from EXAFS spectroscopy and electron and X-ray diffraction. Am Mineral 77:1144–1157

Manceau A, Gorshkov AI, Drits VA (1992b) Structural chemistry of Mn, Fe, Co, and Ni in manganese hydrous oxides: Part I. Information from XANES spectroscopy. Am Mineral 77:113–1143

Manceau A, Drits VA, Silvester E, Bartoli C, Lanson B (1997) Structural mechanism of Co^{2+} oxidation by the phyllomanganate buserite. Am Mineral 82(11–12):1150–1175

Manceau A, Marcus MA, Grangeon S (2012) Determination of Mn valence states in mixed-valent manganates by XANES spectroscopy. Am Mineral 97:816–827

Manceau A, Lanson M, Takahashi Y (2014) Mineralogy and crystal chemistry of Mn, Fe, Co, Ni, and Cu in a deep-sea Pacific polymetallic nodule. Am Mineral 99:2068–2083

Mandernack KW, Post J, Tebo BM (1995) Manganese mineral formation by bacterial spores of the marine *Bacillus*, strain SG-1: evidence for the direct oxidation of Mn(II) to Mn(IV). Geochim Cosmochim Acta 59:4393–4408

Mann S, Sparks NHC, Scott GHE, deVrind-deJong EW (1988) Oxidation of manganese and formation of Mn_3O_4 (hausmannite) by spore coats of a marine *Bacillus sp*. Appl Environ Microbiol 54:2140–2143

McLennan SM (1989) Rare earth elements in sedimentary rocks: influence of provenance and sedimentary processes. In: Lipin BR, McKay GA (eds) Geochemistry and mineralogy of rare earth elements. Rev. Mineral. 21, Mineral. Soc. Am., Washington, pp 169–200

Mewes K, Mogollón JM, Picard A, Rühlemann C, Kuhn T, Nöthen K, Kasten S (2014) The impact of depositional and biogeochemical processes on small scale variations in nodule abundance in the Clarion–Clipperton Fracture Zone. Deep-Sea Res 191:125–141

Miyata N, Maruo K, Tani Y, Tsuno H, Seyama H, Soma M, Iwahori K (2006) Production of biogenic manganese oxides by anamorphic ascomycete fungi isolated from streambed pebbles. Geomicrobiol J 23:63–73

Morgan JJ (2005) Kinetics of reaction between O_2 and Mn (II) species in aqueous solutions. Geochim Cosmochim Acta 69:35–48

Mukhopadhyay R, Ghosh AK (2010) Dynamics of formation of ferromanganese nodules in the Indian Ocean. J Asian Earth Sci 37:394–398

Mukhopadhyay R, Ghosh AK, Iyer SD (2008) The Indian Ocean nodule field. Geology and resource potential. In: Hale M (series editor) Handbook of exploration and environmental geochemistry no. 10. Elsevier, Amsterdam, p 292

Müller PJ, Hartmann M, Suess E (1988) The chemical environment of pelagic sediments. In: Halbach P, Friedrich G, von Stackelberg U (eds) The manganese nodule belt of the Pacific ocean: geological, environment, nodule formation, and mining aspects. Enke, Stuttgart, pp 70–90

Novikov GV. Bogdanova O, Yu (2007) Transformations of ore minerals in genetically different oceanic ferromanganese rocks. Lithol Miner Resour 42:303–317

Peacock CL, Sherman DM (2007a) Sorption of Ni by birnessite: equilibrium controls on Ni in seawater. Chem Geol 238:94–106

Peacock CL, Sherman DM (2007b) Crystal-chemistry of Ni in marine ferromanganese crusts and nodules. Am Mineral 92:1087–1092

Post JE, Appleman DE (1988) Chalcophanite, $ZnMn_3O_7$-$3H_2O$: new crystal-structure determinations. Am Mineral 73:1401–1404

Post JE, Appleman DE (1994) Crystal structure refinement of lithiophorite. Am Mineral 79:370–374

Post JE, Bish DL (1988) Rietveld refinement of the todorokite structure. Am Mineral 73:861–869

Post JE, Veblen DR (1990) Crystal structure determinations of synthetic sodium, magnesium, and potassium birnessite using TEM and the Rietveld method. Am Mineral 75:477–489

Post JE, Heaney PJ, Hanson J (2003) Synchrotron X-ray diffraction of the structure and dehydration behavior of todorokite. Am Mineral 88:142–150

Rogers TDS, Hodkinson RA, Cronan DS (2001) Hydrothermal manganese deposits from the Tonga-Kermadec Ridge and Lau Basin Region, Southwest Pacific. Mar Geores Geotechnol 19:245–268

Rosson RA, Nealson KH (1982) Manganese bacteria and the marine manganese cycle. In: Ernst WG, Morin JG (eds) The environment of the deep sea. Prentice Hall Inc., Englewood Cliffs, pp 206–216

Schweissfurth R (1971) Manganknollen im Meer. Naturwissenschaften 58:344–347

Shaw TJ, Gieskes JM, Jahnke RA (1990) Early diagenesis in differing depositional environments: the response of transition metals in pore water. Geochim Cosmochim Acta 54:1233–1246

SPC (2013) Deep sea minerals: manganese nodules, a physical, biological, environmental, and technical review. In: Baker E, Beaudoin Y (eds) vol 1B. Secretariat of the Pacific Community

Stumm W, Morgan JJ (1981) Aquatic chemistry: an introduction emphasizing chemical equilibria in natural waters, 2nd edn. Wiley, New York, p 780

Takahashi Y, Manceau A, Geoffroy N, Marcus MA, Usui A (2007) Chemical and structural control of the partitioning of Co, Ce, and Pb in marine ferromanganese oxides. Geochim Cosmochim Acta 71:984–1008

Tebo BM, Bargar JR, Clement BG, Dick GJ, Murray KJ, Parker D, Webb SM (2004) Biogenic manganese oxides: properties and mechanisms of formation. Annu Rev Earth Planet Sci 32:287–328

Tebo BM, Johnson HA, McCarthy JK, Templeton AS (2005) Geomicrobiology of manganese (II) oxidation. Trends Microbiol 13:421–428

Tebo BM, Clement BG, Dick GJ (2007) Biotransformations of manganese. In: Hurst CJ, Crawford RL, Garland JL, Lipson DA, Mills AL, Stetzenbach LD (eds) Manual of environmental microbiology, 3rd edn. ASM Press, Washington, pp 1223–1238

Turner S, Buseck PR (1979) Manganese oxide tunnel structures and their intergrowths. Science 203:456–458
Usui A, Mita N (1995) Geochemistry and mineralogy of a modern buserite deposit from a hot spring in Hokkaido, Japan. Clays Clay Miner 43:116–127
Usui A, Mellin TA, Nohara M, Yuasa M (1989) Structural stability of marine 10Å manganates from the Ogasawara (Bonin) Arc: implication for low-temperature hydrothermal activity. Mar Geol 86:41–56
Villalobos M, Toner B, Bargar J, Sposito G (2003) Characterization of the manganese oxide produced by *Pseudomonas putida* strain MnB1. Geochim Cosmochim Acta 67:2649–2662
Visbeck M, Gelpke N (2014) World ocean review 3. Maribus gGmbH, Hamburg, p 163
von Stackelberg, U. (1997). Growth history of manganese nodules and crusts of the Peru Basin. In: Manganese mineralization: geochemistry and mineralogy of terrestrial and marine deposits. Geol Soc Spec Pub, 119, pp 153–176
von Stackelberg U (2000) Manganese nodules of the Peru Basin. In: Cronan DS (ed) Handbook of marine mineral deposits. CRC Press, Boca Raton, pp 197–238
von Stackelberg U, Beiersdorf H (1987) Manganese nodules and sediments in the equatorial North Pacific Ocean, "Sonne" Cruise SO25, 1982. Geol. Jahrb., D87:403 pp
von Stackelberg U, Marchig V (1987) Manganese nodule from the equatorial North Pacific Ocean. Geol Jahrb D87:123–227
Warren BE (1941) X-ray diffraction in random layer lattices. Phys Rev 59:693–698
Webb SM, Tebo BM, Bargar JR (2005) Structural characterization of biogenic Mn oxides produced in seawater by the marine Bacillus sp. strain SG-1. Am Mineral 90:1342–1357
Wegorzewski AV, Kuhn T (2014) The influence of suboxic diagenesis on the formation og manganese nodules in the Clarion Clipperton nodule belt of the Pacific Ocean. Mar Geol 357:123–138
Wegorzewski A, Kuhn T, Dohrmann R, Wirth R, Grangeon S (2015) Mineralogical characterization of individual growth structures of Mn-nodules with different Ni+Cu content from the central Pacific Ocean. Am Mineral 100:2497–2508

Thomas Kuhn is a marine geologist at the German Federal Institute for Geosciences and Natural Resources (BGR). He has specialized in solid-phase associations and structural control of trace elements in ferromanganese precipitates, rocks, and sediments; the automated analysis of seafloor images; geostatistical resource estimation; and the analysis of hydro-acoustic data for the exploration of manganese nodule fields. He has participated in more than 25 research cruises to all major oceans.

Anna V. Wegorzewski is a marine geologist at the German Federal Institute for Geosciences and Natural Resources (BGR). She is working on the mineralogical composition of manganese nodules, especially on the enrichment and incorporation of economically interesting metals into the manganese phases particulary with regard to further metallurgical treatment. Since 2010, she participated in five research cruises in the Pacific and Indian ocean.

Carsten Rühlemann is a marine geologist at the German Federal Institute for Geosciences and Natural Resources (BGR) and is the project manager for the exploration of manganese nodules in the German license area. He has participated in more than 20 ocean-going expeditions.

Annemiek Vink is a marine bio-geologist at the German Federal Institute for Geosciences and Natural Resources (BGR). She is responsible for the coordination of the environmental management program in the German Mn-nodule exploration license area in the CCZ, which focuses strongly on the collection of adequate environmental baseline data as well as the analysis of potential impacts of Mn-nodule exploitation on faunal communities (e.g., due to nodule removal, sediment plume dispersion and settling). She has participated in several research/exploration cruises into the CCZ.

Chapter 3
Marine Co-Rich Ferromanganese Crust Deposits: Description and Formation, Occurrences and Distribution, Estimated World-wide Resources

Peter E. Halbach, Andreas Jahn, and Georgy Cherkashov

Abstract Cobalt-rich ferromanganese crusts from the seafloor are gaining significance due to the presence of a variety of major, minor, and trace metals that are of strategic importance for sustained demands of the industry in future. This chapter describes the occurrence and nature, mineralogy, formation and growth, chemical composition as well as their inter-relationships. The chapter further looks at total and regional metal potentials and proposes a resource assessment model for ferromanganese crust deposits and their economic considerations.

3.1 Introduction

The oceans represent the largest and most prominent feature on the surface configuration of the Earth; no other planet in the solar system has an ocean. The fact that Earth has so much water in the liquid form is unique in the inner Solar System. Most of this liquid water is stored in the ocean (Seibold and Berger 1993). This is of particular importance because water is the major basis for life on Earth. However, this huge water reservoir provides, besides food and energy, minerals and is a permanently acting source-sink system. These energy and material exchanges are taking place particularly at the seafloor, mostly controlled by processes working in the water column and generated by surface bioproductivity, continental material runoff into the oceans, and hydrothermal mass transfer.

The concept of interconnected phenomena and processes applies to many places on Earth including the seafloor where many sink products find their eventual deposition. Ferromanganese crust occurrences, for example, cover as cm- to dm-thick hydrated oxide layers huge seafloor areas in water depths of 1000 to more than

P.E. Halbach (✉) • A. Jahn
Freie Universitaet Berlin, Berlin, Germany
e-mail: hbrumgeo@zedat.fu-berlin.de

G. Cherkashov
Institute of Geology and Mineral Resources, St. Petersburg, Russia

R. Sharma (ed.), *Deep-Sea Mining*, DOI 10.1007/978-3-319-52557-0_3

5000 m. Their growth is provided by particulate mineral substances and planktonic skeletons resulting from oceanic water-column processes (see below). These crusts have a black to brownish-black colour and are one type of the two oxidic mineral resources that incorporate metals supplied and transported from both land (aerosols, continental runoff) and ocean sources (oxygen-minimum zone, hydrothermal alteration of the oceanic crust, dissolution of biogenic skeletons). In contrast to the ferromanganese nodules, the crusts mostly are tightly attached to the surfaces of hard substrate rocks, i.e. the crusts have to be mechanically loosened before a seafloor recovery can technically take place.

For any kind of successful crust mining, it is essential that the crusts will be recovered with minimum portions of the underlying barren rocks. However, up to now this technical problem is not solved. The crusts are polymetallic with regard to their chemical compositon, i.e. besides their main metals Mn and Fe, they contain some interesting minor (Co, Ni, Ti, Cu, and REEs) and trace elements (Mo, W, Nb, Te, Ga, and Pt). Some of these metals or semimetals have a great future potential as innovative high technology elements. However, up to date, it is not clear how far and which of these constituents can be extracted technically under profitable market conditions.

The knowledge of the geochemical and mineralogical bonding relationships and intergrowth conditions is also an important basis for the development of corresponding steps for mineral processing and for metallurgical extraction and enrichment. The concentration levels of the valuable metals within the crusts in relation to the market prices and the areal abundance also define the regional potential of the crust deposits as a future metal resource; these aspects are also considered.

3.2 Occurrence and Nature

Ferromanganese crusts (Fig. 3.1) form by direct precipitation from cold seawater under more or less oxic conditions and consist of hydrated mineral layers (up to 25 cm thick representing several generations of growth) on hard substrate rocks like volcanic hyaloclastites, more or less weathered basaltic rocks, carbonate-fluorapatite, limestone rocks, and consolidated clay deposits. In the crusts, many metals exist in the highest state of oxidation. Crusts do not form in marine areas where thicker, more or less consolidated sediment layers cover the rock surfaces.

Deposits of the Co-rich ferromanganese crusts are found throughout the global oceans; the fact that these deposits are distributed in the Pacific, Atlantic, and Indian Oceans indicate more or less uniform water column conditions (see below) at the time of crust growth. The main geomorphological settings are flanks, terraces, and summits of seamounts, submerged volcanic mountain ranges, and guyot platforms where the ocean currents have kept the seafloor more or less free of sediment for millions of years. The guyot platforms may also have patches of hydrogenetic nodules which show a similar layered set-up and metal composition as surrounding crust deposits (Halbach and Marbler 2009). Some of the estimated 50,000 seamounts

Fig. 3.1 Cobalt-rich manganese crust covering a hyaloclastic substrate rock; thickness of the crust about 8 cm; sample from a seamount slope in the Central Pacific Basin. The fracture surface shows a younger upper and an older lower layer. The latter is strongly impregnated by carbonate-flourapatite

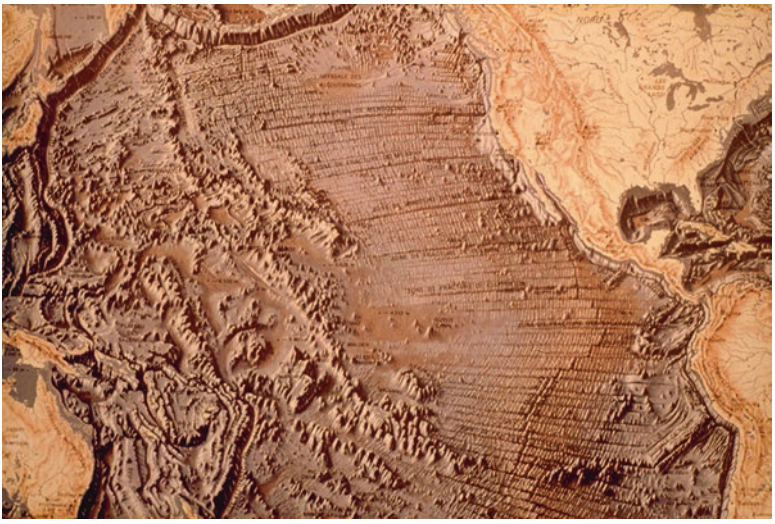

Fig. 3.2 Seafloor morphology of the Northern Pacific Ocean (Berann et al. 1977); the western part is characterized by many submarine extinct volcanoes and seamount chains, often former hot spot systems

which occur, for example, in the western half of the Pacific Ocean (Fig. 3.2), where the richest crust deposits are found, have been mapped and sampled in detail, but also other crust sites in the South Pacific, in the Atlantic, and in the Indian Oceans have been studied.

Thick metal-rich crusts occur on the outer rims of seamount summits, platforms, and on broad saddle structures (Hein et al. 2000). Intermediate slope terraces also have crust coverage where the crusts are often associated with patches of hydrogenetic nodules, which often contain small crust fragments as nuclei. Economically interesting crust deposits exist, in general, between 800 and 3000 m water depth because of higher Co and Ni concentrations (see below). The Atlantic and Indian Oceans contain far fewer seamounts and submarine mountain ranges than the western Pacific and, therefore, are less prospective for crust deposits. Crust distributions and compositions on seamounts are complex and controlled by many factors including seamount morphology, current patterns, mass wasting, substrate rock types, ages of precipitation as well as growth rates, subsidence history and climatic influences including changes in oceanic surface bioproductivity (see below). The regional importance of these potential metal resources finally depends on local crust distribution, as well as on small-scale topography, ore-grade, tonnage, and water-depth range. Often the crust layers imitate the microtopography (Figs. 3.3 and 3.4) of the underlying substrate rocks in the cm-to dm-scale; rounded boulders and blocks as well as former volcanic flow structures are reproduced by the morphology of the crust surfaces; the small-scale surface morphology shows often a knobby texture (Fig. 3.1). If the relative local micromorphological relief exceeds about 20 cm (Figs. 3.3 and 3.4), the technical loosening and recovery process can be significantly impeded. Crusts of 3–5 cm thickness, for example, may have local abundance values of 50–90 kg/m^2 (wet weight), in the case that the substrate rocks are almost entirely coated (Figs. 3.3 and 3.4).

Fig. 3.3 Seafloor image of a ferro-manganese crust field from a seamount slope in the Marshall Islands Area; long edge corresponds to 5 m. The slope has an inclination of 15°–18°. The coverage by crusts is about 90%. The underlying rocks control the micromorphology of the crust surfaces

Fig. 3.4 Seafloor image of a ferromanganese crust field from a seamount slope in the Central Pacific Basin; long edge corresponds to 5 m. The slope has an inclination of 15°–18°. The coverage by crusts is almost 100%. The underlying rocks control the micromorphology of the crust surfaces

In contrast to nodules, the crusts in general are tightly attached to hard substrate rocks. Surprisingly, on some slopes (inclination 16°–18°) of Central Pacific seamounts, it was observed that the crust layers are forming m- to dm-sized plates which are already loosened from the underground by a natural process and are slowly gliding downward (Figs. 3.5 and 3.6; Halbach et al. 2008). Along with this, the loosened plates are also disintegrated and/or fragmented. The microtopography on slopes with detached crust fragments is, in general, very smooth. The crusts of the upper parts of such slope areas show cross patterns of shrinkage cracks which probably formed due to dehydration processes of the original water-rich colloidal precipitates; with increasing maturation of the ferromanganese material, the porosity and the H_2O contents decrease and the grade of material order increases. This loss of volume eventually causes the formation of shrinkage cracks and gravity is responsible for the loosening and gliding down the slope; this downward movement also causes the reduction to smaller crust pieces.

The ferromanganese pavements generally are thin-layered, in cross section the individual layers occur as rhythmic sequences and differ in composition. Thus, the microlayers reflect the consecutive autocatalytic growth process of the crusts and the chemical variety in supply. The respective growth rates are very low and vary between 1 and 10 mm per 1 million year (Hein et al. 2000). In particular, these slow growth rates allow the adsorption and incorporation of large quantities of trace metals to the hydrated oxide and oxyhydroxide-phases in the water column and at the crust surfaces. It can last, therefore, up to several 10s of millions of years to form a

Fig. 3.5 Seafloor image of a ferromanganese crust field from a seamount slope in the Central Pacific Basin (slope inclination about 18°); long edge corresponds to 6 m. The crusts are covered by an unconsolidated thin sediment layer. First shrinkage cracks have already led to detachment of larger crust fragments

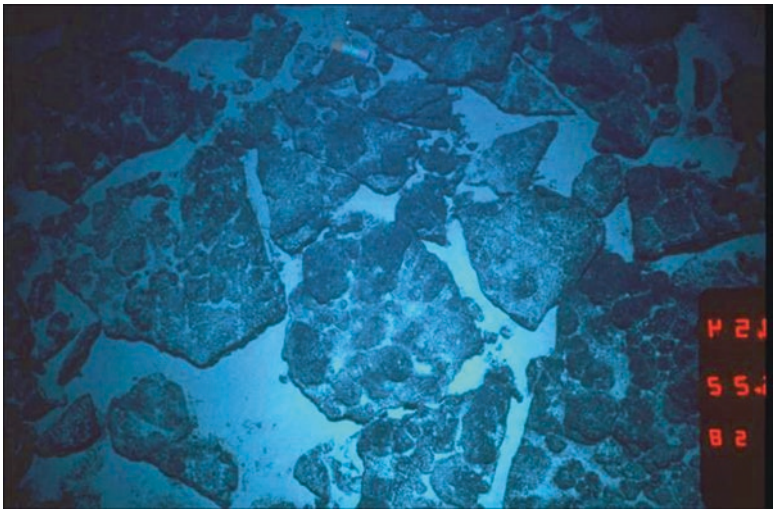

Fig. 3.6 Seafloor image of a ferromanganese crust field from the same slope as in Fig. 2.5 but at a deeper location; long edge corresponds to 6 m. The crusts are fragmented to dm- to m-sized plates which are loosened and glide downward

thick crust; such crusts have maximum ages of 75–80 Ma (Li et al. 2008). However, one very important feature is that crust growth is generally interrupted for millions of years; this hiatus may last for 10–20 Ma and can occur several times in the growth history.

The important result of this is that it can be distinguished between a younger and an older crust generation consisting of several sub-units (Li et al. 2008). During the long-lasting episodes of hydrogenetic growth interruptions, the crust layers are subject to diagenetic processes under the influence of suboxic to reducing conditions of an expanded O_2-minimum zone causing stagnating conditions in a larger part of the water column. This expansion of the O_2-minimum zone is, in general, caused by higher bioproductivity in oceanic surface waters, which is associated with larger amounts and higher fluxes of biomass (particulate organic matter) descending in the oceanic water column. Because of the decomposition of these enhanced masses of organic matter, the thickness of the water layer with both, O_2-deficiency but plenty of dissolved orthophosphate (HPO_4^{2-}), is getting much larger and reaches deeper, thus the crust growth under these conditions will be interrupted. This temporary lack of dissolved O_2 in deeper water layers is probably also connected with reduced cold deep-sea current activity. Even transient calcareous sediment coverages on the crust surfaces may have existed (see below). On the other hand, the ferromanganese crusts, being in contact with the O_2-depleted seawater or pore water, have very high porosities (45–60 vol% in the case of the younger crust generation). Thus, diagenetic processes will take place in the pore spaces of the crusts and may cause Mn-rich remineralizations as well as epigenetic carbonate-fluorapatite impregnations (Halbach et al. 2008). The textural and mineralogical changes caused by this diagenetic overprinting will be considered in a particular chapter (see below). However, all crust units are primarily formed as hydrogenetic precipitates on the seabed. But the older generations were subject to diagenetic overprinting processes after their primary growth.

The overall hydrogenetic process of the marine ferromanganese crust formation is a complex succession of different steps of material state changes. It can, in general, be described as an open and unsteady intraoceanic flow system controlled by changing surface bioproductivity conditions and influenced by different on-the-path chemical reactions such as scavenging mechanisms, water column particle transport, surface adsorption, redox reactions, carbonate dissolution, and colloidal-chemical precipitation. All these interacting reactions finally result in the very slow growth of the ferromanganese crust layers. One important basis to explain this typical precipitation is to understand the changing characteristic stratification of the oceanic water column during the periods of hydrogenetic growth and growth interruptions connected with epigenetic alterations. This particular marine system also is an excellent example to document how biological activity eventually leads to inorganic metal-rich seabed depositions.

3.3 Mineralogy

The internal microtexture of the ferromanganese crusts shows, under the ore-microscope, dendritic columnar zones of concentric layers of different reflectivity due to varying contents of Fe and Mn: the lighter layers are commonly richer in Mn and the darker ones in Fe; the latter ones often show a distinct micro-porosity in the

younger section. Each thin lamina of ferromanganese material represents a short period of uniform hydrogenetic precipitation. Between the colloform growth bodies, elongated pore spaces exist, which are occasionally filled with secondary minerals. This kind of texture is typically well-developed in the younger crust generation (Fig. 3.7).

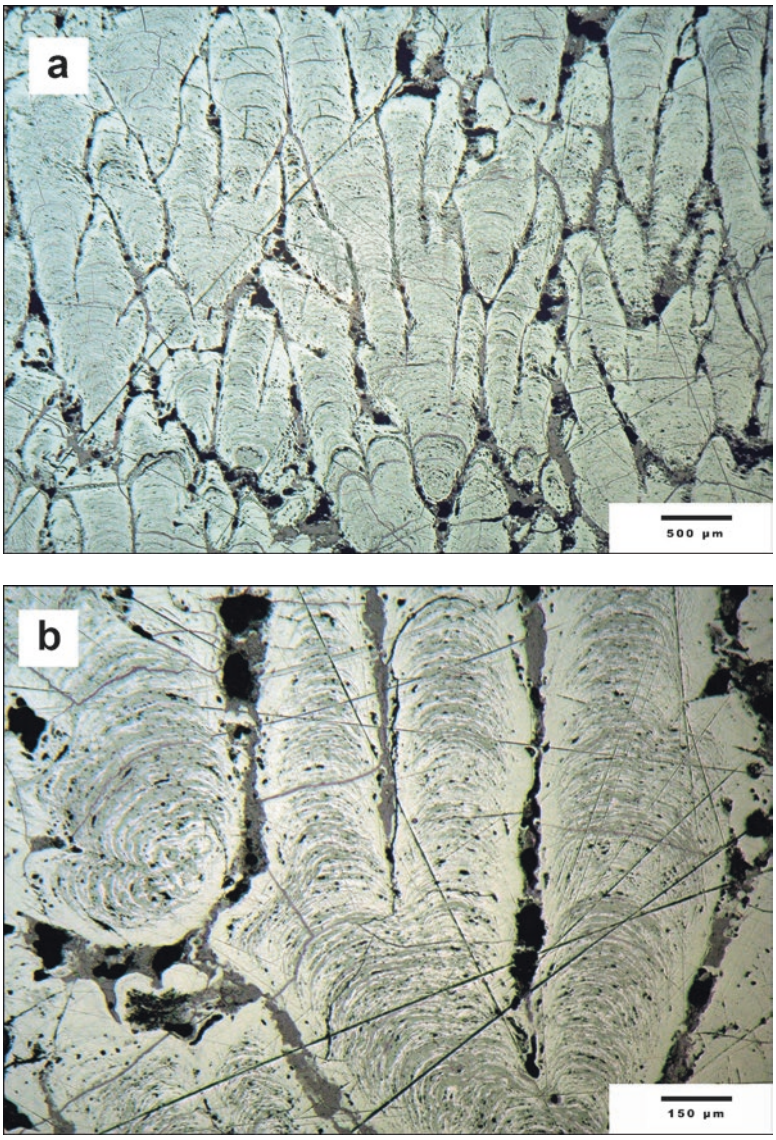

Fig. 3.7 (**a** and **b**) Photomicrographs (parallel polarizers) of a polished section of a ferromanganese crust sample showing the growth textures of the younger generation with typical colloform dendritic patterns of microlayered oxide material. (**a**) Shows an overview picture of the typical growth columns and elongated pore spaces. (**b**) Displays a larger magnification picture, the individual laminae vary in brightness: the lighter ones are richer in Mn and have less Fe than the grey microlayers

The mineralogy of these ferromanganese laminae is relatively simple compared to other ferromanganese precipitates such as diagenetic or hydrothermal Fe-Mn depositions. The dominant cryptocrystalline phase in the laminae is ferruginous δ-$MnO_2 \times H_2O$ (also called vernadite) with two x-ray reflections at about 1.4 Å and 2.4 Å; the sharpness of these two lines varies widely depending on crystallite size and Mn content. The metals mostly associated with the vernadite-phase are also the elements preferentially representing the economic importance of the crusts: these include Mn, Co, Ni, Zn, W, Mo, REEs, Pt, and Te. Ti, which also might have an economic potential, is mainly carried by a mixed Fe-Ti-oxyhydroxide phase. All these elements are highly enriched in the crusts as compared to seawater composition (see below). Another major phase in the crust material is x-ray amorphous FeOOH (Fe-oxyhydroxide), which is commonly epitaxially intergrown with the δ-MnO_2.

The vernadite-phase can constitute more than 90% of the x-ray crystalline phases. Remainder portions in the crusts consist of fine-grained detrital minerals, such as quartz, plagioklase, K-feldspar, pyroxene, phillipsite, and carbonate-fluorapatite (CFA; also called francolite). The quartz and most of the feldspar grains are of eolian dust origin. Goethite (α-FeOOH) can be detected in the innermost layers of the crust, i.e. in the layers of the older generations. Further admixtures in the crust consist of x-ray amorphous aluminosilicate, which was obviously supplied to the crust growth as colloidal substance. Calcite can occur in the surface layers of the younger crust generation as fragments of foraminiferal skeletons. Calcite also exists in the pore spaces of the older generation layers as well as birnessite (7 Å—phyllomanganate; Halbach et al. 2009), which was only identified by ore microscopy (Fig. 3.8). This birnessite is one important new mineral phase resulting from the epigenetic overprinting (see below). This epitaxial microgrowth feature of the Mn and Fe phases is a typical mineralogical feature of the hydrogenetic substance and can be explained by some characteristic mechanisms taking place in the final phase of the seafloor precipitation (see below).

As already mentioned, the ferromanganese crusts usually consist of two distinct growth generations: a younger and an older unit, the latter is composed of several subunits. The older generation is mostly thicker than the younger one and has typically a 3–6 cm thickness. These growth generations reflect climatical and environmental changes in the growth history (see below). However, all crust units were primarily formed as hydrogenetic precipitates on the seafloor (Fig. 3.9). After the older-generation hydrogenetic growth periods, the units in each case were subject to a hiatus of non-growth. During these episodes, the highly porous ferromanganese layers (porosity: 50–65 vol%; the older generation is somewhat less porous than the younger one) were diagenetically influenced by O_2-depleted water of an expanded O_2-minimum zone or by pore water from a transitional sediment coverage.

The most remarkable epigenetic mineral of this diagenesis is the authigenic carbonate-fluorapatite (CFA; see chapter 3.4.2), which may constitute up to 30% in the older part of the crusts, but averages between 9 and 10%. Birnessite is also a result of the diagenetic influence during the hiatus and is typically formed under suboxic conditions as fine-grained pore fillings (Fig. 3.8; see chapter 3.4.2). This birnessite is intimately intergrown with CFA and/or calcite. The typical microtexture containing these diagenetic remineralizations is the so-called “mottled texture” (Fig. 3.8) often combined with dissolution features and ferromanganese replacement textures.

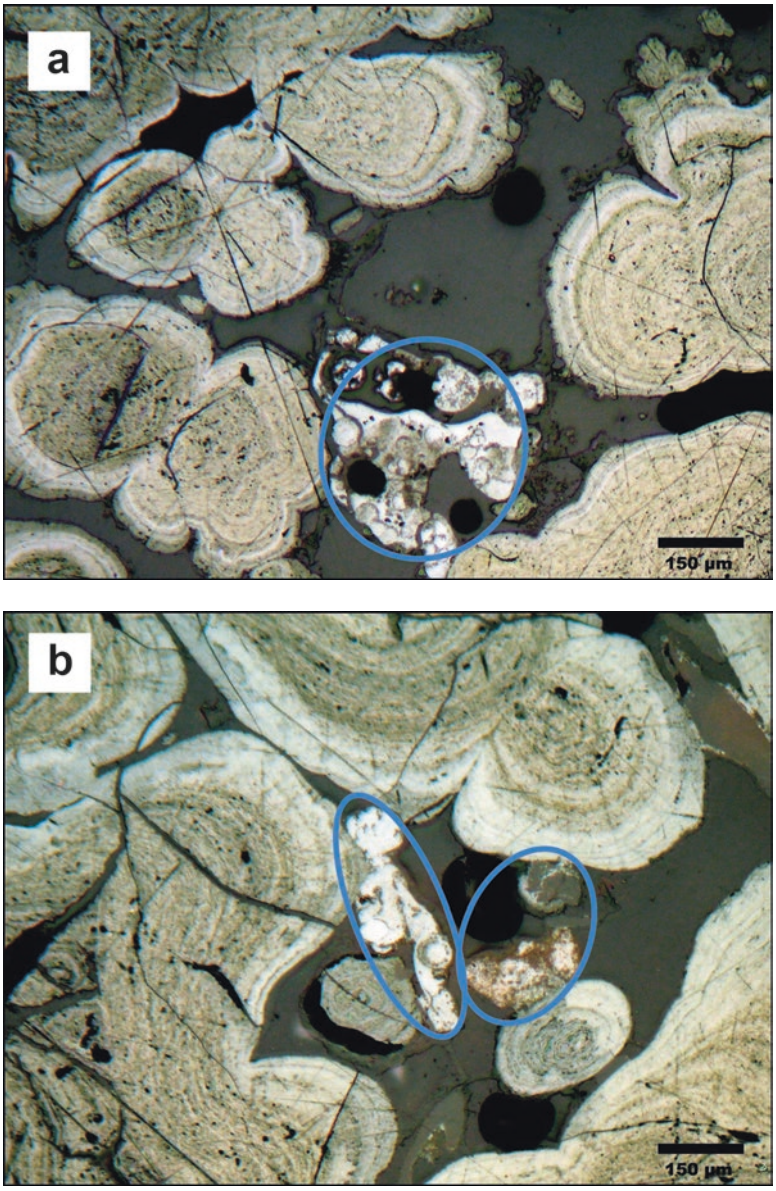

Fig. 3.8 (**a** and **b**) Photomicrographs (parallel polarizers) of a polished section of a ferromanganese crust sample showing the growth textures of the upper zone of the older generation with the typical mottled texture of oxidic rounded growth patterns and larger xenomorphic interstice fillings (diameters around 0.3 mm). The internal textures show typical diagenetic remineralization features. The pore spaces are filled with *grey* apatite and/or calcite. In both pictures (**a** and **b**), within the pores whitish precipitates (*blue circles*) probably consisting of diagenetically formed birnessite are observed. Interestingly, these pore fillings also contain higher Pt values of up to 2.0 ppm according to LA-ICP-MS measurements (Halbach and Marbler 2009)

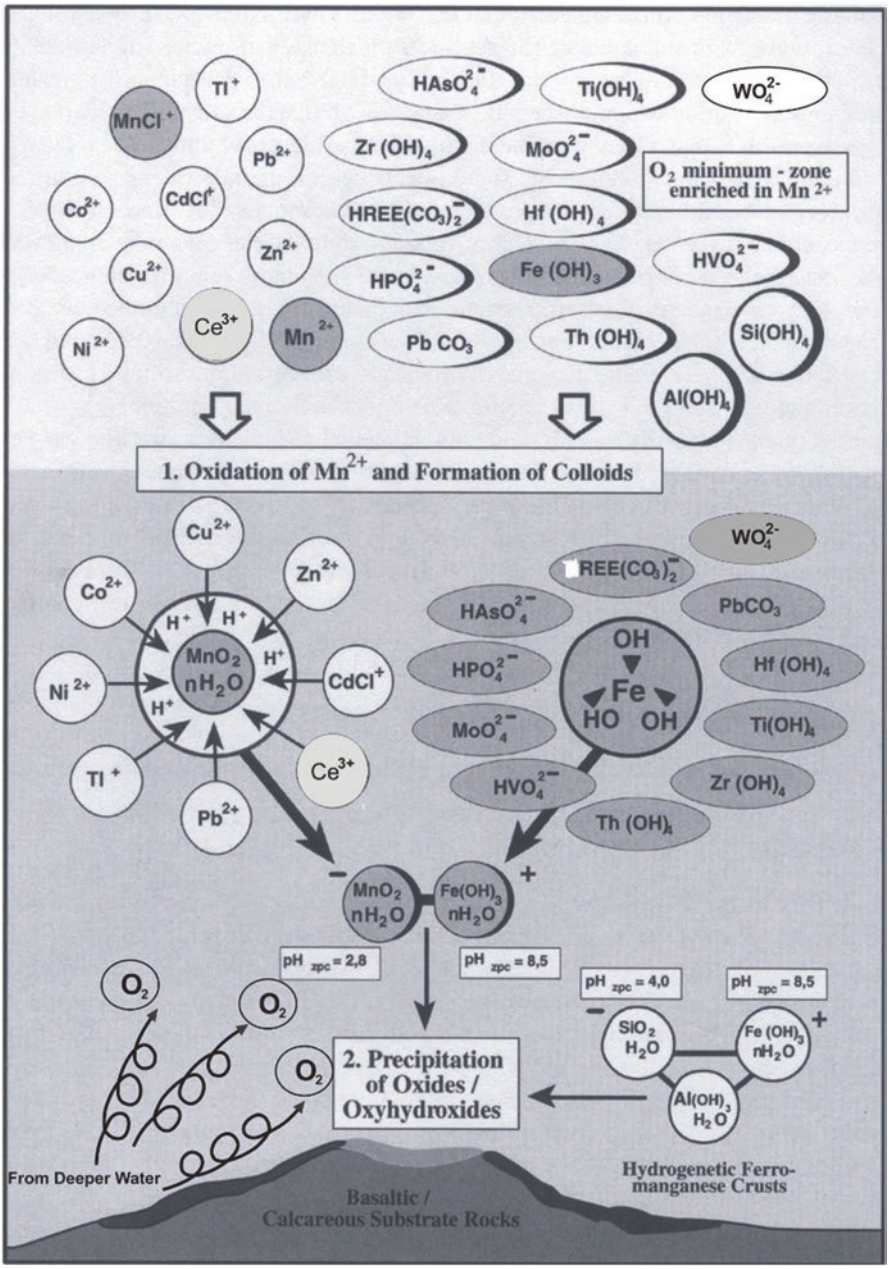

Fig. 3.9 Colloidal-chemical model for the formation of hydrogenetic crusts showing the probable hydrated cations, anion complexes and colloidal phases in seawater, adsorption of metals, the pH of the zero point of charge (zpc), and the precipitation of hydrated oxides on substrate rocks (modified from Koschinsky and Halbach 1995). Dissolved oxygen is supplied from deeper water by turbulent eddy diffusion

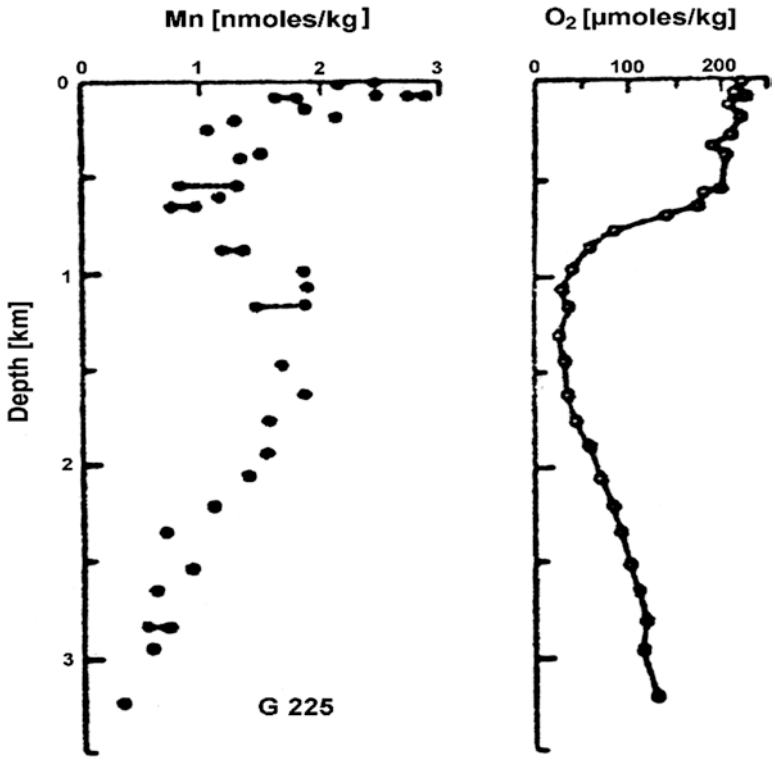

Fig. 3.10 Typical profiles of dissolved O_2 and dissolved Mn from a Central Pacific station (GEOSECS 1975); both constituents behave inversely. The O_2-minimum and the respective Mn maximum lie at water depths between 1000 and 1300 m (central zone of the O_2-minimum zone). This source of dissolved Mn mainly supplies the hydrogenetic accretion. But it has still to be oxidized (see below)

These zones within the older crust generation were analyzed by point measurements, using the laser ablation technique (LA-ICP-MS). The resulting data show the highest concentrations of Pt up to 2.0 ppm in the whole crust profile (see below). Therefore, it is obvious that this secondary Mn mineralization is one main carrier phase for Pt caused by post-depositional enrichment along redox fronts associated with CFA formation (Vonderhaar et al. 2000; see below).

3.4 Formation and Growth Processes

3.4.1 Hydrogenetic Accretion

Co-rich hydrogenetic ferromanganese crusts are a typical interface product of growth processes taking place on sediment-free substrate rocks on the seafloor. They grow preferentially in water depths below the oxygen-minimum zone (OMZ)

and have so far been found in water depths of up to more than 5000 m, i.e. also below the calcite compensation depth (CCD). It is assumed that the O_2-minimum zone is the most important source of dissolved manganese, also the decomposition of faecal pellets contributes to this Mn budget.

The process of hydrogenetic precipitation is basically an inorganic colloidal-chemical as well as a surface-chemical mechanism. Microbial mediations can be assumed, in particular since steps of redox-reactions are involved. Elements in seawater may occur as dissolved hydrated ions or as inorganic as well as organic complexes, which, in general, have either a positive or a negative surface charge depending on the pH of the respective aqueous environment. These complexes form hydrated colloids that interact with each other and with other dissolved hydrous metal ions. Hydrated cations such as Co, Ni, Zn, Sn, and Ce are, for example, attracted by the negatively charged surfaces of colloidal hydrous Mn-oxide particles, whereas hydrated anions and elements forming larger complexes with low-charge densities (e.g. U, As, Pb, Hf, Th, Nb, and REEs) are attracted by the slightly positively charged hydrous Fe-oxyhydroxide particles (Fig. 3.9). In addition to the outer and inner sphere adsorption, coupled redox processes (co-precipitation because of electron interchange) can be assumed to explain trace element enrichments. The main agent to oxidize the Mn^{2+} ions is oxygen, transported upwards from deeper water by turbulent eddy diffusion and turbulent rise processes at seamount slopes (Fig. 3.9).

Studies of the young hydrogenetic ore generation with reflected light microscopy and high-resolution SEM microscope reveal interesting results regarding a possible involvement of fine-grained phytoplankton particles (coccolith platelets) during the growth of the iron-manganese substance. The two main components of the composition of the hydrogenetic substance are hydrated δ-MnO_2 (vernadite) and x-ray amorphous Fe-oxyhydroxide, both of which are heteroepitaxially intergrown with each other within the extremely fine-grained oxidic material. Reflected light microscopy furthermore shows a finely laminated texture in the form of dendritic columns (Fig. 3.7).

The individual cyclic layers are 4–10 μm thick and have differing reflexions under parallel polarizers; according to microprobe measurements, the lighter layers are somewhat richer in Mn whereas the gray layers are richer in Fe. Basically, both metals exist in each of the alternating layers; regarding the chemical bulk composition of the crusts, both elements behave inversely (see below). Under reflected light microscopy, a further difference becomes obvious: whereas the light, Mn-rich micro-layers usually are very dense and massive, the Fe-rich layers often exhibit a micro-porosity restricted to these layers in a range of 2–4 μm.

In order to supply the hydrogenetic growth with the two main metals Mn and Fe, preferentially two sources are assumed (Halbach 1986): (1) Mn (Mn^{2+}) derives as a dissolved species from the oxygen-minimum zone (has yet to be oxidized) and (2) particulate Fe-oxyhydroxide is released during dissolution of carbonate plankton (aragonite and calcite skeletons; Halbach and Puteanus 1984). With the SEM it could be shown that, besides other carbonate skeletons, especially relics of

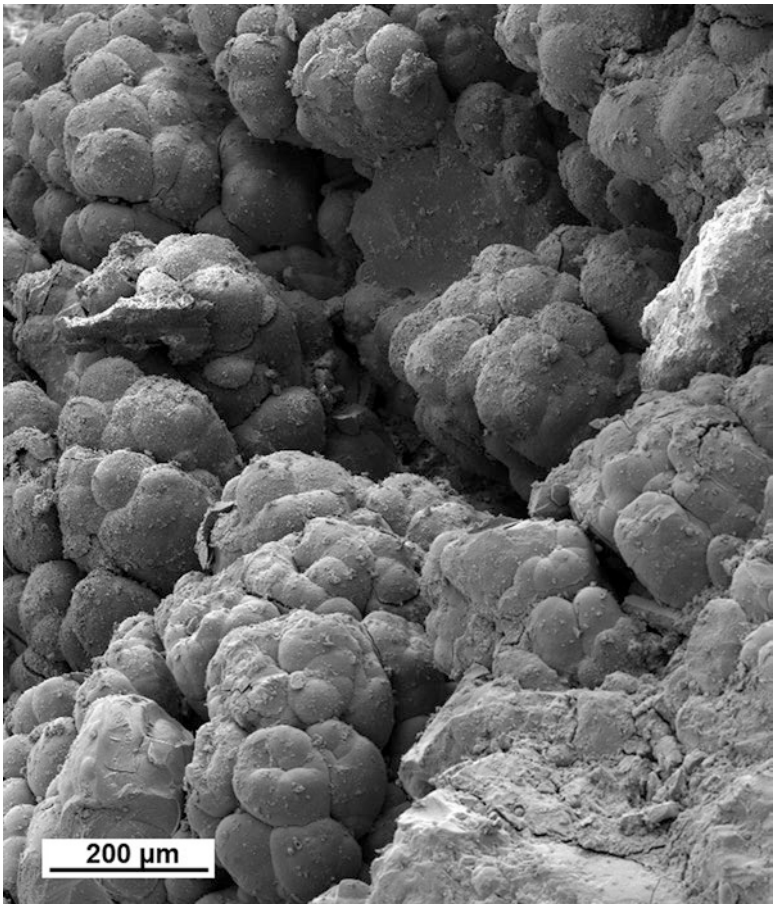

Fig. 3.11 The SEM image of a crust surface shows the typical knobby texture representing the youngest part of the growth columns (younger generation crust from the Manihiki Plateau, Central Pacific, water depth: 3310–3600 m; Halbach et al. 2009). The immediate surfaces are characterized by a micro-roughness consisting of coccoliths and coccolith fragments which are stuck to the surfaces (see Fig. 3.12)

coccolith platelets exist on the surface of hydrogenetic ore crusts (Fig. 3.11), all of them are corroded in various degrees (Fig. 3.12). In the interstices between the growth forms (Fig. 3.8), these planktonic relics often are enriched which is probably due to current influences in the micro-range (more deposition in the leeside of the micromorphology; Fig. 3.13).

Coccoliths are miscroscopically fine discs of calcite (3–10 µm; Fig. 3.15), which form the shell of calcareous algae of the order coccolithophorida. Coccolithophorides belong to the most important primary producers in the surface waters of the oceans

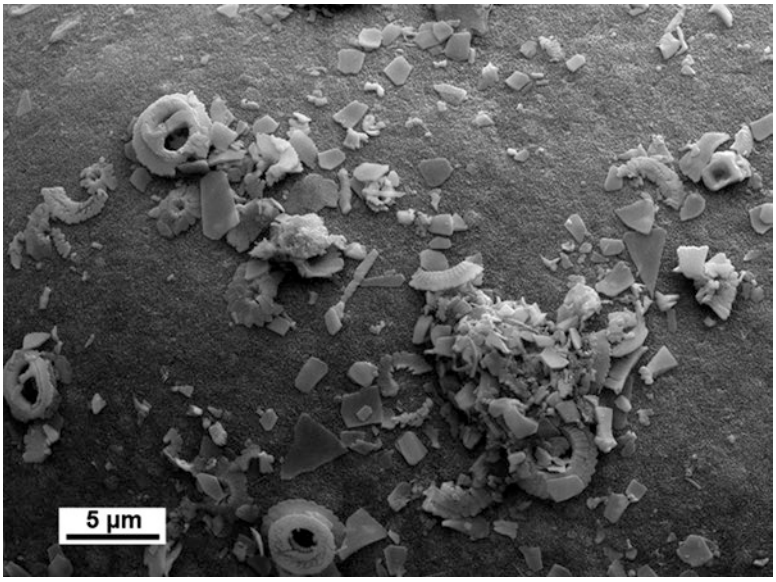

Fig. 3.12 The SEM image shows the surfaces of the columnar ferromanganese growth microstructures covered by corroded coccoliths and coccolith fragments (younger generation crust from the Manihiki Plateau, Central Pacific, water depth: 3310–3600 m; Halbach et al. 2009). The carbonate platelets of the nanoplankton are adhered to the oxide surface layers

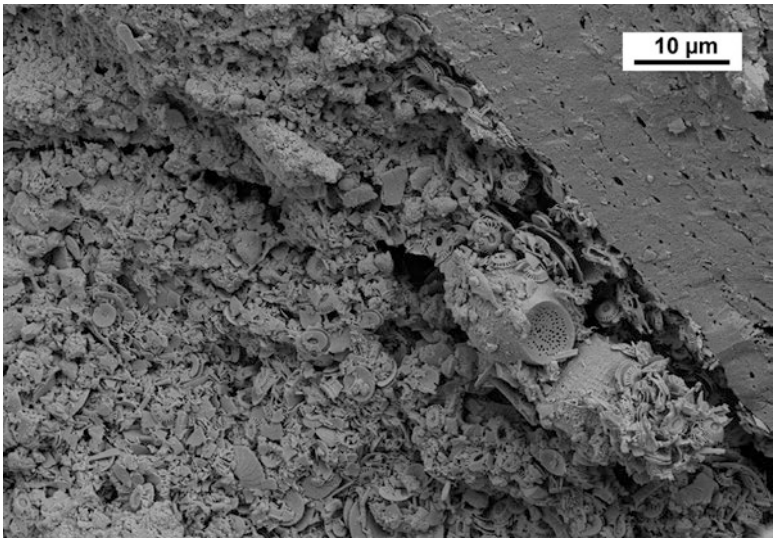

Fig. 3.13 SEM image of a crust sample from the Louisville Ridge (younger generation, water depth: 1540–1770 m, SW-Pacific). Debris of coccolith platelets and globigerina shells accumulate at the leeside of the knobby surface of the ferromanganese crusts. In the upper right corner layered hydrogenetic substance exists. The visible micro-porosity in this substance is obviously arranged in layers parallel to the surface (see also Fig. 3.14)

and are at the base of the food chain. Due to the fineness of the fragile calcareous platelets, a vertical transport and direct sedimentation from the water column is not possible (Kennett 1982). However, the transport within the water column can be explained by faecal pellets. These have grain sizes of 100–300 μm and have an organic pellicle which keeps the enclosed material from dissolving. A single faecal pellet can contain up to 10^5 calcium carbonate platelets. The subsidence rates of faecal pellets are 100–400 m per day (Kennett 1982). Since they are rich in organic substance, they are partly or completely decomposed in the O_2-minimum zone, thus below this water layer a release of coccoliths takes place. However, it is of interest to note that, on crust surfaces from deeper water layers (about 3200 m), also corroded skeletons of globigerina were observed.

Based on these observations, it can be concluded that during corrosion and dissolution of the fine plankton particles in the near-bottom water layer and on the crust surface, Fe-oxyhydroxide substance was released and thus was provided for the growth of the hydrogenetic substance (Halbach et al. 2009). SEM images of deeper crust areas show that the dissolution of the planktonic micro-relics on the surface does not take place completely, but is continued in the deeper layers underneath the surface, finally resulting in a micro-porosity restricted to this layer. Occasionally, closer to the surface these relics of coccoliths are still present (Fig. 3.14).

Due to the chemical dissolution of an obviously very high supply of carbonate plankton relics, a certain Fe enrichment is plausible. But how does this process interact with the dissolved Mn^{2+} from the OMZ and may cause a heteroepitaxial intergrowth?

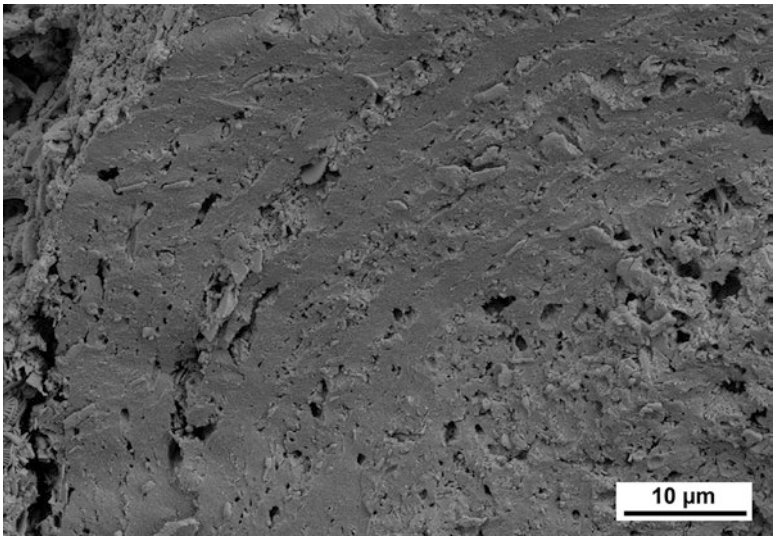

Fig. 3.14 SEM image of a crust sample from the Louisville Ridge (younger generation, water depth: 1540–1770 m, SW-Pacific). Within the layered setup of a single growth column of hydrogenetic substance, the micro-porosity is arranged along the former surfaces in contact to seawater. These layers of micro-porosity are occasionally filled with relics of coccoliths debris

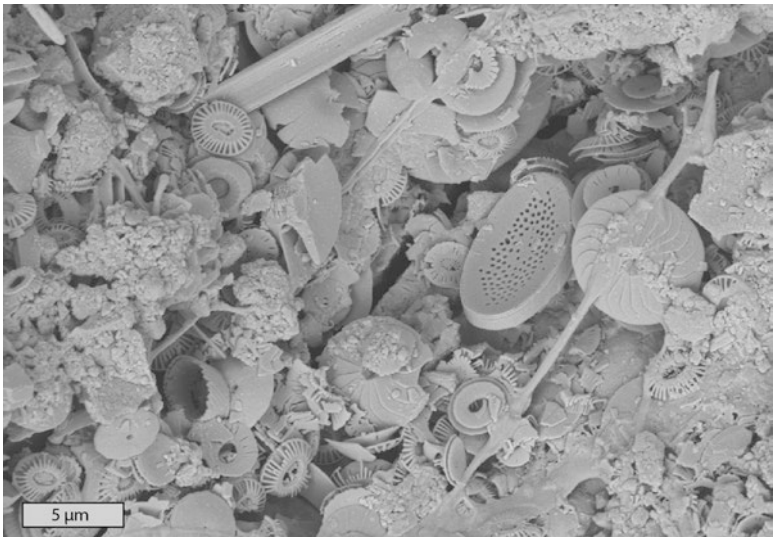

Fig. 3.15 SEM image of a dredged crust sample from the Louisville Ridge in the SW-Pacific (water depth: 1540–1770 m; Halbach et al. 2014). Assemblage of coccolith debris including *Calcidiscus leptoporus* and *Emiliania huxleyi* fragments

Mn present in the OMZ originates mostly from the decomposition of faecal pellets and the associated decomposition of organic substance. A slight input of Mn^{2+} from submarine hydrothermal springs into the OMZ is also possible. This Mn has to be oxidized before it can be incorporated into the hydrogenetic substance as hydrated δ-MnO_2.

Underneath the OMZ, contents of dissolved O_2 increase due to upward transport of oxygen with cold deep currents by turbulent diffusion. Under weakly alkaline conditions, oxidation of Mn^{2+} ions can be described as follows

Reaction (1): $Mn^{2+} + OH^- + ½O_2 \rightarrow MnO_2 + H^+$

According to this reaction, an offer in OH^- anions will promote the Mn oxidation. Comparing this model reaction with the chemical dissolution of skeletal $CaCO_3$, it becomes obvious that during a second process ions are released which promote Mn oxidation:

Reaction (2): $CaCO_3 + H_2O \rightarrow Ca^{2+} + HCO_3^- + OH^-$

According to Stumm and Morgan (1995), the pH value also has a kinetic influence on the oxidation rate of Mn^{2+}, since the presence of OH-ions (see the following equation) clearly promotes the oxidation rate in the alkaline range.

$$\frac{-\mathrm{d}Mn^{2+}}{\mathrm{d}t} = k_o\left[Mn^{2+}\right] + k'\left[OH^-\right]^2\left(Po_2\right)\left[Mn^{2+}\right]\left[MnO_2\right]$$

From these relationships, it can be concluded that oxidation from Mn^{2+} to MnO_2 in the micro-environment on the surfaces is promoted by dissolving planktonic carbonate particles. This microchemical process can also take place within the water column, but will mostly occur on the surface of the hydrogenetic ore crusts. Since also Fe-oxyhydroxide micro-flakes are released during dissolution of the planktonic skeletons, δ-MnO_2 and $Fe(OH)_3 \times H_2O$ will encounter. As colloidal chemical systems, these have opposite surface charges at marine pH values of ca. 8.2 (Stumm and Morgan 1995). This eventually leads to the intensive intergrowth of the two phases. This nano-scale process controlled by carbonate dissolution can be described as a coupled Fe-release and catalytic Mn-oxidation reaction. This leads to the cyclic precipitation of heteroepitaxially intergrown Fe-Mn particles. The two extremely fine-grained hydrous mineral phases are also characterized by very high specific particle surfaces (Halbach et al. 1975), which certainly will influence and promote the rate of absorption of trace metals.

The microscopical studies (see above) show that the light-grey, porous micro-layers of the ore crusts which obviously result from the dissolution of planktonic carbonate particles, containing more Fe than Mn, pass over into white-greyish, very dense, and massive micro-layers which have higher Mn contents than Fe and no microscopically visible pore space.

It is assumed that these two fine-grained ore layers represent one growth cycle of hydrogenetic precipitation, during which at first the intensive deposition of phytoplankton particles released an increased amount of Fe-oxyhydroxide substance. The increasing carbonate dissolution slowly changed the pH value towards a more alkaline range in the microenvironment of the crust surfaces, which eventually leads to increased Mn oxidation and precipitation of δ-MnO_2.

Then a renewed supply of planktonic carbonate particles took place and another, Fe-richer porous micro-layer was generated. This model shows that the biogeochemical control of the laminary nano-growth of the ore crusts is probably due to a cyclic development of bioproductivity in the surface waters.

3.4.2 Diagenesis of and Epigenetic Mineral Formation in Older Crust Layers

Chronostratigraphy and age dating of Pacific and Atlantic crusts display a deep-sea accumulation of layered oxidic metal compounds from late Cretaceous through Pleistocene with distinct hiatuses in growth alternating with time intervals of metal deposition (Halbach and Puteanus 1984; Koschinsky et al. 1997; Li et al. 2008; Pulyaeva and Hein 2011); accordingly, the oldest crust sections have maximum ages from 75 to 80 Ma. Crusts vary from several mm up to about 25 cm in thickness and reveal a layered structure from four to six individual growth intervals (Hein et al. 1993; Li et al. 2008). A very important hiatus identified in crust growth is dated as early to middle Oligocene (Pulyaeva and Hein 2011). It divides the total section of the crusts into older and young growth generations distinguished by a

very important geochemical feature: the older growth generations are strongly impregnated by secondary phosphorite (carbonate-fluorapatite, also called francolite), the young generation has no phosphorite-content; its P concentrations, therefore, are low and, in general, below 0.6% (referred to dry material). This phosphatization and overprint of the older crust units have remarkable compositional consequences regarding the contents in main and trace metals including the REEs. The carbonate-fluorapatite (CFA), for example, is a mineral which also takes up REEs in its mineral lattice.

The growth time of the younger crust generation is dated as Miocene to Pleistocene and contains early to late Miocene and Pliocene to Pleistocene units (Pulyaeva and Hein 2011). However, age dating using Os isotope composition of Co-rich crusts in comparison to geochemical seawater evolution allows a better delimitation of the hiatus intervals (Klemm et al. 2005; Li et al. 2008). If the phosphatization is used as a signal to define the older crust units, the results of Li et al. (2008) indicate that the phosphorite impregnation is older than about 42 Ma (i.e. older than Oligocene), which does not correspond to the results of Pulyaeva and Hein (2011). However, regional influences and variations can also be responsible for these discrepancies.

During the geological intervals with distinctly warmer ocean temperatures, stagnating conditions in the water column controlled by higher surface bioproductivity, and combined with a vertically extended OMZ (enriched in dissolved orthophosphate), the ferromanganese crust growth was interrupted. After the individual hydrogenetic growth periods, and during the following hiatus (see above), the highly porous ferromanganese layer was influenced by suboxic to anoxic waters of the OMZ or even by pore water of a temporarily cover with calcareous sediments.

The observed phosphatization is the main crust feature which indicates the diagenetic overprint of the older crust layers. The mineralogy and texture were strongly changed by this particular epigenetic process. The older ferromanganese crust deposits have phosphate interlayers, inclusions, and fine- to coarser-grained impregnations, but may also overlay phosphorite depositions formed obviously by replacement of calcareous sediments. The distribution of the phosphatized sections within the succession of the older crust units indicates that these mineralogical overprints represent defined episodes.

A model to explain the phosphogenic episodes that impregnated the older crust generations with francolite was already proposed by Halbach et al. (1982, 1989), explaining the mineral changes by an expansion of the oxygen-minimum zone. This phenomenon can be related to increased surface-water bioproductivity causing a suboxic and orthophosphate-rich water layer reaching down to the crust-covered slopes and plateaus, inhibiting further crust growth. Microscopic investigations reveal that in the former surface layers between the different phosphatized subunits, often pores, fissures, and interstitial spaces exist which are occasionally filled with planktonic calcareous sediment particles (mostly globigerina; Halbach et al. 2009). This observation shows that during the hiatuses, the subjacent ferromanganese layers were sometimes covered by calcareous sediment, which may also explain why hydrogenetic precipitation could not take place. Because of this sediment cover,

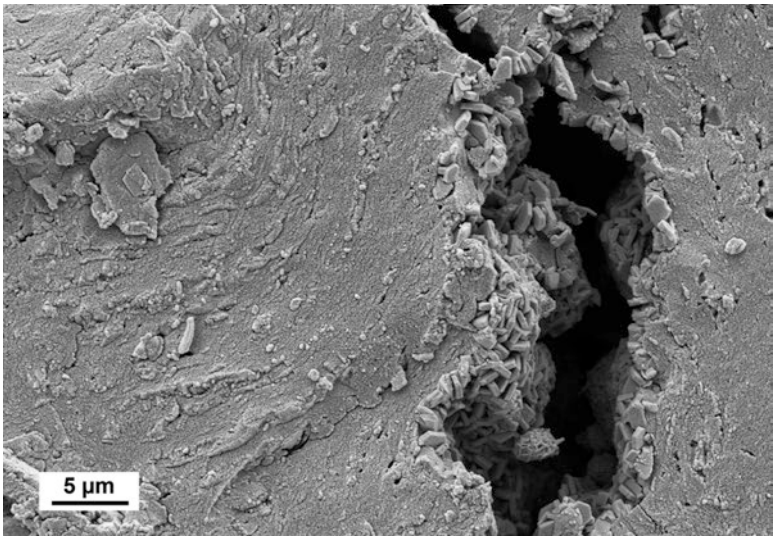

Fig. 3.16 SEM image of an older generation crust sample from the Louisville Ridge (water depth: 1910–2150 m; SW-Pacific). In the elongated cavity between two hydrogenetic growth columns, typical micro-granular tabular hexagonal crystals of apatite are formed. These microcrystals covering the walls of the pore spaces are obviously products of epigenetic overprinting

the ferromanganese units were also subject to sediment diagenesis, resulting in stronger replacement, redeposition, and new mineral formation processes. Basically, the two mentioned processes may also have taken place immediately after each other.

The epigenetic influence started with the phosphorite impregnation of the pore spaces in the hydrogenetic substance. This was promoted by the existence of nuclei surfaces, thus CF-apatite crystallization commenced with the displacement of planktonic carbonate relics by orthophosphate-bearing aqueous solutions. However, with some increase of phosphatization, the apatite formation led also to clusters of micro-granular, ideally crystallized hexagonal platelets in cavities and micro-cracks of the hydrogenetic substance (Figs. 3.16 and 3.17). Also, groups of birnessite lamellae can be observed beside the apatite. The hydrogenetic matter itself remained mainly unaltered. This kind of epigenetic overprint obviously represents a lower degree of alteration.

Under the conditions of a higher-degree diagenetic alteration, the hydrogenetic substance was partially subjected to substantial changes in mineral composition and micro-textures (Koschinsky et al. 1997). It is assumed that this high-degree overprint is mostly related to sediment-covered pore water conditions. The different geochemical pore water environment led to extensive disintegration and rearrangement of the primary hydrous Fe-Mn-oxide phases, mobilizing associated elements as well. Fe and Mn were largely fractionated; the Mn could reprecipitate as buserite, which is a more stable mineral phase under the diagenetic suboxic conditions. Fe was residually enriched in Ti- and Co-bearing Fe-rich collomorphous micro-layers with Fe contents of up to 44%; goethite was observed as new

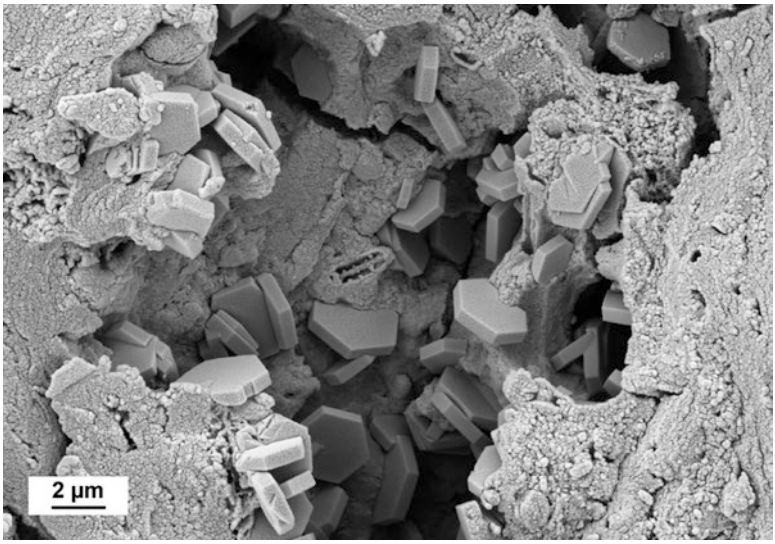

Fig. 3.17 SEM image of an older generation crust sample from the Louisville Ridge (water depth: 1910–2150 m; SW-Pacific). Close-up detail of Fig. 3.16. The hexagonal crystals are irregularly orientated within and on the surface of the hydrogenetic substance. These micro-crystalline phosphate aggregates are grains of 2–4 µm in size

mineral (Koschinsky et al. 1997). Barite needles and euhedral crystals of phillipsite were also observed as new stable mineral formations in the older crust layers. The frequent occurrence of buserite indicates that the Mn mobilized from the hydrogenetic vernadite-phase was recrystallized as 7 Å-manganate; this mineral in the older crust unit is enriched in Ni^{2+}, Cu^{2+}, Zn^{2+}, and Mg^{2+} which substitute for Mn^{2+} in the birnessite lattice; the 7 Å-line of the birnessite spectrum was confirmed by XRD investigation of older crust material (Halbach et al. 2014). Certain elements like Ni, Zn, Cu, Y, and REEs are somewhat enriched in the old crusts compared to the young crust's composition. The intense impregnation with phosphorite also has the technical consequence that the older crust material has the relative mineral hardness of five in the Mohs scale, i.e. this material is distinctly harder than the younger crust material and, therefore, more difficult to loosen and to recover.

The distribution and intensity of the phosphatization in the older crust layers is very irregular and variable, thus it is hardly possible to derive representative regional mean compositions. Investigations by Baturin and Yushina (2007) show this compositional heterogeneity of the phosphatized crust layers. According to their results, the apatite content can even increase up to 53% in maximum. In the sample sets discussed, apatite contents of up to 30% could be observed in high-degree alteration crust samples (Halbach et al. 2014).

Based on these results, it can be distinguished between two sorts of epigenetic overprinting of the hydrogenetic ore substance: (1) phosphorite impregnation which preserved the hydrogenetic substance to a large degree, and (2) phosphorite

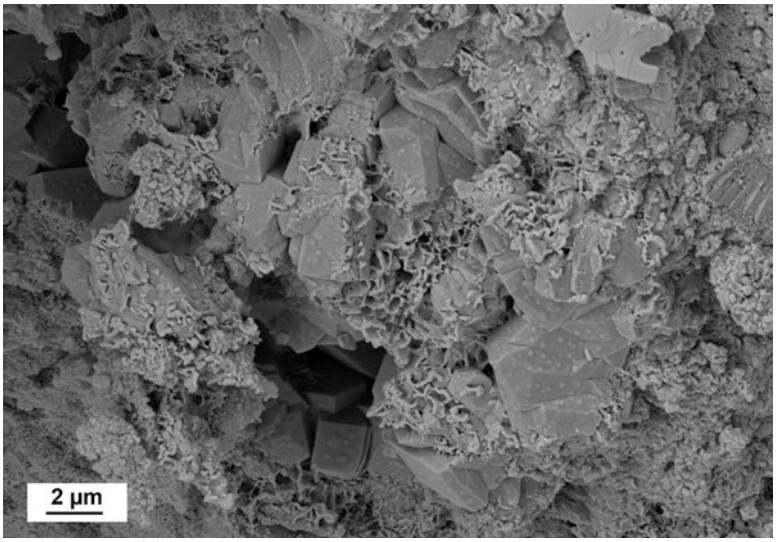

Fig. 3.18 SEM image of an older generation crust sample from the Louisville Ridge (water depth: 1910–2150 m; SW-Pacific). On the surfaces of the tabular hexagonal apatite crystals newly formed fine lamellae of birnessite, which are also a product of the early diagenetic overprinting, are observed. It is assumed that this Mn-rich birnessite aggregates were precipitated after the apatite formation

impregnation during intensified diagenetic conditions due to longer-term sediment cover with partial redistribution of the hydrogenetic substance and formation of new minerals. A typical newly formed mineral mostly intensively intergrown with apatite is lamellar birnessite (Figs. 3.18 and 3.19). Also skeletons of globigerina totally replaced by apatite can be observed (Fig. 3.20). The sediment cover in the second case was only temporary and was removed by later erosional processes; after that, due to changed geochemical O_2-conditions in the water column, normal hydrogenetic crust growth continued anew. The two kinds of overprint are probably also related to the interaction of local seamount morphology and mid-depth current influences, which controlled whether non-depositional conditions with low-degree or sedimentation with high-degree diagenetic alteration prevailed (Halbach and Marbler 2009; Halbach et al. 2014).

The history of crust growth and diagenetic overprint represents a very complicated multiple-parameter evolutionary process. Due to the movement of the Pacific Plate, particularly the crust deposits in the Pacific Ocean were shifted through the equatorial zone of high bioproductivity. However, according to their primary geographic positions, the movement and the path through the bioproductivity belt are responsible for a strongly variable overprinting of the crust layers. The subsidence of the seafloor structures on which the crusts precipitated also played an important role, since in the beginning of the growth history the slopes and platforms submerged to the depth ranges of the oxygen-minimum zone where hydrogenetic precipitation started. So it is evident that the older crust units grew in shallower water and at different geographic locations than they are at present.

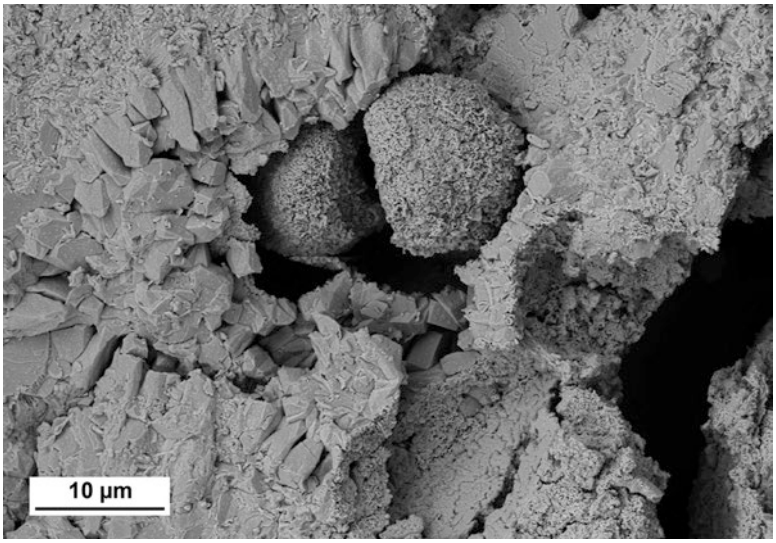

Fig. 3.19 SEM image of an older generation crust sample from the Louisville Ridge (water depth: 1910–2150 m; SW-Pacific). The micro-columnar crystals of apatite were formed by replacement of calcite substance of a former plankton skeleton. In the centre of the apatite-filled interstice are two spherical aggregates consisting of densely packed lamellar birnessite

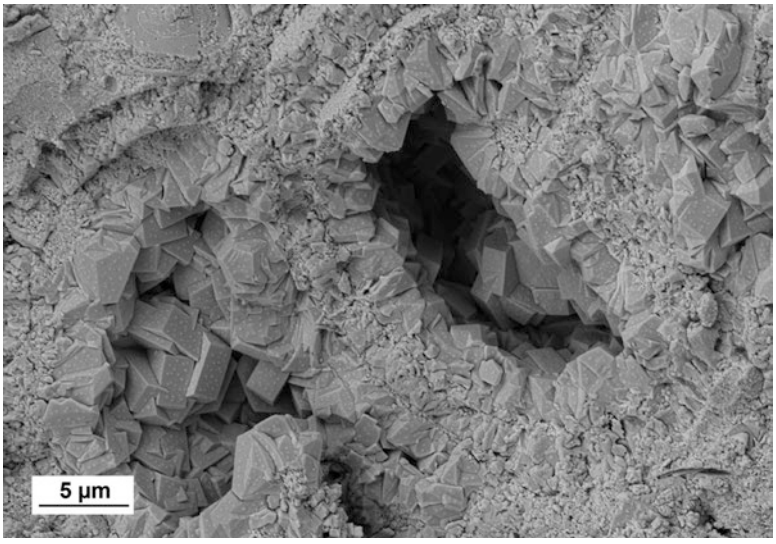

Fig. 3.20 SEM image of an older generation crust sample from the Louisville Ridge (water depth: 1910–2150 m; SW-Pacific). A former globigerina skeleton is replaced by micro-crystalline apatite, which consists in the inner part the micro-cavity of tabular hexagonal crystals

The ocean currents and the circulation of water masses around the seafloor structures as well as the processes in the water column such as the changing carbonate dissolution rate were also of influence since they controlled the Fe budget of the ferromanganese crust precipitation (Halbach and Puteanus 1984). Phosphatization also shows depth dependence and was found to be strong above 2500 m water depth in the Central Pacific, but becomes negligible at greater water depth (Koschinsky et al. 1997). At the Manihiki Plateau, for example, crust samples of the older generation are apatite-free ($P < 0.6\%$) in water depths more than 3300 m (Halbach et al. 2009). For comparison, some deep-water crust samples from the Osbourn Trough in the South Pacific (water depth 4400–4800 m; Halbach et al. 2014) were studied. The sampling sites are now located just underneath the present CCD (Calcite Compensation Depth); the surrounding sediments typically have red clay composition. These crusts do not show any diagenetic overprint and phosphatization. This raises the question whether these crusts were also interrupted in their growth history (see below). However, when reconstructing the water depths during times of growth or phosphate impregnation, it has to be considered that the ore crusts, together with their volcanic underground, slowly subsided within the water column during their geological existence.

3.4.3 Chemical Composition

3.4.3.1 Introduction

In general, ferromanganese crust deposits occur in the Pacific, Atlantic, and Indian Ocean. The deposits in the Pacific Ocean are much more intensively studied than in the other two oceans. Thus, the results of the Pacific Ocean research projects give much more detailed information and explanations with regard to the distribution, formation conditions, and composition and are, therefore, presented profoundly in the following chapters. Furthermore, the Pacific Ocean contains the largest resources compared to the Atlantic and Indian Ocean (Chap. 5). Some information about the different compositions between the three oceanic areas is also given in Sect. 3.5.2 (Economic Considerations).

To consider, to explain, and to evaluate the detailed chemistry of the ferromanganese crusts, a data set of samples from the Central Pacific region was selected. The 32 crust samples from different water depths (Table 3.1) were analysed with respect to major, minor and trace element composition.

The samples were milled and pulverized in an agate mortar; 5 g of each sample were separated and sent to the Activation Laboratories (Actlabs), Ontario, Canada. There the samples were digested and analysed for major, minor, and trace elements. The total number of analysed elements amounts to 56 (Halbach and Marbler 2009). Actlabs has carried out a detailed quality control by comparative measurement with certified reference materials, which proves the high quality of the data (Halbach and

Table 3.1 Location, water depth, and cruise number of analysed ferromanganese crust samples

Ref. no.	Sample code	Cruise no.	Water depth (m)	Longitude	Latitude
1	1DK tot.	SO 33/A	4112	158°22.54′ W	18°41.40′ N
2	2DK 1 young	SO 33/A	2021	158°22.54′ W	18°39.07′ N
3	2DK 3 old.	SO 33/A	2021	158°22.54′ W	18°39.07′ N
4	3DK tot.	SO 33/A	2140	158°22.54′ W	18°39.07′ N
5	6DK tot.	SO 33/A	870	158°22.54′ W	18°40.59′ N
6	17DK tot.	SO 33/A	2448	162°10.41′ W	9°41.36′ N
7	18DK old.	SO 33/A	1755	162°10.57′ W	9°42.06′ N
8	15DK tot.	SO 33/A	1487	162°09.53′ W	9°43.33′ N
9	33DK tot.	SO 33/A	2714	162°57.35′ W	6°16.02′ N
10	39DK tot.	SO 33/A	1217	164°50.05′ W	9°11.28′ N
11	44DK tot.	SO 33/A	1464	164°46.45′ W	9°13.32′ N
12	40DS tot.	SO 37	3049	169°05.11′ W	15°38.42′ N
13	63DK-3 tot.	SO 33	2905	169°15.09′ W	15°30.00′ N
14	64DK-1 tot.	SO 33	2161	169°13.26′ W	15°30.23′ N
15	65GTV-1 tot.	SO 33	1693	169°12.24′ W	15°35.30′ N
16	54GTV-2 tot.	SO 33	1393	169°12.50′ W	15°35.47′ N
17	57DK 1 old.	SO 33	1209	169°12.30′ W	15°35.22′ N
18	57DK 1 young	SO 33	1209	169°12.30′ W	15°35.22′ N
19	6 DK 2 young	SO 33	870	158°18.46′ W	18°40.59′ N
20	6 DK 2 old.	SO 33	870	158°18.46′ W	18°40.59′ N
21	55 DK 1 young	SO 33	1480	169°12.26′ W	15°35.12′ N
22	55 DK 1 old.	SO 33	1480	169°12.26′ W	15°35.12′ N
23	20 DS 1 old.	SO 37	1310	170°23.50′ W	15°39.92′ N
24	20 DS 1 young	SO 37	1310	170°23.50′ W	15°39.92′ N
25	43 DS 4 old.	SO 37	1600	169°12.25′ W	15°37.28′ N
26	43 DS 4 young	SO 37	1600	169°12.25′ W	15°37.28′ N
27	5 DSR 9 old.	SO 66	2500	174°53.60′ W	4°08.85′ S
28	5 DSR 9 young	SO 66	2500	174°53.60′ W	4°08.85′ S
29	43 DSO 5 old.	SO 66	2260	174°52.84′ W	4°08.06′ S
30	43 DSO 5 young	SO 66	2260	174°52.84′ W	4°08.06′ S
31	64 DSK 7 old.	SO 66	2680	177°19.79′ E	8°23.16′ S
32	64 DSK 7 old.	SO 66	2680	177°19.79′ E	8°23.16′ S

All samples originate from Central Pacific areas. Explanation: *tot.* means total crust, *young.* means younger generation, *old.* means older generation. These crust samples originate from seamounts surrounding the Central Pacific Basin (Fig. 3.39: regions 8, 11 and 12)

Marbler 2009). From the total sample set (Table 3.1) 14 subsamples (Table 3.4) were send to the Jacobs University Bremen (Germany) for additional Pt analysis; this was particularly done to compare the Pt contents between the older and the younger crust generation. For the latter reason, it was necessary to manually separate the ferromanganese crusts into an upper and a lower unit along macroscopically

visible transition zones (see above). The determination of the major and minor elements (Mn, Fe, P, Al, Si, K, Mg, Ca, Ni, Ti, Ba, Ce, Pb, Cu) was carried out using a fusion ICP (FUS-ICP, Actlabs, Canada: Lithoquant 4). Only Co was determined by an optical emission spectrometer with inductively coupled plasma (ICP-OES, Actlabs, Canada). The important trace elements Nb, W, Mo, Ga, and REE were also measured by FUS-ICP-MS (Actlabs, Canada: Lithoquant 4); for the determination of Au and Pd, a fire assay mass spectroscopy (FA-MS, Actlabs) and, for Te, the aqua regia MS (AR-MS, Actlabs) were used. Pt was determined with a stripping voltammetric method at the Jacobs University Bremen.

To study the local micro-distribution and interelement relationships in some crust profiles of polished sections, the laser ablation technique coupled with an ICP-MS (LA-ICP-MS) instrument at the University of Mainz was applied. This is an ICP-MS Agilent 750 with pulsated LA-Up 213 New Wave. The data of this method are only semiquantitative since a constant element for internal standardization is not available in the crusts. However, the specific interelement relationships can be interpreted (see below).

3.4.3.2 Major Constituents

The main metals in the ferromanganese crusts are Mn (13–27%) and Fe (6.0–18%; Table 3.2); they show in general an inverse relationship. The sum of these two elements in the bulk composition amounts to about 32%. The Mn/Fe ratio varies between 0.7 and 3.7 (mean value 2.0; Table 3.2). Another geochemical feature is that Fe increases and Mn decreases with water depth (see below). The data are well comparable with crust samples from, e.g., the Marshall Island marine areas (USGS KORDI Open File Report 90-407 1990). However, the results have the tendency to higher quality crust compositions which is also indicated by the high Mn/Fe ratio of 2.0; in the Marshall Islands sample set the respective value amounts only to 1.5.

Table 3.2 Descriptive statistics: average composition of Central Pacific samples from 1000 to 4100 m water depth (Actlabs results)

(%)	Mean	Median	Std. dev	Min	Max
SiO_2	5.22	4.20	3.41	1.37	12.79
Al_2O_3	1.18	0.83	0.91	0.31	3.75
Fe_2O_3	16.23	15.29	4.57	8.66	26.31
Fe	11.35	10.69	3.19	6.05	18.39
MnO	28.24	29.81	4.68	17.19	35.75
Mn	21.01	22.18	3.48	12.79	26.60
Fe + Mn	32.36	32.92	3.57	21.48	37.01
Mn/Fe	2.02	2.11	0.70	0.70	3.68

(continued)

Table 3.2 (continued)

(%)	Mean	Median	Std. dev	Min	Max
MgO	1.50	1.53	0.16	1.08	1.81
CaO	5.63	3.13	4.52	2.51	23.58
Na_2O	1.82	1.86	0.46	0.52	3.05
K_2O	0.47	0.46	0.20	0.01	1.01
TiO_2	1.42	1.35	0.35	0.78	2.57
P_2O_5	2.50	0.94	2.95	0.41	14.57
LOI	31.37	29.96	5.82	22.71	40.71
(ppm)					
Co	6647	6470	2666	2490	11,800
Ni	4326	4170	1501	1670	7250
Cu	573	540	378	170	2220
Zn	514	560	158	140	700
Mo	431	414	148	178	705
W	68	62	26	22	120
Nb	40	42	12	19	56
Te	34	37	12	8	61
Pt	0.273	0.233	0.199	0.106	0.730
Ga	18	21	11	5	40
Rb	5	4	3	2	16
Sr	1320	1324	149	1082	1753
Y	206	207	68	104	417
Zr	423	420	158	184	842
Sn	7	7	2	3	12
Ba	1646	1467	759	1003	5122
La	201	185	62	100	335
Ce	892	892	261	411	1630
Pr	36	29	16	17	73
Nd	136	106	66	64	290
Sm	31	25	16	15	69
Eu	8	7	4	4	17
Gd	30	24	16	15	69
Tb	5	5	2	3	11
Dy	36	33	12	18	65
Ho	8	8	2	4	13
Er	24	23	6	12	36
Tm	4	4	1	2	5
Yb	22	23	5	11	31
Lu	3	3	1	2	5
Tl	69	56	47	0	160
Pb	945	903	646	95	2620
V	481	490	121	255	717

Mean contents of SiO_2 are 5.2%, Al_2O_3 1.2%, MgO 1.5%, Na_2O 1.8%, and K_2O 0.5%; MgO, Na_2O, and K_2O which are fixed mainly to the aluminosilicate fraction show moderate variations (see standard deviations in Table 3.2), whereas SiO_2 and Al_2O_3 as the main constituents of this fraction show high standard deviations according to differing fluxes. A small part of SiO_2 and Al_2O_3 is also contributed by the clastic input. Na_2O and K_2O can also be fixed to detrital feldspar. TiO_2, which also is of economic interest, shows a significantly positive correlation with the Fe-oxyhydroxide phase and a weaker correlation, but also a positive one, with SiO_2 and Al_2O_3. TiO_2 has a mean value of 1.4% and also increases with water depth (see below).

The mean value of CaO is 5.6% with a high standard deviation (Table 3.2). The main portion of CaO is fixed to P_2O_5 forming the carbonate-flourapatite fraction (CFA), which predominantly exists in the older crust generation. The CaO/P_2O_5-ratio of this mineral is around 1.6, thus about 3% CaO forms CFA and 1.7 is fixed to non-apatite minerals, which probably are calcite and feldspar. The respective mean amount of CFA in bulk crust composition amounts to 5.2%. The chemical analyses of the individual crust samples subdivided into older and younger crust subsamples show significant differences in the CFA content (Table 3.3). Young crust generation subsamples have P_2O_5 concentrations of 0.6–0.7%. In contrast, the older generation subsamples show significantly higher P_2O_5 contents varying from 3.5 to 11.4%. It is important to note that the water depth has a considerable influence: subsamples from shallower water depths (1310–1600 m; Table 3.3) show higher concentrations in CFA (about 32% maximum) than the old crust subsamples from deeper water (2260–2680 m; Table 3.3), which have only about 9.7% CFA. Since the apatite is a diagenetic product caused by the O_2-depleted seawater of an expanded O_2-minimum zone and precipitated within the pore spaces of older crust layers (see above), it is obvious that this influence was more intense in shallower water.

Table 3.3 Comparative mean values of Central Pacific ferromanganese crust compositions (young generation and older generation) of two different water depth ranges (Actlabs data)

	Young crust	Young crust		Old crust	Old crust
	Mean (n = 3)	Mean (n = 2)		Mean (n = 3)	Mean (n = 2)
w.d.	2260–2680 m	1310–1600 m		2260–2680 m	1310–1600 m
SiO_2 (%)	4.82	3.42		2.70	2.35
Al_2O_3	1.09	0.57		0.61	0.60
Fe	11.11	10.51	>	8.80	6.98
Mn	22.47	22.48	>	22.59	15.43
Fe + Mn	33.58	32.99		31.38	22.40
Mn/Fe	2.03	2.14		2.59	2.25
MgO	1.47	1.41		1.38	1.16
CaO	2.73	2.65	<	7.20	19.12
Na_2O	1.82	1.80		1.72	1.79
K_2O	0.45	0.38		0.41	0.31
TiO_2	1.32	1.15		1.33	0.88

(continued)

Table 3.3 (continued)

	Young crust	Young crust		Old crust	Old crust
	Mean (n = 3)	Mean (n = 2)		Mean (n = 3)	Mean (n = 2)
P_2O_5	0.64	0.72	<	3.46	11.42
LOI	38.42	39.89		37.46	29.29
Co (ppm)	5983	8185	>	2600	4810
Ni	5657	4040		3455	4900
Cu	637	230		567	350
Zn	667	370		420	225
Mo	369	332	<	380	430
W	55	56		67	67
Nb	33	29		30	22
Te	31	34		37	42
Ga	6	6		8	8
Rb	3	4		3	4
Sr	1192	1209		1315	1529
Y	117	138	<	254	363
Zr	319	211		375	323
Sn	7	5		7	7
Ba	1397	1062	<	1645	1653
La	131	162	<	174	212
Ce	614	719	<	843	880
Pr	22	30		27	28
Nd	83	114		98	103
Sm	18	26		21	22
Eu	5	7		6	6
Gd	15	22		19	21
Tb	3	5		4	4
Dy	24	32		30	32
Ho	5	7		7	8
Er	17	20		22	25
Tm	3	3		3	4
Yb	16	18	<	21	22
Lu	3	3		3	3
Hf	6	4		6	5
Pb	1983	1089		811	312
Th	4	10		4	4
U	11	11		10	10
V	379	399	>	363	283

In Table 3.3, some selected sample analyses have been compiled with regard to younger crust and older crust compositions and distinguished according to two depth ranges (1310–1600 m and 2260–2680 m). The results indicate some very interesting general geochemical trends and information: (1) The Fe-content is

higher in the younger crust than in older crust samples. (2) The CaO and P_2O_5 contents indicate the CFA quantity. In the older crust samples, these constituents are basically higher; however, the older crust samples from shallower water depths are significantly CFA-richer. Thus, the respective CFA-values decrease with increasing water depth in the older crust samples. (3) The Co-contents are significantly higher in the young crust samples, but decrease with water depth. (4) The Mo-concentrations are somewhat higher in the older crust samples. (5) The Y, La, and Ce and Yb concentrations are somewhat higher in the older crust samples. (6) The Ba-content is higher in the older crust samples. (7) The V-contents are somewhat higher in the young crust samples. Some of these results obviously show that the water depth plays an important role for the vertical element distribution in crust samples (see below). For the apatite concentration in the older crust samples even the result has been observed, that in Pacific crust samples (Manihiki Plateau) in water depths below 3300 m, the samples are apatite-free (see above).

3.4.3.3 Minor Elements

Minor elements are defined as elements with contents between about 600 ppm and about 1% in the ferromanganese crusts. Co, which is the metal with the greatest economic market potential in crusts, ranges from 0.3 to 1.2%, the mean value is about 6700 ppm (Table 3.2). Very rarely, the Co concentration in individual crusts can exceed 2% according to Hein et al. (2000). Co is considered to be an element most characteristic of hydrogenetic precipitation in crusts and is assumed to have a constant flux in the water column, regardless of the water depth (Halbach et al. 1983). The observation that the Co concentration in crusts, nevertheless, decreases with increasing water depth (see below) is explained by the increasing growth rate associated with an increase and incorporation of Co-free diluting mineral compounds (predominantly aluminosilicates and Fe-oxyhydroxide). Co exists in seawater mainly as a hydrated divalent cation and is, therefore, adsorbed by hydrous MnO_2 colloids combined with an oxidation to Co^{3+} after outer sphere adsorption (oxidative scavenging; Halbach 1986): the respective enrichment factor compared to seawater composition is about 6×10^9 (Halbach and Marbler 2009).

After Co, also Ni has a positive relationship to Mn and shows a mean value of 4326 ppm in bulk crust composition and varies between 1670 and 7250 ppm (Table 3.2). Co and Ni show, in general, positive correlations with each other (Halbach and Marbler 2009). Both elements are negatively related to Fe, but significantly positively related to Mn (Fig. 3.21). Ni exists in seawater also as a hydrated divalent cation and is fixed to the Mn fraction by adsorption. The respective enrichment factor is only 0.8×10^7 (Halbach and Marbler 2009), since an oxidation of Ni after surface adsorption is thermochemically not possible (Halbach 1986). Also, Ni decreases with increasing water depth, which is typical for the Mn-group metals (see below).

Cu concentrations average 573 ppm and increase up to more than 2000 ppm (Table 3.2). Cu has a low economic potential in the ferromanganese crusts. Contents increase moderately with water depth (see below). The interelement relationship for

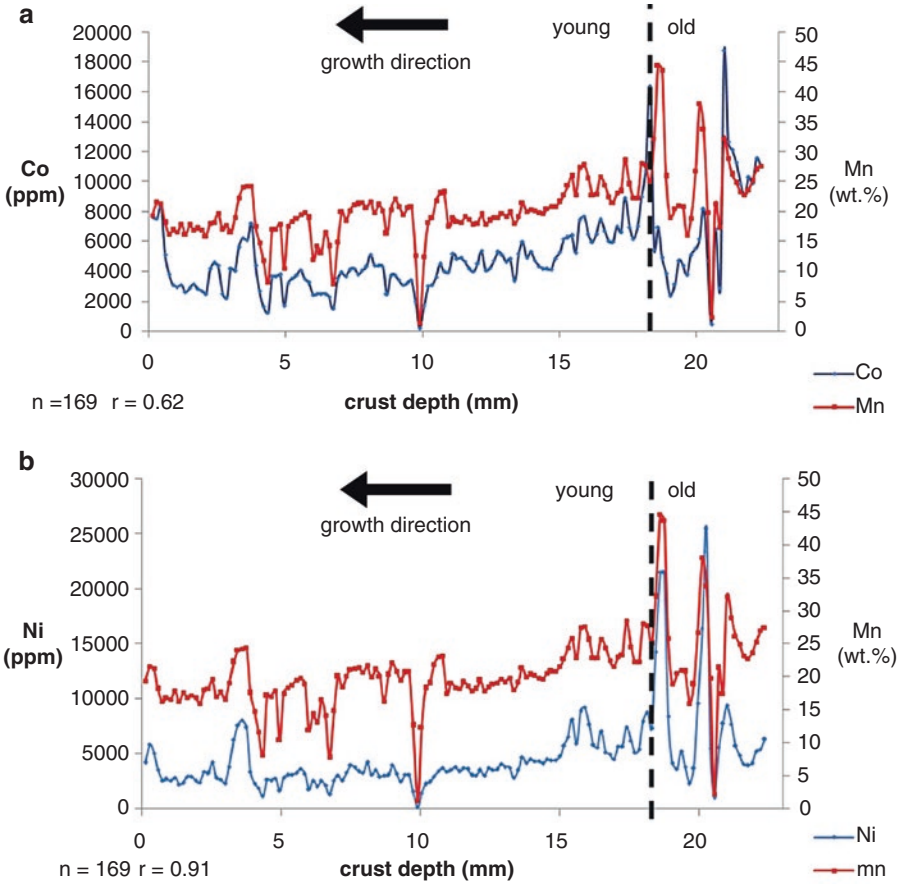

Fig. 3.21 Co and Mn (**a**) and Ni and Mn (**b**) in a ferromanganese crust profile by LA-ICP-MS measurements (HRG). The dashed line marks the boundary (hiatus) between the older and the younger crust generation of sample 43DS-1. The resolution in the profile amounts to 0.14 mm per measurement ($n = 169$). Both diagrams show that the Co and Ni concentrations are closely related to the Mn content. The three maximum peaks of Mn in the older crust part of the profile indicate birnessite clusters in the ore texture (see also Fig. 3.8a, b)

Cu is indifferent. Regarding the bulk composition data and the analytical data vs. water depth, Cu shows a weakly positive relationship to Fe and TiO_2 (see below). In contrast, in the LA-ICP-MS profile of Cu is positively related to Mn, Ni, and Zn. Cu exists in seawater as a hydrated divalent cation as well as a carbonate complex ($CuCO_3^0$); this is probably the reason for the dual nature of Cu vs. Mn or Fe. The respective enrichment factor for Cu amounts to 7.5×10^6 (Halbach and Marbler 2009).

Ba concentrations reach 5122 ppm in the crusts (mean value of 1650 ppm; Table 3.2) and Sr has also relatively high contents with up to 1750 ppm and a mean value of 1320 ppm. Pb concentration averages 945 ppm and increases up to

2620 ppm (Table 3.2). Pb contents are variable and higher in the younger than in the older crust units (Table 3.3).

Some of these minor elements also differ in their contents comparing the older and the younger crust generations. The most obvious feature is the concentration of Co, which, for individual samples, can reach in the younger part more than double the value then in the older one. Mean contents of Co in the younger generation is 6900 ppm, and in the older generation 3930 ppm only (Table 3.3).

3.4.3.4 Trace Elements

Molybdenum and Tungsten

The two heavy metals Mo and W (Table 3.2) are also enriched in ferromanganese crusts and are of moderate economic importance. Both elements have as 6^+ cations a high ionic potential and exist in seawater dominantly as hydrated anion complexes. The contents of Mo reach up to 705 ppm in the Actlabs data set (Table 3.2), with a mean value of 431 ppm in bulk crust composition for the depth range 1000–4100 m. In some crust samples, the contents of Mo are slightly elevated in the older crust unit (Table 3.3), with values up to 635 ppm (SO 33 18DK, older generation). However, no general trend between the two crust generations is obvious in the analysed samples. Because of the high Mo content in seawater of 10^4 ng/kg (10 ppb; Nozaki 1997), the enrichment factor for Mo in crusts in relation to seawater amounts only to 5×10^4 (Halbach and Marbler 2009). Mo shows a clearly positive relationship in the Actlabs data set to Mn ($r = 0.67$), to Ni ($r = 0.83$), to W ($r = 0.79$), and to Te ($r = 0.64$). These data indicate that Mo belongs to the Mn-group of metals. A further geochemical feature is that Mo is inversely related to water depth ($r = -0.69$), which is typical for the Mn-group.

In the LA-ICP-MS profile, these relationships are more distinct. The relationship to Mn has a correlation coefficient of $r = 0.62$ (Fig. 3.22; $n = 169$). This positive correlation is valid for the older and younger crust. One remarkable feature in this Mn-Mo plot is that, after the non-growth hiatus, the concentration in the younger crust starts with higher Mo concentrations, which probably is related to the retreat of the expanded O_2-minimum zone. A very close relationship is shown to W indicated by a correlation coefficient of $r = 0.99$ (Fig. 3.22). To Fe, Mo is inversely related ($r = -0.55$, Fig. 3.22); the plot also shows that, with the beginning of the young crust growth after the hiatus, Fe starts with very low concentrations in the crust.

W contents in the crust samples reach 120 ppm with a mean value of 70 ppm (Table 3.2). The comparison between the older and younger generation data shows no general difference between the two crust units. W belongs to the Mn-group and the respective correlation coefficients are to Mn $r = 0.71$, to Ni $r = 0.78$, to Te $r = 0.64$, and to Mo $r = 0.79$ (Halbach and Marbler 2009).

In the LA-ICP-MS profile, W has a very similar behaviour as Mo. The correlation coefficient to Mn is $r = 0.91$ (Fig. 3.22). Also, W starts with high concentrations in the crust immediately after the non-growth hiatus. The reason for this similarity certainly is that both elements exist in seawater dominantly as highly soluble

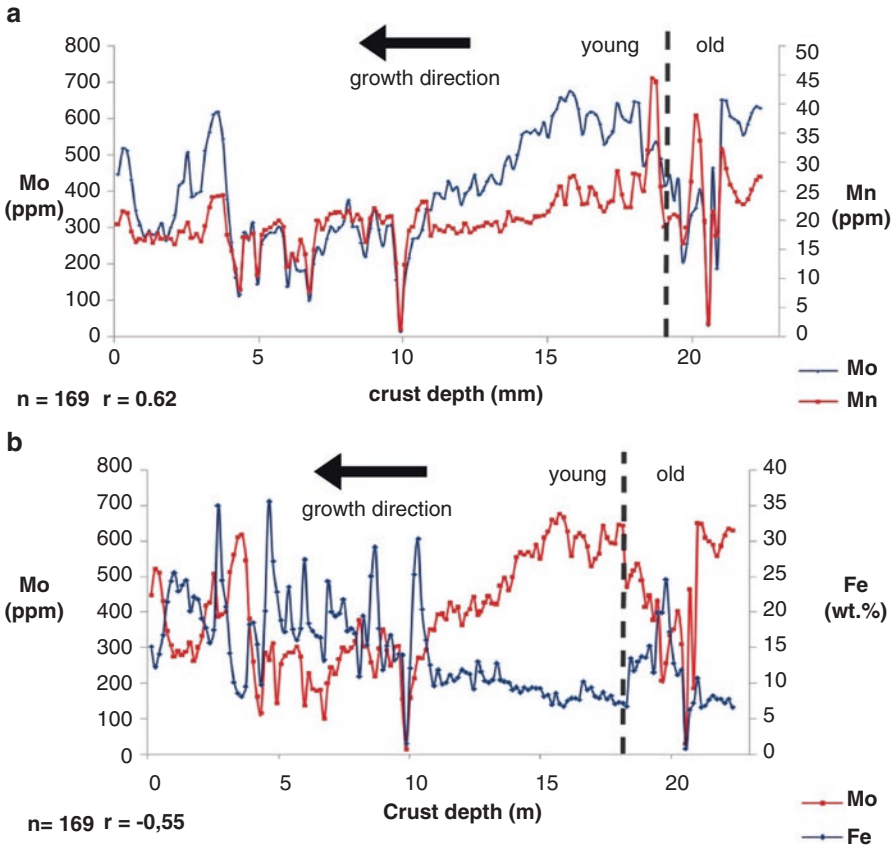

Fig. 3.22 Mo with Mn (**a**), Mo with Fe (**b**), W with Mn (**c**), and W with Mo (**d**) in a ferromanganese crust profile by LA-ICP-MS measurements (HRG). The dashed line marks the boundary between the older and the younger crust generation of sample 43DS-1. The resolution in the profile amounts to 0.14 mm between the measurement points

oxyanionic complexes (MoO_4^{2-}, WO_4^{2-}). According to the anionic character of both complexes, the elements should be adsorbed by the slightly negatively charged Fe-hydroxide particles. However, this does not fit with the data and observations (Halbach et al. 2008). In contrast, a coupled redox process of precipitation with Mn (Halbach and Marbler 2009) is proposed.

Platinum and Palladium

The precious metal Pt exists in the ferromanganese crusts as a trace element and is of economic interest. Compared to concentrations in the Earth's upper continental crust, the marine ferromanganese material contains about 100 times more Pt. The mean

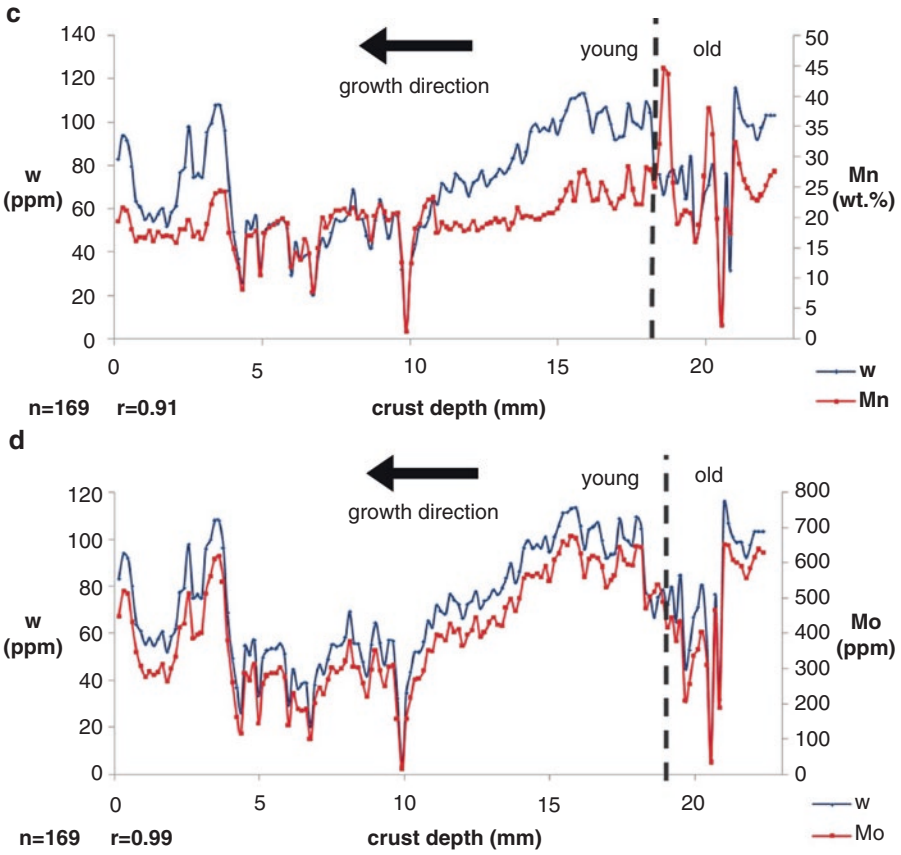

Fig. 3.22 (continued)

concentration of Pt in bulk ferromanganese crusts in the data set is 0.2 ppm; however, according to Halbach et al. (1989), the respective mean value amounts to about 0.5 ppm for shallower crust samples. Thus, 0.4 ppm is regarded as the mean Pt concentration of bulk crust samples in the water depth range of 1000–4100 m. Compared to the seawater concentration of 0.05 ng/kg (Nozaki 1997), the Pt enrichment factor in ferromanganese crusts is about 8×10^6. Regarding the concentration range of Pt in crusts, there are two important controlling parameters: (1) the influence of the water depth which indicates that crust samples from shallower water contain more Pt than deeper crust samples (Table 3.4, 2); the time factor also influences the Pt-content as far as the older crust units are more enriched in Pt than the younger one. In the samples analysed by the Jacobs University, Bremen (determined by stripping voltametric method), the younger crust samples have Pt-contents varying between 221 and 810 ppb, whereas in the older unit the values range from 481 to 1015 ppb (Table 3.4). The mean value of the older generation samples is 705 ppb;

Table 3.4 Contents of Co, Ni, and Pt and the Mn/Fe ratio in 14 analysed ferromanganese crust samples from the Central Pacific distinguishing between older and younger generation (Halbach and Marbler 2009)

Cruise	Sample	Type	Co (ppm)	Ni (ppm)	Pt (ppb)	Mn/Fe	Water depth
SO 33	65GTV-1	Old	8420	6590	**481**	2,12	1693 m
	54GTV-2	Young	11100	2130	**221**	1,82	1393 m
	57DK-1	Old	6450	4910	**730**	2,73	1209 m
	57DK-2	Young	9960	1870	**323**	2,15	1209 m
SO 66	43DS0-1	Old	3630	4640	**690**	2,87	2260 m
	43DS0-2	Young	6050	6240	**258**	1,81	2260 m
	5DSR-1	Old	3820	3960	**656**	2,35	2500 m
	5DSR-2	Young	4860	4720	**652**	2,16	2500 m
	64DSK-1	Old	6980	6100	**1015**	2,54	2680 m
	64DSK-3	Young	7040	6010	**810**	2,11	2680 m
SO 37	20DS-1	Old	2490	3270	**549**	2,55	1310 m
	20DS-3	Young	8770	4620	**405**	2,00	1310 m
	43DS-1	Old	2710	3640	**817**	1,95	1600 m
	43DS-3	Young	7600	3460	**360**	2,27	1600 m

the respective value for the younger generation is 433 ppb for a water depth range from about 1200 to 2700 m. Therefore, Pt has a clear enrichment in the older generation of two to three times compared to the younger one (Table 3.4 and Fig. 3.24). This geochemical feature was already described and evidenced by Halbach et al. (1989) in crust samples from the Central Pacific (Table 3.5).

In addition to the Pt bulk concentrations of older and younger crust samples, Halbach et al. (1989) investigated the distribution of Pt and Pd through a complete ferromanganese crust profile (Table 3.6). The results agree well with the postulated trends mentioned before. They also show that the Pd contents are distinctly lower than the Pt values and do not differ between the older and younger generations (mean value: 16 ppb; Table 3.6). With regard to the Pt/Pd ratio, the two growth generations show significant differences: the Pt/Pd ratio of the older crust generation (41.6) is on an average about twice as high as the ratio of the younger generation (22.6). This result is controlled by the higher Pt values of the older crust layer (Table 3.6). The high Pt/Pd ratios in ferromanganese crusts compared to seawater (Pt/Pd ratio ~ 1; Halbach and Marbler 2009) represent a significant "positive Pt anomaly" caused by chemical fractionation of Pt from Pd.

An additional specimen taken from the upper part of another older crust sample even yielded a Pt content of 1100 ppb (Halbach et al. 1989), which indicates that within the older unit highest Pt concentrations can be found in the upper 15–20 mm.

Vonderhaar et al. (2000) measured a stratigraphic profile (Fig. 3.23) of Pt and other element concentrations such as P_2O_5, CaO, MnO, and Fe_2O_3 in a ferromanganese crust (Hawaiian Archipelago, Schumann seamount) by using the LA-ICP-MS technique. The profile shows a younger generation sample down to 27 mm depth. This point is marked by an arrow, respectively a hiatus. The younger layer has Pt values

Table 3.5 Contents of Co, Ni, and Pt and Mn/Fe ratio of ferromanganese crust samples from the Central Pacific (Halbach et al. 1989)

Cruise	Sample	Gen.	W.d. (m)	Co (%)	Ni (%)	Pt (ppb)	Mn/Fe
SO 18	30 DK2	Young	3780	0.38	0.51	**140**	1.57
	31DK3	Young	2100	1.13	0.56	**280**	2.13
	32DK3	Young	1120	1.18	0.71	**330**	2.54
	111DK5	Young	1240	0.84	0.46	**270**	1.96
	43DK4	Young	3350	0.63	0.53	**280**	1.63
	76DK3	Young	1190	1.38	0.60	**300**	1.86
	58DK3	Old	1510	0.71	0.56	**280**	2.76
	76DK2	Old	1190	0.50	0.62	**840**	2.73
	31DK4	Old	2100	0.53	0.38	**250**	2.09
	32DK4	Old	1120	0.79	0.78	**880**	3.46
	111DK4	Old	1240	0.85	0.82	**780**	3.37
SO 33	48DK4	Young	1350	1.32	0.68	**370**	2.06
	48DK4	Old	1350	0.67	0.63	**350**	2.16
	49DK3	Young	1320	1.17	0.78	**490**	2.85
	49DK3	Old	1320	0.70	0.77	**1020**	2.72
	56DK2	Old	1390	0.70	0.92	**540**	3.92
	56DK8	Young	1390	1.24	0.65	**720**	2.10
	56DK8	Old	1390	0.87	0.86	**880**	2.95
	58DK1	Young	1330	1.04	0.56	**530**	1.81
	58DK1	Old	1330	0.53	0.72	**950**	2.60
	62DK1	Young	1630	1.28	0.68	**620**	2.19
	62DK1	Old	1630	0.57	0.68	**720**	2.18
	69DK1	Young	1500	1.07	0.44	**320**	1.43
	69DK2	Old	1500	0.41	0.79	**400**	2.78
	69DK2	Young	1500	1.01	0.39	**380**	1.32
	69DK2	Old	1500	0.58	0.74	**750**	2.84
	72DK2	Young	1550	1.06	0.41	**590**	1.32
	72DK2	Old	1550	0.72	0.75	**800**	1.64
SO 37	43DS6	Young	1600	1.13	0.69	**300**	2.04
	43DS6	Old	1600	0.66	0.83	**450**	2.58
	47DS2	Young	1490	1.29	0.76	**310**	2.20
	47DS2	Old	1490	0.73	0.97	**410**	3.22
	47DS5	Young	1490	1.03	0.76	**460**	2.18
	47DS5	Old	1490	0.60	0.86	**450**	2.80

The mean values for Pt, Ni, and Co of the younger generation amounts to 393.5 ppb ± 151.8 Pt; 0.60% ± 0.13 Ni; 1.07% ± 0.25 Co; the respective values for the older generation are 632.4 ppb ± 252.1 Pt; 0.75% ± 0.14 Ni; 0.65% ± 0.13 Co. Considering the depth range less than 2000 m, the following concentrations were obtained: younger generation—427.86 ppb ± 142.03 Pt, 0.61% ± 0.14 Ni, 1,15% ± 0.15 Co; older generation—656.25 ppb ± 239.66 Pt, 0.77% ± 0.11 Ni, 0.66% ± 0.13 Co. Ni and Co were determined by AAS, Pt by using fire-assay technique followed by flameless atomic adsorbtion

Table 3.6 Analytical data of fine-grained drilling samples obtained from one ferromanganese crust profile

Depth* (mm)	Pt (ppb)	Pd (ppb)	Pt/Pd ratio
Younger crust generation			
4	310	15	20.7
8	401	17	23.6
12	435	20	21.8
16	417	14	29.8
20	374	12	31.2
24	348	15	23.2
29	308	20	15.4
33	290	15	19.3
Mean	360	16	23.1
Standard deviation	±55	±2.8	±5.2
% deviation	15.2	17.7	22.6
Older crust generation			
38	469	11	42.6
42	651	12	54.3
46	717	25	28.7
50	716	17	42.1
55	611	14	43.6
60	650	16	40.6
38	750	19	39.5
Mean	652	16	41.6
Standard deviation	+94	+4.8	+7.5
% deviation	14.4	29.2	18.0

*The profile starts at the surface of the crust and continues down to the substrate rock (Halbach et al. 1989)

of 100–550 ppb and is not impregnated by CFA. The older generation, impregnated by CFA, starts at 27 mm in the crust profile. Between the older and younger generation, a non-growth period of about 27 Ma duration exists (Vonderhaar et al. 2000). During this long-lasting hiatus, the older crust generation was subject to diagenetic changes due to the influence of O_2-depleted seawater of an expanded O_2-minimum zone or of pore water because of temporary sediment cover (see above). This water entered into the pore spaces of the older crust unit. The LA-ICP-MS results indicate that in the first 2 cm of the older unit (marked in Fig. 3.23 as dark-shaded area), a remarkable Pt enrichment has taken place up to concentrations of 1.8 ppm. This specific increase in Pt concentration probably took place during the hiatus as post-depositional enrichment along redox fronts associated with carbonate-fluorapatite (CFA) deposition. However, the maximum of apatite is located just a little bit underneath the maximum of Pt in the respective plot. The lower part of the older unit shows less CFA impregnation than the upper part. According to polished section images (Fig. 3.8a, b), there was also dissolution and redeposition of ferromanganese

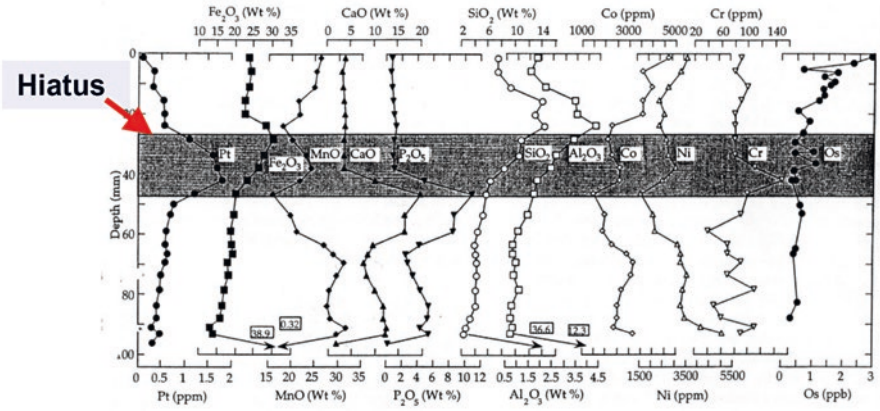

Fig. 3.23 (Vonderhaar et al. 2000) Pt and other element concentrations in a ferromanganese crust profile by LA-ICP-MS measurements (High Resolution Geochemistry: HRG). The *dark area* shows the layer with highest concentrations of Pt in the crust, which also represents the upper part of the older generation unit. The CFA-rich horizon is just underneath the layer with the highest Pt concentrations

material during the time of CFA precipitation. The local Pt enrichment in this layer could be explained by a short-way transport under diagenetic conditions and Pt reprecipitation combined with the birnessite formation.

The high-resolution geochemical (HRG) investigations (0.14 mm per measurement) by LA-ICP-MS in a profile from the younger to the upper part of the older generation in crust sample 43DS-1 show a highly positive correlation between Pt and Mn (Fig. 3.24a; $r = 0.82$) and also a positive correlation between Pt and Mo (Fig. 3.24b; $r = 0.62$). The respective correlation of Pt to Fe is negative (Fig. 3.24c; $r = -0.39$). A strong selective increase of Pt in the older crust generation is also visible and marked in the profile plot by circles (Fig. 3.24a). This suggests that these points of Pt enrichment in the concentration plots are identical with the Mn-rich pore space fillings seen in polished sections (Fig. 3.8a, b).

Based on these observations, it can be concluded that the local higher Pt contents in the upper layer of the older crust unit were obviously caused by post-depositional diagenetic processes, which have taken place in the pore spaces of the older crust unit during the hiatus and under the influence of suboxic to reducing O_2-depleted porewater conditions.

Stüben et al. (1999) carried out a comparison of Pt enrichment with Ce* (Ce-anomalies calculated by Ce/La ratio) and showed that there is no correlation between Pt/Pd- and Ce/La-ratios. This indicates that the Pt bonding mechanism to the Fe-Mn colloids and crust surfaces is not a process of direct oxidative enrichment (i.e. oxidative scavenging), such as it is for Ce and Co. One assumption is that Pt might be fixed as Pt^0 in the ferromanganese crust (Halbach and Marbler 2009).

Two sources may be responsible for the Pt concentration in the ferromanganese crusts: seawater and cosmic spherules. Only very rarely, cosmic spherules were

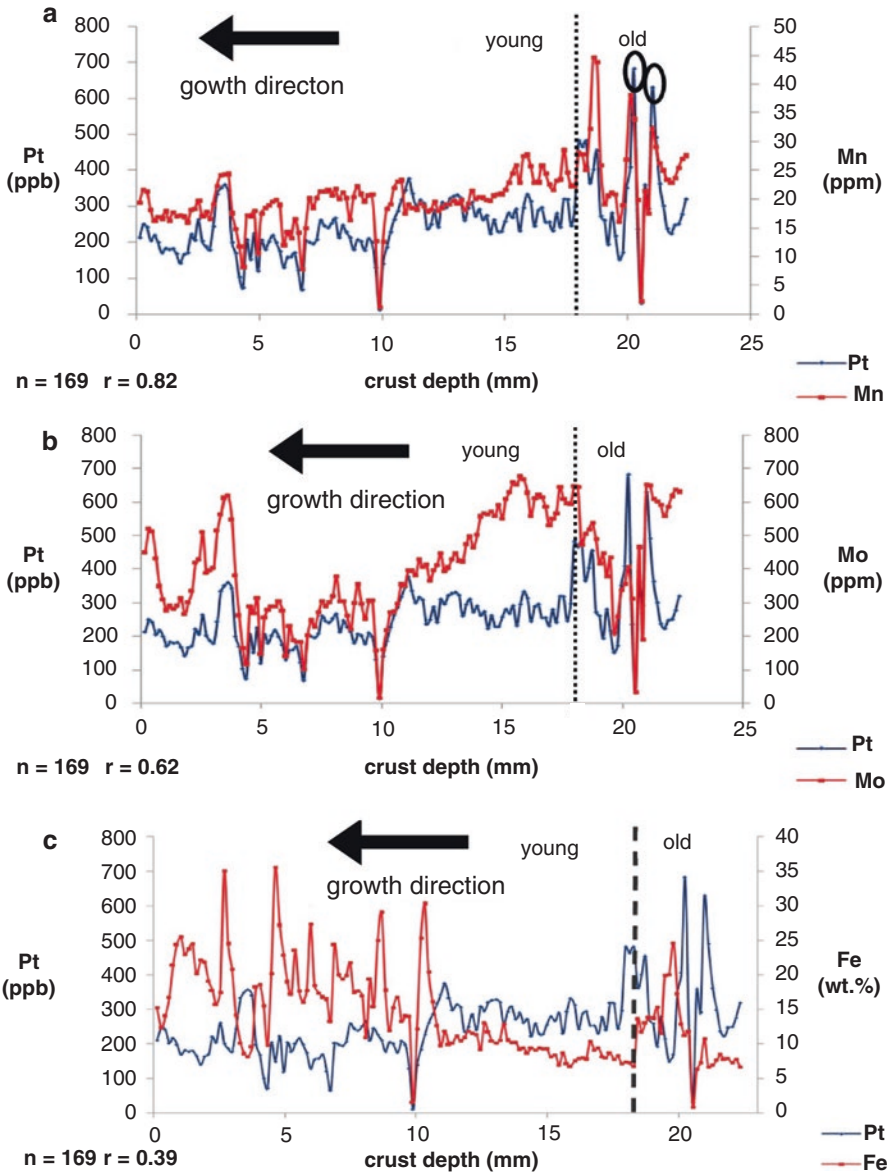

Fig. 3.24 Pt and Mn (**a**), Pt and Mo (**b**), and Pt and Fe (**c**) in a ferromanganese crust profile by LA-ICP-MS measurements (HRG). The dashed line marks the boundary (hiatus) between the older and the younger crust generation of sample 43DS-1. The resolution in the profile amounts to 0.14 mm between the measurement points ($n = 169$). The *two circles* in the Pt plot (**a**) of the older generation part mark the spot-like Pt enrichment in two Mn-rich pore space fillings

observed (Halbach et al. 1989). In general, Pt is two to ten times more enriched in iron meteorites compared to Pd (Wedepohl 1969). Inclusions of cosmic spherules also should lead to very high local enrichments of Pt and other PGEs; however, the ratios of Pt to other PG elements are in general non-chondritic (Vonderhaar et al. 2000). Also, the relatively continuous course of the Pt values, particularly in profiles of the younger generation, rules out a remarkable contribution of cosmic spherules to the Pt budget. Consequently, seawater should be the main Pt source. Thermodynamic calculations by Stüben et al. (1999) show that the main species of dissolved platinum under seawater conditions may be the platinum oxyhydroxide $Pt(OH)_2^0$. Therefore, the following model reaction may describe how the Pt was fixed to the diagenetically formed and reprecipitated Mn-mineral:

$$Pt(OH)^0_2 + Mn^{2+} \rightarrow MnO_2 + Pt^0 + 2H^+.$$

However, the geochemical observation that Pt is positively related to Mn, i.e. Pt is obviously hosted by oxidized MnO_2-bearing mineral phases, might also be explained by another chemical mechanism presented and published by Maeno et al. (2016). This model is based on the assumption that a Pt(II) mixed anion complex $[PtCl_{4-x}(OH)_x]^{2-}$ can be fixed to d-MnO_2 because the Pt(II) is oxidized to Pt(IV), and at the same time, some Mn^{4+} will be reduced to Mn^{2+}. Oxidized Pt(IV) is, in general, coordinated with six oxygen atoms. Thus, an isomorphous substitution between Pt(IV) and Mn(IV) may exist in the MnO_2-lattice. This process is described as a coupled oxidation-reduction scavenging reaction.

Niob and Gallium

Nb has a mean value of 40 ppm in ferromanganese crusts and reaches values of up to 56 ppm (Table 3.2), without any remarkable differences between the older and the young crust generations. Due to analytical problems in the detection of Nb in ocean waters, the concentration of Nb in seawater is not very accurately known. The determination of the Nb concentrations in seawater amounts to approximately 4 ng/kg. With this value, the enrichment of Nb in ferromanganese crusts versus seawater is 10×10^6 (Halbach and Marbler 2009). In the correlation matrix of the LA-ICP-MS profile of sample SO 37 43 DS4 (water depth 1600 m), Nb shows a clearly positive relationship to some elements which belong to the Fe-group (see below): Nb-Al $r = 0.66$, Nb-Si $r = 0.71$, Nb-Ti $r = 0.73$, Nb-Fe $r = 0.80$. However, these positive correlations are not confirmed with the same level of confidence by the interelement considerations of the actlabs data. Nevertheless, a positive relation between the Fe-group elements and Nb may exist. However, this statement needs further investigations. Nb is not considered to be of economic importance, since the concentrations are too low.

Ga is also a low-concentrated trace metal in ferromanganese crusts and has a mean value of only 18 ppm (Table 3.2). It reaches maximum values of up to 40 ppm with slightly higher contents in the older crust unit. The determination of Ga in seawater amounts to approximately 1.2 ng/kg. With this value, an enrichment factor

of 2.3 × 10^7Ga in ferromanganese crusts versus seawater can be calculated. Ga is negatively correlated to Fe ($r = -0.68$) and shows a weakly positive correlation with Mn and Ni (Ga-Mn $r = 0.43$, Ga-Ni $r = 0.64$); however, with other elements of the Mn-group, the respective correlation is less significant. Also, for Ga the clarification of the interelement relationships needs further investigations. Ga is not considered to be of economic importance, since the concentrations are too low.

Tellurium

Te is one of the economically interesting trace metals in ferromanganese crusts Hein et al. (2003). Its concentrations in crusts from different oceanic regions reach over 200 ppm (e.g. for the Atlantic Ocean; Hein et al. 2003). In Pacific crusts, Te varies from a few ppm up to nearly 200 ppm. In the analysed crust samples, the contents of Te range from 8 to 61 ppm (Table 3.2); the older crust generation samples show in general somewhat higher mean concentrations than the younger ones (Table 3.3; older crust generation: 39 ppm, younger crust generation 32 ppm). The enrichment of Te in relation to the seawater concentration (0.07 ng/kg) amounts to about 5 × 10^8 (Halbach and Marbler 2009).

Thermodynamic calculations indicate that dissolved Te predominantly occurs as the Te(VI) species $TeO(OH)_5^-$ and, to a lesser extent, as the Te(IV) species $TeO_2(OH)_2^{2-}$ under seawater conditions; according to Hein et al. (2003), the Te(IV) is less abundant in seawater by factors of 2–3.5 than Te(VI). The anionic speciation of Te in seawater and charge balance considerations suggest that Te should be scavenged by colloidal FeOOH particles which, however, are only slightly positively charged in seawater. In a model proposed by Hein et al. (2003), an oxidative enrichment of Te by preferential outer sphere adsorbtion of Te(IV) on FeOOH and subsequent surface oxidation to Te(VI) should explain the species distribution in seawater and the remarkable enrichment of Te in ferromanganese crusts. A thermodynamical consideration by chemical reaction modelling was not carried out for this assumption. Also, the surface particle reactivity of colloidal FeOOH is fairly weak. A similar adsorbtion process of oxidative scavenging is assumed for Co and Ce at the surfaces of colloidal positively charged MnO_2 particles in crusts. But in that case, it has to be pointed out that the Mn oxide has strong particle reactivity and, therefore, is highly capable for the adsorption of hydrated cations.

Schirmer et al. (2008) investigated the variability of Te concentrations of different crust layers of ferromanganese crust samples and drilled small subsamples in profiles from the surface (youngest layer) down to the layer just above the substrate rock (oldest layer) of two crust samples. With the increasing phosphatization in the old crust layer (sample SO 66 80 DSK-3; Fig. 3.25), a weak trend of increasing Te contents could be observed. At about 3 cm down into the crust, the phosphatization starts. Within the increasing phosphatization, the Te contents increase up to 75 ppm. With a correlation coefficient of $r = 0.6$ for sample 80 DSK-3, there is a strong positive correlation of Te with Mn, suggesting that the enrichment of Te may be coupled to the Mn-phase. Distinct positive correlations of Te are also observed

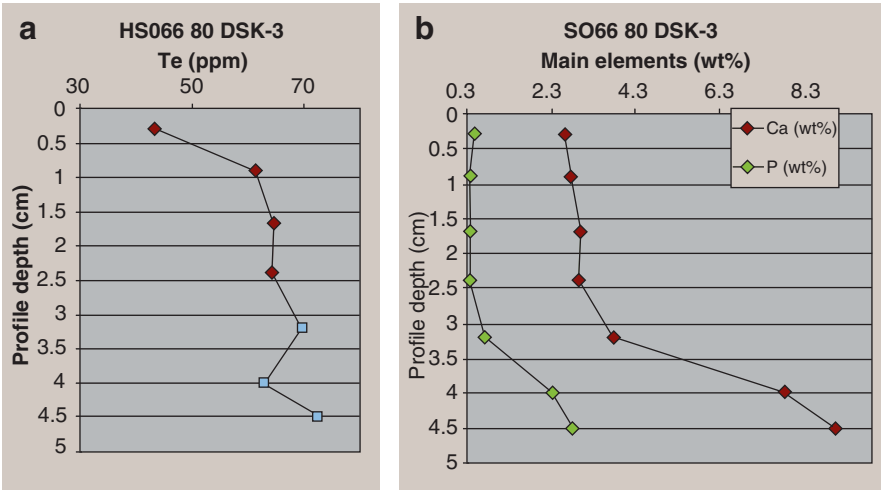

Fig. 3.25 (**a**) Te, (**b**) Ca, and P profiles for crust sample SO66 80 DSK-3, Central Pacific, water depth: 1450 m. The phosphatized old crust unit starts at 3 cm from the crust surface (From: Schirmer et al. 2008)

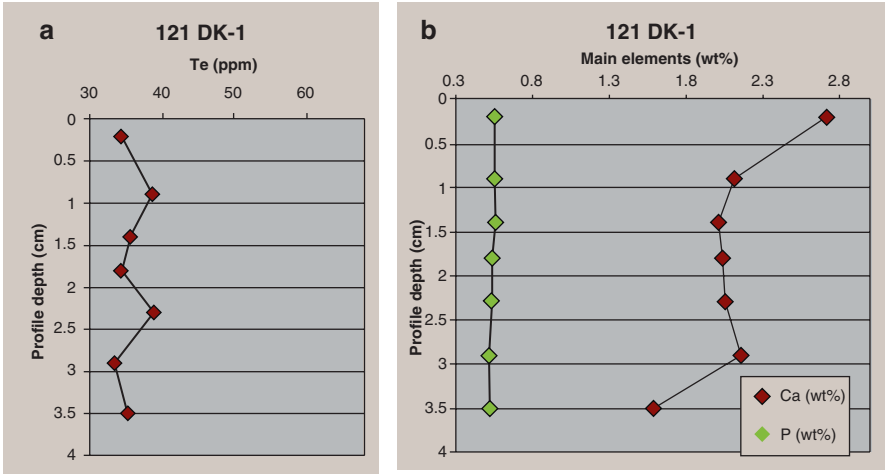

Fig. 3.26 (**a**) Te, (**b**) Ca, and P profiles for crust sample 121 DK-1, NE-Atlantic, water depth 2000 m, with no visibly phosphatized crust unit (From: Schirmer et al. 2008)

with the elements Mo (r = 0.79), Ni (r = 0.77), Zn (r = 0.86), and Ce (r = 0.91; Schirmer et al. 2008).

A second sample from the North East Atlantic (121 DK-1, water depth 2000 m; Schirmer et al. 2008) was studied. Due to a more or less even distribution of Te in the non-phosphatized crust sample, no increase down into the crust was observed for Te (Fig. 3.26). The Te concentrations are between 30 and 40 ppm, and the content of P is

more or less constant. Comparing the results, one important observation can be made: the sample SO 66 80 DSK-3 shows a phosphatized older crust unit where the Te concentrations have enhanced values; the non-phosphatized sample 121 DK-1 has relatively constantly low Te concentrations which approximately correspond to the Te content in the upper younger crust layer of sample SO 66 80 DSK-3.

Halbach and Marbler (2009) have studied with the high resolution ICP-MS method the internal microchemistry of several main, minor, and trace elements in a profile of crust sample SO 37 43 DS4, which is one sample of the crust data set. Although the method is only semiquantitative, the interelement relationships can be correctly evaluated. In Fig. 3.27, the three element pairs Te-Mn, Te-Mo, and Te-Fe were selected. The layered structure of the younger and older generation is reflected by the rhythmic variations of the element plots. Figure 3.27a shows that Te is weakly positively related to Mn and the respective correlation coefficient only is $r = 0.42$. The Fig. 3.27b indicates that also Te correlates positively with Mo at a higher level of significance ($r = 0.66$). Also, the interelement relationship of Te vs. Fe was checked and a weak negative interrelationship ($r = -0.21$) was obtained. These results show that Te shows a positive correlation to Mn and also to Mo. Also important is the information that Te is weakly negatively related to Fe, which does not fit with the model that Te is enriched in the crust by a surface adsorbtion onto the colloidal FeOOH particles.

From the data set of 32 samples (Table 3.2), 12 samples were selected to consider the water depth dependence of the metal composition (see below); Te was also regarded. The depth range of the samples varies from 1217 to 4112 m; within this range, Te shows a clear decrease with increasing water depth. For example, the samples above 2000 m water depth have a mean value of 47 ppm Te, whereas the samples underneath 2000 m show only a mean concentration of 22 ppm Te. The correlation coefficient of Te vs. water depth amounts to $r = -0.79$, which is similar to other negative correlation coefficients like for Mn, Ni, Mo, Co, and W (Table 3.9). In that case, Te also belongs to the manganese group of metals (Type A group, Chapter 3.4.3.5). The respective Fe value in this consideration is $r = 0.78$, i.e. Fe is positively related to the water depth: deeper crust samples contain considerably more Fe than the shallow ones. These geostatistical results contradict also the assumption that Te is fixed to the FeOOH fraction in the ferromanganese material. The positive correlation between the anionic Te complex in seawater and the manganese-phase cannot be explained by an outer sphere adsorbtion, possibly also a coupled redox process with subsequent precipitation can be applied to explain the observed correlation. For economic considerations, it can be stated that crust samples from shallower water are also more enriched with regard to the trace metal Te (Halbach and Marbler 2009).

Rare Earth Elements (REE)

The rare earth elements (REEs) are transition metals and often considered as the 15 lanthanides plus scandium and yttrium; in this chapter, preferentially the lanthanides are regarded. Most of the REEs are not as uncommon in nature as the name implies.

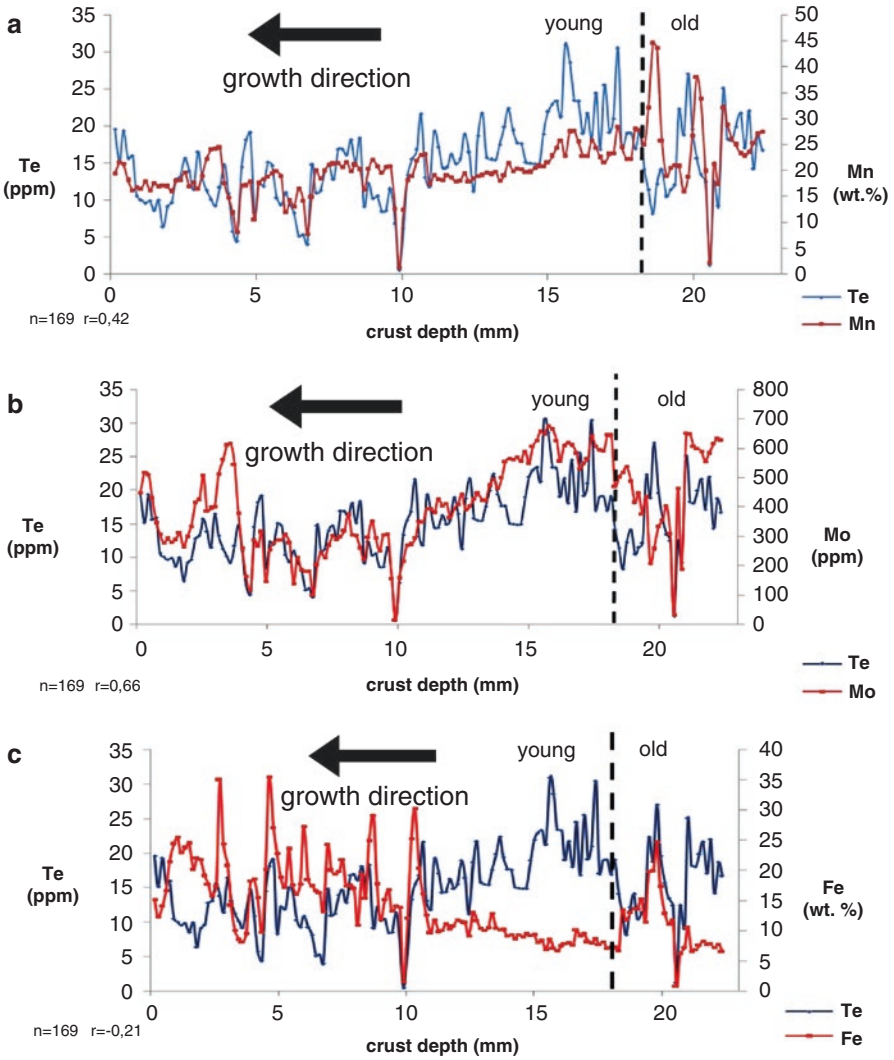

Fig. 3.27 (**a–c**) La-ICP-MS crust profiles of sample SO 37 43 DS4, Central Pacific, water depth 1600 m. The concentration plots (23 mm profile length) vs. crust depth is based on 169 measurements, i.e. the high resolution amounts to 0.14 mm between the measurement points. The main part of the profile comprises the young crust generation; the first part of the old crust generation is also covered by the plot. The element pairs considered are also evaluated by their correlation coefficients

During differentiation of the magmatic rocks, the REEs are successively accumulated in the upper Earth's crust rocks (Table 3.7). Overall, weathering and erosion delivers the REEs to the oceans; but only a few percent of the total REE amount entering the oceans are dissolved. The bulk of the REEs in eroded material are contained in the clay fraction. The absolute and relative concentrations of the REEs in ocean

Table 3.7 Names and chemical symbols of REEs ordered in ascending atomic number; in addition, the absolute abundances in continental crust and chondrite are given

	Element	Symbol	Atomic number	Upper crust abundance [ppm]	Chondrite abundance [ppm]
	Scandium	Sc	21	22	9
	Yttrium	Y	39	22	Na
LREEs	**Lanthanum**	La	57	30	0.34
	Cerium	Ce	58	**64**	0.91
	Praseodymium	Pr	59	7.1	0.121
	Neodymium	Nd	60	26	0.64
	Promethium	Pm	61	Na	Na
	Samarium	Sm	62	4.5	0.195
	Europium	Eu	63	0.88	0.073
HREEs	**Gadolinium**	Gd	64	3.8	0.26
	Terbium	Tb	65	0.64	0.047
	Dysprosium	Dy	66	3.5	0.3
	Holmium	Ho	67	0.8	0.078
	Erbium	Er	68	2.3	0.2
	Thulium	Tm	69	0.33	0.032
	Ytterbium	Yb	70	2.2	0.22
	Lutetium	Lu	71	0.32	0.034
	ΣREE			**146.37**	**3.45**

Na not available. The Table demonstrates the relative enrichment of REEs in the upper crust rocks compared to primitive rocks (Taylor 1964)

waters reflect their input from rivers, eolian transport, and hydrothermal venting as well as the influence of sedimentation and precipitation. Due to their high particle surface reactivity, the REEs have short marine residence times of only about 400 years. The REE concentrations in the oceans display a non-random vertical distribution; concentrations of all REEs increase towards the seafloor (Fig. 3.28).

In seawater, REEs occur mainly as carbonate complexes (Ohta and Kawabe 2000); in the most cases, light rare earth elements (LREEs) form monocarbonate complexes ($REECO_3^+(aq)$) and heavy rare earth elements (HREEs) form bicarbonate complexes ($REE(CO3)_2^-$). The fact that REEs in seawater form cationic and anionic carbonate complexes is used by the two main hydrogenetic constituents hydrous δ-MnO_2 and Fe-oxyhydroxide to fractionate the group of REEs by surface adsorption: the Mn-phase prefers to collect LREE–complexes, the Fe-phase (in contrast) HREE–complexes. Because of the transitional configuration of the filling of the 4^+ lanthanide electron shell, this fractionation is not complete.

The analyzed REEs (lanthanides) are: Ce, La, Pr, Nd, Sm, Eu, Gd, Tb, Dy, Ho, Er, Tm, Yb, and Lu. In the Actlabs data set (Table 3.2), these elements were determined for bulk crust composition. The mean values as well as their minimum and maximum values and standard deviations are shown in Table 3.8. The total sum of the REEs in the Central Pacific data set amounts to a mean value of 1628 ppm; the

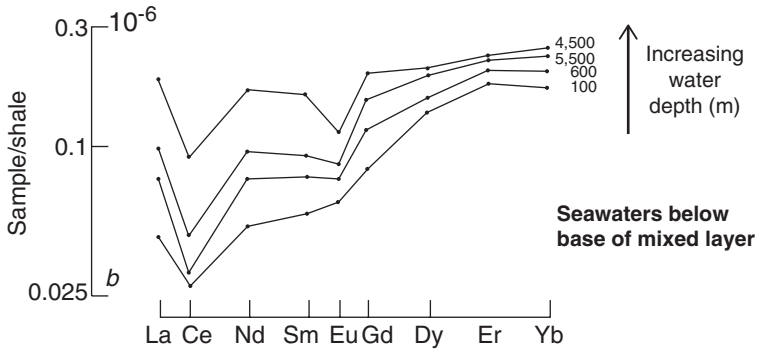

Fig. 3.28 Typical REE patterns (normalized to shale composition, PAAS; McLennon 2001) from seawater below the mixed layer, the considered depth range is 100–4500 m; example North Atlantic Ocean. The distribution graphs show the typical enrichment of REEs with increasing water depth (Elderfield and Greaves 1982). A pronounced negative Cerium anomaly exists in all water depths; i.e. Cerium is distinctly depleted in comparison to shale composition, the heavy REEs are slightly enriched in seawater. This enrichment increases with water depth

Table 3.8 Mean REE concentrations in bulk crust composition (Actlabs data; $n = 18$; Central Pacific samples; Halbach and Marbler 2009)

Elements [ppm]	Mean	Std. dev.	Min.	Max.
La	228	66	100	335
Ce	996	272	456	1630
Pr	42	19	17	73
Nd	163	75	64	290
Sm	38	18	15	69
Eu	10	5	4	17
Gd	38	18	17	69
Tb	6.5	2.7	2.8	11.4
Dy	40	14	18	65
Ho	9	2	4	13
Er	26	6	12	36
Tm	3.8	0.8	1.8	5.2
Yb	24	5	11	31
Lu	3.7	0.7	1.7	4.7
Total sum	**1628**		**724**	**2649**

maximum value even reaches up to 2649 ppm (Table 3.8). The average amount is fairly high compared to the average REE content in the CCZ manganese nodules (about 670 ppm; Halbach and Jahn 2016) and corresponds to an increase of about 240%. The comparative data set of the younger and older crust composition (Table 3.3) indicates that the older crust samples contain 10–20% more REEs than the younger one. The explanation for this chemical trend will be the fact that the older crust generations contain in varying portions CFA (see above), which also carries REEs in its lattice.

The relative distribution of the individual REE mean values of Table 3.8 normalized to shale composition is represented in Fig. 3.29. The curve indicates a remarkably

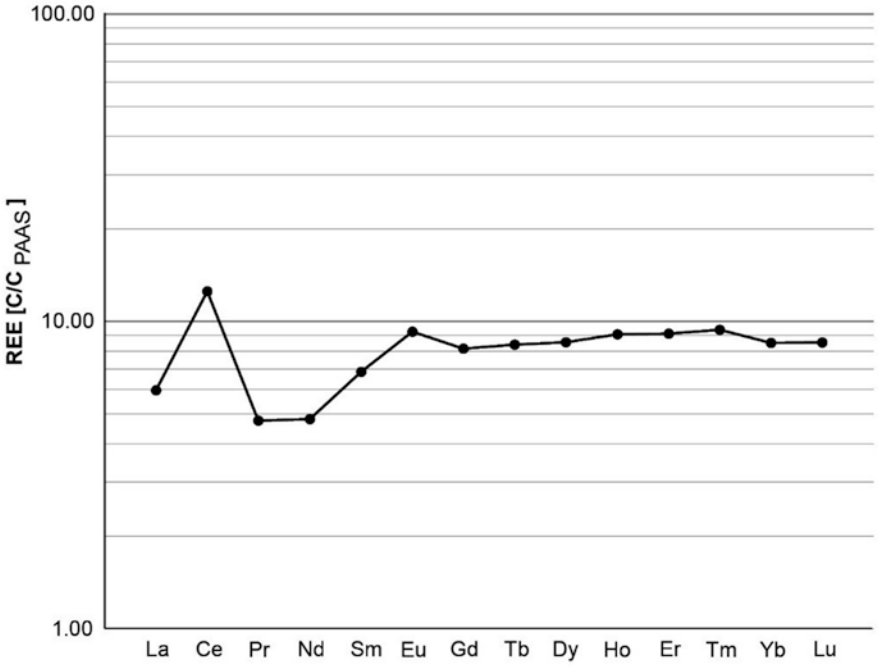

Fig. 3.29 Relative distribution of the REEs (values after Table 3.8) normalized to shale composition (PAAS; McLennon 2001)

positive Ce anomaly, and in relation to the shale composition, an enrichment of the elements from Eu to Lu. Cerium dominates in the 3+ valence state in the suspended load of rivers, which eventually reaches the ocean. There, the absorption reactions on surfaces of the ferromanganese particles control the further fractionation of the REEs (Byrne and Kim 1990). As a result, Ce is oxidized to the highly insoluble 4+ valence state after the absorption which is indicated by the significantly positive Ce anomaly. On the other side, this results in a strong Ce depletion in seawater composition (Fig. 3.28). Nevertheless, the 3+ valence REEs also exhibit interelement fractionation, owing to their formation of complexes with the CO_3^{2-} anion complex. In seawater, the complex species exhibit an increase in their stability with increasing atomic number (Piper and Bau 2013).

The comparative distribution patterns of average ΣREE compositions of ferromanganese crust and nodule groups from several marine regions show interesting differences. Very high REE concentrations are found in Atlantic ferromanganese crusts (ΣREE: 2382 ppm, Halbach et al. 2013). Recent investigations (Marino et al. 2016) of samples from the cretaceous seamounts in the Southern Canary Island Seamount Province (NE Central Atlantic) show that the ΣREEY contents reach average values of 2800 ppm. These crusts are characterized by a high average Fe content of 23.5%. This enrichment in Fe is explained by the influence of Sahara eolian dust and submarine volcanic plumes (Marino et al. 2016). The average content of ΣREEs in Indian Ocean ferromanganese crusts (2436 ppm, Halbach et al. 2013)

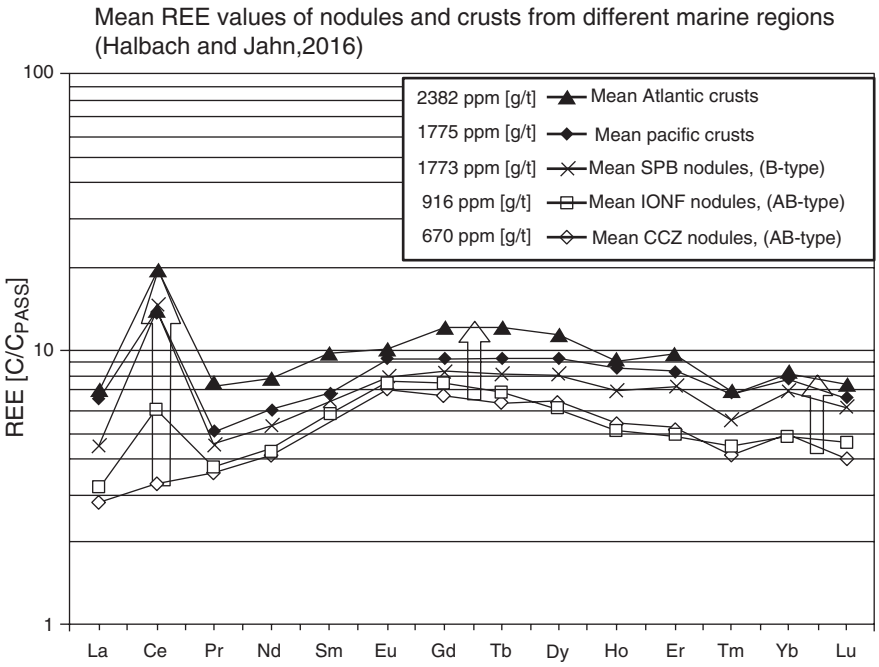

Fig. 3.30 Shale-normalized (PAAS; McLennon 2001) average REE patterns of three nodule and two crust groups from different marine regions. The Atlantic and Indian Ocean crusts are richest in REE and show the largest positive Ce anomaly; the CCZ nodules are relatively poor in REEs and show no distinct Ce anomaly. With increasing hydrogenetic influence, the positive Ce anomaly as well as the concentration in MREE (Eu to Dy) rise. *SPB* South Penrhyn Basin, *IONF* Indian Ocean Nodule Field, *CCZ* Clarion-Clipperton Fracture Zone of the Pacific Ocean. The CCZ nodules only have a very weak positive Ce anomaly. The SPB nodules, which are of hydrogenetic origin, are very similar to the mean composition of the Pacific crusts

is in the same range as the Atlantic ferromanganese crusts. The respective normalized distribution curve is very similar to the Atlantic Ocean one; the curve was, therefore, not included in Fig. 3.30. Both crust groups also have the highest positive Ce anomaly and show the largest enrichment in the group of the MREEs (Eu to Dy). The comparison with the nodule groups indicates the low REE concentrations in the CCZ-nodules and the higher contents in nodules from the South Penrhyn Basin, which are of hydrogenetic origin. The Indian Ocean nodules are somewhat richer in REEs than the CCZ nodules (Halbach et al. 2013).

3.4.3.5 Metal Composition Versus Water Depth

The fact that metal concentrations in ferromanganese crusts vary with water depth was already observed in former publications (Halbach and Manheim 1984; Halbach 1986). In particular, the two metals Co and Ni, which are of high economic importance with regard to the metal value of the crusts, show a very significant

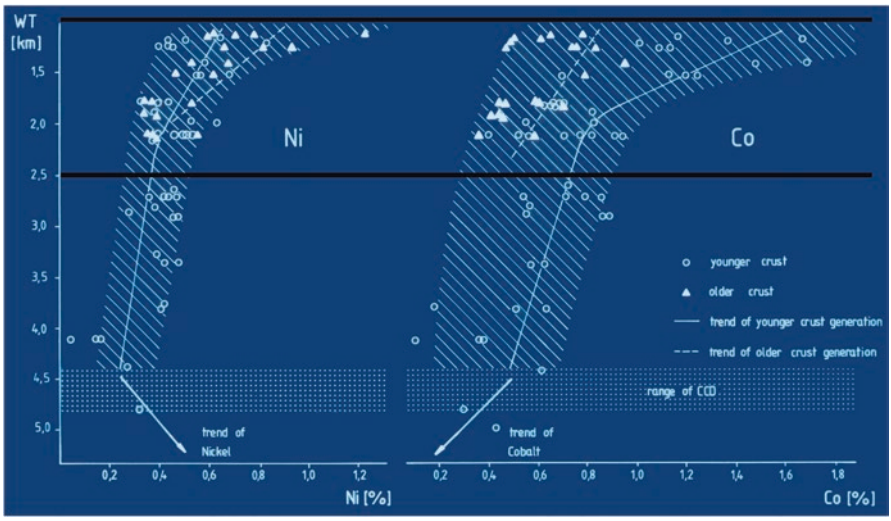

Fig. 3.31 Co and Ni concentrations vs. water depth (Halbach and Manheim 1984). Both metals decrease with increasing water depth. The diagram also shows that the gradient of decrease is steeper in the upper part of the water column. According to the depth-related concentrations, the depth from 1000 to 2500 m was defined as the high-quality and prime depth range of crust recovery. Samples data originate from the Midpac-Cruises (Central Pacific)

variation with the water depth: both metals significantly decrease with increasing water depth and both metals belong to the group of Mn-controlled elements (see below). Therefore, the high quality and prime depth range for a potential recovery of crusts was defined as 1000–2500 m (Fig. 3.31).

The decrease in Co concentrations in the younger crust layer is steeper in the upper part than in the lower part of the water column. Thus, the trends of decreasing Co and Ni concentrations with increasing water depth are more distinct in the upper part. However, also other elements show clear dependencies in concentration on the water depth (Table 3.9). For this consideration, only younger crust samples were used, because the older crust samples are diagenetically overprinted and contain strongly varying apatite contents which disturb the primary geochemical signals of immediate hydrogenetic precipitation and dilute especially the Mn-controlled metal group elements. Another observation is that, in water depths of more than about 3300 m, the older generation crust layers are not phosphatized (see chapter 3.4.2).

Considering the results represented in Table 3.9, it can be distinguished between a Mn-controlled (type A) and a Fe-controlled (type B) element group. The following elements belong to the Mn-group (A): Mn, Ni, Mo, W, Te, and Co; the Fe-group (B) consists of Fe, Ti, Cu, and Nd.

The decrease and/or increase of the studied metals in the crust depends on the release and supply of Fe-oxyhydroxide, which in turn depends on the calcite and aragonite dissolution rate in the water column (Halbach and Puteanus 1984). Thus, the depths of the CCD (Calcite Compensation Depth) and the ACD

Table 3.9 Linear correlation coefficients (r) of the metal concentrations of 12 younger generation crust samples (Central Pacific, Halbach and Marbler 2009) used for the consideration of the depth-dependant composition

	water depth	Al_2O_3	Fe_2O_3	MnO	CaO	TiO_2	Ni	Cu	Ga	Nb	Mo	Nd	W	Te	Co
water depth	1														
Al_2O_3	0.58	1													
Fe_2O_3	0.78	0.26	1												
MnO	-0.76	-0.90	-0.62	1											
CaO	-0.24	0.41	-0.61	-0.10	1										
TiO_2	0.85	0.46	0.81	-0.71	-0.41	1									
Ni	-0.69	-0.56	-0.79	0.83	0.16	-0,73	1								
Cu	0.62	0.08	0.56	-0.29	-0.32	0,69	-0.28	1							
Ga	-0.21	-0.14	-0.56	0.41	0.39	-0.28	0.64	0.15	1						
Nb	0.17	0.27	-0.02	-0.16	0.22	0.26	-0.04	0.32	0.46	1					
Mo	-0.69	-0.74	-0.68	0.88	0.07	-0.60	0.76	-0.18	0.63	0.20	1				
Nd	0.77	0.32	0.82	-0.59	-0.37	0.84	-0.69	0.75	-0.14	0.15	-0.53	1			
W	-0.70	-0.72	-0.72	0.86	0.16	-0.61	0.75	-0.18	0.61	0.19	0.99	-0.56	1		
Te	-0.79	-0.35	-0.92	0.64	0.65	-0.77	0.70	-0.49	0.48	0.06	0.70	-0.80	0.77	1	
Co	-0.84	-0.50	-0.85	0.75	0.34	-0.82	0.68	-0.74	0.28	-0.24	0.66	-0.79	0.68	0.81	1

The type A Mn-group (red) metals have significantly negative, the type B Fe-group metals (blue) significantly positive coefficients, i.e. the Mn group elements decrease and the Fe group elements increase with water depth

(Aragonite Compensation Depth) have an important influence on this geochemical system. Since the depth of the CCD and ACD as well as the intensity of calcite and aragonite dissolution have clearly varied over the growth period of the ore crusts, the detailed circumstances are difficult to reconstruct. Up to now, there is no convincing explanation for the above-mentioned "two-gradients-model". However, because of the higher solubility of aragonite in seawater, the ACD is significantly above the CCD; thus, in shallower water it may be suggested that both, the aragonite dissolution and the calcite dissolution rate, contribute to the budget of Fe-oxyhydroxide available for the hydrogenetic growth process of the crusts (see below).

The Mn-controlled group comprises metals which are related to the colloidal Mn-oxide particles either by outer or inner sphere adsorption or by co-precipitation. Since the main Mn source is the O_2-minimum zone, it can also be assumed that, with increasing water depth from this water layer, the Mn concentrations decrease; also an increase of released Fe-oxyhydroxide particles also may cause a dilution of the Mn-controlled chemical system. The Fe-oxyhydroxide has, in general, two water column sources: release because of enhanced dissolution of biogenetic calcareous tests down to the depth range of the CCD (Halbach and Puteanus 1984), and hydrothermal alteration of the oceanic crust; however, the latter contribution will influence particularly very deep-water crusts (Halbach et al. 2014). For the following considerations, with regard to the metal composition versus the water depth above the CCD, the Fe-oxyhydroxide (released by carbonate dissolution) with its related elements (B-group, see above) will play probably the dominant role.

To study these relationships also in younger crust samples from another Pacific area, 11 samples from the Manihiki Plateau were taken which show an increase in

water depth from 1220 to 5000 m (Halbach et al. 2009). The compositions of these samples are represented in Table 3.10. The elements Co, Ni, Mn, Mo, W, and Zn show a highly significant negative correlation of the concentration versus water depth and belong to the A-group metals. In contrast, the elements Ti, Ce, Nd, and Y correlate with Fe and indicate an increase of concentration with water depth.

Six elements of the data set presented in Table 3.10 were exemplarily plotted versus the water depth: Co, Ni, Fe_2O_3, MnO, Mo, and Nd (Fig. 3.32). The elements Co, Mo, and Ni as well as MnO represent the A–group, Fe_2O_3 and Nd the B–group. In all cases, the exponential regression curves have distinctly higher values of the coefficients of determination as the linear relationships. All four Mn-group members have coefficients of regression of $R^2 = 0.66–0.84$ for the linear regression; the quality of the exponential correlation is even better with coefficients of regression of $R^2 = 0.74$ to $R^2 = 0.89$. The plots of Fe_2O_3 and Nd, which both show the same trend of increasing concentrations with water depth, also have very good coefficients of correlation. The linear correlations are $R^2 = 0.74–0.79$, and the exponential correlations are $R^2 = 0.78–0.84$. Thus, in all the cases, the exponential curves represent a more probable statistical characterization of the considered interrelationship. Already in the data set described by Halbach and Manheim (1984; see Fig. 3.31), the observation that the element plots versus water depth for Ni and Co showed two gradients (a steeper one in shallower water) was made. The element plots of Fig. 3.32 reveal that in water depths above 2500 m the gradients of increase or decrease are somewhat steeper. One explanation for this observation could be that, in the hydrogenetic crusts, the effect of dilution of the chemical Mn-group system by the Fe-oxyhydroxide supply caused by dissolution of two carbonate systems (aragonite and calcite) is higher in shallower water than in deeper water. Underneath the ACD, i.e. in deeper water, only the calcite dissolution down to the CCD takes place and controls the Fe-oxyhydroxide supply of the deeper-water crust growth.

These described relationships show that the crust growth versus the water depth is controlled by two antagonistic chemical systems: the Mn- and the Fe-group system. Basically, the release of the Fe-oxyhydroxide particles, which increase with increasing water depth, shows two different gradients in dependence from varying carbonate dissolution rates. These are influenced in shallower water by aragonite and calcite dissolution, but in deeper water only by calcite dissolution. These relationships are obviously better described by the exponential regression. This water depth dependency of the crust composition elucidates that a representation of chemical average values always has to be accompanied by the corresponding water depth range.

3.4.3.6 Interelement Relationships

For interpretation, explanation, and presentation of the high diversity of the collected geochemical data, three methods of mathematical statistics were carried out:

(a) **Descriptive statistics** to summarize and to describe the collection of data by the calculation of the mean value, the median, the standard deviation as well as the minimum and maximum values from bulk samples.

Table 3.10 XRF—results (main, minor, and trace metals of dried substance) of younger generation crust samples from the Manihiki Plateau ordered according to increasing water depth (Halbach et al. 2009)

Sample	Water depth (m)	SiO_2 (%)	TiO_2 (%)	Al_2O_3 (%)	Fe (%)	Fe_2O_3 (%)	Mn (%)	MnO (%)	Ce (ppm)	Co (ppm)	Cu (ppm)	Mo (ppm)	Nd (ppm)	Ni (ppm)	W (ppm)	Zn (ppm)	Y (ppm)	Mn/Fe
MP 19	1220	1.30	1.09	0.71	7.26	10.39	22.59	29.18	500	9261	944	657	57	7522	114	801	47	3.11
MP 7	1560	2.03	1.23	0.65	7.30	10.45	22.54	29.12	750	8979	1103	794	93	7112	131	741	181	3.09
MP 16	1570	2.88	1.43	0.70	10.04	14.36	19.52	25.23	510	8543	713	401	129	4804	84	569	123	1.95
MP 12	2215	5.68	1.39	1.40	12.83	18.36	18.36	16.28	685	4951	1234	302	113	3522	64	546	154	1.27
MP 6	2600	4.76	1.16	0.92	11.70	16.74	17.82	23.02	378	5602	1108	356	162	4068	79	488	143	1.52
MP 9	3210	1.97	1.07	0.81	12.42	17.77	17.23	22.26	424	4974	954	284	198	3351	56	489	143	1.39
MP 2	3455	12.32	1.31	3.76	12.25	17.52	13.52	17.47	531	3637	1257	213	144	2649	52	467	129	1.10
MP 1	3865	7.53	1.52	1.65	15.42	22.06	14.57	18.83	681	3868	907	273	194	1935	64	436	154	0.95
MP 14	4105	12.42	1.48	3.98	12.74	18.22	12.86	16.62	962	4311	773	213	219	1931	57	382	164	1.01
MP 4	4207	7.91	1.55	2.23	12.57	17.98	15.19	19.63	957	5673	815	192	195	2487	46	397	146	1.21
MP 17	5000	8.71	1.77	2.45	15.71	22.48	12.37	15.98	1017	2753	680	183	201	1183	44	363	144	0.79

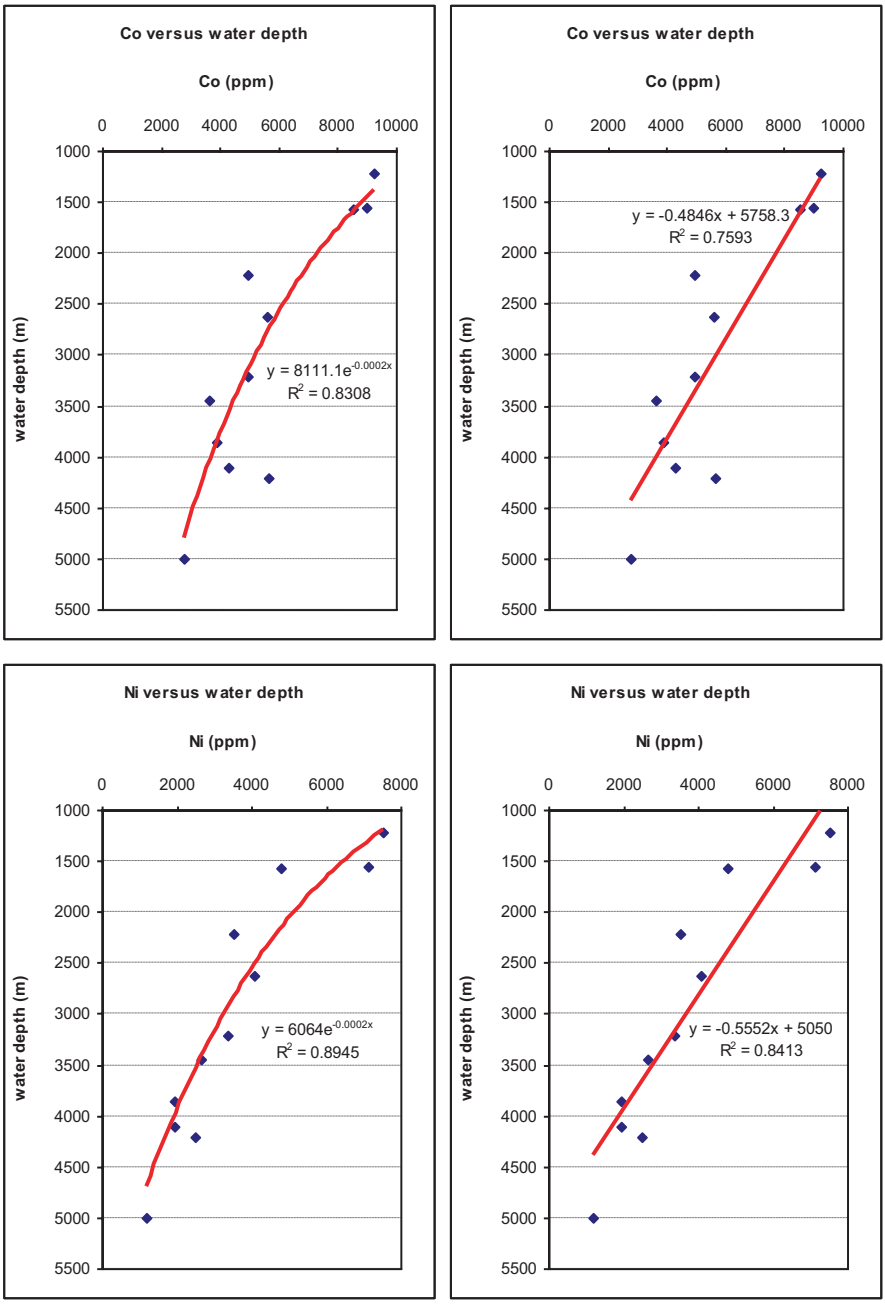

Fig. 3.32 Exemplary plots of element (Co, Ni, Fe_2O_3, MnO, Mo, and Nd) concentrations of younger generation crust samples from the Manihiki Plateau versus the water depths ($n = 11$; Table 3.10). Plots on the left side show the graphical results of the exponential correlation, plots on the right side show linear regression. R^2 indicates the coefficient of determination. These values show that the exponential correlations always have higher values of the coefficient of determination. For further explanation see text

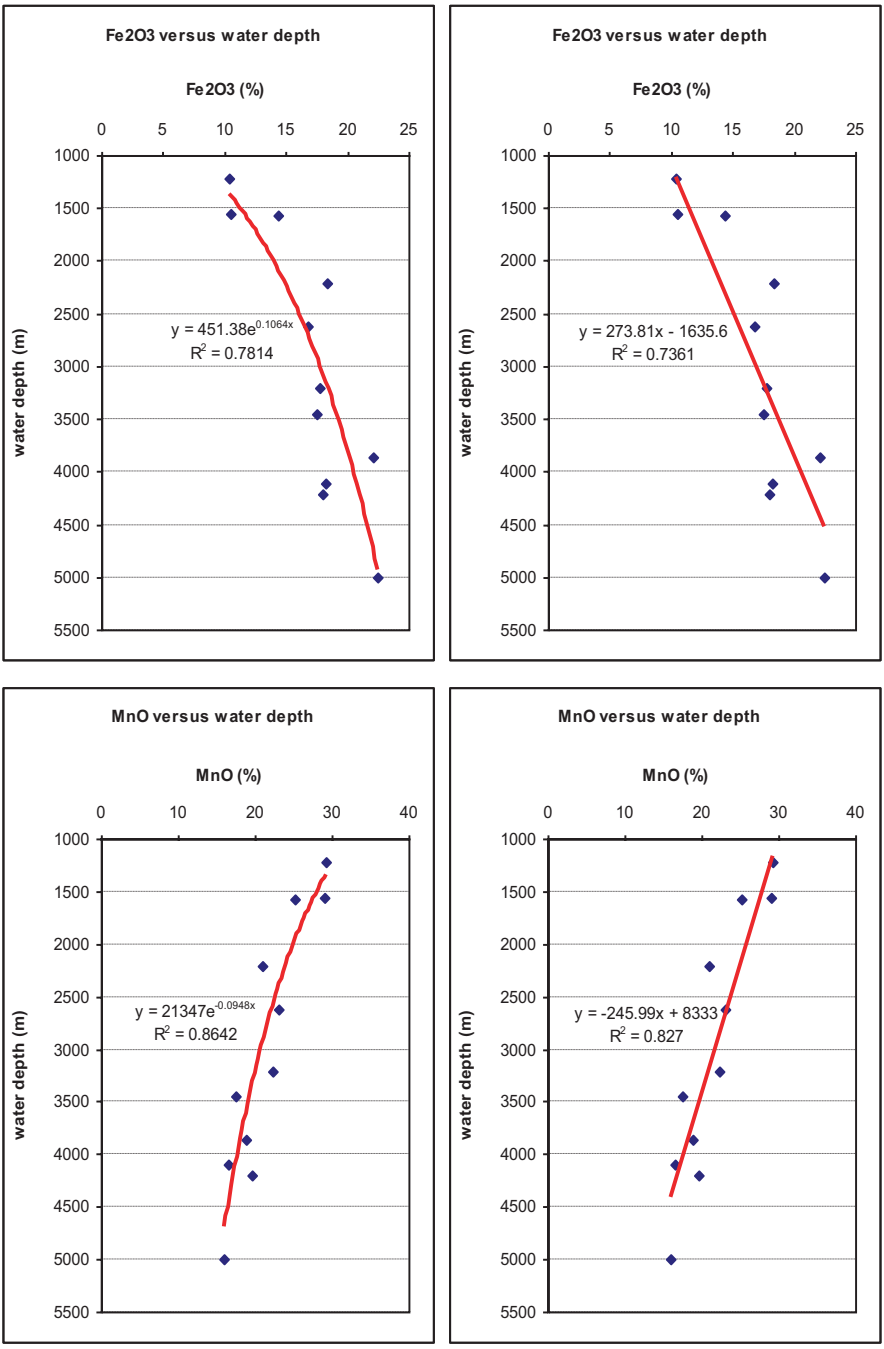

Fig. 3.32 (continued)

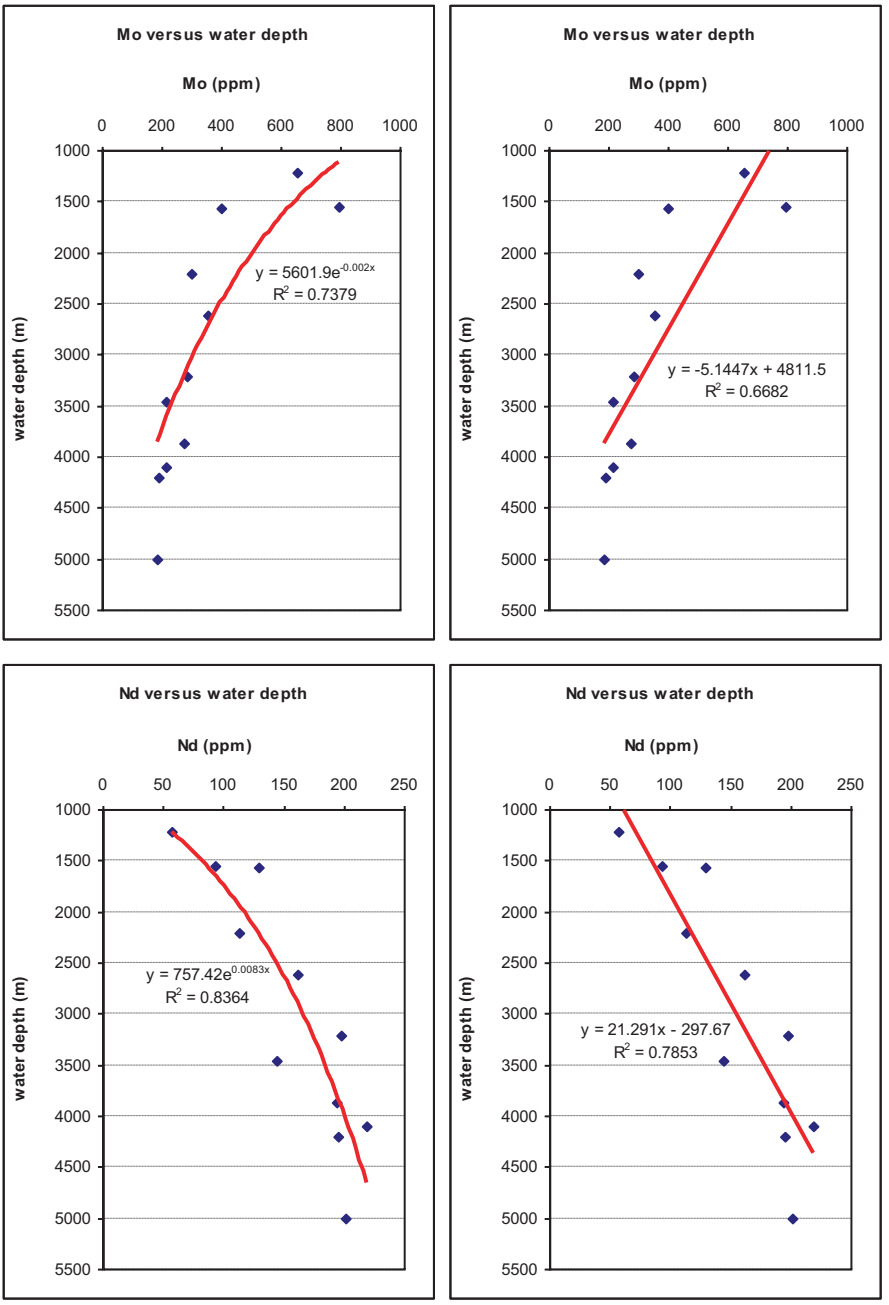

Fig. 3.32 (continued)

(b) **Bivariate statistics**, or bivariate correlations, to calculate the variables for linear or exponential regression. In geochemistry, the correlation coefficients show the relation or accordance of elements to each other in a defined quantity of samples.
(c) **Factor analysis** is a statistical method used for data reduction and to explain variability among observed variables in terms of fewer unobserved variables called factors. The observed variables are modeled as linear combinations of the factors. These factors can be identified through varimax factor analysis, and the possible sources can be suggested by contouring the factor scores. In geochemistry, different factors can correspond to different mineral associations, and thus to the transporting and element-bearing mineral phases or groups. For these considerations, a data set of 31 samples from the Central Pacific (Fig. 3.33; Halbach and Marbler 2009) and an analytical profile of LA-ICP-MS data of one younger generation crust sample (polished section) were used.

The results of the descriptive (a) and bivariate (b) statistics have already been shown and discussed in the individual chapters to demonstrate the respective relationships between individual elements, element pairs, and groups of elements.

All of the elements are associated with one or more mineral phases within the crusts. Interpreting the correlations, the following phases and their associated elements (Halbach and Marbler 2009) were indicated: δ-MnO_2component: Mn, Co, Mo, W, Te, Ni, Zn, Sn, (Pt), (Ce); Fe-oxyhydroxide component—FeOOH: Fe, Ti, Cu, Nb, Nd, and other REEs (Ce only partly); closely related to FeOOH is the aluminosilicate component: Al, Si, Mg, Fe, Ti, Sn, K, Na; carbonate-fluorapatite component (CFA; only in the older crust): Ca, P, Y, Sr, (Pt); residual biogenic component: Ba, Ca, Sr, (Pt). Elements of the aluminosilicate, Fe-oxyhydroxide, and δ-MnO_2components vary, in general, inversely with the CFA. These interelement associations are similar to those determined for crust samples from the Marshall Islands (USGS-KORDI Open File Report 1990).

Between the two crust generations, there are distinct variations in the interelement relationships. The most interesting feature is that elements represented by CFA and residual biogenic phases are combined in the older crust unit. This indicates that in crusts which were not phosphatized (younger crust generation), the elements associated with the older-crust apatite are part of an undifferentiated biogenic phase. Another interesting difference is that Ba, Cu, Ca, P, and Pt often increase within the older crust units. This is caused by the diagenetic overprint indicated by an addition of CFA and newly formed minerals during longer periods of non-growth (hiatus; Koschinsky et al. 1997). Co-contents decrease in the older generation and also with increasing crust thickness and growth rate; therefore, it is most abundant in the younger crust generation from moderate water depths (see above).

Some authors described geographic distributions in the interelement relationships, which probably reflect the regional oxidation potential (Hein et al. 1993). The water depth of the top of the oxygen-minimum zone increases, for example, from the Central Pacific to the north; the maximum amount of depletion of oxygen in seawater

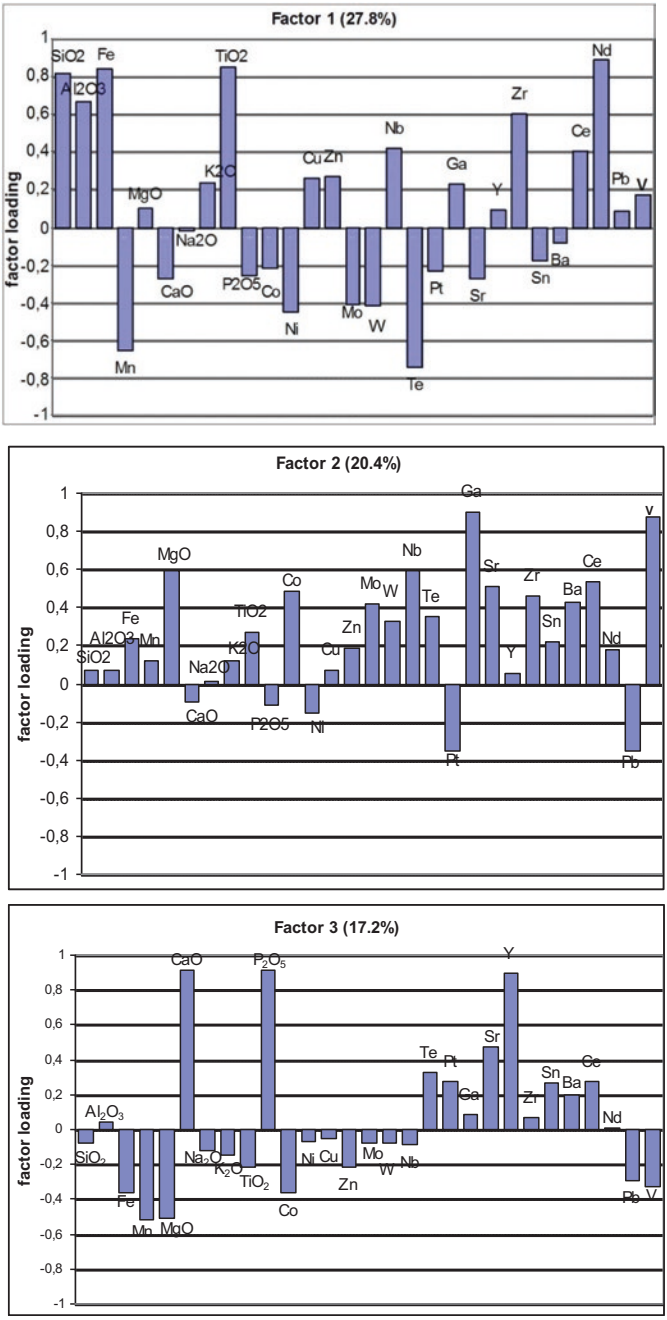

Fig. 3.33 Plots of Varimax rotated components with factor loadings. Actlabs data set (n = 31; Halbach and Marbler 2009)

decreases to the north and the west in the Pacific. The water depth of the greatest oxygen depletion also increases to the west (USGS-KORDI Open File Report 1990). Therefore, the data used originate mainly from the Central Pacific including the Manihiki Plateau since this region is considered to contain best-quality Co-rich ferromanganese crust deposits.

During the up to about 75 Ma history of growth, the crusts with distinguishable older and younger units have changed their geographic position because of plate motions, and their water depth has increased because of subsidence due to cooling of the oceanic crust and changes of the sealevel. Changes in all of these oceanographic and geological conditions over long periods of time would produce crusts with many chemical signatures representative of many different environments. Analysis of thick bulk crusts may average all these individual characteristic geochemical signatures.

The element correlations and variations between younger and older crust generations (see above) indicate that: (1) diagenesis has significantly affected the composition of the old crust units; (2) growth rates affect element associations; (3) P is associated with apatite only in older crust generations, suggesting at least two mechanisms of incorporation of P into crusts; in the younger generation data (Fig. 3.34), P is controlled by the Fe-oxyhydroxyde phase and the aluminosilicate phase. (4) The aluminosilicate fraction varies directly and the Mn-phase inversely with water depth. (5) Co varies inversely with crust thickness and water depth. Koschinsky et al. (1997) showed that Co is even released during the diagenetic overprint.

Fe compounds are less soluble than Mn compounds and the ferrous ion oxidizes more easily than the manganese ion under most naturally occurring pH-Eh conditions (Glasby and Schulz 1999). The results indicate that partial Fe-Mn fractionation must occur within the oxygen-minimum zone, but Fe is preferentially concentrated in crusts forming in deeper water of higher oxidation potential and Mn in the areas where seawater has the lower oxygen contents. However, the fractionation is never complete, but is extensive enough so that the crust compositions reflect the enrichment or depletion of minor and trace metals associated with the Fe- and Mn-phases (Glasby 2006).

Varimax factor analysis was completed for the 31 bulk crust samples (Fig. 3.33) as well as for one LA-ICP-MS profile data set of the younger crust unit (Fig. 3.34). The element groups determined by Varimax can be assigned to show the same crust phases as determined from the analysis of the correlation coefficients.

The five phases determined for the 31 bulk crusts (Fig. 3.33) are interpreted to be:

Factor 1 (27.8%), positive factor loading of the Fe-oxyhydroxide phase including aluminosilicate phase, negative factor loading of the δ-MnO_2 phase; factor 2 (20.4%), positive factor loading of the δ-MnO_2 phase and aluminosilicate phase (including residual biogenic phase), weak negative factor loading of the CFA; factor 3 (17.2%), positive factor loading of the CFA, negative factor loading of a diagenetic Mn-phase (probably birnessite). The data show that the δ-MnO_2 phase controls in particular the elements Co, Ni, Mo, W, Te, Pt, Sn, and Zn. The bulk crust

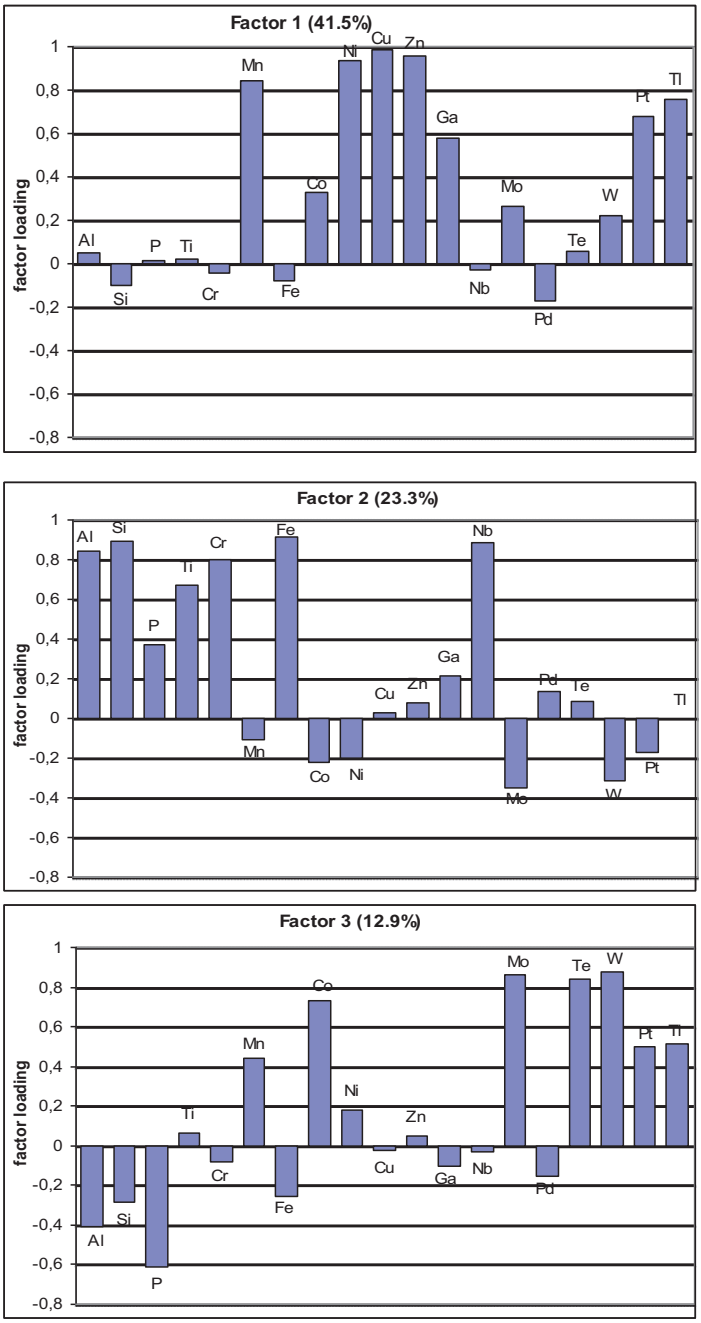

Fig. 3.34 Plots of Varimax rotated components with factor loadings. LA-ICP-MS data set of one profile of a polished section (younger generation crust, sample 43 DS 4, water depth: 1600 m; n = 149 measuring points)

data also indicate that the CFA-phase (CaO, P_2O_5) of the older unit carries REEs (indicated by Ce and Y) and some Pt, Te, and Sr. Ga has a significant signal in factor 2, which probably indicates that Ga is carried by the aluminosilicate phase.

Using the LA-ICP-MS data (Fig. 3.34) of one younger generation crust profile, three phases can be identified and are interpreted to be:

Factor 1 (41.5%), indicating a positive factor loading of the δ-MnO_2 phase; factor 2 (23.3%), positive factor loading of the Fe-oxyhydroxide phase including the aluminosilicate phase, weak negative factor loading again of the δ-MnO_2 phase; factor 3 (12.9%), positive factor loading of the δ-MnO_2 phase, weak negative factor loading of the aluminosilicate phase. The CFA-phase does not exist in the younger generation. Pt is mainly fixed to the δ-MnO_2 phase. In addition to the typical manganophile elements (W, Te, Mo, Co, Ni and Pt), also Cu and Zn are controlled, at least partly, by the δ-MnO_2 phase. Nb is distinctly indicated at factor 2, probably controlled by the Fe-oxyhydroxide phase.

These results show the dominant influence of the hydrated δ-MnO_2 phase together with the respective A-group metals regarding the mineralogical and geochemical compositions of this younger generation crust sample, which originates from a water depth of 1600 m (sample 43 DS 4; Table 3.1). The Fe-oxyhydroxide phase with the B-group element cluster is a second important type of carrier. The aluminosilicate cluster is the third important carrier phase in the younger generation hydrogenetic substance. The data show that several minor and trace elements show multiple carrier phase behaviour which is probably caused by the fact that some of the elements dissolved in seawater have several speciations.

3.5 Total and Regional Metal Potentials

3.5.1 Resource Assessment Model for Ferromanganese Crust Deposits

Co-rich ferromanganese crust deposits exist on slopes, summits, and platforms of seamounts and guyot structures in the oceans. An extensive exploration of these deposits like the nodule deposits in the CCZ does not exist. Nevertheless, in the Pacific Ocean, more areas were investigated than in the Indian and the Atlantic Ocean. Therefore, a linear resource assessment method was developed and used which is based on the assumption that all seamounts and guyots in all three oceans in a defined water depth contain Co-rich ferromanganese crust deposits. The model (Halbach et al. 2013) considers two types of seamounts, the classical cone-shaped seamounts and the guyots. In addition, the roughness of the seafloor, possible thick sediment coverage, and surface obstacles like boulders were regarded and classified as non-mineable sites.

Seamounts and guyots were distinguished by their overall slope angle. Most of the submarine mountains are volcanic structures. Variations of the slope angles of

submarine mountains are also controlled by erosion and subsidence. While seamounts form slopes with more than 12° from the base to the top, guyots have erosional plateaus which reduce their overall height/radius ratio and, therefore, their mean slope angle. Respective slope angles were calculated for all known seamounts which are included in the seamount catalogue of Wessel (2001) and Wessel et al. (2010). These authors compiled the global seamount population deduced by gravity anomalies determined from satellite-based radar altimetry of the ocean surface.

The cumulative mean slope angle curve (Fig. 3.35) for all of the more than 11,000 entries shows two distinct groups of submarine structures: (1) mountains with angles of up to about 12° which are interpreted as guyots and (2) mountains with more than 12° which represent normal conical seamounts. This method to distinguish the two types of seafloor structures by their overall slope angle has been checked and confirmed at several real seamount structures (Halbach et al. 2010).

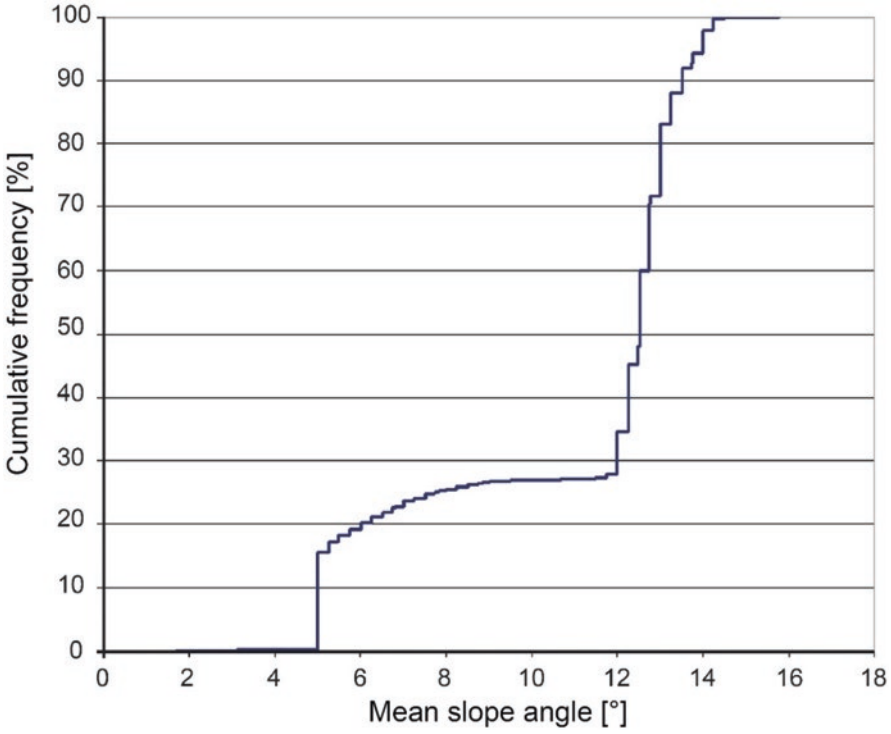

Fig. 3.35 Cumulative curve depicting the mean slope angle of seamounts and guyots versus their cumulative frequency. The diagram shows a bimodal distribution. The first group comprises the slope angles (mean angles from the foot to the top of structure) from 5° to 10° that corresponds to about 28% of the population. The second group starts with 12° and ends with 16°. Group 1 represents guyots, which have a summit plateau that reduces the height/radius ratio. Group 2 stands for seamounts with no or only small summit plateaus. Note: The steep rise of the curve at a mean slope angle of 5° is a result of the stepwise increase of radius and height information in the original data set which masks the onset of the curve

Assuming a mean water depth of 4500 m, the surface areas of all seamounts of the catalogue were inferred empirically by a geometric model that describes the seamount structures as simple cones using the given data for the height and the basis radius. For guyots, it was assumed that the marine mountains can be characterized as truncated cones with slope angles like seamounts (12°) and corresponding plateaus; therefore, the overall slope angle values are considered to be distinctly lower than 12°. Typically, the seamount type structures show slope angles from 12° to 16° (Fig. 3.35). With this distinction, the surface areas for the seamounts slopes as well as the guyot slopes and plateaus could be calculated.

For the assessment of the potential ore resources, the seamounts and guyots of importance were selected by certain criteria:

– Geographic position between 50°N and 50°S,
– Minimum age is early Cenozoic (55 Ma),
– The top of the respective mountain structure must be in a water depth range between 800 and 2500 m below sea level.

The first limiting criterion was chosen because of the bad weather conditions in higher latitudes, which are unfavourable for marine mining activities. The second one is based on the fact that only older seafloor structures are covered with crust deposits of sufficient thickness. The third criterion is based on the observation that Ni and Co concentrations are higher in present-day moderate water depth ranges (chapter 3.4.3.5).

For the assessment procedure, the surface areas of the seamounts and guyots were summed up from 3000 m water depth to the top of the structure (800–2500 m). The platform areas of guyots were taken into consideration only with 30%, which is an empirical value for sediment-free platform portions, based on field observations. With a given dried crust density (1.4 g/cm^3) and an average coverage of ferromanganese crusts determined by thickness (3.5 cm), the potential ore quantity (dried matter) was calculated. Then these numbers were reduced by an empirically derived mineability factor of 50% because of seafloor roughness, local sediment coverage, and obstacles. This mineability factor is deduced from seafloor observations made on many cruises and represents a conservative estimate. In Fig. 3.36, an example of a very favourable crust deposit situation is presented, where the seafloor morphology is very flat and the crust coverage is homogeneous. In contrast, Fig. 3.37 shows an unfavourable microtopography which probably prohibits a selective and successful recovery.

The basic calculation for the inferred resources is as follows:

$$R_i = A_m \times T \times D \times M$$

where:

R_i = Inferred Resources [t]
A_m = Model Area [m^2]
T = Thickness [m]
D = Dry Density [t/m^3]
M = Mineability Factor [50%]

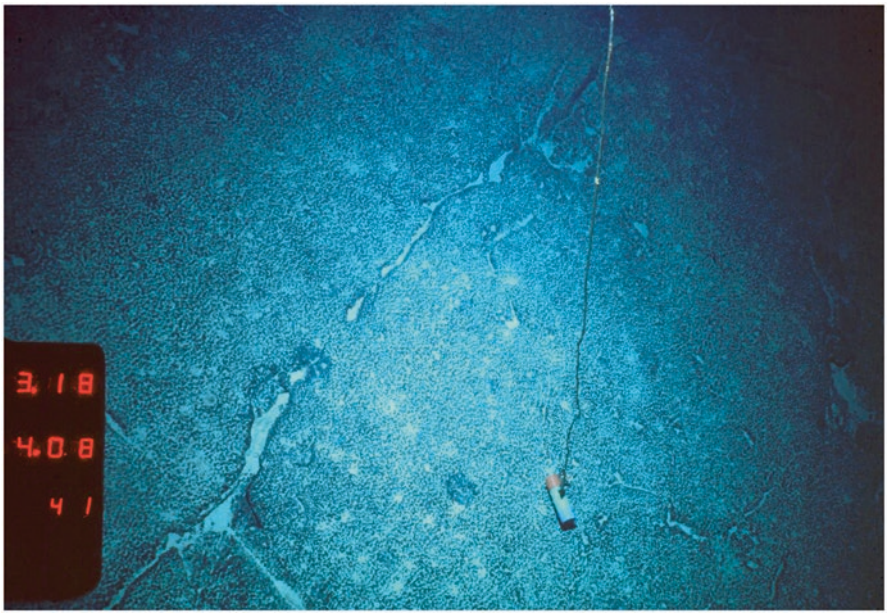

Fig. 3.36 Smooth seafloor microtopography with cracks in the crust coverage (approximately 6 cm crust thickness). Due to the very low roughness, the crust field can be regarded as mineable. The long edge of the picture corresponds to about 4 m

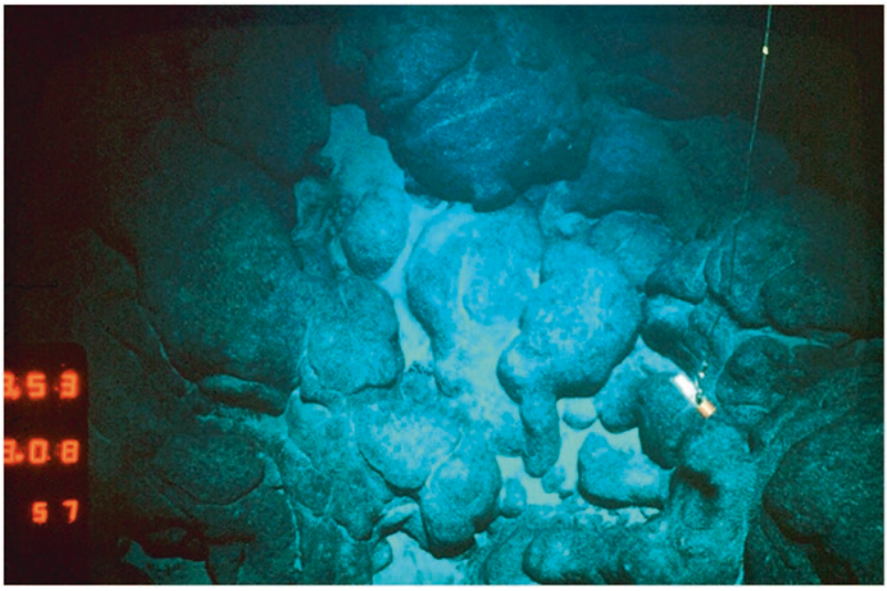

Fig. 3.37 The seafloor image shows former lava outflows forming large pillows covered with ferromanganese crusts and some sediment fillings in pockets. The rough topography and large amount of crust-covered boulders will probably prohibit any successful mining recovery. The long edge of the picture corresponds to about 4 m

The total amount of estimated ferromanganese crust resources for all the oceans assessed by this model calculation results in 35.1×10^9t of ore material (dried matter), whereas this value splits into:

3.7×10^9t (Indian Ocean; 10.6%),
7.8×10^9t (Atlantic Ocean; 22.2%),
23.6×10^9t (Pacific Ocean; 67.2%).

The model calculation leads to some very interesting conclusions: The ocean with the highest number of seamount structures and, therefore, containing the largest amount of ferromanganese crust is the Pacific Ocean, which contains about two thirds of the total resources. Despite the predominant number of individual seamounts (70.5% of the total number of ocean floor structures), the seamounts represent only a relative small portion of the totally considered areas. However, up to 85% of the estimated crust-bearing seafloor areas are located on the flanks or platforms of guyots, which shows the dominant position of the guyot structures for the potential crust resources. Considering the procedure of estimation, it can be stated that based on the three criteria for seamount and guyot selection as well as on the used deposit factors, which are established on some variable assumptions, the respective results can be regarded as quite conservative. For example, an increase of the assumed average thickness from 3.5 to 5 cm would increase the available resources accordingly. However, this would probably imply that also parts of the heterogeneous older crust generation (see chapter 3.4.2), which is apatite-bearing, will be recovered.

The amounts of the suggested estimated resources represent minimum values. The intention of the modelling is to present only a plausible order of magnitude. For example, Hein et al. (2009) have published a rough estimate of the resource quantity of the crusts in the Central Pacific Region being 7.5×10^9t (dry material), which corresponds to 1/3 of the quantity estimated by the model. For all oceanic areas, Hein and Koschinsky (2013) have estimated a global tonnage of crusts to be about 200×10^9t. Comparing this value with the total amount of the 35×10^9t obtained by the model, the order of magnitude of both estimations is similar, since the estimation of Hein and Koschinsky (2013) does not consider any kind of limiting factors.

Regarding the factor “mineability”, it has to be noted that for successful crust recovery it is essential that the ferromanganese crusts should be detached from the seafloor with minimum dilution by substrate rock material. To this day, a corresponding and tested technical method does not exist. Therefore, the presented tonnages of ferromanganese crusts cannot be considered as reserves according to the classification to mineral deposits (USGS 1980) since the term “reserves” implies that the commodity can be economically recovered, extracted, or produced at the time of determination, i.e. reserves include only recoverable materials independent of whether extraction facilities are in place or operative. The proposed classification for the crust deposits is “identified resources”. These are defined by the USGS (1980) as resources whose location, grade, quality, and quantity are known or estimated from specific geologic evidence. “Identified resources” include economic, marginally economic,

and sub-economic components. At present (2016), the metal market is characterized by comparatively low commodity prices. In order to create a profitable deep-sea mining venture, the metal market will need a considerable recovery.

3.5.2 Economic Considerations

The marine ferromanganese crust deposits contain, besides the main elements Mn, Fe, and P (P mainly in the older generation crusts), a number of interesting minor (Co, Ni, Ti, Cu, Zn, Ba, Pb, Sr, and REEs) and trace elements (Mo, V, W, Nb, Te, Ga, Pt, Pd, and Y). Not all of the mentioned elements are considered to be of importance, therefore the economically interesting metals are listed in Table 3.11. This table compares the composition of the crust deposits from the Central Pacific region (water depth range: 800–3000 m) with the average composition from the Atlantic and the Indian Ocean (Hein and Koschinsky 2013). Some differences are obvious. The Atlantic and the Indian Ocean deposits are dominated by Fe (Pacific: 11.0%, Atlantic: 20.9%, and Indian Ocean: 22.3%) and the corresponding Fe-controlled group B elements (see chapter 3.4.3.5). The Mn concentration and the Mn-controlled metals are distinctly lower than in the Pacific data set. Also, the rare earth elements are significantly higher in the Atlantic and Indian Ocean samples (Atlantic: ΣREEs 2221 ppm

Table 3.11 Concentrations of the valuable metals in ferromanganese crusts from different oceanic regions

	Pacific Ocean (Halbach and Marbler 2009)	Atlantic Ocean (Hein and Koschinsky 2013)	Indian Ocean (Hein and Koschinsky 2013)	
Mn	22.5	14.5	17.0	%
Ti	0.7	0.9	0.9	%
Ni	4849	2581	2563	ppm
Co	7084	3608	3291	ppm
Cu	434	861	1105	ppm
V	389	849	634	ppm
Mo	351	409	392	ppm
REEs	1060	2221	2363	ppm
Zn	519	614	531	ppm
Pt	450	567	211	ppb
W	56	79	80	ppm
Nb	31	51	61	ppm
Te	33	43	31	ppm
Y	128	181	178	ppm

The data from the Pacific Ocean are adjusted to the assessment model and represent the composition of crust samples which originate from the considered depth range (see above, chapter 3.5.1) of 800–3000 m water depth. The data for the Atlantic and Indian Ocean were altogether taken from Hein and Koschinsky (2013); a differentiation according to the water depth has not been done. Elements, which are not considered to be of economic interest, are not included

and Indian Ocean: ΣREEs 2363 ppm). In addition, the Ni and Co concentrations are higher in the Pacific Ocean samples, while in contrast, the Cu concentrations are higher in the Atlantic and Indian Ocean deposits. Based on these observations and despite the volatility of the metal market prices, it can be concluded that the Pacific crust occurrences represent a higher market value per tonne of dried ore material than the respective deposits of the Atlantic and Indian Ocean.

The range of the metal concentrations of Nb, Te, and W (Table 3.11 and chapter 3.4.3) shows that in all three oceans these contents are below 100 ppm. The relative portion of the total market value per tonne of ore material (current metal prices in 2016) of these three elements is less than 0.5%. Thus, it is questionable whether these extremely low concentrated elements can be extracted under technical-economical market conditions.

One interesting geochemical feature is the significant water depth dependence of the minor and trace metals. The Mn-group elements Co, Ni, Mo, W, Te, and Pt decrease with increasing water depths. Best concentrations of these metals are in the lower part of, and immediately below, the O_2-minimum zone. On the other hand, the Fe-group elements Ti, Cu, and REEs increase with increasing water depths. Since the Mn-group metals have a much higher metal-marked potential than the Fe-group elements, the shallower water region represents a more interesting depth range. Comparative considerations (Halbach and Marbler 2009) have shown that the decrease of the economic value of the Mn-group elements with increasing water depth down to 4100 m is not compensated by the increasing market value of the Fe-group metals. Typical crusts from very deep water (e.g. Osbourn Trough, 4640 m; Halbach et al. 2014) have, for example, REE-concentrations up to more than 3000 ppm and Ti-contents of up to 1.9% combined with 26% Fe; however, the Mn-, Co-, Ni-, and Mo-concentrations decrease to 12%, 2700 ppm, 1200 ppm, and 180 ppm, respectively.

Table 3.12 lists the land-based reserves (USGS 2016) of the contained valuable metals in comparison to the identified resources of the total ferromanganese crust deposits. Even though the two data sets represent two different classification categories, a rough comparison of the total amounts shows that some commodities are much more abundant in the marine deposits. These metals are: Mn, Ni, Co, Te, and Y, whereby in the following order the ratio increases in the succession Ni, Mn, Y, Co, and Te, the latter element is even 48 times more abundant in the ferromanganese crusts than in the land-based deposits.

Compared with ferromanganese nodules, the crusts exist with their best-quality depth range in a shallower water depth range than the nodules. Thus, it can be expected that the operating expenditures are more favourable in the case of crust recovery. In contrast to the ferromanganese nodules, however, the crusts in general are tightly attached to the hard substrate rocks. Crusts also have with their local coverage density a higher mineral abundance per unit of area than nodules (in CCZ nodule areas in-situ abundances of 10–25 kg/m^2 are considered to be mining sites; a threshold of 6 kg/m^2 in-situ abundance is selected; ISA 2010). An average seamount, for example, with a slope angle of about 14° and a mean crust thickness of about 3.5 cm may have about 8×10^6t of crust material in the depth range between 1000

Table 3.12 Estimated resources for the valuable metals in ferromanganese crust deposits presented in Table 3.11 in comparison to land-based reserves (USGS 2016; see text)

	Pacific Ocean	Atlantic Ocean	Indian Ocean	Total	Land-based Reserves (USGS 2016)	
Proportion of the total crust resources (dry)	23.6 (67.3%)	7.8 (22.2%)	3.7 (10.5%)	**35.1 (100%)**		10^9 t
Mn	5304.1	1131.0	629.0	**7064.1**	620.0	10^6 t
Ti	174.9	71.8	32.6	**279.2**	460.3	10^6 t
Ni	114.4	20.1	9.5	**144.0**	79.0	10^6 t
Co	167.2	28.1	12.2	**207.5**	7.1	10^6 t
Cu	10.2	6.7	4.1	**21.0**	720.0	10^6 t
V	9.2	6.6	2.3	**18.1**	15.0	10^6 t
Mo	8.3	3.2	1.5	**12.9**	11.0	10^6 t
REE	25.0	17.3	8.7	**51.1**	106.0	10^6 t
Zn	12.2	4.8	2.0	**19.0**	200.0	10^6 t
Pt	10,656.0	4422.6	780.7	**15,859.3**	39,600.0	t
W	1314.2	616.2	296.0	**2226.4**	3300.0	10^3t
Nb	734.1	397.0	226.8	**1357.9**	4300.0	10^3t
Te	769.6	335.4	114.7	**1219.7**	25.0	10^3t
Y	3019.2	1411.8	658.6	**5089.6**	393.7	10^3t

and 2500 m. If 50% of this amount is recoverable (micromorphology is one important factor limiting the mineability, see above) the seamount may have a high-quality identified resource of 4×10^6t (wet material). Using this example, the small-scale abundance of the crust amounts to 70 kg/m^2 (wet material).

Regarding the time of realization, the marine Co-rich crust mining is considered to be more distant in time compared to nodule and massive sulfide recovery. However, the particular in-situ conditions at the potential mine sites of crusts require a very sophisticated technical method to separate the crust layers from underlying substrate rocks. Thus, the development of an effective recovery system is a challenging undertaking. Since the crusts also represent an oxidic mineral material comparable in composition to the manganese nodules, respective ore processing techniques will be very similar to nodule extraction flow sheets.

3.5.3 Regional Distribution of Crust Deposits

The Atlantic is the second largest ocean extending as a relatively narrow (about 5000 km wide) S-shaped basin lying between the arctic and sub-antarctic regions (Kennett 1982). The Atlantic has the largest N-S extension of any ocean. It is on the average slightly shallower than the Pacific, which results from large areas of continental shelves and margins. Another particular feature of the Atlantic is that it gets

the greatest amount of fresh water discharge from huge river systems (Kennett 1982). One major result of this phenomenon is that terrigenous sediment input is much higher than in the other oceans.

The most remarkable tectonic and morphological feature is the Mid-Atlantic Ridge (MAR), which controlled the geological opening history and the development and type of seafloor morphology existing nowadays. The opening of the Atlantic started about 150 Ma ago, the spreading is still going on. The MAR has a shape of an inverted question mark and extends from 87°N down to the sub-antarctic Bouvet Island at 45°S. It is the boundary between the American plates in the west and the Eurasian and African plates in the east. The topographic features basically show that the centre of the Atlantic Ocean is shallower because of the spreading ridge.

Since seamounts structures with hydrogenetic ferromanganese crust occurrences should have an age of at least 50–55 Ma, the respective provinces with prospective crust deposits are, therefore, generally located away from the MAR (Fig. 3.38). Manganese crust deposits close to the rift axis mostly are of hydrothermal origin, and thus not of economic interest. The majority of the sites in the Atlantic representing potential areas for hydrogenetic crust deposits are located between the ridge structure and the continental shelf. They mostly consist of seamount groups or seamount chains as it is also typical for the Pacific and the Indian Ocean.

These seafloor structures were, in general, formed by hot-spot volcanism (Seibold and Berger 1993): hot-spot plumes are thought to originate from the lower mantle and constitute an important component of the mantel's convection and rise because of zones of weaknesses in the lithosphere. After their island stage, volcanism ceases and the islands subside. The origin of an island chain is explained by a stationary source of hot magma over which the lithosphere rides (Seibold and Berger 1993). As the oceanic plate moves, a trail of extinct volcanoes forms and eventually develops into a chain of sunken seamounts. The slopes of these seamounts and the platforms of the guyots (flat-topped seamounts with erosional plateaus) are the predominant sites for hydrogenetic precipitation and crust deposit formation.

The distribution of the potential crust deposit provinces in the Atlantic Ocean (Fig. 3.38) strikingly shows that respective crust occurrences may exist only in the older part of the seafloor. The marked sites have been selected based on the specific marine depositional conditions and the respective geological history of formation. Not all of the marked sites have already been studied or checked for crust deposits. However, in some regions such as the Canary Islands (Marino et al. 2016) and the Tropic seamount (Koschinsky et al. 1995; CI and TS in Fig. 3.38) or the Sierra Leone Rise (Asavin et al. 2008; SLR), crust occurrences were studied. Other sites are in the stage of investigation (e.g. Rio Grande Rise; RGR in Fig. 3.38).

Crust samples from the Atlantic Ocean show, compared to those from the Pacific Ocean, that the concentrations of Mn are on the average 7–8 wt% lower and those of Fe about 8–9 wt% higher (Tables 3.2 and 3.11). Correspondingly, the metals Co and Ni which are closely related to Mn also have lower concentrations in the Atlantic ferromanganese crusts (mean value: 3600–4000 ppm Co and 2600–3000 ppm Ni). On the other hand, metals which are controlled by Fe have somewhat higher concentrations in the Atlantic samples (Ti 0.9 wt%, Cu 870 ppm, and some of the

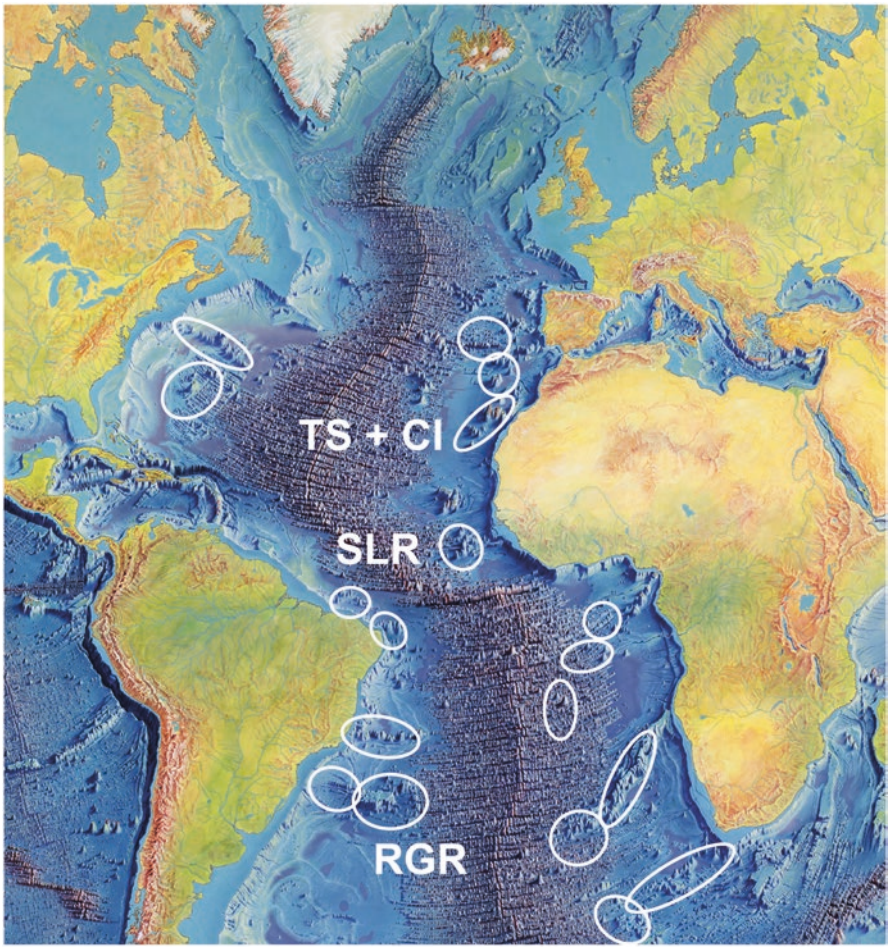

Fig. 3.38 Overview map (Berann et al. 1977) of potential crust deposit provinces in the Atlantic Ocean. Only a few of the potential sites have been studied so far, e.g. the Tropic Seamount (TS) and the Canary Island (CI) region as well as the Sierra Leone Rise (SLR). The Rio Grande Rise (RGR) is currently in the state of investigation

REEs 2460 ppm). One main reason for these differences in metal composition is probably the higher growth rate of the Atlantic crusts caused by more terrigenously influenced and Fe-dominated element sources in the Atlantic, which is supplied by huge river systems flowing into this ocean from the East and the West. Also, the eolian input in the sub-tropical North-Atlantic is large (eolian dust originating from the Sahara Desert). In contrast, the Pacific Ocean is more a closed and isolated marine system with less terrigenous influence.

The Indian Ocean is the third largest ocean and most of its area lies in the southern hemisphere (Kennett 1982). The boundary between the Indian and the Atlantic

Ocean is located south of Africa, while its boundary to the Pacific Ocean follows the Indonesian Islands to Eastern Australia and south of Tasmania (Fig. 3.39). Also, the Indian Ocean has a few islands and it is marked by several plateaus and ridges. The majority of river discharge occurs in the northern part adjacent to Asia (Fig. 3.39). The bathymetry of the Indian Ocean shows that the tectonically active mid-ocean rift system is shaped like a broad inverted Y with links northwest towards the Golf of Aden, southwest towards the South Atlantic, and southeast towards the southern ocean south of Australia (Kennett 1982). Large fracture zones displace the ridge axis; in the central part the three ridges meet at the Rodriguez triple junction (Fig. 3.39). The rough topography of the ridge system contrasts with long aseismic seafloor structures like the Ninety-East ridge, which represents a huge hot-spot track indicating that a stationary plume period may even last as long as 100 Ma (Seibold and Berger 1993). Similar as in the Atlantic Ocean, potential sites with prospective crust deposits may only be distributed in the older part of the oceanic seafloor. Correspondingly, some regions are marked in Fig. 3.39. In three of the indicated regions, crust deposits have already been sampled and studied: Ninetyeast Ridge (NER in Fig. 3.39; Hein et al. 2016), Mozambique Ridge (MR; Perritt and Watkeys 2007), and Afanasiy-Nikitin Seamount (Rajani et al. 2005). The known crust deposits of the Indian Ocean are also characterized by higher Fe and lower Mn-contents than the crust deposits of the Pacific Ocean (Tables 3.2 and 3.11).

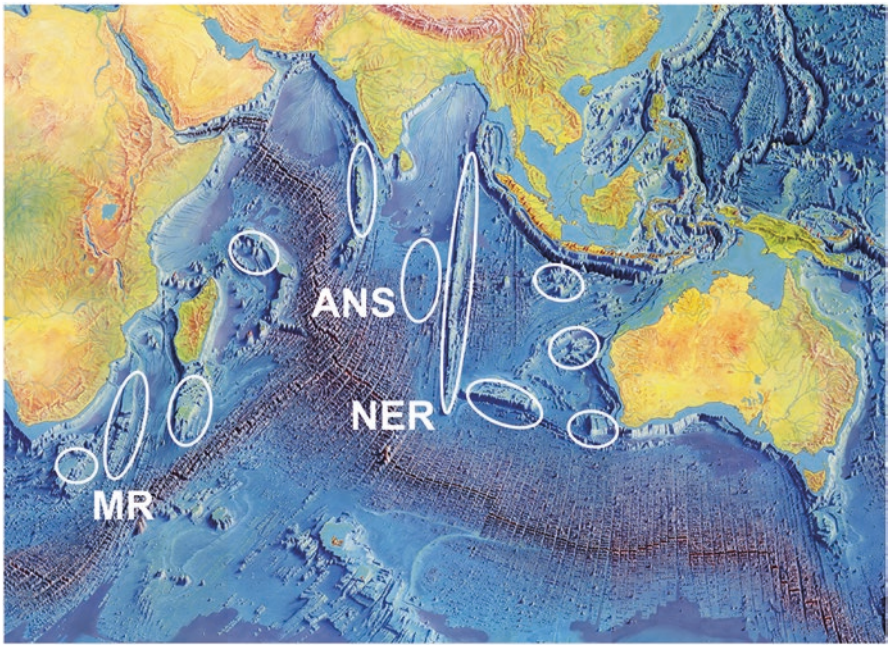

Fig. 3.39 Overview topography (Berann et al. 1977) and map of distribution of potential crust deposit provinces in the Indian Ocean. From some of the potential crust provinces, data are already available as from the Mozambique Ridge (MR), the Afanasiy-Nikitin Seamount (ANS), and the Ninetyeast Ridge (NER)

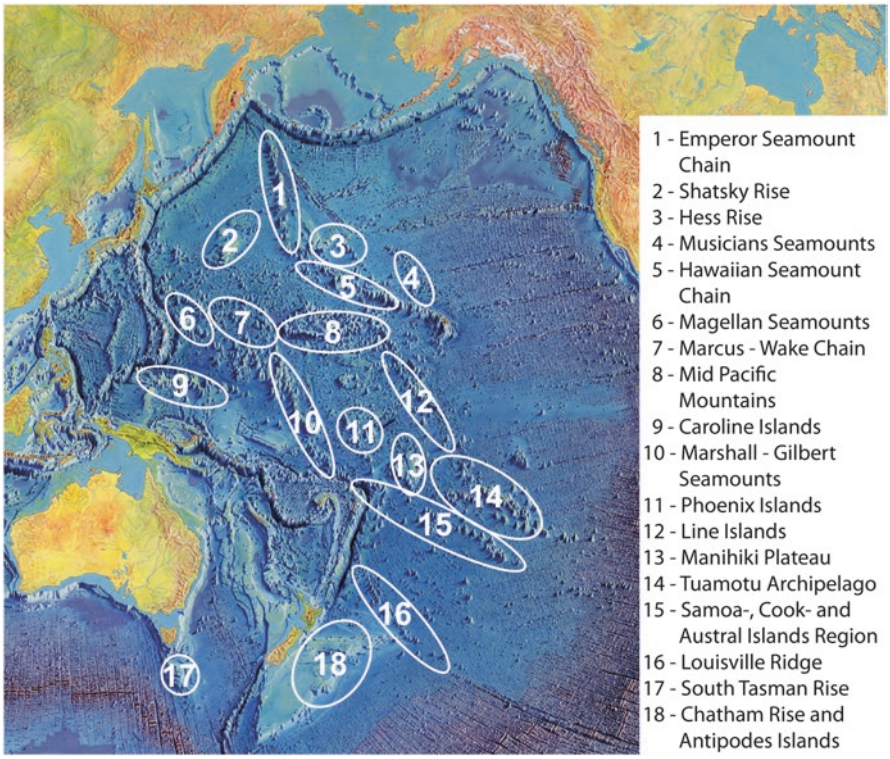

Fig. 3.40 Overview topography (Berann et al. 1977) and map of distribution of potential crust deposit provinces in the Pacific Ocean

The largest ocean is the Pacific (Fig. 3.40), which occupies more than one third of the Earth's surface (Kennett 1982). The Pacific is surrounded mainly by linear mountain chains, trenches as parts of subduction systems, and island arc systems that effectively isolate the deep-sea basins from the influence of continental terrigeneuos sedimentation. The fact that the Pacific Ocean is less influenced by terrigenous sources of continental run-off probably causes the higher Mn concentrations compared to the Fe contents in the crust material combined with higher concentrations of Ni and Co (Tables 3.2 and 3.11).

The continental shelves of this ocean are narrow forming only a small proportion of the total Pacific area compared with the other oceans (Kennett 1982). Two further distinct features of the Pacific include large numbers of volcanic islands and fossil sunken seamount chains, especially in the western and central parts as well as the presence of marginal basins which act as important sediment traps. One of the oldest records of seafloor spreading is in the Northwest Pacific. There, the magnetic lineations are of early Cretaceous to Jurassic age (Kennett 1982). Spreading from the East-Pacific Rise and its precursors has resulted in a northward to northwestward increase in age of the seafloor. The modern East Pacific Rise is a relatively

young feature in the eastern part with some remarkable fracture zones; between the fracture zones, abyssal plains are distributed.

The most frequent and prospective regions with Co-rich crust deposits are found in the Northwest and Central Pacific Ocean (Fig. 3.40; Halbach and Manheim 1984; Hein et al. 2000). There, the ancient seafloor consists of Mesozoic plates with numerous seamount chains of Cretaceous age. But also younger hot-spot systems, still active nowadays like the Hawaiian Island chain, can be observed. Several pole rotations of the Pacific plate have also controlled the movement trails as it can be seen, for example, by the different strike directions of the Emperor and Hawaiin chains.

The western part of the Pacific Ocean has a lot of island states; thus, a large part of the crust deposits are located within their Exclusive Economic Zones (EEZ). Those areas outside of the EEZs are administered by the International Seabed Authority (ISA, Kingston/Jamaica). Draft regulations on prospecting and exploration for Co-rich ferromanganese crusts in the ISA-Area were already published in 2006 (ISA 2006). In the meantime, exploration licences for this type of marine minerals have also been given to some contractors.

3.6 Conclusions

1. Cobalt-rich ferromanganese crusts are one type of the oxidic metallic mineral resources in the deep ocean. They directly precipitate from cold seawater under oxic to suboxic conditions in a thin-layered set-up on hard substrate rocks and incorporate metals supplied and transported from both land (aerosols, continental run-off) and sea sources (oxygen-minimum zone, dissolution of carbonate skeletons, hydrothermal alteration of the oceanic crust). The very slow process of hydrogenetic precipitation is basically an inorganic colloidal-chemical and surface-chemical mechanism. The ferromanganese crusts consist of a very fine-grained mixture of ferruginous vernadite (mainly δ-$MnO_2 \times H_2O$) and X-ray amorphous Fe-oxyhydroxide, as well as aluminosilicate phases, carbonate-fluorapatite (secondary in the older crust generation) and minor admixtures of fine-grained, detrital quartz, and feldspar as well as residual biogenetic phases. A consecutive process to explain the heteroepitaxial intergrowth of the Mn- and Fe-phases controlled by bioproductive processes in surface waters is presented.
2. A very important feature is that crust growth was interrupted for millions of years; this hiatus may last for 10–25 my and may occur several times in the growth history. During long-lasting paleo-oceanographic episodes of growth interruptions, the crusts are subject to diagenetic processes under the influence of suboxic to reducing conditions of an expanded O_2-minimum zone, occasionally even combined with a temporary sediment cover. The most important result of the diagenetic process is an impregnation with apatite.
3. The marine ferromanganese crust deposits contain Mn and Fe as main elements. A number of very interesting minor (Co, Ni, Ti, Co, and Ce) and trace elements (Mo, W, Nb, Te, Ga, Pt, Pd, and REEs) are highly enriched in crusts compared to

seawater composition and average crustal abundance. Some of these elements have a great future potential as innovative high-technology and green-technology constituents.

4. One interesting geochemical feature described is the significant water depth dependence of minor and trace metals. The Mn-group elements Co, Ni, Mo, W, Te, and Pt decrease with increasing water depths. Best concentrations of these metals in the crusts are observed immediately below the O_2-minimum zone, i.e. in shallower water depths. On the other hand, the Fe-group elements Ti, Cu, and REEs increase with increasing water depths. Since the Mn-group metals have a higher metal market potential than the Fe-group elements, the shallower oceanic water regions represent more interesting depth ranges. Comparative considerations show that the decrease of the economic value of the Mn-group elements with increasing water depth down to 4100 m is not compensated by the increasing market value of the Fe-group metals.
5. The total and regional metal potentials are calculated based on a resource assessment model using some limiting factors. Basically, crust deposits occur in all three oceans; however, compositional differences can be observed. But, due to the particular geological and oceanographic conditions in the Pacific Ocean, by far the largest and best deposits exist there.
6. In contrast to ferromanganese nodules, crusts are tightly attached to hard substrate rocks. These particular in-situ conditions at potential mine sites of crusts will require a very sophisticated technical method to separate the crust material from the underlying substrate rocks.
7. Regarding the factor "mineability", it has to be stated that, for successful crust recovery, it is essential that the ferromanganese crusts must be detached from the seafloor with minimum dilution by substrate rock material. To this day, a corresponding and tested technical method does not exist. The presented tonnages of ferromanganese crusts cannot be considered as reserves according to the classification of mineral deposits (USGS 1980) since the term "reserves" implies that the commodity can be economically recovered, extracted, or produced at the time of determination, i.e. reserves include only recoverable materials independent from existing extraction facilities being in place or operative. The proposed classification for the crust deposits, therefore, is "identified resources". These are defined by the USGS as resources whose location, grade, quality, and quantity are known or estimated from specific geologic evidence. "Identified resources" include economic, marginally economic, and sub-economic components.
8. Regarding the time of realization, marine Co-rich crust mining is considered to be more distant in time compared to nodule and massive sulfide recovery. However, the particular in-situ conditions at the potential mining sites of crusts require a very specific 2-step method to separate (detachment technology) and to recover (lifting technology) the crust material. Thus, the development of an effective mining system is a challenging undertaking. Since the crusts have an oxidic mineral composition comparable to the manganese nodules, respective ore processing techniques will be very similar to nodule extraction flow sheets.

References

Asavin AM, Anikeeva LI, Kazakova VA, Andreev SI, Sapozhnikov DA, Roshchina IA, Kogarko LN (2008) Trace element and PGE distributionin layered ferromanganese crusts. Geochem Int 46(12):1179–1205

Baturin GN, Yushina IG (2007) Rare earth elements in phosphate-ferromanganese crusts on Pacific seamounts. Lithol Min Resour 42(2):101–117

Berann HC, Heezen BC, Tharp M (1977) Manuscript painting of Heezen-Tharp "World ocean floor" map by Berann. Library of Congress. https://www.loc.gov/item/2010586277/

Byrne RH, Kim KH (1990) Rare element scavenging in seawater. Geochim Cosmochim Acta 54:2645–2656

Elderfield H, Greaves MJ (1982) The rare earth elements in seawater. Nature 296:214–219

GEOSECS (1975) The Geochemical Ocean Section Study: a program for the International Decade of Ocean Exploration: 1975. National Science Foundation (U.S.)

Glasby GP (2006) Manganese: predominant role of nodules and crusts. In: Schulz HD, Zabel M (eds) Marine geochemistry. Springer, Berlin, pp 371–427

Glasby GP, Schulz HD (1999) EH, pH diagrams for Mn, Fe, Co, Ni, Cu and As under seawater conditions: application of two new types of EH, pH diagrams to the study of specific problems in marine geochemistry. Aquatic Geochem 5:227–248

Halbach P (1986) Processes controlling the heavy metal distribution in Pacific ferromanganese nodules and crusts. Geol Rundsch 75:235–247

Halbach P, Jahn A (2016) Concentrations and metal potentials of REEs in marine polymetallic nodule and Co-rich crust deposits. In: Abramowski T (ed) Deep sea mining value chain: organization, technology and development. IOM, Szczecin, pp 119–132

Halbach P, Manheim FT (1984) Potential of cobalt and other metals in ferromanganese crusts on seamounts of the Central Pacific Basin. Mar Mining 4(4):319–336

Halbach P, Marbler H (2009) Marine ferromanganese crusts: contents, distribution and enrichment of strategic minor and trace elements. BGR-Report, Hannover, Project No: 211-4500042565, pp 1–73

Halbach P, Puteanus D (1984) The influence of the carbonate dissolution rate on the growth and composition of Co-rich ferromanganese crusts from Central Pacific seamount areas. Earth Planet Sci Lett 68:73–87

Halbach P, Özkara M, Hense J (1975) The influence of metal content on the physical and mineralogical properties of pelagic manganese nodules. Miner Deposita 10:397–411

Halbach P, Giovanoli R, von Borstel D (1982) Geochemical processes controlling the relationship between Co, Mn, and Fe in early diagenetic deep-sea nodules. Earth Planet Sci Lett 60(2):226–236

Halbach P, Segl M, Puteanus D, Mangini A (1983) Co-fluxes and growth rates in ferromanganese deposits from Central Pacific seamount areas. Nature 304:716–719

Halbach P, Kriete C, Prause B, Puteanus D (1989) Mechanisms to explain the platinum concentration in ferromanganese seamount crusts. Chem Geol 76(1–2):95–106

Halbach P, Schwarz-Schampera U, Marbler H (2008) Platinum and some other trace metals in ferromanganese crusts-geochemical models to explain contradictions. In: UMI 2008, marine minerals: technological solutions and environmental challenges, conference abstracts, Oxford, MS, USA, 6 pages

Halbach P, Jahn A, Lucka M (2009) Geochemical–mineralogical investigations about the distribution, the interelement relationships and the bonding processes of economically important minor and trace metals in marine ferromanganese crusts (Marine Ferromanganese Crusts II). BGR-project No. 207-4500051248, pp 1–63

Halbach P, Jahn A, Lucka M, Post J (2010) Vorkommen von kobaltreichen Manganerzkrusten an Seebergen und technische Konzeption für das Ablösen vom Untergrund, CoCrusts Modul B. Bundesanstalt für Geowissenschaften und Rohstoffe, project number: 201-4500052339, pp 1–108

Halbach P, Schneider S, Jahn A, Cherkashov G (2013) The potential of rare-earth elements in oxidic deep-sea mineral deposits (ferromanganese nodules and crusts). In: Martens PN (Hrsg.) Mineral resources and mine development. Verlag Glückauf GmbH, Essen, pp 161–174

Halbach P, Abram A, Jahn A (2014) Louisville Project Study Report, Geoscientific Report for Bundesanstalt für Geowissenschaften und Rohstoffe (BGR), Hannover, Germany, BGR-Project No.: 204-10061918, pp 1–116

Hein JR, Koschinsky A, Halliday AN (2003) Global occurrence of tellurium-rich ferromanganese crusts and a model for the enrichment of tellurium. Geochim Cosmochim Acta 67(6):1117–1127

Hein JR, Koschinsky A (2013) Deep-ocean ferromanganese crusts and nodules. In: Scott S (ed) Treatise on geochemistry, vol 13, 2nd edn, Chapter 11, pp 273–291

Hein JR, Yeh HW, Gunn SH, Sliter WV, Benninger LM, Wang C-H (1993) Two major Cenozoic episodes of phosphogenesis recorded in equatorial Pacific seamount deposits. Paleoceanography 8:293–311

Hein JR, Koschinsky A, Bau M, Manheim FT, Kang J-K, Roberts L (2000) Cobalt-rich ferromanganese crusts in the Pacific. In: Cronan DS (ed) Handbook of marine mineral deposits. CRC Press, London, pp 239–279

Hein JR, Conrad TA, Dunham RE (2009) Seamount characteristics and mine-site model applied to exploration- and mining-lease-block selection for cobalt-rich ferromanganese crusts. Mar Georesour Geotechnol 27:160–176

Hein JR, Conrad T, Mizell K, Banakar VK, Frey FA, Sager WW (2016) Controls on ferromanganese crust composition and reconnaissance resource potential, Ninetyeast Ridge, Indian Ocean. Deep Sea Res I 110:1–19

ISA (2006) Exploration and mine site model applied to block selection for cobalt-rich ferromanganese crusts and polymetallic sulphides. International Seabed Authority, ISBA/12/C/3, Kingston, Jamaica, pp 1–14

ISA (2010) A geological model of polymetallic nodule deposits in the Clarion Clipperton Fracture Zone, Technical study no. 6. International Seabed Authority, Kingston, Jamaica, pp 1–211

Kennett JP (1982) Marine geology. Prentice Hall, Inc, London, pp 1–813

Klemm V, Levasseur S, Frank M, Hein JR, Halliday AN (2005) Osmium isotope stratigraphy of a marine ferromanganese crust. Earth Planet Sci Lett 238:42–48

Koschinsky A, Halbach P (1995) Sequential leaching of ferromanganese precipitates: genetic implications. Geochim Cosmochim Acta 59(24):5113–5132

Koschinsky A, van Gerven M, Halbach P (1995) First investigations of massive ferromanganese crusts in the NE Atlantic in comparison with hydrogenetic Pacific occurrences. Mar Georesour Geotechnol 13(4):375–391

Koschinsky A, Stascheit A, Bau M, Halbach P (1997) Effects of phosphatization on the geochemical and mineralogical composition of marine ferromanganese crusts. Geochim Cosmochim Acta 61(19):4079–4094

Li JS, Fang NQ, Qu WJ, Ding X, Gao LF, Wu CH, Zhang ZG (2008) Os isotope dating and growth hiatuses of Co-rich crust from central Pacific. Sci China Ser D Earth Sci 51(10):1452–1459

Maeno MY, Ohashi H, Yonezu K, Miyazaki A, Okaue Y, Watanabe K, Ishida K, Tokunaga M, Yokoyama T (2016) Sorption behavior of the Pt(II) complex anion on manganese dioxide (δ-MnO2): a model reaction to elucidate the mechanism by which Pt is concentrated into a marine ferromanganese crust. Miner Deposita 51:211–218

Marino E, Gonzales FJ, Somoza L, Lunar R, Ortega L, Vazquez JT, Reyes J, Bellido E (2016) Strategic metals, rare earths and platinum group elements in Mesozoic-Cenozoic cobalt-rich ferromanganese crusts from long-lived seamounts in the Canary Island Seamount Province (NE Central Atlantic). Ore Geol Rev

McLennon SM (2001) Relationship between the trace element composition of sedimentary rocks and upper continental crust. Geochem Geophys Geosyst 2:1–24

Nozaki Y (1997) A fresh look at element distribution in the North Pacific. Eos 78(21):221–222

Ohta A, Kawabe I (2000) REE(III) adsorption onto Mn dioxide (δ-MnO2) and Fe oxyhydroxide: Ce(III) oxidation by δ-MnO2. Geochim Cosmochim Acta 65(5):695–703

Perritt S, Watkeys MK (2007) The effect of enviromental controls on the metal content in ferromanganese crusts and nodules from the Mozambique Ridge and in the Mozambique Basin, Southwestern Indian Ocean. South Afr J Geol 110:295–310

Piper DZ, Bau M (2013) Normalized rare earth elements in water, sediments, and wine: identifying sources and environmental redox conditions. Am J Anal Chem 4:69–83

Pulyaeva IA, Hein JR (2011) Hydrogenetic Fe-Mn crusts from the atlantic and pacific oceans: geological evolution and conditions of formation. Marine minerals: recent innovations in technology. UMI, Hawaii, 11 pages

Rajani RP, Banakar VK, Parthiban G, Mudholkar AV, Chodankar AR (2005) Compositional variation and genesis of ferromanganese crusts of the Afanasiy Nikitin Seamount, Equatorial Indian Ocean. J Earth Syst Sci 114(1):51–61

Schirmer T, Koschinsky A, Bau M, Marbler H, Hein JR, Savard D (2008) Te–Se systematics of marine iron manganese crusts and nodules. Unpublished report

Seibold E, Berger WH (1993) The sea floor – an introduction to marine geology, Springer, Berlin, pp 1–356

Stüben D, Glasby GB, Eckhardt JD, Berner Z, Mountain BW, Usui A (1999) Enrichments of platinum-group elements in hydrogenous, diagenetic and hydrothermal marine manganese and iron deposits. Explor Min Geol 8(3–4):233–250

Stumm W, Morgan JJ (1995) Aquatic chemistry: chemical equilibria and rates in natural waters, 3rd edn. Wiley-Interscience, pp 1–1040

Taylor SR (1964) Trace element abundances and the chondrite Earth model. Geochim Cosmochim Acta 28(12):1989–1998

USGS (1980) Geological survey circular 831. Publications of the geological survey, 1962-1970, Permanent Catalog, U.S. Geological Survey, Federal Center, Denver, pp 1–5

USGS (2016) Mineral commodity summaries. http://minerals.usgs.gov/minerals/pubs/mcs/

USGS KORDI Open File Report 90-407 (1990) Geological, geochemical, geophysical, and oceanographic data and interpretations of seamounts and Co-rich ferromanganese crusts from the Marshall Islands, USGS-KORDI R.V. FARNELLA cruise F10-89-CP. U.S. Geological Survey, pp 1–246

Vonderhaar DL, Garbe-Schönberg D, Stüben D, Esser BK (2000) Platinum and other related element enrichment in Pacific ferromanganese crust deposits. Spec Publ SEPM 66:287–308

Wedepohl KH (1969) Handbook of geochemistry, vol 1. Springer, Berlin, pp 1–442

Wessel P (2001) Global distribution of seamounts inferred from gridded Geosat/ERS-1 altimetry. J Geophys Res 106 (B9)(19):431–419, 441

Wessel P, Sandwell DT, Kim S-S (2010) The global seamount census. Oceanography 23(1):24–33

Prof. Peter Halbach (Dr.-Ing., Dr. habil, Dr. h.c.) was Dean of the Department of Geoscience at the Technical University of Clausthal, full professorship in 1988 and Director of the Center for Marine Raw Materials Research (1990–1992); 1992–2005 full professor at the Free University of Berlin (Chair for Economic and Environmental Geology). Prof. Halbach has more than 150 scientific publications, was leader of many international marine projects and research cruises. In 2001, he was awarded the Moore Medal from the IMMS. At present, he is the chairman of the Advisory Board of the Deep-Sea Mining Alliance (DSMA, Germany). Prof. Halbach is presently still active in scientific research and advising.

Andreas Jahn has more than a decade of experience in the field of geologic investigation with a particular specialization in marine mineral exploration and deposit assessment (manganese nodules, ferromanganese crusts, and seafloor massive sulfides). In close collaboration with Prof. Halbach, he was consultant to various companies and institutions including the German BGR and the ISA. Within this scope, he participated in the publication of numerous advisory reports regarding the delineation, evaluation, and the economic realization of exploitation of different kinds of marine mineral deposits. Andreas Jahn holds an MSc in geology from the Free University Berlin (Germany).

Georgy Cherkashov is Deputy Director of the Institute for Geology and Mineral Resources of the Ocean (VNIIOkeangeologia, St. Petersburg, Russia) of the Ministry of Natural Resources (since 1996). He holds a Dr. Sci. for research of seafloor massive sulfide (SMS) deposits of the Mid-Atlantic Ridge. He has been the Chief Scientist of 13 ocean-going Russian and international expeditions for prospecting of SMS deposits in the Pacific, Atlantic, and Indian Oceans (1983–2007). He was also the President of International Marine Minerals Society (2011–2012), member of the Legal and Technical Commission of the International Seabed Authority (since 2012), and is part-time Professor at St. Petersburg State University (Marine Geology) (since 2005).

Chapter 4
Seafloor Massive Sulfide Deposits: Distribution and Prospecting

Georgy Cherkashov

Abstract Discovery of hydrothermal vents and seafloor massive sulfides (SMS) that contain metals of economic importance due to their high concentrations has generated significant interest among researchers as well as entrepreneurs as an alternative source that can be mined in future. This chapter provides a brief historical review of hydrothermal systems, the distribution, geological setting, morphology, composition, and age as well as formation and source of metals in SMS deposits. The chapter also looks at the criteria for recognition and exploration technologies for SMS deposits.

4.1 Introduction

Seafloor massive sulfide (SMS) deposits present the third (and last discovered) type of a short list of deep-sea minerals after ferromanganese nodules and cobalt-rich ferromanganese crusts. The discovery of hydrothermal vents and associated massive sulfides in the end of 1970s was recognized as one of the main events in marine science in the twentieth century. This discovery had not only fundamental but also economic importance due to extraordinary concentrations of metals being discharged from hot vents to the sea bottom. It was confirmed that mid-ocean spreading ridges and arc systems where SMS deposits are accumulated, along with deep-sea basins and seamounts that are hosts of fields of nodules and crusts, have comparable resources with continental metallogenic potential.

Seafloor massive sulfides are considered as modern analogues of land-based volcanogenic massive sulfide (VMS) deposits which were formed over the entire history of our planet evolution from the Archean to the Cenozoic (Hannington et al. 2005; Franklin et al. 2005). VMS provided more than half of the past global production of zinc and lead, 7% of the copper, 18% of the silver, and a significant amount of gold and other by-product metals (Singer 1995). Taking into account relatively short period of geological history for modern SMS accumulation the estimated

G. Cherkashov (✉)
Institute for Geology and Mineral Resources of the Ocean (VNIIOkeangeologia), Institute of Earth Sciences, St Petersburg State University, St. Petersburg, Russia
e-mail: gcherkashov@gmail.com

R. Sharma (ed.), *Deep-Sea Mining*, DOI 10.1007/978-3-319-52557-0_4

resources are not as huge as VMS, nevertheless they are considered as the real source of metals for long-term development of global economy. Also, the technologies for future mining are in process of being designed and methods of metals extraction from SMS already exist being similar to that of VMS.

4.2 Historical Review of Hydrothermal Systems and SMS Deposits Study

The discovery and study of hydrothermal vents and seafloor massive sulfides has a long history of expeditionary researches and theoretical predictions. The initial findings related to the indicators of hydrothermal activity in the near-bottom waters and bottom sediments were hydrothermal plumes and metalliferous sediments.

Anomalies of temperature and salinity in the near-bottom waters were first recorded in the late nineteenth century in the expedition on the Russian vessel "Vityaz" (1886–1889) in the Red Sea. However, this discovery as well as similar data obtained during cruise on the RV "Albatross" (Sweden) from the Red Sea half a century later (1948) was not noticed by the scientific community.

The first samples of metalliferous sediments were recovered from the ocean floor during the famous expedition of the HMS "Challenger" (1873–1876). Sediments characterized by high iron and low aluminum content were dredged near the East Pacific Rise (EPR). Such unusual deposits were collected again in the 1940s on the USS "Carnegie" (Revelle 1944). However, these data did not get an explanation and was overlooked.

Here, the theory of continental drift by Alfred Wegener, published in 1915, should be mentioned revolutionary in its novelty as the discovery of oceanic hydrothermal systems was an excellent proof of the plate tectonics theory.

Only in the 1960s, Skornyakova (1964) and Boström and Peterson (1966), as well as Bonatti and Joensuu (1966) published papers in which the accumulation of metalliferous sediments and crusts enriched in iron and manganese hydroxides was determined and related to hydrothermal activity. For the first time ancient metalliferous sediments were collected during Leg 2 of the Deep Sea Drilling Project (DSDP) in the basal layer of the sedimentary cover of the Atlantic seabed (Peterson et al. 1970).

Large-scale oceanographic researches in the framework of the International Indian Ocean Expedition (1963–1965) on Research Vessels Discovery, Chain, Atlantis-II and Meteor held in the Red Sea led to the discovery of metalliferous muds in numerous deeps (Miller et al. 1966). It was also found that some deeps contain hot brines up to 180 m thick (Degens and Ross 1969). The explanation for this phenomenon, associated with the dissolution of salt-bearing strata exposed on the rift slopes, was given later (Bäcker 1982).

High-temperature disseminated sulfide mineralization represented by iron and copper sulfides has been detected in the volcanic rock samples dredged from the mid-ocean ridges starting from 1967 (Baturin and Rozanova 1972).

At the same time increasing number of data indicating the presence of unknown sources of energy and metals in the ocean allowed to formulate theoretical background to the discovery of oceanic hydrothermal systems. Sillitoe (1972) suggested the presence of similar complexes in the modern ocean to the ancient ophiolites, which are composed of rocks occurring on the seabed and associated pyrite ores. The idea of the fluid circulation in the oceanic rocks proposed on the basis of differences in the values of the theoretically calculated and the actually observed heat flux in the ocean was suggested by Wolery and Sleep (1976).

Subsequently, more information and new data have been collected. The new sea technology and particularly deep-towed systems and submersibles played key role in the research. In 1976, Kathleen Crane from the Scripps Oceanographic Institute using Deep Tow system got an image of large white clams on black basalts at a depth of 2500 m on the Galapagos ridge. The temperature anomaly of up to 2.5 °C was also observed. Seeps of warm fluids (17 °C) discharging through cracks in the basalt lavas were recorded in the same area in 1977. This seepage zones in basalts were marked by clusters of clams and tubeworms that were later defined as representatives of a special «hydrothermal» fauna (Corliss et al. 1979).

The first sample of the massive sulfide was recovered in 1978 at the 21°N EPR during the international expedition CYAMEX (France, USA, and Mexico) by French submersible Cyana (Cyamex 1978; Francheteau et al. 1979). The presence of sulfide minerals was detected only after the land-based laboratory analysis. Subsequently during the expedition in the following year in the same area with Alvin submersible, the first images of *black smoke* from sulfide chimney standing on a basalt base was recorded with measured temperatures of the discharged fluids being as high as 350 °C (Spiess et al. 1980). Unique biological chemosynthetic communities associated with these hot vents added to the importance of *black smokers* discovery.

The process of the new hydrothermal vents discovery was very dynamic and the initial 5 years all these discoveries were concentrated in the Pacific—at the Galapagos ridge, the northern and southern part of the EPR, and ridges in the north-east Pacific (Gorda, Juan de Fuca, and Explorer). In other oceans, smokers were not found. It was proposed that the hydrothermal system might be formed only in intermediate- and fast-spreading ridges, which included ridges of the Pacific with the full spreading rate between 6 and 18 cm/year. However, the first hydrothermal field was discovered in 1985 at the Mid-Atlantic ridge (MAR) with the spreading rate of less than 4 cm/year. Thus, slow- and ultraslow-spreading ridges which accounts for about 60% of the total length of the mid-ocean ridges (Hannington et al. 2010) have been recognized as promising areas for hydrothermal systems and SMS deposits occurrences as well. The hydrothermal field at the 26°08′N of the MAR was called the TAG as discovered during the project of **T**rans-**A**tlantic **G**eotraverse project (Rona et al. 1986). It was observed that the hydrothermal mound in such a field can attain a size as large as 200 m in diameter and 50–60 m in height. Later it was proved that such large sizes of SMS deposits are specific to the slow-spreading ridges setting.

Other findings of fundamental importance were the discovery of hydrothermal chimneys in the subduction-related volcanic arc systems (Booth et al. 1986). After following several discoveries in arc and back-arc settings (Tonga-Kermadec, Izu-Bonin, Mariana, Manus basin), the connection between hydrothermal systems and convergent zones of oceanic plates has been established (Ishibashi and Urabe 1995; Binns and Scott 1993). Thus, two basic geological settings of hydrothermal systems associated with the boundaries of lithospheric plates have been identified: divergent (the system of mid-ocean ridges) and convergent (the system of island arcs).

Analyses of the samples of massive sulfides testified that a new type of marine minerals, which contains high concentrations of copper, zinc, lead, gold, silver, and rare metals such as cobalt, cadmium, molybdenum, indium, tellurium, selenium, bismuth, and germanium, were discovered.

The detailed history of SMS exploration since the discovery of the first black smokers on the East Pacific Rise can be followed in reviews by Rona and Scott (1993), Lowell et al. (1995), and Ishibashi and Urabe (1995).

4.3 Distribution and Geological Setting of SMS Deposits

The distribution of hydrothermal systems and seafloor massive sulfides has global character (Fig. 4.1). Currently, the number of known sites of hydrothermal activity is close to 500, and it is estimated that the number could increase by three times

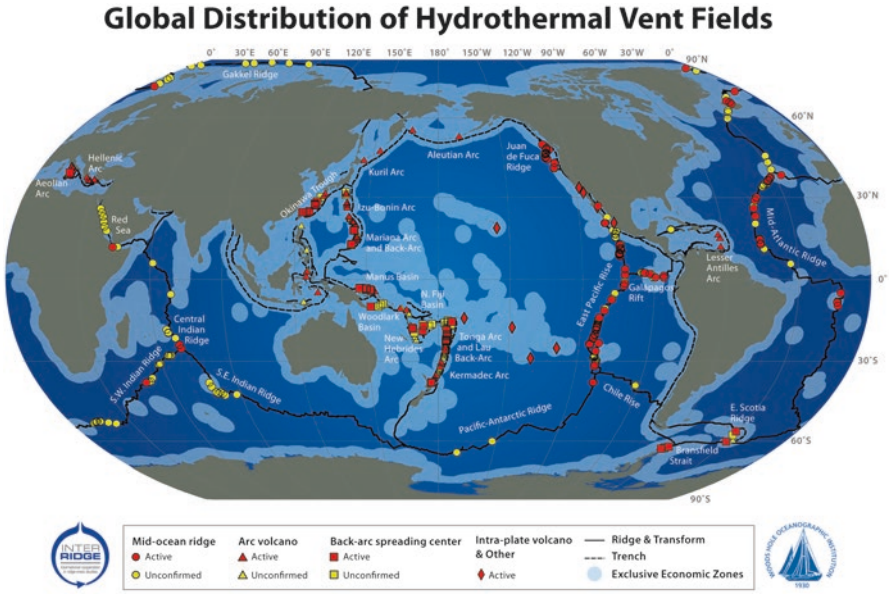

Fig. 4.1 Global distribution of hydrothermal systems (from InterRidge at http:/www.interridge.org/irvents/)

(Beaulieu et al. 2015). Another estimates of the abundance and distribution of known sulfide deposits in well-studied areas indicate that between 1000 and 5000 large sulfide deposits may exist on the modern seafloor (Petersen et al. 2016). "Geopolitical" statistics shows that from the area that should be explored for SMS deposits, 58% is located beyond the national jurisdiction, 36% within EEZs, and 6% are included in proposals for extensions of continental shelf by different countries (Petersen et al. 2016).

A wide variety ("geodiversity") is typical for SMS deposits related to different geological settings (German 2008; Fouquet et al. 2010). Two global structures—Mid-Ocean Ridges (MOR) and Island Arc Systems (IAS)—could be considered as a first level of geodiversity. Two-thirds of hydrothermal systems are connected with Mid-Ocean Ridges and one-third with Island Arc System, which directly correlates with the length of MOR and IAS (66,000 km and 22,000 km, respectively).

Mid-ocean ridges are characterized by different spreading rates, varying from 1 to 18 cm/year (full rate):

- Ultrafast >12.0 cm/year
- Fast 8.0–12.0 cm/year
- Intermediate 4–8 cm/year
- Slow 2.0–4.0 cm/year
- Ultraslow <2.0 cm/year

The ridges with different spreading rate vary in morphology, segmentation and mode of accretion, as well as geophysical and geochemical characteristics. Variety of hydrothermal deposits (both in terms of the size and composition) of different spreading ridges are considered as the second level of geodiversity of MOR system. In turn, hydrothermal systems in arc environments, the settings in which the majority of ancient VMS districts are thought to have formed (Franklin et al. 2005), are also subdivided on this level. Among them are SMS deposits related to frontal arc volcanoes, arc-related rifts, and back-arc spreading centers. Transitional arc volcanoes and volcanoes in continental margin arcs can also host significant seafloor massive sulfide deposits (Monecke et al. 2014).

Initially the first hydrothermal vents were discovered in the mid-ocean ridge of the East Pacific Rise and maximum number of hydrothermal fields are situated on this global structure. There is a clear link between the frequency of occurrence of vents and their spreading rates, which determines the intensity of magmatic processes. Thus, the magmatic control determines the formation and intensity of hydrothermal processes in a fast- and intermediate-spreading ridges. Another situation occurs in the ranges of conditions characterized by slow- and ultraslow-spreading centers. In this case, the main importance is the tectonic factor.

As a result, there are two types of hydrothermal systems within the mid-ocean ridges, which differ in a number of parameters, the main of which is a resource potential of SMS deposits (Table. 4.1).

The estimates of SMS tonnage within ridges of different spreading rates (Hannington et al. 2010, 2011; Beaulieu et al. 2015; German et al. 2016) show the higher resource potential of slow- and ultraslow ridges comparable with fast- and intermediate ones (Fig. 4.2).

Table 4.1 Geological setting and parameters of SMS deposits at the East Pacific Rise (EPR) and at the Mid-Atlantic Ridge (MAR)

Parameters		EPR	MAR
Tectonics/magmatism			
Spreading (mm/year)		6–16	<2–4
Host rocks		Basalts	Basalts, Gabbro-peridotites
Ore-control structures		Central graben, off-axial smts	AVR, OCC
SMS deposits			
Age of SMS (years)		$n \times 10^0$–$n \times 10^3$	$n \times 10^0$–$n \times 10^5$
Av. size of single mound (m)		$n \times 10^0$	$n \times 10^0$–$n \times 10^2$
Av. size of cluster mounds (m)		$n \times 10^1$	$n \times 10^1$–$n \times 10^3$
Distance between hydrothermal fields (km)		$n \times 10^0$–10^1	$n \times 10^1$–$n \times 10^2$
Estimated resources (t)		$n \times 10^1$–$n \times 10^3$	$n \times 10^3$–$n \times 10^6$
Metals	Cu/Zn	Lower	Higher
	Au	Lower	Higher

AVR axial volcanic ridge, *OCC* oceanic core complex

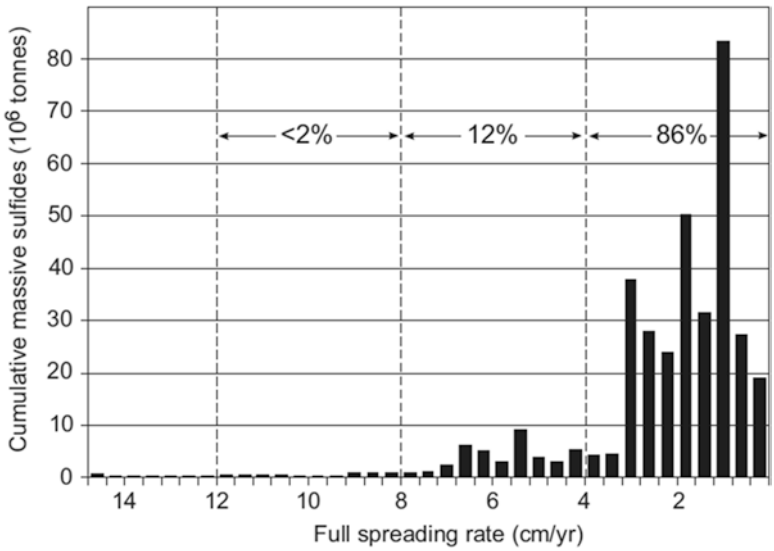

Fig. 4.2 Expected distribution of seafloor massive sulfide deposits on the mid-ocean ridges as a function of spreading rate (German et al. 2016)

Apparent contradiction between frequency and resource potential of SMS in different spreading rate ridges could be explained by combination of small size but numerous amount ore accumulations within fast- and intermediate-spreading ridges.

The next level of geodiversity is connected with variety of the SMS deposits related to ridges with different spreading rates. The most contrasting diversity could

Table 4.2 Geological setting of SMS deposits at the northern equatorial MAR

Structural setting				
Mode of accretion				
Symmetrical			Asymmetrical	
Setting in the rift zone				
Axial		Off-axial		
Association with OCC/detachments				
Not associated			Associated	
			Hanging wall	Footwall
Hosted rocks				
Basalts				Gabbro-peridotites
E-MORB	N-MORB			
Menez Gwen	*Puis des Folles*	*Krasnov*	*Semenov*	
Lucky Strike	*Snake Pit*	*Peterburgskoye*	*Ashadze-4*	*Ashadze-1, 2*
	Broken Spur	*Zenith-Victory*	*TAG*	*Irinovskoye*
	Squid Forest	*Yubileynoye*		*Logatchev*
		Surprize		*Pobeda*
				24° 30′ N
				Rainbow

be observed at the slow-spreading ridges. Based on the mode of accretion and type of hosted rocks, two geological settings of SMS deposits at slow-spreading ridges could be divided: symmetrical mode of accretion with basalts and asymmetrical accretion with gabbro-peridotites (Escartin et al. 2008). The same division of the MAR as a typical slow-spreading ridge is described as "magmatic" (with domination of volcanic processes) and "tectonic" segments where magmatism is reduced and tectonism is dominant (German et al. 2016). Half of the SMS deposits at the Northern Equatorial part of the MAR are associated with basalts at magmatic segments and another half with lower crust and mantle rocks (gabbro-peridotites) of the oceanic core complex (OCC) at tectonic segments (Table 4.2). OCC is tectonically uplifted along detachment faults, which exhume from the footwall deep-seated gabbro-peridotite rocks onto the seafloor and may provide pathways for hydrothermal fluids (Smith et al. 2006; MacLeod et al. 2009; Tivey et al. 2003; McCaig et al. 2007). Basalt-hosted deposits can be located in the axial part of the rift valley; in this case, they are often confined to neovolcanic zones (axial volcanic ridge)—the youngest manifestations of basaltic volcanism. The basalt-hosted deposits could also be located at off-axis setting associated with slopes of the rift valley or tops of the rift mountains. This setting is typical for ultramafic-hosted deposits as well. The last level of geodiversity within slow-spreading ridges is based on the association of SMS deposits with footwall or hanging wall of detachment faults at the tectonic segments of the ridge (Table 4.2).

4.4 Morphology of SMS Deposits

Morphology of SMS deposits depends on the stage of hydrothermal system evolution and varies in different geological settings. Individual active and/or inactive black smokers/chimneys are typical for the initial (immature) stage of SMS deposit formation and have height from few centimeters up to 45 m (Petersen et al. 2016) (Figs. 4.3 and 4.4)

A typical young (up to few thousand years) basalt-hosted active vent field at the Endeavor segment of the intermediate-spreading Juan de Fuca Ridge has been described as follows: "the active vent fields are characterized by steep-sided sulfide edifices that commonly rise several tens of meters above the seafloor and can each contain multiple active points of high-temperature discharge" (Jamieson et al. 2014) (Fig. 4.5).

"Forest-like" chimney accumulations with numerous (up to ten) 30–40 cm high edifices per 1 m^2 have been observed at ultramafic basement of slow-spreading Mid-Atlantic Ridge (Firstova et al. 2016) (Fig. 4.6). This hydrothermal field (Ashadze-1) is also rather young (7.2 ka) but has different way of occurrence comparable with the same age deposits associated with basalts. Besides smokers, another type of individual hydrothermal edifices—beehive-like diffusers—have been observed at the TAG and other hydrothermal fields (Fig. 4.7).

Over a period of time, chimneys collapse and the sulfide debris accumulates as a mound. The mound-like structures with apron of disintegrated chimneys are widely

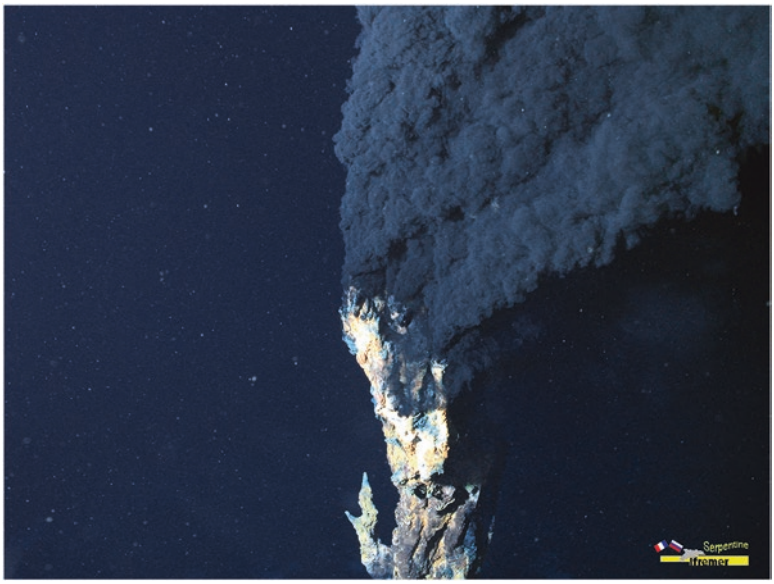

Fig. 4.3 Black smoker at the Ashadze-1 hydrothermal field. Photo by ROV Victor in French–Russian expedition Serpentine (2007). Copyright IFREMER

Fig. 4.4 Inactive chimney from the Mid-Atlantic Ridge (Photo V. Malin)

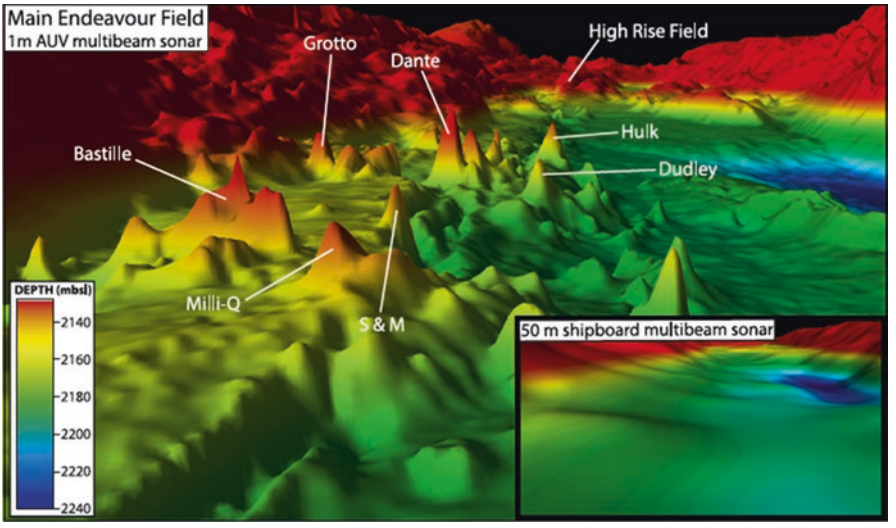

Fig. 4.5 3-D image of the Endeavor Segment of the Juan de Fuca Ridge with sulfide edifices. Bathymetric data were generated from multibeam sonar collected with MBARI AUV D. Allan B and gridded at 1 m. Inset image is of the same scene using shipboard multibeam data gridded at 50 m. At this resolution, sulfide edifices at Endeavor cannot be resolved (Jamieson et al. 2014)

Fig. 4.6 Cluster of small chimneys at the ultramafic-hosted Ashadze-1 deposit (MAR). Chimneys are in different degrees of oxidization. White actinias indicate present-day hydrothermal activity. Photo made by ROV Victor in French–Russian expedition Serpentine (2007). Copyright IFREMER

Fig. 4.7 White smoker (*left*) and diffuser (*right*). Manus Basin. Southwest Pacific (Photo P. Halbach)

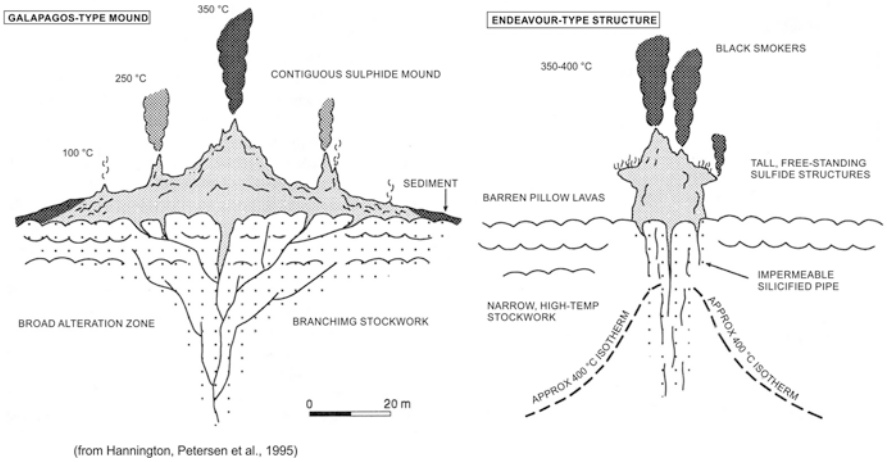

Fig. 4.8 Morphology of seafloor massive sulfides in the Pacific ocean (Hannington et al. 1995)

distributed (Fig. 4.8). They have been observed at the Galapagos Ridge, Juan de Fuca Ridge (the Zephyr Mound with a diameter of ~90 m and a height of 26 m is the largest single sulfide accumulation so far discovered along the Endeavor Segment (Jamieson et al. 2013)), and at many other sites. But the largest basalt-hosted mounds were discovered at the TAG hydrothermal area where Active and Mir Mounds reach 200 m in diameter and 40–50 m in height.

The large size of these mounds could be explained by long-term process of their formation —up to 50 thousand years (Lalou et al. 1995), which is typical for slow-spreading ridges. A huge mound-like structures are also formed in another geological setting, i.e., within sediment-filled rift valley. Mounds up to 300 m in diameter and 50 m in height are formed where sediments allow for efficient trapping of the metals due to metal precipitation below the seafloor (as in Middle Valley and Okinawa Trough) (Zierenberg et al. 1998; Takai et al. 2012).

The final transformation of SMS accumulation is represented by coalescence mounds and products of their destruction. Morphology of SMS deposit on the matured stage of evolution could be illustrated by Solwara-1 hydrothermal field located in the Bismark Sea (Southwest Pacific). The 3-D image of this best studied ore body prepared for mining operations has been designed based on high-resolution near-bottom bathymetry and EM profiling (Fig. 4.9).

As for basaltic hosted hydrothermal fields, the morphology of ultramafic-hosted sulfide deposits is controlled by several local factors such as depth, phase separation, hydraulic fracturing, and permeability (Fouquet 1997). In ultramafic environments, the discharge is clearly less focused than at basaltic sites. This “diffuse” discharge through more permeable hydrothermally altered ultramafics produces relatively flat deposits without clearly organized mounds. The latter are quite different from basaltic environments where conical mounds are typically formed (Fig. 4.10). In addition,

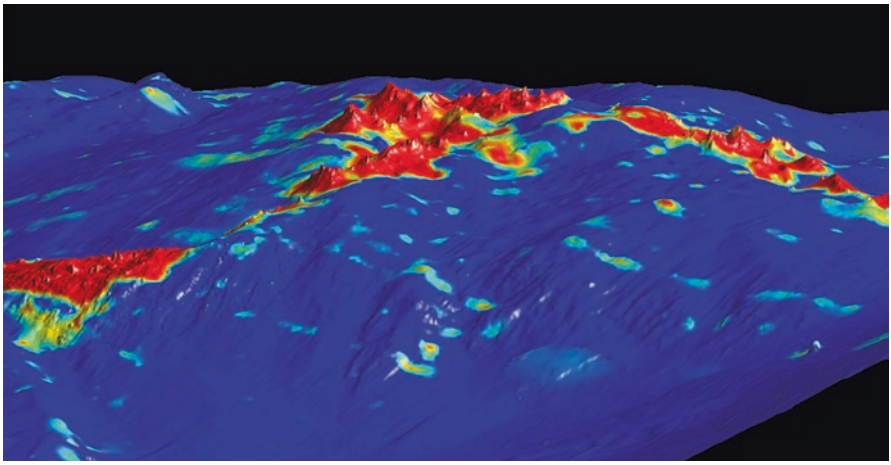

Fig. 4.9 3-D image of Solwara-1 SMS deposit (Lipton 2012)

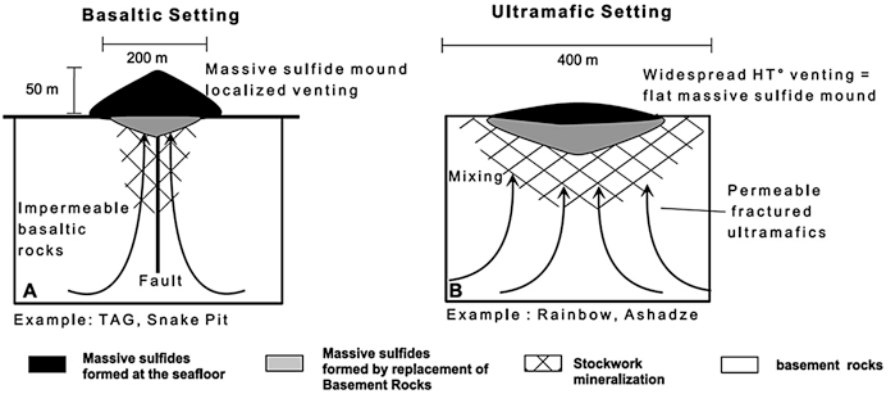

Fig. 4.10 Differences in the morphology of deposits and type of discharge between basaltic and ultramafic hydrothermal deposits. Compared to (**a**) basaltic hosted fields, discharge is less focused in (**b**) ultramafic environments, and no real mound is formed; part of the deposit may occur as replacement of the ultramafic rocks (Fouquet et al. 2010)

pervasive near-surface high-temperature circulation generates highly altered areas and enhances subsurface sulfide precipitation, large stockwork mineralization, and completes replacement of the ultramafic rocks by massive sulfides (Fouquet et al. 2010).

One more specific SMS structure found in ultramafic environment at the MAR is "smoking crater" 20–25 m wide and 1–3 m deep with small black smokers on the rim and at the bottom of the crater (Bogdanov et al. 1997; Koschinsky et al. 2006; Fouquet et al. 2008; Petersen et al. 2009). It was suggested that crater shape structure was formed as a result of explosive event due to overpressure conditions inside of the hydrothermal «protomound» (Fouquet et al. 2008, 2010).

4.5 Composition and Aging of SMS Deposits

The composition of hydrothermal sulfide deposits can vary considerably according to the geodynamic environment, the nature of basement rocks affected by hydrothermal circulation, the water depth, the phase separation processes, and the maturity of deposits (Fouquet and Lacroix 2014).

The major minerals forming SMS deposits include iron sulfides, such as pyrite and marcasite, as well as the minerals of the most economic interest—chalcopyrite (copper sulfide) and sphalerite (zinc sulfide). All other minerals of SMS deposits are considered as minor (by-product) ones. According to the name of deposits, most minerals are represented by sulfides but not only: for example, copper oxychloride (atacamite) is widely distributed in SMS deposits at the Mid-Atlantic ridge. The precious metals gold and silver mainly occur in native form. Minor and rare metals either form their own accessory minerals or occur as isomophous phase in another carrier mineral.

Genetically SMS minerals could have primary (generated directly from the hydrothermal fluid) or secondary (formed during alteration of the primary minerals) nature. The zonation of mounds and chimneys is temperature-dependent and involves the replacement of early relatively low-temperature zinc-rich assemblages may with higher temperature copper-rich assemblages. Weathering of SMS on the seabed results in the formation of secondary copper-rich sulfides. High- and low-temperature hydrothermal minerals are recognized as well. High-temperature sulfide minerals often associated with low-temperature precipitates which are predominantly represented by non-sulfide minerals: sulfates, carbonates, and silicates (Table 4.3).

High grade of copper and zinc (up to tens of percent), gold and silver (tens and hundreds of ppm, respectively) in comparison with VMS and other on-land deposits determines economic interest to SMS as a source of these metals. The rare elements—bismuth, cadmium, gallium, germanium, antimony, tellurium, thallium, and indium—which are critical for high-tech industry can significantly enrich some deposits, especially those that were formed at volcanic arcs.

The mean metal content of seafloor massive sulfide deposits with respect to their geological setting demonstrates big varieties (Table 4.4).

The deposits associated with relatively homogenous basalts (in particular on fast- and intermediate-spreading ridges) are enriched in zinc, silver, and selenium. SMS

Table 4.3 Minerals of hydrothermal precipitates

High temperature			Low temperature				
Sulfides			Oxyhydroxides				
Iron	Copper	Zinc	Iron	Manganese	Silica	Carbonates	Sulfates
Pyrite	Chalcopyrite	Sphalerite	Goethite	Todorokite	Quartz	Aragonite	Anhydrite
Marcasite	Bornite	Wurtzite	Hydrogoethite	Birnessite	Opal	Calcite	Barite
Pyrrhotite	Chalcosite		Hematite	Vernadite			
	Isocubanite		Amorphous				

Table 4.4 The mean metal content of seafloor massive sulfide deposits with respect to their tectonic setting

Setting	*N*	Cu,% (wt%)	Zn,% (wt%)	Pb,% (wt%)	Fe,% (wt%)	Au, ppm (ppm)	Ag, ppm (ppm)
Sediment-free MOR	51	4.5	8.3	0.2	27.0	1.3	94
Ultramafic-hosted MOR*	349	17.9	7.1	0.02	24.8	10.0	56
Sediment-hosted MOR	3	0.8	2.7	0.4	18.6	0.4	64
Intraoceanic back-arc	36	2.7	17.0	0.7	15.5	4.9	202
Transitional back-arcs	13	6.8	17.5	1.5	8.8	13.2	326
Intracontinental rifted arc	5	2.8	14.6	9.7	5.5	4.1	1260
Volcanic arcs	17	4.5	9.5	2.0	9.2	10.2	197

Source: GEOMAR and VNIIOkeangeologia* (Petersen et al. 2016 with additions)

deposits related to mantle rocks are characterized by high values of copper, gold, and cobalt. Sediment-hosted deposits have low concentrations of metals due to the dilution by non-ore material but sometimes are enriched in lead and arsenic. At volcanic arc systems, such as in the western Pacific, the source rocks (mainly andesites and rhyolites) are more variable in composition. It is directly reflected in the composition of the massive sulfides, which are often higher in copper, zinc, lead, silver, and gold.

Regarding geochemical associations, metals are connected with two major elements: copper and zinc. Cobalt, nickel, selenium, and indium are mainly associated with copper, whereas cadmium, lead, arsenic, silver, antimony, and germanium are associated with zinc. Gold shows more complex behavior and may be associated with either copper or zinc.

4.5.1 Age of SMS Deposits

Age of SMS occurrence and duration of ore formation are parameters which characterize maturity of hydrothermal system and determine the size of deposit. The age varies in wide interval: from the first years to hundreds of thousand years depending on the setting of deposit. Short-lived hydrothermal systems with the age up to first thousand years are typical for the fast- and intermediate-spreading ridges as well as for volcanic arc structures (de Ronde et al. 2011; Jamieson et al. 2013). The long-lived systems (tens and hundreds of thousand years) are related to the slow- and ultraslow-spreading centers (Cherkashov et al. 2010). The age of the oldest deposit at the Mid-Atlantic Ridge (Peterburgskoye) is estimated at ca 223 ka (Kuznetsov et al. 2015). The formation of SMS deposits is episodic: active and inactive periods alternate.

4.6 Formation and Source of Metals in SMS Deposits

Seafloor massive sulfide deposits are formed from the hot vents on the seabed as a result of the interaction of seawater with a heat source in the sub-seafloor. The general scheme of the hydrothermal system is given in Fig. 4.11.

It is assumed that the seawater changes its characteristics (especially temperature, redox potential, salinity, and metals content) in the course of the penetration through cracks and circulation in the subsurface of the seafloor. The heated seawater leaches out metals from the surrounding rocks. The chemical reactions that take place in this process result in a hot (up to 400 °C), acidic, reduced and enriched in dissolved metals and sulfur fluid. The hydrothermal circulation is initiated by near-surface magma chamber. Thus, the first prerequisite of hydrothermal circulation and SMS deposit formation is the existence of the heat source.

The second necessary condition for fluid circulation is the increased permeability of seabed rocks provided by seismic/tectonic activity.

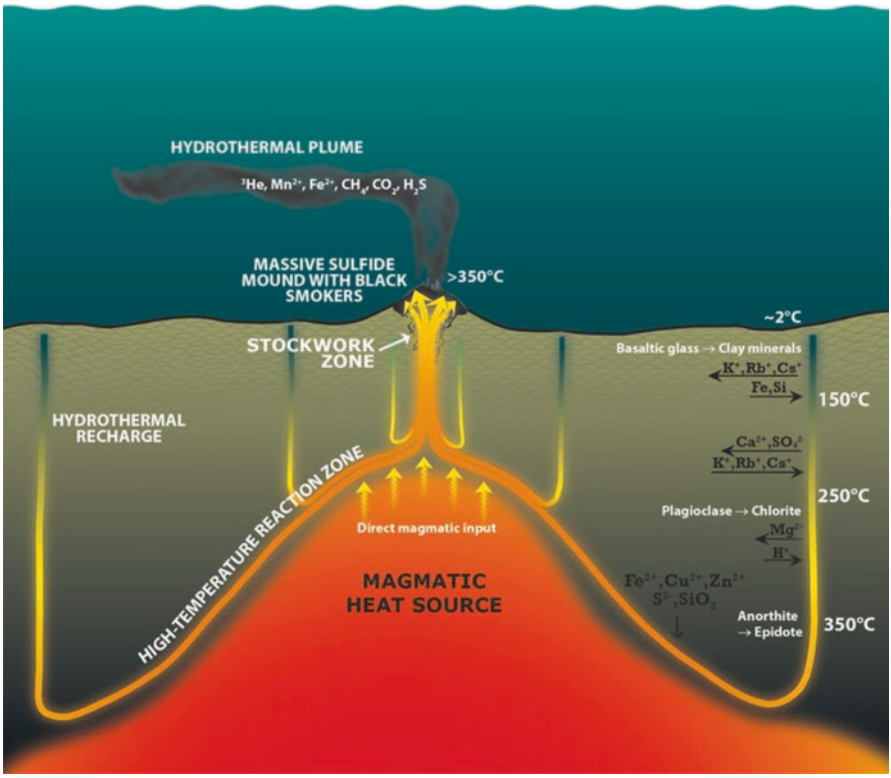

Fig. 4.11 General scheme of hydrothermal system (Jamieson et al. 2016)

These two conditions are realized on the borders of the lithospheric plates, where volcanic and tectonic activity is the most intensive at our planet. Thus, hydrothermal systems in the ocean are related to the main geological and tectonic structures on the seabed—mid-ocean ridges and island arc systems.

Hydrothermal minerals forming chimney and smoke precipitate in zone of hot (up to 400 °C) hydrothermal fluid discharge to the cold (2–4 °C) near-bottom seawater. The color of hydrothermal vents depends on their temperature: black smoke with suspended sulfide minerals has temperature > 300 °C while white smoke with non-sulfide minerals (sulfates and carbonates) is characterized by lower temperature (<200 °C) (Fig. 4.7). A vertical jet-like discharge is replaced by horizontal spreading, after the density of the rising fluid becomes equal to density of the bottom waters at corresponding horizon. This lens of hydrothermal plume usually occurs at a depth of 200–300 m above the bottom. Plume has a thickness of 50–100 m and is characterized by anomalies of transparency/turbidity, gases (methane, hydrogen), and metals (manganese, iron) concentrations. Exploration methods of the active hydrothermal fields with associated sulfide mineralization are based on determination of these parameters in the near-bottom waters (see next section).

Rona (1984) has estimated that only about 5% of the metal amount from hydrothermal fluids accumulates in massive sulfides and 95% disperses as smoke and plume in near-bottom waters with further oxidation and forming layers of metalliferous sediments around hydrothermal fields.

According to the recycling model of SMS formation, the hosted rocks are considered as a source of metals. However, there is geological setting where metals in SMS could be provided by magmatic fluids. This is typical for the sites where seafloor massive sulfide deposits are forming in close association with subduction-related volcanic centers. Hydrothermal vents at submarine arc volcanoes show clear evidence of the direct input of magmatic volatiles, similar to magmatic-hydrothermal systems in subaerial volcanic arcs (Yang and Scott 1996, 2006).

Thus, for the formation of hydrothermal systems, a combination of two main factors—the magmatic and tectonic—is necessary; the main mechanism leading to the formation of hydrothermal fluids at the mid-ocean ridges is the circulation of seawater in the rocks of the seafloor, while direct magmatic supply of metals is also evident in island arcs environment.

4.7 Criteria for Recognition and Strategy of SMS Exploration

Current exploration for seafloor massive sulfides is based on detection of hydrophysical and geochemical anomalies around hydrothermal fields as well as geophysical anomalies associated directly with ore bodies. Similar methods are used in prospecting of on-land deposits but marine environment dictates specific approaches in their application.

The following parameters are used for recognition of hydrothermal systems:

- Hydrological: transparency/turbidity, methane and manganese concentrations in near-bottom waters. These components are characterized by the contrasting anomalies in the plumes above active hydrothermal fields. This approach is based on the fact that the size of anomalous area is considerably higher than the source of this anomaly (hydrothermal field) dimensions.
- Geochemical and mineralogical: metals (iron, manganese, copper, and zinc) and minerals (high-temperature—sulfides, and low-temperature—hydroxides of iron and manganese, sulfates and carbonates) in the sediments. These components form dispersed haloes due to result of fall-out of particles from the plume, same as in process of mass transfer during weathering of sulfide ore bodies. The abovementioned consideration regarding the sizes of anomalies and source of them is true for these type of anomalies as well as for the hydrological ones.
- Geophysical: electric self-potential and magnetic susceptibility in the near-bottom waters. These parameters differ distinctly sulfides from the host rocks and sediments. It is recommended to couple electromagnetic methods to get synergetic effect for prospecting of the SMS deposits.

Currently, exploration for massive sulfide deposits is carried out in two main stages: regional (large-scale) and detailed. Bathymetric and sonar survey for the mapping of the area as well as geological sampling and hydrocast profiling for identification of anomalies in bottom waters and sediments are conducted during the regional exploration stage. Detailed works in the local areas are performed for the groundtruthing of the anomalies and targets revealed on the previous regional stage. Besides sampling of the sulfides, video- and photo profiling for delineation of the deposits are included in the set of methods on this stage.

4.8 Exploration Technologies

Sea technologies used for SMS exploration are based on the criteria for their recognition described in previous section. Here is the brief overview of the technological systems currently applied during cruises either under the conducting of “Contracts with International Seabed Authority for exploration of polymetallic sulfides” or in course of scientific research of oceanic hydrothermal systems.

4.8.1 Hydrological Tools

CTD-rosette system is of considerable use for detection of the hydrothermal plumes generated by hot vents associated with massive sulfides. Plumes can be also detected from water columns surveys using purposefully designed Miniature Autonomous Plume Recorders (MAPRs) instruments that “has revolutionized the international

community's ability to explore for hydrothermal activity" (German et al. 2016). MAPRs are used both on vertical profile stations and in conjunction with deep-towed instrument packages (e.g., sonar mapping systems).

4.8.2 Geological Sampling Tools

Different types of grabs (i.e., TV-equipped), cores (gravity, piston, hydraulic, box), and dredges are used to obtain geological samples (rocks, ores, sediments) studied on-board and further in the onshore laboratories.

4.8.3 Remote and Autonomous Operating Vehicles

Towed vehicles (Remote Operating Vehicles—ROV) together with the autonomous (Autonomous Operating Vehicles—AUV) are currently the main technological systems employed on regional and detailed stages for SMS exploration. Deepwater ROVs are linked to a host ship by a load-carry umbilical cable and have modular structure. Depending on the purpose of dive, ROV may be equipped with a manipulator, still/video camera, echosounder, sonar, magnetometer, water sampler, and different sensors that can measure self-potential and other water parameters. AUVs may also carry varied payload sensors such as sonar, echosounder, sub-bottom profiler, laser profiler, magnetometer, and still image camera. The main advantages of unmanned vehicles are their versatility, high efficiency, and safety which cannot be guaranteed in the case of manned submersibles. All these factors make the ROV and AUV most high-tech and demanded complexes in the search for and study of submarine hydrothermal systems.

4.8.4 Drilling Systems

To study the internal structure of the sulfide ore bodies and to estimate their resources drilling is needed. There are two types of drilling systems:

- On-board drilling system (Derrick type)
- Seabed system by using a drilling rig

The first method executed from the specialized vessel allows to drill deep wells and to use Logging-while-Drilling technique. However, this method is extremely complex from a technological point of view and the cost of these works is very high. The using of the second type of drilling systems could be done from non-specialized vessel. This way is more efficient, less expensive, and most widely used in modern practice.

4.8.5 Manned Submersibles

The role of submersibles in the discovery and study of hydrothermal systems is very high. Discoveries and observations made on-board Cyana, Alvin, Pisces, Nautilus, Mir, Shinkai will remain in the history of oceanographic research. Many divers believe that no one device can replace the human eye (especially an expert eye); therefore, each dive of submersible is unique in terms of the information obtained. However, it is clear that the mainstream of ocean technology development is associated with robotic systems.

References

Bäcker H (1982) Metalliferous sediments of hydrothermal origin from the Red Sea. In: Halbach P, Winter P (eds) Marine mineral deposits. Glückauf, Essen, pp 102–136

Baturin GN, Rozanova TV (1972) Ore mineralization in the rift zone of the Indian ocean. In: Research of oceanic rift zones. pp 190–202

Beaulieu SE, Baker ET, German CR (2015) Where are the undiscovered hydrothermal vents on oceanic spreading ridges? Deep Sea Res II. http://dx.doi.org/10.1016/j.dsr2.2015.05.001

Bogdanov Y, Bortnikov N, Vikentiev I (1997) New type of modern mineral-forming system: black smokers of hydrothermal field at 14°45′ N, Mid-Atlantic Ridge. Ore Deposit Geol 39(1):68–90 (in Russian)

Bonatti E, Joensuu O (1966) Deep-sea iron deposits from the South Pacific. Science 154(3749): 643–645

Booth R, Crook K, Taylor B et al (1986) Hydrothermal chimneys and associated fauna in the Manus back-arc basin, Papua New Guinea. Eos 67(21):489–490

Boström K, Peterson MNA (1966) Precipitates from hydrothermal exhalations on the East Pacific Rise. Econ Geol 61(7):1258–1265

Cherkashov G, Poroshina I, Stepanova T, Ivanov V, Bel'tenev V, Lazareva L, Rozhdestvenskaya I, Samovarov M, Shilov V, Glasby G (2010) Seafloor massive sulfides from the northern equatorial Mid-Atlantic Ridge: new discoveries and perspectives. Mar Georesour Geotechnol 28:222–239

Corliss JB, Dymond J, Gordon LI, Edmond JM, Von Herzen RP, Ballard RD, Green K, Williams D, Bainbridge A, Crane K, Van Andel TH (1979) Submarine thermal springs on the Galapagos Rift. Science 203:1073–1083

Cyamex (1978) Découverte par submersible de sulfures polymétalliques massifs sur la dorsale du Pacifique oriental, par 21°N (projet "Rita"). C R Acad Sci 287:1365–1368

de Ronde CEJ, Massoth GJ, Butterfield DA, Christenson BW, Ishibashi J, Ditchburn RG, Hannington MD, Brathwaite RL, Lupton JE, Kamenetsky VS, Graham IJ, Zellmer GF, Dziak RP, Embley RW, Dekov VM, Munnik F, Lahr J, Evans LJ, Takai K (2011) Submarine hydrothermal activity and gold-rich mineralization at Brothers Volcano, Kermadec Arc, New Zealand. Miner Deposita 46:541–584

Degens ET, Ross DA (eds) (1969) Hot brines and recent heavy metal deposits in the Red Sea. Springer, New York

Escartın J, Smith DK, Cann J, Schouten H, Langmuir CH, Escrig S (2008) Central role of detachment faults in accretion of slow-spreading oceanic lithosphere. Nature 455:790–795

Firstova A, Stepanova T, Cherkashov G, Goncharov A, Babaeva S (2016) Composition and formation of gabbro-peridotite hosted seafloor massive sulfide deposits from the Ashadze-1 hydrothermal field, Mid-Atlantic Ridge. Minerals 6:19. doi:10.3390/min6010019

Fouquet Y (1997) Where are the large hydrothermal sulphide deposits in the oceans? Philos Trans R Soc Lond Ser A 355(1723):427–440

Fouquet Y, Lacroix D (2014) Deep marine mineral resources. Springer, Heidelberg
Fouquet Y, Cherkashov G, Charlou JL, Ondreas H, Birot D, Cannat M, Bortnikov N, Silantyev S, Sudarikov S, Cambon-Bonavita MA, Desbruyeres D, Fabri MC, Querellou J, Hourdez S, Gebruk A, Sokolova T, Hoise E, Mercier E, Kohn C, Donval JP, Etoubleau J, Normand A, Stephan M, Briand P, Crozon J, Fernagu P, Buffier E (2008) Serpentine cruise—ultramafic hosted hydrothermal deposits on the Mid-Atlantic Ridge: first submersible studies on Ashadze 1 and 2, Logatchev 2 and Krasnov vent fields. Inter Ridge News 17:15–19
Fouquet Y, Cambon P, Etoubleau J, Charlou JL, Ondreas H, Barriga FJAS, Cherkashov G, Semkova T, Poroshina I, Bohn M, Donval JP, Henry K, Murphy P, Rouxel O (2010) Geodiversity of hydrothermal processes along the Mid-Atlantic Ridge and ultramafic hosted mineralization: a new type of oceanic Cu-Zn-Co-Au volcanogenic massive sulfide deposit. In: Rona PA, Devey CW et al (eds) Diversity of submarine hydrothermal systems on slow spreading ocean ridges. Geophysical monograph, vol 188. AGU, Washington, pp 297–320
Francheteau J, Needham HD, Choukroune P, Juteau J, Seguret M, Ballard RD, Fox PJ, Normark W, Carranza A, Cordoba A, Guerrero J, Rangin C, Bougault H, Cambon P, Hekinina R (1979) Massive deep sea sulphide ore deposit discovered on the East Pacific Rise. Nature 277:523–528
Franklin JM, Gibson HL, Jonasson IR, Galley AG (2005) Volcanogenic massive sulfide deposits: Economic Geology 100th Anniversary Volume: 523–560
German C (2008) Global distribution and geodiversity of high-temperature seafloor venting. Deep-sea mining: a reality for science and society in the 21st century. Science and policy workshop, 10
German C, Petersen S, Hannington MD (2016) Hydrothermal exploration of mid-ocean ridges: where might the largest sulfide deposits occur? Chem Geol 420:114–126. doi:10.1016/j.chemgeo.2015.11.006
Hannington MD, Jonasson IR, Herzig PM, Petersen S (1995) Physical and chemical processes of seafloor mineralization at mid-ocean Ridges. In: Geophysical Monograph, vol 91. AGU, Washington, pp 115–157
Hannington MD, de Ronde C, Petersen S (2005) Sea-floor tectonicsand submarine hydrothermal systems. In: Hedenquist JW et al (eds) Economic Geology 100th Anniversary Volume, pp 111–141
Hannington MD, Jamieson J, Monecke T, Petersen S (2010) Modern sea-floor massive sulfides and base metal resources: toward an estimate of global sea-floor massive sulfide potential. Spec Publ Soc Econ Geol 15:317–338
Hannington M, Jamieson J, Monecke T, Petersen S, Beaulieu S (2011) The abundance of seafloor massive sulfide deposits. Geology 39:1155–1158 http://dx.doi.org/10.1130/G32468.1
Ishibashi J, Urabe T (1995) Hydrothermal activity related to arc-backarc magmatism in the Western Pacific. In Taylor B (ed) Backarc basins: Tectonics and magmatism. New York, Plenum Press, pp 451–495
Jamieson JW, Hannington MD, Clague DA, Kelley DS, Delaney JR, Holden JF et al. (2013) Sulfide geochronology along the Endeavour segment of the Juan de Fuca ridge. Geochem Geophys Geosyst. doi: 10.1002/ggge.20133
Jamieson JW, Clague DA, Hannington M (2014) Hydrothermal sulfide accumulation along the Endeavour Segment, Juan de Fuca Ridge. Earth Planet Sci Lett 395:136–148
Jamieson JW, Petersen S, Bach W (2016) Hydrothermalism. In: Harff J, Meschede M, Petersen S, Thiede J (eds) Encyclopedia of marine geosciences. pp 344–357
Koschinsky A et al (2006) Discovery of new hydrothermal vents on the southern Mid-Atlantic Ridge (4S–10S) during cruise M68/1. Inter Ridge News 15: 9–15
Kuznetsov V, Tabuns E, Kuksa K, Cherkashov G, Maksimov F, Bel'tenev V, Lazareva L, Zherebtsov I, Grigoriev V, Baranova N (2015) The oldest seafloor massive sulfide deposits at the Mid-Atlantic Ridge: 230Th/U chronology and composition. Geochronometria 42(1):100–106
Lalou C, Reyss JL, Brichet E, Rona PA, Thompson G (1995) Hydrothermal activity on a 10(5)-year scale at a slow-spreading ridge, TAG hydrothermal field, mid-Atlantic Ridge 26-degrees-N. J Geophys Res 100:17855–17862

Lipton I (2012) Mineral Resource Estimate: Solwara Project, Bismarck Sea, PNG. Technical Report compiled under NI43–101. Golder Associates, for Nautilus Minerals Nuigini Inc.
Lowell RP, Rona PA, Von Herzen RP (1995) Seafloor hydrothermal systems. J Geophys Res 100(B1):327–352
MacLeod CJ, Searle RC, Casey JF, Mallows C, Unsworth M, Achenbach K, Harris M (2009) Life cycle of oceanic core complexes. Earth Planet Sci Lett 287:333–344
McCaig AM, Cliff B, Escartin J, Fallick AE, MacLeod CJ (2007) Oceanic detachment faults focus very large volumes of black smoker fluids. Geology 35:935–938
Miller AR, Densmore CD, Degens ET, Hathaway JC, Manheim FT, Mcfarlin PF, Pocklington R, Jokela A (1966) Hot brines and recent iron deposits of the Red Sea. Geochim Cosmochim Acta 30(3):341–359
Monecke T, Petersen S, Hannington MD (2014) Constraints on water depth of massive sulfide formation: evidence from modern seafloor hydrothermal systems in arc-related settings, Econ Geol 109:2079–2101. http://dx.doi.org/10.2113/econgeo.109.8.2079
Petersen S, Kuhn K, Kuhn T, Augustin N, Hékinian R, Franz L, Borowski C (2009) The geological setting of the ultramafic-hosted Logatchev hydrothermal field (14°45′N, Mid-Atlantic Ridge) and its influence on massive sulfide formation. Lithos 112:40–56
Petersen S, Kratschell A, Augustin N, Jamieson J, Hein JR, Hannington MD (2016) News from the seabed—geological characteristics and resource potential of deep-sea mineral resources. Mar Policy 70:175–187. doi:10.1016/j.marpol.2016.03.012i
Peterson MNA, Edgar NT, Von der Borch CC, Rex RW (1970) Cruise leg summary and discussion. In: Init Reports DSDP, vol 2. US Govt Print-Office, Washington
Revelle RR (1944) Marine bottom samples collected in the Pacific Ocean by the "Carnegie" on her seventh cruise. Carnegie Inst Publ 556. Carnegie Inst, Washington
Rona PA (1984) Hydrothermal mineralization at seafloor spreading centers. Earth Sci Rev 20(1):1–104
Rona PA, Scott SD (1993) A special issue on sea-floor hydrothermal mineralization; new perspectives; preface. Econ Geol 88(8):1933–1973
Rona PA, Klinkhammer G, Nelson TA, Trefry JH, Elderfield H (1986) Black smokers, massive sulfides, and vent biota at the Mid-Atlantic Ridge. Nature 321(6065):33–37
Sillitoe RH (1972) Formation of certain massive sulphide deposits at sites of spreading. Trans Inst Min Metall 81(789):13141–13148
Singer DA (1995) World class base and precious metal deposits—a quantitative analysis. Econ Geol 90:88–104
Skornyakova NS (1964) Dispersed iron and manganese in Pacific sediments. Lithol Min Deposit 5:3–20 (in Russian)
Smith DK, Cann JR, Escartin J (2006) Widespread active detachment faulting and core complex formation near 13 N on the Mid-Atlantic Ridge. Nature 443:440–444
Spiess FN, Macdonald KS, Atwater T, Ballard R, Carranza A, Cordoba D, Cox C, Diazgarsia VM, Francheteau J, Guerrero J, Hawkins J, Hamon R, Hessler R, Juteau T, Kastner M, Larson R, Luyendik B, Macdougall JD, Miller S, Normark W, Orcutt J, Rangin C (1980) East Pacific Rise; hot springs and geophysical experiments. Science 207(4438):1421–1433
Takai K, Mottl MJ, Nielsen SHH, Birrien JL, Bowden S, Brandt L, Breuker A, Corona JC, Eckert S, Hartnett H, Hollis SP, House CH, Ijiri A, Ishibashi J, Masaki Y, McAllister S, McManus J, Moyer C, Nishizawa M, Noguchi T, Nunoura T, Southam G, Yanagawa K, Yang S, Yeats C (2012) IODP expedition 331: strong and expansive subseafloor hydrothermal activities in the Okinawa Trough. Sci Drill 13:9–26
Tivey MA, Schouten H, Kleinrock MC (2003) A near-bottom magnetic survey of the Mid-Atlantic Ridge axis at 26°N: implications for the tectonic evolution of the TAG segment. J Geophys Res 108:2277. doi:10.1029/2002JB001967
Wolery TJ, Sleep NH (1976) Hydrothermal circulation and geochemical flux at mid-ocean ridges. J Geol 84(3):249–275
Yang K, Scott SD (1996) Possible contribution of a metal-rich magmatic fluid to a sea-floor hydrothermal system. Nature 383(6659):420–423

Yang K, Scott SD (2006) Magmatic fluids as a source of metals in arc/back-arc hydrothermal systems: evidence from melt inclusions and vesicles. In: Christie DM, Fisher CR, Lee S-M (eds) Back Arc spreading systems: geological, biological, chemical and physical interactions, vol 166. American Geophysical Union, Geophysical Monograph, Washington, pp 163–184

Zierenberg RA et al (1998) The deep structure of a sea-floor hydrothermal deposit. Nature 392(6675):485–488

Georgy Cherkashov is Deputy Director of the Institute for Geology and Mineral Resources of the Ocean (VNIIOkeangeologia, St. Petersburg, Russia) of the Ministry of Natural Resources (since 1996). He holds a Dr. Sci. for research of seafloor massive sulfide (SMS) deposits of the Mid-Atlantic Ridge. He has been the Chief Scientist of 13 ocean-going Russian and international expeditions for prospecting of SMS deposits in the Pacific, Atlantic, and Indian Oceans (1983–2007). He was also the President of International Marine Minerals Society (2011–2012), member of the Legal and Technical Commission of the International Seabed Authority (since 2012) and is Professor at St. Petersburg State University (Marine Geology), part time (since 2005).

Chapter 5
Submarine Phosphorites: The Deposits of the Chatham Rise, New Zealand, off Namibia and Baja California, Mexico—Origin, Exploration, Mining, and Environmental Issues

Hermann Kudrass, Ray Wood, and Robin Falconer

Abstract Rising consumption and increasing prices of phosphate fertilizers initiated the commercial exploration of offshore phosphorite deposits. Origin of the phosphorite, state of exploration, and mining concepts are described for three of the most advanced projects. The phosphorites of the Chatham Rise/New Zealand are located in 400 m water depth, about 500 km offshore and originated by Late Miocene phosphatization of a hemipelagic chalk. The gravel-sized phosphorites form a residual decimeter-thick layer with an inferred resource of 24 million tons. The authigenic, sand-sized phosphorites at the outer shelf of Namibia form a meter-thick layer with estimated resources of 60 million tons. The sand-sized phosphorites on the mid-shelf off the Baja California/Mexico contain an estimated resource of about 300 million tons. In all three projects, the phosphorites are planned to be recovered by a trailing suction hopper dredge and enriched by onboard size screening. Mining licenses were granted, but environmental considerations have delayed the economically feasible exploitation of these marine phosphorites.

5.1 Introduction

Onshore phosphorite reserves are well-explored and can supply the worldwide consumption of phosphate fertilizer for the next hundred years (Orris and Chernoff 2002). But the deposits are not evenly distributed around the world and not always close to agriculture centers. The continents on the southern hemisphere are

H. Kudrass (✉)
MARUM, Leobener Straße, Bremen, Germany
e-mail: kudrass@gmx.de

R. Wood • R. Falconer
Chatham Rise Rock Phosphate, 93 The Terrace, Wellington, New Zealand
e-mail: raywood@crpl.co.nz; robinfalconerassociates@paradise.net.nz

R. Sharma (ed.), *Deep-Sea Mining*, DOI 10.1007/978-3-319-52557-0_5

especially lacking in significant production of phosphorite. The main phosphorite resources are the widespread deposits of northern Africa and the Nubian Shield, which originated in shallow-water along the former southern margin of the Late Cretaceous Tethys Ocean and the Paleocene to Eocene Atlantic Ocean (Soudry et al. 2006). Other economically important deposits are the Miocene phosphorites of Florida and the Permian Phosphoria Formation, both of which mainly serve the North American fertilizer markets. Sedimentary deposits from the Late Proterozoic in China produce exclusively for local consumption (Li 1986).

In contrast to the concentration of mineable onshore phosphorite deposits in the northern hemisphere, occurrences of submarine phosphorites are widely distributed in both hemispheres. They commonly are found along the western side of the continents, where they are associated with intense upwelling and an extended oxygen-minimum zone underlying the highly fertile surface water (Föllmi 1996, Fig. 5.1). Many of the marine phosphorites lie on the outer shelf and have gained considerable commercial interest. The origin and resource aspects of the best explored phosphorite deposits at the Chatham Rise, New Zealand, off Namibia and Baja California, Mexico, are discussed in the following sections.

5.2 Authigenic and Diagenetic Formation of Phosphorite

Phosphorus is used in many essential biological processes, and along with nitrate, silicate, and sometimes iron, it is one of the constituents limiting the primary biological production in the oceans. Due to its intense biological consumption in the photic zone, phosphorus is strongly depleted in the surface waters. Marine organic material sinking through the water column usually contains about 1% phosphorus. Decomposition of organic particles in the deeper ocean releases some phosphorus, which remains dissolved in the deeper water or is scavenged by sinking iron oxides and clay particles (Benitez-Nelson 2000; Compton et al. 2000). The ocean floor sediment is hence a first-order sink for organic matter, iron oxides, clay, and phosphorus.

In areas with slow sediment accumulation and oxic bottom water, the organic material is mostly consumed by bottom fauna and phosphorus is recycled into the water. In areas with rapid accumulation, organic matter and phosphorus are buried in the sediments. In special conditions of upwelling zones, the high flux of the sinking organic matter from the fertile surface water results in suboxic to anoxic bottom waters and the organic matter is partly consumed by highly specialized sulfide-oxidizing bacteria, which store polyphosphate as energy resources in their cells (Fig. 5.2). Changes in bottom water conditions can cause the sulfide-oxidizing bacteria to release phosphate in such high concentrations (Schulz and Schulz 2005;Goldhammer et al. 2010; Lomnitz et al. 2015) that Ca-phosphate precipitates, probably in an amorphous, highly reactive form (Schenau et al. 2000; Arning et al. 2009). Additional phosphate can be supplied by dissolution of fish debris (Suess 1981; Noffke et al. 2012) and desorption from iron oxides (e.g., Froelich et al. 1988). This authigenic precipitate can form ooids, pellets, peloids, laminae, nodules or crusts and is later transformed into microcrystalline francolite, a carbonate flourapatite with the approximate composition $Ca_{10}\,(PO_4)_{4.8}\,(CO_3)_{1.2}\,F_{3.2}$ (McCellan and Gremillion 1980).

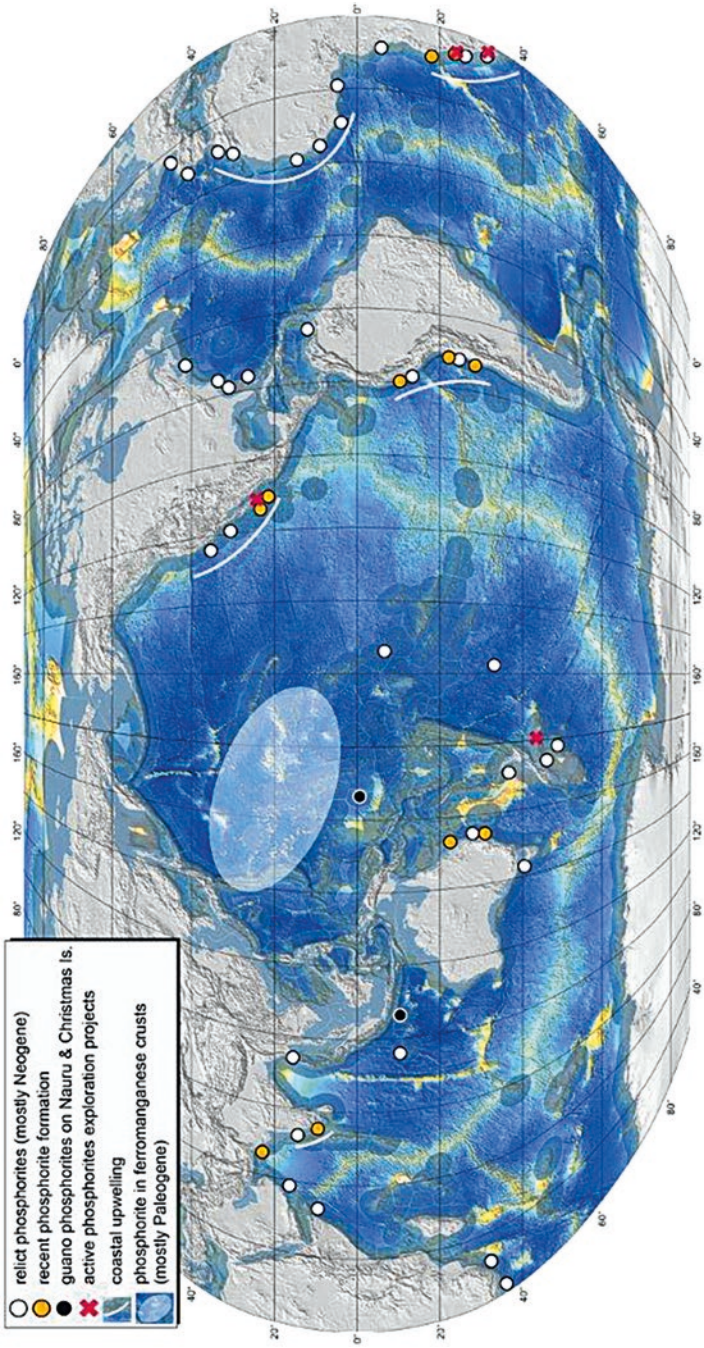

Fig. 5.1 Distribution of submarine phosphorites

Fig. 5.2 (**a**) Mats of sulphide-oxidizing bacteria at the sediment surface in the upwelling system of Peru, water depth 132 m, station SO147-FS 93 (picture size 1 m^2). (**b**) Section through a sediment core with white strings of sulphide-oxidizing bacteria Thioploca, off Peru, core diameter 12 cm

Diagenetic phosphorite forms when phosphorus is released by the bacteria and reacts directly with chalk or replaces carbonate biogenic material. This phosphatization produces irregular slabs, cobbles, or an armor of cemented sediments, frequently containing glauconite (Birch 1980). Authigenic and diagenetic phosphorites are chemically and mechanically stable in most marine sedimentary environments and tend to accumulate in condensed sequences (Bentor 1980; Föllmi 1996). Sizable phosphorite resources can only accumulate if the conditions for phosphorite precipitation in the muds under upwelling systems frequently alternate between periods of anoxic mud sedimentation and phosphorite deposition and periods of winnowing and erosion. Pleistocene sea level changes could have produced these alternating sedimentary regimes. The more frequent changes of El Nino to La Nina conditions in the upwelling systems of the eastern Pacific Ocean provide another cycle of concentrating phosphorites at the outer margin of the shelf. The larger grain size and the higher density of authigenic or diagenetic phosphatic particles favor local enrichment as a lag deposit, whereas the finer non-phosphatized or terrigenous particles are more easily mobilized and transported into deeper or other depositional centers.

5.3 The Chatham Rise Phosphorite

5.3.1 Regional Setting and Seafloor Morphology

The Chatham Rise extends about 1000 km east from the South Island of New Zealand into the southwest Pacific (Fig. 5.3). The rise is an elongated continental fragment with a Permo-Triassic basement and its crest is generally 200–400 m deep.

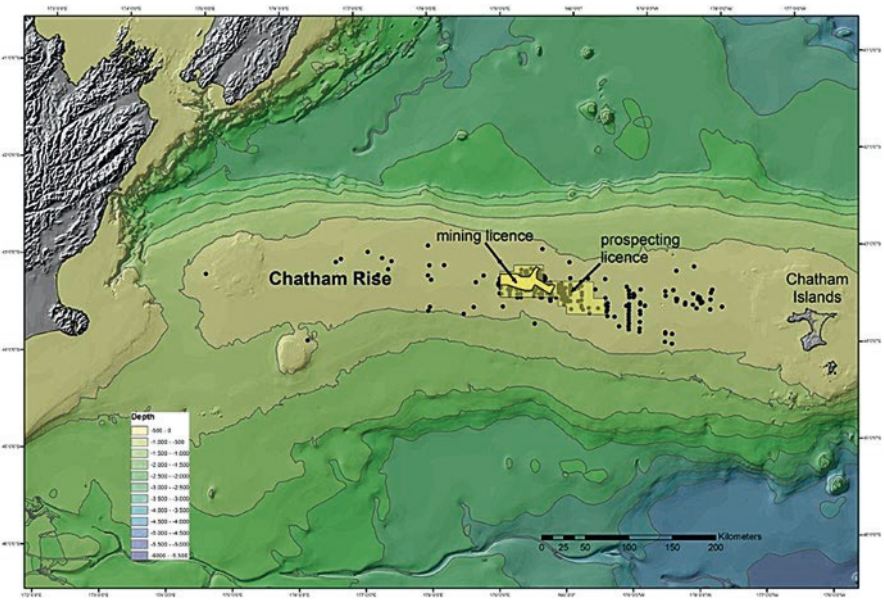

Fig. 5.3 Bathymetry of the Chatham Rise, phosphorite samples (*black dots*), and the mining and prospecting licences of Chatham Rock Phosphate (CRP)

It is capped by Oligocene to Late Miocene chalk (Falconer et al. 1984). The main body of the phosphorite deposit is confined to a 400 m-deep saddle on the crest of the rise midway between the South Island and the Chatham Islands. The small-scale morphology of this saddle is dominated by the impact of iceberg keels on the seafloor (Fig. 5.4). Furrows caused by northward movement of grounded icebergs and pits produced by rotating and overturning icebergs are the most important small-scale seafloor elements, ranging in scale from a few meters to tens of kilometers. These impacts shaped the seafloor by disrupting the seafloor sediments to a depth of 15 m along furrows and in the pit marks. The phosphoritic sand and underlying chalk were excavated and deposited along the rims of the furrows and pit depressions (Fig. 5.5).

During the long interglacial periods, the seafloor was smoothened and the phosphorite redistributed by winnowing of the sand, filling of the depressions, and burrowing and dissolution of the exposed chalk. The most prominent furrow was caused by a double-keeled iceberg crossing the eastern part of the saddle. The direction and width of the two parallel furrows change several times along the 35 km long track, which implies that shifting tidal currents were driving the at least 300 m-thick iceberg. Some large furrows are superimposed by younger ones and presumably had been produced during former glacial events. Similar massive impacts were probably repeated at the end of the five main Pleistocene glacial periods. Distribution of ice-rafted debris on the Campbell Plateau, south of the Chatham Rise, indicates that the flow of icebergs from the destabilized Antarctic ice shelves during the last deglaciation was more frequent than during the former glacial/interglacial transition (130,000 years ago) (Carter et al. 2002).

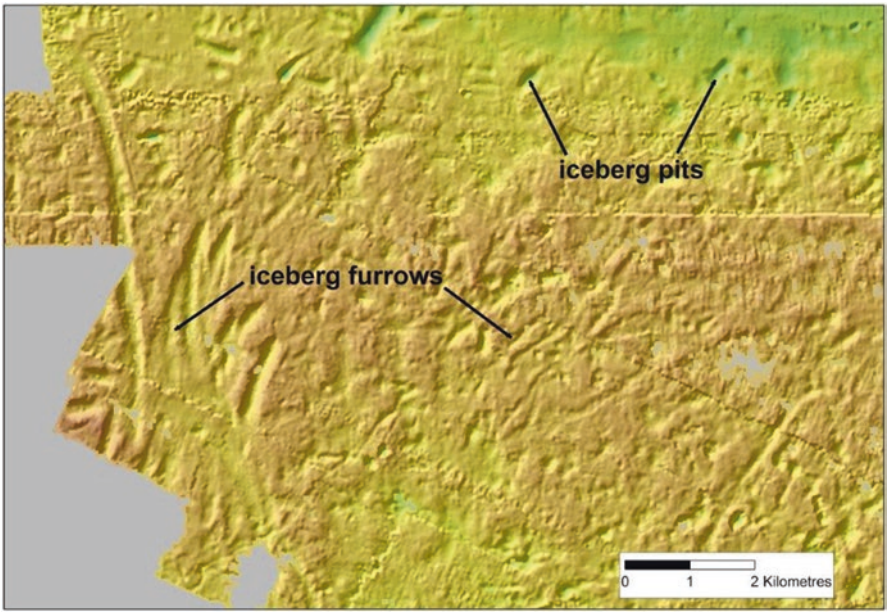

Fig. 5.4 Bathymetry with iceberg furrows and pits in the western part of the CRP mining licence

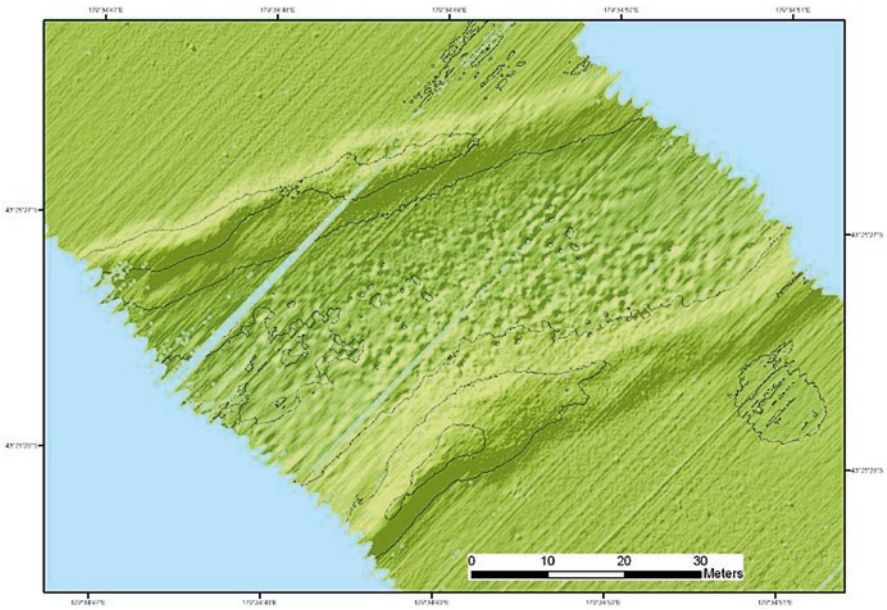

Fig. 5.5 Iceberg furrow with intensely bioturbated seafloor at the bottom of the furrow

5.3.2 Oceanographic Setting

The large-scale oceanographic environment is dominated by the Subtropical Convergence, which lies along the crest Chatham Rise and separates colder, less saline sub-Antarctic water to the south from warmer subtropical water to the north (Heath 1985). Bottom currents, monitored by turbidity and current meters during the autumn, winter, and spring seasons of 2011, are dominated by tidal currents with a predominately northwesterly direction and with velocities of possibly more than 40 cm s^{-1}.

Absolute values of the near-bottom turbidity are poorly constrained, but they are generally low and show little correlation with current velocities. Formation of a lag deposit indicates that, over long periods, currents are strong enough to remove fine material. Scour marks around glacial boulders, occasional ripples, and sediment on benthic organisms are evidence of this process. They indicate that peak current velocities can mobilize the muddy sand of the uppermost seafloor sediments. The intense bioturbation at the bottom of depressions and channels also indicates lateral sediment transport, which supplies organic-rich fine sediments into these local depositional centers (Fig. 5.5).

5.3.3 Formation of the Chatham Rise Phosphorites

In comparison to other phosphorite deposits, the Chatham Rise phosphorite is unique with respect to its origin in a pelagic environment. The phosphorites of the Chatham Rise consist of carbonate fluorapatite (francolite), which replaced an early to middle Miocene nannochalk (Cullen 1980; Kudrass and von Rad 1984). Before the diagenetic alteration, the Miocene chalk was exposed at the seafloor, forming a hardground and was intensively bored and partly impregnated by iron hydroxides (Von Rad and Rösch 1984). The diagenetic phosphatization preserved the shape of large chalk lumps and their cm-sized bore holes. Most of the phosphorite consists of fine to medium-sized gravel with subrounded irregular shapes. Shark teeth and bone fragments of cetaceans, especially the earbones of dolphins, were also phosphatized and are well-preserved. Kudrass and von Rad (1984) postulated that the Chatham Rise phosphorites, like all other sedimentary phosphorites, formed in the sediments of an upwelling system. Two Sr-isotope analyses of the phosphorite constrain its formation to 5.2 Ma (McArthur et al. 1990). K-Ar ages from the glauconite grains and the glauconitic rim of phosphorite, however, have a much longer range from 10.8 to 3.8 Ma (Kreuzer 1984).ODP drill site 1125 on the northeastern slope of the Chatham Rise recovered a continuous pelagic sequence, which recorded "a strong frontal productivity signal in the late Miocene—early Pliocene with enhanced sedimentation rates up to 13 cm/k.y. and a nutrient-enriched $\delta^{13}C$ signature between 5.8 and 4.8 Ma" (Carter et al. 2004). This period of high productivity correlates well with the Sr-isotope age of the postulated upwelling and formation of phosphorite on the Chatham Rise crest.

Considering the present oceanographic setting, a situation with upwelling and anoxic bottom water seems to be difficult to establish. Since the opening of the Drake Passage in the Oligocene, the current system in the southern ocean has not fundamentally changed and therefore the present position of the Subtropical Convergence with its slight meridional shifting across the Chatham Rise should not have changed considerably (Carter et al. 2004). Changes in the paleogeography of New Zealand west of the Chatham Rise may offer a possible explanation for a relatively short-lived change in oceanographic conditions. Paleogeographic reconstructions indicate a marine seaway developed briefly through central New Zealand about 5 Ma (Wood and Stagpoole 2007). In addition, changes in morphology and water depth of the central Chatham Rise, where about 50 m of Mid-Oligocene and Late Miocene chalk have been eroded since the formation of the phosphorite (Falconer et al. 1984, Fig. 5.7), may have had some local influence.

After phosphatization of the chalk surface, probably achieved in many cycles of mud deposition, phosphate release, mud erosion, and repeated deposition, the non-phosphatized Miocene chalk was slowly eroded. Probably during that time, the phosphorites were coated by a thin veneer of glauconite (Fig. 5.6), which protected

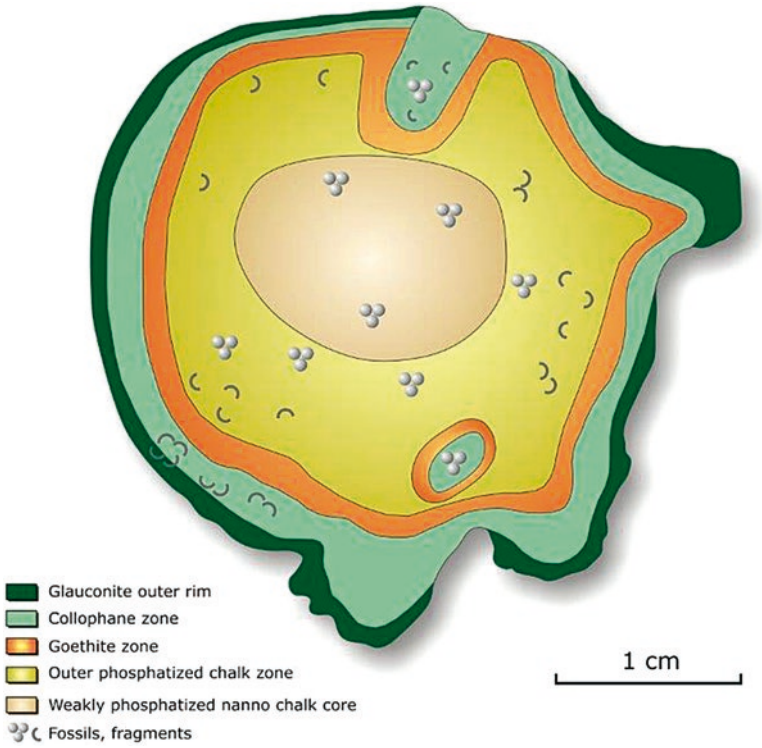

Fig. 5.6 Schematic cross-section of a typical phosphorite from the Chatham Rise (modified from von Rad and Rösch 1984)

them from corrosion at the sediment–seawater interface. Unprotected phosphorite and especially the phosphatized whale bones without a glauconitic rim are deeply pitted by dissolution (Cullen 1980). During the 5 Ma following the formation of the phosphorites, more glauconitic sand was deposited and about 50 m of chalk were removed by burrowing, winnowing, and dissolution. The highly corroded appearance of modern biogenic debris, mostly foraminiferal tests and echinoid spines, indicates that this dissolution is ongoing. During the Pleistocene, volcanic ash and ice-rafted terrigenous material were added, which comprise about 10% of the surface sediments.

The result of these five million-year-long processes of deposition (Fig. 5.7), chemical and biogenic alteration, and erosion is a sandy-gravelly lag deposit of Miocene phosphorites, mixed with glauconitic grains, foraminiferal tests, and minor terrigenous material (Fig. 5.8). The portion of fine silt and clay-sized material is small and mainly consists of calcareous nannoplankton and various clay minerals. The lag deposit varies in thickness from almost nothing to at least 70 cm and covers an intensively bored surface of Oligocene semi-consolidated chalk.

5.3.4 Distribution and Composition of the Chatham Rise Phosphorites

Phosphorites are widespread on the Chatham Rise, but commercial concentrations are confined to a saddle on the crest of the rise (Fig. 5.3). The rich deposit covers an area of about 400 km^2 between 179° 05` E and 179°45` E. The phosphorites have a grain size of 1 mm to > 100 mm (Fig. 5.8) and are evenly distributed throughout a completely bioturbated, decimeter-thick, glauconitic foraminiferal fine sand (Fig. 5.9). The phosphorites comprise on an average about 15% of the surficial sediments. Towards the north and south, the phosphorite deposit thins or is buried by the glauconitic sand, which increases in thickness to the deeper levels at both sides of the saddle. In the east-west direction, phosphorites have been sampled over a distance of 300 km along the rise crest and may constitute a semi-continuous deposit interrupted by local banks and depressions (Fig. 5.3).

Within the area of highest concentration, the horizontal variation of the phosphorite content is high (Kudrass 1984). Cone-penetration measurements show that the thickness of the phosphorite-bearing sand shows no continuity over distances of 50 m. This high spatial variability is caused by iceberg scouring, which probably ploughed the surface of the saddle during the five glacial periods in the Pleistocene and disrupted the original relatively even distribution of phosphorite.

In the long intervals between the glacial periods, phosphorite partly buried by the chalk resurfaced by the combined effects of chalk dissolution, boring, and winnowing of the glauconitic sand. Thus, the original coverage was more or less restored, but modified into a locally high variability mostly reflecting the iceberg disturbance of the last glacial period about 18,000 years ago.

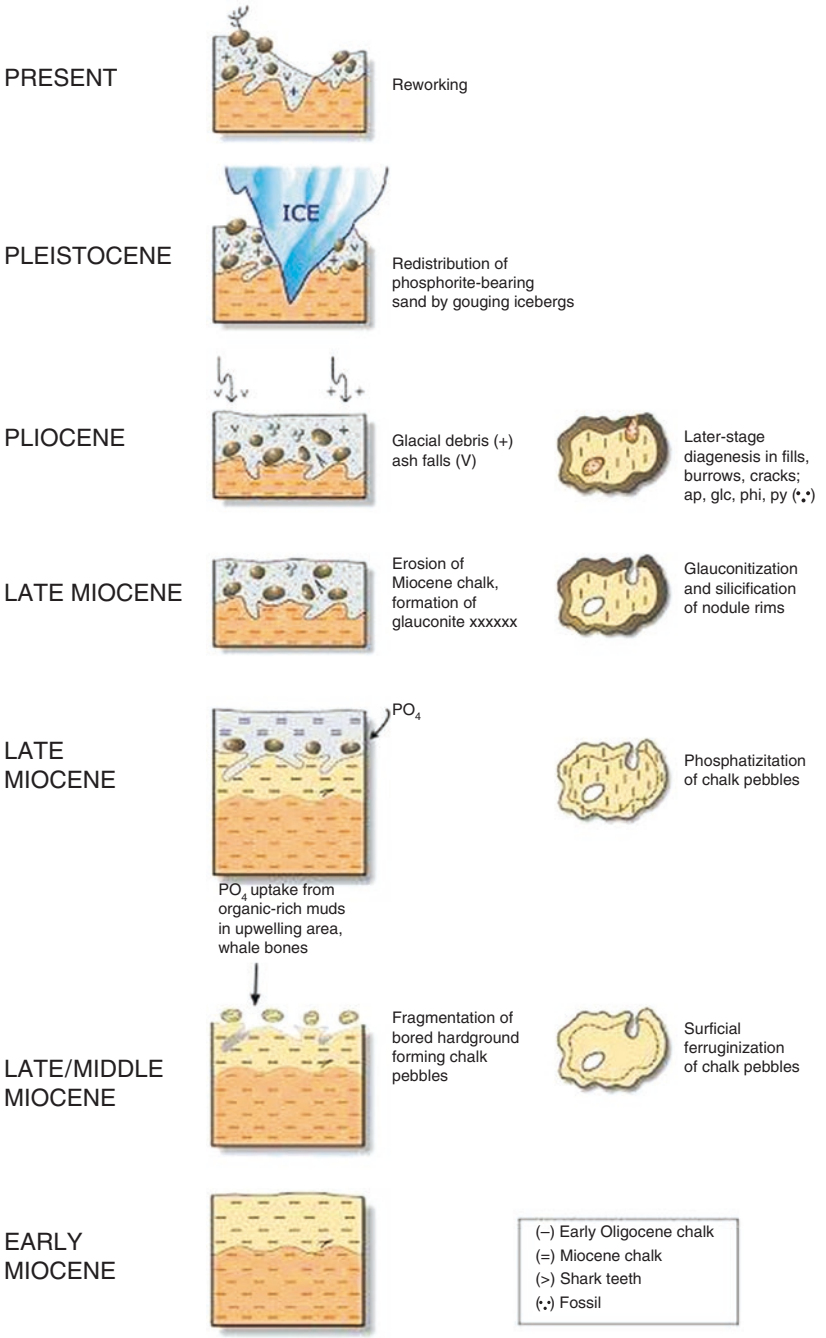

Fig. 5.7 Scheme of the Neogene sedimentary evolution of the central Chatham Rise and origin of the phosphorite, note the erosion of early to late Miocene chalk after the phosphatization event at about 5 Ma (modified from Kudrass and von Rad 1984)

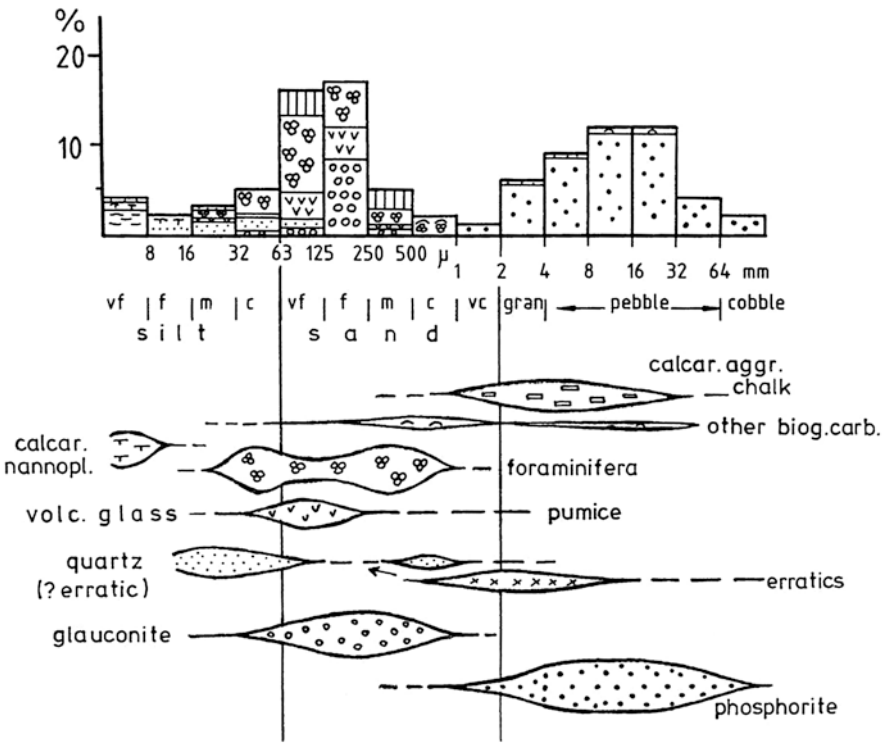

Fig. 5.8 Bimodel grain-size frequency of sample (SO17-17GG) and generalized composition of a phosphorite-rich sample, note the concentration of phosphorities in the fraction > 1mm (from von Rad and Rösch 1984)

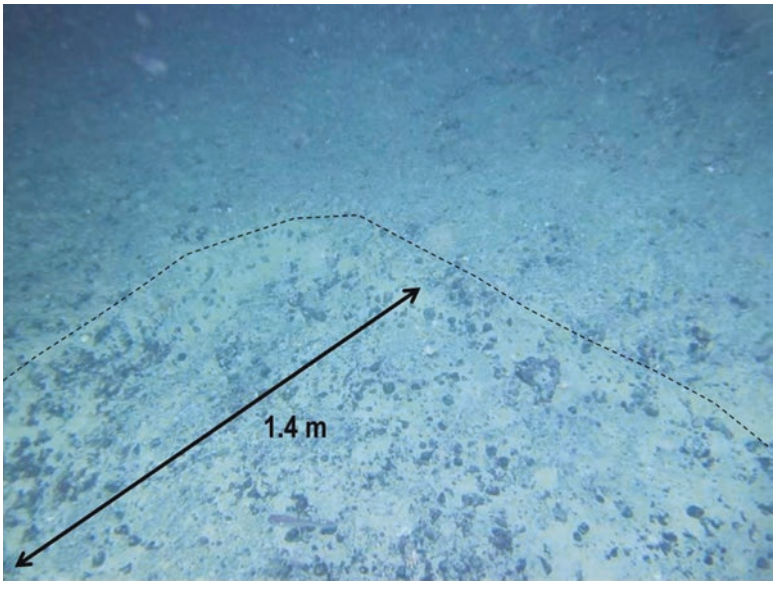

Fig. 5.9 Bottom photograph with phosphorite embedded in glauconitic foraminiferal sand

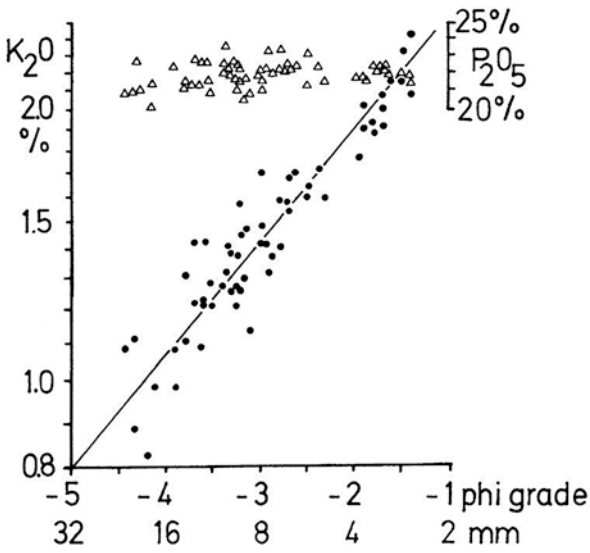

Fig. 5.10 K_2O% and P_2O_5% versus the grain size of phosphorite (from Kudrass and Cullen 1982)

The chemical composition of the phosphorites depends on their grain size. Large phosphorites (>8 mm) usually have a core with lower phosphatization and a higher Ca-carbonate component, including Sr and U (with an average of 158 mg kg^{-1}). The smaller fractions (1–8 mm) are completely phosphatized, but with decreasing grain size the relative portion of the elements associated with the glauconitic cover, such as Si, Al, Fe, K, many trace metals, and REEs, increase (Fig. 5.10). The P_2O_5 concentrations remain relatively stable between 19.4% (coarse) and 21.8% (fine fraction). The relatively low concentration of Cd (0.2 mg kg^{-1}) and Pb (10 mg kg^{-1}) in the Chatham Rise phosphorites is probably due to the low terrigenous supply to the former upwelling sediments.

5.3.5 Resource Estimation and Mining Concept

Analysis of the grab samples obtained by cruises with Valdivia (1978) and SONNE (1981) cruises predicted that the deposit contains 25 million tons of phosphorite with an average coverage of 66 kg m^{-2} in an area of 378 km^2 (Kudrass 1984). This resource estimation is a conservative estimate, as the grab sampler did not always penetrate the entire phosphorite-bearing glauconitic sand. Based on the correlation between the phosphorite-rich areas and seismic facies (Falconer et al. 1984), additional resources of approximately the same magnitude may be found in neighboring areas, but concentrations and coverage could be much lower. A recent reassessment of the phosphorite resource, including data collected by Chatham Rise Rock Phosphate Limited (CRP), has estimated and inferred resource of 23.4 million tons of phosphorite with a cut-off grade of 100 kg m^{-2}. This estimation is compliant with the "Australasian Code for Reporting of Exploration Results, Mineral Resources and Ore Reserves".

The average concentration of phosphorite in the surficial sediment is about 15 wt %. Their assessment revealed that adjacent areas of the resource could have an additional 8–12 million tons of phosphorite (Sterk 2014).

The recovery of the phosphorite nodules is achieved by a conventional trailing suction hopper dredger (Fig. 5.11). The phosphorite-bearing glauconitic sand is mobilized by jet streams within the drag head to a depth of approximate 50 cm.

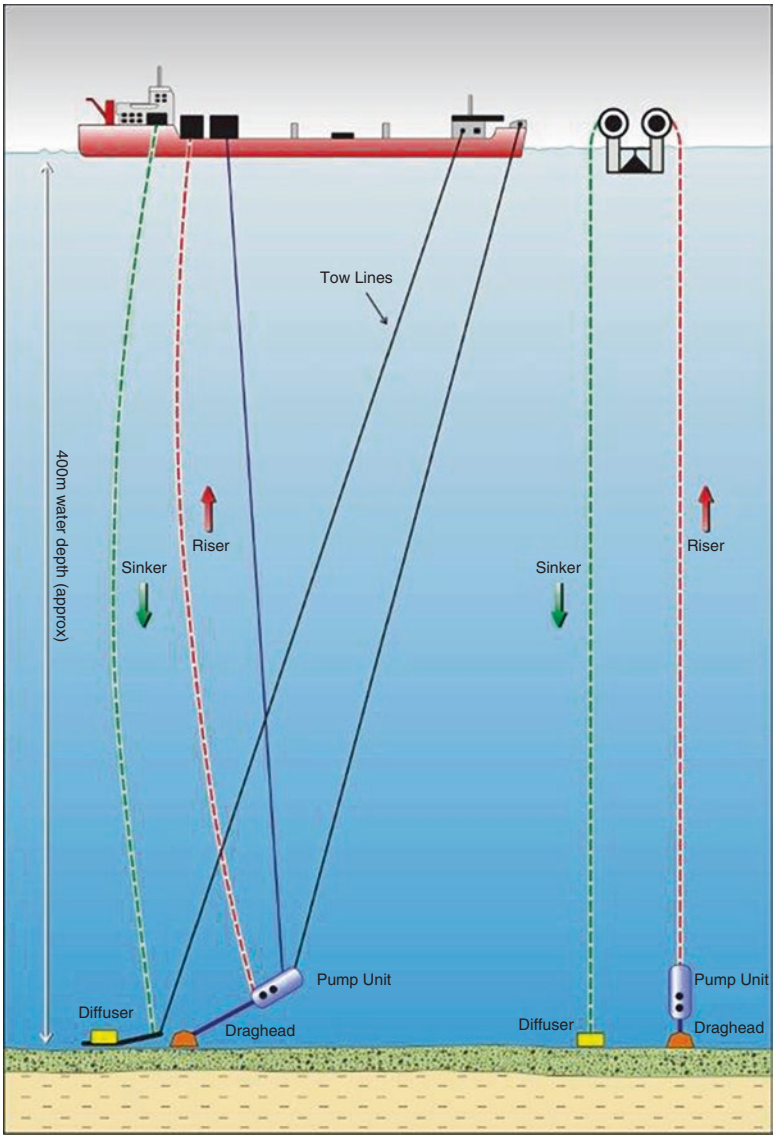

Fig. 5.11 Layout of the mining system of a trailing suction hopper dredge. The seabed sediment goes up through the drag-head and riser, is processed on the mining vessel, and the non-phosphorite sediments are returned to the seabed through the sinker and diffuser.

The trailing drag-arm carrying the suction head and pump unit is suspended from the vessel by wires and is decoupled from the ship´s vertical movements by a hinge. The mixture of phosphorites and sand is pumped through a riser pipe to the vessel where the phosphorites (>2 mm) are separated and stored. The undersized material, mostly sand and coarse silt (Fig. 5.8), is returned via a sinker pipe to the seabed. At the end of the sinker pipe, a diffuser reduces the outflow velocities and most of the tailings settle near the path of the drag head. When the vessel's holds are full, the vessel proceeds to a port in New Zealand where the phosphorite is unloaded. Under this scenario, 1.5 Mt of phosphorite can be recovered per annum by mining of three 10 km^2 mining blocks. The mining would initially target areas of high-resource value and therefore are spaced throughout the mining license area.

5.3.6 Exploration History and Present Status (2015)

Phosphorites from the Chatham Rise were first described by Reed and Hornibrook (1952). Pasho (1976) sampled the phosphorite with dredges, determined its lateral extent, and tried to estimate the size of the resource. Cullen (1980) described the deposit and its formation. In 1978 and 1981, two sampling and profiling expeditions with the research vessels Vadivia and Sonne thoroughly investigated the distribution and origin of the deposit and produced the first reliable estimate of the size of the resource (Kudrass and Cullen 1982; von Rad and Kudrass 1984). As a result of this work, a prospecting license was granted to a consortium with industrial partners from New Zealand and Germany (Fletcher Challenge, Preussag). However, the license was dropped before mining started because of the drop in phosphate prices and the technical challenges of deep-sea mining.

Due to the exhaustion of the phosphorite deposits at Nauru and Christmas Island, New Zealand had to import phosphorite from very distant sources such as those in Morocco. The long transport distance significantly increased the costs for fertilizer in New Zealand. Consequently, the Chatham Rise phosphorites were again considered as an alternative resource for the agriculture industry, which annually imports about one million tons of phosphorite. Field tests have also demonstrated that the phosphorite can be used as a direct fertilizer (Mackay et al. 1984).

In 2008, Chatham Rise Rock Phosphate Limited (CRP) received an exploration permit covering an area of 3900 km^2, and after a series of exploration and environmental campaigns with the research vessels Tangoroa, Tranquil Image, and Dorado Discovery, CRP received a mining permit covering 820 km^2 in 2011 (Fig. 5.3). After a public hearing and discussion of the Environmental Impact Assessment, the environmental consent required to mine the deposit was declined in February 2015 due to the decision making committee's uncertainty about the nature and extent of environmental disturbances.

5.4 Phosphorite Deposits off South Africa and Namibia

5.4.1 Diagenetic Phosphorites off South Africa

The shelf sediments of the South African and Namibian phosphorite province contain a large variety of phosphorites (Birch 1980). Diagenetic phosphorite, which originated by phosphatization of carbonate rocks and biogenic debris, forms a 0.5 m thick pavement across large parts of the shelf off the southern tip of Africa (Fig. 5.12). The phosphorites occur as lumps, pebbles, and gravel-sized, irregular fragments, which originally consisted of foraminiferal limestone, glauconitic, or limonitic sandstone. The age of phosphatization varies from the earliest Miocene to the Quaternary. Many pebbles originated during several events of phosphatization

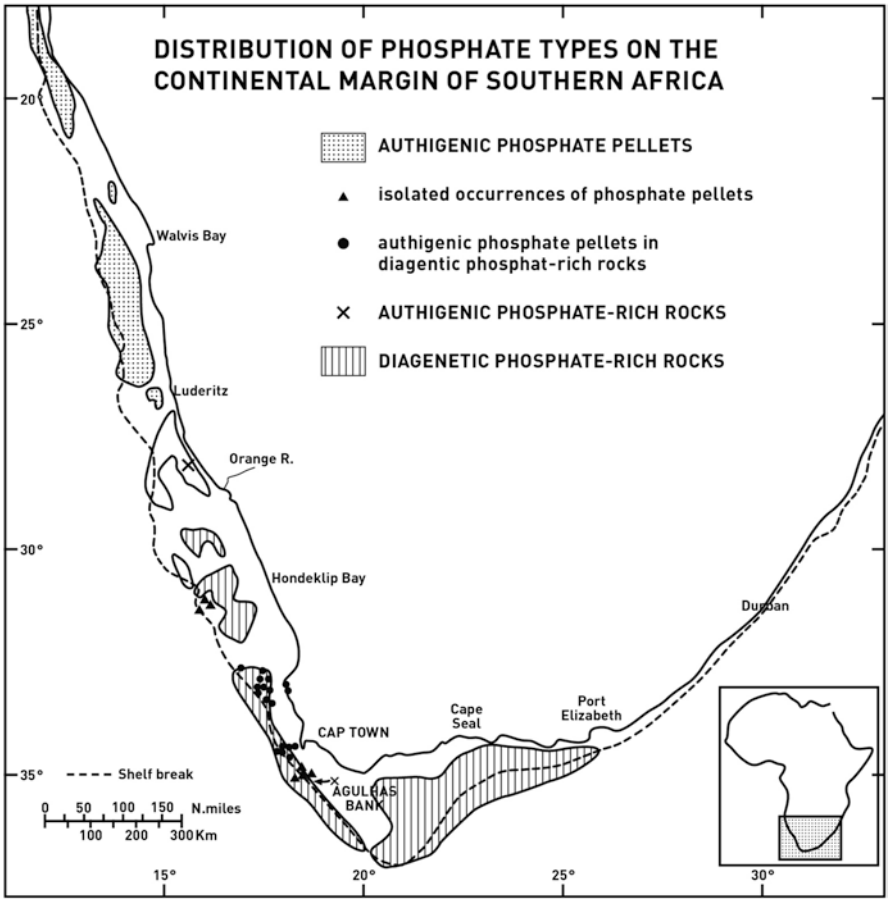

Fig. 5.12 Distribution of authigenic and diagenetic phosphorites on the continental shelf and upper slope off South Africa and Namibia (from Birch 1980)

separated by millions of years (Compton et al. 2002). Commercial exploration has started at the southeastern Agulhas Bank, where the widespread phosphorite cover is winnowed by the strong Agulhas Current, but detailed results are not available.

5.4.2 *Authigenic Phosphorites off Namibia*

Authigenic phosphorite is the dominant phosphoritic component off Namibia, which has formed by precipitation of sand-sized pellets in the organic-rich muds (Birch 1980). The phosphorite-rich sediments form a meter-thick continuous layer at the outer shelf and upper slope in water depths of 180–300 m (Bentor 1980, Compton and Bergh 2016, Fig. 5.13). Data from gravity cores show that the phosphorite-rich sediment consists of two layers (Sandpiper Project, EIA 2012). The upper layer has a thickness of 0.1–1.0 m and consists of coarse molluscan shell debris embedded in a dark brown matrix of fine-sandy phosphoritic pellets. The shell fragments decrease in size and abundance with depth and the pellets and mud content increase.

The fining downward of the top layer grades into the second layer whose thickness varies between a few centimeters to more than 2 m. The dark brown to blackish

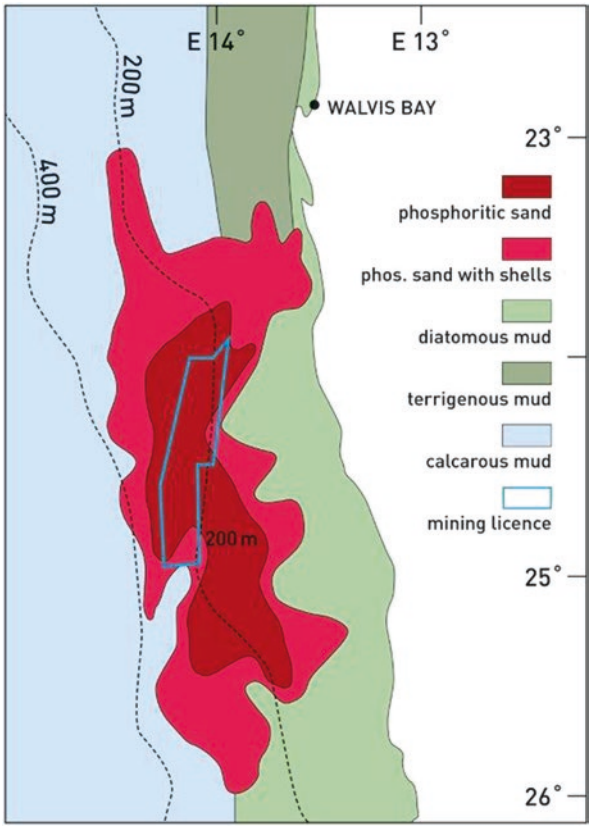

Fig. 5.13 Sediments of the Namibian shelf (modified from Baturin 2000) and the approximate position of the mining license area of the Sandpiper Project

layer consists of slightly muddy, fine phosphoritic sand. This layer overlies with a sharp contact firm grey marine Miocene clay. The erosional surface of the Miocene clay is burrowed and the holes are filled with the phosphoritic sand. The two layers have a high spatial continuity parallel to the shelf break. Local topographic depressions of the Miocene clay are filled with thicker sand deposits.

The depositional history of the phosphoritic sequences is not well-understood. The poor preservation of the mollusc shells points to long exposure (Bremner 1980) and the high C:N ratio of the organic matter indicates recycling from the highly productive inner shelf zone (van der Plas et al. 2007). As the Sr-ages of phosphorites range from latest Miocene to the Quaternary (McArthur et al. 1990; Compton et al. 2002; Compton and Bergh 2016), the present accumulation of the rich phosphorite deposit resulted from a complex, frequently repeated sequence of phosphorite precipitation in organic-rich muds beneath an upwelling system, followed by reworking of the mud and concentration of the phosphoritic pellets during changes of sea level and changing current systems.

5.4.2.1 The Sandpiper Prospect

Namibia Marine Phosphate received an exploration license in 2005 and 2006 for a 25 km wide and 100 km long area along the 200 m isobath at the outer shelf break. Subsequently, it also received a mining license in 2011 for the most prospective area (Fig. 5.13). More than 1500 sites in the exploration license area have been sampled by a large grab and a 3 m-long gravity corer. The most prospective inner segment was sampled at a 400 m grid and the outer areas were sampled along 4 km-long profiles with a1.6 km spacing.

This exploration identified an area of 220 $km^2$with 60 Mt of phosphoritic sediment with an average concentration of about 20.8% P_2O_5 (Sandpiper Project 2012; Sterk and Stein 2015). The phosphoritic pellets are from 100 to 500 µm in diameter, most of them between 150 and 250 µm. The refined phosphorite contains about 27%P_2O_5.The higher concentrations of K_2O (1.2%), Fe_2O_3 (4%), Al_2O_3 (5.5%), and SiO_2 (15%) of the lower layer are related to an increased glauconitic component. Trace elements such as Cd (70 mg kg^{-1}), As(70 mg kg^{-1}), and U (107 mg kg^{-1}) are within the normal range of sedimentary phosphorites (Sandpiper EIA 2012).

In the entire area of the mining license, an additional 140 Mt of resource are predicted, although with a somewhat lower concentration of P_2O_5. The area of the exploration license may contain up to 2000 Mt of phosphoritic sediments with an average grade of 10% P_2O_5.

5.4.2.2 Mining Concept

The richest phosphorite concentrations at a water depth of about 220 m are the first mining targets. Mining has not started, but the proposal is for the phosphorites to be recovered by a conventional trailing suction hopper dredge and the slurry is stored onboard. The configuration of the mining ship is comparable to that proposed for

the Chatham Rise project (Fig. 5.11). The drag head recovers about 50 cm of sand and several passes are needed to excavate the complete section of the thickest layer. The mining operations will leave a decimeter-thick layer of the phosphoritic sand as a cover on the Miocene clay. The excess water will be discharged below the ship in a low-density sediment plume which contains most of the fine particles (< 125 μm) from the slurry, amounting to 10–20% of the dredged sediment. When full, the vessel will sail about 100 km to the coast south of Walvis Bay and pump the slurry through a pipeline into a buffer pond onshore. Treatment of the phosphorites includes screening to remove the coarse grained biodetritus (> 1 mm) and washing in spiral cones to separate the fine mud particles and to enhance the concentration of phosphorite. The water for the processing plant will be produced in a desalination plant. After processing, the final product is expected to contain about 28% P_2O_5. Annual production is expected to be about 3 Mt (Sandpiper Project 2012).

5.4.2.3 Environmental Issues

The Sandpiper prospect lies at the offshore fringe of the oxygen minimum zone, which is fully developed under the coastal upwelling zone with its associated intense biological production (Birch 1980; Shannon 1985). A highly specialized benthic fauna has adapted to the low oxygen concentrations of the bottom water and is characterized by a low diversity with a local high abundance (Levin 2003; van der Plas et al. 2007). The macrofauna are dominated by annelid worms and crustaceans are poorly represented (Sandpiper Project 2012).

The environmental impact assessment identified the most evident effects of mining as:

- loss of benthic fauna in the mined section,
- disturbance of benthic fauna adjacent to the mining tracks by the redeposition of mobilization of bottom sediments, which are mobilized by the drag head, and
- disturbance of the pelagic ecology from modifications of the water column by the settling of fine-grained particles and dissolved elements from the excess slurry water.

The impacts on the benthic fauna are assumed to be transient, as recolonization seems to be possible, if the phosphoritic sand is not completely removed. Also, the effects on the water column are considered to have no significant effect on the ecology, especially as the impacted area is a small fraction of the Namibian fishing grounds.

However, the fishing industry, a major component of Namibia's economy, and environmental groups oppose the mining plans. They are concerned that the assessment of toxic effects or oxygen depletion from the overspill and drag head disturbances is not well-understood as no data on the concentrations of organic matter, methane, hydrogen sulphide, and dissolved trace metals like Cd, Ni, As in the anoxic porewater of the deeper sediments are available. In addition, the high seasonal variability of surface and bottom currents seems not to be sufficiently considered in the evaluation. After a public hearing in 2013, the Namibian Government issued a moratorium to investigate the environmental impacts of mining on the marine ecosystem in more detail before

allowing mining to proceed. After a re-evaluation of the environmental impact assessment, the proposed phosphorite mining received the Environmental Certificate Clearance in October 2016.

5.5 Authigenic Phosphorites off Baja California

Onshore and offshore phosphorites and their relation to the upwelling system off the peninsula of Baja California, Mexico, have been investigated for many years. At the top of isolated offshore platforms, phosphatization has cemented dolomite and Miocene foraminiferal limestone. The highest concentrations of authigenic phosphoritic pellets are located on the middle shelf near the center of the peninsula (D'Anglejan 1967). On the narrow shelf, the phosphorites occur as well rounded, sorted black pellets with a grain size of 125–250 μm embedded in muddy terrigenous sand. In the well-sorted sand fraction, the grainsize of phosphorite and non-phosphatic grains indicates similar histories of transportation or reworking. The phosphorites reach highest concentrations up to 40% in water depths of 50–100 m. Recently formed phosphoritic pellets have been described from several deeper shelf sites (Jahnke et al. 1983), but the majority of the phosphorite on the shelf is interpreted as a long-term residual deposit, which was concentrated during periods of low sea level (D'Anglejan 1967).

The phosphorite-rich segment of the shelf was investigated by Odyssey Marine Exploration, which received an exploration license for a prospect called "Don Diego". The area lies 40 km offshore from Ulloa Bay in water depths of 70–90 m, between latitudes 25°50´ and 26°20´ N. Based on 199 cores, the potential resources are estimated as 327 Mt with an average grade 18.5% P_2O_5. The phosphorite-bearing sediments will be recovered with a trailing suction dredge. On board the hopper ship, a sized concentrate with the phosphorite will be removed by screening and stored ready for transshipment to cargo vessels. The remaining coarse and fine material (approx. 50%) will be returned to the seabed via a vertical fall pipe. Numerical models predict the sediment plume will spread to a maximum distance of 4 km. The impacts of the proposed mining on the environment, especially on the fisheries, whales, and turtles, are predicted to be insignificant. However, numerous stakeholders including environmentalist groups and the fishing and tourist industries are concerned about the possible negative impacts of marine mining. Odyssey has prepared a refined environmental impact assessment and is in discussion with Mexican government regulators about the environmental consent.

5.6 Future Development Prospects

This chapter has briefly described three highly prospective areas that are being considered for development (Fig. 5.1): Chatham Rise, New Zealand; Namibia and Baja California, Mexico. These deposits are all very close to their potential consumers,

which will considerably reduce the transportation costs from the present onshore deposits in the northern hemisphere. Other advantages of marine mining over onshore mining include the relatively low cost and mobility of infrastructure, the mining vessel can be easily moved or modified for another project, and the ability to deliver the product to a variety of harbors for onshore distribution. Exploitation of these phosphorite resources will require increased knowledge of the potential environmental impact of mining as well as their commercial and technical viability.

Several other highly prospective areas have only been investigated for scientific purposes. For example, the extensive upwelling areas at the outer shelf off Peru and Chile could be a future target for phosphorite exploration as research data indicate that the diluting effect of terrigenous detritus could be small and the frequent oceanographic variations from La Nina to El Nino may drive changes in the redox conditions and bottom currents required for precipitation of phosphorite and its concentration by erosion and winnowing.

Experience to date shows that the environmental consent is the primary barrier to the development of these projects. With increasing knowledge, the mining impacts on the local fisheries and on the marine ecosystems can be better estimated and eventually reduced to an acceptable level. Convincing diverse groups of stakeholders with the present knowledge that the benefits of the project outweigh the uncertain environmental impacts is a significant challenge.

References

Arning ET, Lückge A, Breuer C, Gussone N, Birgel D, Peckmann J (2009) Genesis of phosphorite crusts off Peru. Mar Geol 262(1–4):68–81. doi:10.1016/j.margeo.2009.03.006

Baturin GN (2000) Formation and evolution of phosphorite grains and nodules on the Namibian shelf, from recent to Pleistocene. In: Glenn CR, Prevot-Lucas L, Lucas J (eds) Marine authigenesis: from global to microbial, vol 66. Society of Economic Paleontologists and Mineralogists, Special Publication, pp 185–199

Benitez-Nelson CR (2000) The biogeochemical cycling of phosphorus in marine systems. Earth-Sci Rev 51:109–135

Bentor YK (ed) (1980) Marine phosphorites—geochemistry, occurrence, genesis, vol 29. Society of Economic Paleontologists and Mineralogists, Special Publication, pp 1–249

Birch GF, (1980) A model of penecontemporaneousphosphatizationby diagenetic and authigenic mechanisms from thewestern margin of southern Africa. In: Bentor YK (ed) Marine phosphorites: geochemistry, occurrence, genesis, vol 29. Society of Economic Paleontologists and Mineralogists, Special Publication, pp 33–18

Bremner JM (1980) Concretionary Phosphorite from SW Africa. J Geol Soc Lond 1980(137): 773–786

Carter L, Neil HL, Northcote L (2002) Late Quaternary ice-rafted events in the SW Pacific Ocean, off eastern New Zealand. Mar Geol 191:19–35

Carter RM, McCave IN, Carter L (2004) Leg 181 synthesis: fronts, flows, drifts, volcanoes and the evolution of the southwestern gateway to the Pacific Ocean, Eastern New Zealand. In: Richter C (ed) Proceedings of ODP, Scientific Results. doi:10.2973/odp.proc.sr.181.210.2004

Compton JS, Bergh EW (2016) Phosphorite deposits of the Namibian shelf. Mar Geol 380:290–314. http://dx.doi.org/10.1016/j.margeo.2016.04.006

Compton JS, Mallinson D, Glenn CR, Filippelli G,Föllmi K, Shields G, Zanin, Y (2000) Variations in theglobal phosphorus cycle. In: Glenn CR, Prevot-Lucas L, Lucas, J (eds) Marine authigenesis: from global to microbiology, vol 66. Society of Economic Paleontologists and Mineralogists, Special Publication, pp 21–33

Compton JS, Mulabasina J, McMillan IK (2002) Origin and age of phosphorite from the Last Glacial Maximum to Holocene transgressive succession off the Orange River, South Africa. Mar Geol 186:243–261

Cullen DJ (1980) Distribution,composition and age of phosphorites on the Chatham Rise, east of New Zealand, vol 29. Society of Economic Paleontologists and Mineralogists, Special Publication, pp 139–148

D'Anglejan BF (1967) Origin of marine phosphorites off Baja California, Mexico. Mar Geol 5:15–44

Falconer RKH, Von Rad U, Wood R (1984) Regional structure and high-resolution seismic stratigraphy of the central Chatham Rise (New Zealand). Geologisches Jahrbuch D65:29–56

Föllmi B (1996) The phosphorus cycle, phosphogenesis and marine phosphate-rich deposits. Earth-Sci Rev 40:55–124

Froelich PN, Arthur MA, Burnett WC, Deakin N, Hensley V, Jahnke R, Kaul L, Kim K-H, Roe K, Soutar A, Vathakanon C (1988) Early diagenesis of organic matter in Peru continental margin sediments: phosphorite precipitation. Mar Geol 80:309–343

Goldhammer T, Brüchert V, Ferdelmann TG, Zabel M (2010) Microbial sequestration of phosphorus in anoxic upwelling sediments. Nat Geosci 3:557–561. doi:10.1038/NGEO913

Heath RA (1985) A review of the physical oceanography of the seas around New Zealand—1982. NewZeal J Freshwater and Mar Res 19:79

Jahnke RA, Emerson SR, Roe KK, Burnett WC (1983) The present day formation of apatite in the Mexican continental margin sediments. Geochim Cosmochim Acta 47:259–266

Kreuzer H (1984) K-Ar dating of glauconitic rims of phosphorite nodules (Chatham Rise, New Zealand). Geologisches Jahrbuch D65:121–127

Kudrass HR (1984) The distribution and reserves of phosphorite on the central Chatham Rise (SONNE-17 Cruise 1981). Geol Jahrb D65:179–194

Kudrass HR, Cullen DJ (1982) Submarine phosphorite nodules from the central Chatham Rise off New Zealand—composition, distribution, and resources (Valdivia cruise 1978). Geol Jahrb D51:3–41

Kudrass HR, von Rad U (1984) Geology and some mining aspects of the Chatham Rise phosphorite: a synthesis of the SONNE-17-results. Geologisches Jahrbuch D65:233–252

Levin J (2003) Oxygen minimum zone benthos: adaption and community response to hypoxia. Oceanogr Mar Biol Annu Rev 41:1–45

Li Y (1986) Proterozoic and Cambrian phosphorites-regional review: China. In: Cook PJ, Shergold JH (eds) Proterozoic and Cambrian phosphate deposits of the world, Volume 1—Proterozoic and Cambrian phosphorites. Cambridge University Press, Cambridge, pp 42–62

Lomnitz U, Sommer S, Dale AW, Löscher CR, Noke A, Wallmann K, Hensen C (2015) Benthic phosphorus cycling in the Peruvian oxygen minimum zone. Biogeosciences 12(16755–16801):2015. doi:10.5194/bgd-12-16755-2015

Mackay AD, Gregg PEH, Syers JK (1984) Field evaluation of Chatham Rise phosphorite as a phosphatic fertiliser for pasture. New Zeal J Agric Res 27(1):65–82

McArthur J et al (1990) Dating phosphogensis with strontium isotopes. Geochim Cosmochim Acta 54:1343–1351

McCellan GH, Gremillion LR (1980) Evaluation of phosphatic raw material. In: Khasawneh FE et al (eds) The role of phosphorus in agriculture. American Society Agronomy, Madison, pp 43–80

Noffke A, Hensen C, Sommer S, Scholz F, Bohlen L, Mosch T, Graco M, Wallmann K (2012) Benthic iron and phosphorus fluxes across the Peruvian margin. Limnol Oceanogr 57(3):851–867. doi:10.4319/lo.2012.57.3.0851

Orris GJ, Chernoff CB (2002) Data set of world phosphate mines, deposits, and occurrences. USGS, Open File Report 02-156

Pasho DW (1976) Distribution and morphology of Chatham Rise phosphorites, vol 77. Memoir of the New Zealand Oceanographic Institute, Wellington, pp 1–27

Reed JJ, Hornibrook N d B (1952) Sediments from the Chatham Rise, vol 77. Memoir of the New Zealand Oceanographic Institute, Wellington, pp 173–188
Sandpiper Project (2012) 80th Annual IFA Conference May 2012, Doha Qatar
Sandpiper Project: Environmental Impact Assessment Report for the Marine Consent, Draft Report (2012) http://www.namphos.com/project/sandpiper/environment/item/57-environmental-marine-impact
Schenau SJ, Slomp CP, De Lange GJ (2000) Phosphogenesis and active formation in sediments from the Arabian Sea oxygen minimum zone. Mar Geol 169:1–20
Schulz HN, Schulz HD (2005) Large sulphur bacteria and the formation of phosphorite. Science 307:416–414
Shannon LV (1985) The Benguelaecosystem.Part I. Evolution of the Benguela, physical features and processes. Oceanogr Mar Biol Annu Rev 23:105–182
Soudry D, Glenn CR, Nathan Y, Segal ID, VonderHaar ID (2006) Evolution of Tethyan phosphogenesis along the northern edges of the Arabian–African shield during the Cretaceous–Eocene as deduced from temporal variations of Ca and Nd isotopes and rates of P accumulation. Earth Sci Rev 78:27–57
Sterk R (2014) Technical report and mineral resource estimate on the Chatham Rise Project in New Zealand, NI43 101
Sterk R, Stein JK (2015) Seabed mineral deposits: a review of current mineral resources and future developments. Deep Sea Mining Summit. Aberdeen, Scotland, 10 February 2015, p 37
Suess E (1981) Phosphate regeneration from sediments of the Peru continental margin by dissolution of fish debris. Geochim Cosmochim Acta 45:577–588
Von Rad U, Rösch H (1984) Geochemistry, texture, and petrography of phosphorite nodules and associated foraminiferal glauconite sands (Chatham Rise, New Zealand). Geologisches Jahrbuch D65:129–178
van der Plas AK, Monteiro PMS, Pascall A (2007) Crossshelf biogeochemical characteristics of sediments in the central Benguela and their relationship to overlying water column hypoxia. Afr J Mar Sci 29:37–47
Wood RA, Stagpoole VM (2007) Validation of tectonic reconstructions by crustal volume balance: New Zealand through the Cenozoic. Geol Soc Am Bull 119:933–943

Hermann Kudrass spent most of his professional life as a marine geologist with the Geological Survey of Germany, Hannover (BGR). He investigated resources of sand and gravel, heavy minerals, phosphorites, manganese nodules, and crusts in many parts of the oceans. His paleoclimatic investigations and sea level research were focused in Southeast Asia. Since his retirement in 2007, he serves as scientific adviser for Marum/University Bremen and Chatham Rise Rock Phosphate Limited, New Zealand.

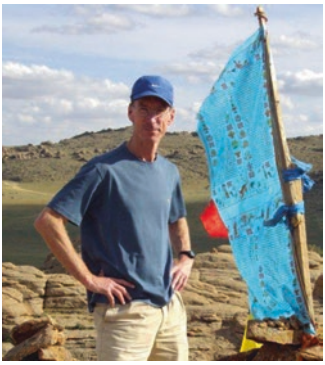

Ray Wood retired from GNS Science after a 34-year career as a marine geoscientist in New Zealand. He led and/or contributed to marine surveys that explored the geology, resources, and tectonic history of New Zealand's EEZ. He is currently the Chief Operating Officer for Chatham Rock Phosphate, a company that plans to mine phosphorite from New Zealand's sea floor, and the leader of the technical team that is helping Oman define the outer limits of its continental shelf beyond the 200 M EEZ.

Robin Falconer is the principal of consulting firm Robin Falconer Associates Ltd. He is the former General Manager Research at GNS Science and Natural Hazards Group Manager (1995–2008). Prior to that, for 14 years an independent consultant in marine research and surveys; and earlier with the Canadian Geological Survey. He has worked in New Zealand and internationally on a range of topics including: marine mineral and oil exploration, seabed surveys, weather analyses, oceanography, environmental studies, geographic information systems, geological hazard assessment, and computer mapping. Robin started working on Chatham Rise phosphate in 1980. He has been involved as a consultant to Chatham Rock Phosphate Ltd (CRP) for the last 6 years. He is currently a Director of CRP.

Chapter 6
Predictive Mapping of the Nodule Abundance and Mineral Resource Estimation in the Clarion-Clipperton Zone Using Artificial Neural Networks and Classical Geostatistical Methods

Andreas Knobloch, Thomas Kuhn, Carsten Rühlemann, Thomas Hertwig, Karl-Otto Zeissler, and Silke Noack

Abstract The licence areas for the exploration of manganese nodule fields in the equatorial Pacific Ocean cover 75,000 km^2 each. The purpose of this study was to predict the nodule abundance of nodule fields over an entire licence area using artificial neural network statistics. Bathymetry and backscatter information of the seafloor and different derived datasets, as well as sampling point data (box core stations), were used as model input data. Based on the prediction results, mineral resources of manganese nodules at different cut-off grades were calculated and the estimated resources were classified according to international codes. In principle, the estimation of tonnages of metals such as nickel, copper, cobalt, manganese, molybdenum, etc. is also possible based on the prediction results and the average metal contents of the nodules.

6.1 Introduction

6.1.1 Scope of Work

The exploration of manganese (Mn) nodules requires the investigation of vast areas of the seafloor since Mn nodules are a two-dimensional deposit sitting on top of deep-sea sediments. Such exploration of nodule fields can be realised in a reasonable amount of time using hydro-acoustic data such as bathymetry and backscatter

A. Knobloch • T. Hertwig • K.-O. Zeissler • S. Noack
Beak Consultants GmbH, Am St Niclas Schacht 13, Freiberg 09599, Germany
e-mail: andreas.knobloch@beak.de

T. Kuhn (✉) • C. Rühlemann
Federal Institute for Geosciences and Natural Resources (BGR),
Stilleweg 2, Hannover 30655, Germany
e-mail: thomas.kuhn@bgr.de

R. Sharma (ed.), *Deep-Sea Mining*, DOI 10.1007/978-3-319-52557-0_6

(Kuhn et al. 2012). However, the major parameters for the economic evaluation of Mn nodule fields are the metal content and the nodule abundance (i.e., the mass per area). It has been shown that the metal content is rather constant in areas covering several thousand square kilometres. For instance, the combined Ni-Cu-Co content in the eastern part of the Clarion-Clipperton Zone (CCZ) has a coefficient of variation (CoV), which is less than 10%. In contrast, the nodule abundance varies over the same area with a CoV of more than 30% (Kuhn et al. 2012).

However, nodule abundance and metal content can only be measured from single point box core stations. Naturally, the amount of such sampling is very limited compared to the vast areal extent of the exploration areas (75,000 km^2). Normally, they amount to a few hundreds of box core stations as compared to several millions of measuring points from bathymetric and backscatter surveys. This limited number of stations is not sufficient to execute resource estimation over larger parts of an exploration area using conventional geostatistical methods. Therefore, the approach we have undertaken was to understand factors controlling the distribution of manganese nodules in relation to the available data, i.e. bathymetric and backscatter data, by using the artificial neural network approach. This chapter provides a general workflow on how to determine the spatial distribution of manganese nodules with artificial neural networks, to compare this approach to classical geostatistics (kriging), and to use the results for estimation and classification of the manganese nodule mineral resources.

6.1.2 Data Used

The basic data used for the investigation are included in the list below:

- digital elevation model (bathymetry data) with a ground resolution of ~100 m,
- backscatter data with a ground resolution of ~100 m,
- measured values of manganese nodules abundance in kg/m^2 and metal contents of nodules,
- ship tracks of the surveying vessel during its sampling campaigns (Wiedicke-Hombach and Shipboard Scientific Party 2009, 2010).

In addition to this, the following data sources were obtained and used:

- average seasonal and annual chlorophyll-a-concentration in the ocean water in mg/m^3, derived from MODIS Aqua data, at a 4 km resolution (NASA 2014);
- average seasonal and annual night-time water temperature at the ocean water surface in °C, derived from MODIS Aqua data, at a 4 km resolution (NASA 2014);
- average seasonal and annual content of particulate organic carbon (POC) of ocean waters in mg/m^3, derived from MODIS Aqua data, at a 4 km resolution (NASA 2014);
- average water currents in u- and v-vector direction in m/s at water depths of 0, 4200 and 4899 m, at a 1/3 degree resolution (approximately 37 km; NOAA 2014).

6.1.3 Software Used

Modelling was run using advangeo® prediction software. This software was developed by Beak Consultants between 2007 and 2012 and provides artificial neural network (ANN) for predictive modelling to GIS users working with Esri ArcGIS version 10 (Beak 2012). Supplementing this approach, classical geostatistics (universal and block kriging) were applied using the Geostatistical Analyst extension of Esri ArcGIS version 10.

All data were converted to ArcGIS-compatible shapefiles or gridfiles, i.e. either vector or raster data. In order to use the ANN tool with advangeo® and ArcGIS, all input data had to be converted to raster format. Results were also compiled in raster format, i.e. *x*, *y*-data with a *z*-value describing the modelled value—in this case the manganese nodule abundance on the ocean floor in kg/m^2.

6.2 Description of Study Area

6.2.1 Bathymetry

For this study, bathymetry data of an area of about 75,000 km^2, located in the eastern and central Clarion-Clipperton Zone within the equatorial northeast Pacific Ocean, have been used (Wiedicke-Hombach and Shipboard Scientific Party 2009, 2010). Bathymetric surveys have been carried out using a SIMRAD EM120 multibeam echo sounder with a frequency of 12 kHz installed on the hull of the US-American R/V Kilo Moana (Wiedicke-Hombach and Shipboard Scientific Party 2009, 2010). The resolution of the gridded hydro-acoustic data from the EM 120 system in ~4000–5000 m water depth is between 100 and 125 m grid cell size. The working areas are situated in the CCZ between Mexico and Hawaii and covers a typical licence area for the exploration of manganese nodules granted by the International Seabed Authority (Fig. 6.1). Water depth in the working area varies between 1460 and 5200 m and the seafloor is generally characterised by horst and graben structures as well as ridges that are several kilometers wide, tens of kilometers long and up to a few hundred meters high. These structures are interpreted as fossil traces of the East Pacific Rise. Seamounts are other characteristic seafloor features which range from small single seamounts rising a few hundreds of meters above the surrounding seafloor to complex seamount structures or chains rising up to more than 2500 m above their surrounding seafloor (Fig. 6.2). Despite the rather complex and diverse seafloor morphology, ~70% of the working area is characterised by seafloor slopes $\leq 3°$.

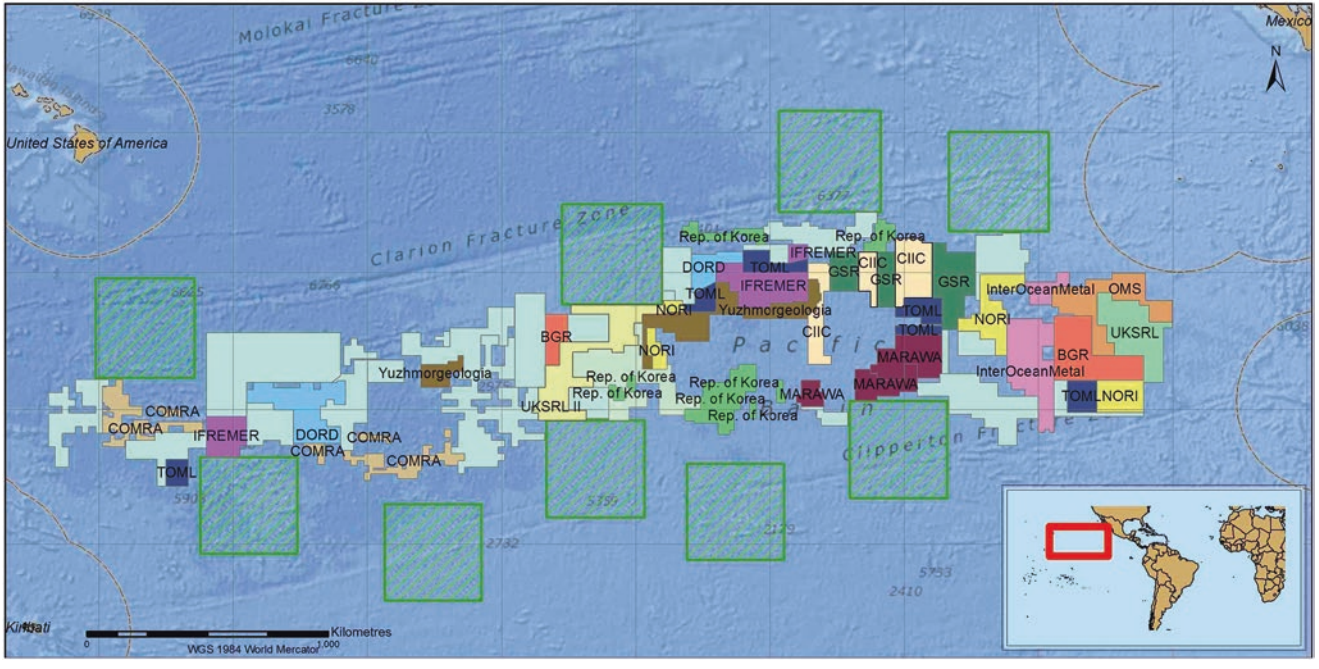

Fig. 6.1 Polymetallic nodules exploration areas in the Clarion-Clipperton Fracture Zone (CCZ) of the NE Pacific (© International Seabed Authority). Note that the exploration area of each licence holder covers 75,000 km^2

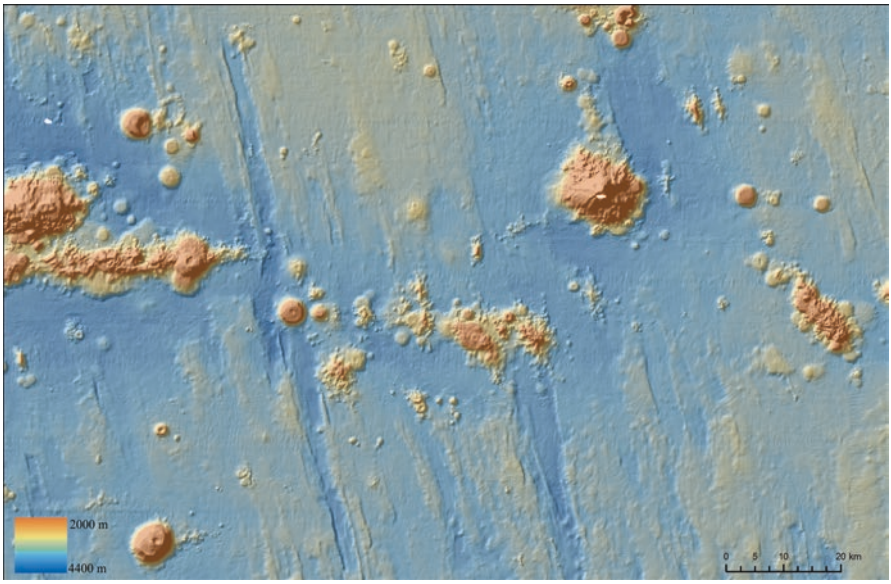

Fig. 6.2 Bathymetry of a typical part of the CCZ indicating the occurrence of large flat seafloor areas as well as different seamount types and ridges

6.2.2 Backscatter Data

Multibeam acoustic imagery (backscatter) data have simultaneously been collected during seafloor bathymetric mapping using the SIMRAD EM120 multibeam echo sounder (Wiedicke-Hombach and Shipboard Scientific Party 2009, 2010). Backscatter data were processed for along-track and across-track errors and eventually transferred into geo-referenced 8-bit grey values (Fig. 6.3; Wiedicke-Hombach and Shipboard Scientific Party 2009, 2010). Backscatter data provide information on the geological conditions of the seafloor. The higher the value the more likely it is to have hard rocks on the ocean floor, while lower backscatter values indicate unconsolidated, water-saturated sediments. Since the difference in relative backscatter strength between a flat, sediment-covered seafloor with and without nodules is between +11 and +13 dB for frequencies between 6.5 and 160 kHz, it is possible to distinguish nodule fields on the seafloor from areas devoid of nodules (Scanlon and Masson 1992; Mitchell 1993). Moreover, the analysis of backscatter data of a 12 kHz multibeam system also allows for the discrimination between seafloor areas dominated by small-sized nodules (long axis of the nodules is generally smaller than 4 cm) and seafloor areas dominated by medium to large-sized nodules (>4 cm; Rühlemann et al. 2013). Fields of small-sized nodules have, in turn, a generally lower nodule abundance compared to fields of medium- to large-sized nodules.

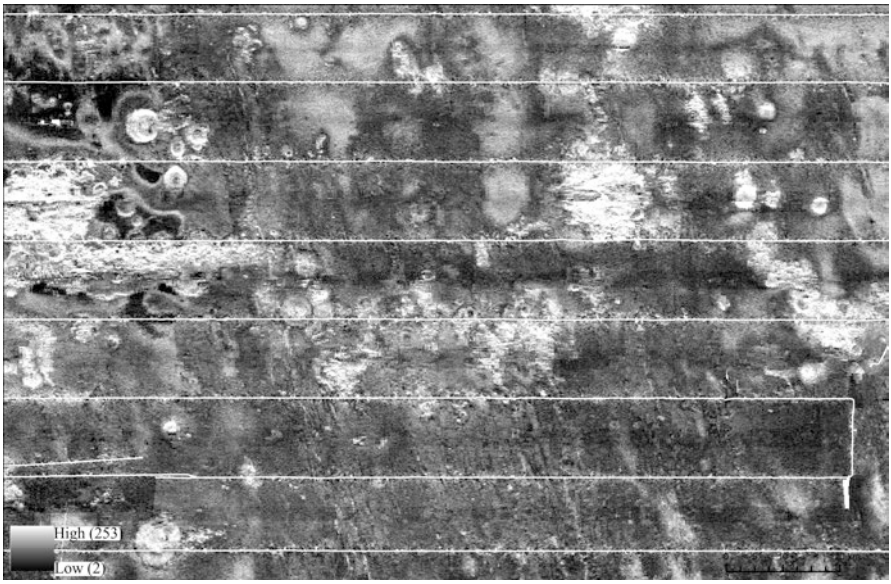

Fig. 6.3 Multibeam acoustic imagery (backscatter) of the seafloor displayed as 8-bit grey values. The *white horizontal stripes* are vessel tracks. Those data were omitted from further analysis. Map section as in Fig. 6.2

The physical principles, which control the correlation between backscatter data and nodule occurrence, allow the prediction of nodule abundance mainly based on hydro-acoustic data in areas without box core samples. However, there is no linear and simple correlation between the hydro-acoustic data and the nodule abundance. Therefore, we have used first- and second-order statistics on the hydro-acoustic data and have analysed the influence of each parameter (both from original data and their derivates) on the nodule abundance using the artificial neuronal network approach.

6.3 Predictive Mapping of Manganese Nodule Abundance

6.3.1 Theoretical Background

6.3.1.1 Artificial Neural Networks (ANN)

In general, two main types of approaches can be used for predictive mapping. These can be distinguished as the so-called knowledge-driven or data-driven approaches. Knowledge-driven approaches are methods such as fuzzy logic or the pure ranking of influencing parameters based on the expert's knowledge. Data-driven approaches are methods such as weights of evidence, artificial neural networks, logistic regression, or random forest. The data-driven artificial neural network approach may also,

however, be influenced by knowledge, since the preparation and processing of data that goes into the artificial neural network is based on knowledge and experience of the expert using the approach.

Artificial neural networks (ANN; Hassoun 1995; Kasabov 1996; Haykins 1998; Bishop 2008) are a powerful tool to integrate data containing different types of information (Brown et al. 2003; Lamothe 2009), such as geology, geophysics, or geochemistry, and to find patterns or relationships in the data. Since many geoscientific events or phenomena (such as ore grades) are influenced by multiple parameters, it is often very difficult to understand the relationship between the parameters that lead to the event or phenomena, especially if very large data sets are being analysed. Because of this, a multivariate geostatistical method such as ANN is capable of investigating and helping to explain geoscientific and other questions.

The functionality of artificial neural networks is based on the functionality of a biological neural system. It consists of artificial neuron cells, which are connected in a network with multiple layers. The biological processes of receipt of information, processing of information, and forwarding of information are simulated in the software by simple mathematical equations. The connection between the neuron cells in the different layers of the network is defined by so-called interconnection weights. The weights define how quick information is forwarded in the ANN. They can be directed in either direction to or from any neuron cell and can be changed with training just as in a biological neural network.

One neuron cell can receive information or data from several connected other neuron cells. This information is then processed to one single information output by a propagation function. Most of the time, a simple sum function is used. The activation function computes the output status of a neuron cell and defines how and when information is forwarded to the connected neuron cells. Very often, a sigmoid function is used as activation function.

The network topology describes the setup of the neurons in layers. It defines the number of hidden layers and neurons in the hidden layers and the number of neurons in the output layer. The number of neurons in the input layers is defined automatically by the amount of available different types of input information. The topology also defines rules such as how many links are between the neurons and how information can run through the network. In this case study, a multilayer perceptron was used. It is a simple network with one input layer with n input neurons, one hidden layer, and one neuron in the output layer. Information can only be processed feed-forward. Figure 6.4 provides a schematic overview of the network setup and the functions used for receiving and forwarding information to and from any neuron within the artificial neural network.

For training of the network, a back-propagation-of-error approach was used. It adapts the weights between the neurons by considering the degree of error from the output signal so that it is minimised. Training itself is an iterative process conducted over a defined number of training runs, where the network is "fed" with data from known events or phenomena in the modelling area. The network then reduces or increases the weights in order to minimise the total error of the network to predict the data at the known locations, correctly.

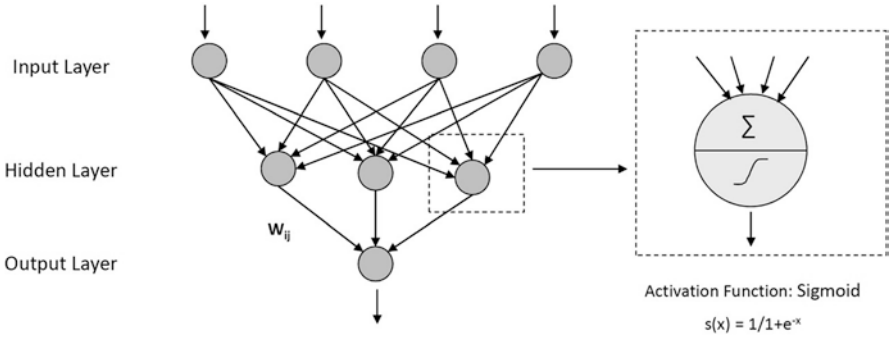

Fig. 6.4 Topology of a Multi-Layer-Perceptron (*left*) and schematic overview of used propagation and activation functions (*right*) (Barth et al. 2014)

6.3.1.2 Classical Geostatistics (Kriging)

Kriging is a well-known geostatistical method for interpolation of point data. Its advantage compared to other classical interpolation methods is that it accounts for the spatial variance of a value, which can be determined and described by a variogram. The variogram model mathematically specifies the spatial variability of the data set in each geographical direction. Scale, range, and nugget effect of the variogram model are required input parameters for kriging (Akin and Siemens 1988). The range of the variogram defines the maximum distance between sample points at which samples statistically influence each other. The scale represents the non-random component of the variability of the data set and the nugget effect stands for the random component.

For prediction at any unknown location, the values from the neighbouring known locations are weighted by keeping the estimation error variance low. This error depends on the fitting quality of the variogram function. In this case study, universal kriging and block kriging were used.

6.3.2 Data Processing

In order to use the available base data in the ANN, several steps involving data pre-processing were necessary. Due to the different statistical distributions of the values from the bathymetric and backscatter datasets in the working area with different variance and average value, the datasets had to be z-transformed and re-scaled. As a result, the data distributions were transformed to have the same average value and to have a variance twice as wide as the standard deviation.

In the next pre-processing step, the bathymetry and backscatter datasets were filtered using a smoothening average filter. It is a moving average box, averaging the surrounding data values. A 3 × 3 filter was used for bathymetry and 5 × 5 filter for

backscatter. Next, based on previous investigations (Rühlemann et al. 2013), the backscatter dataset was interpreted and classified into four classes: class 1—sedimentary flat areas without any manganese nodules, class 2—small nodules (<4 cm of long axis), class 3—medium to large nodules (>4 cm long axis), and class 4—hard reflector, indicating rocks without nodules.

Different derivatives were then calculated from the processed datasets of bathymetry and backscatter using the Spatial Analyst extension of ArcGIS. These were the slope of the surface (first derivative), aspect and curvature (second derivative). For the aspect of the surface, which is the exposition or direction of the steepest slope at any point, two different raster datasets were calculated for the N/S- and the W/E--striking slopes. For curvature, three different types were calculated—vertical curvature, which is the curvature in the direction of the steepest slope; horizontal curvature, which is the curvature in the direction of the contours of the surface, i.e. in the direction perpendicular to the steepest slope; and the maximum curvature, by combining both vertical and horizontal curvature. In addition, flow direction and flow accumulation were calculated from the bathymetry dataset, to explain possible pathways of bottom currents.

One problem with the measured backscatter data was the clear change of the absolute values along the vessel tracks during the measurement. In order not to use such data during training of the ANN, a buffer distance of 500 m was applied on both sides of the known tracks. Any sampling point within this buffer distance was not used for the training of the ANN. Furthermore, areas with submarine volcanoes, so-called seamounts, were not considered during the predictive modelling. This is due to the fact of the general understanding that no mineable manganese resources can be found there. As a result, these areas were completely masked out during processing, modelling, and presentation of the prediction results. As outer limits for delineation of the seamounts-mask, the lower foot of the hillside slopes of the seamounts was used.

In addition, linear structures and lineaments have been digitised based on the bathymetry and its derivatives—slope and curvature. Finally, special raster datasets were calculated to be used as an additional dataset in the artificial neural network, which have the distance to the nearest lineament or seamount assigned to any specific raster cell. These distances were calculated by using the Euclidian distance tool from the Spatial Analyst of ArcGIS. Lower values indicate a shorter distance to the closest lineament/structure or seamount. These raster datasets were used in order to include information about the spatial distribution of the manganese nodule abundance in relationship to the formation of the structures and seamounts in the ANN.

The last but most important pre-processing step required was the selection and processing of the training data. It is necessary to train and calibrate the ANN model. As mentioned before, the known values of the manganese nodules abundance (wet weight) were used to train the model. In total, 214 values of manganese nodule abundance were available; after a plausibility test of the original data, only 209 values were judged sufficient for training purposes. Some of the values had also to be averaged since they were too close together. This is due to the intended resolution of the prediction of 100 m. All data points closer together than 100 m were averaged

so that only 200 values remained. Lastly, the before-mentioned buffer of 500 m around the ship tracks was used to filter data points from areas with influenced backscatter data. Finally, 182 values could be used for further analysis.

6.3.3 Model Development and Calibration

For modelling with the ANN, all previously described data layers were imported and used as separate input layers and assigned to separate neurons. Overall, 73 separate input data layers were created to be used in the ANN. In addition, all input data were mapped and transformed to raster datasets with exactly the same raster extent concerning the outer limits and their raster resolution, which was 100 m.

All input data layers were normalised from their original values and re-sampled to values between 0 and 1 in order to bring them to the same order of magnitude as the prediction result of the ANN model, which will range between 0 and 1. The training data (Mn nodule abundances in kg/m^2), with the original measurement values, had also to be re-sampled between 0 and 1 in order to use it as training data. After the initial computations, the result of the final output layer had to be re-converted to its original data distribution in order to interpret it.

The main idea of the model development and calibration with the training data is to find the pattern in the input data, which correlates with the values of the training data at the sites of the training data. Input data layers with high correlations will be weighted higher than layers with lower correlation. The difficult exercise is to find these correlations in the multi-variate space, since the ANN is using all input layers at once for the training and not one by one. Since some layers might not contain relevant information, which correlates with the distribution of the manganese nodule abundance of the sample points, these layers will be weighted less or can be completely left out of the ANN model. This can be tested by training ANN models with different combinations of input data layers. Models with combinations of data layers with only high correlation will have lower prediction errors than models, where input layers are included with only noisy information.

Training itself was run over 1000 iterations/epochs. Overall, 117 different combinations of input layers were used to train the ANN. The prediction error of each model was calculated as the model's root mean squared error (RMSE) of the originally measured abundance value minus the predicted/modelled value for all 182 training locations.

6.4 Modelling Results

The lowest error was determined for the ANN model using the combination of the following input layers:

- backscatter (filtered, classified): class 1—sedimentary, flat areas without nodules,
- backscatter (filtered, classified): class 2—small nodules,

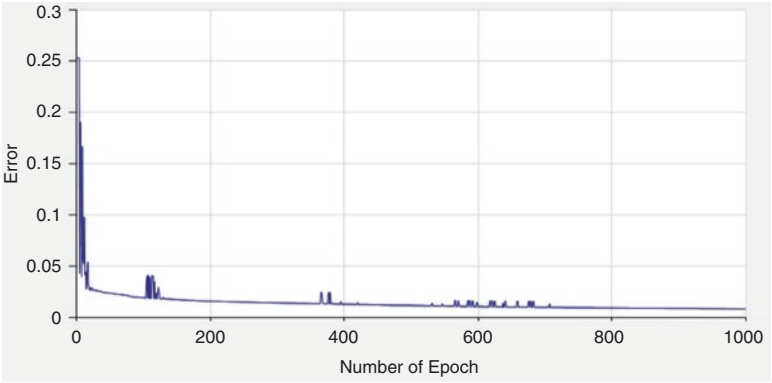

Fig. 6.5 Training curve of the final ANN model using a combination of 17 different input layers

- backscatter (filtered, classified): class 3—medium-large nodules,
- backscatter (filtered, classified): class 4—hard reflector,
- backscatter (z-transformed, filtered): absolute value,
- bathymetry (filtered): flow accumulation,
- bathymetry (filtered): slope,
- bathymetry (z-transformed, filtered): absolute value, inversely scaled,
- lineaments: Euclidian distance with 15 km maximum,
- seamounts: Euclidian distance with 13.5 km maximum, inversely scaled,
- chlorophyll-a-concentration: yearly average from spring,
- temperature of the ocean water surface at night: yearly average from spring,
- content of particulate organic carbon: yearly average from spring,
- water current at 4200 m water depth: average of u-vector,
- water current at 4899 m water depth: average of u-vector,
- water current at 4200 m water depth: average of v-vector,
- water current at 4899 m water depth: average of v-vector.

Figure 6.5 shows the change of the training error (RMSE) over 1000 training iterations. It shows that a stable plateau was found and no more oscillations occur after 700 iterations. In addition, Fig. 6.6 provides the correlation curve between observed/measured manganese abundance and modelled/predicted abundance at the training locations. The goodness of the correlation curve is $R^2 = 0.8016$, indicating a satisfactory prediction result. The prediction result was compiled (see example in Fig. 6.7) as a raster map in ArcGIS, containing the predicted manganese nodules abundance across the investigation area in absolute values of kg/m^2. A comparison between Figs. 6.2 and 6.3 with Fig. 6.7 indicates the influence of the backscatter data, the slope of the bathymetry as well as the distance to the linear structures and seamounts on the nodule abundance.

In order to understand the influence of the different input layers that led to the prediction results, the weights of all neurons within the whole network were evaluated. This was done by using the approaches of Olden (Olden and Jackson 2002; Olden et al. 2004), in which the so-called connection weights are calculated.

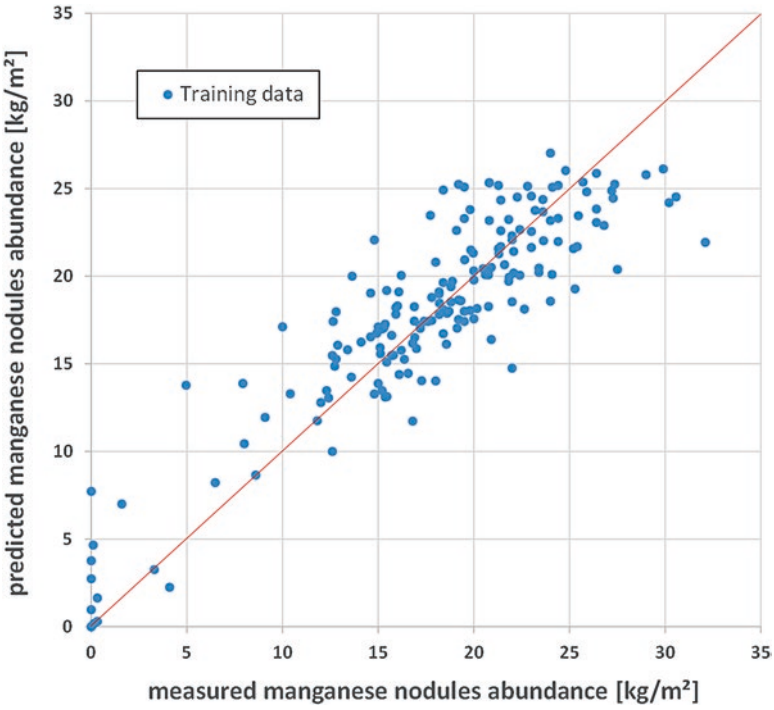

Fig. 6.6 Correlation curve of measured/observed vs. modelled/predicted manganese nodules abundance [kg/m^2] at the training points (positions of box cores). RMSE = 2.98 kg/m^2; $R^2 = 0.8016$

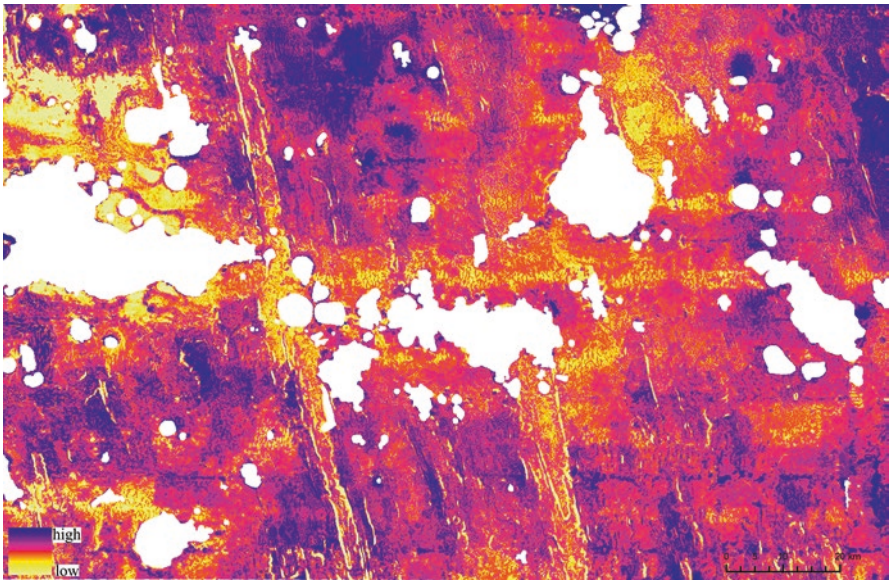

Fig. 6.7 Prediction map showing the manganese nodules abundance in kg/m^2 in one part of the CCZ. Map section as in Fig. 6.2

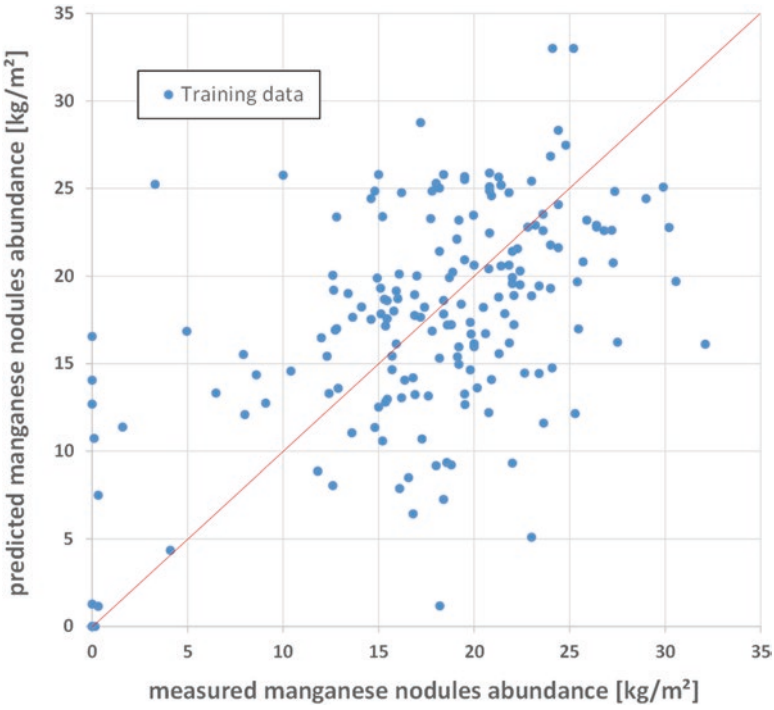

Fig. 6.8 Cross validation curve of measured/observed vs. modelled/predicted manganese nodules abundance [kg/m^2] at the training points (positions of box cores). RSME = 6.332 kg/m^2, $R^2 = 0.2662$

This is done by summing up all weights that are connected or originated at one certain neuron of an input layer. In addition, with the help of the so-called Garson's algorithm, the percentage of the weight for a single input layer can be calculated in proportion to the overall weighting of all neurons in the network.

Based on the Garson's algorithm, the most significant input data layers are (in order of significance):

- backscatter (filtered, classified): class 1—sedimentary, flat areas without nodules → 43%,
- bathymetry (filtered): slope → 15%,
- water current at 4899 m water depth: average of v-vector → 13%,
- bathymetry (z-transformed, filtered): absolute value, inverse scaled → 11%.

Finally, goodness of the prediction result was tested by using leave-one-out-cross-validation (LOOCV). It provides information about the robustness of a parameter and training data constellation and their representation of the spatial distribution of the manganese nodules abundance. A total of 182 cross validation models were run by leaving out one training value at a time and determining the predicted value of the model at the location of the training point, which was not used for the training. The resulting cross-validation-curve in Fig. 6.8 shows the good general fit of

the model. However, the RMSE of the cross validation of 6.332 kg/m^2 implies an average relative error regarding the prediction of the nodule abundance of approximately 35%. This rather high RMSE indicates the sensitivity of the models for one training point. Problems especially arise with values close to 0 kg/m^2 nodule abundance with most of these values being predicted too high. Moreover, the large difference of the resolution of the training points (box core stations with a surface area of 0.25 m^2) and the hydro-acoustic data (the area of each hydro-acoustic "pixel" is 10,000 m^2) may also be a reason for the rather high RMSE.

In addition to the prediction model based on the ANN trained over the whole area, a smaller prediction model was created for four sub-clusters inside the working area by using universal kriging as an interpolation tool, based on the training data values (box core samples). In these four sub-areas (sub-cluster 11, 12, 61 and 62; Fig. 6.10), the density of sample points and available measurements of the nodule abundance were high enough to apply such an interpolation method. A spherical variogram model was used for all four sub-clusters. The range values used in the kriging model are between 3000 and 7000 m, indicating the spatial variance of manganese nodules abundance. The nugget values for the nodules abundance used in the variograms range between 2 and 3 kg/m^2; only sub-cluster 12 has a rather high nugget value of 18 kg/m^2. These nugget values make up 16–23% of the total variance of the data set except for sub-cluster 12 with 71% of the total variance.

6.5 Resource Estimation of Manganese Nodules

6.5.1 Resource Estimation Based on the ANN Model

The mining of manganese nodules will require a minimum amount of nodules per year to be mined to render it economic. Since nodule collectors can only have a limited size, can move with a limited speed over ground, and have a collecting efficiency somewhere between 30 and 80%, a certain minimum nodules abundance is necessary to guarantee that enough nodules can be collected. This threshold is called the cut-off value. It is not clear yet what the cut-off for an economic nodule mining might be. However, with our approach, it is possible to determine the mineable areas at different cut-off grades of manganese nodules abundance based on the area-wide prediction results. Using the resulting total remaining surface area at each cut-off and multiplying it by the average manganese abundance for the specific area covered at a certain cut-off grade, the total weight of manganese nodules was calculated for the different cut-off grades.

Figure 6.9 schematically shows the estimated total resources in tonnes at different cut-off grades for one licence area for the exploration of manganese nodules (75,000 km^2). A clear break point is visible where the resource decreases stronger. This indicates the value of the cut-off above which mining will be less economic, because the covered areas may become too small, too spread out, and the total

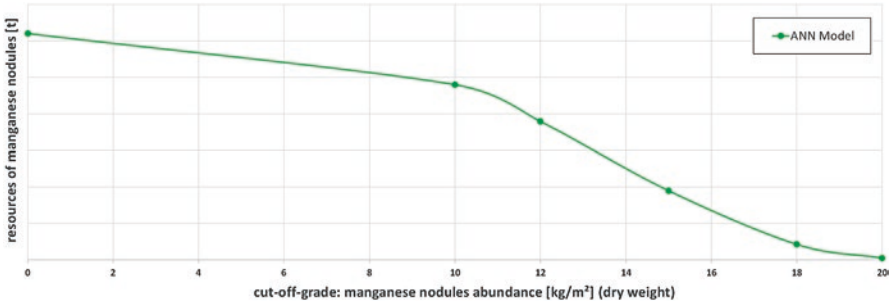

Fig. 6.9 Calculated resources of manganese nodules [t] in the working area at different cut-off grades of manganese nodules abundance [kg/m^2] (dry weight). A clear break point is visible at 10 kg/m^2 dry weight, which corresponds to ~15 kg/m^2 wet weight of manganese nodules abundance

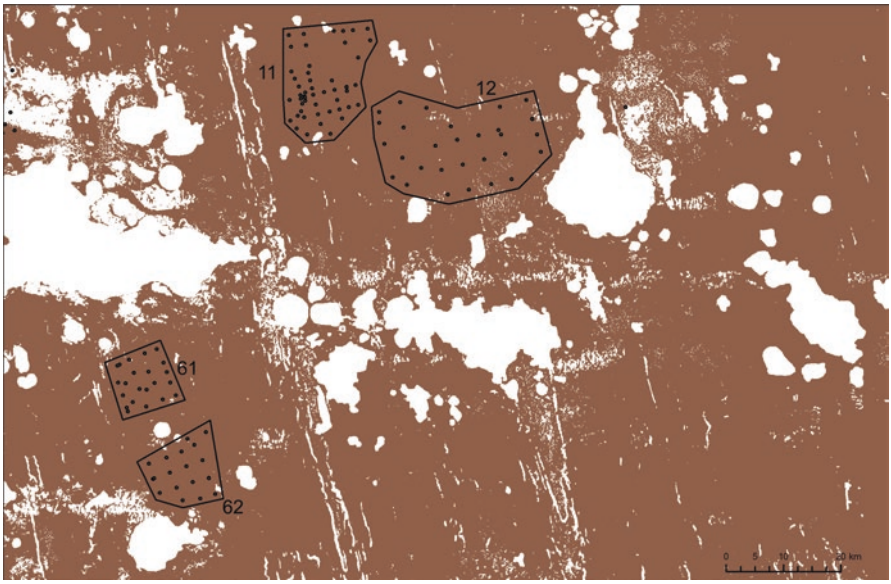

Fig. 6.10 Distribution of manganese nodule fields with a minimum abundance of 15 kg/m^2 (so-called cut-off value; based on wet weight). Locations and designation of four sub-clusters and sites of box core stations are also shown. Such maps are the basis for the selection of prospective nodule fields (i.e., the sub-clusters). Map section as in Fig. 6.2

nodule tonnages may be too low across the study area. The break point is in line with the currently assumed cut-off grade for mining based on technical equipment and economic evaluations, which is around 15 kg/m^2 (based on wet weight; i.e. ~10 kg/m^2 based on dry weight).

Based on different cut-off values of the nodule abundance, it is possible to map prospective regions, i.e. areas with a high percentage above the respective cut-off (Fig. 6.10).

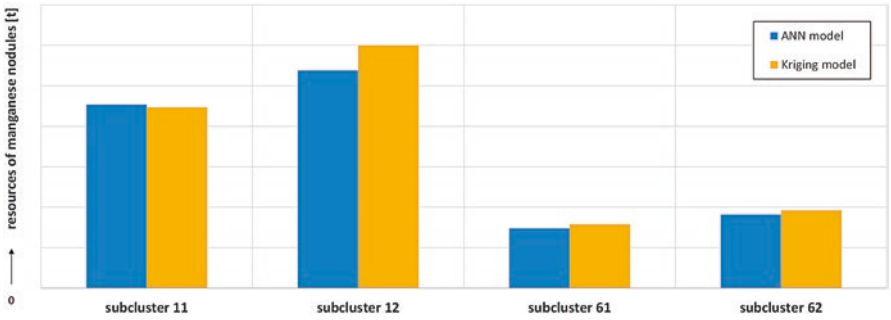

Fig. 6.11 Calculated resources of manganese nodules [t] in the four clusters in the eastern part of the working area at a cut-off-grade of 15 kg/m^2 of nodule abundance (wet weight)—comparison of calculations between the artificial neural network and universal kriging model

Based on the average metal content of the manganese nodules from each box core station, it is also possible to calculate metal tonnages according to the different cut-offs. In order to do this, it is necessary, though, to determine the nodule abundance based on dry weight.

6.5.2 Resource Estimation Based on the Kriging Model

Using the same approach as applied for the resource estimation based on the ANN model, resources of manganese nodules were calculated for four smaller sub-cluster areas (Fig. 6.10) using the results of the universal kriging model.

Figure 6.11 shows the estimated manganese resources based on the universal kriging prediction results in all four sub-clusters compared to the resource calculations based on the ANN prediction model. It shows the similarities between the two different approaches and validates the prediction results of the model based on ANN directly with the independent results based on the kriging model. Nevertheless, it has to be noted that even though the overall manganese nodules resources are almost the same using both approaches, the predicted spatial distribution of manganese nodules differs.

One advantage of the kriging approach versus the ANN approach is that the absolute prediction error can be calculated for any point in the modelled area within the four sub-clusters with kriging. This provides an overview of the spatial distribution of the prediction error and shows areas with lack of training data to interpolate correctly. A relative prediction error (RPE) was calculated. It was defined as the true value, which is distributed with 95% probability within the interval between:

$$\left[PV - RPE\left(in\%\right); PV + RPE\left(in\%\right)\right]$$

with PV as the predicted value—in our case the manganese nodule abundance in kg/m^2. The relative prediction error (RPE) in percent can then be calculated as:

$$RPE\left[\%\right] = 2 * PE / PV^{*}100$$

with PE—absolute prediction error.

Block kriging was applied on the universal kriging results (i.e. point kriging with 100 m resolution) in order to estimate the absolute and relative prediction error at different block sizes of 500 × 500 m, 1000 × 1000 m, 2000 × 2000 m, and 5000 × 5000 m.

By comparing the values of the absolute and relative prediction error of the kriging model, it can be derived that the models with larger block sizes result in smaller prediction errors. At block sizes of 500 × 500 m or 1000 × 1000 m, the block kriging results are very similar to the point kriging result. With block sizes of 1000 × 1000 m, 2000 × 2000 m, or even 5000 × 5000 m, the results become more generalised. At an assumed technical block size of 2000 × 2000 m, the relative prediction error in the four clusters ranges between 16 and 26% (Fig. 6.12).

6.6 Classification of Manganese Mineral Resources

Based on the calculated mineral resources of manganese nodules, the mineral resources for the described four sub-clusters were classified by using geostatistical key values. In general, mineral resources can be classified based on the degree of geological knowledge. According to CRIRSCO (2012), resources are defined as a concentration or occurrence of a raw material with economic relevance within or above the earth's crust. Based on the geometry, content, quality, and amount of the raw material, it can be assumed that the raw material can be mined economically.

Regarding the grade of geological knowledge, three mineral resource classes can be defined after JORC (2012; with increasing level of knowledge): inferred mineral resources, indicated mineral resources, and measured mineral resources. According to Benndorf (2015), the following two criteria can be used to evaluate the geological knowledge of a mineral resource based on statistical key values:

- Accuracy of the calculated mineral resources with a certain defined confidence interval,
- Continuity of the mineral resource and its measured content.

Based on this statement, the relative prediction error and the range value of the kriging model can be used to classify the estimated mineral resources. It has to be stated that there is no definition of the absolute degree of the accuracy required after JORC (2012) to classify any mineral resource into one of the described three classes. In addition, one has to be well aware that the accuracy has always to be stated together with the assumed confidence interval.

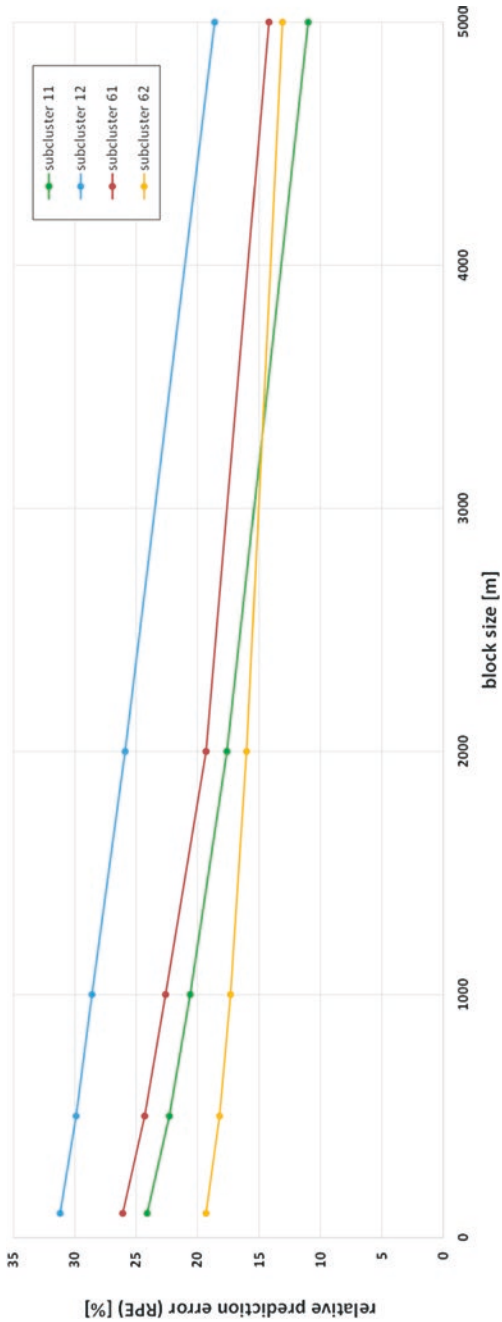

Fig. 6.12 Plot of the relative prediction error (%) of the nodule abundance (wet weight) based on block kriging and different block sizes

Table 6.1 JORC classification of nodule resources of sub-clusters based either on accuracy of the calculation (prediction error) or continuity (range of variogram) of the resource

Sub-cluster	Block size (m)	Relative prediction error (%)	Confidence level (%)	JORC classification	Range of variogram (m)	Average sample distance (m)	JORC classification
11	2000	17.6	95	Indicated	3000	2380	Indicated
12	2000	25.9	95	Inferred	4000	4679	Inferred
61	2000	19.3	95	Indicated	4000	2592	Indicated
62	2000	16.0	95	Indicated	7000	3049	Measured

As mentioned before, based on the kriging results, a relative prediction error was determined with a 5% confidence interval, which is a 95% confidence level. Knowing this, the mineral resources in the four cluster areas can be classified based on GDMB (1983). In GDMB (1983), a table is provided, which links the verbal knowledge classes used in JORC to maximum acceptable average prediction errors for each class. Based on it, measured mineral resources are assumed to have a relative prediction error of less than 10%; indicated mineral resources to have a relative prediction error between 10 and 20%; and inferred mineral resources to have a relative prediction error between 20 and 30%.

As a result, assuming a cut-off grade of 15 kg/m^2 (wet weight) and a block size for mining of 2000 m, three of the four smaller cluster areas can be classified as indicated mineral resources, while cluster 12 can be classified as inferred mineral resources, only (Table 6.1). As discussed, the range value of the kriging model can be used to evaluate the continuity of the raw material and its grade. This can be done by comparing the average sampling distance within a certain area with the range value of the variogram. According to Benndorf (2015), the classification can be done as follows: measured mineral resources are assumed to have an underlying average sampling distance of less than half of the range value; indicated mineral resources are assumed to have an average sampling distance between half of the range value and the range value; and inferred mineral resources are assumed to have an average sampling distance of larger than the range value (Fig. 6.13). As a result, the same mineral resource classification can be done for three out of the four smaller cluster areas compared to the classification based on the relative prediction error. For cluster 62, the mineral resources can be classified as measured (compared to a previously indicated mineral resource; Table 6.1).

6.7 Conclusions and Recommendations

In summary, the manganese nodule abundance was successfully predicted across an area of 75,000 km^2 in the Pacific Ocean using an artificial neural networks approach. This approach allows precise statements to be made about the spatial distribution of the manganese nodules abundance with a spatial resolution of 100 × 100 m. The prediction is based on a final model composed of 17 different input data layers.

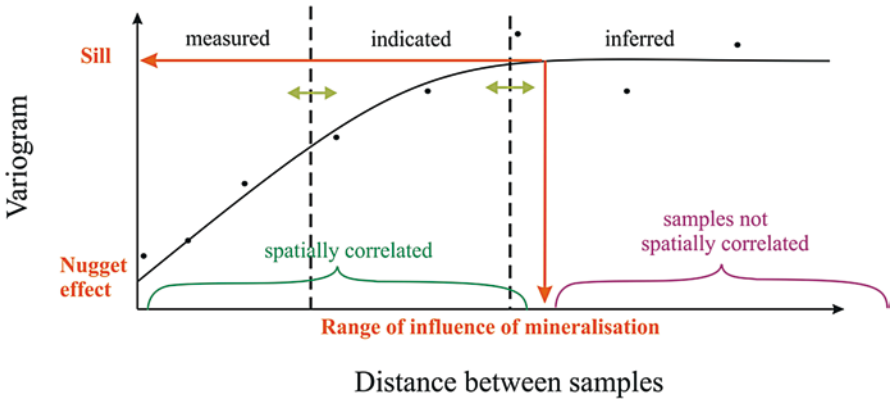

Fig. 6.13 Resource classification based on the continuity of the deposit using the variogram range (after Benndorf 2015)

The most important sources of information were the flat areas without manganese nodules derived from the backscatter data and the slope derived from the available bathymetry dataset. The model was trained with 182 sampling points with measured values of the manganese nodules abundance in kg/m^2. The model was verified with cross validation. In addition, it was fully validated by using an independent model approach with kriging, which led to the same prediction results in four selected smaller cluster areas within the working area.

Based on the predicted area-wide abundance, the total wet weight of the nodules was calculated. Derived from this amount, the total mineral resources of manganese nodules were estimated at different cut-off-grades in tonnes. In addition to this, the absolute and relative prediction error was determined at different block sizes for the resource estimation based on kriging results within the four sub-clusters. The error ranges between 16 and 26%. Based on this relative prediction error, the four cluster areas could be classified as either indicated or inferred mineral resources assuming a confidence level of the prediction of 95%. The mineral resources were classified as well based on comparison of the range value of the variogram model with the average sampling distance within the four sub-clusters. With this approach, the four areas were classified to be indicated or even measured mineral resources.

In order to improve the mineral resources classification, the relative prediction error needs to be lowered. This can be achieved by increasing the sample density and hence decreasing the average sample distance. By decreasing the sample distance compared to an average range value of the variogram used for kriging, the mineral resource classification can also be improved. To simulate the improvement of the sample density, additional kriging models were already run with artificially densified sample networks with artificial sample points, which were assigned with values from the original kriging model. Later, the prediction error was re-calculated. By interpolating the change of the relative prediction error compared to the change of the sample density, the required average sample distance can be stated in order to classify the mineral resources as measured.

A further general improvement of the prediction result based on ANN can be achieved by adding further important and relevant input data layers as well as using more training points. The analysis of underwater images, which yield information about nodule coverage and nodule size distribution, and the correlation of such information with hydro-acoustic data (e.g. with backscatter data) are such relevant input data. Another improvement can be expected by adding data providing information about the water currents. As shown with the few, low-resolution datasets of water currents from NOAA used in this study, this type of data shows some kind of relationship to the distribution of the manganese nodules.

It is recommended to further investigate the proposed densification of the sample network within a smaller area inside one of the four sub-clusters in the working area. Only by doing this, it can be proven whether the increase of the recommended sample density will lead to the forecasted decrease of the prediction error, which is required to classify the mineral resources as measured.

References

Akin H, Siemens H (1988) Praktische Geostatistik: Eine Einführung für den Bergbau und die Geowissenschaften. Springer, Berlin, p 304

Barth A, Knobloch A, Noack S, Schmidt F (2014) Neural network based spatial modeling of natural phenomena and events. In: Khosrow-Pour M (ed) Systems and software development, modeling, and analysis: new perspectives and methodologies. IGI Global, p 186–211. ISBN 13: 9781466660984

Beak (2012) advangeo® prediction software user's guide. Version 2.0 for ArcGIS 10.0. Beak Consultants GmbH, Freiberg, 2007–2012

Benndorf J (2015) Vorratsklassifikation nach internationalen Standards–Anforderungen und Modellansätze in der Lagerstättenbearbeitung. Markscheidewesen 122(2–3):6–14

Bishop MC (2008) Neural networks for pattern recognition. Oxford University Press, Oxford

Brown W, Groves D, Gedeon T (2003) Use of Fuzzy membership input layers to combine subjective geological knowledge and empirical data in a neural network method for mineral-potential mapping. Nat Resour Res 12(3):183–200. doi:10.1023/A:1025175904545

CRIRSCO (2012) International Reporting Template for the public reporting of Exploration Results, Mineral Resources and Mineral Reserves. Committee for Mineral Reserves International Reporting Standards, ICMM, Nov 2013. http://www.crirsco.com/templates/international_reporting_template_november_2013.pdf. Accessed 31 Jan 2015

GDMB (1983) Klassifikation von Lagerstättenvorräten mit Hilfe der Geostatistik: Vorträge einer Diskussionstagung der Fachsektion Lagerstättenforschung in der GMDB. Schriftenreihe der GDMB; Heft 29. Herausgeber: Gesellschaft Deutscher Metallhütten-und Bergleute r. V., Clausthal-Zellerfeld. Wissenschaftliche Redaktion: W. Ehrismann und H. W. Walter. Verlag Chemie, Weinheim, Deerfield Beach, Basel

Hassoun M (1995) Fundamentals of artificial neural networks. MIT Press, Cambridge, p 537

Haykins S (1998) Neural networks: a comprehensive foundation, 2nd edn. Prentice Hall, Upper Saddle River

JORC (2012) The JORC code. Australasian code for reporting of exploration results, mineral resources and ore reserves. AusIMM, Carlton. http://www.jorc.org/docs/jorc_code2012.pdf. Accessed 31 Jan 2016

Kasabov NK (1996) Foundations of neural networks, fuzzy logic, and knowledge engineering. MIT Press, Cambridge

Kuhn T, Rühlemann C, Wiedicke-Hombach M (2012) Developing a strategy for the exploration of vast seafloor areas for prospective manganese nodule fields. In: Zhou H, Morgan CL (eds) Marine minerals: finding the right balance of sustainable development and environmental protection. The Underwater Mining Institute, Shanghai, K1-9

Lamothe D (2009) Assessment of the mineral potential for porphyry Cu-Au ± Mo deposits in the Baie-James region. Document published by Géologie Québec (EP 2009-02). http://collections.banq.qc.ca/ark:/52327/bs1905189. Accessed 24 Oct 2010

Mitchell NC (1993) Comment on the mapping of iron-manganese nodule fields using reconnaissance sonars such as GLORIA. Geo-Mar Lett 13:244–247

NASA (2014) Ocean Color Web: Data Access-Level 3 Browser. Aqua MODIS Data. Ocean Biology Processing Group (OBPG), NASA Goddard Space Flight Center. http://oceancolor.gsfc.nasa.gov/cgi/l3. Accessed 5 Nov 2014

NOAA (2014) OSCAR: Ocean Surface Current Analyses–Real time. Data Download for Ocean Surface Currents. OSCAR Project Office, Earth and Space Research. http://www.oscar.noaa.gov/datadisplay/oscar_datadownload.php. Accessed 5 Nov 2014

Olden JO, Jackson DA (2002) Illuminating the "black box": a randomization approach for understanding variable contributions in artificial neural networks. Ecol Model 154:135–150

Olden JD, Joy MK, Death RG (2004) An accurate comparison of methods for quantifying variable importance in artificial neural networks using simulated data. Ecol Model 178:389–397

Rühlemann C, Kuhn T, Vink A, Wiedicke M (2013) Methods of manganese nodule exploration in the German license area. In: Morgan CL (ed) Recent developments in Atlantic seabed minerals exploration and other topics of timely interest. The Underwater Mining Institute, Rio de Janeiro, p 7

Scanlon KM, Masson DG (1992) Fe-Mn nodule field indicated by GLORIA, North of the Puerto Rico Trench. Geo-Mar Lett 12:208–213

Wiedicke-Hombach M, Shipboard Scientific Party (2009) Cruise Report "Mangan 2008", RV Kilo Moana, 13 Oct–22 Nov 2008. Bundesanstalt für Geowissenschaften und Rohstoffe, Hannover, 89 pp

Wiedicke-Hombach M, Shipboard Scientific Party (2010) Cruise Report "Mangan 2009", RV Kilo Moana, 20 Oct–27 Nov 2009. Bundesanstalt für Geowissenschaften und Rohstoffe, Hannover, 64 pp

Andreas Knobloch is a geologist and Head of the Department for International Activities at Beak Consultants GmbH from Germany. He has specialised in exploration targeting, mineral resource management, and information system development. Since 2010, he is responsible for predictive mapping of the manganese nodules in the German licence area in the CCZ on behalf of the German Federal Institute for Geoscience and Natural Resources (BGR) using artificial neural networks and geostatistics.

Thomas Kuhn is a marine geologist at the German Federal Institute for Geosciences and Natural Resources (BGR). He has specialised in solid-phase associations and structural control of trace elements in ferromanganese precipitates, rocks, and sediments, the automated analysis of seafloor images, geostatistical resource estimation, and the analysis of hydro-acoustic data for the exploration of manganese nodule fields. He has participated in more than 25 research cruises to all major oceans.

Carsten Rühlemann is a marine geologist at the German Federal Institute for Geosciences and Natural Resources (BGR) and is the project manager for the exploration of manganese nodules in the German licence area. He has participated in more than 20 ocean-going expeditions.

Thomas Hertwig is a geochemist and Head of the Department for Geosciences and Environment at Beak Consultants GmbH from Germany. He has specialised in exploration of barite, fluorite, copper, tin and gold deposits, mineral resource management, geostatistics, and soil sciences.

Karl-Otto Zeissler is a geomathematician and works as GIS developer and analyst at Beak Consultants GmbH from Germany. He has specialised in application of mathematical methods for geological reconnaissance mapping and the development of computer-aided technologies for the exploration of raw materials.

Silke Noack is an engineer for mine surveying and works as database and GIS developer at Beak Consultants GmbH from Germany. Since 2008, she is responsible for the development of the advangeo® Prediction Software and specialised in artificial neural networks and other analysis technologies.

Chapter 7
Statistical Properties of Distribution of Manganese Nodules in Indian and Pacific Oceans and Their Applications in Assessing Commonality Levels and in Exploration Planning

T.R.P. Singh and M. Sudhakar

Abstract This chapter presents results of analysis of available statistical data on distribution of manganese (polymetallic) nodules on the seafloor of Indian and Pacific Oceans. It is concluded that the nodule fields of varying sizes within each of the two oceans share common distribution patterns. More importantly, the study brings out striking similarity between the distribution characteristics of nodule fields in the two oceans in terms of coefficients of variation of nodule abundance, variographic parameters including similar but high level of nugget coefficients and the unimodal lognormal frequency distribution of abundance values. The computations of estimation variances for study areas in Indian and Pacific Oceans establish the constancy of the product of variance of error and the area of nodule field under given conditions. Finally, since nodule abundance forms the governing parameter for exploration planning as brought out by the data, estimation variances for selected sizes of nodule fields have been computed for varying sampling grids for both the oceans. It is concluded that a given sampling grid of say, 0.15° over a given size of nodule field of 75,000 km^2, produces an identical estimation error of less than ±10% of the respective mean abundance values in Indian as well as Pacific Oceans.

7.1 Introduction

It is well known that manganese nodules containing copper, nickel, cobalt and manganese occur extensively in the Clarion-Clipperton Fracture Zone (CCZ) in the Equatorial North Pacific Ocean as well as Central Indian Ocean Basin (CIOB) in the Indian Ocean. Currently, a large number of State or State-sponsored agencies are registered as the contractors with International Seabed Authority (ISA) in the CCZ

T.R.P. Singh (✉) • M. Sudhakar
Ministry of Earth Sciences, Prithvi Bhavan, Lodi Road, New Delhi 110 003, India
e-mail: trp_singh@yahoo.com; m.sudhakar@nic.in

R. Sharma (ed.), *Deep-Sea Mining*, DOI 10.1007/978-3-319-52557-0_7

while India is the only contractor engaged in exploration for nodules in CIOB. Extensive sampling of nodules for measurement of abundance (kg/m^2) and metal grades leading to estimation of nodule resources have been carried out in CCZ and CIOB, in addition to bathymetric surveys. This chapter, however, is restricted to the study of sampling data originating from exploration by a large number of contractors and other agencies. As the original raw sampling data are not available for CCZ or for CIOB in public domain, summary statistical data including the variographic models have been used for this study to make some meaningful inferences on the statistical properties of the distribution of nodules in the two oceans. Variographic parameters allow prediction of estimation accuracies for given sizes of nodule fields as also planning of exploration density for achieving pre-specified estimation accuracies.

Almost the entire sampling carried out in CIOB is through free-fall grab samplers with five to seven operations for each sampling station (Jauhari et al. 2001). Box coring operations were limited. Similarly, virtually all the sampling data obtained from CCZ by all investigators/contractors were also from free-fall grab samplers (ISA 2010, Technical Study: No. 6). It has been widely recognized that free-fall grab samplers represent the best tools for assessment of nodule abundance (Hennigar et al. 1986). Uniformity of sampling tools across CCZ and CIOB provides the necessary basis for comparing statistical parameters of nodule distribution.

The objectives of the present study are to (a) present the relative variability of nodule abundance and grades for various study areas of CCZ as well as CIOB leading to identification of the governing parameter for exploration planning, (b) demonstrate the validity of Area-Estimation Variance relationship for various sizes of study areas in CCZ as well as CIOB, (c) provide graphic solutions for prediction of estimation accuracies for varying sizes of nodule fields and finally to (d) investigate the extent to which some generalizations may be made on the commonality of statistical properties of distribution of nodules in the two oceans.

7.2 Nature of Data and Sources Used in the Study

The data used in the present study primarily includes mean values and variances/standard deviations of abundance and metal grades for all study areas of CCZ as well as CIOB listed below. The variogram models for abundance resulting from experimental variograms for CCZ as well as CIOB as also the frequency distribution charts for abundance have also been used.

7.2.1 Major Sources of the Data Include

1. ISA Technical Study: No. 6 (ISA 2010) and Workshop Volume (ISA 2009) for study areas in CCZ (ISA 1–ISA 4 and Total Study Area (TCCZ)) (Fig. 7.1)
2. Nautilus minerals: Press release, November 22, 2012 for the area allocated to Tonga Offshore Mining Limited (TOML) as well as for the Reserved Areas

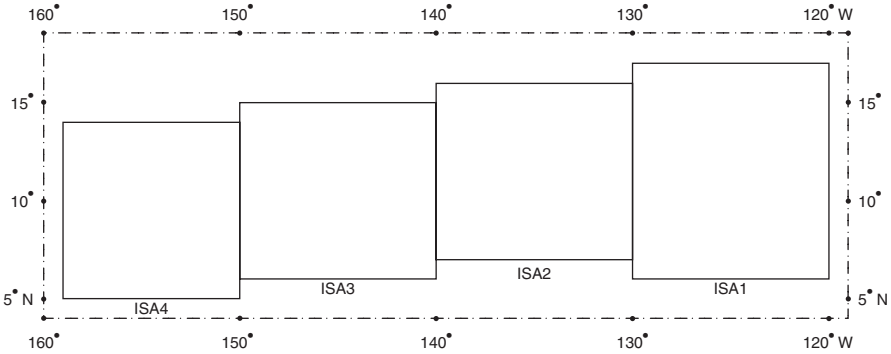

Fig. 7.1 Location of study areas in CCZ

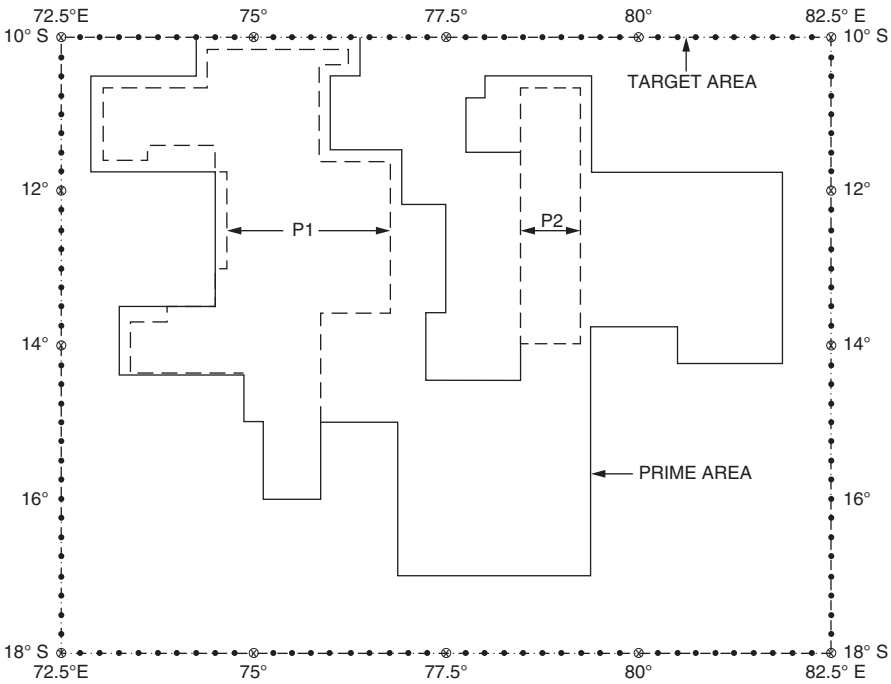

Fig. 7.2 Location of study areas in CIOB

outside the TOML contract area within CCZ. The TOML contract area represents areas mainly contributed by the three contractors: DORD of Japan, AFERNOD of France, Yuzhmorgeologiya of the Russian Federation.

3. Unpublished Thesis (Sudhakar 1993) for all study areas of CIOB (Target Area, Prime Area, Pioneer Area—Part P1, Pioneer Area—Part P2 and Total Pioneer Area P) (Fig. 7.2)

Since the data sources are clearly defined as above, they will not be referenced further in the body of the chapter to avoid repeated referencing.

7.3 Studies on Variabilities of Abundance and Metal Grades in Nodule Deposits

It is intended to discuss the variability of nodule abundance (kg/m^2) and of metal grades for Cu, Ni, Co, and Mn. The simplest measure of natural variability is sample variance. However, for many purposes, the coefficient of variation is most informative because it gives a relative measure of variability which takes into account both the mean and the variance (Koch and Link 1971). The coefficient of variation is the ratio of standard deviation to mean and may be expressed in percent term. It is particularly useful for comparing variabilities of two or more variables like abundance and metal grades as also for comparing variability of a single variable across two or more areas.

Table 7.1 presents the coefficients of variation (CV) for nodule abundance and metal grades for all study areas of CIOB. The data in Table 7.1 lead to the following two interesting observations.

1. The values for CVs for abundance as well as metal grades are strikingly similar across all study areas irrespective of the sizes of the study areas. Thus, area P1 (118,000 km^2), area P2 (32,000 km^2), area P (150,000 km^2), Prime Area (405,750 km^2) and the Target Area (960,000 km^2) share similar values of CVs for abundance and metal grades. The relatively higher value of CV for abundance in Target Area is on account of inclusion of some barren zones resulting in significantly lower values of mean abundance.
2. The variability expressed as CV for nodule abundance is significantly higher than the CVs of metal grade for all study areas of CIOB.

It is interesting to compare the variability of nodule abundance as well as metal grades for the study areas in CCZ as presented in Table 7.2.
The following observations are interesting for CCZ:

1. The order of magnitude values for CVs for nodule abundance as well as metal grades like Mn, Co, Ni and Cu are strikingly similar for almost all study areas within CCZ. It may be noted that except for TOML blocks having sizes smaller than 15,000 km^2 (four TOML blocks account for 50,000 km^2), all other study areas represent vast areas each of 0.5 million km^2 or more. The smaller sizes of TOML blocks may contribute to slightly lower value of CVs for abundance while the CVs for metal grades show an excellent similarity.

Table 7.1 Coefficients of variation for abundance and metal grades in CIOB (Expressed in %)

Study areas of CIOB(Area in km^2)	Abundance	Mn	Co	Ni	Cu
Target area (960,000)	111	16	36	26	35
Prime area (405,750)	82	17	37	28	40
Pioneer area—Part P1 (118,000)	77	14	38	24	28
Pioneer area—Part P2 (32,000)	80	14	29	20	30
Pioneer area—Total P (150,000) = P1 + P2	78	14	38	23	29

Table 7.2 Coefficients of variation for abundance and metal grades in CCZ (expressed in %)

Study areas of CCZ (Area in km^2)	Abundance	Mn	Co	Ni	Cu
TOML area					
1. Ex-DORD (<15,000)	50	10	18	21	35
2. EX-Yuzhmorgeologiya (<15,000)	67	16	22	20	27
3. Ex-AFERNOD (<15,000)	42	8	13	8	13
4. Ex-DORD (<15,000)	53	5	10	6	8
Reserved areas outside TOML area (>400,000)	74	15	40	16	24
As per study by ISA					
1. Total study area (TCCZ) (4,190,000)	85	13	21	15	21
2. ISA 1 (1,056,000)	89				
3. ISA 2 (1,405,000)	87				
4. ISA 3 (966,000)	70				
5. ISA 4 (764,000)	61				

Areas for TOML and Reserved Area outside TOML Area extrapolated from data in Press Release by Nautilus Minerals

2. In CCZ also, the variability expressed as CVs for abundance is significantly higher than the CVs for metal grades for all study areas.

Based on the above observations for CCZ as well as CIOB, it is reasonable to conclude that

- On a regional scale, the variability of abundance as well as metal grades expressed in terms of coefficient of variation is similar for all study areas within CCZ as well as CIOB. In addition and more interestingly, variabilities of abundance as well as metal grades are strikingly comparable for all the study areas across the two nodule bearing oceanic regions, the CCZ and CIOB. Thus, except for smaller areas of TOML blocks in CCZ and Target Area for CIOB, all study areas in CCZ as well as CIOB share a common variability characteristic.
- The variability for nodule abundance far exceeds the variability for metal grades for all study areas across CIOB and CCZ. Consequently, for all exploration planning and targeted estimation accuracy objectives, nodule abundance becomes the governing factor and metal grades need not be targeted independently or additionally for defining exploration density.

7.4 Further Studies on Statistical Properties of Distribution of Nodule Abundance

Having established that nodule abundance (kg/m^2) is the governing parameter for exploration planning, it is now proposed to discuss the statistical properties of distribution of nodule abundance in CIOB and CCZ and their implications. Tables 7.3 and 7.4 summarize the values of mean, standard deviation/variance and range for abundance values

Table 7.3 Basic statistics of abundance in study areas of CCZ

Study areas of CIOB (*N*, *d*)	Mean (kg/m^2)	Standard deviation (kg/m^2) (Variance) (kg/m^2)^2	Range (kg/m^2)
Target area (*N* = 1412, *d* = 0.15°–0.30°, Av.d = 0.24°)	3.6	4 (16)	0–20
Prime area (*N* = 903, *d* = 0.15°–0.24°, Av.d = 0.19°)	5.12	4.2 (17.6)	
Pioneer area—Part P1 (*N* = 429, *d* = 0.15°)	5.6	4.3 (18.5)	
Pioneer area—Part P2 (*N* = 107, *d* = 0.15°)	5.1	4.1 (16.8)	
Pioneer area—P (P1 + P2) (*N* = 536, *d* = 0.15°)	5.5	4.3 (18.5)	0–20

N = No. of Counts, *d* = mean sampling grid

Table 7.4 Basic statistics of abundance in study areas of CCZ

Study areas of CCZ (*N*, *d*)	Mean (kg/m^2)	Standard deviation (kg/m^2) (Variance) (kg/m^2)^2	Range (kg/m^2)
TOML area			
1. Ex-DORD (*N* = 18, *d* = 0.27°)	10.12	5.08 (25.8)	2.7–18.0
2. EX-Yuzhmorgeologiya (*N* = 88, *d* = 0.12°)	8.82	5.87 (34.5)	0.0–26.0
3. Ex-AFERNOD (*N* = 78, *d* = 0.13°)	9.98	4.2 (17.6)	1.3–21.0
4. Ex-DORD (*N* = 42, *d* = 0.18°)	7.68	4.09 (16.7)	0.1–16.4
Reserved areas outside TOML area (*N* = 2188, *d* = 0.14°)	8.21	6.06 (36.7)	0.0–52.2
As per study by ISA			
1. Total study area (TCCZ) (*N* = 3611, *d* = 0.34°)	6.72	5.52 (30.5)	0.0–44.0
2. ISA 1 (*N* = 791, *d* = 0.36°)	6.6	5.9 (34.8)	0.0–44.0
3. ISA 2 (*N* = 1051, *d* = 0.36°)	7.9	6.9 (47.6)	0.0–38.2
4. ISA 3 (*N* = 958, *d* = 0.317°)	5	3.5 (12.3)	0.0–21.0
5. ISA 4 (*N* = 811, *d* = 0.307°)	7.2	4.4 (19.4)	0.0–26.0

N = No. of Counts, *d* = mean sampling grid

together with number of counts *N* and the mean sampling grids *d* for the study areas of CIOB and CCZ, respectively. Additionally, spherical variogram models for abundance resulting from the respective experimental variograms for CIOB and CCZ have the following form:

$$\gamma(h) = C_o + C\left[\frac{3}{2}\cdot\frac{h}{a} - \frac{1}{2}\left(\frac{h}{a}\right)^3\right],\ h \le a$$

where the parameters have the following values for CIOB and CCZ:

Parameter	CIOB	CCZ
C_o = Nugget variance	5.0 units	13.0 units
C = Structural variance	11.0 units	17.5 units
a = Range	1°	3°

It is relevant to bring out, for subsequent analysis, that for corresponding exponential variogram model, $\gamma(h) = C_o + C(1 - e^{-h/a})$, the parameters C_o and C remain the same but a (exponential) = 0.5a (spherical) (Singh 1980).

From the data presented in Table 7.3 for CIOB, it emerges that the mean value for abundance is remarkably similar for all study areas like P1, P2, P and Prime Area except for Target Area where the mean value drops significantly since it includes, as explained earlier, some barren zones. The values of standard deviations and variances are again nearly uniform for all study areas. The variance resulting from variographic modelling at 16 units also matches closely with the sample variance values for each of the study areas. However, the nugget variance, representing the chaotic component of the total variance is significantly high at 31%.

The data for CCZ presented in Table 7.4 need to be analysed against the background that the study areas vary from less than 15,000 km^2 to as large as 4 million km^2. Yet, the mean abundance values show reasonable similarity across the study areas and if the smaller blocks of TOML are excluded, the similarity is significant. The standard deviation for abundance varies in a close range generally between 4 and 6 units. The variance obtained from variogram modelling at 30.5 units matches with the sample variance observed for the Total Study Area of about 4 million km^2 and is also comparable with other larger study areas. However, the nugget variance in this case also is significantly high at 43% of the total variance.

7.5 Comparative Variability Studies Between CIOB and CCZ

The data presented in Tables 7.3 and 7.4 for CIOB and CCZ, respectively, lead to the following observations:

1. The mean values of abundance for all study areas in CIOB show a general uniformity. Similarly, the large study areas of CCZ also display similarity of mean values of nodule abundance. Homogeneity in the distribution of nodules on the seafloor on a regional scale is also reflected in the unimodal lognormal frequency distribution of nodule abundance values in CIOB as well as CCZ (Singh and Sudhakar 2015). It is interesting to note, however, that CCZ includes a much larger nodule bearing area, say 4 million km^2 against only about 0.4 million km^2 of nodule bearing area of CIOB. Further, the mean abundance value for any study area in CCZ is significantly higher than every study area in CIOB.

2. While the standard deviation/variance values are generally uniformly distributed across study areas in CIOB as well as CCZ, these values are higher for CCZ than CIOB. The standard deviation values lie between 4 and 4.5 units for CIOB, the spread is larger between 4 and 6 units for CCZ. Higher variances in the study areas of CCZ are on account of larger range of abundance values from 0 to 52 kg/m^2 in CCZ than a smaller range from 0 to 20 kg/m^2 in CIOB with correspondingly higher mean abundance values in CCZ than CIOB.
3. The value of range for abundance derived from the variograms is much larger (3°) for CCZ than the corresponding value of 1° for CIOB. This is consistent with the size of uniformly distributed nodule fields in CCZ (about 4 million km^2) which is nearly 10 times larger than similar field in CIOB.

7.6 Estimation Variance in Relation to Area of Nodule Field

It is well known that unlike most mineral deposits, nodule deposits form a single layer on the sea floor. Consequently, the Volume-Estimation Variance relationship for nodule deposits reduces to the Area-Estimation Variance relationship. It is proposed to investigate if some simple working relationship between an area of a nodule field and estimation variance (a measure of estimation accuracy) for the given size of nodule field may be used for some practical applications. For this, as a starting step, a general expression for the estimation variance is provided in the following section.

Let us consider a general case of nodule bearing two-dimensional block of extensions S and T in the X and Y directions, respectively. Let the block be sampled at n points with spacing $\Delta y(\Delta y = T/n)$ in the Y direction and at m points with spacing $\Delta x(\Delta x = S/m)$ in the X-direction so that the total number of sample points is $m.n$. Let us now define a discrete function $Z_{ij} = Z(X_i, Y_j)$, $i = 1, \ldots m$; $j = 1, \ldots ; n$ over a mesh of $m.n$ points where (X_i, Y_j) denotes the location of sample points and Z denotes the nodule abundance (kg/m^2). We estimate the mean

$Z_e(S, T)$ of the block of extensions (S, T) as,

$$Z_e(S,T) = \sum_{i=1}^{m}\sum_{j=1}^{n} Z_{ij} / m.n$$

The true mean of a block of dimensions (S, T) denoted by $Z_t(S, T)$ may be expressed as,

$$Z_t(S,T) = \underset{m.n\to\infty}{Lim.}(Z_e(S,T)) = (1/S\cdot T)\iint_{S}^{T} Z(x,y)\mathrm{dxdy}$$

Estimation accuracy or estimation variance refers to the variance of difference e between the estimated and true mean values and is denoted by Var(e). The estimation variance, Var(e), is given by,

$$\begin{aligned} Var(e) &= E(e)^2 = E\left\{\left[Z_e(S,T)\right]-\left[Z_t(S,T)\right]\right\}^2 \\ &= Var\left(Z_e(S,T)\right)+Var\left(Z_t(S,T)\right)-2Cov.\left[Z_e(S,T)\cdot Z_t(S,T)\right] \end{aligned} \tag{7.1}$$

The expression for Var(e) in (7.1) may be evaluated using any admissible covariance function for varying block dimensions and sample spacings. Unfortunately, there is no analytical equivalent of the above expression (7.1), and it has to be numerically evaluated each time. A graphic solution, however, has been provided by Singh (1978) using exponential covariance function of the form $r(h) = C{\cdot}e^{-h/a}$ where C denotes the structural variance and a represents a characteristic parameter related to range of corresponding spherical function. This parameter, for practical applications is related as, a (exponential model) = 0.5a (spherical model). The graphic solution provides Var(e) in terms of structural variance C for varying b/a ($b = \sqrt{(S{\cdot}T)}$, being the side of equivalent square expressed in terms of parameter a of exponential covariance model) and for varying d/a (d being the side of equivalent square grid).

The relationship between the given area and corresponding estimation variance, Var(e), for given sampling grids may be evaluated through numerical evaluation of the expression (7.1) above even though it is highly cumbersome. However, the graphic solution discussed above may be used to define the underlying relationship. The following relationships may be established assuming uncorrelated errors:

1.

$$b^2{\bullet}Var(e) = Block\ Area.Var(e) = Constant\ for\ given\ sampling\ grid\ d \tag{7.2}$$

2. For the two sample spacings d_1 and d_2, and the corresponding variance of error Var(e_1) and Var(e_2),

$$Var(e_1)/Var(e_2) = (d_1/d_2)^2\ for\ the\ same\ block\ size \tag{7.3}$$

The above relationships are of practical utility since (a) they can be used to predict the variance of error for a different block size from the value of Var(e) from a given block size, (Var(e) being inversely proportional to the block area) and (b) they may also be used to predict the Var(e) for another sample spacing from a value known for the given sample spacing for the same block.

Once Var(e) has been obtained, the corresponding confidence interval at 95% confidence level around the estimated mean is calculated as $\pm 2\sqrt{(\text{Var}(e))}$, where $\sqrt{(\text{Var}(e))}$ represents standard error. The confidence interval is also sometimes expressed in terms of estimated mean $\bar{Z}$ as relative standard error or relative confidence interval as $\pm 2\sqrt{\left(Var(e)\right)}/\bar{Z}$ expressed in percent.

Table 7.5 Estimation variance-area relationship for abundance in CIOB

Study areas	Var(e) = (C_o/N) + f·C	Var(e)·Area
P1 (d = 0.15°)	0.01715 (f = 0.0005)	2024
P2 (d = 0.15°)	0.06433 (f = 0.0016)	2058
P (d = 0.15°)	0.01427 (f = 0.00045)	2140
Prime (d = 0.15°–0.24°) Av.d = 0.19°	0.00883 (f = 0.0003)	3583 (2239)
Target (d = 0.15°–0.30°) Av.d = 0.24°	0.00574 (f = 0.0002)	5510 (2152)

Figs. for the product Var(e)·Area in parentheses represent recalculated products for Prime and Target Area corresponding to d = 0.15°
Factor f is read from graphic solution (Singh 1978) for block size b/a and sample spacing d/a

Table 7.6 Estimation variance-area relationship for abundance in CCZ

Study areas	Var(e) = (C_o/N) + f·C	Var(e)·Area
ISA 1 (d = 0.36°)	0.0209 (f = 0.00026)	22,070
ISA 2 (d = 0.36°)	0.0159 (f = 0.00021)	22,339
ISA 3 (d = 0.317°)	0.0179 (f = 0.00025)	17,291 (2230)
ISA 4 (d = 0.307°)	0.0209 (f = 0.00028)	15,967 (2187)
TCCZ (ISA 1–ISA 4) (d = 0.34°)	0.0045 (f = 0.00005)	18,855 (21138)

Figs. for the product Var(e)·Area in parentheses represent recalculated products for ISA 3, ISA 4 and TCCZ corresponding to d = 0.36°
Factor f is read from graphic solution (Singh 1978) for block size b/a and sample spacing d/a

7.6.1 Verification of the Var(e)·Area Relationship

- *Case of CIOB*
  The expression in (7.2) may be verified using data available for CIOB and CCZ. Table 7.5 presents the Var(e) as well as the product (Var(e)·Area) for different study areas of CIOB. It may be observed that the products are nearly constant for the three study areas P_1, P_2 and P, where the sample spacing in these areas is nearly identical. For Prime and Target Area, the products vary on account of different sample spacings. However, when the new products are recalculated corresponding to grid of 0.15°, the products for these two areas also match the products for the three study areas—P1, P2 and P.
- *Case of CCZ*
  The data relating to Var(e) as also the products (Var(e)·Area) for various study areas are presented in Table 7.6. The products for ISA 1 and ISA 2 are nearly constant, where the sample spacing is also nearly identical for the two areas. The products for ISA 3 and ISA 4 and also for Total Area (TCCZ) are somewhat different on account of difference in sample spacing. If the products are recalculated for sample spacing d = 0.36°, the resultant products show an excellent agreement with ISA 1 and ISA 2.

The computations for CIOB as well as CCZ thus validate the constancy concept of the products Var(e)·Area within the range of block sizes and sample spacing considered. Useful practical deductions may be made using the relationship.

7.7 Estimation Variance Computations for Selected Areas in CIOB and CCZ

With the spherical variogram functions available for CIOB as well as CCZ as discussed in the earlier sections and using the relationship a(spherical) = 2·a (exponential), estimation variances have been computed for various sizes of nodule fields and varying sample spacings in CIOB and CCZ using graphic solution (Singh 1978). For practical reasons, following four sizes of nodule fields have been selected that have relevance to the third United Nations Convention on the Law of the Sea (UNCLOS-III) (United Nations 1982):

- 300,000 km^2 being the maximum size of an Application Area that an applicant may submit to ISA.
- 150,000 km^2 being the maximum size of the Area that may be allocated to a contractor by ISA for exclusive exploration and subsequent relinquishment.
- 75,000 km^2 being the maximum size of the Area that may be retained by the contractor for exclusive exploration after relinquishment.
- 7500 km^2 being the most possible size that may contain nodule resources for about 20 years eventual mine life. This may be a single nodule field or an aggregate of multiple nodule fields and is termed here as the First-Generation Mine site (FGM). (This is outside the provisions of UNCLOS-III).

Typically, three levels of sample spacing d at 0.075°, 0.15° and 0.30° have been used for the computations of estimation variances. Tables 7.7 and 7.8 present the estimation variance Var(e) values for the above sizes of nodule fields and varying sample spacings for CIOB and CCZ, respectively. Same results are plotted in Figs. 7.3 and 7.4 for CIOB and CCZ, respectively. The graphic solutions presented may, however, be used for any size of the nodule fields and for any sample spacings within the given ranges.

Table 7.7 Estimation variance for varying area sizes and varying sampling grids in CIOB

Area sizes (Area in km^2)	d = 0.075°	d = 0.15°	d = 0.30°
7500	0.0560 (0.236)	0.2285 (0.478)	0.9950 (0.997)
75,000	0.0059 (0.077)	0.0238 (0.154)	0.1031 (0.321)
1,50,000	0.0029 (0.054)	0.0124 (0.111)	0.0521 (0.228)
3,00,000	0.0014 (0.037)	0.0062 (0.078)	0.026 (0.161)
Range for the product Var(e)·Area	420–440	1715–1860	7200–7800

Figs. in parentheses are standard deviations of error/mean

Table 7.8 Estimation variance for varying area sizes and varying sampling grids in CCZ

Area sizes (Area in km^2)	$d = 0.075°$	$d = 0.15°$	$d = 0.30°$
7500	0.119 (0.345)	0.479 (0.690)	1.97 (1.403)
75,000	0.012 (0.109)	0.0487 (0.220)	0.191 (0.437)
1,50,000	0.0060 (0.077)	0.0242 (0.155)	0.0957 (0.309)
3,00,000	0.0031 (0.056)	0.0123 (0.111)	0.0495 (0.222)
Range for the product Var(e)·Area	895–930	3600–3690	14,400–14,850

Figs. in parentheses are standard deviations of error/mean

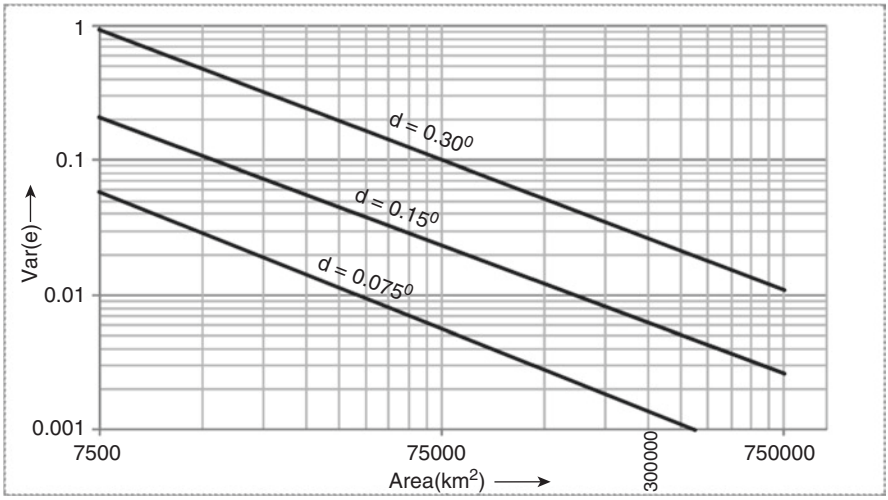

Fig. 7.3 Area vs. Var(e) for varying sampling grids (d) in CIOB

7.7.1 Observations on the Estimation Variance Values

Following important observations may be made from the results of computation of estimation variance values:

1. The data presented in Tables 7.7 and 7.8 further validate the assumption of uncorrelated errors for the sizes of nodule fields and sampling grids considered since the product Var(e)·Area is nearly constant for all selected areas for CIOB as well as CCZ. Also, the relationship between estimation variances and sampling grids as presented earlier is also validated.
2. The nugget effect being high contributes significantly to the overall estimation variance for any size of the area and any sample spacing. It is easily verified from the data presented in Tables 7.5 and 7.6 that the contribution to Var(e) by nugget variance is always higher than the contribution by structural variance for CIOB as well as CCZ.

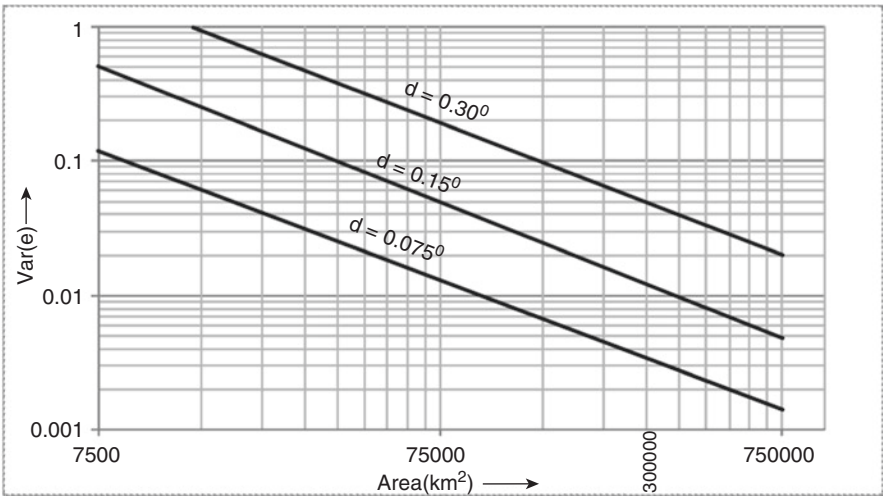

Fig. 7.4 Area vs. Var(*e*) for varying sampling grids (*d*) in CCZ

3. As expected, estimation variance (or estimation error) decreases with increasing size of the area for the same sample spacing. Thus, typically, for an area of 75,000 km^2 and sample spacing of $d = 0.15°$ in CIOB, the Var(*e*) work out to 0.0238 units and standard error as 0.154 units. This implies that the confidence interval at 95% confidence level will be about ±0.30 units around the mean or say ±6% of the estimated mean abundance of about 5 units. The confidence interval under similar cases in CCZ works out to ±0.40 units around the estimated abundance mean, or say, ±5% of the estimated abundance mean of 8 units. Thus, even though numerical value of standard error for CCZ may be higher than CIOB for the same area, the relative errors for both CIOB and CCZ are comparable due to higher mean values in CCZ. It therefore implies that a given sample spacing will produce nearly identical relative estimation accuracy for a given area in CIOB as well as CCZ. Thus, at the level of retained area of 75,000 km^2 in both CIOB and CCZ, the sampling density at 0.15° is adequate for estimating abundance with a confidence interval of about ±5% of the respective mean values of abundance.
4. It is also clear that while a sample spacing of 0.15° may be adequate for an area of 75,000 km^2, it does not produce same level of estimation accuracy for smaller area, say for 7500 km^2. In case of CIOB, the confidence interval works out to ±1.0 unit around the estimated mean abundance while it works out to ±1.4 units in case of CCZ for the same area of 7500 km^2. A sample spacing of 0.075° or less will be needed both for CIOB and CCZ for such an area to achieve similar level of relative accuracy as for 75,000 km^2, say less than ±10%.

It must be remarked that the above discussions hold at the global level for the given area and not for sub-components within the area under consideration. The above results may be useful in planning of exploration for nodules for existing as well as future contractors.

7.8 Commonality in Distribution Characteristics of Nodules in CIOB and CCZ

All the above observations lead to some significant generalizations on the distribution of nodules on the seafloors in CIOB as well as CCZ. On a regional scale, the distribution of nodules shows remarkable uniformity in terms of mean and variance of nodule abundance values within CIOB as well as CCZ. It implies that any nodule field within Prime Area of CIOB of area larger than say 30,000 km^2 will have mean and variance of nodule abundance similar to any other nodule field of similar size within the Prime Area. Similarly, any nodule field within CCZ of area larger than say 100,000 km^2 will have similar values of mean and variance of nodule abundance to any other nodule field of similar size within CCZ. In terms of relative variability expressed as coefficient of variation for abundance as well as metal grades, the nodule fields in CIOB display striking commonality with similar fields in CCZ. The homogeneity of distribution of nodule abundance on regional scale is also reflected by unimodal lognormal frequency distribution of abundance values for CIOB as well as CCZ. The variographic parameters are also relatively similar. The distribution of nodule abundance values suggest that, while there is uniformity on a regional scale, the abundance behaves highly erratic locally due to high value of nugget coefficient for nodule fields of CIOB as well as CCZ.

The commonality in the distribution patterns of nodules is so significant that a given sampling density in a given size of nodule field in CIOB as well as CCZ produces nearly identical value of relative estimation accuracy for abundance. This implies identical strategy for sampling of nodules for CIOB as well as CCZ. However, the commonality disappears when the size of nodule fields and absolute abundance values are considered. It emerges that not only the total area of the nodule fields in CCZ is effectively 10 times larger than the size of the nodule field in CIOB; the mean abundance values are also significantly higher than those of CIOB. This is reflected in the cluster of existing contractors as well as potential cluster of future contracts in CCZ. It is also consistent with the conclusion that while there is a potential of 18 additional mine site contracts with ISA in the CCZ, it is unlikely that there may be a second application for a mine site in CIOB in the foreseeable future (Singh and Sudhakar 2015). It is also relevant to suggest that the First-Generation Mine site covering the most favourable areas for initial 20 years of mine life may only need about 10% of the contracted mine site of 75,000 km^2 in the CCZ.

7.9 Conclusions

A review of available data from various sources leads to a clear conclusion that the variability (expressed as coefficient of variation) of nodule abundance as well as metal grades is comparable within as well as across all study areas in CIOB and CCZ. It is also concluded that the variability of nodule abundance in any nodule field is much higher than the variability in the metal grades and hence forms the governing parameter for exploration planning.

Based on variographic parameters available, estimation variances have been computed for all study areas in CIOB as well as CCZ. The results validate that, for the sizes of the area and the sampling grids considered, the products of estimation variance and the area of nodule field remain a constant for a given sampling grid. The results also show that the estimation variances Var(e_1) and Var(e_2) corresponding to the two sampling grids d_1 and d_2 for the given nodule field are related as:

$$Var\left(e_1\right) / Var\left(e_2\right) = \left(d_1 / d_2\right)^2$$

These results are useful for practical applications in exploration planning campaigns.

Finally, computations for estimation variances as a function of sampling grids have been made for selected sizes of nodule fields that have relevance for the existing or future contractors in CIOB or CCZ. These results show that for any given size of nodule field, either in CIOB or in CCZ, a given sampling grid produces identical value of relative estimation error for abundance. Thus, for an area of size 75,000 km^2, a sampling grid of 0.15° will lead to an estimation error of less than ±10% of the respective mean abundance for CIOB as well as CCZ.

The study brings out striking similarity in the distribution characteristics of nodules in both CIOB as well as CCZ. It is concluded that on a regional scale, there is a high degree of uniformity in distribution of nodule abundance in both CIOB and CCZ. Locally, however, the nodule abundance behaves erratic due to high level of nugget coefficient in CIOB as well as CCZ.

While there is a great similarity in the relative characteristics of nodule distribution in CIOB and CCZ, the commonality disappears when the size of nodule field and absolute abundance values are considered. The size of nodule fields in CCZ is more than 10 times the size of nodule fields in CIOB with the mean abundance values in CCZ being significantly higher than in the CIOB. There is therefore a greater attention for the future potential contractors in CCZ than in CIOB.

Acknowledgements The authors gratefully acknowledge the Secretary, Ministry of Earth Sciences, Govt. of India for his overall encouragement and support. The authors also thankfully acknowledge the approval of the International Sea Bed Authority to use relevant data and map. Special thanks to Dr. HS Mandal for supporting the graphics.

References

Hennigar HF, RE Dick, Foell EJ (1986) Derivation of abundance estimates for manganese nodule deposits; Grab sampler recoveries to ore reserve. In: Offshore technology conference, OTC 5237, Houston, May 1986, 5 p

ISA (2009) Workshop on the results of a project to develop a geological model of polymetallic nodule deposits in the Clarion-Clipperton zone International Seabed Authority, Kingston, 14–17 Dec 2009

ISA (2010) A geological model of polymetallic nodule deposits in the Clarion-Clipperton fracture zone, 2010. Technical Study: No. 6. eBook by the International Seabed Authority, Kingston. ISBN: 978-976-95268-2-2, p 211

Jauhari P, Kodagali VN, Sankar SJ (2001) Optimum sampling interval for evaluating ferromanganese nodule resources in the Central Indian Ocean. Geo-Mar Lett 21:176–182
Koch GS Jr, Link RF (1971) The coefficient of variation—a guide to the sampling of ore deposits. Econ Geol 66:293–301
Nautilus Minerals: Press Release (Nov 2012) Nautilus Minerals Defines 410 million tonne inferred mineral resource. http://www.nautilusminerals.com
Singh TRP (1978) Estimation accuracy in relation to control spacing in sampling of ore deposits: Graphic solutions. J Math Geol 10(6):691–697
Singh TRP (1980) An investigation on the relationship among the models of covariances function used in Geology. Indian J Earth Sci 7(2):109–118
Singh TRP, Sudhakar M (2015) Estimating potential of additional mine sites for polymetallic nodules in Pacific and Indian Oceans. Int J Earth Sci Eng 8(4):1938–1941
Sudhakar M (1993) Geostatistical analysis of polymetallic nodules from the Indian Ocean and a comparative studies from the Pacific Ocean deposits. Unpublished Ph.D. thesis, Indian School of Mines, Dhanbad, p 287
United Nations (1982) United Nations Convention on Law of the Sea (UNCLOS). United Nations, New York

Dr. T.R.P. Singh obtained his Masters in Applied Geology from IIT Kharagpur, Diploma in Mining and Exploration and M.Sc. in Ore Evaluation from Delft, The Netherlands, and Ph.D. in Mining Geostatistics from Osmania University. After serving NMDC, Dr. Singh joined Engineers India (EIL) in 1981. While at EIL, Dr. Singh worked as a Project Manager for the Seabed Mining Programs of Dept. of Ocean Development, Govt. of India and also served as a member of UN Group of Technical Experts on Deep Seabed Mining during PREPCOM period. Dr. Singh continues to be a member of Standing Committee of Ministry of Earth Sciences (MOES) and is also currently Hon Adviser, MOES.

Dr. Maruthadu Sudhakar holds a Ph.D. in Applied Geology, from Indian School of Mines, Dhanbad, and M.Sc. in Law of the Sea and Marine Policy from the London School of Economics and Political Science. He has served for more than 34 years in major national institutes/agencies viz., NIO, NCAOR, MoES, NCESS and now as the Director, Centre for Marine Living Resources and Ecology. He has contributed to the understanding of deep-sea bed resources, oceanographic surveys and polar sciences; spent about 1500 days at sea also a leader of several expeditions to Indian and Southern Oceans and Antarctica. He has also been an elected Member of Legal and Technical Commission (LTC) of the International Seabed Authority since 2007 and is associated with many professional bodies.

Chapter 8
Assessment of Distribution Characteristics of Polymetallic Nodules and Their Implications on Deep-Sea Mining

Rahul Sharma

Abstract This chapter looks at the distribution characteristics of nodules and associated seafloor features so as to provide this information to the industry for designing a suitable mining system. Further, it also looks at different scenarios emerging from mining rates ranging from 1 to 3 Mt year^{-1}, in order to optimize mining rate while addressing the environmental concerns. It also suggests certain formulae that can be adopted for estimating any deep-sea mineral with necessary modifications.

8.1 Introduction

Polymetallic nodules continue to fascinate researchers due to their shear abundance in deep-sea basins of all major oceans in the world (Cronan 2000), and also because of 3% growth rate of consumption of metals they contain (Mn, Cu, Ni, Co) in the last four decades (Sudhakar and Das 2009). Although the actual exploitation and extraction have been on hold owing to fluctuating metal prices in the world market, projections suggest that these mineral deposits are expected to be the alternative source of metals in the twenty-first century (Lenoble 2000; Kotlinski 2001). Whereas, in view of relatively shallow depths and proximity to the shore, some entrepreneurs have plans to initially start mining massive sulfides from within the EEZ of island countries (Gleason 2008); given the ongoing development in technology, deep-sea nodule mining could well become a reality in future, as they are found loosely strewn on the seafloor (Fig. 8.1) and just have to be scooped up, which makes them relatively easy to mine as compared to massive sulfides and ferromanganese crusts that are "stuck" to the seafloor.

R. Sharma (✉)
CSIR-National Institute of Oceanography (Council of Scientific and Industrial Research), Dona Paula, 403004, Goa, India
e-mail: rsharma@nio.org; rsharmagoa@gmail.com

R. Sharma (ed.), *Deep-Sea Mining*, DOI 10.1007/978-3-319-52557-0_8

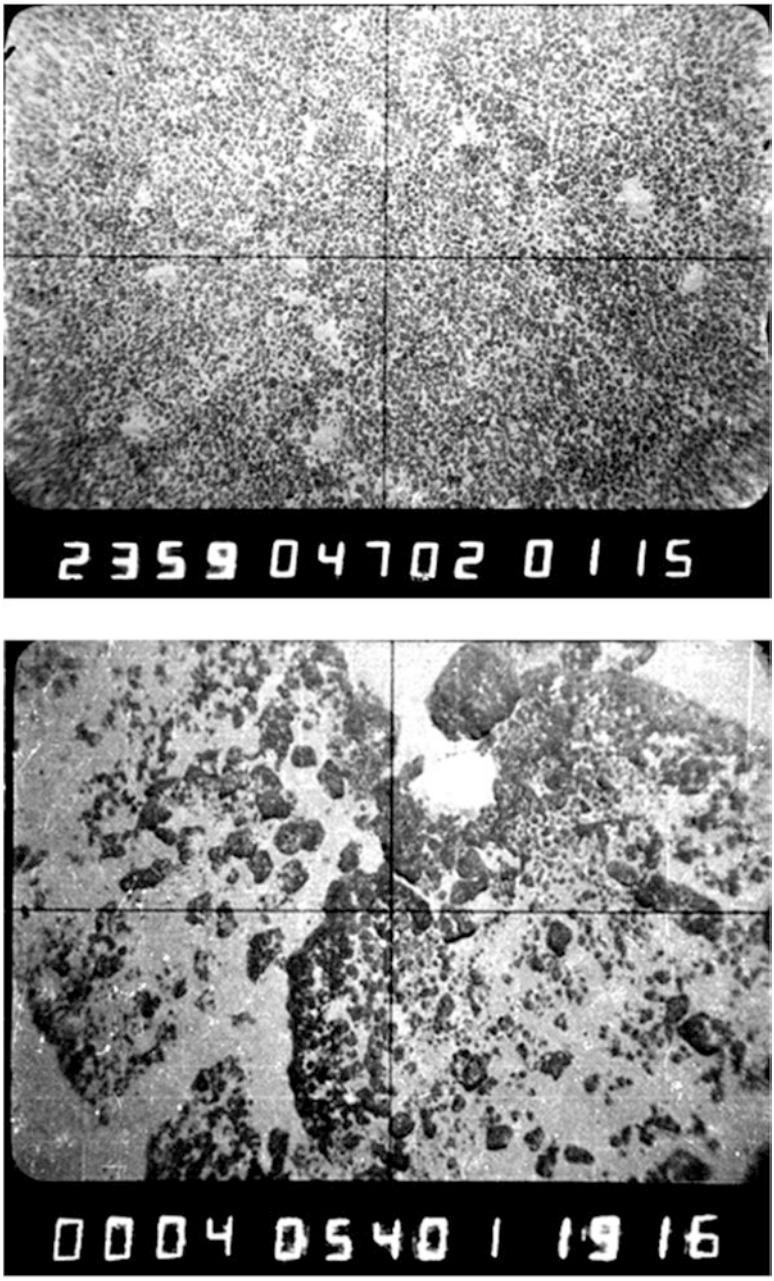

Fig. 8.1 Nodules and crusts on the seafloor

This chapter looks at the distribution characteristics of nodules and associated seafloor features and their influence on different mining scenarios based on mining rates (ranging from 1 to 3 Mt year^{-1}), so as to provide useful information to the

industry for designing a suitable mining system and optimizing the mining rate, while addressing the environmental concerns. This chapter also proposes certain equations for evaluating the relationships of polymetallic nodules with associated seafloor features as well as computing different mining estimates that can be applied to other deep-sea minerals.

8.2 Estimation of Nodule Characteristics and Associated Features

Data relating to distribution, quantity, and association of nodules with different substrates and topography on the seafloor is collected using freefall grabs, vanveen grabs, TV grabs, corers as well as sounding and sub-bottom profiling techniques (Kunzendorf 1986). Seafloor photography with single-shot underwater cameras and deep-towed seafloor photography systems have also proved to be effective tools for supplementing the data on distribution of nodules (Bastien-Thiry 1979; Fewkes et al. 1979; Sharma 1993). Estimation of nodule characteristics can be approached as follows.

8.2.1 Measurement of Area Covered on the Seafloor

Measurement of area and volume of a deposit recovered during sampling can be calculated based on the dimensions of the sampling device. While making any estimates from seafloor photographs, the area covered by the photograph on the seafloor is calculated by using the altitude (distance *X)* of camera above seafloor and camera lens angle (θ) (Fig. 8.2) as:

$$D = X \tan\theta \tag{8.1}$$

where D = ½ of length (L in meters)

so, $2D = L$ (length of area covered on seafloor in meters) and $2/3\ L = B$ (breadth of area covered on seafloor in meters)

Hence, area covered on seafloor

$$(A) = L \times B\left(\text{in m}^2\right) \tag{8.2}$$

Further, the dimensions of the features of interest (e.g., size or diameter of nodules or crusts) are measured from the vertical photographs, by using the scale factor *(*S_f) which is derived as:

$$S_f = \left(A / A_p\right)^{1/2} \tag{8.3}$$

where A_p is the area of the photograph.

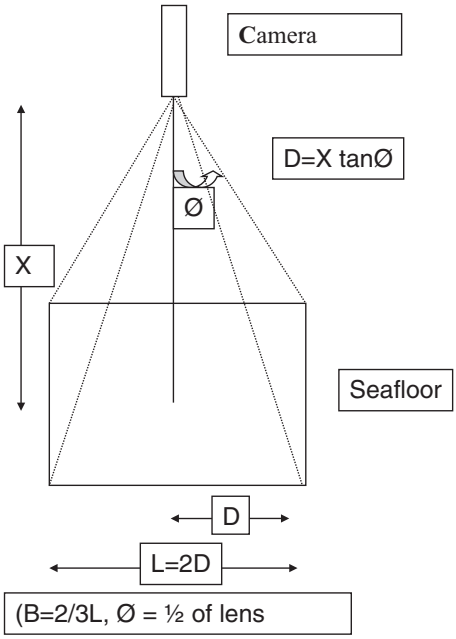

Fig. 8.2 Calculation of area photographed on the seafloor

Coverage (C) which refers to the area covered by a feature (nodules or crusts in this case) with respect to the area photographed on the seafloor is expressed in % and is calculated as:

$$C = \left(A_c / A_p\right) \times 100 \tag{8.4}$$

where A_c is the total area covered by nodules (or crusts) in the photograph.

A_c can be estimated using different methods such as point counting manually (Fewkes et al. 1979) and also image analyses electronically (Park et al. 1997; Sharma et al. 2013).

8.2.2 Calculation of Nodule Abundance

Nodule abundance from grab (N_g) or core samples is estimated by dividing the weight of recovered nodules with the area of the grab or corer and expressed in kgm^{-2} (Frazer et al. 1978). Researchers have also attempted abundance estimation of the nodules based on photographs (Felix 1980; Handa and Tsurusaki 1981; Lenoble 1982; Sharma 1993). Of these the simplest method of estimating nodule abundance from photographs as described by Handa and Tsurusaki (1981) is as follows:

$$N_p = 7.7 \times C \times D / 100 \tag{8.5}$$

where N_p is the abundance in the photograph (kg m^{-2}), C is the nodule coverage (%), and D is average nodule diameter (cm). Here, coverage (C) is calculated as in Eq. (8.4) and the average nodule diameter (D) is computed using the scale factor (S_f) as in Eq. (8.3). Here, it is suggested that for better accuracy of the estimation the constant factor (7.7 in this case) may have to be derived independently for each deposit based on local conditions.

As the photographs record the exposed nodules only and the grabs recover the buried nodules as well, it is observed that nodule abundance estimated from grabs and photographs at the same location may not agree. Here, relative abundance (R_a) gives the percentage of agreement between the photo abundance (N_p) and the grab abundance (N_g) and is calculated as (Sharma 1993):

$$R_a = \left(N_p / N_g\right) \times 100 \tag{8.6}$$

The complementary value of the relative abundance could also be used as an indicator of buried nodules for planning the depth of excavation in an area during mining.

8.3 Distribution of Nodule Characteristics and Associated Features

Frequency distributions of nodule characteristics that can influence mining were evaluated from different basins in the Pacific and Indian Oceans (Tables 8.1 and 8.2) based on sample data from research publications. Here, it must be noted that these studies were conducted over large areas in different ocean basins for the purpose of understanding the distribution characteristics of nodules with respect to geological setting and not for resource estimation in potential mine-sites that would normally have higher concentration of nodules in relatively small areas.

8.3.1 Frequency Distribution of Nodule: Size, Coverage, Abundance

8.3.1.1 Nodule Size

Classification of nodules from different basins in the Pacific Ocean in size classes of 2 cm shows that a large number of samples (49–58%) belong to 2–4 cm size class, followed by <2 cm size class (11–40%) as well as 4–6 cm size class (up to 31%) and few nodules (0.5–7%) in higher (6–8 and >8 cm) size classes. However, when nodules from other basins were classified in 3 cm size classes, a majority of them (72–89%) fell in <3 cm size class. Similarly in the Indian Ocean, a large number of the nodules (23–67%) belong to 2–4 cm size class in Central Indian Basin, followed by 4–6 cm (20–53%); whereas the nodules from the Exclusive Economic Zone of Mauritius

Table 8.1 Frequency (%) distribution of nodule characteristics in Pacific Ocean

Parameter/location (no. of samples)	Classification (nos. in % samples)										References
Size (cm)	<2	2–4	4–6	6–8	>8						
Central Pacific basin (3512) #	40	49	9	1.5	0.5						Usui (1986)
Magellan trough (61) #	11	49	31	7	2						Usui and Nakao (1984)
Penrhyn basin (84) #	40	58	1	1	–						Usui (1994)
Size (cm)	<3	3–6	>6								
Samoan basin (947) #	89	10	1								Glasby et al. (1980)
SW of Rarotonga (1003) #	72	26	2								Glasby et al. (1980)
South of Rarotonga (1526) #	78	18	4								Glasby et al. (1980)
Coverage (%)	0	<10	10–20	20–30	30–40	40–50	50–60	60–70	70–80	>80	
Central Pacific basin (125) +	76	10	8	3	2	1					Usui (1986)
Magellan trough (57) +	14	4	26	21	9	14	9	4	-	-	Usui and Nakao (1984)
Penrhyn basin (68) +	0	4	15	10	15	10	3	13	19	10	Usui (1994)
Abundance(kg m^{-2})	<5	5–10	10–15	15–20	20–25	>25					
Central Pacific basin(90) +	67	14	12	7	–	–					Usui (1986)
Magellan trough (61) +	36	16	12	8	16	11					Usui and Nakao (1984)
Penrhyn basin (84) +	32	13	12	17	5	21					Usui (1994)
Nodule burial (cm)	0–50	50–100	100–200	200–300	300–400	400–500	500–600	>600			
Peru basin (54) #	13	0	0	10	18	37	9	13			Cronan (2000)
Peru basin (12) #	33.3	58.3	8.3								Stoffers et al. (1982)
Central Pacific basin (29) #	86							14			Usui (1986)

Key: + = no. of operations, # = no. of nodules

Table 8.2 Frequency (%) distribution of nodule characteristics in Indian Ocean

Parameter/location (no. of samples)	Classification (nos. in % samples)										References
Size (cm)	<2	2–4	4–6	6–8	>8						
CIOB (9000)#	9×	67	20	3	1						Sharma (1998)
CIOB (171)#	1	23	53	16	7						Sarkar et al. (2008)
EEZ of Mauritius (635)#	35	58	6	0.5	0.5						Nath and Prasad (1991)
Wt%/size	<2	2–4	4–6	6–8	>8 cm						
CIOB (9000)#	9×	40	35	11	5						Sharma (1998)
EEZ of Mauritius (635)#	8	65	16	7	4						Nath and Prasad (1991)
Coverage (%)	0	<10	10–20	20–30	30–40	40–50	50–60	60–70	70–80	>80	
CIOB (988)+	67	18	6.5	3	2.8	1.8	0.6	0.5	0.1	0.1	Sharma (1998)
Abundance (kg m^{-2})	<5	5–10	10–15	15–20	20–25						
CIOB (725)+	56	25	13	5.5	0.5						Sharma (1998)
CIOB (479)+	67	23	8	2	–						Kodagali and Sudhakar (1993)
CIOB (47)+	38	19	28	15	–						Sarkar et al. (2008)
CIOB (23)*+	43	48	9	–	–						Jauhari et al. (2001)
EEZ of Mauritius (13)+	77	23	–	–	–						Nath and Prasad (1991)
Nodule burial	0–50	50–100	100–200	200–300	300–400	400–500	>500 cm				
CIOB (57)#	33	11	16	14	14	7	5				Pattan and Parthiban (2007)

Key: * = Average abundance at each location, × = including broken fragments, + = no. of operations, # = no. of nodules

had many nodules (35%) in <2 cm size class. By weight (%), a majority of nodules (40–65%) fall in 2–4 cm size class, followed by 4–6 cm size (16–35%). Hence, by number as well as by weight, nodules between 2–4 cm size contribute the most to the total population of nodules, and many of the remaining nodules belong to <2 and 4–6 cm. Combining the data from both size classifications indicates that 2–3 cm could be the dominant size range for nodules in different ocean basins.

8.3.1.2 Nodule Coverage

In the Central Pacific Ocean as well as Central Indian Ocean, a majority of the locations (68–76%) had nil nodule coverage as observed from the seafloor photographs, followed by <10% coverage (in 10–18% locations) and higher (>10%) nodule coverage in very few locations (1–8%). However, Magellan Trough and Penrhyn Basin in the Pacific Ocean had relatively more locations (15–26%) with 10–20% nodule coverage indicating that different basins within the same ocean could have higher nodule coverage based on local geological conditions. It was also observed that many of seafloor photographs in the Pacific as well as Indian Oceans do not show higher coverages due to partial or complete burial of nodules under the sediment cover (Fewkes et al. 1979; Sharma 1989a).

8.3.1.3 Nodule Abundance

In the Pacific Ocean, a majority of the grab sampling locations (32–67%) had submarginal nodule abundance (<5 kgm^{-2}), whereas the frequency ranged from 7 to 21% for different classes of paramarginal deposits (5–10, 10–15, 15–20, 20–25, >25 kg m^{-2}) (Table 8.1). Similarly in the Indian Ocean, many locations (38–77%) from different basins had submarginal nodule abundance, with the remaining accounting for different classes of paramarginal deposits (Table 8.2). However these studies are based on basin scale studies, whereas it is reasonable to expect that the first-generation mine-sites identified after detailed resource estimation, would contain higher average nodule abundances so as to maintain the techno-economic feasibility of the mining venture.

Comparison of 964 photographs along with grab sample data from the same locations in Central Indian Ocean Basin showed that whereas nodules were recorded in both at 426 (44%) locations, no nodules were recorded in either at 206 (21%) locations indicating that these locations are totally devoid of nodules. Of the remaining 332 (35%) locations, nodules were recorded in photographs alone at 56 (6%) locations and only in grabs at 276 (29%) locations (Fig. 8.3). Of the locations where nodules were recorded in both, 71% had very high agreement (R_a ~ 100%) and at the remaining locations, the agreement between photos and grabs varied from 30 to 90%. This shows that whereas at many locations, a large number of nodules are exposed which have been captured by photographs as well as collected by grabs and at the other locations, a few nodules are buried and their degree of burial ranges from 10 to 70% (R_a = 30–90%). Also, occurrence of low abundance (<5 kgm^{-2}) in

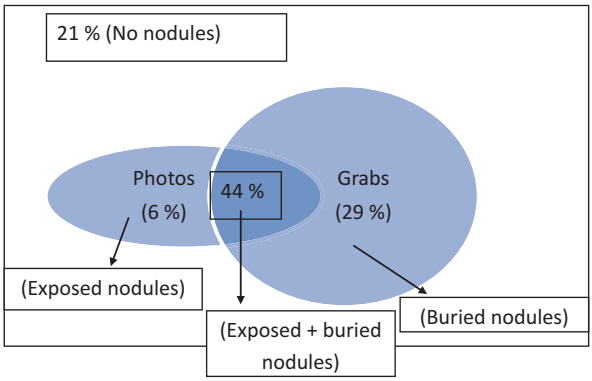

Fig. 8.3 Venn diagram of nodule occurrence in grabs and photographs

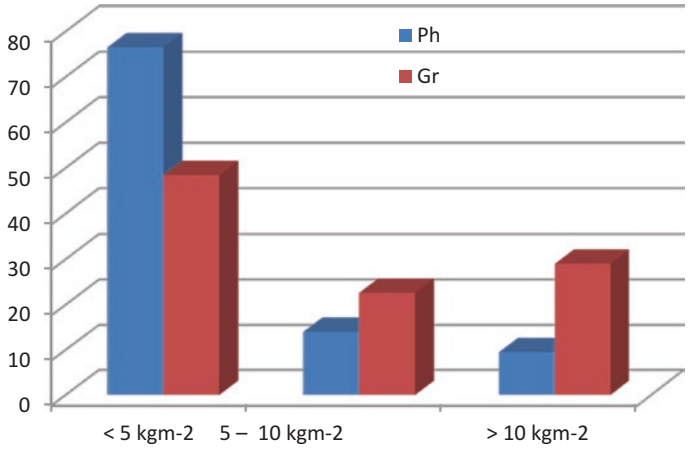

Fig. 8.4 Distribution of nodule abundances in grabs (Gr) and photographs (Ph)

majority of the photographs (76.5%) as compared to about half of the grab samples (48.4%) in contrast to high abundance (>5 kgm^{-2}) in few photographs and many grabs (51.6%) indicates the occurrence of buried nodules (Fig. 8.4).

Whereas, grab samplers are capable of collecting nodules in top 20–30 cm, core samplers that can penetrate deeper down to several meters have shown that the occurrence of buried nodules is generally within the top 1–2 m (Stoffers et al. 1982), but occasionally these also occur at deeper depths of more than 5 m in the Pacific (Usui 1986; Cronan 2000) as well as Indian Oceans (Pattan and Parthiban 2007).

8.3.2 Association of Nodules with Different Substrates

Nodule deposits are associated with different substrates, such as sediments and rocks that could have a bearing on mining of nodules. It is observed that generally R_a is high (>50%) in the areas of thin sediment, that gradually becomes less in the

sediments of intermediate thickness, and is even less in thick sediments because of the increase in the number of buried nodules. On the other hand, in the area of rock exposures, there is very good agreement (R_a = 90–100%) between photography data and grab data at the locations with no sediment patches, and low agreement (R_a < 60%) where sediment patches are seen in the micro relief of the rock outcrops (Sharma 1993).

8.3.2.1 Effect of Sediment Cover

An evaluation of ~20,000 photographs in the Indian Ocean has shown that almost two-thirds (65%) of the photographs have nil nodule coverage (i.e., no exposed nodules), whereas many (17–21%) of the remaining photos have low nodule coverage (1–20% coverage), some (~11%) have moderate coverage (20–50% coverage) and very few have higher nodule coverage (50–80%) (Sharma et al. 2010). The fact that at many of the locations where no nodules are exposed in the photographs, nodules have been collected in grab samples as observed earlier, indicates at the occurrence of buried nodules under sediment–water interface boundary layer (Sharma 1989a). Analyses of sounding data on thickness of the acoustically transparent layer in the nodule areas have shown that the thickness of this uppermost sediment layer is highly variable from a few meters to several tens of meters (Sharma et al. 2013).

Studies in the Pacific Ocean also have shown that the "Sediment–Water Interface Boundary (SWIB)" layer is known to bury the nodules and obscure them from camera view at some locations (Fewkes et al. 1979) and whereas these buried nodules cannot be accounted for in the photographs, they are collected in the grab samplers. The extent of nodule burial depends on the size and shape of nodules and thickness of SWIB layer (Cronan and Tooms 1967; Felix 1980). Hence, photography data and grab sample data can be used to complement each other for evaluating the distribution of nodules in terms of their occurrence and also exposure or burial.

Due to "fractionation" effect, nodules look smaller and the nodule abundance estimates are lower in the photographs, as the average diameter of the nodules is less that results in an underestimation of nodule abundance at these locations (Sharma 1989a). Nodule coverage and abundance in the photographs and grabs have an inverse relation with SWIB thickness because thicker the SWIB layer, the more is the burial resulting in a lower number of nodules being seen in the photographs and collected in the grabs (Sharma 1989b). Horn et al. (1973) also observed that in the Pacific Ocean, barren areas have resulted either through burial by sediments or prevention of nodule development by covering the potential nuclei.

8.3.2.2 Distribution of Rock Exposures

Rock exposures are observed as hard, dark colored substrates in the seafloor photographs (Fig. 8.1) that generally have a coating of ferromanganese oxides, also called as encrustations or "crusts." Distribution of rock outcrops/crusts in a part of

the Pacific Ocean showed that their coverage ranged from 1 to 100% and a majority of them (63.5%) had low (<20%) coverage, few (14%) had medium (20–50%) coverage, and the remaining (22.5%) had high (>50%) coverage (Yamazaki and Sharma 1998). Similar observations from seafloor photographs in the Central Indian Ocean showed that these had a wide range of coverage (from 1 to 100%) with about half (48%) having low coverage (<20%); one-third (34%) having medium coverage (20–50%) and the remaining (17%) having higher coverage (>50%) on the seafloor (Sharma et al. 2010).

These outcrops when broken up due to submarine erosion act as sources of nucleating material that originates from weathered basalts that are the products of volcanic eruptions represented by the present day seamounts (Iyer and Karisiddaiah 1988). The broken fragments from the rocky outcrops, which are eroded and transported along the slopes and flanks of the seamounts and abyssal hills, act as nuclei for accretion of the oxides from the hydrogenous as well as digenetic sources of metals on the seafloor, thereby resulting in large concentrations of nodules in these areas (Iyer and Sharma 1990). This phenomenon has been explained as "seed" hypothesis wherein the nodule population is controlled by the distribution of the "seeds" or rock fragments that act as nuclei for nodules (Horn et al. 1973).

8.3.3 Nodule Distribution in Different Topographic Settings

When nodule and crust coverage data were plotted with respect to depth and distance in the Central Indian Ocean, it showed that whereas the crust/rock outcrops were predominantly exposed on the top of a seamount/abyssal hill, more nodules were exposed on the lower slopes where sediment accumulation is less as compared to flat abyssal plains and valleys (Iyer and Sharma 1990; Sharma and Kodagali 1993; Sharma et al. 2010) indicating that the topographic settings appeared to control the distribution of nodules, rocks, and sediment as follows:

- Rock exposures (and Fe-Mn encrustations) at the summits with no sediment cover or nodules
- Transition zone between rock outcrops with encrustations and thin sediment cover with nodules on upper slopes
- Nodule fields with thin sediment cover on lower slopes
- Partial to complete burial (or absence) of nodules due to variable thickness of the sediment cover in the plains and valleys

Similar study on distribution of nodules, rock outcrops/encrustations and sediment with respect to slope angles in the Pacific Ocean (Yamazaki and Sharma 2000) revealed the following topographic control:

1. 15–40° slope angle: crust-dominant zone
2. 7–15° slope angle: transition zone between nodule fields and crusts
3. 3–7° slope angle: sediment-dominant zone
4. 0–3° slope angle: nodule-dominant zone

These indicate that whereas the overall distribution patterns are similar, there could be minor variations depending on local geological conditions between different ocean basins.

8.4 Estimation of Mining-Related Variables

On the basis of characteristics of the mineral deposits in an area, several variables related to mining can be estimated which are demonstrated in this section, based on the cut-off abundance of 5 kg m^{-2} and life of a mine-site as 20 years (UNOET 1987).

8.4.1 Estimation of Mining Rates

Mining rate is generally expressed in terms of rate of mining of dry nodules that will eventually be available for further processing. However, higher quantities of wet nodules will have to be mined to account for loss of water (moisture) content before processing. These can be estimated as follows:

1. If mining rate is given for dry nodules, i.e., $MR_{(dry)}$, then

$$MR_{(wet)} = 100 \times MR_{(dry)} / \left(100 - W_{C(nod)}\right) \tag{8.7}$$

2. If mining rate is given for wet nodules, i.e., $MR_{(wet)}$, then

$$MR_{(dry)} = MR_{(wet)} - \left(W_{C(nod)} \times MR_{(wet)} / 100\right) \tag{8.8}$$

where $MR_{(wet)}$, $MR_{(dry)}$ are in Mt $year^{-1}$
$W_{C(nod)}$ = Water (moisture) content of nodule is in %

8.4.2 Estimation of Metal Production (M_P)

$$M_P = T_{MC} \times MR_{(dry)} \tag{8.9}$$

where T_{MC} = total concentration of extractable metals (%) and $MR_{(dry)}$ and M_P are in Mt $year^{-1}$

8.4.3 Estimation of Metal Value (M_V)

$$M_{\mathrm{V}} = M_{\mathrm{P}} \times mp \times 1000 \tag{8.10}$$

where M_P = metal production (Mt) and mp = metal price (in \$ kg^{-1})
Note: Here, mp is multiplied by 1000 to convert from tonnes to kg (an mp is per kg).

8.4.4 Estimating Total Mineable Area (M) According to UNOET (1987)

$$M = A_{\mathrm{t}} - \left(A_{\mathrm{u}} + A_{\mathrm{g}} + A_{\mathrm{a}}\right) \tag{8.11}$$

where

A_t = the total area
A_u = area un-mineable due to the topography
A_g = area below cut-off grade
A_a = area below cut-off abundance

8.4.5 Size (or Area) of Mine-Site (A_s) According to UNOET (1987) Is

$$A_{\mathrm{s}} = A_{\mathrm{r}} \times D / \left(A_{\mathrm{n}} \times E \times M\right) \tag{8.12}$$

where

A_s = size of mine-site (km^2)
A_r = annual nodule recovery rate or mining rate (dry tonnes per year)
D = duration of mining operation (years)
A_n = average nodule abundance in the mineable areas (Kg m^{-2})
E = efficiency of the mining device (%)
M = proportion of mineable area (as fraction of total area)

8.4.6 Area of Contact/Year (A_c)

$$A_{\mathrm{c}} = MR_{(dry)} / A_{\mathrm{n}} \tag{8.13}$$

where A_n = average nodule abundance (Kg m^{-2}).

8.4.7 Ore Production/Day (O_p)

$$O_{\mathrm{p}} = MR_{(dry)} / D \tag{8.14}$$

where D = no. of days of operation.

8.4.8 Volume of Sediment Disturbed at the Seafloor (V_s in m^3)

$$V_{\mathrm{s}} = A_{\mathrm{c}} \times D_{\mathrm{p}} \times C_{\mathrm{s}} / 100 \tag{8.15}$$

where

A_{c} = area of contact
D_{p} = depth of penetration (m)
C_{s} = coverage of sediment (%)

8.4.9 Wt. of Disturbed Sediment (Wet) or Water Laden Sediment ($W_{s(wet)}$ in t)

$$W_{\mathrm{s}(wet)} = V_{\mathrm{s}} \times D_s \tag{8.16}$$

where D_s = density of sediment (g cm^{-3}).
Note: Density in g cm^{-3} to be multiplied by 1000 to convert into Kg m^{-3}.

8.4.10 Wt. of Disturbed Sediment (Dry) or without Water ($W_{s(dry)}$ in t)

$$W_{\mathrm{s}(dry)} = W_{\mathrm{s}(wet)} \times \left(100 - W_{\mathrm{C}(sed)}\right) / 100 \tag{8.17}$$

where $W_{\mathrm{C(sed)}}$ = Water content of sediment (%).

8.4.11 Wt. of Unwanted Material (M_u) to be Disposed Off (in Mt)

$$M_{\mathrm{u}} = MR_{(dry)} \times \left(100 - T_{MC}\right) / 100 \tag{8.18}$$

where T_{MC} = total concentration of extractable metals (%).

8.5 Mining Estimates Based on Geological Factors

8.5.1 Estimation of Mining Rates for Dry and Wet Nodules

Literature on nodule mining shows that over the years different mining rates ranging from 1 to 25 Mt year^{-1} have been suggested by various workers (Table 8.3). Considering water (moisture) content of nodules as 25% (Mero 1977), the eventual mining rates for 1.5 Mt year^{-1} (as suggested in ISA 2008), and 3 Mt year^{-1} (as per UNOET 1987) have been estimated (Table 8.4). Accordingly, at least 2 Mt of wet nodules will have to be mined annually to achieve the target of 1.5 Mt of dry nodules. On the other hand, only 1.125 Mt of nodules will be mined annually if the mining rate is considered for 1.5 Mt of wet nodules. These quantities will be doubled in case of mining rate of 3 Mt year^{-1}. However, in order to avoid the confusion between mining rates for dry and wet nodules, it is proposed that henceforth the mining rates should be expressed clearly either in terms of dry nodules or as wet nodules. Mining

Table 8.3 Proposed mining rates for polymetallic nodules

Sr. no.	Proposed by	Mining rate
1	Flipse et al. (1973)	1–5 Mt year^{-1} (dry)
2	Kaufman (1974)	1 Mt year^{-1} (dry)
3	Siapno (1975)	1 Mt year^{-1} (dry)
4	Pearson (1975)	1–25 Mt year^{-1} (dry)
5	Lenoble (1980)	2.1–3 Mt year^{-1} (dry)
6	OMI (1982)	3 Mt year^{-1} (dry)
7	OMA (1982)	2.1 Mt year^{-1} (dry)
8	Academie des Sciences (1984)	3 Mt year^{-1} (dry)
9	Dick (1985)	1–2 Mt year^{-1} (dry)
10	UNOET (1987)	3 Mt year^{-1} (dry)
11	Herrouin et al. (1991)	1.5 Mt year^{-1} (dry)
12	ISA (2008)	1.5 Mt year^{-1} (wet)
	Average (considering all individual values as well as median values in case of range)	2.9 Mt year^{-1}
	Average (considering all individual values as well as median values in case of range and excluding anomalous range of Sr. no. 4)	2.1 Mt year^{-1}

Note: All proposed mining rates are for dry nodules, except at Sr. no. 12

Table 8.4 Actual and eventual mining rates based on water content in nodules

Actual mining rate	Water content in nodules (%)	Eventual mining rate
1.5 Mt year^{-1} (dry)	25	2.000 Mt year^{-1} (wet)
3.0 Mt year^{-1} (dry)	25	4.000 Mt year^{-1} (wet)
1.5 Mt year^{-1} (wet)	25	1.125 Mt year^{-1} (dry)
3.0 Mt year^{-1} (wet)	25	2.250 Mt year^{-1} (dry)

Table 8.5 Estimated metal production (Mt) for different mining rates

		Mining rate (Mt year^{-1}) of dry nodules			
Metal[a]	1.0	1.5	2.0	2.5	3.0
Mn	0.24	0.36	0.48	0.6	0.72
Ni	0.011	0.165	0.022	0.0275	0.033
Cu	0.0104	0.0156	0.0208	0.0350	0.312
Co	0.001	0.0015	0.002	0.0025	0.0030
Total/year	0.2624	0.3936	0.5248	0.6560	0.7872
Total (in 20 years)[b]	5.248	7.872	10.496	13.120	15.744

[a]Mn = 24%, Ni = 1.1%, Cu = 1.04%, Co = 0.1% (Jauhari and Pattan 2000)
[b]As life of a mine-site is expected to be 20 years (UNOET 1987)

rate for dry nodules expressed as $MR_{(dry)}$ is the quantity that will eventually be available for further processing; whereas, mining rate for wet nodules expressed as $MR_{(wet)}$ should be used to represent the mining rate at which wet nodules will have to be mined so as to achieve the $MR_{(dry)}$.

For a given $MR_{(wet)}$, $MR_{(dry)}$ may vary from place to place depending upon the average moisture/water content in nodules which will have to be estimated for each mine-site during exploration in order to fix the target quantity of wet nodules to be mined to achieve the required rate of mining of dry nodules.

8.5.2 Metal Production for Different Mining Rates

Estimation of metal production at different mining rates ranging from 1 to 3 Mt year^{-1} of dry nodules reveals that Mn production would range between 0.24 and 0.72 Mt, Ni between 0.011 and 0.033 Mt, Cu between 0.0104 and 0.312 Mt and Co between 0.001 and 0.003 Mt annually, the total metal yield ranging from 0.2624 Mt (for 1 Mt year^{-1} mining rate) to 0.7872 Mt (for 3 Mt year^{-1} mining rate) for a certain concentration of these metals (Table 8.5).

8.5.3 Mining Estimates for Different Mining Rates

Estimates for various parameters related to mining of polymetallic nodules have been worked out for mining rates ranging from 1 to 3 Mt year^{-1} of dry nodules (Table 8.6), and their implications have been discussed in this section.

8.5.3.1 Estimation of Mineable Area

According to Eq. (8.5), estimation of mineable area can be made by subtracting the un-mineable areas due to factors such as unfavorable topography (A_u), grade (A_g), and abundance (A_a) from the total area (A_t) available to a contractor. Considering A_u

as 20% (UNOET 1987), and assuming A_g as 15% and A_a as 15% and subtracting them from A_t = 75,000 km^2 (maximum area allotted to each Contractor); the total mineable area *(M)* will be 37,500 km^2 (Sharma 2011). However, this would vary for each "Contractor" depending upon the actual area allotted and also other ground conditions in different mining areas with respect to topography, grade, and abundance.

8.5.3.2 Area (Size) of Mine-Site

As per Eq. (8.6), the area (size) of the mine-site could vary from 4267 to 12,800 km^2 for different mining rates (Table 8.6) for the nodule abundance (A_n) of 5 kg m^{-2} and efficiency (E) of the mining system as 25% (as suggested by UNOET 1987). The other components being constant, variation in A_n and E could alter the size of the mine-site (A_s). Also, it is reasonable to expect a higher average nodule abundance *(A_n* = 8–10 kg m^{-2}) in the potential first-generation mine-sites and a higher efficiency *(E)* of the mining system with advancement in technology. This would reduce the size of the mine-site (A_s) considerably restricting the mining activities to a smaller area, hence reducing the environmental impacts, especially as first-generation mining would start in areas of high nodule abundances.

8.5.3.3 Area of Contact

Whereas the estimation of area of mine-site takes into consideration the duration and efficiency of mining, the area of contact is the actual area that will be scraped during mining and has a bearing on the volume of associated sediment that will be disturbed leading to environmental impact on the benthic ecosystem. For different mining rates and average nodule abundance of 5 kg m^{-2}, with an annual operation time of ~300 days, the actual area of contact (scraped) will vary between 200 and 600 km^2 year^{-1} that is 0.66–2 km^2 day^{-1} (Table 8.6) which are in effect miniscule with respect to the area of the ocean basins where these nodules are found. Also, as the average nodule abundance is expected to be higher in the actual mine-site than the cut-off value considered here, the actual area scraped (or the "area of contact" on the seafloor) will be much smaller than those estimated here.

8.5.3.4 Ore Production

Irrespective of nodule abundance, mining of 1–3 Mt of nodules for ~300 working days in a year, would lead to production of 3333–10,000 t of ore per day (Table 8.6) that will not only require lift mechanism to bring them to the surface through >5 km of water column, as well as other infrastructure on the mining platform. Concerns have been raised over the effect of large-scale mining on the prices of the metals extracted because of the disparity between the ratios of constituent metals in the nodules and the ratio of their world demand (Pearson 1975). Hence, optimum

Table 8.6 Estimates for mining of polymetallic nodules at different mining rates

Estimates for operation of 300 days year^{-1}	Mining rate (dry nodules)					Remark
	1.0 Mt year^{-1}	1.5 Mt year^{-1}	2.0 Mt year^{-1}	2.5 Mt year^{-1}	3.0 Mt year^{-1}	
Area (Size) of mine-site[a]	4267 Km^2	6400 Km^2	8533 Km^2	10,667 Km^2	12,800 Km^2	Negligible with respect to area covered by ocean basins
Area of contact per year[a]	200 Km^2	300 Km^2	400 Km^2	500 Km^2	600 Km^2	i.e., 0.66–2 km^2 day^{-1}
Ore production/day	3333.3 t day^{-1}	5000 t day^{-1}	6666.6 t day^{-1}	8333.25 t day^{-1}	10,000 t day^{-1}	Proportionate storage and transport facility required
Volume of sediment disturbed at seafloor	60,000 m^3 day^{-1}	90,000 m^3 day^{-1}	120,000 m^3 day^{-1}	150,000 m^3 day^{-1}	180,000 m^3 day^{-1}	Major source of environmental impact
Wt. of disturbed sediment (wet) (@1.15 g cm^{-3} density)	69,000 t day^{-1}	103,500 t day^{-1}	138,000 t day^{-1}	172,500 t day^{-1}	207,000 t day^{-1}	In slurry form that can travel with bottom currents to adjacent areas
Wt. of disturbed sediment (dry) (@ 80% water content)	13,800 t day^{-1}	20,700 t day^{-1}	27,600 t day^{-1}	34,500 t day^{-1}	41,400 t day^{-1}	Dominant (50–60%) fine clays, may remain suspended for longer periods
Unwanted material to be disposed off (@ 26% of metal content)	0.74 Mt year^{-1}	1.11 Mt year^{-1}	1.48 Mt year^{-1}	1.85 Mt year^{-1}	2.22 Mt year^{-1}	Find constructive use or environment friendly disposal mechanism

[a]For cut-off abundance of 5 kg m-2 (minimum required for nodule mining, UNOET (1987))

production of ore, containing the desired composition of metals would be necessary to maintain a balance in the metal prices because over-production (more than the demand) could lead to lowering of metal prices, eventually making deep-sea mining uneconomical.

8.5.3.5 Volume and Weight of Disturbed Sediment

According to a study, the ratio of nodule to sediment on the seafloor is 1:9 (Sharma 2011), and so during mining, a large volume of sediments will be disturbed. Considering a minimum penetration of nodule collector in the sediment as 10 cm, the total volume of sediment disturbed on the seafloor will range from 60,000 to 180,000 m^3 day^{-1} depending on the mining rate (Table 8.6) which will be a major source of environmental impact that will require certain measures to restrict it to the seafloor, instead of being transported to the surface or even discharged midway through the water column. The key factor in plume dispersion is the high proportion (>50%) of clay sized particles (<4 u) that can remain in suspension over long period of time, whereas nodule debris will settle faster. Even if it is expected that the areas being mined would have relatively higher nodule abundances and hence lower nodule to sediment ratio, it would be desirable to screen out as much sediment as possible close to the seafloor before lifting the nodules so as to contain the area from environmental impacts.

Since wet density of sediments is 1.15 g cm^{-3} (Khadge and Valsangkar 2008), i.e., 1150 kg m^{-3}, the total weight of the water laden sediment would range between 69,000 and 207,000 t day^{-1} depending upon the mining rate (Table 8.6). Also, as ~80% of the total weight of wet sediment is water (Khadge and Valsangkar 2008), the weight of solid particles would vary between 13,800 and 41,400 t (Table 8.6) that will be disturbed for each day of mining. Once again, the nodule to sediment ratio considered here is for a large area that includes locations without any nodule coverage and low nodule coverage as well, and whereas the first-generation mine-sites are expected to be in areas of dense nodule populations, where the associated sediments would be proportionately less, leading to lesser disturbed sediment particles.

8.5.3.6 Unwanted Material After Metallurgical Processing

If four metals (Mn, Cu, Ni, Co) are extracted with a total metal content of ~26% (Jauhari and Pattan 2000), the remaining 74% of unwanted material in the range of 0.74–2.22 Mt $year^{-1}$ (Table 8.6) will have to be disposed off, which could pose a major environmental challenge, specially because the processing is expected to be in land-based plants and generation of such large quantities of material will require proper disposal or alternative use will have to be thought of.

8.6 Influence of Geological Factors on Mining Design

8.6.1 Nodule Characteristics

Since nodule sizes vary from <1 to 10 cm and the size distribution is variable between different locations, the mining system will have to be designed for an optimum nodule size for efficient recovery and for pumping them to the surface. Use of a crusher on the nodule collector may help in maintaining the consistency in size of the nodules to be lifted to the surface, and use of buffer may help in storing them at an intermediate level before pumping them in fixed quantities to the mining platform for energy conservation. Nodule concentration on the seafloor would have a direct bearing on the amount of nodules recovered by the mining system, as for higher abundance, larger quantities can be recovered in a shorter duration, and vice versa. Higher concentration of nodules along the rugged topography and lower slopes at the base of seamounts and abyssal hills might enhance the recovery of nodules, as compared to the low nodule concentrations in the valleys and plains. Moreover, the local topographic variations and sediment thickness as well as patchy distribution of nodules may also affect the performance of the collector. Hence, it is proposed that the collector system should be capable of detecting the zones of higher nodule concentrations, acoustically or photographically, before sweeping the seafloor (Sharma 1993).

8.6.2 Association with Different Substrates

The mining head will encounter substrates such as sediments and rocks associated with nodules on the seafloor. The effect of sediment cover in burying the nodules (Felix 1980) can pose problems in nodule recovery and as the extent of nodule burial varies from 0 to 100% (Sharma 1989b), the nodule collector will have to be designed to penetrate within the sediments to collect at least a part of the buried nodules in order to be efficient. The binding strength of nodules to the sediment will also be a critical factor in the design of the nodule collector for which use of water jets may help dislodge the nodules from the seabed. Pumping of large quantities of sediments along with nodules will not only increase the energy consumption, but will also cause a major environmental problem if disposal of debris is at or close the surface. Hence, the sediments may have to be discharged in deeper areas below the photic zone to reduce the impact on marine life in the water column. Alternatively, there should be a mechanism to wash them out near the seafloor to enable pumping of nodules only.

Rock outcrops, which appear to extend up to a few tens of meters on the seafloor, and at times occur in the nodule fields along the slopes of seamounts as well as abyssal plains, may act as obstruction to the nodule collector. These areas need to be mapped carefully in order to identify locations where the mining system may not be

able to operate or is likely to get damaged due to the occurrence of hard substrates. Also the photographs, in which nodules and crusts co-occur, indicate transition zones between the outcrops and nodule fields (Fig. 8.1), mapping of which is required for deciphering the margins of the nodule mining areas. Hence, the nodule collector should be capable of sensing such zones, as well as being "driven" around or "flown" over these outcrops in order to avoid any damage to the mining equipment.

8.6.3 Relation with Topography

As the seafloor is made up of abyssal hills (>200 m relief), seamounts (>1000 m), and abyssal plains and valleys, the collector should be designed to negotiate certain gradients, but steeper areas and those with more frequent undulation may pose problems in operation of the nodule collector. Morphometric analysis in a part of the CIOB has shown that a majority (92%) of the area has 0°–3° slope, the remaining areas have higher slopes (up to 15°) (Kodagali 1989). Slope angle studies in a nodule field in the Pacific Ocean had identified <3° slope angles as being nodule dominant, 3°–7° slope angles as sediment dominant, 7°–15° slope angles as a transition zone and >15° slope angles as rock/crust-dominant zones (Yamazaki and Sharma 2000). Hence, the collector system would have to negotiate the changes on the seabed characteristics in terms of reliefs, substrates, and nodule concentrations for better efficiency as well as safety.

8.6.4 Optimization of Mining Rates

The annual recovery rate would be determined by the requirement of providing adequate feed to the large-scale processing facility (UNOET 1987). Considering the metal production (Table 8.5) for different mining rates, it appears that an optimum mining rate of nodules would be 1.5 Mt year^{-1} of dry nodules at the least (preferably 2.0 Mt year^{-1}), so as to yield reasonable quantities of metals as well as net returns for the investment. This is especially for those metals such as cobalt which are available in very small concentrations as only 1500 t of cobalt will be produced at mining rate of 1.5 Mt year^{-1} (dry).

8.6.5 Ore Production and Area of Mine-Site

Estimates show that between 3333 and 10,000 t of nodules (ore) will be recovered every day with the area of the mine-site varying between 4267 and 12,800 km^2 for different mining rates (Table 8.6). The area of the mine-site would be determined on the basis of mean nodule abundance and efficiency of the collector mechanism.

This mine-site will be a small portion within the mineable area that would be delineated based on the best combination of nodule grade, abundance and topographic conditions, and the first such site where mining would commence is termed as First-Generation Mine-site (FGM). The area of the mine-site (~4200–12,800 km^2) as well as the area of contact (that will be actually scraped) on the seafloor (<1–2 km^2 day^{-1}) for a cut-off abundance of 5 kg m^{-2}, would be extremely small in proportion to the mineable area.

8.6.6 Environmental Impact and Waste Disposal

The main source of environmental impact on the seafloor would be the movement of nodule collector while picking up the nodules (Thiel et al. 1998). Earlier studies have indicated that the overall impact of deep-sea mining will be small compared to natural, large-scale processes of ocean circulation and sediment redistribution (Amos et al. 1977). Estimates have also been worked out for benthic and surface discharges during mining operation (Morgan et al. 1999). Current estimates show that the actual area of the mine-site as well as the area scraped by the mining system (i.e., the area of contact) would be extremely small (Table 8.6) even for the lowest nodule abundance (5 kg m^{-2}). Moreover, expecting a higher nodule abundance in FGM, these could still be smaller (Figs. 8.5 and 8.6), restricting actual mining to a tiny speck in the area allotted to the contractor. However, the total volume of sediment disturbed (60,000–180,000 m^3 day^{-1}) as well as the weight of the wet sediment, i.e., in slurry form (69,000–207,000 t day^{-1}) and also the weight of dry sediment, i.e., as solid particles (13,800–41,400 t day^{-1}) appears to be significant but not enormous considering the area and volume of the water column.

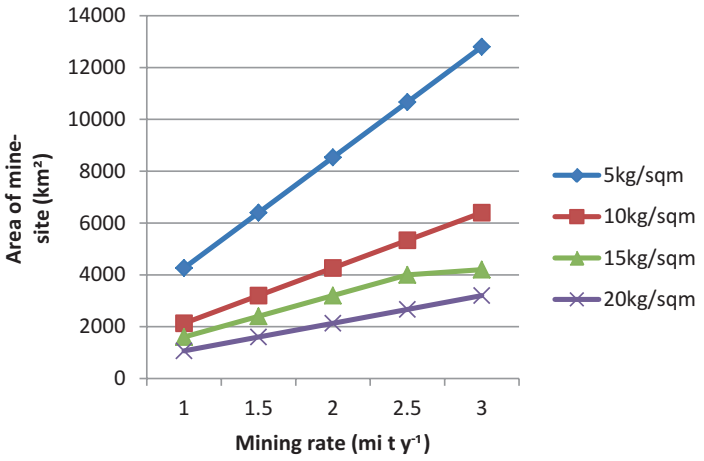

Fig. 8.5 Area of mine-site for different mining rates and nodule abundances

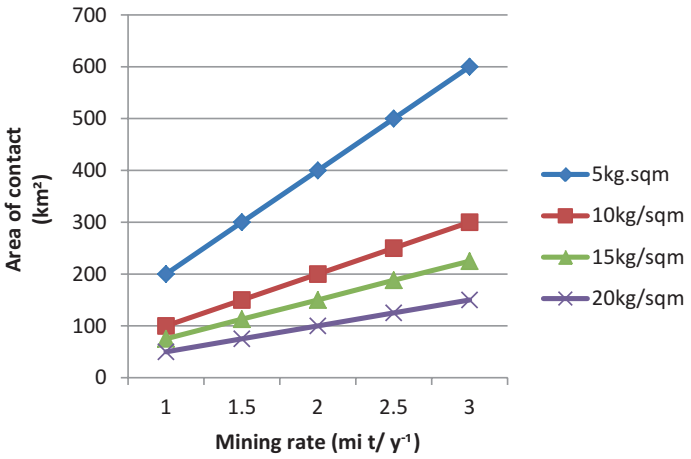

Fig. 8.6 Area of contact for different mining rates and nodule abundances

Care is needed to ensure that these sediments are discharged as close to the seafloor as possible, so as to avoid being transported to adjacent areas by currents. Also, clays (<4 u) being the dominant component (>50%) of these sediments (Khadge and Valsangkar 2008) are likely to remain in suspension for considerable period of time. Hence, suitable mechanisms will have to be devised to ensure that most of the sediment associated with nodules is not discharged into the water column, but as close to the seafloor as possible, so as to reduce the impact on physico-chemical conditions that could in turn affect the biological communities in the marine ecosystem.

Besides lifting of nodules from the seafloor to the mining platform, another environmental concern is discharge or spillage of ore during pre-processing and at-sea transfer and also transport to shore that could increase turbidity in surface waters, affecting the biological productivity in these areas. Also in case of at-sea processing, discharge of waste chemical products could be more hazardous than the discharge of mining effluent (Amos et al. 1977). Finally, the disposal of unwanted material (0.74–2.22 Mt year^{-1}) left over after metallurgical processing is the major issue that will have to be addressed. Finding an alternative use such as those for land reclamation or as agricultural material (Wiltshire 2000, Wiltshire, this publication) could be some of the options.

8.7 Conclusions

Several formulae suggested in this chapter can be adopted for evaluating different mineral characteristics that can be used for designing different components of the mining system. Equations have also been proposed for making estimates associated

with mining such as metal production (and values), area (size) of mine-site, ore production, as well as volume and weight of sediments that will be disturbed for different mining rates. Considering the metal values and estimated expenditures, it is suggested that the mining rate for nodules should be at least 1.5 Mt year^{-1} or more, preferably 2 Mt year^{-1}, as for lower mining rates, the metal production will be extremely low especially for metals of low concentrations such as cobalt.

It is proposed that mining rates should be mentioned in terms of dry nodules and termed as "Mining Rate (dry)," as it represents an absolute quantity of nodules that will be supplied to the processing plant for metallurgical extraction. The term "Mining Rate (wet)" may be used for describing the quantity of wet nodules that will have to be mined to achieve the Mining Rate (dry), after removal of average water (moisture) content in nodules that could vary between different mine-sites.

Wide range in nodule distribution characteristics in terms of their size (0–10 cm), coverage (1–90%), abundance (5–25 Kg m^{-2}) and burial (few cm to few m); as well as their association with substrates such as sediments and rocks; and also the influence of topography on their distribution are critical geological factors for designing the nodule mining system. The nodule collector will have to be an intelligent device to negotiate the variable slopes, patchy distribution as well as partial to complete nodule burial under the sediment–water interface and occurrence of rocks/crust outcrops in the nodule fields. As estimations from photography data consider only the exposed nodules and the abundance data from grabs considers only a part of the buried nodules (down to the "biting" depth of the grab), their calculation may be an underestimate at times, implying that in effect there may be more nodules at a given location.

An area claimed by a Contractor will comprise the following:

1. Exploration area—The area eventually retained by a Contractor or allotted by ISA to a Contractor with exclusive rights for exploration.
2. Mineable area—The portion of the allotted area that is mineable after subtracting the un-mineable areas due to unfavorable topography, grade and abundance.
3. Mine-site—The final site within the allotted area in which mining operation will be conducted.

Although, large areas may be allotted to different contractors, the final area that will be scraped (or area of contact) on the seafloor, would be much smaller in size with respect to the area of the ocean basins as well as the allotted areas; even if several mine-sites are located in it.

In view of the large quantities of associated sediments expected to be disturbed while mining the nodules, necessary measures need to be taken, so as to restrict them within the mine-site on the seafloor and minimize the chances of being transported to adjacent areas. Another area that requires attention is the disposal or "constructive" use (at least partially) of large quantities of unwanted material that will be left over after extraction of metals.

Whereas, research has been mainly concentrated in core areas of designing the technology for mining as well as processing of nodules, some attention also needs to be paid towards logistic support in terms of ore handling, storage and

power generation facilities on the mining platform, as well as supply vessels for transportation of ore, supplies and personnel, especially considering the large distances and uncertain weather conditions of the mining areas.

With the depletion of land resources and lack of other alternative sources of metals for industrial use, nodule mining could become a reality in future, the timing of which will be determined by the cost of bringing them to market under prevailing conditions (Rona 2003). As Morgan (2000) has optimistically concluded: "If the international regulation of seabed mining can be accomplished without imposing untenable restrictions on the development of the deep seabed, commercial development of these deposits will surely occur."

References

Academie des Sciences (1984) Les nodules polymetalliques. Faut-il exploiter les mines oceaniques? Gauthier-Villiars, Paris

Amos AF, Roels OA, Garside C, Malone TC, Paul AZ (1977) Environmental aspects of nodule mining. In: Glasby GP (ed) Marine manganese deposits. Elsevier, Amsterdam, pp 391–437

Bastien-Thiry H (1979) Sampling and surveying techniques. In: Manganese nodules: dimensions and perspectives, UNOET. Reidel, Dodrecht, pp 7–19

Cronan DS (ed) (2000) Marine mineral deposits handbook. CRC Press, Boca Raton

Cronan DS, Tooms JS (1967) Subsurface concentration of manganese nodules in Pacific sediments. Deep-Sea Res 14:112–119

Dick R (1985) Deep-sea mining versus land based mining. In: Donges JB (ed) The economics of deep-sea mining. Springer, Berlin, pp 2–60

Felix D (1980) Some problems in making nodule abundance estimates from seafloor photographs. Mar Min 2:293–302

Fewkes RH, McFarland WD, Reinhart WR Sorem RK (1979) Development of a reliable method for evaluation of deep sea manganese nodule deposits. Bureau of Mines Open File Report 64-80, US Department of the Interior Bureau of Mines, p 91

Flipse JE, Dubs MA, Greenwald RJ, (1973) Pre-production manganese nodules activities and requirements. Mineral resources of the deep seabed, hearings of the sub-committee on minerals, materials and fuels of the US Senate Committee on Interior and Insular affairs (15 March), pp 602–700

Frazer JZ, Fisk MB, Elliott J, White M, Wilson L (1978) Availability of copper, nickel, cobalt and manganese from ocean ferromanganese nodules. Annual Report, June 30, 1977-August 31, 1978, US Department of Commerce, SIO Reference 78-25, pp 105–138

Glasby GP, Meylan MA, Margolis SV, Backer H (1980) Manganese deposits of the Southwestern Pacific Basin. In: Varentsov IM, Grasselly GY (eds) Geology and geochemistry of manganese, vol III. Hungarian Academy of Science, Budapest, pp 137–183

Gleason WM (2008) Companies turning to seafloor in advance of next great metals rush. Min Eng 60:14–16

Handa K, Tsurusaki K (1981) Manganese nodules: relationship between coverage and abundance in the northern part of Central Pacific Basin, vol 15. Geological Survey of Japan, pp 184–217

Herrouin G, Lenoble JP, Charles C, Mauviel F, Bernard J, Taine B (1991) French study indicates profit potential for industrial manganese nodule venture. Trans Soc Min Metall Explor 288:1893–1899

Horn DR, Horn BM, Delach MN (1973) Factors which control the distribution of ferromanganese nodules and proposed research vessel's track, North Pacific. Technical report No 8, NSF-GX33616, Washington DC, p 19

ISA (2008) Report on the International Seabed Authority's workshop on Polymetallic nodule mining technology: current status and challenges ahead. International Seabed Authority, Jamaica. ISBA/14/LTC/3, p 4
Iyer SD, Karisiddaiah SM (1988) Morphology and petrography of pumice from the Central Indian Ocean Basin. Indian J Mar Sci 17:333–334
Iyer SD, Sharma R (1990) Correlation between occurrence of manganese nodules and rocks in a part of the Central Indian Ocean Basin. Mar Geol 92:127–138
Jauhari PJ, Pattan JN (2000) Ferromanganese nodules from the Central Indian Ocean Basin. In: Cronan DS (ed) Handbook of marine mineral deposits. CRC Press, Boca Raton, pp 171–195
Jauhari P, Kodagali VN, Sankar SJ (2001) Optimum sampling interval for evaluating ferromanganese nodule resources in the Central Indian Ocean. Geo-Mar Lett 21:176–182
Kaufman R (1974) The selection and sizing of tracts comprising a manganese nodule ore body. In: Pre-prints offshore technology conference, vol. II. Houston, pp 283–289
Khadge NH, Valsangkar AB (2008) Geotechnical characteristics of siliceous sediments from the Central Indian Basin. Curr Sci 94:1570–1573
Kodagali VN (1989) Morphometric studies on a part of Central Indian Ocean. J Geol Soc India 33:547–555
Kodagali VN, Sudhakar M (1993) Manganese nodule distribution in different topographic domain of the Central Indian Basin. Mar Georesour Geotechnol 11:293–209
Kotlinski R (2001) Mineral resources of the world's ocean—their importance for global economy in the 21st century. In: Proceedings of the ISOPE Ocean mining symposium, Szczecin, Poland, pp 1–7
Kunzendorf H (1986) Marine mineral exploration. Elsevier, Amsterdam, p 300
Lenoble JP (1980) Polymetallic nodules resources and reserves in the North Pacific from the data collected by AFERNOD. Oceanol Int 80:11–18
Lenoble JP (1982) Technical problems in ocean mining evaluation. In: Varentsov IM, Grasselly GY (eds) Geology and geochemistry of manganese, vol III. Hungarian Academy of Science, Budapest, pp 327–342
Lenoble JP (2000) A comparison of possible economic returns from mining deep-sea polymetallic nodules, polymetallic massive sulphides and cobalt-rich ferromanganese crusts. In: Proceedings of the workshop on mineral resources, International Seabed Authority, Jamaica, pp 1–22
Mero JL (1977) Economic aspects of nodule mining. In: Glasby GP (ed) Marine manganese deposits. Elsevier, Amsterdam, pp 327–355
Morgan CL, Odunton N, Jones AT (1999) Synthesis of environmental impacts of deep seabed mining. Mar Georesour Geotechnol 17:307–357
Morgan CL (2000) Resource estimates of the Clarion-Clipperton manganese nodule deposits. In: Cronan DS (ed) A handbook of marine mineral deposits. CRC Press, Boca Raton, pp 145–170
Nath BN, Prasad MS (1991) Manganese nodules in the exclusive economic zone of Mauritius. Mar Min 10:303–335
OMA (1982) Application by Ocean Mining Associates for an exploration license, filed with NOAA, US Dept. of Commerce (18-2-1982)
OMI (1982) Application for and notice of claim to exclusive exploration rights for manganese nodule deposits in the NE Equatorial Pacific Ocean, filed with NOAA, US Dept. of Commerce (19-2-1982)
Park SH, Kim DH, Kim C, Park CY, Kang JK (1997) Estimation of coverage and size distribution of manganese nodules based on image processing techniques. In: Proceedings of the second Ocean mining symposium, Seoul, 24–26 Nov, pp 40–44
Pattan JN, Parthiban G (2007) Do manganese nodules grow or dissolve after burial? Results from the Central Indian Ocean Basin. J Asian Earth Sci 30:696–705
Pearson JS (1975) Ocean floor mining. Noyes Data Corporation, New Jersey
Rona PA (2003) Resources of the ocean floor. Science 299:673–674

Sarkar C, Iyer SD, Hazra S (2008) Inter-relationship between nuclei and gross characteristics of manganese nodules, Central Indian Ocean basin. Mar Georesour Geotechnol 26:259–289
Sharma R (1989a) Effect of sediment-layer boundary layer on exposure and abundance of nodules: a study from seabed photographs. J Geol Soc India 34:310–317
Sharma R (1989b) Computation of nodule abundance from seabed photographs. In: Proceedings of offshore technology conference, Houston, 1–4 May, pp 201–212
Sharma R (1993) Quantitative estimation of seafloor features from photographs and their application to nodule mining. Mar Georesour Geotechnol 11(4):311–331
Sharma R (1998) Nodule distribution characteristics and associated seafloor features: factors for exploitation of deep-sea Fe-Mn deposits. Society for Mining, Metallurgy and Exploration INC, vol 304, pp 16–22
Sharma R (2011) Deep-sea mining: economic, technical, technological and environmental consideration for sustainable development. Mar Technol Soc J 45:28–41
Sharma R, Kodagali VN (1993) Influence of seabed topography on the distribution of manganese nodules and associated features in the Central Indian Basin: a study based on photographic observations. Marine Geology, 110(1–2):153–162
Sharma R, Sankar SJ, Samanta S, Sardar AA, Gracious D (2010) Image analysis of seafloor photographs for estimation of deep-sea minerals. Geo-Mar Lett 30:617–626
Sharma R, Khadge NH, Jai Sankar S (2013) Assessing the distribution and abundance of seabed minerals from seafloor photographic data in the Central Indian Ocean Basin. Int J Remote Sens 34:1691–1706
Siapno WD (1975) Exploration technology and ocean mining parameters. American Mining Congress Convention, San Fransisco, p 24
Stoffers P, Sioulas A, Glasby GP, Thijssen T (1982) Geochemical and sedimentological studies of box core from western sector of the Peru Basin. Mar Geol 48:225–240
Sudhakar M, Das SK (2009) Future of deep seabed mining and demand-supply trends in Indian scenario. In: Proceedings of ISOPE Ocean mining symposium, Chennai, pp 191–196
Thiel H, Angel MV, Foell EJ, Rice AL, Schreiver G (1998) Environmental risks from large scale ecological research in the deep-sea: a desk study. In: Marine science and technology, official publication of the European Communities, vol XIV, p 210
UNOET (1987) Delineation of mine sites and potential in different sea areas. UN Ocean Economics and Technology Branch and Graham & Trotman Limited, London
Usui A (1986) Local variability of manganese nodule deposits around the small hills in the GH81-4 area. In: Nakao S (ed) Marine geology, geophysics and manganese nodules around deep-sea hills in Central Pacific basin, report of Geological Survey of Japan no. 21, pp 98–159
Usui A (1994) Manganese nodule facies in the western part of the Penrhyn Basin, south Pacific (GH83-3 Area). In: Usui A (ed) Marine geology, geophysics and manganese nodules in the Penrhyn Basin, South Pacific, report of Geological Survey of Japan no. 23, pp 87–164
Usui A, Nakao S (1984) Local variability of manganese nodule deposits in GH80-5 area. In: Nakao S, Moritani T (eds) Marine geology, geophysics and manganese nodules in the northern vicinity of Magellan Trough, report of Geological Survey of Japan no. 20, pp 106–121
Wiltshire JC (2000) Innovations in marine ferro-manganese oxide tailings disposal. In: Cronan DS (ed) Handbook of marine mineral deposits. CRC Press, Boca Raton, pp 281–308
Wiltshire J.C., (this publication). Sustainable Development and its Application to Mine Tailings of Deep Sea Minerals. In: Sharma R. (Ed.) Deep-sea mining: resource potential, technical and environmental considerations, Springer, Pp. ___
Yamazaki T, Sharma R (1998) Distribution characteristics of co-rich manganese deposits on a seamount in the Central Pacific Ocean. Mar Georesour Geotechnol 16:283–305
Yamazaki T, Sharma R (2000) Morphological features of Co-rich manganese deposits and their relation to seabed slopes. Mar Georesour Geotechnol 18:43–76

Dr. Rahul Sharma has been working as a Scientist at the CSIR-National Institute of Oceanography in Goa, India, and has led a multidisciplinary group on "Environmental studies for marine mining." He has a master's degree in Geology and a doctorate in Marine Science. His professional interests include application of exploration and environmental data to deep-sea mining. He has edited 3 special issues of scientific journals, 1 symposium proceeding, published scientific 35 papers, 20 articles, and presented 50 papers at international symposia.

His international assignments include Visiting Scientist to Japan, Visiting Professor to Saudi Arabia, member of the UNIDO mission "to assess the status of Deep-sea mining technologies" in Europe, the USA, and Japan, invited speaker and consultant for the International Seabed Authority, Jamaica, and has contributed to the "World Ocean Assessment report I" of the United Nations.

Part II
Deep-Sea Mining Technology: Concepts and Applications

Chapter 9
Fundamental Geotechnical Considerations for Design of Deep-Sea Mining Systems

Tetsuo Yamazaki

Abstract The importance of manganese nodules, seafloor massive sulfides, and cobalt-rich manganese crusts as future metal sources has been well recognized. However, less geotechnical information of the resources is available to aid the design of mining system. The results of fundamental studies for geotechnical characteristics of the resources and sediments associated with the resources are presented in this chapter. Effects of the characteristics on the design of mining system are examined. Some additional engineering and economic considerations for the design are also discussed.

9.1 Introduction

Manganese nodules, seafloor massive sulfides, and cobalt-rich manganese crusts in deep-sea areas have been focused as future metal sources (Mero 1965; Halbach 1982; Lenoble 2000). Lack of the geotechnical information is one of the reasons why they still remain out of commercial ventures.

Manganese nodules are the first recognized deep-sea mineral resources (Mero 1965; Cronan 1980) and many efforts have been concentrated into the R&D of the mining system (Welling 1981; Herrouin et al. 1989; Yamada and Yamazaki 1998) and the environmental impacts (Burns et al. 1980; Foell et al. 1990; Yamazaki and Kajitani 1999). Deep-sea sediments are the bed of manganese nodules and a key objective of the design of mining system (Richards and Chaney 1981). Some important geotechnical characteristics of manganese nodules and deep-sea sediments are summarized in this chapter.

Recent active exploration surveys on seafloor massive sulfides and cobalt-rich manganese crusts have been conducted by Japan in the North Pacific (Usui and Someya 1997; Nishikawa 2001). The results reveal a larger potential for metal sources (Yamazaki 1993; Iizasa et al. 1999). On the other hand, less information is available in the literature for the design of their mining systems (Halkyards 1985;

T. Yamazaki (✉)
Osaka Prefecture University, 1-1 Gakuen-cho. Naka-ku, Sakai, Osaka 599-8531, Japan
e-mail: yamazaki@marine.osakafu-u.ac.jp

R. Sharma (ed.), *Deep-Sea Mining*, DOI 10.1007/978-3-319-52557-0_9

Yamazaki et al. 1990). Example data of geotechnical characteristics of seafloor massive sulfides and cobalt-rich manganese crusts, and seamount sediments associated with them are introduced, though the data accumulation is still insufficient.

9.2 Importance of Geotechnical Characteristics on Design of Mining System

General concept of mining system expected for deep-sea mineral resources is shown in Fig. 9.1. Mining vessel, ore lift system with pipeline and pump, and seafloor miner are the components. Depending on the distribution depths, such as about 5000 m for manganese nodules, about 1500 m for seafloor massive sulfides, about 2000 m for cobalt-rich manganese crusts, and the production rates, the sizes and capacities of the vessels and lift systems will be different. Although the overall mining mechanisms could be similar, the miners are expected to be quite different due to distribution and geotechnical characteristics of the resources.

Manganese nodules are usually distributed on ocean floor at water depths of 4000–6000 m, and the Clarion-Clipperton Fracture Zones (CCFZ) in the Pacific is known for their dense and high quality deposits (Padan 1990; ISA 2008). These nodules are generally about 1–15 cm in diameter and half buried in soft deep-sea sediments. In accordance with the exploration results of CCFZ, the first stage commercial nodule mining is expected in a certain area which has 10 kg/m^2 of average wet nodule abundance (Herrouin et al. 1989). Figure 9.2 shows a simple model of such nodule distribution. The coverage of nodules is only 15% in the case. The importance of geotechnical characteristics of deep-sea sediments for nodule miner design is easily recognized from the figure. A hydraulic nodule pick-up device shown in Fig. 9.3 may be adapted to the collection mechanism because its high pick-up efficiency and reliability were established in the scale model test (Yamada and Yamazaki 1998). Mechanical and hybrid nodule collection devices have also been studied for the collection mechanisms (Hong et al. 1999; Schulte et al. 2001).

In any case, the most basic parameter for the design is the geotechnical characteristics of the sediments. Both towed and self-propulsive types developed for the propulsion mechanisms are also seriously affected with the sediment properties (Yamazaki et al. 1989; Hong and Choi 2001). A large amount of deep-sea sediment is remolded and resuspended with the nodule pick-up and propulsion. A seafloor plume is created with the sediments as illustrated in Fig. 9.1. Some of the sediments are transported through the lift system to the mining vessel with bottom water and the nodules. The sediments and the nodule fragments that cannot be separated from the water might be discharged from the vessel into surface waters creating a turbid plume as illustrated in Fig. 9.1. These plumes may cause environmental impacts on ocean ecosystem (Ozturgut et al. 1978; Foell et al. 1990). Some fundamental impacts have been studied during and after the mining tests and the artificial experiments (Burns et al. 1980; Ozturgut et al. 1980; Thiel and Forschungsverbund Tiefsee-Umweltsschutz 1995; Yamazaki and Kajitani 1999). On the other hand, in

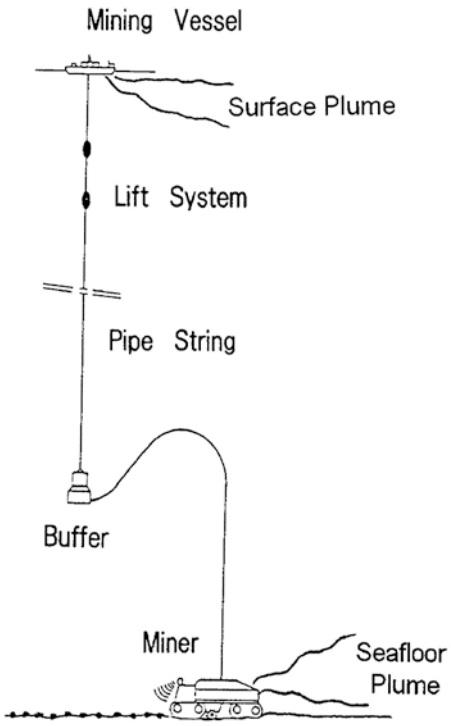

Fig. 9.1 Image of mining system and plumes created by the operation

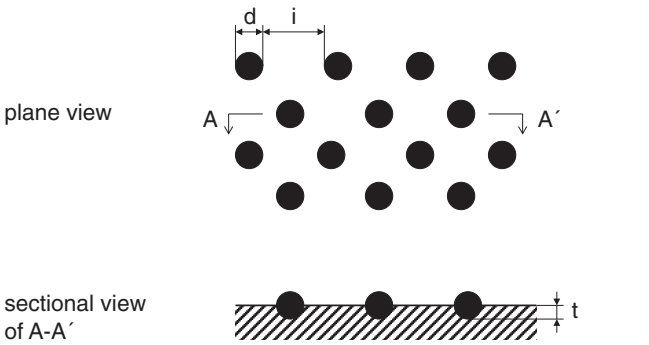

d: diameter = 5.0 cm
i: interval = 11.2 cm
t: burial depth = 2.5 cm
ρ_n : nodule density = 2.0 g/cm^3 (bulk, wet)
ρ_s : sediment density = 1.2 g/cm^3 (bulk, wet)
c: coverage = 15 %

Fig. 9.2 Model distribution of 10 kg/m^2 (wet) nodule population

view of recent environmental concerns, discharge of sediment and nodule-laden water into the bottom layers has been proposed (Agarwal et al. 2012). The plume behavior in the water column in the both cases is influenced by the geotechnical characteristics of the sediments.

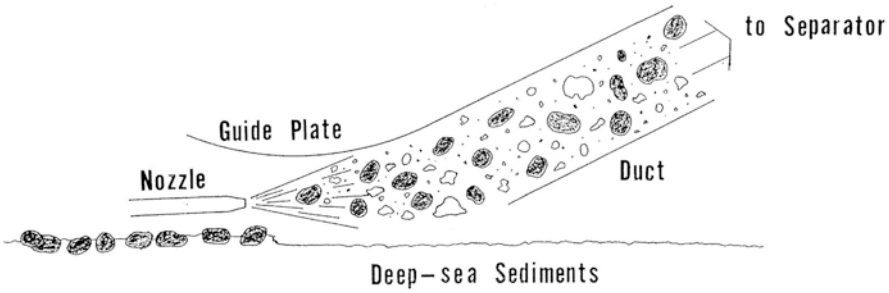

Fig. 9.3 Hydraulic pick-up device for nodule collection

Table 9.1 General distribution characteristics of seafloor massive sulfides comparing with the other deep-sea mineral resources

	Manganese nodule	Seafloor massive sulfide	Cobalt-rich manganese crust
Water depth	4000–6000 m	700–3500 m	800–2500 m
Topography	Flat ocean floor	Spreading center of rise, back arc, etc.	Island and seamount slopes
			Top of guyots
Substrate	Sediments	Basalt	Basalt
		Metamorphic rock	Hyaloclastite
			Limestone
Morphology	Nodule	Chimney and mound on seafloor	Crust
			Nodule
Deposit aspect	Coverage: <50%	Massive ore body of tens million tons	Thickness: <20 cm
	Abundance: <40 kg/m^2		Coverage: <100%
			Abundance: <200 kg/m^2
Metal content	Co: <0.5%	Au: <20 ppm	Pt: <2 ppm
	Ni: <2%	Ag: <1%	Co: <2%
	Cu: <2%	Cu: <15%	Ni: <1%
	Mn: <35%	Pb: <25%	Cu: <0.5%
	Fe: <25%	Zn: <25%	Mn: <35%
		Fe: <40%	Fe: <25%

Seafloor massive sulfides are formed by hydrothermal processes associated with the spreading centers due to plate tectonic activity at water depths of 1200–3500 m generally (Rona and Scott 1993). Their general distribution characteristics are shown in Table 9.1 as compared to the other deep-sea mineral resources. The gold- and silver-rich Kuroko type deposits have been found near Japan in Okinawa and Izu-Ogasawara regions at water depths of 700–1800 m (Halbach et al. 1989; Iizasa et al. 1999). Geotechnical characteristics of the sulfides are primary factors for the design of excavation and propulsion mechanisms of the seafloor miner.

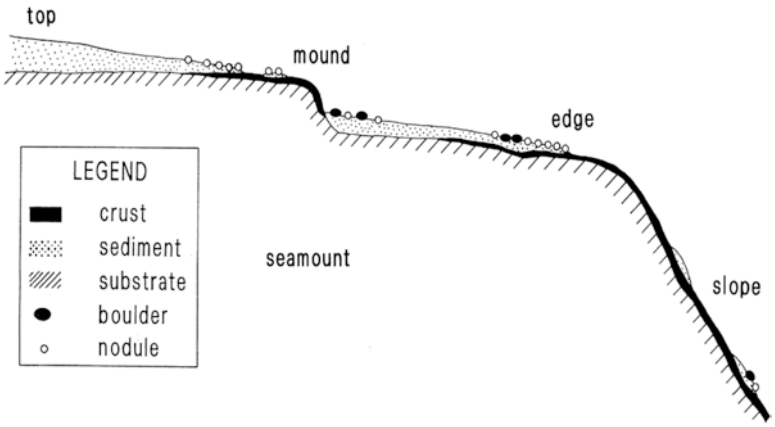

Fig. 9.4 Schematic distribution aspect of cobalt-rich manganese crust

From geotechnical viewpoint, however, the sulfides are the least known of the three resources as little information is available (Crawford et al. 1984; Yamazaki and Park 2003) for their general characteristics. Because of a current commercial interest in mining the sulfides (Malnic 2001), some geotechnical characteristics in the area have been evaluated (Nautilus Minerals, Inc. 2007). If active hydrothermal venting sites with chemosynthetic community exist near the mining area, a quite different ecosystem response can be expected.

Cobalt-rich manganese crusts are distributed on seamounts at water depths of 800–2500 m. The equatorial Pacific is considered as the high potential area (Halbach 1982; Manheim 1986). As recognized from the model distribution in Fig. 9.4, geotechnical characteristics of not only the crusts and their substrates but also the seamount sediments are very important factors for the design of the seafloor miner. The environmental effects may be similar to that of manganese nodule mining.

Because all the three resources are in deep waters, their stress condition is under highly confined pressure. A linear increase on compressive strength of materials with the confined pressure is known. However, no or less effects with the pressure on the tensile and shear strengths, ruling factors on the failures, are recognized (Yamaguchi and Nishimatsu 1991). To clarify tensile strengths of the rocky materials and shear strengths of the sediments is the most important for the geotechnical understanding. Other geotechnical characteristics such as the densities and compressive strengths are also important parameters for example for the machinery designs of the ore lift mechanism in the mining system and the ore crusher in the post-mining ore treatment. Particle size distributions of the sediments, on the other hand, are the key factor for plume behavior.

9.3 Geotechnical Characteristics of Deep-Sea Minerals

9.3.1 Manganese Nodules and Deep-Sea Sediments

9.3.1.1 Manganese Nodules

Density and porosity were measured as physical properties of manganese nodules. The nodules tested were saturated by water in a vacuum water pot for 48 h. Then the weights in water and air under water-saturated condition were measured. After being dried at 105°C for 24 h, the weight in air under fully dried condition was measured. The bulk and solid densities, and the porosity were calculated using the following equations:

$$\rho_b = \frac{W_w}{(W_w - W_s)/\rho_w}$$

$$n = \frac{W_w - W_o}{W_w - W_s}$$

$$\rho_s = \frac{\rho_b - n\rho_w}{1-n}$$

where

ρ_b: bulk density under water-saturated condition
ρ_s: density of solid
ρ_w: density of water
W_w: water-saturated weight in air
W_s: water-saturated weight in water
W_o: dried weight in air
n: porosity

Compressive strength, tensile strength, work index, Protodyakonov's coefficient, Shore hardness, and micro-Vickers hardness were measured as the engineering properties. The nodules formed like cylindrical test pieces under water-saturated condition were used for the uniaxial compressive strength measurements and the nodules themselves without any treatment for the point load tensile strength measurements. The tensile strength is calculated using the following equation (Hiramatsu et al. 1965):

$$S_t = 0.9P_p / d^2$$

where

S_t: tensile strength
d: distance between loading points
P_p: load at failure under point loading

Table 9.2 Geotechnical properties of manganese nodules

Nodule type	r	s	s.r
Bulk density (g/cm^3)	1.98	–	2.02
Compressive strength (MPa)	1.4–4.0	–	0.4–1.1
Tensile strength (MPa)	0.2–0.3	–	0.1–0.3
Work index (kWh/t)	8.27	–	10.4
Protodyakonov's coefficient	1.33	–	1.11
Shore hardness	13–27	20–32	14–21
Micro-Vickers hardness	11–26	16–28	12–27

Note: s (smooth surface nodules), r (rough surface nodules), s.r (nodules of intermediate surface feature)

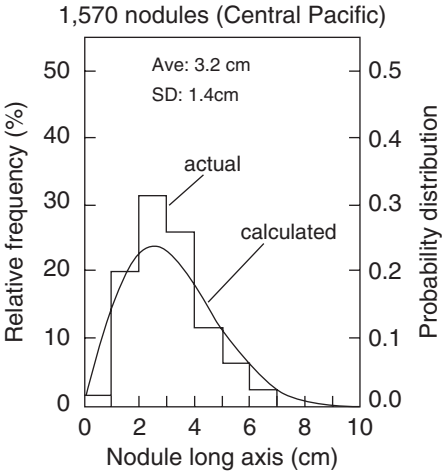

Fig. 9.5 Fitting by Weibull probability distribution for relative frequency with nodule long axis

The samples collected with dredging during GH81-4 Cruise (GSJ 1986) from the Central Pacific Basin were tested. The results are summarized in Table 9.2. Depending on a nodule classification mentioned in a paper (Usui 1986) of the cruise report, three classifications are used in the table.

The sizes of manganese nodules are important data for not only the design of the collection mechanism but also the remote acoustic analysis of the potential mining site (Magnuson 1983). Some example distributions were introduced in Sundkvist (1983). In the paper, as a representative equation of the relative frequency with the cross-sectional areas of the nodules in seafloor photos, the Rayleigh probability distribution was introduced. From the data during R/V Hakurei-maru Cruise GH79-1 in the Central Pacific Basin, the Weibull probability distribution for the relative frequency with the nodule long axis and the Gaussian probability distribution for the cumulative frequency with the nodule long axis were obtained (NRIPR 1989) as shown in Figs. 9.5 and 9.6. These numerical modeling of the nodule size distributions are very important for the geotechnical understanding of the potential mining sites.

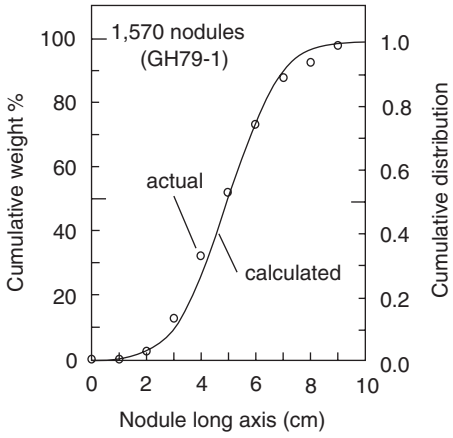

Fig. 9.6 Fitting by Gaussian probability distribution for cumulative frequency with nodule long axis

9.3.1.2 Deep-Sea Sediments

Sediment Sampling

Geotechnical characteristics of deep-sea sediments, such as size distribution, solid density, bulk density, water content, cone penetrating resistance, and shear strength, are essential data for the design of manganese nodule mining system. The importance was discussed in Richards and Chaney (1981).

Normally the spade box corer of which the core cube side is 50 cm in length is used for the bulk sampling of the surface sediment layer. A sub-core, about 10 cm in diameter and 40–50 cm in length, sampled from the box core is carried back to on-land laboratory for the geotechnical testing. Some characteristics, such as water content and vane shear strength with depth, are measured on-board in the box core for every 6 cm intervals from the surface (Yamazaki et al. 1995a).

For the deeper sampling, the piston corer of which the core tube inner diameter is about 6 cm is used. The water content and vane shear strength are measured on-board only for every 50 cm intervals from the surface. A large-diameter gravity corer (LC) described in detail in the next section was tried once for deeper sampling of the deep-sea sediments in 1994. The core was carried back to on-land laboratory for the geotechnical measurements.

Static Characteristics

The geotechnical characteristics including the water content and vane shear strength are measured in on-land laboratory. Comparison of the values of water content and vane shear strength measured on-board and on land is good for understanding the sub-core condition during the transportation. The size distribution, consistency, such as Atterberg liquid limit and Atterberg plastic limit, uniaxial compressive strength,

and unconsolidated-undrained triaxial compressive strength are also measured in on-land laboratory. The strength reduction of the sediments after some physical disturbances is an important factor for the design of propulsion mechanism of the seafloor miner (Richards and Chaney 1981). The sensitivity defined with the following equation is the one in shear strength. After the original vane shear strength is measured at each position in the core, the vane tester is fully turned around several times and the value is measured as the remolded one at the same position as follows:

$$s = \tau_0 / \tau_r$$

where

s: sensitivity
τ_0: original vane shear strength
τ_r: remolded vane shear strength

Example data of the geotechnical characteristics including the internal frictional angles and cohesion calculated from the triaxial compressive strength data are shown in Figs. 9.7, 9.8, 9.9, 9.10, 9.11, and 9.12 and Table 9.3. The geotechnical characteristics measured in the LC core are summarized in Fig. 9.13. The internal friction angle and cohesion are given as a tangential line of Mohr's failure circles under different confined pressures of multiple specimens, each 35 mm in diameter and 70 mm in length.

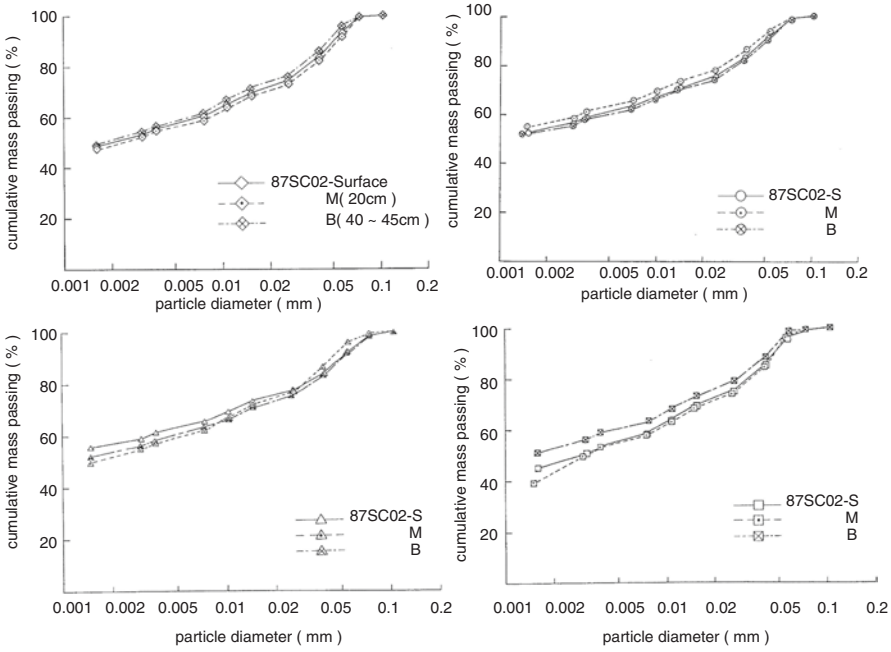

Fig. 9.7 Example size distribution of deep-sea sediments

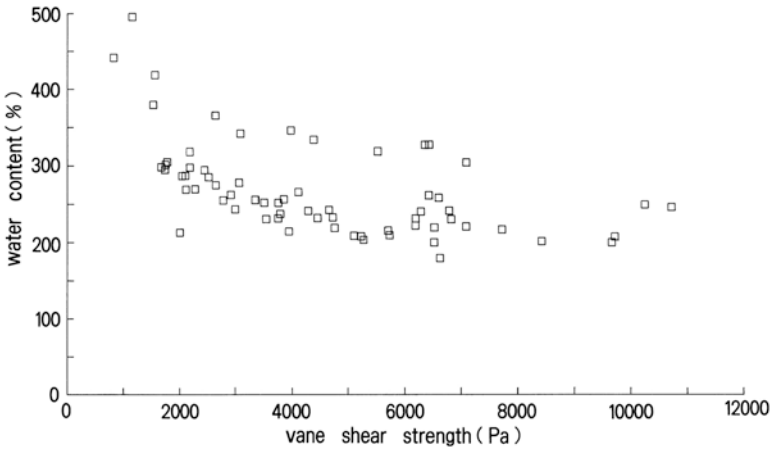

Fig. 9.8 Relationship between original vane shear strength and water content of deep-sea sediments

Dynamic Characteristics

The dynamic response of deep-sea sediments was measured using a newly developed method (Yamazaki et al. 1995c). This method is based on measurement of falling behavior of a disk collider on a cylindrical specimen or into a sub-core sample of the sediments with time. The collider was 500 g in mass and 35 mm in diameter. The free-fall height of the collider was set about 15 cm above the specimen or the sample in order to get about 1 m/s of the contact speed. The schematic outline of dynamic test is introduced in Fig. 9.14. Displacement of the collider, from about 0.05 s before its contact on the specimen or the sample to the end of the collider movement, was measured. The data was analyzed by applying a Voigt's model, which is a parallel connection of a spring and a dashpot as shown in Fig. 9.15, and a stress-strain equation for the sediments. The equation of motion of the collider is written as follows:

$$x'' + \frac{A\eta}{lm}x' + \frac{Ak}{lm}x - g = 0$$

where

x: displacement of collider
A: cross-sectional area of sediments
l: length of sediments
η: dynamic modulus of viscosity of sediments
k: dynamic modulus of elasticity of sediments
m: mass of collider
g: acceleration of gravity
$'$: once differentiation with respect to time
$''$: twice differentiation with respect to time

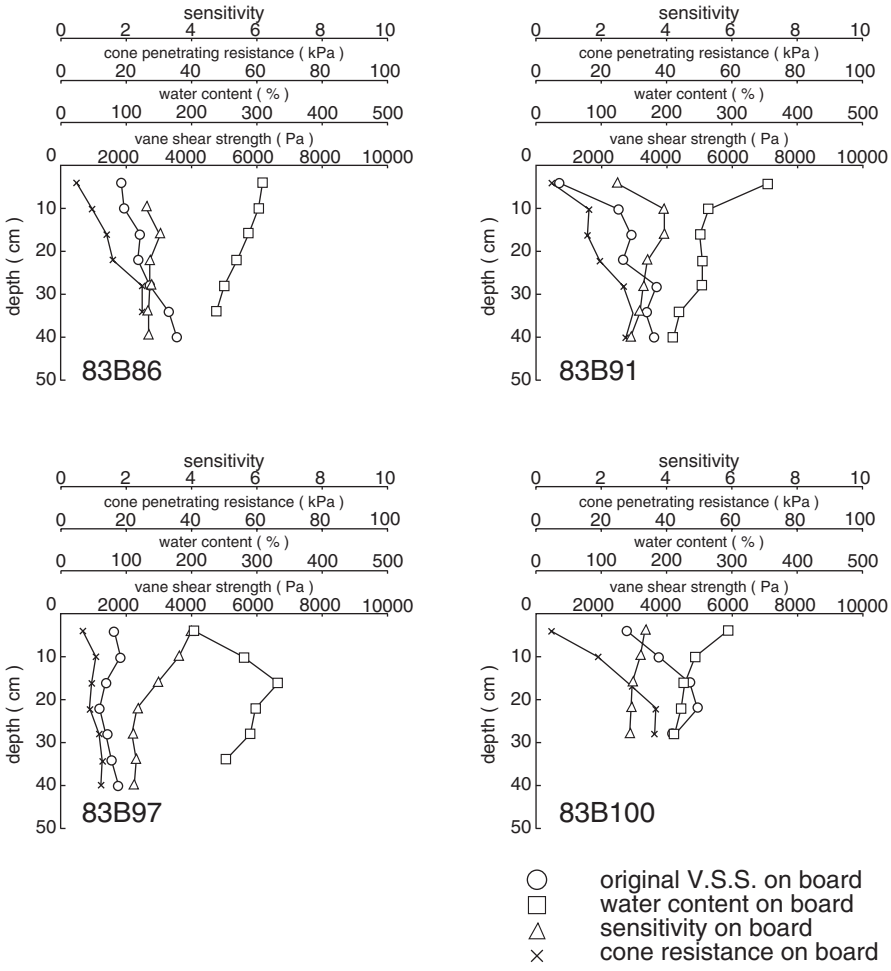

Fig. 9.9 Example results of on-board measurement

If the cross-sectional area and length of the sediments are given, it is possible to calculate the dynamic moduli of elasticity and viscosity from the simultaneous equations induced from the equation by substituting the measured displacement data and the numerically calculated speed and deceleration (Yamazaki et al. 1995c).

Because of the low strength and high sensitivity characteristics, it is impossible to form the cylindrical specimens from the sub-core samples with less than about 4 kPa in the vane shear strength. Most of the superficial layers, which have important roles for estimation of the dynamic response of the sediments in situ, are usually less than about 4 kPa. A direct measurement of the dynamic response on the sub-core sample is required. In case of the sub-core sample, however, it is impossible to specify the cross-sectional area and the length related to the deformation

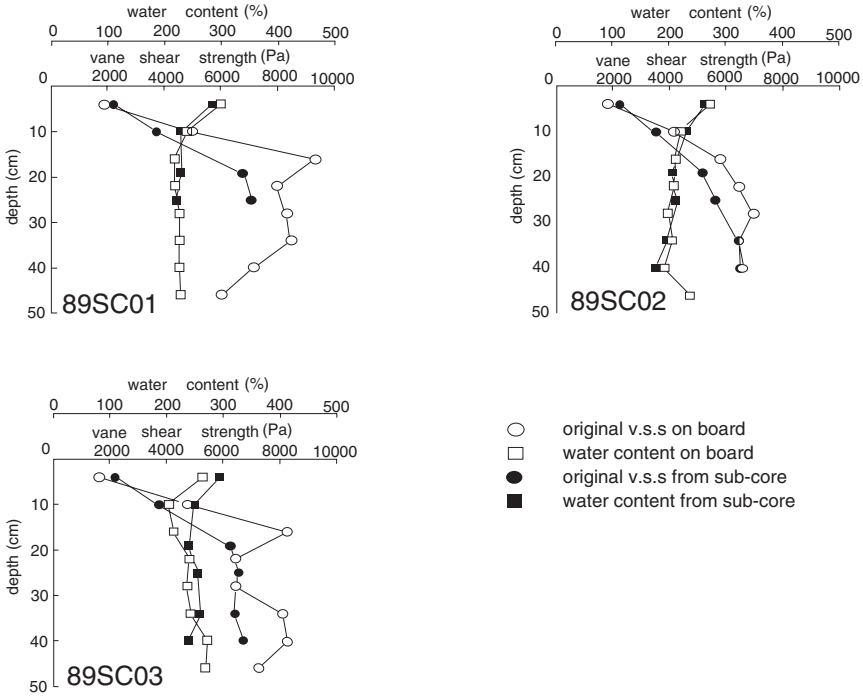

Fig. 9.10 Example results of comparison of on-board and on-land measurements

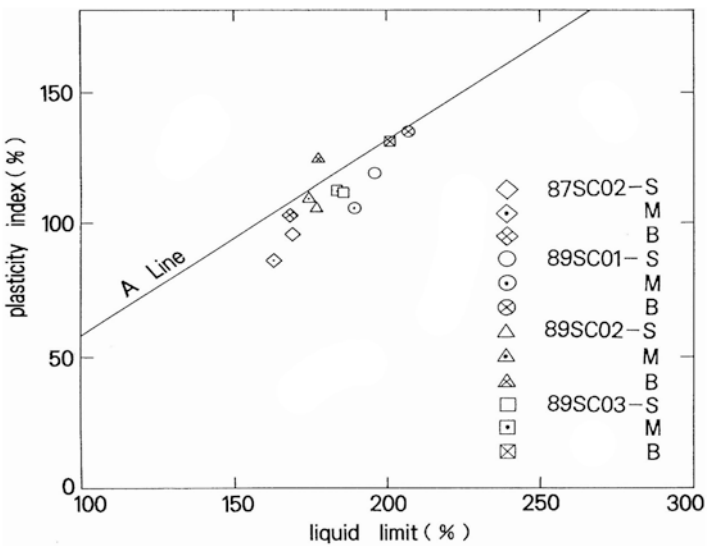

Fig. 9.11 Consistency of deep-sea sediments

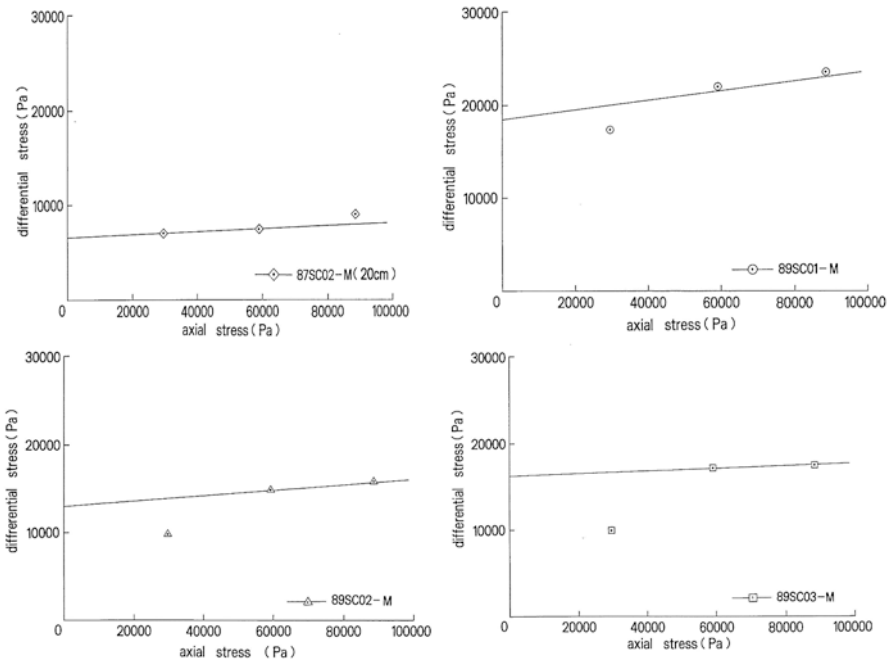

Fig. 9.12 Example results of triaxial tests of deep-sea sediments

Table 9.3 Cohesion and internal friction angle calculated from Fig. 9.12

Sample no.	Cohesion (kPa)	Internal friction angle (degree)
87SC02	3.3	0.4
89SC01	9.2	1.5
89SC02	6.5	0.8
89SC03	8.1	0.4

created by the collider contact. In order to solve the problem, a method assuming the ratio of the cross-sectional area to the length in the sub-core sample by an extrapolation was developed (Yamazaki et al. 1995c). In the method, a pair of falls of the collider, both to the sub-core sample and to the cylindrical specimen, was measured in the possible strength range for the formation of a specimen, i. e., stronger than about 4 kPa in the vane shear strength. The dynamic moduli of elasticity and viscosity, from the result of the collider test to the specimen, were derived from the data. The ratio of the cross-sectional area to the length was set as an unknown factor in the analysis of the result of the collider test to the sub-core sample on the other hand. The ratio was calculated this time because the derived dynamic moduli of elasticity and viscosity were given. It was assumed that the ratio of the cross-sectional area to the length in the strength range less than about 4 kPa in the vane shear strength was able to extrapolate from the strength range more than about 4 kPa

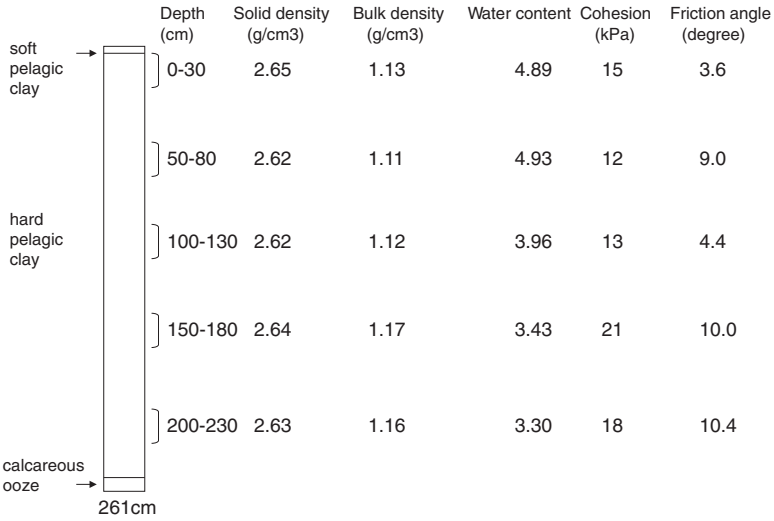

Fig. 9.13 Recovered core column by large-diameter gravity corer and geotechnical characteristics of deeper part of deep-sea sediments

in the continuous extrapolation procedure. The background of this assumption comes from continuities of some factors related to the sediment strength. For example, as shown in Fig. 9.7, a continuous close relationship between the water content and the vane shear strength are obvious in the studied range. The relationship seems almost linear within a limited range. The dynamic moduli of elasticity and viscosity induced from these procedures are summarized in Figs. 9.16 and 9.17.

In Situ Measurement

In situ measurement is the best way to understand geotechnical properties of deep-sea sediments because they are too sensitive to carry back to on-board and on-land laboratories. A pioneer trial and a proposal were made by the author (Tsurusaki et al. 1984; Yamazaki et al. 2005). A successful result has been reported by Babu et al. (2013).

9.3.2 Seafloor Massive Sulfides

Density, porosity, and P wave velocity were measured as fundamental physical characteristics of the seafloor massive sulfides with the same procedures like manganese nodules. The saturated density and the porosity were calculated using the same equations with the nodules.

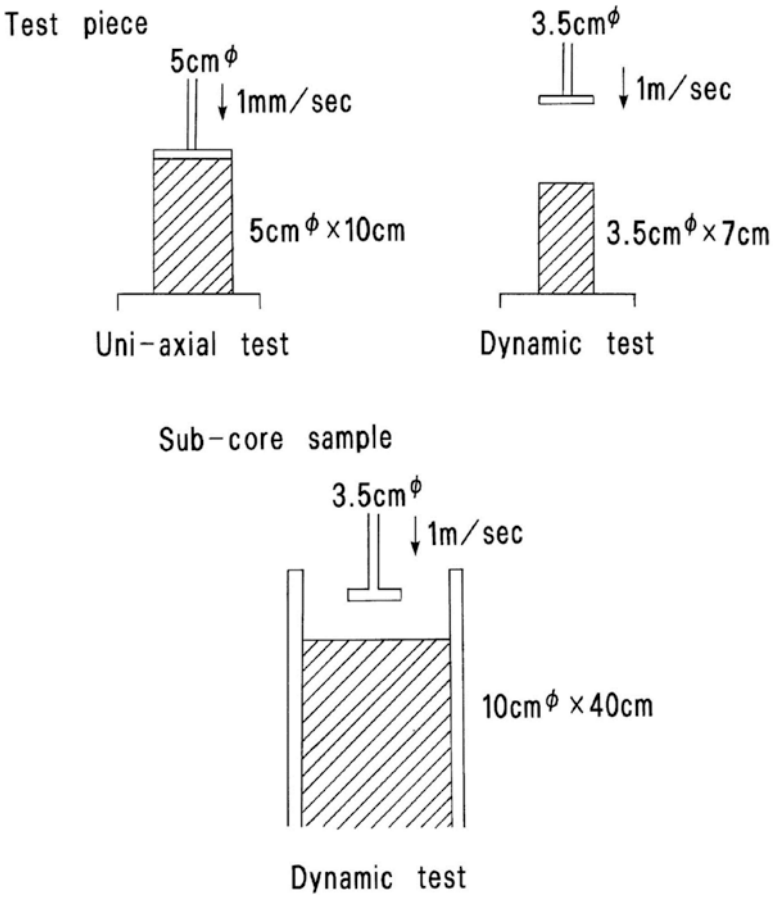

Fig. 9.14 Schematic comparison of static uniaxial and dynamic tests for cylindrical specimens, and dynamic test for sub-core sample

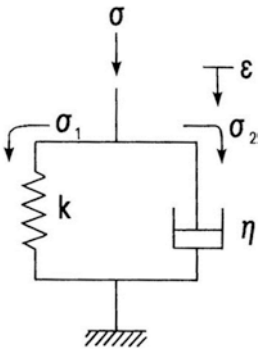

Fig. 9.15 Physical model for analysis of dynamic characteristics

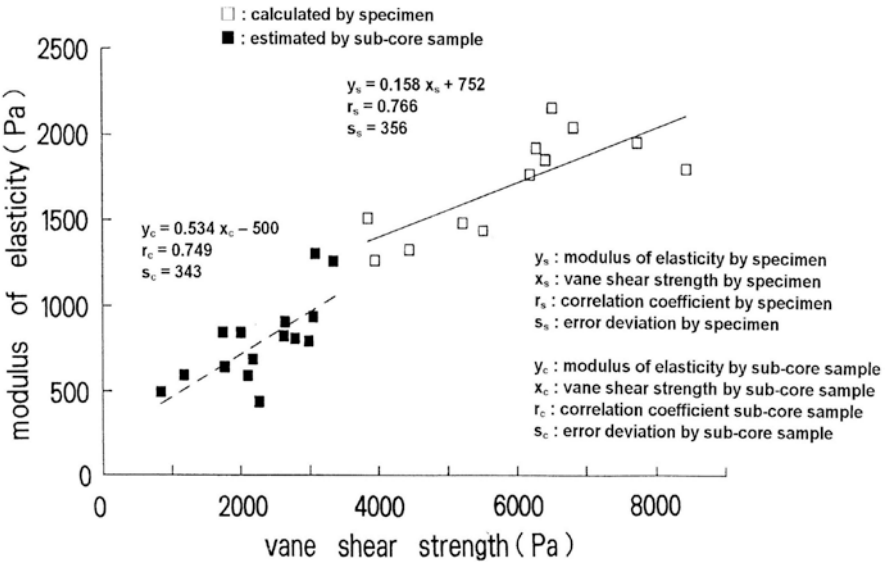

Fig. 9.16 Relationship between dynamic modulus of elasticity and vane shear strength of deep-sea sediments

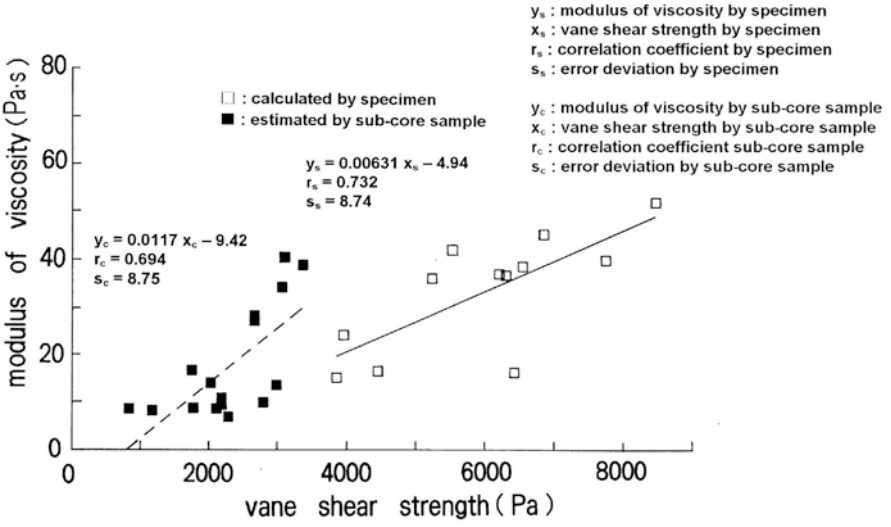

Fig. 9.17 Relationship between dynamic modulus of viscosity and vane shear strength of deep-sea sediments

Compressive strength, tensile strength, Young's modulus, Poisson's ratio, Shore hardness, and micro-Vickers hardness were measured as the geotechnical characteristics. Because quantity of the samples was not sufficient, it was difficult to core the standard cylindrical test pieces in some cases. Therefore, rectangular column

test pieces of 20 mm × 20 mm × 40 mm in length, width, and height, respectively, were used for the uniaxial compressive strength measurements and irregularly shaped test pieces for the point load tensile strength measurements in these cases. The tensile strength is calculated using the same equations with the nodules.

The samples collected with manned submersibles and dredging from Gorda Ridge at East Pacific Rise (Malahoff 1981) and Izena Calderon at Okinawa Trough (Halbach et al. 1989) were tested. The results (Yamazaki et al. 1990; Yamazaki and Park 2003) are summarized in Table 9.4. The metal contents analyzed upon some of them were also summarized in Table 9.5. Some good correlations among the geotechnical characteristics and between the metal contents and geotechnical characteristics were recognized (Yamazaki and Park 2003). Examples of the correlations are shown in Fig. 9.18.

9.3.3 Cobalt-Rich Manganese Crusts and Seamount Sediments

9.3.3.1 Crusts and Substrates

Measured items and methods of geotechnical characteristics for cobalt-rich manganese crusts and their substrates are almost the same as seafloor massive sulfides. Only one difference is the compressive strengths. Because the crusts and some of the substrates were too weak and quantity of the samples was not sufficient, it was difficult to get even the rectangular column type test pieces. Therefore, a substitute method using irregularly shaped test pieces for the compressive strength measurements was chosen. In order to avoid the size effect, the fragmental specimens with weight ranging from 30 to 50 g under water-saturated condition were used for the tests. The compressive strength was calculated from the ordinary uniaxial load testing method for the specimens using the following equation (Protodyakonov 1960):

$$S_c = 5.26 P_l / V^{2/3}$$

where

S_c: compressive strength
P_o: load at failure under ordinary loading
V: volume of specimen

The samples dredged from the equatorial region of the Central Pacific, the southeast and southwest regions of Marcus Island, and around Okinotori-shima Island were tested. The results are summarized in Table 9.6. Frequency distributions of the densities, the compressive strengths, and the tensile strengths are shown in Figs. 9.19, 9.20, and 9.21.

Table 9.4 Geotechnical properties of seafloor massive sulfides

Engineering properties	A	B	C	D	E	F	G	H1	H2	I1	I2	J1	J2	K
Bulk wet density (g/cm^3)	3.298	4.022	3.1406	2.801	2.914	2.387	3.358	2.554	2.668	3.861	3.682	3.388	3.349	3.364
Water content	0.1155	0.0384	0.1467	0.165	0.141	0.207	0.126	0.214	0.174	0.059	0.081	0.128	0.148	0.095
Solid density (g/cm^3)	4.63	4.55	4.49	4.25	4.17	3.64	4.976	4.273	4.008	4.66	4.765	5.095	5.49	4.413
Porosity (%)	37	15	39	45	40	48	41	53	45	22	29	42	48	31
P-wave velocity (km/s)	3.4	3.5	3.1	1.9	2.3	1.8	3.55	2.76	2.49	3.2	2.93	2.45	2.65	2.56
Compressive strength (MPa)	24	38.2	21	3.45	6.37	3.13	11.05	10.26	12.58	18.1	14.93	18.52	11.69	19.22
Tensile strength (MPa)	2.23	4.09	3.04	0.61	0.8	0.14	2.4	2.54	1.81	4.54	2.42	5.21	2.18	2.33
Young's modulus (GPa)	21.9	35.2	18.5	5.7	7.8	22.5	1.448	1.794	3.836	4.51	5.108	4.859	1.745	5.813
Poisson's ratio	0.15	0.28	0.47	0.31	0.27	0.31	−0.022	0.009	0.133	0.025	0.053	0.032	0.01	0.039
Shore hardness	10.2	18.3	14.6	1.6	9.4	5.2	39.01	1.8	7.65	23.32	14.41	12.3	16.94	10.54
Micro-Vickers hardness	162	218	154	0	59	0	635	137	0	188	0	0	0	291

Table 9.5 Metal content of seafloor massive sulfides

Assay	A	B	C	G	H	I	J	K
Au (g/t)	12.8	6.3	5.9	1.3	5.72	0.55	3.98	0.82
Au (g/t)	967	491	676	65.8	500+	500+	476	500+
Cu (%)	13.33	0.895	8.14	0.16	0.01	2.75	1.03	4.7
Pb (%)	16.05	18.75	21.29	0.08	0.14	16.86	10.18	20.25
Zn (%)	29.95	50.2	28.45	0.86	0.6	44.1	20.98	31.83
Fe (%)	2.98	3.41	5.37	44.4	0.77	4.16	19.39	4.15

"500+" in Ag means the value was in the overanalysis range

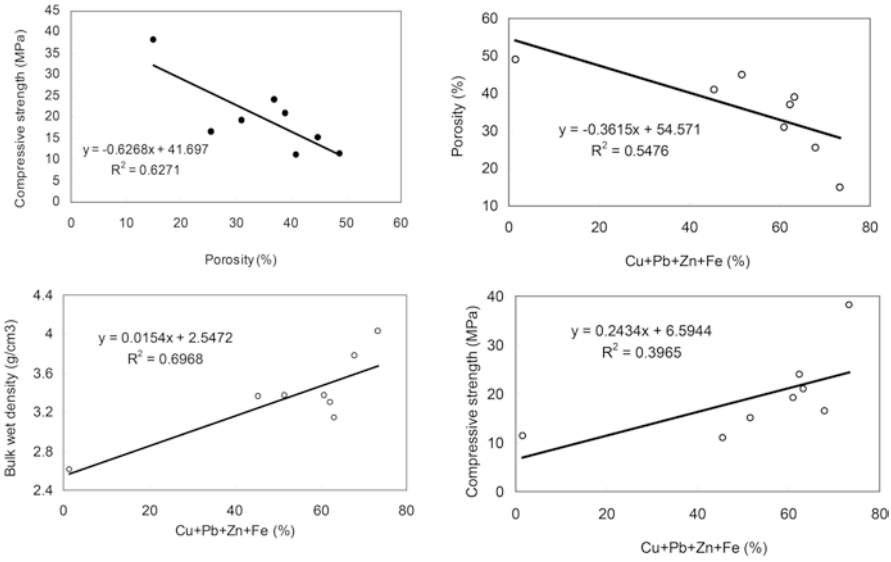

Fig. 9.18 Examples of good correlations among geotechnical characteristics and between metal contents and geotechnical characteristics of SMS

Table 9.6 Geotechnical characteristics of cobalt-rich manganese crusts and their substrates

Engineering properties	Crusts	Substrate
Density (g/cm^3)	1.65–2.17	1.44–2.92
Porosity (%)	43–74	7–69
P wave velocity (m/s)	2090–3390	1760–5860
Compressive strength (MPa)	0.5–16.8	0.1–68.2
Tensile strength (MPa)	0.1–2.3	0.0–18.9

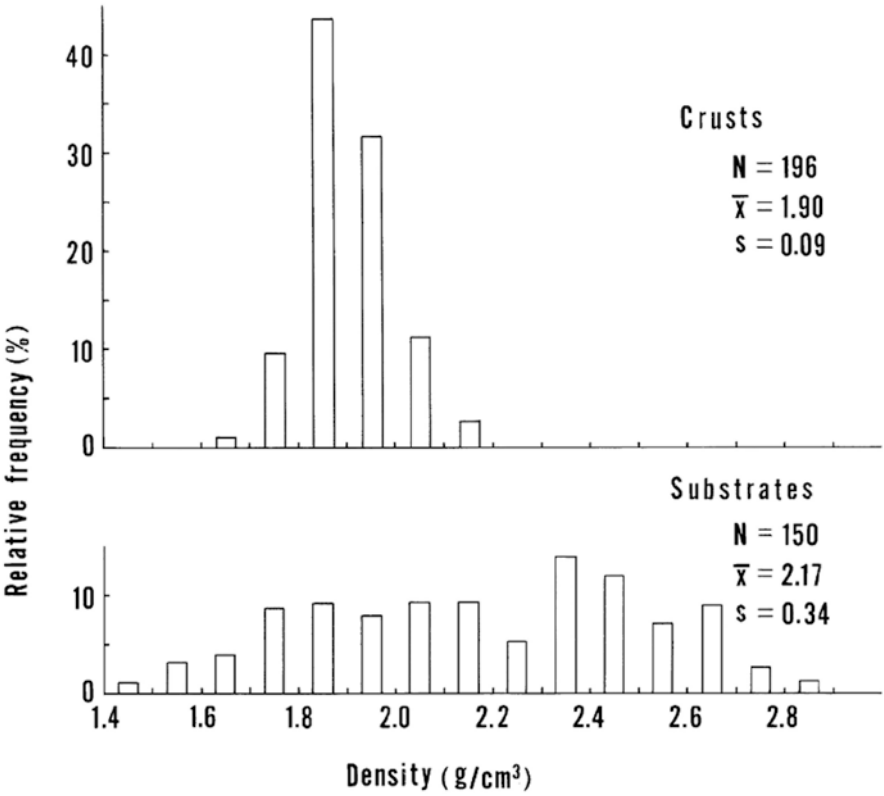

Fig. 9.19 Frequency distribution of density of crusts and substrates

9.3.3.2 Seamount Sediments

Sediment Sampling

Geotechnical characteristics of the seamount sediments, such as size distribution, solid density, bulk density, water content, and strength, are essential data for the design of cobalt-rich manganese crust mining system. However, these characteristics have not yet been examined and made available to the literature. Only their geological size classification is available (Nishimura 1989).

The large-diameter gravity corer (LC) was used for the sampling of the crusts and associated seamount sediments from 1991 (Yamazaki et al. 1993). A schematic setup of LC is shown in Fig. 9.22. The mass of LC head was 350 kg, and the core barrel 160 kg. The free-fall height of LC was positioned 3 m above the seafloor. The core barrel was 4 m in length and 140 mm in outer diameter. The outer diameter of the bit was 150 mm, which was slightly larger than the core barrel. The inner diameter of the core tube inserted in the core barrel was 110 mm. Two core catchers were installed

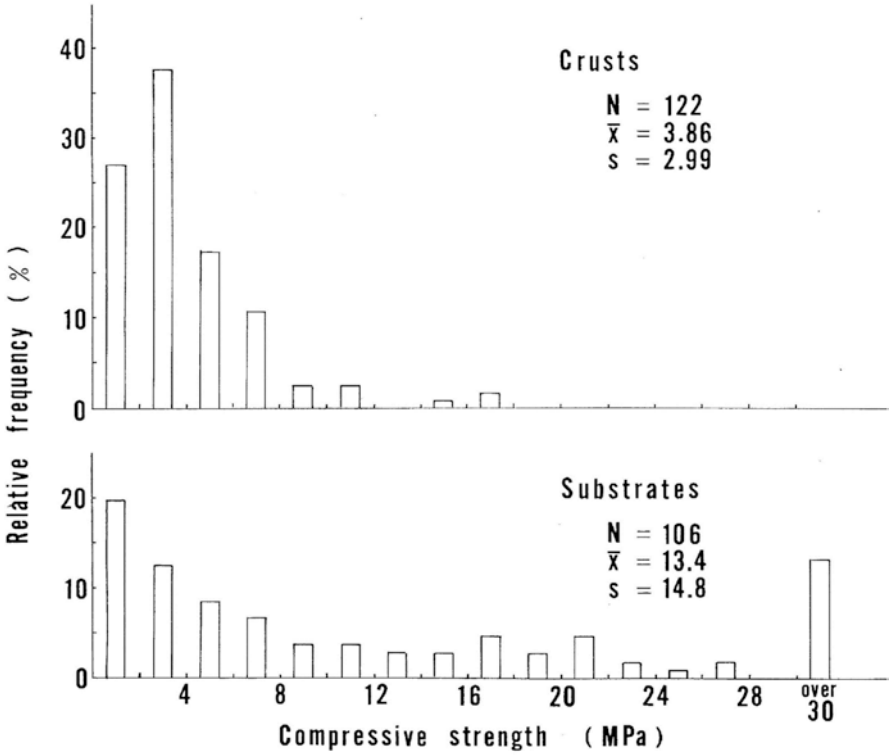

Fig. 9.20 Frequency distribution of compressive strength of crusts and substrates

behind the bit for protecting the core from the dropout during the recovery operation (Yamazaki et al. 1996). Examples of the recovered core column sketches used for the geotechnical analyses are shown in Fig. 9.23. The samples are expected being disturbed, especially near the core tube wall, during LC penetration. Dewatering from the cores was also observed while recovering LC from the sea to the shipboard. This was because the upper part of the 4-m core tube was a water column. The measurements of the geotechnical characteristics of the sediment samples were still important and useful, although they might have been disturbed.

Geotechnical Characteristics

Size distribution, solid density, bulk density, and water content of the surface and the top of every 50-cm unit of the column are measured as the fundamental physical characteristics of the seamount sediments. The relationships among the solid density, the bulk density, and the water content are expressed as follows:

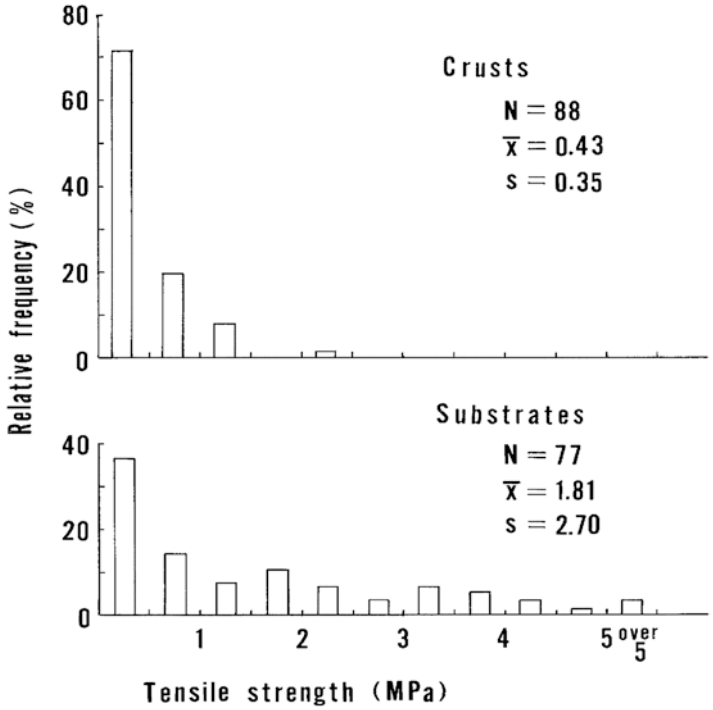

Fig. 9.21 Frequency distribution of tensile strength of crusts and substrates

$$\rho_b = \frac{1+w}{1/\rho_s + w/\rho_w}$$

where

w: water content

The depths of sub-sampling for the measurements are marked along the column sketches in Fig. 9.23. The parts used for unconsolidated-undrained triaxial compressive strength tests are selected according to the size distribution data and the depths. They are also marked in Fig. 9.23. In the triaxial compressive strength tests, two test pieces from a cross section and another two from the adjacent cross section were used. This was because the disturbance near the tube wall by the shearing action was considered to be serious. The consistency, such as Atterberg liquid limit and Atterberg plastic limit, was measured, but no plasticity was found to exist in the seamount sediments.

The size distributions and the results of the triaxial tests are shown in Figs. 9.24 and 9.25. The other characteristics are summarized in Tables 9.7 and 9.8. It must be noticed that most of the sandy samples that were not selected for the triaxial test are less cohesive than the ones tested. These size distributions and the cohesiveness are wider, and the solid density and the water content are higher than the data obtained at the Blake Plateau by Lee (1976).

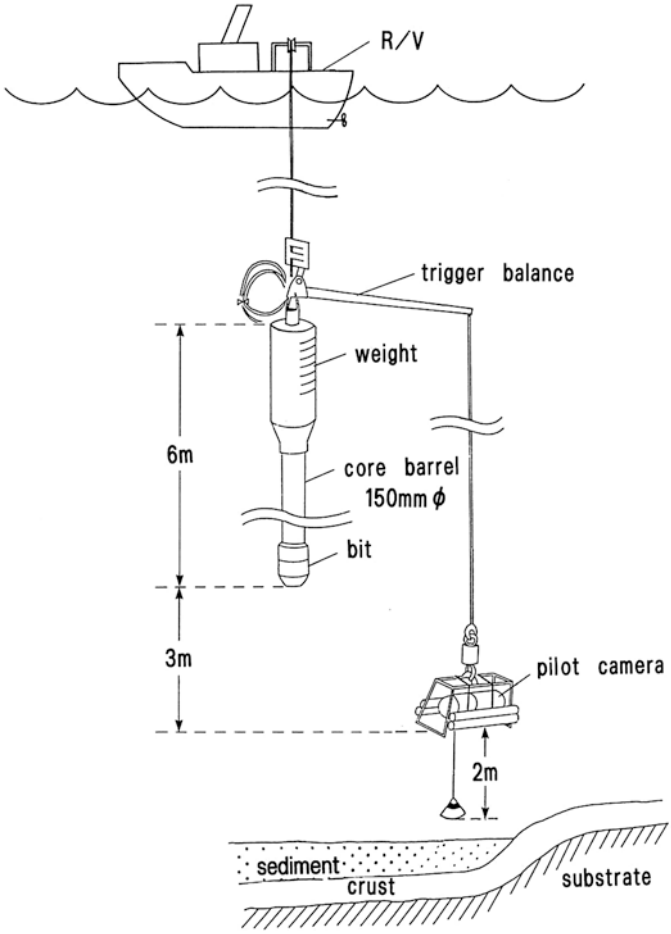

Fig. 9.22 Schematic image of large-diameter gravity coring

9.4 Interactions with Mining Systems

9.4.1 Interactions with Miner

9.4.1.1 Drag

There are two types of soil strength, frictional and cohesive, associated with two quite different kinds of soil, sand and clay, respectively, as Coulomb (1776) pointed out. The deep-sea sediments and the finer seamount sediments are classified into clay and the coarser seamount sediments into sand, respectively, from the size distributions.

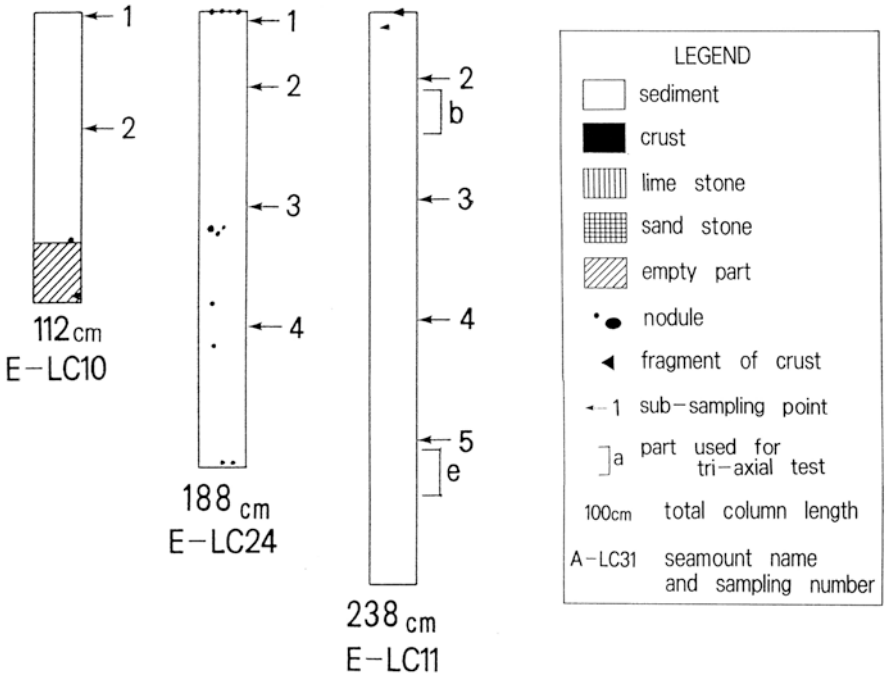

Fig. 9.23 Recovered core column of seamount sediments

The drag resistance from seafloor sediments acting on the miner in case of towed type one is expressed with the following equation (Yamazaki et al. 1989):

$$F_{\mathrm{d}} = F_{\mathrm{f}} + F_{\mathrm{a}} = k_{\mathrm{f}} q_{\mathrm{d}} A + k_{\mathrm{a}} cA$$

where

F_{d}: lateral drag resistance
F_{f}: frictional resistance
F_{a}: lateral adhesive resistance
k_{f}: coefficient of friction
k_{a}: coefficient of lateral adhesion
q_{d}: contact pressure
A: contact area
c: cohesion of sediments

The cutting resistance caused by the sinkage into sediments of the miner is expressed with the following equation:

$$F_{\mathrm{c}} = k_{\mathrm{c}} cBD$$

where

F_{c}: cutting resistance
k_{c}: coefficient of cohesion

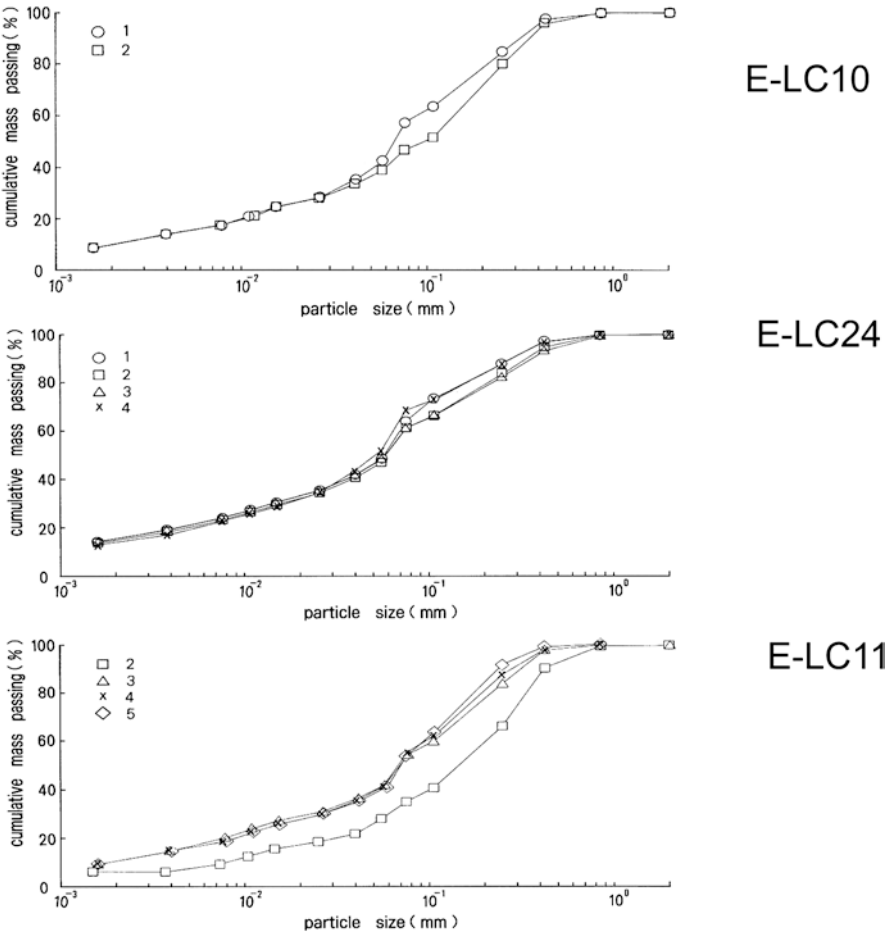

Fig. 9.24 Example size distribution of seamount sediments

B: width of miner
D: sinkage

The total resistance acting on the miner is the sum of the drag and cutting resistances.

$$F_t = F_d + F_c$$

where

F_t: total resistance

The coefficients obtained from small-scale experiments are $k_f = 0.12$, $k_a = 0.08$, and $k_c = 8.2$ for the deep-sea sediments. Because of the sandy nature, only $k_f = 0.35$ is available for the seamount sediments.

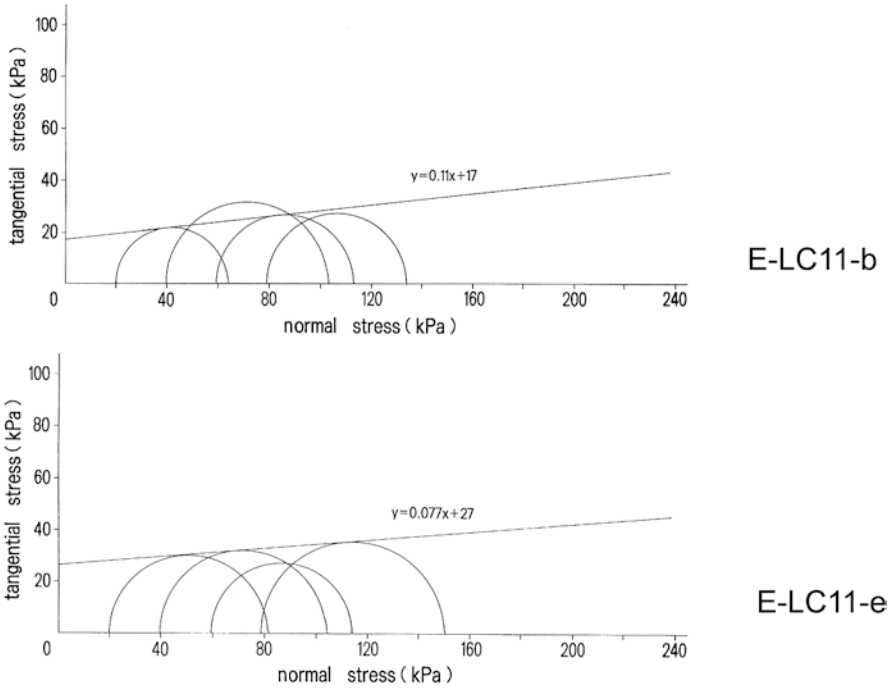

Fig. 9.25 Example results of triaxial tests of seamount sediments

Table 9.7 Densities and water content of seamount sediments

Sample name	Solid density (g/cm^3)	Bulk density (g/cm^3)	Water content
E-LC10-1	2.74	1.50	0.90
E-LC10-2	2.72	1.46	1.00
E-LC11-2	2.78	1.50	0.92
E-LC11-3	2.72	1.50	0.91
E-LC11-4	2.80	1.54	0.83
E-LC11-5	2.70	1.53	0.80
E-LC24-1	2.72	1.46	1.02
E-LC24-2	2.74	1.41	1.17
E-LC24-3	2.74	1.48	0.97
E-LC24-4	2.70	1.43	1.08

Table 9.8 Cohesion and internal friction angle of seamount sediments

Sample name (depth)	Cohesion (kPa)	Internal friction angle (degree)
E-LC11-b (40 cm)	17	6.3
E-LC11-e (190 cm)	27	4.4

The traction force required for the self-propulsive miner is the same as the resistances except interactions between the propulsive mechanism and the sediments. The traction force and the shape effect of grouser on soft sediment layer have been studied experimentally with Hong and Choi (2001).

9.4.1.2 Separating Force

The vertical adhesive resistance while a breakout of embedded object in clay has been studied in the geotechnical engineering field. The primary resistance is the mud suction and the adhesive one is a small fraction while the breakout. Vesic (1971) suggested some contribution of the adhesion on the breakout force. Ninomiya et al. (1971, 1972) formulized the adhesive resistance and showed its effective cases. Muga (1967), Liu (1969), Roderick and Lubbard (1975), Foda (1983), and Das and Suwandhaputra (1987) studied relationships between the load duration and breakout time, and the breakout force. Foda (1983) and Das and Suwandhaputra (1987) pointed out the effect of contact pressure on the breakout force also. In the seafloor miner operation, it is recognized that the effect of the mud suction should be rarely considered from these studies. The adhesive resistance acting on the object on sediments when it is pulled up vertically is expressed with two ways (Yamazaki et al. 1989).

$$F_s = k_p q_d A \left(\text{in case of } q_d / c < 1\right)$$

$$F_s = k_s c A \left(\text{in case of } q_d / c \geq 1\right)$$

where

F_s: separating force
k_p: coefficient of vertical adhesion (in case of $q_d/c < 1$)
k_s: coefficient of vertical adhesion (in case of $q_d/c \geq 1$)

The miner recovery from the seafloor and the nodule pick-up from the sediment surface are typical examples that we need to consider the separation force. The coefficients obtained from a small-scale experiment are $k_s = 0.42$ for the deep-sea sediments and $k_p = 0.04$ for the seamount sediments. They were too weak and too strong are the reasons why only these coefficients were available from the experiment.

9.4.1.3 Seafloor Plume

Size distribution of the sediments is one of key factors to estimate three-dimensional sizes of both the dispersion and resedimentation of the seafloor plume created with the seafloor miner. An artificial seafloor plume was created with a towed disturber in 1994 in CCFZ (Fukushima 1995). Twelve mooring systems with sediment traps and current meters were deployed around the tow area. The resuspended deep-sea

sediments were collected and the current speeds and directions were measured during the experiment. Spatial extent of the resedimentation was clarified with a seafloor camera system in the post-experiment observations and the heavy resedimentation area within 100 m from the towed tracks was recognized (Yamazaki and Kajitani 1999). Using the data, the dispersion and resedimentation behavior of the seafloor plume was analyzed with a computer simulation (Nakata et al. 1997). However, the heavy resedimentation around the disturber tracks was difficult to recreate in the simulation.

Two major factors affected to settling behavior of the plume are the actual effective size distribution of the resuspended and discharged deep-sea sediments and the density effect of discharge in the plume (Jankowski et al. 1996). However, in Nakata's simulation, a particle size distribution of the sediments obtained from the Micro Track size distribution analysis and the Stokes' equation were used and neither aggregation of the sediment particles nor the density effect was considered.

An experimental approach to clarify the aggregation is a size distribution analysis without dispersant in seawater (Yamazaki et al. 2000). In the standard geotechnical analysis, such as ASTM D422 and JIS A1204, the particle settling velocities with dispersant like sodium hexametaphosphate in distilled water are measured and the size distribution is calculated from the velocities by applying Stokes' equation. The Micro Track size distribution analysis is the same method with the geotechnical ones. The results of the experimental approach are compared in Fig. 9.26 with the ones of standard analysis. The mean diameters at 50% cumulative mass finer ranged

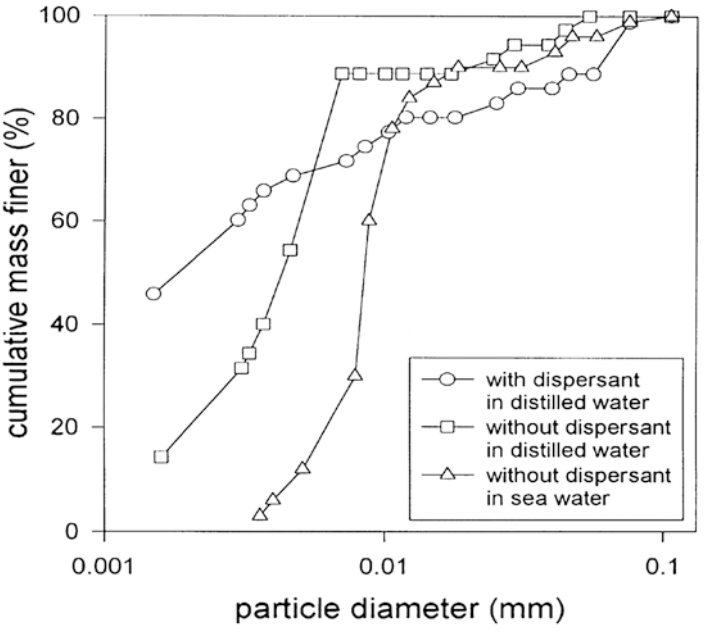

Fig. 9.26 Experimental approach to clarify sediment aggregation

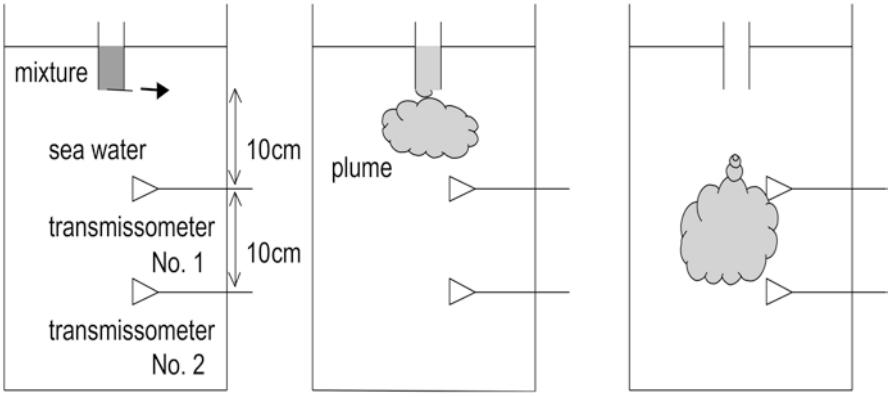

Fig. 9.27 Setup and procedure for clarifying plume behavior

1.2–1.9 micron-meters from the standard measurements, but 8–9.5 micron-meters from without dispersant in seawater, respectively. The mean diameters increased 3–8 times compared with the standard ones. A flocculation of the sediment particles was observed visually in the cases without dispersant in seawater.

A preliminary experiment in a small seawater tank was conducted to observe the density effect (Yamazaki et al. 2000). The setup and procedure are shown in Fig. 9.27. It must be notified that not only the density effect but also the others, such as wall and bottom effect, countercurrent effect, and flocculation of the sediment particles between the mixing and the releasing, are included in the results. Sediment concentration of the mixture was about 5% in weight and settling velocity of the plume was calculated from the concentration record of the transmissometers. The plume settled very quickly mainly as a result of downward density flow in the experiment. Applying Stokes' equation with the results, an equivalent size distribution of the downward density flow measured in the experiment is calculated. An example comparison of the equivalent size distribution with the other size distribution analysis is shown in Fig. 9.28. The mean diameter increased about 100 times compared with the standard one.

9.4.2 Interactions with Lift System

9.4.2.1 Abrasion of Nodules

Abrasion of the ore is expected during the hydraulic lifting through the pipeline from the seafloor to the surface. The abrasion of manganese nodules was tested in a 30 m pump-lift facility shown in Fig. 9.29 by circulating the nodules and water until the passage times through the pump became equal to the ones of expected commercial pump stages for the 5000 m lifting (Yamazaki et al. 1991). Very large amount of fine

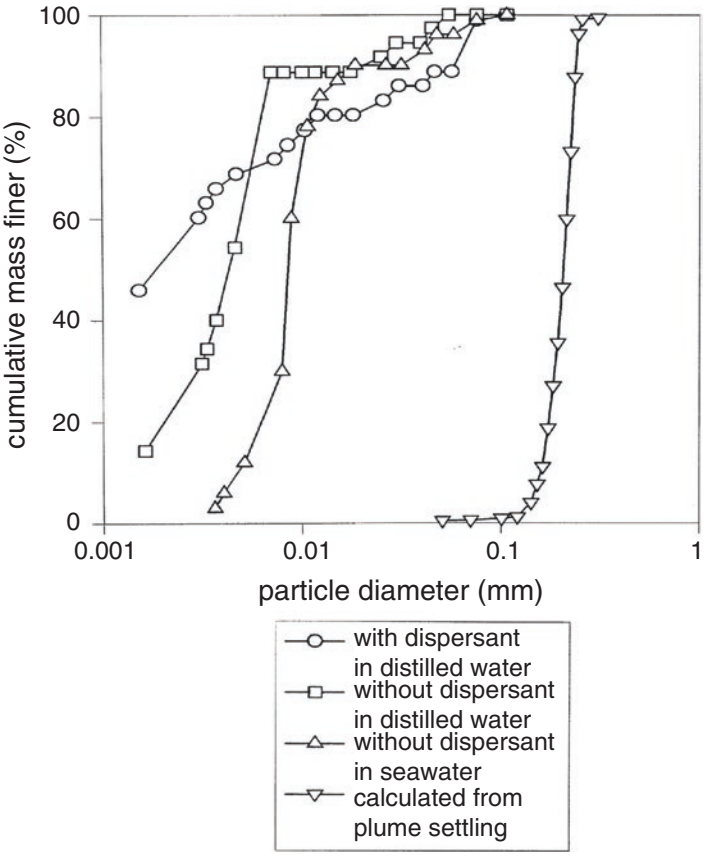

Fig. 9.28 Equivalent size distribution calculated from plume settling velocity

powder was produced by the test. The final size distribution of the abraded nodules is shown in Fig. 9.30 in comparison with the original one. The finer part overlaps the size distribution of the deep-sea sediments.

9.4.2.2 Powderization of Sediments

Because powderization of the sediments during the hydraulic lifting was not known as compared with the abrasion of manganese nodules mentioned in the previous section, an attempt to monitor the powderization was conducted by circulating the sediments in a small-scale setup of pipes and a pump (Yamazaki and Sharma 2001a). The experimental setup is introduced in Fig. 9.31.Comparing the two size distribution curves of the sediments before and after the circulation shown in Figs. 9.32 and 9.33, it was recognized that the relatively larger particles got powderized to smaller ones after circulation. Moreover, amount of the smallest particles less than 3–4 μm

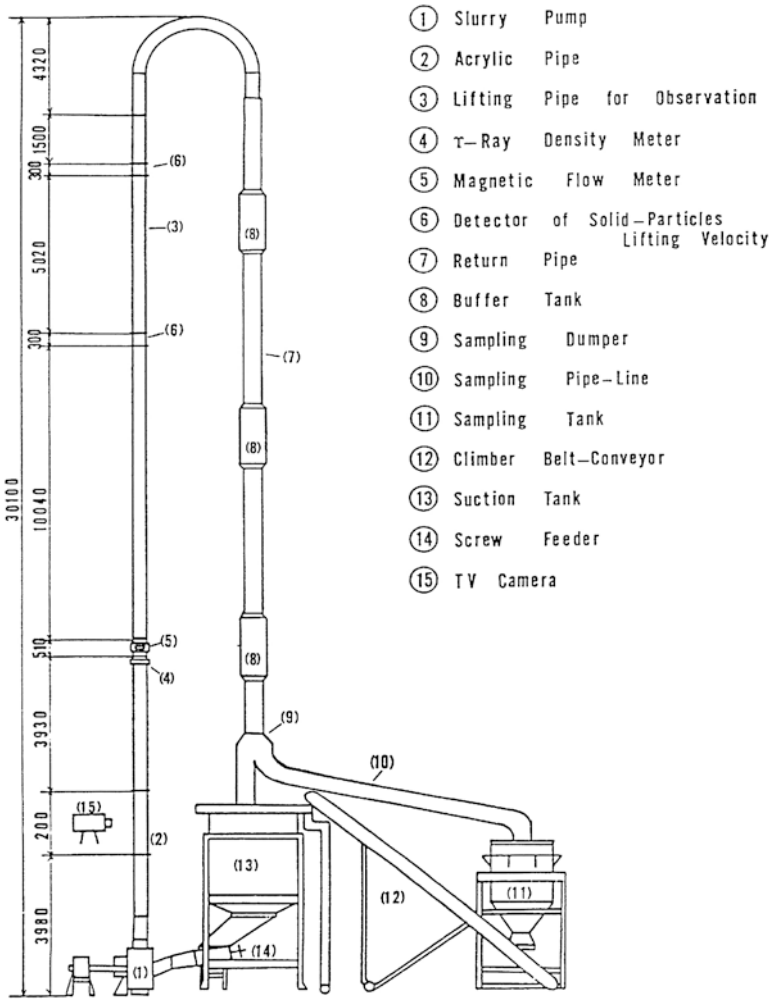

Fig. 9.29 Setup for nodule abrasion experiment

kept the same level after the circulation, indicating that the powderization did not create the smallest size particles. For further understanding of the powderization, larger scale experiments are necessary.

9.5 Actual Design of Deep-Sea Mining System

Though no actual mining system for deep-sea mineral resources has been under operation yet, several engineering approaches have been progressing in the last 40 years. In the 1960s and 1970s, the international consortia were the main players in the

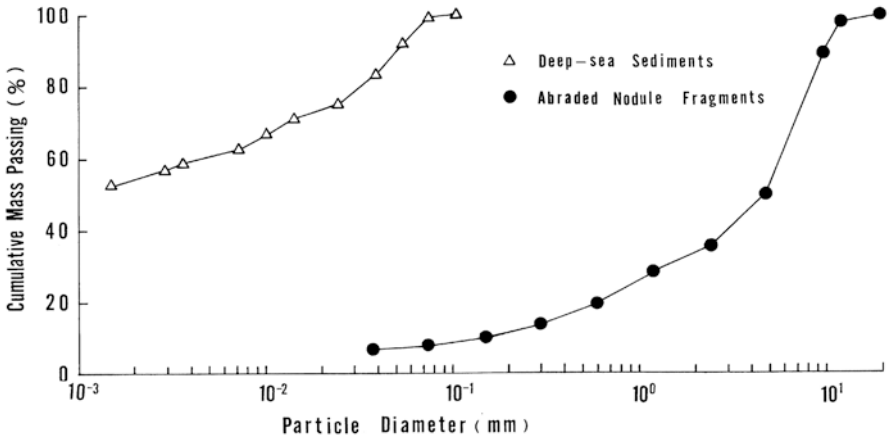

Fig. 9.30 Comparison of size distribution of abraded nodule fragments with deep-sea sediments

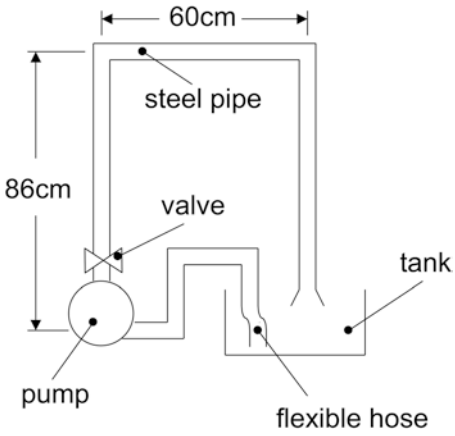

Fig. 9.31 Schematic outline of circulation test setup

R&D activities for manganese nodule mining technologies. Three of them, Ocean Mining Associates, Ocean Mining Inc., and Ocean Minerals Company-Lockheed, conducted some form of tests of prototype mining systems and components in CCFZ (Welling 1981; Kaufman et al. 1985; Bath 1989; Shaw 1993). In the 1980s and 1990s, the mining technologies have been developed by several national projects (Herrouin et al. 1989; Inokuma 1995; Yang and Wang 1997; Hong and Kim 1999; Muthunayagam and Das 1999). Though some of the technically important data remain secret, the outlines of the mining systems are recognized from the technical publications. Many of them are related with the mining system design (Amsbaugh 1982; Welling 1982; Kollwentz 1990;Schwarz 2001; Deepak et al. 2001; Handschuh et al. 2001; Deepak et al. 2007; Abramowski and Cepowski 2013), the riser structures and behaviors (Grote and Burns 1981; Chung et al. 1981; Rogers and Abramson 1981; Yasukawa et al. 1995; Ohta and Morikawa 1997;

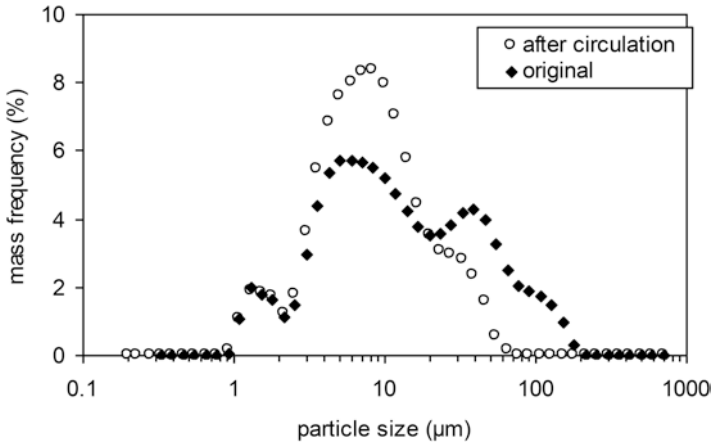

Fig. 9.32 Comparison of particle size distribution of original and after circulation in case of deep-sea sediments sampled in the Clarion-Clipperton Fracture Zones in the Pacific

Yasukawa et al. 1999;Yoon et al. 2003; Hong et al. 2011; Min et al. 2013), the lift system design and the flow dynamics in riser (Clauss 1978; Burns and Suh 1979; Bernard et al. 1987; Shimizu et al. 1992; Xia et al. 1997; Yoon et al. 2000, 2001, 2005; Chung et al. 2001; Hong et al. 2003a, b; Park et al. 2005, 2007a, b, 2009; Sobota et al. 2005, 2007a, b, 2013; Palarski et al. 2007; Vlasak and Chara 2007; Hubinský et al. 2013; Vlasak et al. 2011; Petryka et al. 2013; Ramesh et al. 2013), and the seafloor miner technologies (Li and Zhang 1997; Hong et al. 1997; Hong et al. 1999; Deepak et al. 1999; Yamazaki et al. 1999; Choi et al. 2003; Kim et al. 2003; Lee et al. 2003; Schulte et al. 2003; Choi et al. 2005; Grebe and Schulte 2005;Jung et al. 2005; Kim et al. 2005; Won et al. 2005; Lee et al. 2009; Schulte and Schwarz 2009; Wang et al. 2009; Kim et al. 2011; Lee et al. 2011; Rajesh et al. 2011; Cho et al. 2013; Kim et al. 2013; Lee et al. 2013; Zheng et al. 2013). Depending on recent advancement of robotic technologies, publications related to the mining system and the miner control have been increasing (Schulte et al. 2001; Wang et al. 2003; Hong and Kim 2005; Yeu et al. 2005; Dai et al. 2011; Han et al. 2011; Wang et al. 2011; Han and Liu 2013; Liu et al. 2013; Yeu et al. 2013: Yoon et al. 2013).

Because of the immediate commercial interest of seafloor massive sulfides, with few publications (Parenteau 2010; Stanton and Yu 2010; Smith 2010) the construction of actual mining system has been progressing. The mining system of 4000 tons per day will start the operation in 2018 (Nautilus Minerals, Inc. 2015).

Less R&D has been conducted for the ones for cobalt-rich manganese crust (Halkyard 1985; Latimer and Kaufman 1985; Aso et al. 1992; Chung 1994, 1998; Yamazaki et al. 1995b, 1996).

Components of the final mining system for deep-sea mineral resources from these R&D are mining vessel or platform, ore lift pipeline with submersible pumps or air-lift system, and seafloor towed collector or self-propelled miner. Main parameters

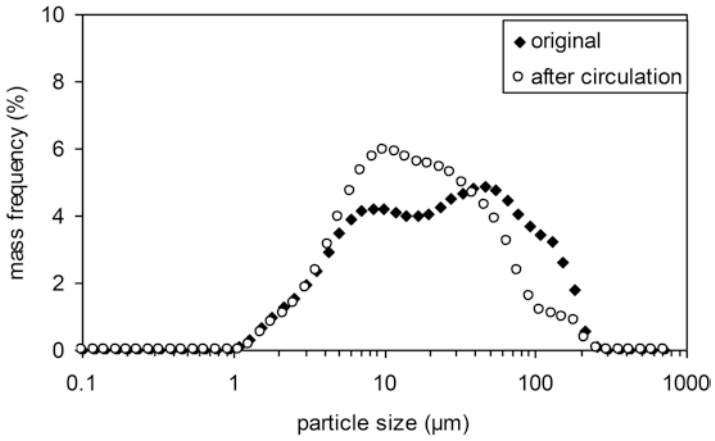

Fig. 9.33 Comparison of particle size distribution of original and after circulation in case of deep-sea sediments sampled in the Central Indian Basin in the Indian Ocean

required for the design of mining system for deep-sea mineral resources are the production rate, operation time, and distribution characteristics including the geotechnical characteristics. The values from one and a half million to three million tons per year in dry weight were presented as the commercial scale nodule recovery rate (Flipse 1983; Johnson and Otto 1986; Herrouin et al. 1989). The days from 250 to 300 per year were expected for the operation time of the ocean mining system (Andrews et al. 1983; Hillman and Gosling 1985; Herrouin et al. 1989).

9.6 Environmental Impact Studies and Scale of BIEs

It is anticipated that the potential for serious environmental impacts will be greatest at the seafloor and at the depth zones of discharge of mining tailings and effluent (Thiel et al. 1998). Certainly, the impacts at the seafloor and in the water column cannot be avoided, but they must be taken into account during the development of the mining equipment and in planning the mining operations to minimize the effects.

The Deep Ocean Mining Environment Study (DOMES) conducted by the National Oceanic and Atmospheric Administration (NOAA), USA from 1972 to 1981 in CCFZ investigated the baseline conditions and monitored environmental impacts during the two pilot-scale mining tests conducted by Ocean Mining Inc. and Ocean Mining Associates in 1978 in the Pacific Ocean (Ozturgut et al. 1978, 1980; Burns et al. 1980). The study measured the concentration of particulate in the discharge, and assessed the biological impacts on the surface as well as seafloor plumes.

Further study and evaluation of the deep-sea environmental impacts were conducted by Germany and USA. The disturbance and recolonization experiment in a manganese nodule area of the Deep South Pacific Ocean (DISCOL) was started in 1988 by a German group. The seafloor disturbance was in 1989 and the latest

post-disturbance monitoring was in 1996, 7 years after the disturbance (Thiel and Forschungsverbund Tiefsee-Umweltsschutz 1995; Schriever et al. 1997). The Benthic Impact Experiments (BIE I&II) were conducted by NOAA from 1991 to 1995 in CCFZ. The seafloor disturbance in 1993 and measurement methods were very systematic (Ozturgut et al. 1997) and have subsequently been followed by other groups. However, the project was stopped in 1995 and the results have been partially reported (Trueblood et al. 1997). Japan in 1994 in CCFZ (JET: Fukushima 1995), Interoceanmetal Joint Organization (IOM) in 1995 in CCFZ (IOM-BIE: Kotlinski and Tkatchenko 1997), and India in 1997 in the Indian Ocean (INDEX: Desa 1997) did the same type BIE using the same disturber as NOAA. The mechanism for disturbing the seafloor was different between DISCOL and the BIEs. In DISCOL, the emphasis was on plowing the seafloor; the BIEs concentrated on sediment resuspension.

The operation time of DISCOL was for 2 weeks and the BIEs were for several tens of hours and the distances covered by the paths of disturbers in the BIEs vary from 33 to 144 km in a narrow width of 200–300 m. The other scale factors of the BIEs' disturbances were analyzed by Yamazaki and Sharma (2001b) using the geotechnical characteristics of the sediments as the key factors. The outlines of disturbances of the BIEs, for example, were summarized in Table 9.9. The quite smaller disturbances than the expected commercial mining are observed.

A new Japan's BIE named DIETS (Direct Impact ExperimenT on Seamount) that focused on analyzing the direct destruction of benthos occurring in the running tracks of a seafloor miner was conducted in a cobalt-rich manganese nodule distribution area on a Pacific seamount in 1999 (Yamazaki et al. 2001). In the experiment, towing a system called a "scraper," the nodules and sediments on the seafloor surface were partially removed. Then effects of the removal on the seafloor ecosystem were monitored. The vertical profile of water contents in sediment columns obtained before and immediately after the experiment shown in Fig. 9.34 clearly means that the top surface sediment layer 1–2 cm deep, in which the water content is quite high, was cut and taken away with nodules in the nodule-removed area.

Another environmental approach related to seafloor massive sulfide mining has been studied in Japan's R&D program. Both the direct destruction of benthos and the effect of resedimentation are estimated and assessed (Toyohara et al. 2011).

9.7 Conclusions

Geotechnical characteristics of deep-sea mineral resources such as manganese nodules, seafloor massive sulfides and cobalt-rich manganese crusts, and sediments accompanied with the resources are introduced. Interactions of the characteristics with the mining system are discussed. Important roles of the characteristics in designing the mining system and analyzing the environmental impacts are notified. The data introduced here are effective for primary understanding of geotechnical characteristics of the resources. However, detailed data collection is necessary for designing specific features of a mining system suitable for a target area.

Table 9.9 Outlines of disturbances of the BIEs

Experiment name	No. of tows	Duration of disturbance (min)	Distance covered (km)	Average speed (km/h)	Water content (%)	Density (g/cm^3)	Sediment concent. (g/L)	Weight of sediment		Volume of sediment[a]		Depth of excavation (mm)
								Dry (t)	Wet (t)	Recovered (m^3)	Discharged (m^3)	
(a) JET	19	1227	32.7	1.6+	78.5+	2.7+	38.3	355+	1651+	1427+	2495+	44+
(b) INDEX	26	2534	88.3	2.1+	84.5+	2.6+	30.23	580+	3737+	3380+	6015+	38+
(c) NOAA BIE	49	5290	141+	1.6+	73+	2.7+	33.3	1500 (1332+)	4888	4000 (4049+)	4328 (6951+)	29+
(d) IOM BIE	14	1130	35	1.8+	80	2.7+	42.1+	360+	1800	1573+	1300 (2693+)	45+

[a]Denotes total volumes in situ, of wet sediment recovered from seafloor and of simulated plume discharged

Numbers given in the table with (+) are estimated by authors, the others are taken from:

(a) Fukushima (1995)

(b) Sharma and Nath (1997); Sharma et al. (1997); Khadge (1999)

(c) Trueblood (1993); Nakata et al. (1997); Gloumov et al. (1997)

(d) Tkatchenko et al. (1996); Kotlinski (personal communication)

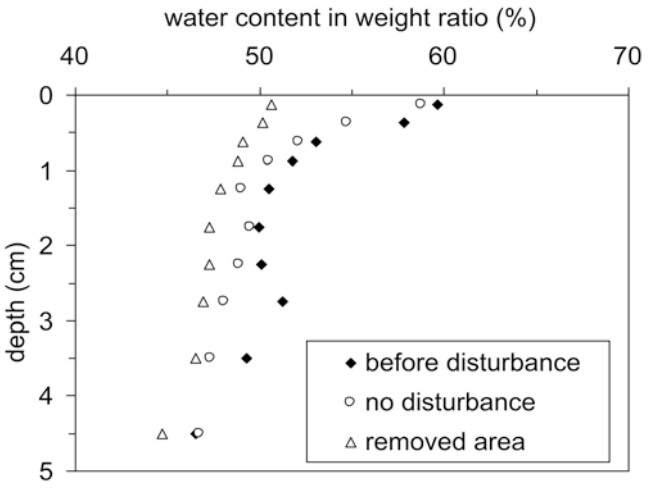

Fig. 9.34 Comparison of vertical profile of water content immediately after scraping

References

Abramowski T, Cepowski T (2013) Preliminary design considerations for a ship to mine polymetallic nodules in the Clarion-Clipperton zone. In: Proceedings of 10th ISOPE Ocean mining symposium, Szczecin, pp 198–203

Agarwal B, Hu P, Placidi M, Santo H, Zhou JJ (2012) Feasibility study on manganese nodules recovery in the Clarion-Clipperton zone. LRET collegium 2012 series, vol 2. University of Southampton, Southampton

Amsbaugh JK (1982) Air-lift mining: text from the DEEPSEA VENTURES, INC. Film "Deep Ocean Mining". In: Humphrey PB (ed) Marine mining: a new beginning. Hawaii Department of Planning and Economic Development, pp 72–81

Andrews BV, Flipse JE, Brown FC (1983) Economic viability of a four-metal pioneer deep Ocean mining venture. US Dept. of Commerce, PB84-122563

Aso K, Kan K, Doki H, Iwato K (1992) Effect of vibration absorbers on the longitudinal vibration of a pipe string in the deep sea—Part 1: in case of mining cobalt crusts. Int J Offshore Polar Eng 2(4):309–317

Babu SM, Ramesh NR, Muthuvel P, Ramesh R, Deepak CR, Atmanand MA (2013) In-situ soil testing in the Central Indian Ocean basin at 5462-m water depth. In: Proceedings of 10th ISOPE Ocean mining symposium, Szczecin, pp 190–197

Bath AR (1989) Deep sea mining technology: recent developments and future projects. In: Proceedings of 21st offshore technology conference, Paper No. 5998

Bernard J, Bath A, Greger B (1987) Analysis and comparison of nodule hydraulic transport systems. In: Proceedings of 19th offshore technology conference, Paper No. 5476

Burns JQ, Suh SL (1979) Design and analysis of hydraulic lift systems for deep Ocean mining. In: Proceedings of 11th offshore technology conference, Paper No. 3366

Burns RE, Erickson BH, Lavelle JW, Ozturgut E (1980) Observation and measurements during the monitoring of deep Ocean manganese nodule mining tests in the North Pacific, March-May 1978, NOAA Technical Memorandum ERL MESA-47

Cho S-G, Park S-H, Choi S-S, Lee T-H, Lee M-U, Choi J-S, Kim H-W, Lee C-H, Hong S (2013) Multi-objective design optimization for manganese nodule pilot miner considering collecting

performance and manoeuver of vehicle. In: Proceedings of 10th ISOPE Ocean mining symposium, Szczecin, pp 253–260
Choi J-S, Hong S, Kim H-W, Lee T-H (2003) An experimental study on tractive performance of tracked vehicle on cohesive soft soil. In: Proceedings of 5th ISOPE Ocean mining symposium, Tsukuba, pp 139–143
Choi J-S, Hong S, Kim H-W, Yeu T-K, Lee T-H (2005) Design evaluation of a deepsea manganese nodule miner based on axiomatic design. In: Proceedings of 6th ISOPE Ocean mining symposium, Changsha, pp 163–167
Chung JS (1994) Deep-Ocean cobalt-rich crust mining systems concepts. In: Proceedings of MTS-94, Washington, DC, pp 95–101
Chung JS (1998) An articulated pipe-miner system with thrust control for deep-Ocean crust mining. Mar Georesour Geotechnol 16(4):253–271
Chung JS, Whitney AK, Loden WA (1981) Nonlinear transient motion of deep Ocean mining pipe. J Energy Resour Technol 103:2–10
Chung JS, Lee K, Tischler A, Yarim G (2001) Effect of particle size and concentration on pressure gradient in two-phase vertically upward transport. In: Proceedings of 4th ISOPE Ocean mining symposium, Szczecin, pp 132–138
Clauss G (1978) Hydraulic lifting in deep-sea mining. Mar Min 1(3):189–208
Coulomb CA (1776) An attempt to apply the rules of maxima and minima to several problems of stability related to architecture. Mem Acad R Sci, Paris 7:343–382
Crawford AM, Hollingshead SC, Scott SD (1984) Geotechnical engineering properties of deep-Ocean polymetallic sulfides from 21°N, East Pacific Rise. Mar Min 4:337–354
Cronan DS (1980) Underwater minerals. Academic Press, London, 362
Dai Y, Liu S, Cao X, Li Y (2011) Establishment of an improved dynamic model of the total deep Ocean mining system and its integrated operation simulation. In: Proceedings of 9th ISOPE Ocean mining symposium, Maui, pp 116–123
Das BM, Suwandhaputra H (1987) Bottom breakout of objects resting on soft clay sediment. In: Proceedings of the 8th national conference on soil mechanics and foundation engineering, Warsaw, pp 189–194
Deepak CR, Pugazhandi M, Paul S, Shajahan MA, Janakiraman G, Atmanand MA, Annamalai K, Jeyamani R, Ravindran M, Schulte E, Panthel J, Grebe H, Schwarz W (1999) Underwater sand mining system for shallow waters. In: Proceedings of the 3rd ISOPE Ocean mining symposium, Goa, pp 78–83
Deepak CR, Shajahan MA, Atmanand MA, Annamalai K, Jeyamani R, Ravindran M, Schulte E, Handschuh R, Panthel J, Grebe H, Schwarz W (2001) Developmental test on the underwater mining system using flexible riser concept. In: Proceedings of the 4th ISOPE Ocean mining symposium, Szczecin, pp 94–98
Deepak CR, Ramji S, Ramesh NR, Babu SM, Abraham R, Shajahan MA, Atmanand MA (2007) Development and testing of underwater mining systems for long term operations using flexible riser concept. In: Proceedings of the 7th ISOPE Ocean mining symposium, Lisbon, pp 166–170
Desa E (1997) Initial results of India's environmental impact assessment of nodule mining. In: Proceedings of the international symposium on environmental studies for deep-sea mining, Metal Mining Agency of Japan, Tokyo, pp 49–63
Flipse JE (1983) Deep-Ocean mining economics. In: Proceedings of the 15th offshore technology conference, Paper No. 4491
Foda MA (1983) Breakout theory for offshore structures seated on sea-bed. In: Proceedings of the conference on geotechnical practice in offshore engineering, Austin, pp 288–299
Foell EJ, Thiel H, Schriever G (1990) DISCOL: a longterm largescale disturbance—recolonisation experiment in the Abyssal Eastern Tropical Pacific Ocean. In: Proceedings of the 22nd offshore technology conference, Paper No. 6328
Fukushima T (1995) Overview "Japan Deep-sea Impact Experiment = JET". In: Proceedings of the 1st ISOPE Ocean mining symposium, Tsukuba, pp 47–53
Gloumov I, Ozturgut E, Pilipchuk M (1997) BIE in the Pacific: concept, methodology and basic results. In: Proceedings of the international symposium on environmental studies for deep-sea mining, Metal Mining Agency of Japan, Tokyo, pp 45–47

Grebe H, Schulte E (2005) Determination of soil parameters based on the operational data of a ground operated tracked vehicle. In: Proceedings of the 6th ISOPE Ocean mining symposium, Changsha, pp 149–156

Grote PB, Burns JQ (1981) System design considerations in deep Ocean mining lift system. Mar Min 2(4):357–383

GSJ (1986) Marine geology, geophysics, and manganese nodules around deep-sea hills in the Central Pacific Basin August-October 1981(GH81-4 Cruise), Geological Survey of Japan, 257 p

Halbach P (1982) Co-rich ferromanganese seamount deposits of the Central Pacific Basin. In: Halbach P, Winter P (eds) Marine mineral deposits—new research results and economic prospects, Marine Rohstoffe und Meerestechnik, Bd 6. Verlag Gluckkauf, Essen, pp 60–85

Halbach P, Nakamura K, Wahsner M, Lange J, Kaselitz L, Hansen R-D, Yamano M, Post J, Prause B, Seifert R, Michaelis W, Teichmann F, Kinoshita M, Marten A, Ishibashi J, Czerwinski S, Blum N (1989) Probable modern analogue of Kuroko-type massive sulfide deposit in the Okinawa Trough back-arc basin. Nature 338:496–499

Halkyard JE (1985) Technology for mining cobalt rich manganese crusts from seamounts. In: Proceedings of the OCEANS'85, vol 1, pp 352–374

Han Q, Liu S (2013) A new path tracking control algorithm of deepsea tracked miner. In: Proceedings of the 10th ISOPE Ocean mining symposium, Szczecin, pp 273–278

Han Q, Liu S, Dai Y, Hu X (2011) Dynamic analysis and path tracking control of tracked underwater miner in working condition. In: Proceedings of the 9th ISOPE Ocean mining symposium, Maui, pp 92–96

Handschuh R, Grebe H, Panthel J, Schulte E, Wenzlawski B, Schwarz W, Atmanand MA, Jeyamani R, Shajahan MA, Deepak CR, Ravindran M (2001) Innovative deep-Ocean mining concept based on flexible riser and self-propelled mining machine. In: Proceedings of the 4thth ISOPE Ocean mining symposium, Szczecin, pp 99–107

Herrouin G, Lenoble J, Charles C, Mauviel F, Bernard J, Taine B (1989) A manganese nodule industrial venture would be profitable—summary of a 4-year study in France. In: Proceedings of the 21st offshore technology conference, Paper No. 5997

Hillman CT, Gosling BB (1985) Mining deep Ocean manganese nodules: description and economic analysis of a potential venture. US Bureau of Mines, IC 9015

Hiramatsu Y, Oka Y, Kiyama H (1965) Rapid determination of the tensile strength of rocks with irregular test piece. J Min Metall Inst Jpn 81(932):1024–1030 (in Japanese with English abstract)

Hong S, Choi J-S (2001) Experimental study on Grouser shape effects on trafficability of extremely soft seabed.In: Proceedings of the 4th ISOPE Ocean mining symposium, Szczecin, pp 115–118

Hong S, Kim K-H (1999) Research and development of deep seabed mining technologies for polymetallic nodules in Korea. In: Proceedings of the proposed technologies for mining deep-seabed polymetallic nodules, International Seabed Authority, pp 261–283

Hong S, Kim H-W (2005) Coupled dynamic analysis of underwater tracked vehicle and long flexible pipe. In: Proceedings of the 6th ISOPE Ocean mining symposium, Changsha, pp 132–140

Hong S, Choi J-S, Shim J-Y (1997) A kinematic and sensitivity analysis of pickup device of deep-sea manganese nodule collector. In: Proceedings of the 2nd ISOPE Ocean mining symposium, Seoul, pp 100–104

Hong S, Choi J-S, Kim J-H, Yang C-K (1999) Experimental study on hydraulic performance of hybrid pickup device of manganese nodule collector. In: Proceedings of the 3rd ISOPE Ocean mining symposium, Goa, pp 69–77

Hong S, Kim H-W, Choi J-S (2003a) A new method using Euler parameters for 3D nonlinear analysis of marine risers/pipelines. In: Proceedings of the 5th ISOPE Ocean mining symposium, Tsukuba, pp 83–90

Hong S, Choi J-S, Kim H-W (2003b) Effects of internal flow on dynamics of underwater flexible pipes. In: Proceedings of the 5th ISOPE Ocean mining symposium, Tsukuba, pp 91–98

Hong S, Choi J-S, Kim H-W, Yeu T-K, Kim J-H, Kim Y-S, Kang S-G, Rheem C-K (2011) Experimental study on vortex-induced vibration of a long flexible pipe in sheared flows. In: Proceedings of the 9th ISOPE Ocean mining symposium, Maui, pp 70–77

Hubinský P, Rodina J, Hanzel J, Rudolf B (2013) Identification of vertical deep-Ocean pipe end-point position. In: Proceedings of the 10th ISOPE Ocean mining symposium, Szczecin, pp 234–238

Iizasa K, Fiske RS, Ishizuka O, Yuasa M, Hashimoto J, Ishibashi J, Naka J, Horii Y, Fujiwara Y, Imai A, Koyama S (1999) A Kuroko-type polymetallic sulfide deposit in a submarine silicic caldera. Science 283:975–977

Inokuma A (1995) Current status of deep-sea mineral resources development in Japan. In: Proceedings of the 1st ISOPE Ocean mining symposium, Tsukuba, pp 9–13

International Seabed Authority (ISA) (2008) Polymetallic nodule mining technology—current trends and challenges ahead. In: Proceedings of the Workshop jointly organized by the International Seabead Authority and the Ministry of Earth Sciences, Government of India, National, Institute of Ocean Technology, Chennai, 18–22 Feb 2008, ISBN 978-976-8241-08-5 (pbk)

Jankowski JA, Malcherek A, Zielke W (1996) Numerical modeling of suspended sediment due to deep-sea mining. J Geophys Res 101(C2):3545–3560

Johnson CJ, Otto JM (1986) Manganese nodule project economics: factors relating to the pacific region. Resour Policy 12(1):17–28

Jung J-J, Yoo J-H, Lee T-H, Hong S, Kim H-W, Choi J-S (2005) Metamodel-based multidisciplinary design optimization of Ocean-mining vehicle system. In: Proceedings of the 6th ISOPE Ocean mining symposium, Changsha, pp 157–162

Kaufman R, Latimer JP, Tolefson DC (1985) The design and operation of a Pacific Ocean deep Ocean mining test ship: R/V Deepsea Miner II. In: Proceedings of the 17th offshore technology conference, Paper No. 4901

Khadge, NH (1999) Effects of benthic disturbance on geotechnical characteristics of sediment from nodule mining area in the Central Indian Basin. In Proceedings of 3rd ISOPE Ocean mining symposium, Goa, pp 138–144

Kim H-W, Hong S, Choi J-S (2003) Comparative study on tracked vehicle dynamics on soft soil: single-body dynamics vs. multi-body dynamics. In: Proceedings of the 5th ISOPE Ocean mining symposium, Tsukuba, pp 141–148

Kim H-W, Hong S, Choi J-S, Yeu T-K (2005) Dynamic analysis of underwater tracked vehicle on extremely soft soil by using Euler parameters. In: Proceedings of the 6th ISOPE Ocean mining symposium, Changsha, pp 132–140

Kim H-W, Hong S, Lee C-H, Choi J-S, Yeu T-K, Kim SM (2011) Dynamic analysis of an articulated tracked vehicle on undulating and inclined ground. In: Proceedings of teh 9th ISOPE Ocean mining symposium, Maui, pp 70–77

Kim H-W, Lee C-H, Hong S, Oh J-W, Min C-H, Yeu T-K, Choi J-S (2013) Dynamic analysis of a tracked vehicle based on a subsystem synthesis method. In: Proceedings of the 10th ISOPE Ocean mining symposium, Szczecin, pp 279–285

Kollwentz W (1990) Lessons learned in the development of nodule mining technology. Mater Soc 14(3/4):285–298

Kotlinski R, Tkatchenko G (1997) Preliminary results of IOM environmental research. In: Proceedings of the international symposium environmental studies for deep-sea mining, Metal Mining Agency of Japan, Tokyo, pp 35–44

Latimer JP, Kaufman R (1985) Preliminary considerations for the design of cobalt crusts mining system in the U.S. EEZ. In: Proceedings of the OCEANS‘85, vol 1, pp 378–399

Lee HJ (1976) DOSIST II—an investigation of the in-place strength behavior of marine sediments. Technical Note N-1438, Naval Civil Engineering Laboratory, Port Hueneme

Lee T-H, Lee C-S, Jung J-J, Kim H-W, Hong S, Choi J-S (2003) Prediction of the motion of tracked vehicle on soft soil using Kriging metamodel. In: Proceedings of teh 5th ISOPE Ocean mining symposium, Tsukuba, pp 144–149

Lee T-H, Lee M-U, Choi J-S, Kim H-W, Hong S (2009) Method of metamodel-based multidisciplinary design optimization for development of a test miner. In: Proceedings of the 8th ISOPE Ocean mining symposium, Chennai, pp 270–275

Lee C-H, Kim H-W, Hong S, Kim S-M (2011) A study on the driving performance of a tracked vehicle on an inclined plane according to the position of buoyancy. In: Proceedings of the 9th ISOPE Ocean mining symposium, Maui, pp 104–109

Lee C-H, Kim H-W, Hong S (2013) A study on dynamic behaviors of pilot mining robot according to extremely cohesive soft soil properties. In: Proceedings of the 10th ISOPE Ocean mining symposium, Szczecin, pp 210–214

Lenoble J-P (2000) A comparison of possible economic returns from mining deep-sea polymetallic nodules, polymetallic massive sulphides and cobalt-rich ferromanganese crusts. In: Proceedings of the workshop on mineral resources of the international seabed area, International Seabed Authority, Lenoble, pp 1–22

Li L, Zhang J (1997) The China's manganese nodules miner. In: Proceedings of the 2nd ISOPE Ocean mining symposium, Seoul, pp 95–99

Liu CL (1969) Ocean sediment holding strength against breakout of partially embedded objects. In: Proceedings of the conference on civil engineering in the Oceans II, ASCE, Miami, pp 105–116

Liu S, Wang G, Li L, Wang Z, Xu Y (2013) Virtual reality research of Ocean poly-metallic nodule mining based on COMRA's mining system. In: Proceedings of the 5th ISOPE Ocean mining symposium, Tsukuba, pp 104–111

Magnuson AH (1983) Manganese nodule abundance and size from bottom reflectivity measurements. Mar Min 4:265–296

Malahoff A (1981) Comparison between Galapagos and Gorda spreading centers. In: Proceedings of the 13th offshore technology conference, Paper No. 4129

Malnic J (2001) Terrestrial mines in the sea; Industry, research and government. In: Proceedings of the proposed technology for mining deep-seabed polymetallic nodules, International Seabed Authority, pp 315–331

Manheim FT (1986) Marine cobalt resources. Science 232:600–608

Mero JL (1965) The mineral resources of the sea. Elsevier Oceanography Series, vol 1, Amsterdam

Min C-H, Hong S, Kim H-W, Choi J-S, Yeu T-K (2013) Structural health monitoring for top-tensioned riser with response data of damaged model. In: Proceedings of the 10th ISOPE Ocean mining symposium, Szczecin, pp 239–245

Muga BJ (1967) Bottom breakout forces. In: Proceedings of the conference on civil engineering in the Oceans I, ASCE, San Francisco, pp 596–600

Muthunayagam AE, Das SK (1999) Indian polymetallic nodule program. In: Proceedings of the 3rd ISOPE Ocean mining symposium, Goa, pp 1–5

Nakata K, Kubota M, Aoki S, Taguchi K (1997) Dispersion of resuspended sediments by Ocean mining activity-modeling study. In: Proceedings of the international symposium on environmental studies for deep-sea mining, Metal Mining Agency of Japan, Tokyo, pp 169–186

Nautilus Minerals, Inc. (2007) Presentation slide in BMORoadshow, Oct 2007

Nautilus Minerals, Inc. (2015) Presentation slide of Annual General Meeting (AGM) in Toronto, on Tuesday, 16 June 2015

Ninomiya K, Tagaya K, Murase Y (1971) A study on suction breaker and scouring of a submersible offshore structure. In: Proceedings of the 3rd offshore technology conference, Paper No. 1445

Ninomiya K, Tagaya K, Murase Y (1972) A study on suction and scouring of sit-on-bottom type offshore structure. In: Proceedings of the 4th offshore technology conference, Paper No. 1605

Nishikawa N (2001) Drilling survey at the Suiyo seamount in the Izu-Ogasawara Arc, Japan. In: Proceedings of the 4th ISOPE Ocean mining symposium, Szczecin, pp 25–30

Nishimura A (1989) Seafloor sediments in Izu and Ogasawara region. In: Res. rep. of study on evaluation methods of hard mineral resources associated with submarine hydrothermal activities for F.Y. 1988, Geological Survey of Japan, pp 52–57 (in Japanese)

NRIPR (1989) Annual Research Report of R&D for manganese nodule mining system, National Research Institute of Pollution and Resources, 119 p (in Japanese)

Ohta T, Morikawa M (1997) Bending strength of lifting pipes handling of pipe connection in manganese mining system. In: Proceedings of the 2nd ISOPE Ocean mining symposium, Seoul, pp 68–74

Ozturgut E, Anderson GC, Burns RE, Lavelle JW, Swift SA (1978) Deep Ocean mining of manganese nodules in the North Pacific: pre-mining environmental conditions and anticipated mining effects. NOAA Technical Memorandum ERL MESA-33

Ozturgut E, Lavelle JW, Steffin O, Swift SA (1980) Environmental investigation during manganese nodule mining tests in the North Equatorial Pacific, in November 1978. NOAA Technical Memorandum ERL MESA-48

Ozturgut E, Trueblood DD, Lawless J (1997) An overview of the United States' benthic impact experiment. In: Proceedings of the international symposium on environmental studies for deep-sea mining, Metal Mining Agency of Japan, Tokyo, pp 23–31

Padan JW (1990) Commercial Recovery of Deep- Seabed Manganese Nodules: Twenty Years of Accomplishments. Mar Min 9:87–103

Palarski J, Plewa F, Sobota J, Strozik G (2007) Analysis of two-phase mixture flow in vertical pipeline, pump. In: Proceedings of the 7th ISOPE Ocean mining symposium, Lisbon, pp 201–204

Parenteau T (2010) Flow assurance for deepwater mining. In: Proceedings of the 29th international conference on Ocean, offshore and Arctic engineering, Shanghai, OMAE2010-20185

Park Y-C, Yoon C-H, Lee D-K, Kwon S-K (2005) Design of hydrocyclone for solid separation. In: Proceedings of the 6th ISOPE Ocean mining symposium, Changsha, pp 119–123

Park J-M, Yoon C-H, Park Y-C, Kim Y-J, Lee D-K, Kwon S-K (2007a) Three dimensional solid-liquid flow analysis for design of two-stage lifting pump. In: Proceedings of the 7th ISOPE Ocean mining symposium, Lisbon, pp 171–176

Park Y-C, Yoon C-H, Kim Y-J, Lee D-K, Park J-M, Kwon S-K (2007b) Separation of manganese nodules from solid-liquid mixture using hydrocyclone. In: Proceedings of the 7th ISOPE Ocean mining symposium, Lisbon, pp 158–161

Park J-M, Yoon C-H, Kang J-S (2009) Numerical prediction of a lifting pump for deep-sea mining. In: Proceedings of the 8th ISOPE Ocean mining symposium, Chennai, pp 229–232

Petryka L, Zych M, Hanus R, Sobota J, Vlasak P (2013) Application of the cross-correlation method to determine solid and liquid velocities during flow in a vertical pipeline. In: Proceedings of the 10th ISOPE Ocean mining symposium, Szczecin, pp 234–238

Protodyakonov MM (1960) New methods of determining mechanical properties of rocks. In: Proceedings of the international conference on strata control, Paris, Paper No. C2

Rajesh S, Gnanaraj AA, Velmurugan A, Ramesh R, Muthuvel P, Babu MK, Ramesh NR, Deepak CR, Atmanand MA (2011) Qualification tests on underwater mining system with manganese nodule collection and crushing devices. In: Proceedings of the 9th ISOPE Ocean mining symposium, Maui, pp 110–115

Ramesh NR, Thirumurugan K, Rajesh S, Deepak CR, Atmanand MA (2013) Experimental and computational investigation of turbulent pulsatile flow through a flexible hose. In: Proceedings of the 10th ISOPE Ocean mining symposium, Szczecin, pp 246–252

Richards AF, Chaney RC (1981) Present and future geotechnical research needs in deep Ocean mining. Mar Min 2(4):315–337

Roderick GL, Lubbard A (1975) Effect of object in situ time on bottom breakout. In: Proceedings of the 7th offshore technology conference, Paper No. 2184

Rogers AC, Abramson HN (1981) Flow-induced excitation of long pipe strings for deep Ocean mining applications. Mar Min 2(4):347–355

Rona PA, Scott SD (1993) A special issue on sea-floor hydrothermal mineralization: new perspectives. Econ Geol 88:1935–1975

Schriever G, Ahnert A, Borowski C, Thiel H (1997) Results of the large scale deep-sea impact study DISCOL during eight years of Investigation. In: Proceedings of the international symposium on environmental studies for deep-sea mining, Metal Mining Agency of Japan, Tokyo, pp 197–208

Schulte E, Schwarz W (2009) Simulation of tracked vehicle performance on deep sea soil based on soil mechanical laboratory measurements in Bentonite soil. In: Proceedings of the 8th ISOPE Ocean mining symposium, Chennai, pp 276–284

Schulte E, Grebe H, Handschuh R, Panthel J, Wenzlawski B, Schwarz W, Atmanand MA, Deepak CR, Jeyamani R, Shajahan MA, Ravindran M (2001) Instrumentation and control system of a sand mining system for shallow water. In: Proceedings of the 4th ISOPE Ocean mining symposium, Szczecin, pp 108–114

Schulte E, Handschuh R, Schwarz W (2003) Transferability of soil mechanical parameters to traction potential calculation of a tracked vehicle. In: Proceedings of the 5th ISOPE Ocean mining symposium, Tsukuba, pp 123–131

Schwarz W (2001) An advanced nodule mining system. In: Proceedings of the proposed technologies for mining deep-seabed polymetallic nodules, International Seabed Authority, pp 39–54

Sharma R, Nath BN (1997) Benthic disturbance and monitoring experiment in Central Indian Ocean Basin. In: Proceedings of the 2nd ISOPE-Ocean mining symposium, Seoul, pp 146–153

Sharma R, Parthiban G, Sivakholundu KM, Valsangkar AB, Sardar A (1997) Performance of benthic disturber in Central Indian Ocean, National Institute of Oceanography, Goa, Tech. Report NIO/TR-4/97, 22

Shaw JL (1993) Nodule mining—three miles deep! Mar Georesour Geotechnol 11:181–197

Shimizu Y, Tojo C, Suzuki M, Takagaki Y, Saito T (1992) A study on the air-lift pumping system for manganese nodule mining. In: Proceedings of the 2nd international offshore and polar engineering conference, vol 1, pp 490–497

Smith G (2010) Deepwater seafloor resource production—development of the World's next offshore frontier. In: Proceedings of the 29th international conference on Ocean, offshore and Arctic engineering, Paper No OMAE2010-20350

Sobota J, Boczarski S, Petryka L, Zych M (2005) Measurement of velocity and concentration of nodules in vertical hydrotransport. In: Proceedings of the 6th ISOPE Ocean mining symposium, Changsha, pp 251–256

Sobota J, Palarski J, Plewa F, Strozik G (2007a) Movement of solid particles in vertical pipe. In: Proceedings of the 7th ISOPE Ocean mining symposium, Lisbon, pp 197–200

Sobota J, Vlasak P, Strozik G, Plewa F (2007b) Vertical distribution of concentration in horizontal pipeline - density and particle size influence. In: Proceedings of the 8th ISOPE Ocean mining symposium, Chennai, pp 220–224

Sobota J, Vlasak P, Petryka L, Zych M (2013) Slip velocities in mixture vertical pipe flow. In: Proceedings of the 10th ISOPE Ocean mining symposium, Szczecin, pp 221–224

Stanton P, Yu A (2010) Interim use of API codes for the design of dynamic riser systems for the deepsea mining industry. In: Proceedings of the 29th international conference on Ocean, offshore and Arctic engineering, Paper No OMAE2010-20189

Sundkvist KE (1983) Size distribution of manganese nodules. Mar Min 4:305–316

Thiel H, Forschungsverbund Tiefsee-Umweltsschutz (1995) The German environmental impact research for manganese nodule mining in the SE Pacific Ocean. In: Proceedings of the 1st ISOPE Ocean mining symposium, Tsukuba, pp 39–45

Thiel H, Angel MV, Foel EJ, Rice AL, Schriever G (1998) Marine science and technology—environmental risks from large-scale ecological research: a desk study. Contract No. MAS2-CT94-0086, Office for Official Publications of European Communities

Tkatchenko G, Radziejewska T, Stoyanova V, Modlitba I, Parizek A (1996) Benthic impact experiment in the IOM Pioneer Area : testing for effects of deep-sea disturbance. In: Proceedings of the international seminar on deep sea-bed mining technology, China Ocean Mineral Resources R&D Assc., Beijing, pp C55–C68

Toyohara T et al (2011) Environmental researches within Japan's approach for Seafloor Massive Sulfide (SMS) mining. In: Proceedings of the 30th international conference on Ocean, offshore and Arctic engineering, Paper No. OMAE2011-49906

Trueblood DD (1993) US cruise report for BIE – II cruise, NOAA Technical Report. Mem. OCRS 4, National Oceanic and Atmospheric Administration, 51 p

Trueblood DD, Ozturgut E, Pilipchuk M, Gloumov IF (1997) The ecological impacts of the Joint U.S.-Russian Benthic Impact Experiment. In: Proceedings of the 2nd ISOPE Ocean mining symposium, Seoul, pp 139–145

Tsurusaki K, Itoh F, Yamazaki T (1984) Development of in-situ measuring apparatus of geotechnical elements of sea floor. In: Proceedings of the 16th offshore technology conference, Paper No. 4681

Usui A (1986) Local variability of manganese nodule deposits around the small hills in the GH81-4 area. Marine geology, geophysics, and manganese nodules around deep-sea hills in the Central Pacific basin August-October 1981(GH81-4 Cruise), Geological Survey of Japan, pp 98–159

Usui A, Someya M (1997) Distribution and composition of marine hydrogenetic and hydrothermal manganese deposits in the Northwest Pacific. In: Nicholson K, Hein JR, Buhn B, Dasgupta S (eds) Manganese mineralization: geochemistry and mineralogy of terrestrial and marine deposits. Geol. Soc. London Spec. Publ., London, pp 177–198

Vesic AS (1971) Breakout resistance of objects embedded in Ocean bottom. J Soil Mech Found Div Am Soc Civ Eng 97(SM9):1183–1203

Vlasak P, Chara Z (2007) Effect of particle size and concentration on flow behavior of complex slurries. In: Proceedings of the 7th ISOPE Ocean mining symposium, Lisbon, pp 181–187

Vlasak P, Chara Z, Kysela B, Sobota J (2011) Flow behavior of coarse-grained slurries in pipes. In: Proceedings of the 9th ISOPE Ocean mining symposium, Maui, pp 158–164

Wang Z, Liu S, Li L, Yuan B, Wang G (2003) Dynamic simulation of COMRA's self-propelled vehicle for deep Ocean mining system. In: Proceedings of the 5th ISOPE Ocean mining symposium, Tsukuba, pp 112–118

Wang S-P, Gui W-H, Ning X-L (2009) Research on the path planning for deep-seabed mining vehicle. In: Proceedings of the 8th ISOPE Ocean mining symposium, Chennai, pp 295–298

Wang Z, Rao Q, Liu S (2011) Dynamic analysis of seabed-mining machine-flexible hose coupling in deep sea mining. In: Proceedings of the 9th ISOPE Ocean mining symposium, Maui, pp 143–148

Welling CG (1981) An advanced design deep sea mining system. In: Proceedings of the 13th Offshore technology conference, Paper No. 4094

Welling CG (1982) R.C.V. Air-lift mining: text from the Film "Harvesting the Bounty of Ocean". In: Humphrey PB (ed) Marine mining: a new beginning. Hawaii Department of Planning and Economic Development, pp 82–92

Won M-C, Cha H-S, Shin S-C (2005) Development of an extended Kalman filter algorithm for the localization of underwater mining vehicles. In: Proceedings of the 6th ISOPE Ocean mining symposium, Changsha, pp 175–180

Xia J, Xie L, Zou W, Tang D, Huang J, Wang S (1997) Studies on reasonable hydraulic lifting parameters of manganese nodules. In: Proceedings of the 2nd ISOPE Ocean mining symposium, Seoul, pp 112–116

Yamada H, Yamazaki T (1998) Japan's Ocean test of the nodule mining system. In: Proceedings of the 8th international offshore and polar engineering conference, pp 3–19

Yamaguchi U, Nishimatsu Y (1991) Introduction of Rock mechanics. University of Tokyo Press, 331 p (in Japanese)

Yamazaki T (1993) A re-evaluation of cobalt-rich crust abundance on the Pacific seamounts. Int J Offshore Polar Eng 3:258–263

Yamazaki T, Kajitani Y (1999) Deep-sea environment and impact experiment to it. In: Proceedings of the 9th international offshore and polar engineering conference, pp 374–381

Yamazaki T, Park S-H (2003) Relationship between geotechnical engineering properties and assay of seafloor massive sulfides. In: Proceedings of the 13th international offshore and polar engineering conference, pp 310–316

Yamazaki T, Sharma R (2001a) Preliminary experiment on powderization of deep-sea sediment during hydraulic transportation. In: Proceedings of the 4th ISOPE Ocean mining symposium, Szczecin, pp 44–49

Yamazaki T, Sharma R (2001b) Estimation of sediment properties during benthic impact experiments. Mar Georesour Geotechnol 19(4):269–289

Yamazaki T, Tomishima Y, Handa K, Tsurusaki K (1989) Experimental study of adhesion appearing between plate and clay. In: Proceedings of the 8th international conference on offshore mechanics and Arctic engineering, vol 1, pp 573–579

Yamazaki T, Tomishima Y, Handa K, Tsurusaki K (1990) Engineering properties of deep-sea mineral resources. In: Proceedings of the 4th Pacific congress on marine science and technology, pp 385–392

Yamazaki T, Tsurusaki K, Handa K (1991) Discharge from manganese nodule mining system. In: Proceedings of the 1st international offshore and polar engineering conference, pp 440–446
Yamazaki T, Igarashi Y, Maeda K (1993) Buried cobalt rich manganese deposits on seamounts. Resource Geology Special Issue, Tokyo, No. 17, pp 76–82
Yamazaki T, Tsurusaki K, Handa K, Inagaki T (1995a) Geotechnical properties of deep Ocean sediment layer. J Min Mater Process Inst Jpn 111:309–315 (in Japanese with English abstract)
Yamazaki T, Chung JS, Tsurusaki K (1995b) Geotechnical parameters and distribution characteristics of the cobalt-rich manganese crust for the miner design. Int J Offshore Polar Eng 5(1):75–79
Yamazaki T, Tsurusaki K, Inagaki T (1995c) Determination of dynamic geotechnical properties of very fine and weak clayey soils by using a collision test. J Jpn Geotech Soc 47(12):23–27 (in Japanese)
Yamazaki T, Tsurusaki K, Chung JS (1996) A gravity coring technique as applied to cobalt-rich manganese deposits in the Pacific Ocean. Mar Georesour Geotechnol 14:315–334
Yamazaki T, Kuboki E, Yoshida H (1999) Tracing collector passes and preliminary analysis of collector operation. In: Proceedings of the 3rd ISOPE Ocean mining symposium, Goa, pp 55–62
Yamazaki T, Kuboki E, Yoshida H, Suzuki T (2000) A consideration on size distribution of resuspended deep-sea sediments. In: Proceedings of the 10th international offshore and polar engineering conference, vol 1, pp 507–514
Yamazaki T, Kuboki E, Matsui T (2001) DIETS: a new benthic impact experiment on a seamount. In: Proceedings of the 4th ISOPE Ocean mining symposium, pp 69–76
Yamazaki T, Komine T, Kawakami T (2005) Geotechnical properties of deep-sea sediments and the in-situ measurement techniques. In: Proceedings of the 6th ISOPE Ocean mining symposium, Changsha, pp 48–55
Yang N, Wang M (1997) New era for China manganese nodules mining: summary of last five years' research activities and prospective. In: Proceedings of the 2nd ISOPE Ocean mining symposium, Seoul, pp 8–11
Yasukawa H, Ikegami K, Minami T (1995) Simulation study on motions of a towed collector for a manganese nodule mining system. In: Proceedings of the 1st ISOPE Ocean mining symposium, Tsukuba, pp 61–68
Yasukawa H, Ikegami K, Minami T (1999) Motion analysis of a towed collector for manganese nodule mining in Ocean test. In: Proceedings of the 9th international offshore and polar engineering conference, vol 1, pp 100–107
Yeu T-K, Hong S, Kim H-W, Choi J-S (2005) Path tracking control of tracked vehicle on soft cohesive soil. In: Proceedings of the 6th ISOPE Ocean mining symposium, Changsha, pp 168–174
Yeu T-K, Yoon S-M, Hong S, Kim J-H, Kim H-W, Choi J-S, Min C-H (2013) Operating system of KIOST pilot mining robot in inshore test. In: Proceedings of the 10th ISOPE Ocean mining symposium, Szczecin, pp 265–268
Yoon C-H, Kwon K-S, Kwon O-K, Kwon S-K, Kim I-K, Lee D-K, Lee H-S (2000) An experimental study on lab scale air-lift pump flowing solid-liquid-air three-phase mixture. In: Proceedings of the 10th international offshore and polar engineering conference, vol 1, pp 515–521
Yoon C-H, Kwon K-S, Kwon S-K, Lee D-K, Park Y-C, Kwon O-K (2001) An experimental study on the flow characteristics of solid-liquid two-phase mixture in a flexible hose. In: Proceedings of the 4th ISOPE Ocean mining symposium, Szczecin, pp 122–126
Yoon C-H, Park Y-C, Lee D-K, Kwon K-S, Kwon S-K, Sung W-M (2003) Behavior of deep sea mining pipe and its effect on internal flow. In: Proceedings of the 5th ISOPE Ocean mining symposium, Tsukuba, pp 76–82
Yoon C-H, Park Y-C, Lee D-K, Kwon S-K, Lee J-N (2005) Flow analysis of solid-liquid mixture in a lifting pump. In: Proceedings of the 6th ISOPE Ocean mining symposium, Changsha, pp 101–105
Yoon S-M, Yeu T-K, Hong S, Kim H-W, Choi J-S, Min C-H, Kim S-B (2013) Study on geometric path tracking algorithm for tracked vehicle model. In: Proceedings of the 10th ISOPE Ocean mining symposium, Szczecin, pp 265–268
Zheng H, Hu Q, Yang N, Chen Y, Yang B (2013) Suspension principle of deep-sea miner and drag tests. In: Proceedings of the 10th ISOPE Ocean mining symposium, Szczecin, pp 286–290

Tetsuo Yamazaki holds degrees in Bachelor of Engineering (1976), Master of Engineering (1978), and Doctor of Engineering (1981) from Hokkaido University. He has been working as a Researcher at the National Institute for Resources and Environment since 1981 and as a Senior Researcher at National Institute for Advanced Industrial Science and Technology since 2001, following which he has been a Professor at Osaka Prefecture University since 2008. His research areas include geotechnical properties of deep-sea mineral resources, deep-sea mining technologies, environmental impacts monitoring and assessment techniques, and economic evaluation of deep-sea mining.

Chapter 10
Concepts of Deep-Sea Mining Technologies

M.A. Atmanand and G.A. Ramadass

Abstract The contents of this chapter are from published literature by the team working in the area of deep-sea mining at National Institute of Ocean Technology (NIOT). It starts with a brief introduction on deep-sea mining technologies. This is followed by the historical perspectives and the present-day work and execution in phases towards deep-sea mining in India. Some of the subsystems and infrastructure for deep-sea-related activities are described which is followed by operation of laying and pickup of artificial nodules at a depth of 500-m water depth. In situ soil tester designed, developed, and tested is described and the future work on the deep-sea mining system for 6000 m is finally explained. Many of these works have been reported in conferences and journals and are cited as references in the end of the chapter.

10.1 Introduction

The world oceans cover about 2/3 of the earth's surface, extending over 360 million square kilometers. They dominate the surface of our planet. Even today their features and potential are not fully explored and are poorly understood. Though today we have a good understanding of the extent and surface behavior of the oceans of the world and their connections, we still know very little of what lies under the waters. Man knows more about the surface of the moon that is far away than the seabed which is close to us. While the coastal areas have been explored and utilized, the exploration into deep seas started much later. The first scientific voyages were taken up during 1831–1836 by the H.M.S. Beagle which also carried Charles Darwin.

Deep-sea exploration is a challenging frontier area of ocean engineering for several reasons.

- The marine environment is at its hostile best.
- The duration of operation is large (several years).
- The location is at a great distance from shore.
- Long-term climate forecast is unreliable and difficult.

M.A. Atmanand (✉) • G.A. Ramadass
National Institute of Ocean Technology, Velachery-Tambaram Road,
Pallikaranai, Chennai 600 100, India
e-mail: atma@niot.res.in

R. Sharma (ed.), *Deep-Sea Mining*, DOI 10.1007/978-3-319-52557-0_10

- Operational depth is too large to fall back on previous experience.
- High pressure environment, in which the survival of components of any engineering system is difficult.

Added to this are the questions of redundancy and reliability of the system and its components to withstand long service hours (approximately 3000 h) between intervals of maintenance. Each one of these aspects poses engineering challenges in design, construction, maintenance, and economics of deep-sea system.

Ever since the voyage of HMS Challenger during the period 1873–1876 in the Atlantic Ocean, when for the first time, the "dark brown rock-like nodules" containing iron and manganese littering large areas of the deepest part of the ocean floor were discovered, mankind has come a long way to make the economic exploitation of these nodules a distinct possibility in the early half of the twenty-first century. These nodules remained largely a scientific curiosity for more than 80 years, and from then onwards rapidly became the object of vigorous scientific research owing to tremendous technological development in the latter half of the twentieth century in conducting oceanographic research in deep sea. Owing to steady development of technology and occasional breakthroughs, the deep seabed exploration has conclusively established the polymetallic nodules as a significant mineral resource for manganese, copper, cobalt, and nickel in the near future, given the depletion of land-based resources. In the meantime, the first ever pilot mining tests in 1978 (by OMI of USA, Japan, Canada, and Germany in the Pacific Ocean, recovering 800 tons of nodules from 5500-m water depth, and subsequent tests by OMA and OMCO in 1978) have conclusively established that the exploitation of this resource is technically feasible, though it will require further significant progress in technology (Halkyard 1985).

Manganese nodules are cm- to dm-size potato-shaped lumps of manganese and iron oxides that litter much of the ocean's sedimented abyssal plains at about 5500-m water depth (Figs. 10.1 and 10.2). These are found in abundant quantities covering large of the seafloor, such as the Clarion-Clipperton Zone of the central-eastern Pacific in international waters southeast of Hawaii and in the Central Indian Ocean, and are considered to be potentially economic. These areas are under the jurisdiction of the United Nations Law of the Sea, which came into effect in November 1994, and are administered by the International Seabed Authority based in Kingston, Jamaica. The better deposits, perhaps representing 10% of the total area of nodule accumulation, average about 2.4% of Cu + Ni + Co, a grade similar to that of terrestrial sulfide Ni-Cu ores such as at Sudbury, Ontario (Exon et al. 1992). Seafloor nodules as a copper resource are about 10% of known land reserves. Manganese, an essential element in steel making that also has other industrial uses, constitutes 20–25% of the higher grade nodules and may someday itself become economic to recover as land mines wane.

The concentrations and grades of the nodules tend to be highest well away from land, where dilution from sediment settling in the water column is lowest, and where biological productivity is high. The latter is important because the metals are delivered to the seafloor primarily by degradation of calcareous microorganisms that are falling through the water column.

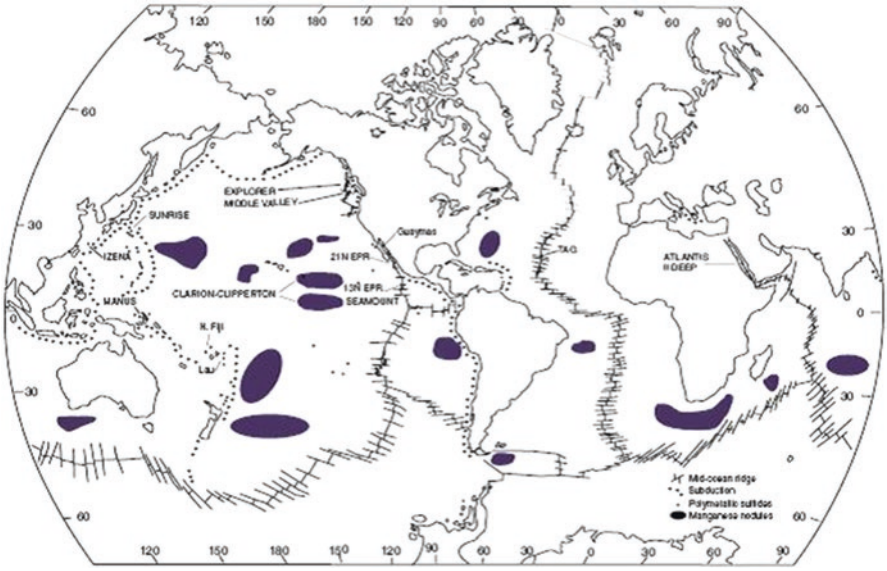

Fig. 10.1 Manganese nodule fields and seafloor massive sulfides (Scott 2001)

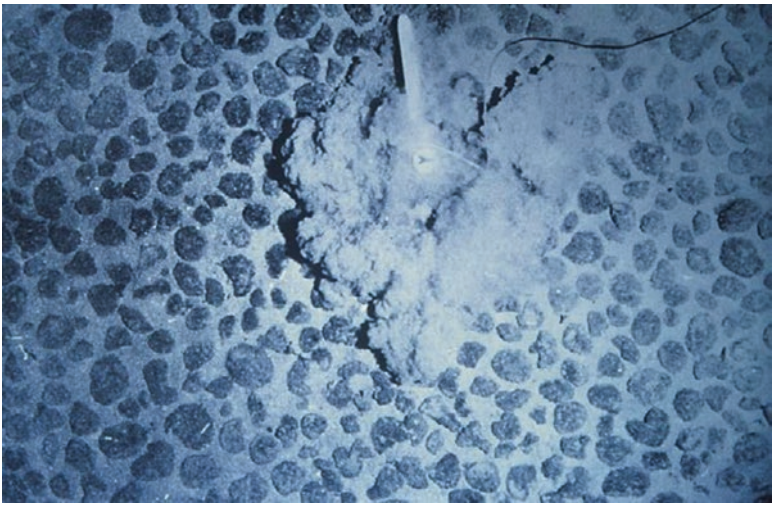

Fig. 10.2 Manganese nodules on the Pacific Ocean floor. Note the sediment cloud produced by contact of the photograph trigger (15 cm outer diameter) with the seafloor. Photograph courtesy of United States Geological Survey

10.2 Historical Perspective

India has been allotted a mining site in the Central Indian Ocean Basin (CIOB) by the International Seabed Authority and is keen on developing technologies to mine manganese nodules. Deep-sea mining of manganese nodules from soft ocean floor at 5000–6000-m depth is a major technological challenge. India, with its strong science and technology base, is carrying out the exploration and exploitation of polymetallic nodules under the Polymetallic Nodule (PMN) program of the Ministry of Earth Sciences (MoES), Government of India. This is one of the major R & D efforts of the MoES towards the development and use of ocean science and technology for exploration of marine nonliving resources for the socioeconomic benefit of the society. This multidisciplinary program is executed by multi-institutional participation. On 26th January 1981, the Indian Oceanographic Research Vessel "Gaveshani" collected the first sample of polymetallic nodules from the Indian Ocean. Continued efforts by India led to the identification of a prospective site with polymetallic nodules in the Indian Ocean and recognition of India as a Pioneer Investor in 1982. Subsequently, India became the first Registered Pioneer Investor in August 1987 along with Japan, France, and the Soviet Union (now Russia) to be allotted large areas with exclusive rights for exploration of polymetallic nodules. Today, India is the only country with a site allocated for polymetallic nodules in the Indian Ocean, while all other sites are located in the Pacific Ocean. The Indian mining site is shown in Fig. 10.3. Under the PMN program of MoES, survey and exploration, mining technology, extractive metallurgy, and environmental impact analysis are the four areas where the Indian efforts are directed.

India has no known resources of cobalt and nickel. The resources of copper in land are also depleting. The dependence on imports for these metals has been increasing yearly at a substantial rate. Polymetallic nodules in the Central Indian Ocean Basin (CIOB) offer the closest possible solution to meet this demand and reduce dependency on imports. The resources available in 1,50,000 sq. km of Pioneer area are 759 MMT of wet and 607 MMT of dry polymetallic nodules, from which 0.85 MMT of cobalt, 7.00 MMT of nickel, and 6.5 MMT of copper can be extracted. The proposed mining for economic viability is 2–3 MMT of nodules per annum, implying that mining can be carried out for several hundred years.

Considering the present consumption rate of copper, nickel, and cobalt in India, the deep-sea resources will satisfy a major portion of the Indian consumption requirement in future. The content of manganese in these nodules is not attractive. However, in the process of extraction of copper, cobalt, and nickel, it has been found that ferromanganese can also be extracted to a large extent. Extraction of all these four metals will enhance the metal value of the nodules. The value of the resources available in the Indian Pioneer area after relinquishment based on average market prices in the last 2 years will approximately be Rs. 12 trillion (approximately USD 170 billion).

India is the only country with the mine site allocated for polymetallic nodules in the Indian Ocean while all others are in Pacific Ocean. Under this program, survey and exploration, mining technology, extractive metallurgy, and environmental

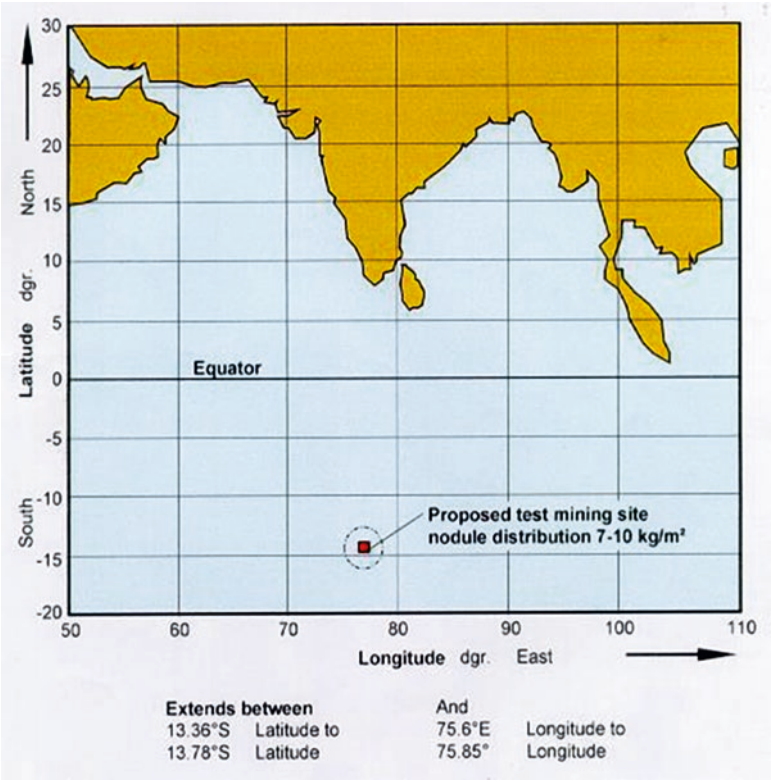

Fig. 10.3 Indian mining site

impact analysis are the four areas where the Indian efforts are directed. During the last 20 years, systematic grid sampling and surveys were taken up in a phased manner with definite objectives by the National Institute of Oceanography (NIO), Goa. The surveys were carried out onboard the Indian Research Vessels Gaveshani and SagarKanya, supported by Charter Vessels Skandi Surveyor, Farnella, G A Reay, Nand Rachit, Sidorenko, and Boris Petrov. Area of over 4 million sq. km. was explored and more than 10,000 locations were sampled for nodules using sampling devices such as freefall grabs, corers, multi-beam bathymetric surveys, and deep-tow photographic surveys. The vast data thus acquired provided insights on the topography of the basin and the resource potential. Environmental impact assessments were also carried out at many locations and recolonization studies done. India has already relinquished 50% of its allocated area as per the stipulations of Resolutions II of UNCLOS III and identified a first generation mining site for carrying out technological development for deep-sea mining.

Deep-sea mining of polymetallic nodules from the soft ocean floor at a depth of 5000–6000 m is a major technological challenge. India has been working on developing this complex technology in a phase-wise manner. To minimize development costs and

associated risks, initial efforts are focused on realization and qualification of machinery for long-term operations in shallow waters, followed by further development of machinery for deep waters. An initial study was done on the various deep-sea mining concepts and the flexible riser concept (Grebe 1997) was chosen for development. An underwater mining system was developed and the flexible riser concept was validated in the Indian seas at 410-m water depth in 2000 (Deepak et al. 2001a, b) jointly by National Institute of Ocean Technology (NIOT) and Institut für Konstruktion (IKS) of University of Siegen, Germany. The tests gave confidence for carrying out further studies that led to enhancements in the mining system and the mother vessel, which were cost effective. The modified system was tested for long-term operations at 451-m depth off Goa coast during March 2006.

10.3 Present-Day Technology

Deep-sea mining of manganese nodules from soft ocean floor at 5000–6000-m depth is a major technological challenge. Most of the existing deep-sea mining concepts are based on the tests carried out by various consortia in the late twentieth century (Brink and Chung 1981; Chung et al. 1980; Chung and Tsurusaki 1994). The systems had either a self-propelled nodule collector (Chung and Tsurusaki 1994) or a towed collector (Heine and Suh 1978; Chung and Olagnon 1996) which collects and pumps nodules from the ocean floor to the lifting system, either directly or through an intermediate storage buffer unit. The lifting system has been either hydraulic or airlift. Hydraulic lift systems had multistage centrifugal pumps installed at three different depths (Kuntz 1979; Chung 1996; Deepak et al. 2001a, b). In the case of airlift systems, compressed air was injected at intermediate depths and the solids were lifted up as a three-phase mixture. An underwater mining system was developed for operations and the flexible riser concept was validated in the Indian seas at 410-m water depth in 2000 jointly by National Institute of Ocean Technology (NIOT) and Institut für Konstruktion (IKS) of University of Siegen, Germany (Atmanand et al. 2000).

The flexible riser system is one of the novel deep-sea mining systems being developed after the Law of the Sea treaty (UNCLOS-III) became effective as of 1994. A crawler-based underwater mining machine collects the nodules as it moves along the ocean floor and is self-propelled and remotely controlled. The presence of multiple mining machines (Fig. 10.4), a flexible riser system instead of a rigid riser system, and a single positive displacement pump instead of multiple centrifugal pumps are the main differences of this system when compared to pipe lift systems. The complete system has been discussed in detail in Handschuh et al. (2001).

The flexible riser system was proposed to be realized in four phases:

- First phase of validation of the flexible riser concept at 400–500-m water depth for underwater mining operations (Deepak et al. 2007).
- Second phase of evaluation of the performance of the system developed in the first phase for long-term operations by equipping the mother vessel with a dynamic positioning system.

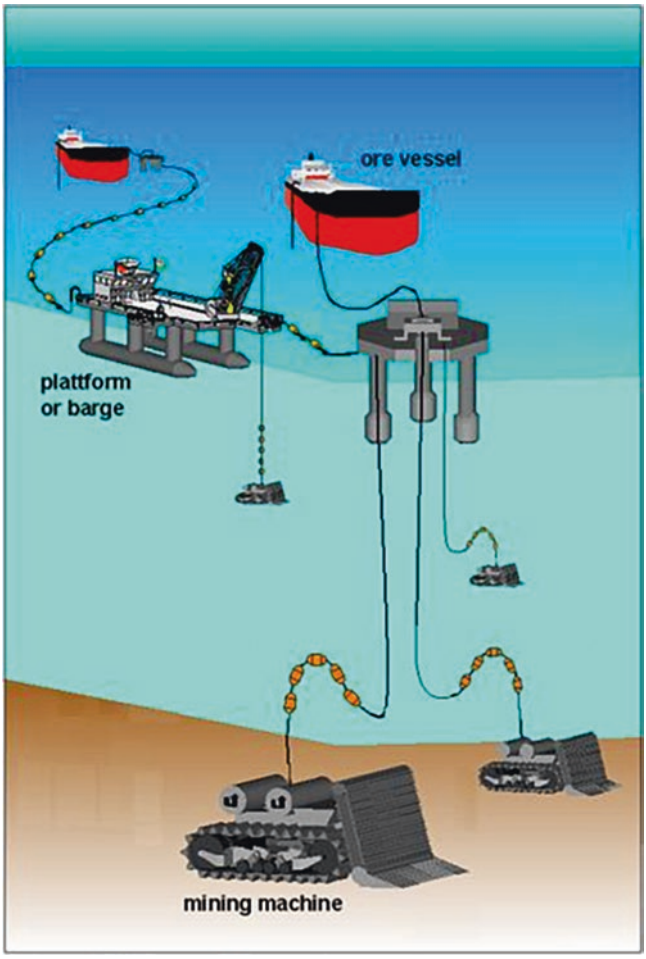

Fig. 10.4 Integrated mining system using flexible riser concept

- Third phase of realization of nodule collection and crusher systems and their addition to the underwater mining machine developed in the second phase.
- Fourth phase of validation of the flexible riser concept for manganese nodule mining operations in the Central Indian Ocean Basin using one underwater mining system.

Further development of this complex deep-sea mining technology was planned with multi-institutional and multinational participation to derive the maximum benefit of the existing technologies, resources, and potential within and outside India. For this purpose, India had a joint developmental program on deep-sea nodule mining technology with the participation of NIOT, Chennai, the technical arm of the then Department of Ocean Development, now the Ministry of Earth Sciences

Enhanced Underwater Mining System for 500 m depth

Underwater Mining System with manipulator and cutter for 500 m depth

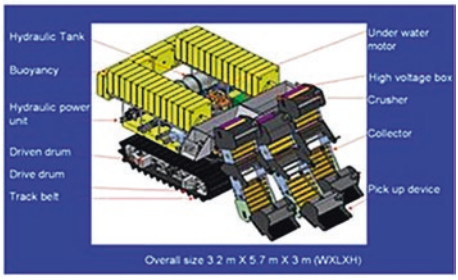

Underwater Mining System with Collector and Crusher for 500 m depth (2008-2009)

Fig. 10.5 Underwater mining system developed by NIOT for 500-m depth

(MoES), and the Institute for Design Engineering and Materials Handling (IKS) of University of Siegen, Germany. IKS was involved for over 18 years in the development of technology and testing of modern equipment for underwater mining at a depth of 6000 m. IKS has also developed a crawler for operating at 500-m water depth. All but the last phase has been completed by NIOT.

Demonstration of deep-sea mining using flexible riser concept was taken up at a depth of 500 m in the first phase. For this purpose, the crawler developed by IKS was augmented by the joint NIOT–IKS team, with a sand mining system, manipulator, pumping system, and other accessories for demonstrating the shallow bed mining technology in Indian seas (Fig. 10.5). The basic crawler was designed for operations up to 6000-m water depth. The involute profile of the rubber track belts compacts the seabed and minimizes the disturbance to the sediments when the

crawler moves along the seabed. After two preliminary tests in 60-m and 120-m water depth (during October '98 and April '99), the final test was carried out during the months of March and September 2000, successfully demonstrating the Integrated Mining System (IMS) by mining sand. In order to overcome the difficulties faced during the trials, the department's research vessel ORV SagarKanya was equipped with a Dynamic Position System (DPS) and a Launching and Retrieval System (LARS). Also, the crawler was enhanced with buoyancy and other systems for better operability on seabed and for pumping sand slurry. The enhanced system was tested at a depth of 451 m with locomotion and pumping, and later on at 515 m with pumping alone. These trials instilled confidence for taking up this technology further with the nodule mining system.

In the third phase, development and qualification of collector and crusher system in shallow waters, mining of artificially laid nodules has been undertaken by maximum utilization of the systems developed under Phase I activities.

Realization of IMS for mining nodules from 6000-m water depth calls for development and qualification of newly developed and critical components, which were not part of sand mining system, namely the collector and crusher. To minimize the technical uncertainties, it is always advisable that such new systems are developed, tested, and qualified for 6000-m applications before going in for cost intensive commercial scale investments. Hence, to achieve the final goal of developing technology for mining nodules from 6000 m, the developmental activities are proposed in phases.

10.3.1 Technical Specification of Underwater Mining System

Underwater mining machine		Hose–cable joints	At 6 m intervals
Overall length	3400 mm	Hose winch	500 kg (SWL)
Overall width	3450 mm	Hose speed	0.5 m/s (max.)
Weight in air	13 tons	*Power supply, control and instrumentation system*	
Weight in water	7.2 tons		
Depth of operation	500 m	Cable	Electromechanical multiconductor
Operational speed	0.5 m/s		
Max speed	0.75 m/s	Breaking strength	400 kN
Max slope	8.5°	Power	120 kW at 3000 V
Slurry discharge	Upto 45 m^3/h	Signal transmission	Two optical lines TCP/IP
Concentration	30% (max.)	Data acquisition	PXI-based system
Mining output	12 tons/h (max.)	Transducers	Velocity, heading, pitch, roll vision
Particle size (max.)	8 mm	Winch for cable	1.6 m dia. × 1.4 m length
Flexible riser system		Cable spool speed	0.5 m/s
Hose size	75 mm		
Hose spool length	100 m		

10.4 Studies Involved in Shallow Water Testing of Underwater Mining System

Many subsystem studies were taken up during the course of development. Some of them are:

- Developmental studies on hydraulic devices for deep sea in hyperbaric chamber
- Developmental studies on Acoustic Positioning and Imaging Systems
- Investigations on interaction of the seabed with nodule collector
- Developmental studies on underwater crushing systems
- Flexible riser system
- Development of testing facilities like Hyperbaric Chamber, Test Pond, Winch Testing Facility, and indigenous deep-sea devices

10.4.1 Developmental Studies on Hydraulic Devices for Deep Sea in Hyperbaric Chamber

Hydraulic systems comprising hydraulic power packs, hydraulic motors, control valves like directional control valves, servo valves, proportional control valves and other devices like pressure compensators and relief valves used in underwater mining machines are generally land-based systems modified for deep-sea mining applications. These systems have to be qualified in hyperbaric chambers before they can be used for deep-sea mining. Circuits simulating loads that occur in deep-sea mining have been designed and the systems realized and tested in the hyperbaric chamber. A hyperbaric test session in progress for underwater Hydraulic Power Unit (HPU), axial piston motor, and proportional control valve for underwater crawler is shown in Fig. 10.6.

10.4.2 Developmental Studies on Acoustic Positioning Systems

Accurate positioning of the underwater mining system is essential for effective mining to be carried out. Underwater acoustic positioning systems with a deep sea transducer and transponders in long baseline modes are viewed to be the most accurate systems for positioning. However, their performance in deep waters is yet to be proved. Developmental studies on positioning systems have been undertaken with subsea acoustic companies and a System 408S of Kongsberg has been realized and initial shallow water tests have been carried out (Fig. 10.7).

A hydro acoustic positioning system consists of both a transmitter (transducer) and a receiver (transponder). A signal (pulse) is sent from the transducer which is mounted on the crawler, and is aimed towards the seabed transponders.

Fig. 10.6 Testing of underwater hydraulic systems in hyperbaric chamber

This pulse activates the transponders which are placed on the seabed and it responds immediately to the transducer. The transducer with its corresponding electronics calculates an accurate position of the transponder relative to the vessel. The realized system operates under Medium Frequency (MF) mode of 21,000–32,500 Hz and Low Frequency (LF) mode of 9500–15,750 Hz. The transducer beam width is ±30°.

10.4.3 Underwater Nodule Imaging System

As underwater cameras are usually unsuccessful in visualizing the bottom-lying polymetallic nodules owing to turbidity generated by the crawler during operations, it is necessary to find an alternative solution to visualize the nodules by using video quality bottom-looking SONAR. Since SONARS which can distinguish the nodules from sediments are not readily available, it was developed initially for shallow waters by interactions with manufacturers. An experiment was performed at a test pond of NIOT using a high frequency SONAR (DIDSON make SONAR). The images of nodules obtained during the tests are shown in Fig. 10.8, which were acceptable. In the next phase, the system will be modified for deep-sea applications.

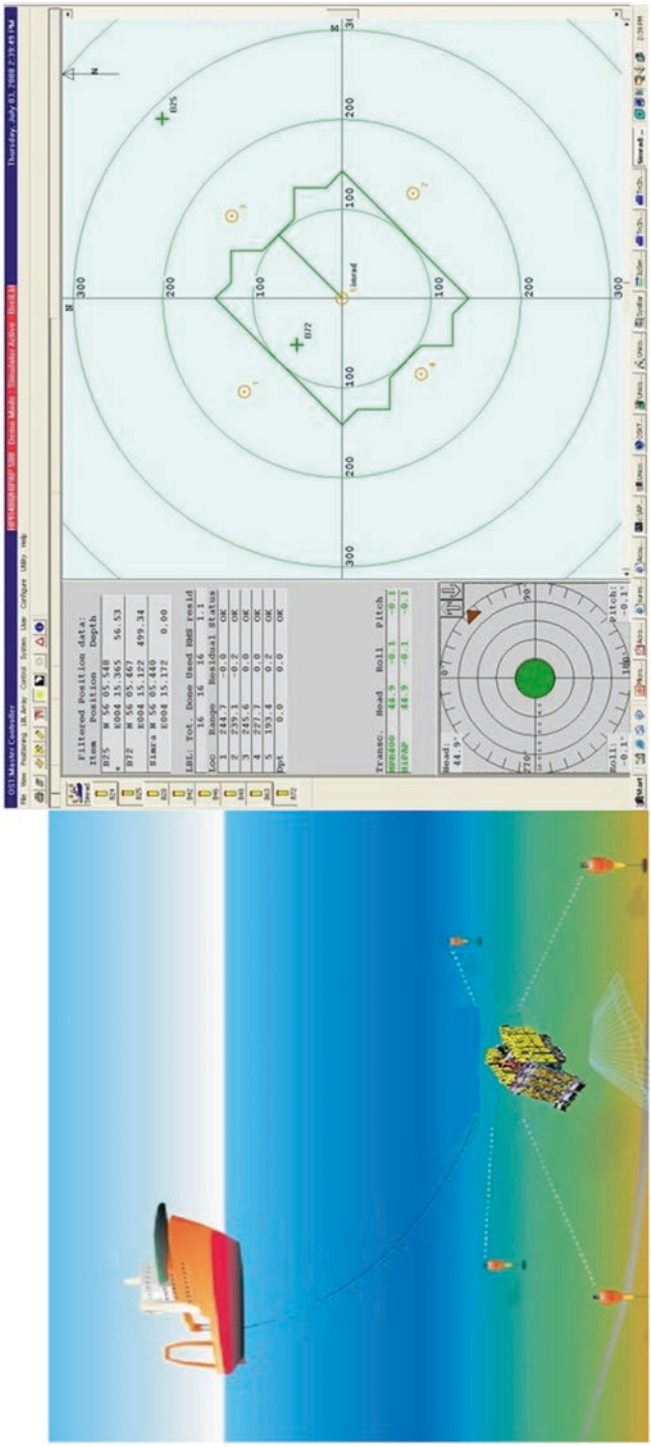

Fig. 10.7 HPR 408S system for deep-sea mining schematic and position obtained during tests

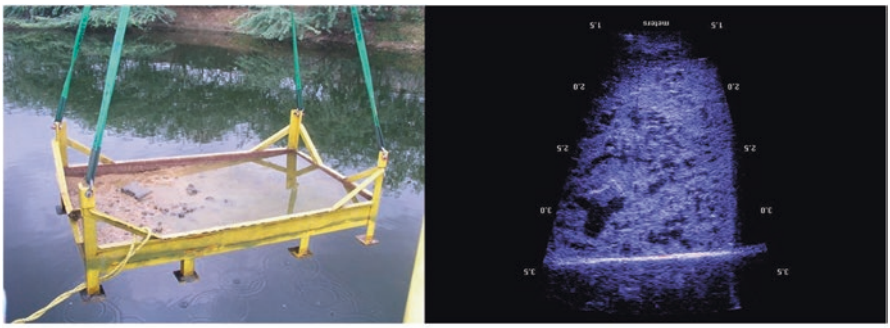

Fig. 10.8 Photo shows real image of nodules laid on the bentonite floor before being lowered into the test pond

10.4.4 Investigations on Interactions of the Seabed with Nodule Collector

Realization of an effective mining system for mining manganese nodules requires extensive studies to be carried out on pickup devices and their interaction with the sea floor. Different forces acting on the pickup devices during mining operations have to be studied in detail. Theoretical approaches and experimental studies were carried out for evaluating the forces for lifting nodules, cutting through sediments and moving the sediment–nodule material as a mass, time spacing, depth of penetration, etc. A test setup was designed and fabricated for carrying out these studies experimentally (Fig. 10.9).

The experiments were performed in a tank by simulating the geotechnical properties of the deep-sea sediments, which was made of bentonite–water mixture and a special consolidation procedure adopted for obtaining shear strength similar to that of the sediments (Fig. 10.10). The results from the tests have been used for design of deep-sea pickup devices and collector.

10.4.5 Developmental Studies on Underwater Crushing Systems

Polymetallic nodules collected from the ocean floor will have to be crushed to less than 30 mm size to facilitate transport through flexible hoses. The crushing properties of the nodules have been studied in detail and an underwater spike crusher with lateral conveying capabilities has been developed. Studies have been carried out on the developed crusher using both manganese nodules and artificial nodules (Fig. 10.11).

Fig. 10.9 Experimental studies on pickup devices for manganese nodule mining

10.4.6 Flexible Riser System

Extensive studies have to be carried out to estimate the pressure losses in the system to arrive at the sizing of the positive displacement pump. Further experimental studies need to be carried out for understanding the possibility of plugging for the flexible riser system. The facilities augmented by NIOT at the Mechanical Handling Laboratory of IIT Madras (Fig. 10.12) have been effectively utilized along with additional facilities available to carry out the studies. Understanding the performance of the system at the maximum particle size and the maximum expected concentration is the most critical element of the study. Materials of different sizes will be mixed to obtain the size distribution similar to that obtained in the CIOB and tests will be carried out to study the pressure drop characteristics.

Attempts shall be made to develop a hawser for the flexible riser. The hawser will be made of special materials to withstand the pressure developed by the slurry pump and also to handle the weight of the crawler and its own weight during the salvage/retrieval operations. The hose and cable will be attached together to form the hawser. Floats will be attached at regular intervals to obtain the catenary shape of the umbilical. The flexible riser system will be analyzed and the results would be used to design the final system.

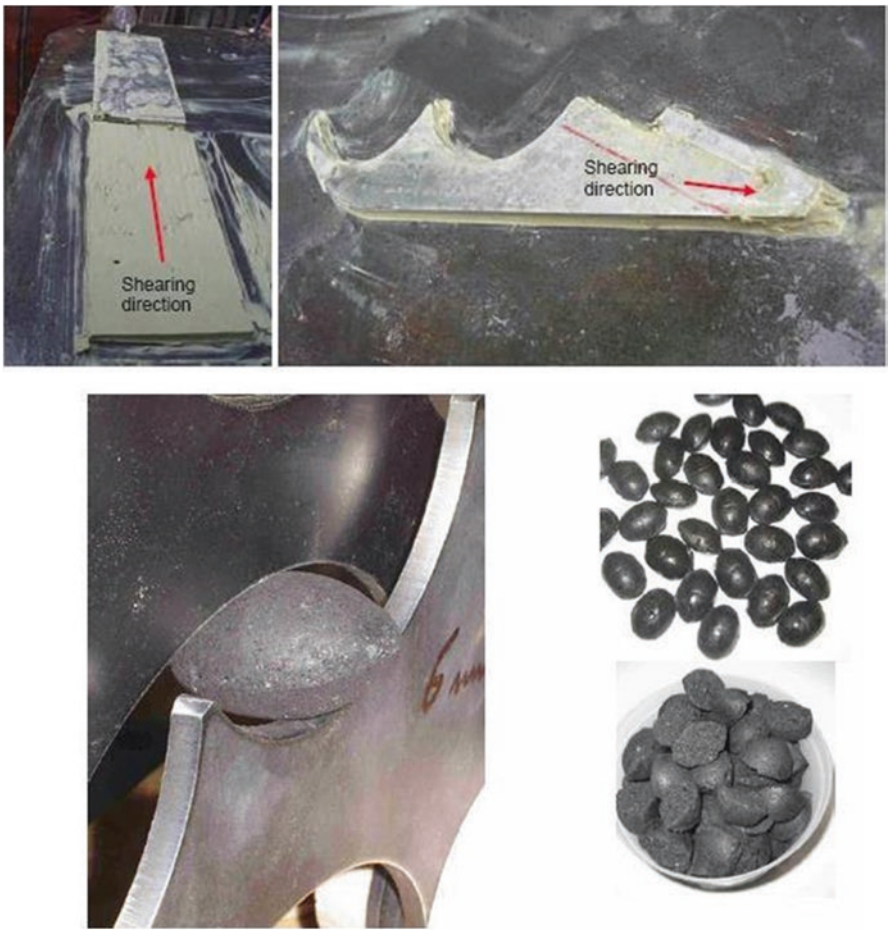

Fig. 10.10 Experimental studies to determine forces for breaking nodules

10.4.7 Development of Testing Facilities and Indigenous Deep-Sea Devices

Facilities developed in the institute for testing deep-sea subsystems, components, and integrated systems include a hyperbaric chamber for testing components and devices up to 900 bar pressure. The chamber has a testing space of 1-m diameter and 3-m length. A test pond has been developed by deepening the existing water body in NIOT and building an access jetty. This test pond is 4-m deep and will facilitate shallow water testing of underwater mining systems (Fig. 10.13). A facility for testing deep-sea winches up to 15 tons capacity has been developed in the Integration Bay of NIOT. Other facilities developed include devices for testing deep ocean electrical, electronics, and fiber-optic communication systems.

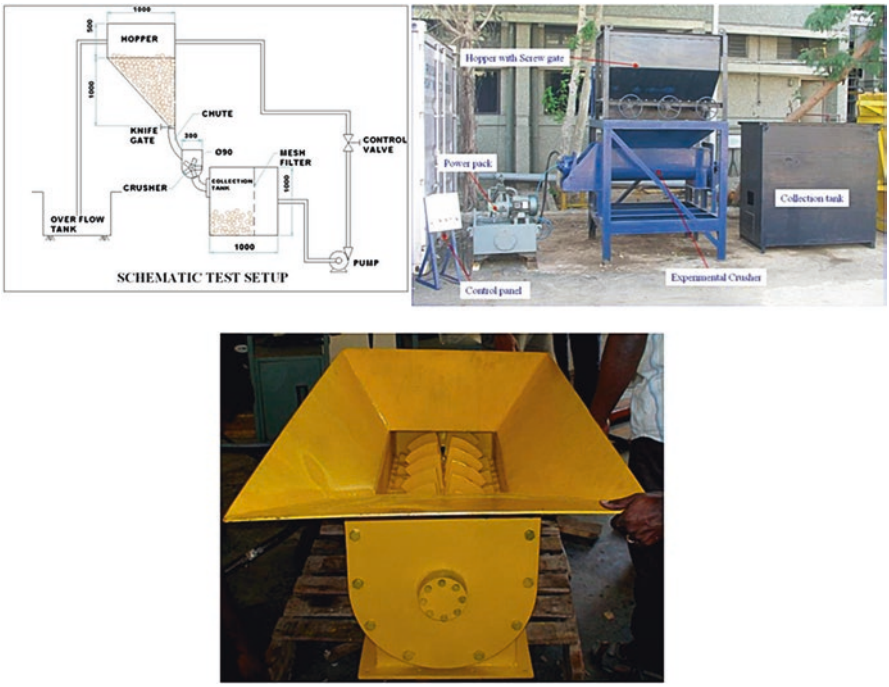

Fig. 10.11 Test setup for study of crusher for manganese nodules

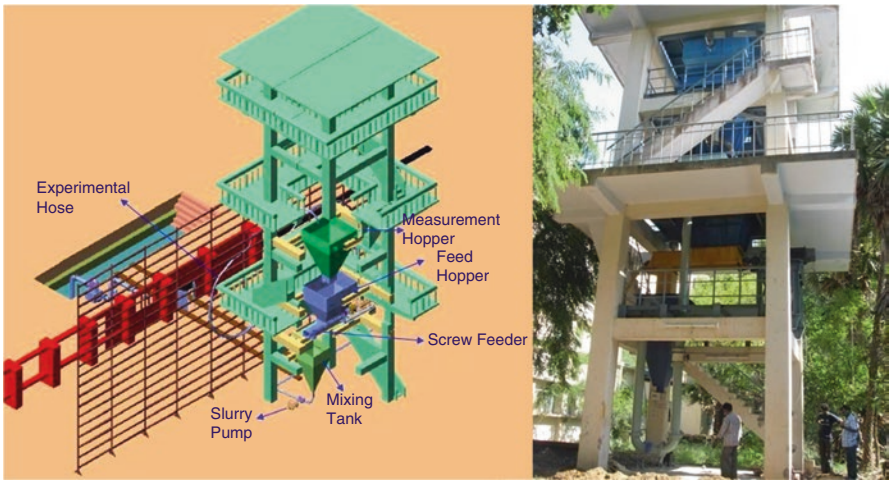

Fig. 10.12 Experimental setup for study of manganese nodule flow through hoses

Fig. 10.13 Underwater machinery test pond

10.5 Laying of Artificial Nodules and Mining of Them at Shallow Waters

In order to go through the next phase of operation, it is necessary to design and develop a nodule mining system and test it at depths of 500 m. As there are no nodules at 500-m water depth, artificial nodules are to be prepared, laid on the seabed, and mined. This section describes a system for laying of artificial nodules and the mining of the same.

The remotely operated artificial nodule laying system consists of a subsea hopper with positioning thrusters, rotary vane feeder, hydraulic power pack, servo valve pack, sonar, cameras, depth sensor, altimeter, Sonar, motion reference unit (MRU), data acquisition system, fiber-optic multiplexing and communication systems (Fig. 10.14). The nodule laying system is powered and operated remotely from the surface through an umbilical cable. The cable also handles the weight of the nodule laying system during launching and retrieval from the ship. The subsea system is towed from the ship which is dynamically positioned for maintaining a desired path. The thrusters in the subsea nodule laying system are used to maintain the orientation of the hopper during motion by maintaining heading with respect to vessel through closed loop control. The system can be operated in a sea state of 3. The thruster's movement can also be controlled individually or as a pair by manual control.

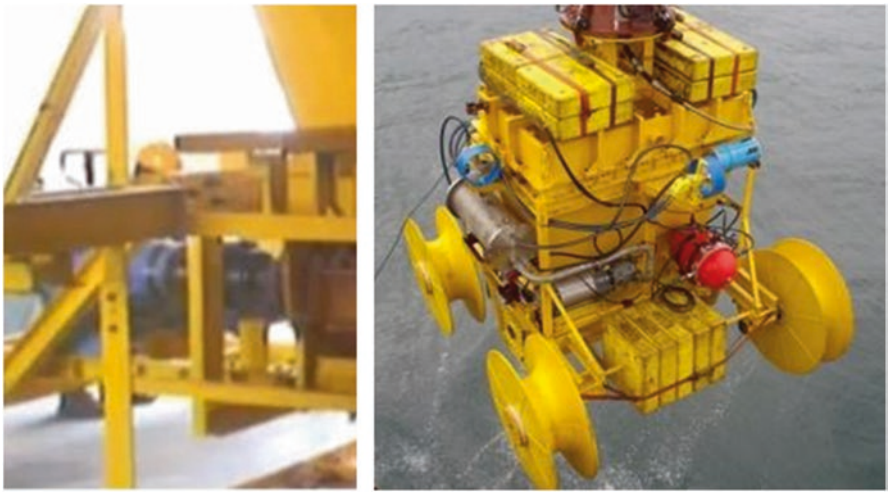

Fig. 10.14 Vane feeder with artificial nodules laying system

10.5.1 Mechanical Systems

The main drives of the artificial nodule laying system are hydraulically operated. The circuit diagram of the hydraulic systems is shown in Fig. 10.15. The hydraulic system consists of the following main subsystems.

10.5.2 Hydraulic Power Pack

The main hydraulic pump is a variable displacement axial piston pump of swash plate design for hydrostatic open circuit systems. The pump has a displacement 100 cc and is set for operations at 200 bar pressure.

10.5.3 Servo Valve Pack

The servo valve pack operates the hydraulic thrusters and the vane feeder. It contains eight servo valves that have low-pressure drop and are used for standard applications. The eight servo valves are rated for 77 lpm full flow at 70 bar pressure drop and would operate in normal conditions with a flow rate of 40 lpm resulting in a pressure drop of 19 bar. These valves are driven by a current amplifier. The servo valve pack operates at a maximum input pressure of 280 bar and a maximum flow rate of 350 lpm. The hydraulic pump is driven by an electric motor operating at a speed of 1450 rpm.

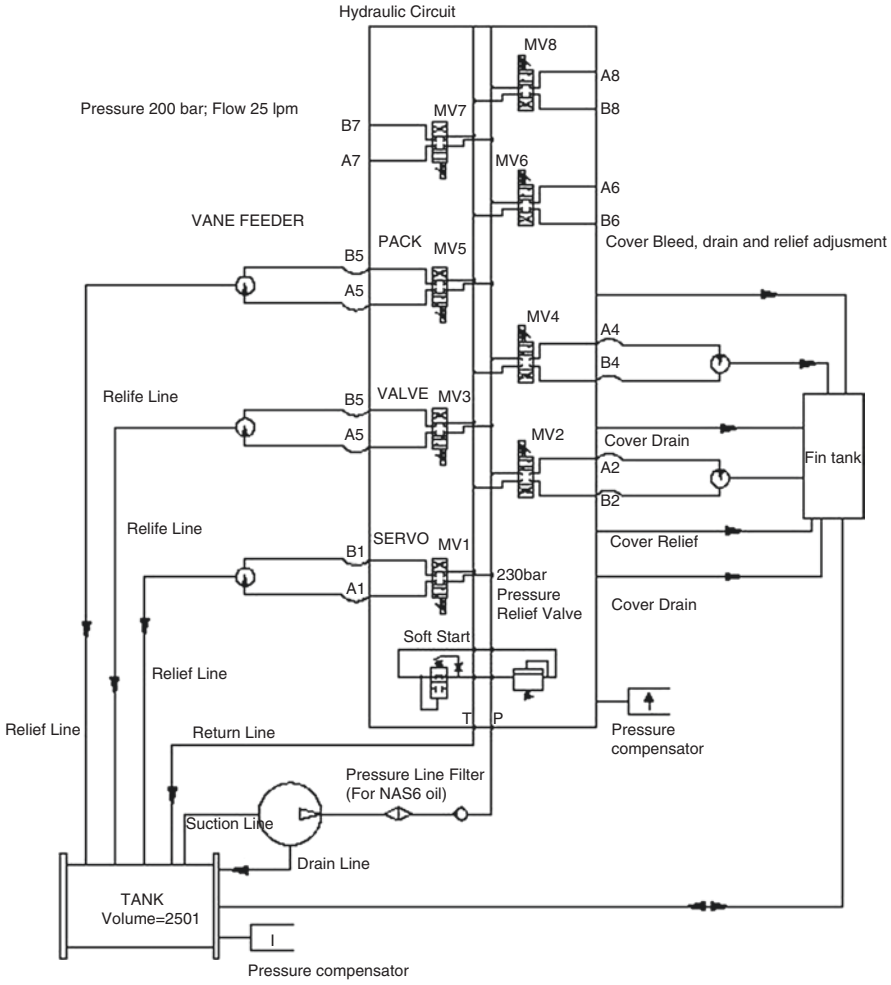

Fig. 10.15 Schematic of hydraulic system

10.5.4 Vane Feeder

A subsea vane feeder has been designed and developed for laying artificial nodules from the hopper. Vane feeder is a device for conveying nodules and it is coupled with the radial piston motor through a planetary gear box. The feeder draws the nodules from the hopper and lays it at a controlled and uniform speed to obtain a nodule carpeted site. The speed of the vane feeder is 0–5 rpm.

10.5.5 Thrusters

Four hydraulic propeller type thrusters driven by a bent axial piston hydraulic motor with displacement of about 28 cc are provided for forward and sideward movements. The thrust produced at 250 bar, 25 lpm is 250 N at 1.5 knots speed. The corresponding flow rate required for the thruster is about 25 lpm for a single thruster.

10.5.6 Electrical Power Distribution System

The electrical power for the powered hopper system is realized from a 500 kVA, 660 V/380 V, 50 Hz, 3-phase transformer available on board ship ORV SagarKanya. The power from this transformer is distributed to various subsystems through a dedicated power distribution panel installed in the ship. A separate 75 kVA, 380 V/380 V, 3 ph, 50 Hz isolation transformer is used to provide power for various sensitive electronic devices and computer systems on deck and well to subsea systems. The isolation transformer provides complete galvanic isolation from other power devices operating on deck. The details of the electrical power distribution scheme are shown in Fig. 10.16.

The hydraulic power unit (HPU) of the hopper system is powered by a 60 kW subsea motor operating at 3000 V, 3-phase, 50 Hz AC. The electrical power to this motor is obtained from a separate 500 kVA High Tension (HT) step-up transformer (500 kVA, 380 V/3000 V, 3 ph, 50 Hz) mounted on the deck. The HPU motor is operated through a medium voltage soft starter installed on the deck. The soft starter enables the motor to have a smooth starting there by avoiding heavy current surge during starting.

The electrical power to the hopper system is transmitted through an 800-m subsea electro-optic cable which is handled from a deep-sea winch. The electrical power and telemetry signals are coupled to the rotating cable drum of winch through a HT slip ring mounted on the winch and terminated at the subsea end to hopper through a custom designed pressure compensated terminated assembly.

10.5.7 Telemetry

The Data Acquisition and Control System (DACS) for the hopper implements a modular DACS with stand-alone embedded controller, which is more versatile for system configuration, programming and avails more local support. The hardware system is a Compact Field Point (cFP) system working on LabVIEW real-time graphical programming software module.

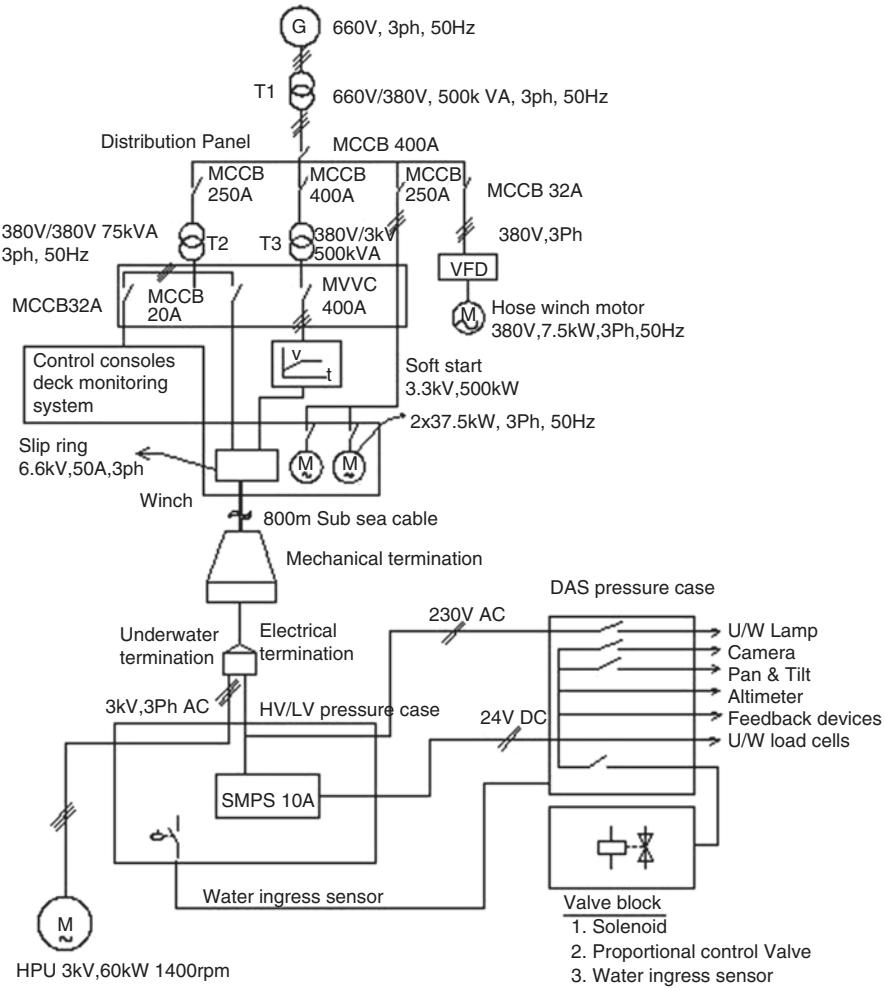

Fig. 10.16 Electrical system

The subsea part of the system has various subsea transducers and control devices interfaced with the cFP and industrial control process connect modules (ICPcon's) stand-alone embedded controller (SAEC) based modular data acquisition system. The block diagram of the DACS and telemetry system, which broadly details the hardware architecture, is shown in Fig. 10.17. The x86-based modular embedded controller (cFP2020) has an integrated 10/100 Base TX Ethernet, RS-485 port, and three RS-232 ports. The Stand-Alone Embedded Controller (SAEC) (ICP CON 7188XA) system, which is acting as the real time target at ship control console, takes interfaces from all user interface devices and communicates with ship subsystems. The industrial PCs acting as the GUI interface center between the operator and

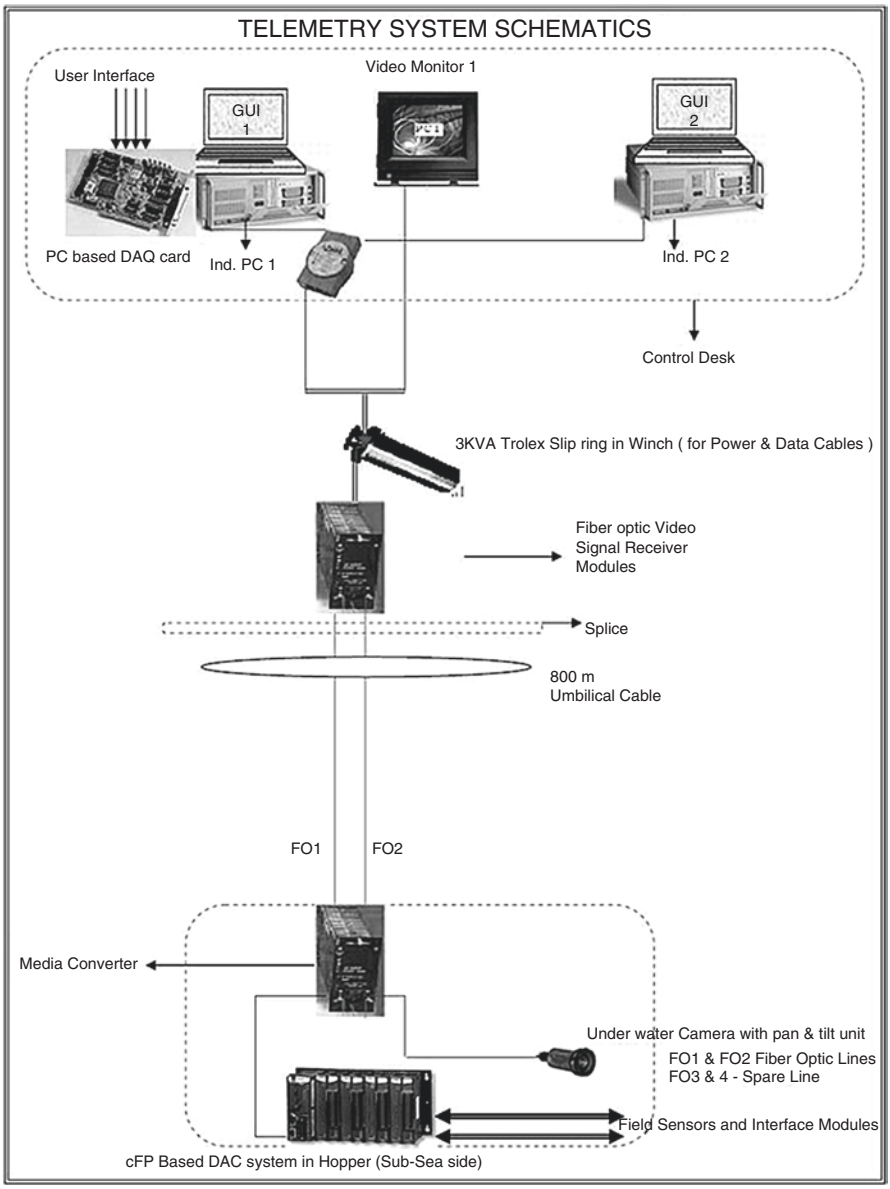

Fig. 10.17 Telemetry system schematics

the DAC system is networked to the SAEC-cFP network. The SAEC has necessary data/control interface cards on its platform for analog and digital data interface from the ship and user interface devices.

10.5.8 Software

The software implemented is LabVIEW®, a user-friendly graphical programming language from National Instruments. The hardware system, SAEC-Compact Field Point (cFP) system, works on LabVIEW® real-time graphical programming software module. Since both are from the same manufacturer, it ensures tight hardware-software integration and flexibility for hardware configuration.

10.5.9 Artificial Nodules Development

Artificial nodules were developed with clay mixed with sawdust as kernel and plain clay as shell (Figs. 10.18 and 10.19). The nodules were cured in air for around 4 days and later fired in the kiln for 3 days. Various materials like fly ash and husk in various proportions were made as kernel to achieve the density, hardness, and texture nearest to that of manganese nodule. It was observed that the combination of brick clay and sawdust in the kernel and brick clay in the shell after curing and firing was having density, hardness, and aggregate impact test value closest as that of actual manganese nodules. Development of artificial nodules for hydro transport studies has also been reported in Yoon (2008). The artificial nodules were produced in various sizes in proportion with the distribution of manganese nodules in the Central Indian Ocean Basin i.e., size 25–30 mm—15%, 40–50 mm—40%, 60–70 mm—35%, greater than 70 mm—10%.

Sl. no.	Description	Polymetallic nodules	Artificial nodules
1.	Density	1500 kg/m^3	1500–1600 kg/m^3
2.	MoHS hardness	1–2	1–2
3.	Aggregate impact test index	56%	55%

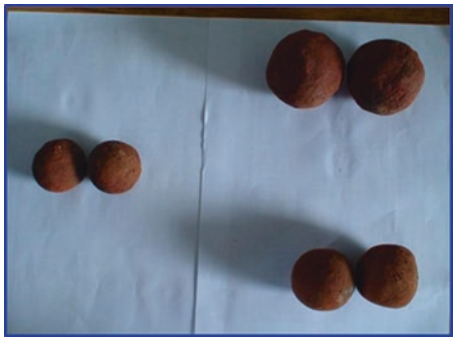

Fig. 10.18 Artificial nodules

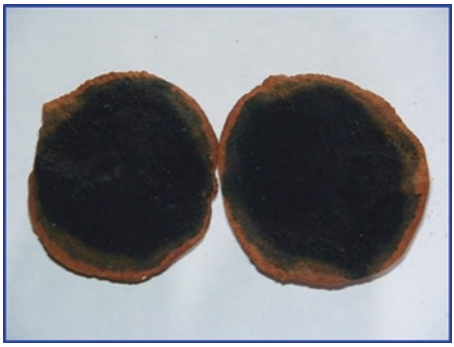

Fig. 10.19 Enlarged sectional view of artificial nodules

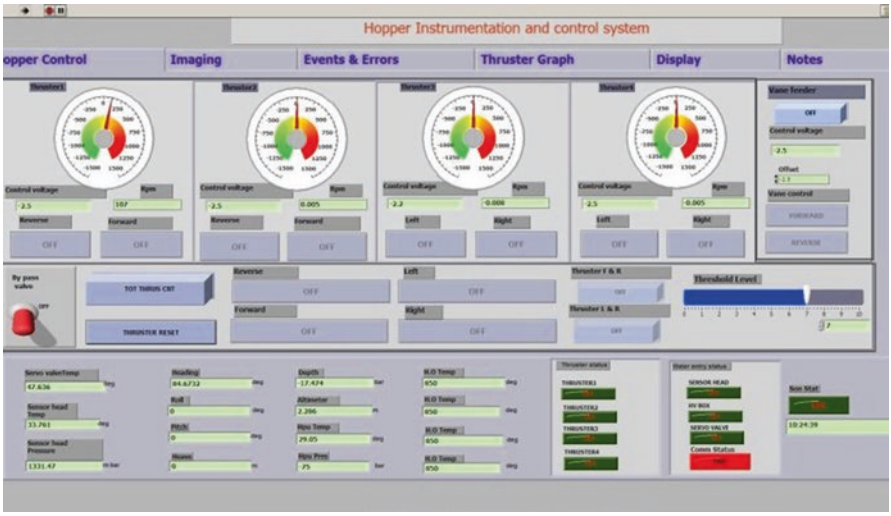

Fig. 10.20 Instrumentation and control system

10.5.10 Control and Operations

The operations of the nodule laying system can be controlled through the front end of a PC-based data acquisition system. The front end has been developed using LabVIEW™ software. Necessary control switches for Feeder and Thrusters have been built-in and the movement can be controlled individually or together, provided by the function in software. The parameters such as HPU temperature, HPU pressure, altimeter, electronics enclosure temperature, electronics enclosure pressure, depth, heading, pitch, roll, and sinking depth can be viewed in the window. The front end control window is shown in Fig. 10.20.

Before the actual deployment, a shallow water test was done in order to qualify the working of the nodule laying system at a depth of 20 m. The hopper system was loaded with 700 kg of artificial nodules. The system was launched using the docked Launching and Retrieval System (LARS) of SagarKanya. At 20-m depth the vane feeder was rotated and nodules were laid on the seabed. The laying of nodules was viewed through both cameras and imaging SONAR and the image of the laid nodules captured.

10.5.11 Sea Trials at 520-m Water Depth

The artificial nodule laying system with 1.5 tons of nodules weight (air) was launched off Chennai coast (13.3 N 80.7 E). The system was suspended at 520-m depth at about 2 m above the ocean floor. The deployment was done using Launching and Recovery System (LARS). The working condition of the systems was tested at intermittent depths of 20 and 300 m during launching. After initial checks on health of subsystems, the nodules were laid on the seabed by operating the vane feeder and moving the hopper using thrusters. The ship was dynamically positioned and moved at very low speed of less than 0.5 knots. The orientation of the hopper was controlled by operating thrusters. Images of nodule discharging from the hopper were captured through sonar and underwater camera (Figs. 10.21, 10.22, 10.23, and 10.24). After the laying of nodules the ship was moved back along the path where nodules were laid to view the nodule carpeted sea floor.

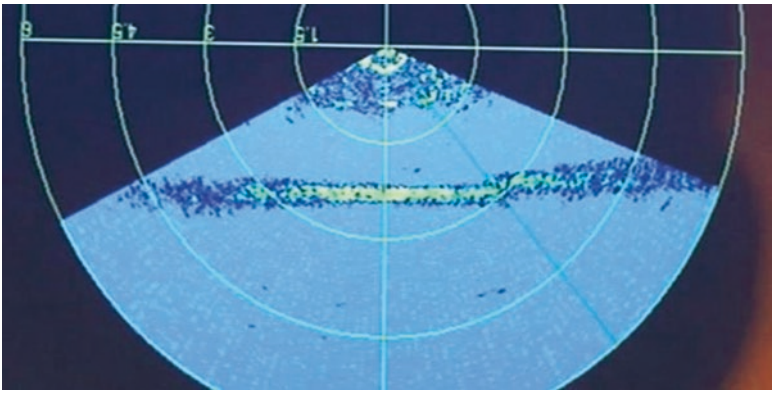

Fig. 10.21 SONAR image before laying the nodules

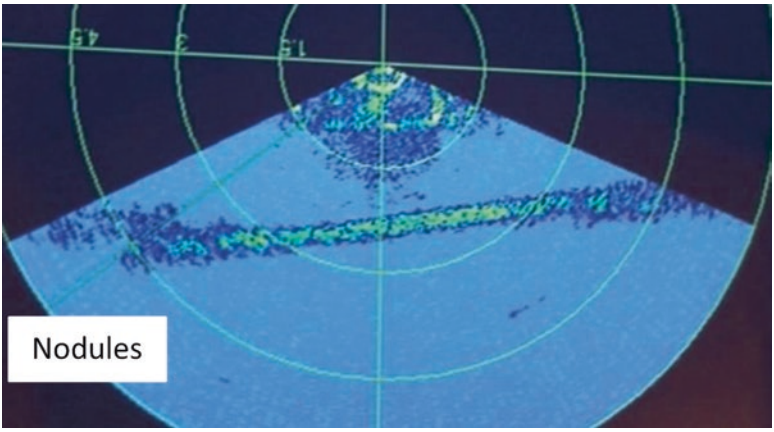

Fig. 10.22 SONAR image during the laying of nodules

Fig. 10.23 Laying of artificial nodules being dropped from vane feeder

Fig. 10.24 Artificial nodule carpeted sea floor viewed through underwater camera

10.6 Development of Mining System for Mining of Artificial Nodules

A remotely operable artificial nodule laying system explained in the previous section was used to lay artificial nodules and the system qualified off Chennai coast in 2007 (Amudha et al. 2009). The same system was used to create a nodule carpeted track to facilitate testing of the underwater mining system with collector and crusher in October 2010 (Fig. 10.25).

The subsea artificial nodule laying system was towed from the ship which is dynamically positioned for maintaining a desired path. The thrusters in the subsea nodule laying system are used to maintain the orientation of the hopper during motion by maintaining heading with respect to vessel through closed loop control. The system can be operated in a sea state of 3. The thruster's movement can also be controlled individually or as a pair by manual control. Motion control algorithm is embedded in the system to position itself in-line with the vessel's heading and done by controlling the trajectory parameters with reference to the ship heading and acoustic positioning system.

10.6.1 Mining Machine

The underwater mining machine consists of tracked crawler vehicle, mechanical tined pickup device, cleated belt conveyor, crusher, twin cylinder positive displacement pump, with large solids transportation system. The model of the mining

Fig. 10.25 Artificial nodule laying system being launched

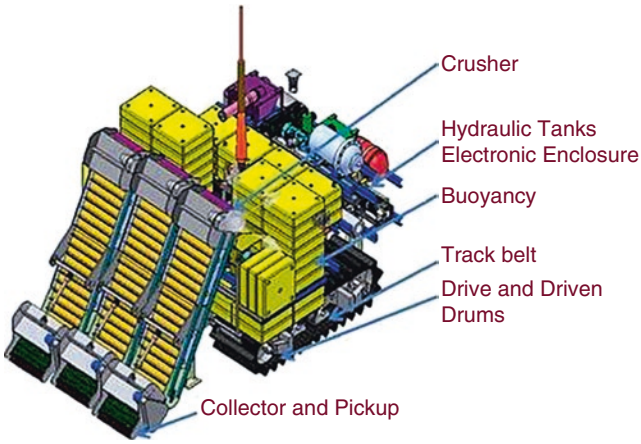

Fig. 10.26 Model of underwater mining machine

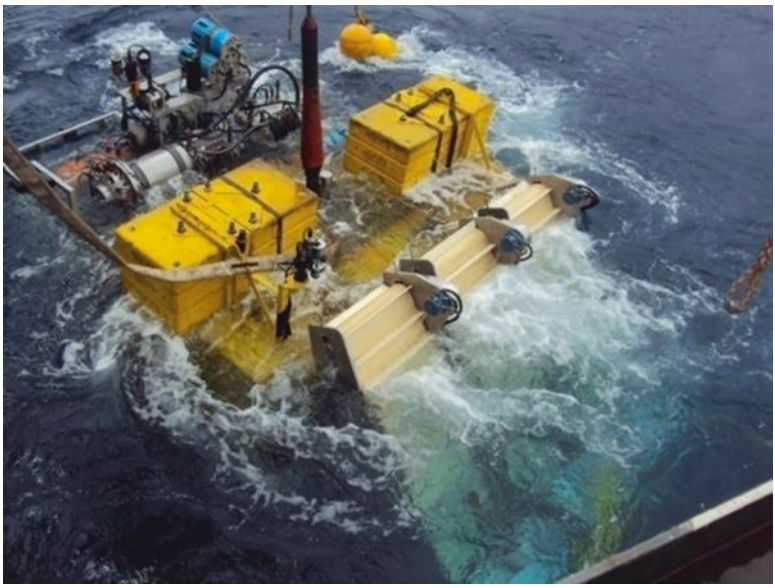

Fig. 10.27 Underwater mining machine being launched

machine is shown in Fig. 10.26. The machine is a remotely operated electrohydraulic machine, augmented with three pickup devices with cleated belt conveyor modules, crushing system, and flexible riser slurry pumping system (Fig. 10.27). It is maneuvered over the seafloor driven by the drive drums at a speed of 0.15–0.5 m/s. During mining operations the machine moves at 0.15/s and travels without mining at 0.5 m/s. Dedicated controllers for instrumentation system were incorporated to communicate through fiber-optic cable embedded in the umbilical cable and commanded from the control console onboard mother vessel.

10.6.2 Specification of Underwater Mining Machine

Overall length	6200 mm
Overall width	3400 mm
Weight in air	20.8 tons
Weight in water	8.8 tons
Depth of operation	500 m
Operational speed	0.15 m/s
Max speed	0.5 m/s
Max slope	8.5°
Slurry discharge	Upto 45 m^3/h
Concentration	30% (max.)
Mining output	8 tons/h (max.)
Particle size (max.)	25 mm
Flexible riser system	
Hose size	75 mm
Hose spool length	100 m
Hose–cable joints	At 6 m intervals
Hose winch	500 kg (SWL)
Hose spool speed	0.5 m/s (max.)
Cable electromechanical multiconductor	
Breaking strength	500 kN
Power	180 kW at 3000 V
Signal transmission	Two optical lines TCP/IP
Data acquisition	PXI-based system
Transducers	Velocity, heading, pitch, roll, vision
Winch for cable	1.6 m dia. × 1.4 m length
Auxiliary winch	12 Tonnes—2 Nos
Cable spool speed	0.5 m/s

10.6.3 Data Acquisition System on Ship

The ship-side system has interfaces for all electrical and data signals from the subsea crawler unit. The control console housed in a mobile container is the Human Machine Interface (HMI) control center for all operations of the mining system. In addition to the status of subsea systems, the control room will have information from a network of onboard Closed-Circuit Televisions (CCTVs) for monitoring various ship deck operations.

The ship-side Data Acquisition and Control System (DACS) is configured with a real-time controller and two industrial PCs working as master and slave controller. The schematic of the ship-side DACS is shown in Fig. 10.28. All the user interface devices like joysticks and toggle switches are interfaced directly to the input/output cards, through a terminal box. The real-time controller, master and slave systems along with

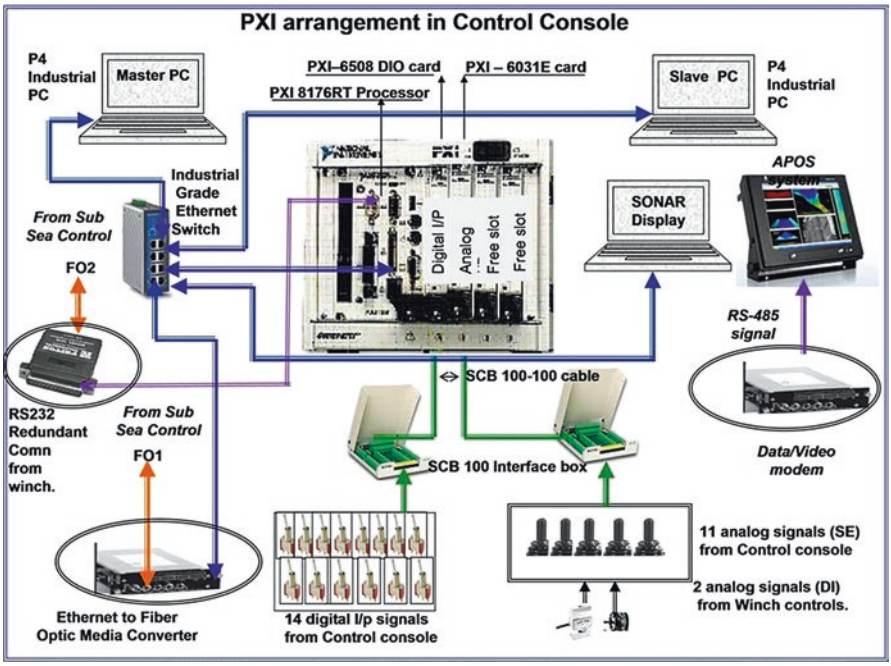

Fig. 10.28 Schematic of ship-side DACS

subsea side controller form a network with TCP/IP protocol and act as the HMI center. The software user command from master and slave and hardware command from joysticks and toggle switches are accessed and routed to ship-based real-time controller to subsea DAC system for necessary operations as described in Fig. 10.28.

The electrical power supply required for the underwater mining machine is transmitted through an 800-m long subsea electro-optic cable from the ship feeder (3 kV, 3-phase, AC supply for the medium voltage subsea motors and 220 V, AC supply for the DAC system). This electro-optic cable is handled from an onboard winch. The electrical power and telemetry signals are coupled to the rotating cable drum through a High Tension (HT) slip ring mounted on the winch and terminated at crawler end through a customized pressure compensated termination assembly namely Field Installable Terminal Assembly (FITA). The electrical and fiber-optic cables from FITA are separated and terminated with a High Voltage Enclosure (HVE) and Electronics enclosure, respectively. Both the 3 kV and 220 V power lines are distributed from the HVE to the subsystems. The transducers and control devices are powered by 24 V DC power supply, provided from Low Voltage Enclosure (LVE) by using Switch Mode Power Supply (SMPS). The gross power requirement of the crawler during mining is approximately 160 kW, out of this 5 kW is consumed by the DAC system.

The control of the crawler from the ship is through the master PC during automatic operation and through joysticks and toggle switches during manual operation

Fig. 10.29 View of onboard control room

as shown in Fig. 10.29. This PC is also configured as a DACS having virtual digital and analog I/Os. The on/off control signal for thrusters, bypass valve of hydraulic pump, slurry pump, camera selection, camera operation, and lights are given as input to the subsea DACS from the control panel of master and slave PCs.

10.6.4 Telemetry System

The data-video telemetry system provides communication link between the mother ship and subsea DACS through a winch and an umbilical cable for monitoring and controlling of crawler operation. The communication link is an electro-optical system which is realized by a 9/125 μm single mode fiber-optical line in the umbilical cable. The optical signal propagates typically at wavelength of 1310 and 1550 μm. A set of media converters are placed in the electronics enclosures at subsea side and inside the winch drum at the ship side. The optical signal which is converted to an electrical signal of video and data information by media converter is passed through electrical slip ring in the winch. The total telemetry system utilizes three fiber-optic lines, out of six in the umbilical cable. The first fiber line is used for a media converter for primary Ethernet data link (100 Mbps). The second fiber line is used for another media converter, which has 10 Mbps Ethernet data, two videos, and two RS232 links as back up to the Ethernet and video link. And the third one is used for a media converter for four video and two RS485 signals as a primary video link. The overall data video telemetry system is shown in Fig. 10.30.

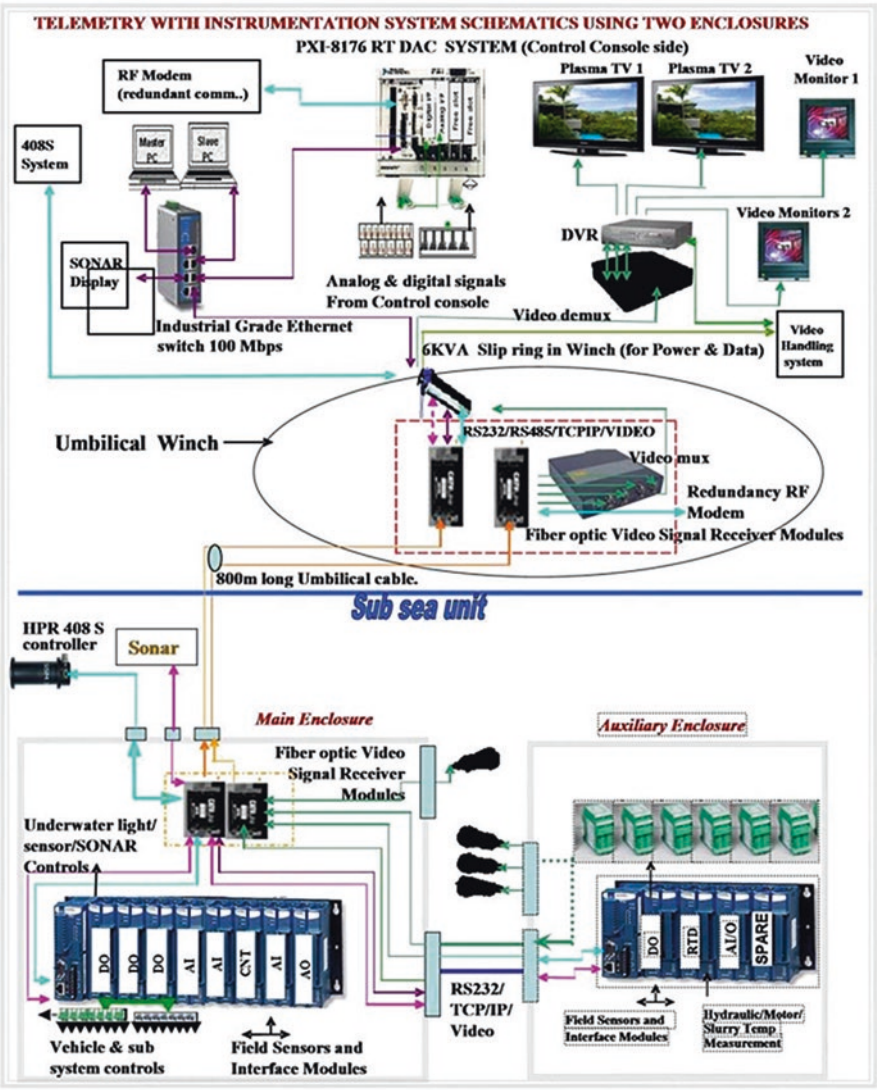

Fig. 10.30 Data-video telemetry system

10.6.5 Dynamic Positioning System

Dynamic Positioning System (DP) is a computer-controlled system for controlling the position of a vessel without the use of mooring anchors, with reference to Dynamic Global Positioning system (DGPS) and various input parameters like wind speed, underwater current speed, heading, pitch, roll, and heave. The station

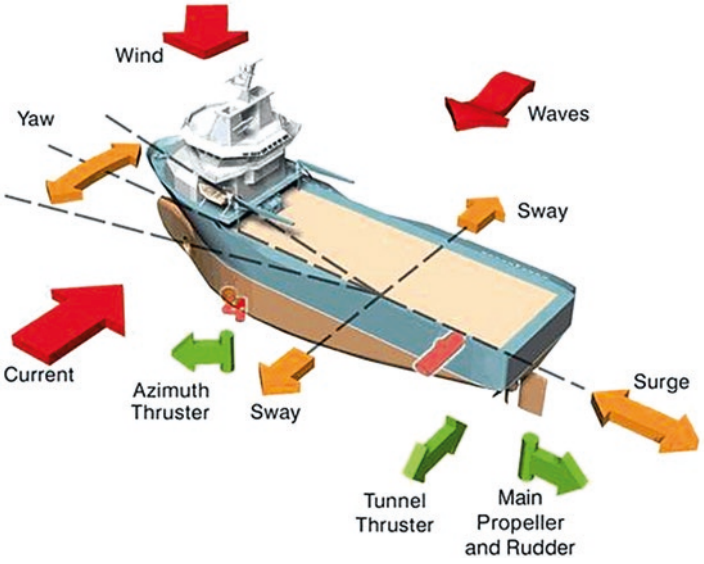

Fig. 10.31 Model of vessel with DP control (Courtesy: Kongsberg-Maritime)

keeping of the ship with respect to the underwater mining machine was done by operating the vessel in DP mode. The DP system also facilitates following the path of the mining machine under follow target mode. Figure 10.31 shows a schematic of typical dynamic positioning system installed in the vessel Sagar Nidhi controlled with various inputs (Courtesy: Kongsberg-Maritime)

10.6.6 Acoustic Positioning System

High Precision Acoustic Positioning (HiPAP) system installed in the ORV Sagar Nidhi mother ship provides underwater position of the crawler with respect to the mother ship. Acoustic positioning software traces the crawler in Super Short Baseline (SSBL) mode.

Crawler integrated with the multipurpose transponders is mainly used as an underwater reference unit. The vehicle maneuvers in a planned mining area with specified tracks which is monitored on the workstation namely APC11 through SSBL positioning mode as shown in Fig. 10.32. This system helps to avoid the overlapping of mining tracks and increase its efficiency. A hydro acoustic positioning system consists of a transmitter (transducer) and a set of receivers (transponder array) on the umbilical cable. On the receipt of signal to the transceiver, the transponders communicates acoustically and responds to the transducer mounted on the crawler.

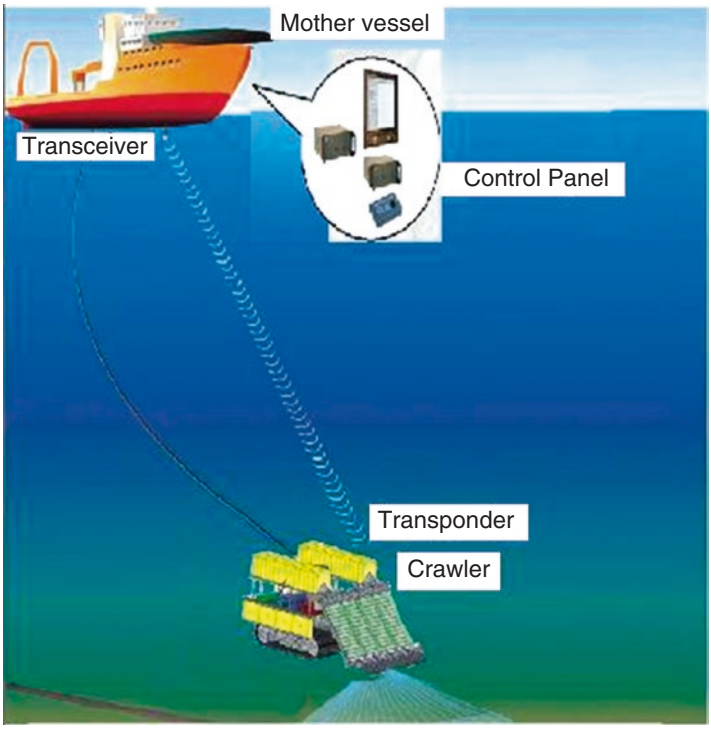

Fig. 10.32 SSBL configuration

10.6.7 Testing of System

The underwater mining machine with collector and crusher system was tested at Angria bank (Lat: 16°13.600′ N and Lon: 72°04.427 E off Malvan coast of India) at 512-m depth. Figure 10.33 shows the test site Angria Bank as viewed in the ship's Console. On reaching the site at Angria bank, core samples (Fig. 10.34 results of core sample) were taken in two locations to determine the most suitable site for testing the mining machine. Multi-beam surveys were done after soil testing to determine the gradient of seafloor for testing the maneuverability of the machine. Figure 10.35 shows the terrain of the site in Angria bank.

10.6.8 Launching and Retrieval System

Underwater mining machine was launched through the A-frame of the Ocean Research Vessel Sagar Nidhi a DP Class II vessel owned by Ministry of Earth Sciences of the Indian Government. The crawler-based collector crusher was launched after creating the artificial nodule carpeted track at the specified location

Fig. 10.33 Test site off Malvan coast of India

Fig. 10.34 Core sample results

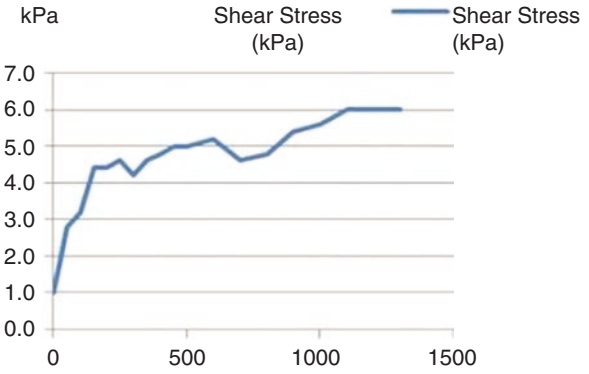

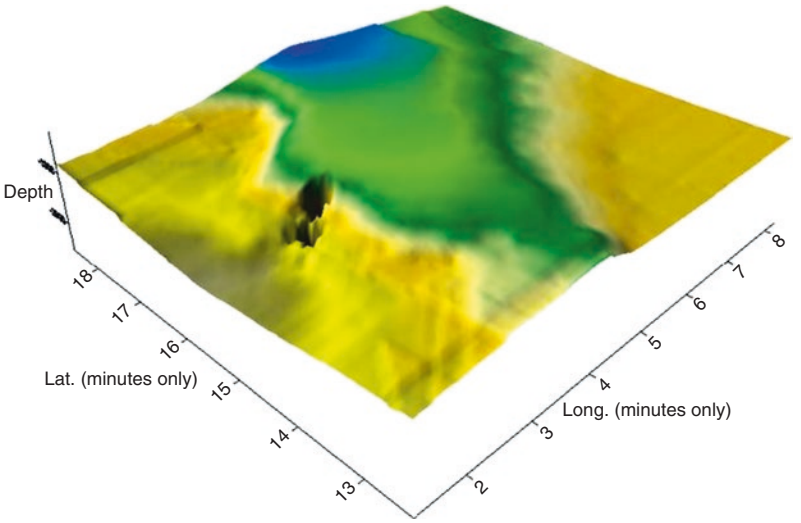

Fig. 10.35 Topography of the sea floor in Angria Bank Test site

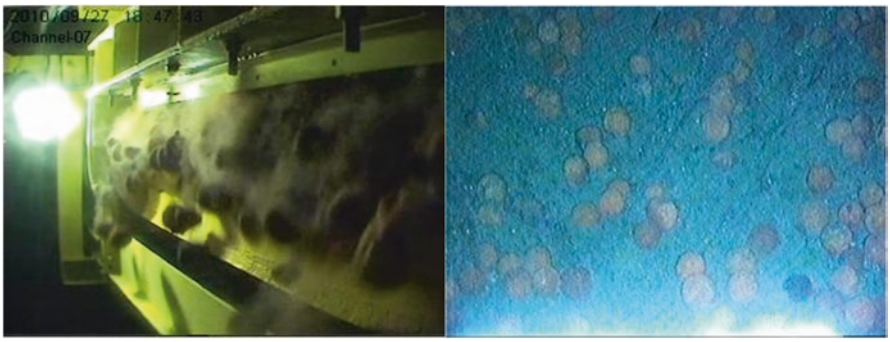

Fig. 10.36 Operations of vane feeder and sea floor with nodules

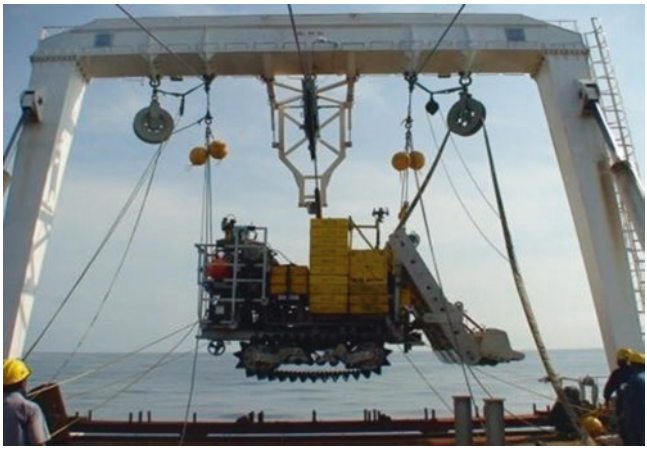

Fig. 10.37 Launching of underwater mining machine

using the artificial nodule laying system. Planned mining path was created by moving the vessel at a speed upto 0.5 knots using dynamic positioning system and operating the vane feeder of hopper to discharge artificial nodules to create track of 10–15 kg/m^2 abundance as shown in Fig. 10.36.

Mining machine system was launched using two auxiliary winches in additional to the main umbilical winch till it crosses the wave zone as shown in Fig. 10.37. The electromechanical armored cable was attached with the hose and buoyancy modules at regular intervals and the cable (SWL 15 tons) handles the weight of the machine after it crosses the wave zone.

Before touchdown of the underwater mining machine it is essential to locate the nodules laid over the seabed. The Acoustic Positioning System (APOS) onboard Sagar Nidhi and dynamic positioning system provided excellent coordination in launching and positioning the mining machine on the nodule path. After touchdown of the mining machine at a depth of 520 m, the vessel was moved in steps of 2 m to a distance of 30 m to the forward side, in coordination with the cable reel-out.

The cable was spooled out after touchdown and S-shaped profile was formed. Pumping of seawater was performed operating the slurry pumping system with 10, 20, 30, and 45 m^3/h and the mining machine moved with path traced on the APOS system with reference of the transponder. The machine moved up to 30 m collecting artificial nodules, crushing them, and pumping to the surface, thereby qualifying the system (Rajesh et al. 2011).

10.7 In Situ Soil Tester

The optimum design of an integrated mining system for polymetallic nodule mining is mainly dictated by the soil properties of extremely soft seabed at 5000–6000-m depth. During design, the entire weight distribution and traction of the mining machine has to be configured considering the bearing strength and shear strength parameters of the soil. The shear strength of the soil also provides useful information for the maneuverability and control of the mining machine. It is also imperative that the mining area be delineated to eliminate vulnerable areas of low strength where the equipment may sink suddenly beyond recovery due to anchoring of the machine. A remotely operable in situ soil tester has been developed for 6000 m operations with a cone tester and a shear vane tester for soft soils and shallow depth of penetration. Soil property measurements and equipment's performance at 5462-m water depth in the Central Indian Ocean Basin have been successfully done (Muthukrishna Babu et al. 2014).

References

Amudha K, Rajesh S, Ramesh NR, Babu M, Abraham R, Deepak CR, Atmanand MA (2009) Development and testing of remotely operated artificial nodule laying system at 500 m water depth. In: Proceedings of 8th ocean mining symposium of international society of offshore and polar engineers, Chennai, 20–24 Sept 2009, pp 233–238

Atmanand MA, Shajahan MA, Deepak CR, Jeyamani R, Ravindran M, Schulte E, Panthel J, Grebe H, Schwarz W (2000) Instrumentation for underwater crawler for mining in shallow waters. In: Proceedings of international symposium of autonomous robots and agents, Singapore, 26 May 2000

Brink AW, Chung JS (1981) Automatic position control of 300000 tons ship during ocean mining operations. In: Proceedings of offshore technology conference, Houston, OTC 4081, pp 205–224

Chung JS (1996) Deep ocean mining: technologies for manganese nodules and crusts. Int J Offshore Polar Eng 6(4):244–254

Chung JS, Olagnon M (1996) New research directions in deep-ocean technology developments for underwater vehicles and resources. Int J Offshore Polar Eng 6(4):241–243

Chung JS, Tsurusaki K (1994) Advances in deep-ocean mining research. In: Proceedings of 4th international offshore and polar engineering conference, ISOPE, vol 1, Osaka, pp 18–31

Chung JS, Whitney AK, Loden WA (1980) Nonlinear transient motion of deep ocean mining pipe. In: Proceedings of offshore technology conference, Houston, OTC 3832, pp 341–352

Deepak CR, Shajahan MA, Atmanand MA, Annamalai K, Jeyamani R, Ravindran M, Schulte E, Handschuh R, Panthel J, Grebe H, Schwarz W (2001a) Developmental tests on the underwater

mining system using flexible riser concept. In: Proceedings of 4th ocean mining symposium of international society of offshore and polar engineers, Szczecin, 23–27 Sept 2001

Deepak CR, Shajahan MA, Atmanand MA, Annamalai K, Jeyamani R, Ravindran M, Schulte E, Panthel J, Grebe H, Schwarz W (2001b) Developmental tests on the underwater mining system using flexible riser concept. In: Proceedings of 4th ocean mining symposium of international society of offshore and polar engineers, Szczecin, 23–27 Sept 2001

Deepak CR, Ramji S, Ramesh NR, Babu SM, Abraham R, Shajahan MA, Atmanand MA (2007) Development and testing of underwater mining systems for long term operations using flexible riser concept. In: Proceedings of 7th ocean mining symposium of international society of offshore and polar engineers, Lisbon, 1–6 July 2007, pp 166–171

Exon NF, Bogdanov NA, Francheteau J, Garrett C, Hsü KJ, Mienert J, Ricken W, Scott SD, Stein RH, Thiede J, von Stackelberg U (1992) Group report: what is the resource potential of the deep ocean? In: Hsü KJ, Thiede J (eds) Use and misuse of the seafloor. Wiley, Chichester, pp 7–27

Grebe H (1997) General mathematical model for the hose connections between the mobile deep sea devices and their mother stations. Ph.D. Thesis, IKS, University of Siegen, Siegen

Halkyard J (1985) Technology for mining cobalt rich manganese crusts from seamounts. In: Proceedings IEEE oceans ‘85 conference, San Diego, pp 352–374

Handschuh R, Grebe H, Panthel J, Schulte E, Wenzlawski B, Schwarz W, Atmanand MA, Jeyamani R, Shajahan MA, Deepak CR, Ravindran M (2001) Innovative deep ocean mining concept based on flexible riser and self-propelled mining machines. In: Proceedings of 4th ocean mining symposium of international society of offshore and polar engineers, Szczecin, 23–27 Sept 2001

Heine OR, Suh SL (1978) An experimental nodule collection vehicle design and testing. In: Proceedings of offshore technology conference, Houston, OTC 3138, pp 741–749

Kuntz G (1979) The technical advantages of submersible motor pumps in deep sea technology and the delivery of manganese nodules. In: Proceedings of offshore technology conference, Houston, OTC 3367, pp 85–93

Muthukrishna Babu S, Ramesh NR, Muthuvel P, Ramesh R, Deepak CR, Atmanand MA (2014) In-situ soil testing in the Central Indian Ocean basin at 5462 m water depth. Int J Offshore Polar Eng 24(32):213–217

Rajesh S, Gnanaraj AA, Velmurugan A, Ramesh R, Muthuvel P, Babu MK, Ramesh NR, Deepak CR, Atmanand MA (2011) Qualification tests on underwater mining system with manganese nodule collection and crushing devices. In: Proceedings of 9th ocean mining symposium of international society of offshore and polar engineers, Maui, 19–24 June 2011

Scott SD (2001) Deep ocean mining. J Geol Assoc Can 28(2):87–96

Yoon CH (2008) Solid-liquid flow experiment with real and artificial manganese nodules in flexible hoses. In: Proceedings of the eighteenth international offshore and polar engineering conference, 6–11 July 2008, Vancouver, Canada

Dr. M.A. Atmanand Scientist "G" and Former Director of National Institute of Ocean Technology and Former Project Director of Integrated Coastal and Marine Area Management. An Instrumentation and Control Engineer by profession, he took his undergraduate degree from University of Calicut, Master's and doctorate degrees from Indian Institute of Technology, Madras. He has done pioneering work in the area of deep-sea technologies in India such as development of underwater crawler for deep-sea operation, in situ soil tester for deep-sea sediments and remotely operable vehicle. Dr. M. A. Atmanand has published 90 papers including international journals, national and international conferences, and book chapters. He is the founder Chair of IEEE Oceanic Engineering Society in India. He has served IEEE Madras section in various capacities and he is the current Chair.

Dr. G.A. Ramadass Scientist, National Institute of Ocean Technology, Chennai, India, holds a Ph.D. Degree (Physics) from Indian Institute of Technology, Madras, India. He is the head of the Deep-sea Technology Group and has been involved in development of technology for remotely operable vehicle, deep water drilling system, gas hydrate exploration, and mining of polymetallic nodules. He has four patents (two international, two national) and has published several scientific papers in international journals as well as national and international conferences.

Chapter 11
An Application of Ocean Mining Technology: Deep Ocean Water Utilization

Koji Otsuka and Kazuyuki Ouchi

Abstract Deep ocean water (DOW) is seawater found at depth of several-hundred meters or lower, and has attracted special interest as one of the renewable resources with great potential, since large amount of cold and stable DOW is renewed in thermohaline circulation such as the great global conveyer. DOW has also been focused as important resource for enhancing marine primary production because DOW contains much inorganic nutrients, such as nitrogen, phosphorus, and silica. In this chapter, we describe fundamental features of DOW and discuss the importance of utilization of DOW, from the viewpoint of sustainability of global environment. We also introduce several technologies of DOW utilizations, such as ocean thermal energy conversion (OTEC), air conditioning, fisheries application, agricultural application, freshwater production, and so forth. Finally, we propose a multipurpose DOW complex float, which generates electric power, freshwater, rare metal and fish ground from only DOW and surface seawater as a sustainable infrastructure.

11.1 Introduction

World population has increased rapidly following the industrial revolution, reaching 7.3 billion in 2016 (U.S. Census Bureau 2016). Several forecasts estimate that this number will rise to about eight billion in 2025 (see Fig. 11.1). Meadows et al. (2004) reveal serious problems concerning global water, food, and energy supply to meet the needs of this growing population. Growth in these resource productions has been accomplished through tremendous use of freshwater, chemical fertilizer, and fossil fuels. This, in turn, has resulted in depletion of water resources, expanding areas of infertile land, climate change, and so forth.

K. Otsuka (✉)
Osaka Prefecture University, 1-1, Gakuencho, Sakai, Osaka 599-8531, Japan
e-mail: otsuka@marine.osakafu-u.ac.jp

K. Ouchi (✉)
Ouchi Ocean Consultant Inc., 193-111 Nagakura, Karuizawa, Nagano 389-0111, Japan
e-mail: ouchi@athena.ocn.ne.jp

R. Sharma (ed.), *Deep-Sea Mining*, DOI 10.1007/978-3-319-52557-0_11

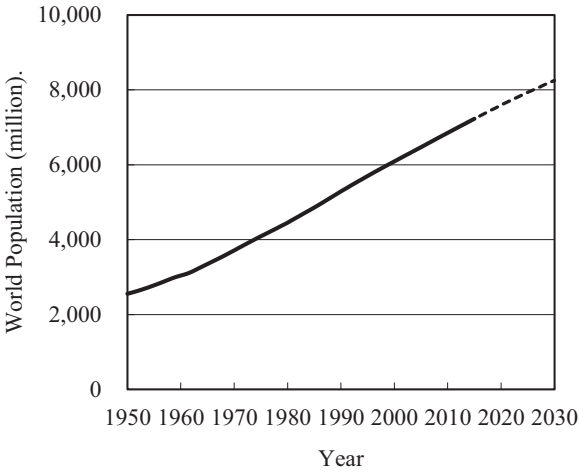

Fig. 11.1 Recent trend of world population (*solid curve*: statistical data, *dotted curve*: estimated data) (U.S. Census Bureau 2016)

It is well known that 70% of the earth surface area is covered by the ocean. The difference of three-dimensional capacity between ocean and land is much bigger than that of the surface area. While the average height of the land is 840 m, the average depth of the ocean is 3800 m. The ocean is also abundant in water and carbon resources, which are fundamental materials of organisms, and stores 97% of water and 85% of carbon on the earth. Therefore, it is necessary to change the land-based conventional production systems into the ocean utilization systems for sustaining human life with increasing world population.

Deep ocean water (DOW) is seawater found at depth of several-hundred meters or lower, and has attracted special interest as one of the renewable resources with great potential, since the large amount of cold and stable DOW is renewed in thermohaline circulation such as great global conveyer. DOW has also been focused as important resource for enhancing marine primary production because DOW contains much inorganic nutrients, such as nitrogen, phosphorus, and silica.

In this chapter, we describe fundamental features of DOW and discuss the importance of utilization of DOW, one of the renewable resources with great potential, from the viewpoint of sustainability of global environment. We also introduce several technologies of DOW utilizations, such as ocean thermal energy conversion (OTEC), air conditioning, fisheries application, agricultural application, freshwater production, and so forth. Finally, we propose a multipurpose DOW complex float, which generates electric power, freshwater, rare metal and fish ground from only DOW and surface seawater as a sustainable infrastructure. This could be one of the significant applications of deep-sea mining technologies as it involves circulation of deep ocean waters while lifting minerals from the seafloor to the surface.

11.2 Features of Deep Ocean Water

DOW has several remarkable features, such as low temperature, high nutrient concentration, and low viable bacterial count, in comparison with surface ocean water. In this section, we describe those fundamental features and their causes, and discuss about consumable capacity from the viewpoint of sustainability of global environment.

11.2.1 Water Temperature

Figure 11.2 shows a typical vertical profile of year-averaged water temperature in subtropical area in Pacific Ocean. Water temperature in the surface mixed layer is around 25 °C, while the temperature drastically decreases with increasing water depth at −100 m or lower, and reaches 5 °C at the depth of 1000 m.

This "low temperature" characteristic is caused by global thermohaline circulation. Stommel and Arons (1960) proposed an abyssal circulation model, which is based on a lot of ocean monitoring data and geophysical theory. They estimated budget of transports in various portions of the world ocean using the model. The estimated results suggest that seawater of 40 Mt/s circulates in deep layer and distributes to each ocean in proportion to the volume of each ocean as shown in Fig. 11.3. This means that those amounts of DOW are renewed by a great global conveyer.

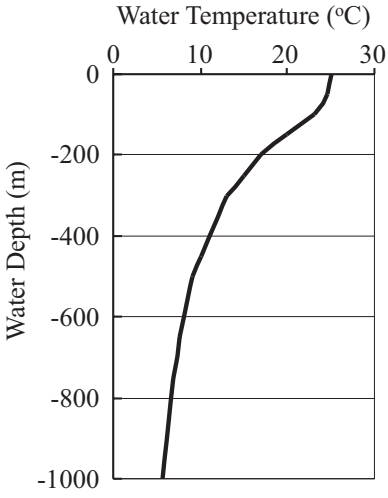

Fig. 11.2 Typical vertical profile of year-averaged water temperature in subtropical area in Pacific Ocean

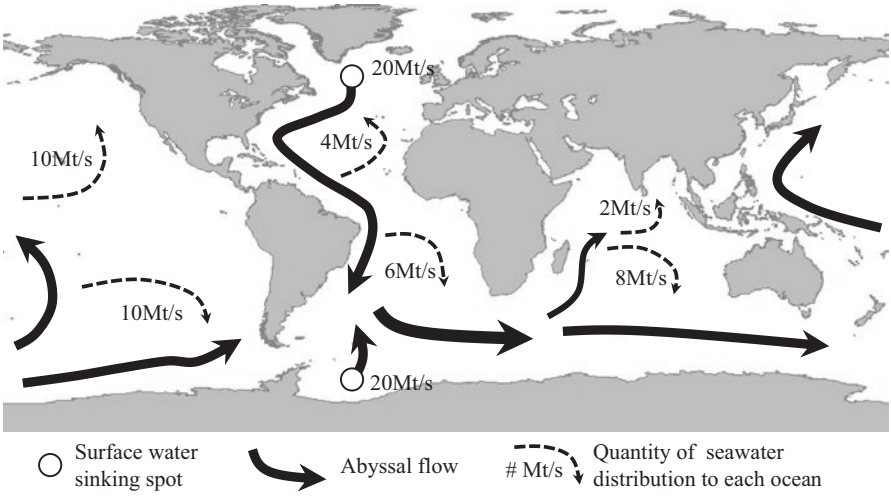

Fig. 11.3 Sketch of abyssal circulation and quantity of seawater distribution to each ocean (based on sketches by Stommel and Arons 1960)

11.2.2 Nutrient Concentration

Figure 11.4 shows a typical profile of year-averaged nitrate concentration in subtropical area in Pacific Ocean. While the nitrate concentration is almost zero at the surface layer, the value drastically increases with increasing water depth, and has a peak at the depth of −700 m.

This "high nutrient concentration" characteristic is caused by biological pump. Inorganic nutrients in euphotic zone are rapidly utilized by primary producers, such as phytoplankton in the photosynthesis process. The organisms thus produced finally change into detritus via grazing, feeding, evacuation, and natural death. This detritus sinks to the deep ocean with decomposition by bacteria. The nutrients reproduced by the decomposition are stored in the deep ocean since there is not enough light intensity for photosynthesis. Therefore, DOW contains a lot of inorganic nutrients and very little organic matters and its dependent bacteria (see Fig. 11.5).

11.2.3 Viable Bacterial Count

Figure 11.6 shows a typical profile of year-averaged viable bacterial count in subtropical area in Pacific Ocean. The viable bacterial count in the surface layer is large, because of active material circulation and large detritus concentration as shown in the previous section. However, the value drastically decreases with increasing water depth, and reaches close to zero at the depth of −500 m or deeper, since only decomposition occurs in the intermediate or deep layers. This "low viable bacterial count" is also caused by biological pump.

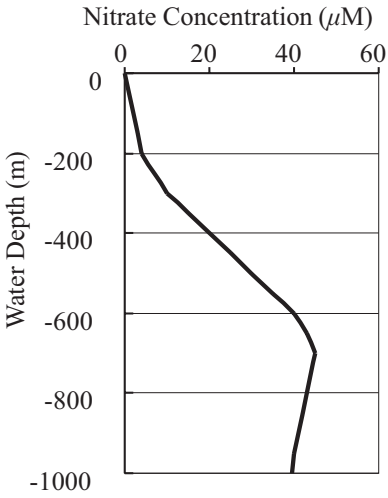

Fig. 11.4 Typical vertical profile of year-averaged nitrate concentration in subtropical area in Pacific Ocean

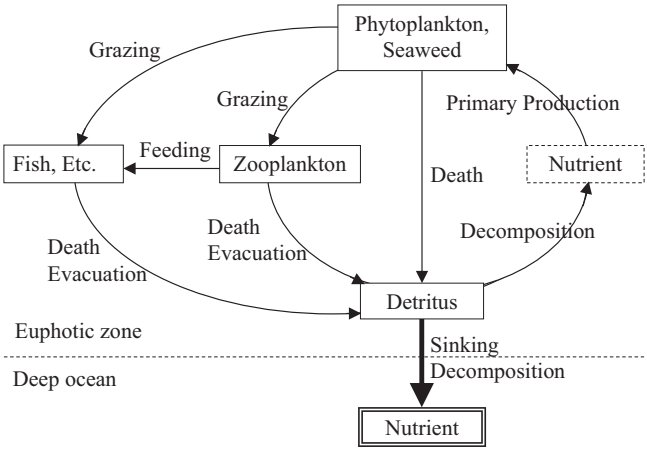

Fig. 11.5 A conceptual diagram of simplified marine material circulation

11.2.4 Consumable Capacity of DOW

Some researches on total capacity of ocean thermal energy have been carried out (e.g., Avery and Wu 1994). However, these estimations are based on the capacity of seawater as a thermal energy reservoir. Takano (1984) suggested that the great global conveyer is strongly linked with the climate system, and proposed that the consumable capacity of DOW may be 10% of the production rate of North Atlantic Deep Water (NADW) as the limit for keeping the driving force of the great global conveyer. It is very important to decide the consumable capacity based on the reproduction rate (or flux) when we consider the sustainable development of the

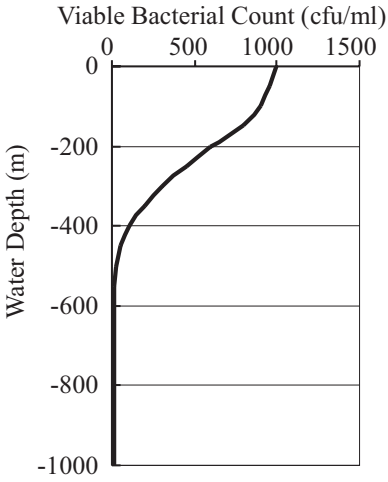

Fig. 11.6 Typical vertical profile of year-averaged viable bacterial count in subtropical area in Pacific Ocean

Table 11.1 Consumable capacity of DOW in each ocean, assuming that 1% of reproduced DOW is consumable

	DOW flux (Mt/s)	Consumable capacity	
		(Mt/s)	(Mt/day)
North Pacific Ocean	10	0.10	8640
South Pacific Ocean	10	0.10	8640
North Atlantic Ocean	4	0.04	3460
South Atlantic Ocean	6	0.06	5180
North Indian Ocean	2	0.02	1730
South Indian Ocean	8	0.08	6910

renewable resources. However, it is very difficult to fix the percentage of production rate to keep the present climate steady. For example, to know the limiting condition for keeping the driving force of the great global conveyer, we need to develop a huge scale computer program, which can accurately simulate the relationship between the climate system and the great global conveyer. Though many researchers claim to have developed such a program, it still remains long way to obtain some reliable results. However in this section, it is assumed that only 1% of reproduction rate (or flux) is consumable as a temporary standard.

Table 11.1 shows the DOW fluxes derived from great global conveyer in each ocean shown in Fig. 11.3, and consumable capacities based on the above assumption. The consumable capacity in each ocean can be obtained by multiplying the each DOW flux to 1%. The right column of the table shows the consumable capacity as a flow rate per day. These numbers represent the maximum numbers of 1 Mt/day-size DOW utilization facilities, which are possible to install in each area. 1 Mt/day-size system approximately corresponds to 5 MW-size OTEC plant. This table demonstrates that huge amount of DOW is consumable in each ocean.

11.3 Deep Ocean Water Applications

DOW has three significant features, such as low temperature, high nutrient concentration, and low viable bacterial count. Utilizing these features, various DOW applications have been developed as shown in Table 11.2. In this section, we introduce several technologies of DOW utilizations, such as OTEC, air conditioning/refrigeration, fisheries application, agricultural application, freshwater production, and so forth.

11.3.1 Ocean Thermal Energy Conversion (OTEC)

Ocean thermal energy conversion (OTEC) is based on the use of the temperature differential between cold DOW and warm surface water to generate electricity. There are two basic types of OTEC systems (Avery and Wu 1994). In the closed-cycle system (CC-OTEC) , a low boiling point working fluid (e.g., ammonia) is alternately evaporated by the surface water and condensed by the DOW (see Fig. 11.7). A turbine generator is employed to extract a portion of the thermal energy received from the warm surface water. For the open-cycle system (OC-OTEC), surface water is flash-evaporated in vacuum chamber and condensed by the DOW. This process can produce desalinated freshwater as a by-product.

Recently, two prototype OTEC facilities have been constructed in Japan and Hawaii one after another. In April 2013, an operation of a 50 kW-scale OTEC pilot plant started in Kumejima Island in Okinawa, Japan. In August 2015, another 100 kW-scale OTEC experimental facility opened in Big Island in Hawaii.

11.3.2 Air Conditioning

Air conditioning systems utilizing DOW use only small fractions of the electrical power required for conventional systems and have been demonstrated to be reliable and cost-effective (Van Ryzin and Leraand 2000). Additional benefits cited include

Table 11.2 Various DOW applications and the features that they utilize

Applications	Low temperature	High nutrient concentration	Low viable bacterial count
OTEC[a]	O		
Air conditioning	O		
Refrigeration	O		
Fisheries application	O	O	O
Agricultural application	O		O
Freshwater production			O
Food production			O
Medical application			O
Healthcare application			O

[a]Ocean thermal energy conversion

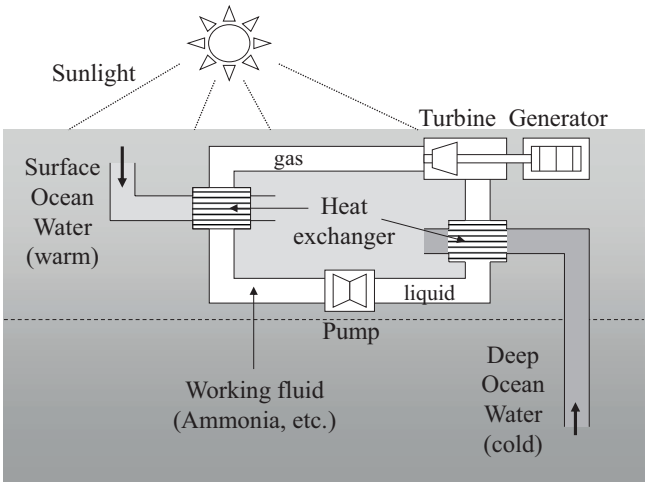

Fig. 11.7 Conceptual sketch of closed-cycle ocean thermal energy conversion (CC-OTEC)

the availability of the refrigeration for food storage system, and ice production. A typical example of air conditioning can be observed at an office building of Natural Energy Laboratory of Hawaii Authority (NELHA) in Big Island, Hawaii. NELHA Gateway Center building is also a good place to learn a technology of DOW air conditioning.

11.3.3 Fisheries Application

Land-based DOW aquaculture was first conducted in the U.S. Virgin Island (Roels et al. 1979). These experiments demonstrated that the utilization of the nutrient-rich DOW significantly raises the yields of microalgae and seaweed, and the high purity and the ability of water temperature control of DOW greatly increase growth rates of fish, shellfish, lobsters, and so forth. At present, several commercial fisheries facilities using DOW operate at NELHA in Hawaii, and Kumejima Island in Japan.

11.3.4 Agricultural Application

Soil temperature control for agriculture was first performed at NELHA in Big Island, Hawaii (Daniel, 1992). Thin cold water pipes are stretched around cultivated lands to cool the soil. Dewdrops made on the thin cold water pipes give moistures. Some vegetables and fruits, which are usually cultivated in cold district, can be harvested in such a tropical island. This technology is applied to several vegetable cultivation research facilities in Japan (e.g., Okinawa Prefectural Deep Seawater Research Center in Kumejima Island).

11.3.5 Freshwater Production

There are two types of desalination processes. One is a thermal process, such as single or multistage flash distillation. The open-cycle OTEC includes this process as shown above. Another is a membrane process, including reverse osmosis (RO) and electrodialysis. Surface water desalination using the membrane process requires troublesome pre- and posttreatments, such as suspended material filtration and sludge drain. These treatments can be omitted in the membrane desalination using DOW containing very little suspended materials. In Japan, most of desalination systems adopt the membrane process because of the cost-effectiveness.

11.3.6 Other Applications

Medical and health care uses were focused as one of the DOW applications in Japan since 1990s. Researches on treatment of allergic dermatitis have been carried out in some places in Japan. DOW applications for cosmetics have been also focused in Japan and Taiwan. A thalassotherapy facility using DOW opened in 1998 in Toyama prefecture in Japan. After that, some similar facilities have been constructed. The other DOW applications are in production of beverages and eatables. A lot of merchandises are sold in Japanese and Taiwanese markets. They are very popular, because they are tasty and good for health.

11.4 Multipurpose DOW Complex Float

There are many isolated islands in the ocean and almost all of those islands were made by volcanic activity of the earth. The shape of the islands is very similar to a volcanic mountain on land but the base is at the ocean seafloor about 4000 m under the sea surface. Hence, it is relatively easy to make use of DOW because the surrounding sea is very deep.

These isolated islands suffer from unstable supply of basic resources such as energy, water, and food. Stable, reliable, and independent infrastructure is required for the security of such islands. Research on multiple utilization of DOW is carried out in order to fulfill such demands of infrastructure for these isolated islands. Ouchi et al. (2007) proposed spar type tethered floating construction around the island, which draws DOW from 800 m depth and surface water. The installation produces electric power, freshwater, phytoplankton, and lithium from the DOW and surface water.

11.4.1 Concept of the Float

Figure 11.8 shows a schematic diagram of the offshore DOW float which is performing as an infrastructure for generating electric power, freshwater, lithium, and phytoplankton. In this case, the length and width of the island are 4 km and 1 km,

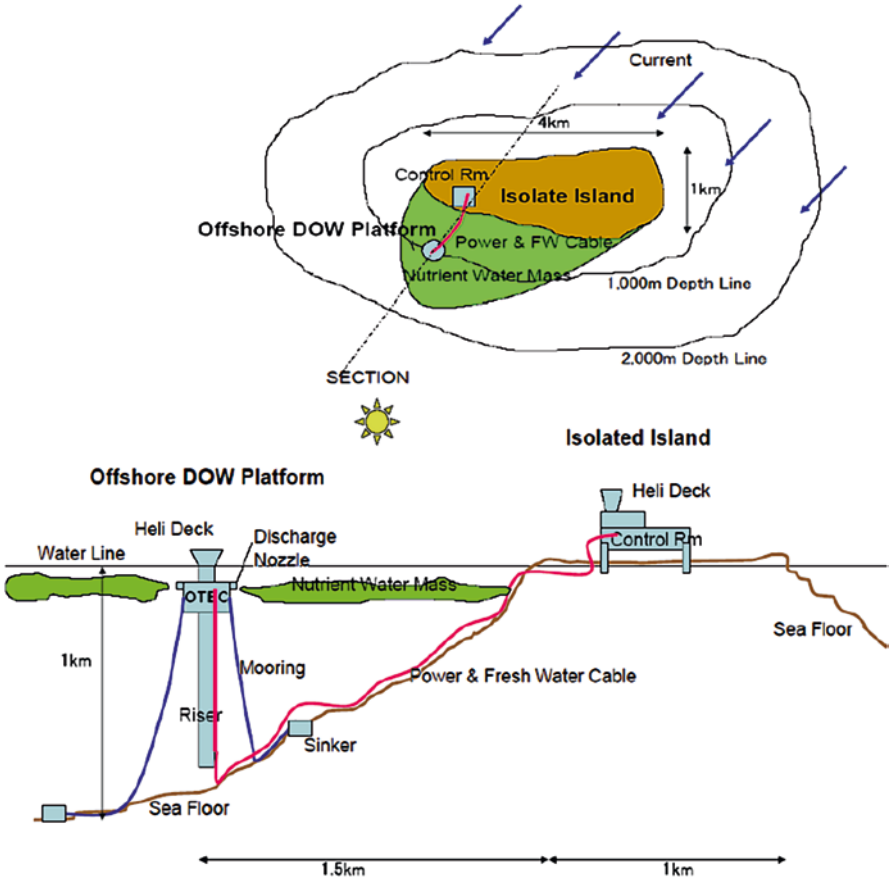

Fig. 11.8 Setup of the offshore DOW float (plan)

respectively, and current direction is almost same through the year. The float is set with mooring chain/wire and anchors on the other side of the island where seawater is not affected by the currents as shown in Fig. 11.8. The length of DOW riser pipe is about 800 m to take enough cold and nutrient-rich water.

11.4.2 Function of Multiple Systems

The principal function and multiple systems of the offshore DOW float systems are as follows, and comprehensive skeleton diagram is shown in Fig. 11.9.

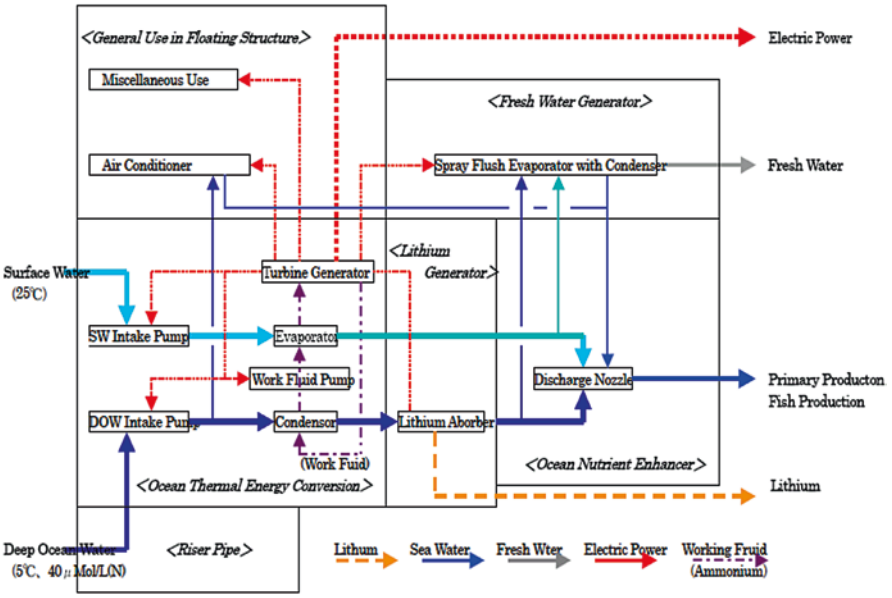

Fig. 11.9 Flow diagram and functions of the DOW complex float

11.4.2.1 Material Input

- *Deep ocean water (DOW)*
  Depth: 800 m, Temperature: 5 °C, Nitrate Salt Density: 40 μmol/L
- *Surface water*
  Depth: 5 m, Temperature: 25 °C

11.4.2.2 Production Output

- *Electric power*
  OTEC (Ocean Thermal Energy Conversion) using Uehara cycle generates significant net electric power (70% of gross power), and the power is sent to the island with an electric power cable in the seafloor.
  - *Freshwater*
    Freshwater is generated as a by-product of OTEC power generation
  - *Phytoplankton*
    After using DOW as the OTEC condenser cooling water, DOW is mixed with surface water and discharged on the surface layer. Nutrient-rich salt of DOW enhances primary productivity due to photosynthesis in the sea which is the base of food chain in the sea.

- *Lithium*
  Lithium whose demand is increasing for advanced battery is collected more effectively from DOW.

11.4.2.3 Means and Apparatus

- *Spar type semi-submerged hull*
  The hull has a column of small water plane area in order to avoid the wave motion, and upper and lower structure those are allotted for control space and engine plant space, respectively. This concept of hull design is well established at the ocean nutrient enhancer TAKUMI in Sagami Bay by one of the authors (Ouchi) in the period of 2003–2008.
- *Riser pipe and drawing pumps*
  The pumps cause upwelling of DOW with the long vertical riser pipe suspended from the hull, drawing the surface water and sending them to the heat exchangers of OTEC plant.
- *OTEC plant*
  The plant generates electric power using advanced OTEC technology "Uehara Cycle" which is fitted with new concept titanium plate heat exchanger and using ammonium/water mixture working fluid. The net output power generation excluding self-consuming power such as pumps, control devices, is 70% of gross power generation in case of 25 °C temperature difference between DOW and surface water.
- *Freshwater production plant*
  The spray-flush type freshwater generator produces significant amount of freshwater using remaining temperature difference after OTEC operation.
- *Lithium absorber*
  The absorber is fitted in the huge waterway of DOW in order to absorb lithium in the seawater efficiently in low temperature condition.
- *Ocean nutrient enhancer*
  The DOW still having rich nutrient salt after the above operation is mixed with surface water and discharged into the euphotic layer of the sea where the sunlight is enough to create photosynthesis, with the density current generator proposed by Ouchi et al. (2008) in the enclosed bay of Gokasyo-wan and Ouchi et al. (2002) in the open sea of Sagami-wan.
- *Transportation apparatus*
  The hull is fitted with helicopter port on the upper deck, boat mouth near the water revel, and elevator lift from the upper deck to the bottom of lower hull.
- *Draft adjustment apparatus*
  For the maintenance of hull, OTEC and other plants, water ballast tanks and filling/discharging pumps are provided.
- *Accommodation and control room*
  Watch and Control rooms and accommodations are provided for the operation crew.

11.4.2.4 Method of Operation

- *Operation crew*
  For operating the multiple systems of the float, the crew stays in the float continuously.
- *Maintenance*
  Periodical maintenance is done by land-based team.

11.4.3 Design of the 5 MW Type DOW Float

The basic design of 5 MW (gross) type DOW complex float is carried out in order to supply electric power, freshwater and fishing ground for the small isolated island whose population is about 3000 people. It is assumed that the island is located in the pacific equatorial ocean, so that design conditions are very severe as below.

Maximum wind velocity: 50 m/s
Significant wave height: 12 m
Maximum wave period: 14 s

Table 11.3 and Fig. 11.10 show principal particulars and general arrangement of the 5 MW-Class Offshore DOW complex float.

Table 11.3 Key particulars of the 5 MW-class DOW float

Floating structure	Spar type with submerged floating structure
Height	65 m
Diameter	54 m
Draft (opening)	40 m (except for riser pipe)
Draft (surfacing)	16 m (except for riser pipe)
Discharge seawater	48,000 t/h
Volume of plant room	23,000 m^3
Volume of water ballast tank	15,000 m^3
Volume of pool for SOW	1420 m^3
Volume of pool for DOW	780 m^3
Volume of pool for discharge seawater	2600 m^3
Diameter of riser pipe × depth	2.6 m × 760 m
Intake of DOW × depth	625,000 m^3/day × 800 m
Intake of SOW × depth	1,250,000 m^3/day × 5 m
Discharge seawater × depth	1,875,000 m^3/day × 20 m
Power generation (gross)	5000 kW
Power generation (net)	3000 kW
Mooring system	Multipoint catenary mooring with anchor, chain, and wire
Power cable	Laying on the bottom of the sea with intermediate buoy. Composite cable with power cable, optical cable, and pipe for water

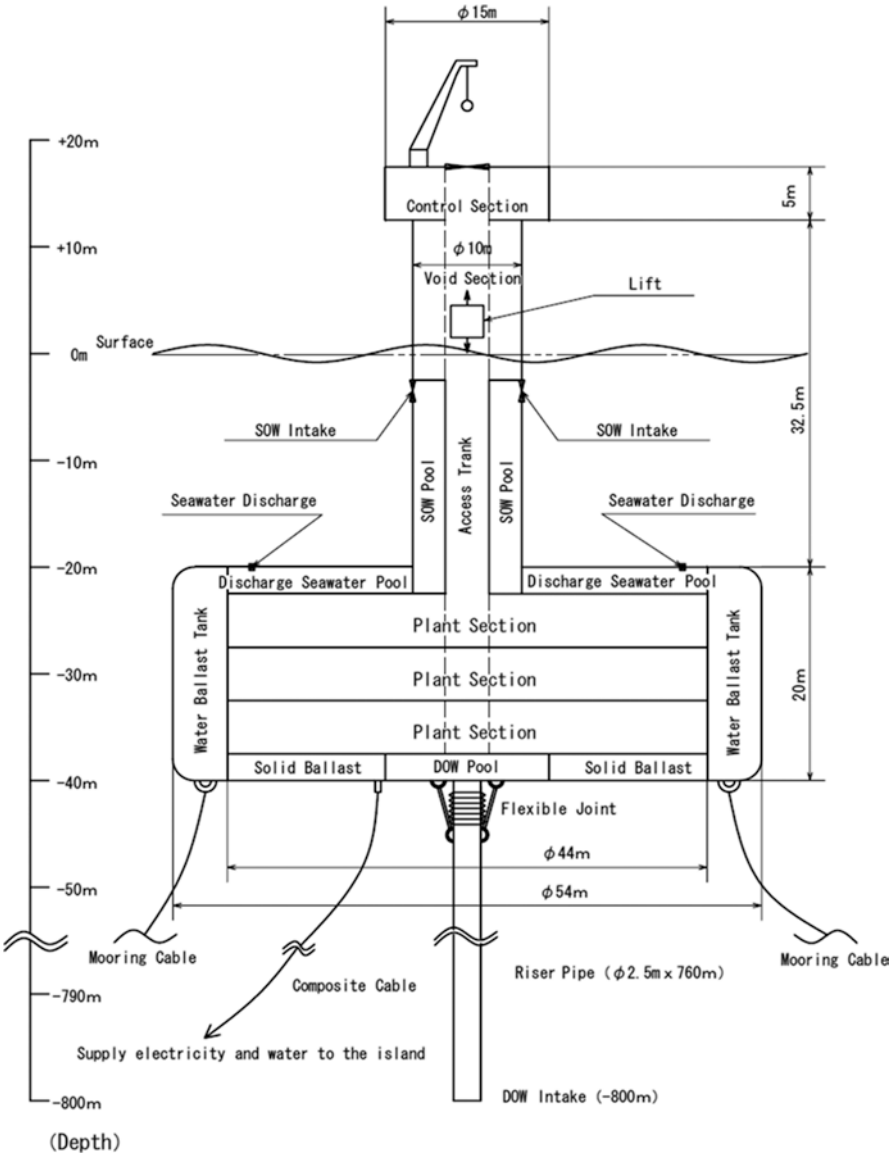

Fig. 11.10 General arrangement of the 5 MW-class DOW float

In order to maintain the reliability of moorings and stability of operations, reduction of the ship motion against rough sea condition is very important. Hence, small water plane mono-column spar type construction as shown in Fig. 11.10 was adopted.

The float is fitted with permanent solid ballast for stability and the water ballast tanks are provided for lifting up the float to the level of the maintenance draft by discharging the ballast water. The solid ballast, water ballast tank and water pool are located outside the engine plant area to prevent collision from outside.

The multi-wire/chain catenary mooring system is adopted in order to restrict turning of the float to avoid winding around the power cable to the shore.

11.4.4 Feasibility Study on the DOW Float

The estimation of price, cost, and profit for manufacturing, setting-up, operation, and running is carried out in case of 1 MW-, 10 MW-, and 100 MW-class DOW complex floats that can produce electricity, freshwater and enhance fisheries, but does not include lithium production. Table 11.4 shows the summary of the estimation and as it is known that the larger system is more profitable than smaller one. From this study, profit of the 5 MW-class DOW complex float seems almost on the breakeven point. Whereas, OTEC alone works out high cost for power generation, the multiple DOW complex float is able to produce not only electricity but also freshwater, fisheries, and lithium. The cost of the platform is shared with each production and it offers significant competitiveness against other renewable power generation systems such as solar heat, photovoltaic, wind turbine, and others.

11.4.5 Conclusion

New concept to make multiple use of DOW is proposed as the offshore DOW platform which produces electric power, freshwater, lithium, and enhances fish production via phytoplankton bloom. The integrated study on each system is carried out and the 5 MW-Class DOW complex float is designed for an isolated island in the equatorial ocean. Also, the estimation of production price and running cost is carried out for various sizes of DOW complex floats. From these studies, it is known that the proposed offshore DOW complex float is profitable in case of more than 5 MW-class size, whose illustration is shown in Fig. 11.11.

We would like to call the system of the isolated island with such a DOW complex float “Ekmene in the Sea.” Here, Ekmene originated from Greek term means the place where the humans can live.

Table 11.4 Price cost and profit estimation of the offshore DOW float "Ekmene in the Sea"

	Item	Unit	0.2×10^6 m^3/day	2×10^6 m^3/day	20×10^6 m^3/day	Remarks
Size	Upwelling capacity	m^3/h	8,333	83,333	833,333	SOW: 25 °C, DOW: 5 °C
	Temperature difference	°C	20	20	20	
	Diameter of riser pipe	m	1.2	3.8	12.1	Velocity in pipe: 2.0 m/s
	Diameter of float	m	30	95	300	
	Displacement of float	ton	4,500	45,00	450,000	
Price	Gross output power	kW	1,083	10,833	108,333	0.13 kW/m^3/h
	Net output power	kW	758	7,583	75,833	70% of gross output power
	Energy (incl. desalination)	10^5 kWh/year	598	5,979	59,787	Rate of operation: 0.9 × 365 days
	Energy (excl. desalination)	10^5 kWh/year	434	4,336	43,362	Rate of operation: 0.9 × 365 days
	Selling price of electricity	10^6 US$/year	0.7	6.5	65.0	US$0.15/kWh, ¥/US$=100
	Fresh water (0.5% of DOW)	ton/year	328,500	3,285,000	32,850,000	Rate of operation: 0.9 × 365 days
	Energy consumption for desalination	10^5 kWh/year	164	1643	16425	Required energy: 5 kWh/ton
	Selling price of fresh water	10^6 US$/year	0.3	3.3	32.9	US$1.5/ton, ¥/US$=100
	Primary production (carbon weight)	ton/year	233	2,328	23,279	Density of nitrate: 40 μmol/L
	Fish production (wet weight)	ton/year	931	9,312	93,116	In terms of Anchovy (Iseki 2000)
	Selling price of fish	10^6 US$/year	0.5	9.3	93.1	50% catch, US$1.0/kg, ¥/US$=100
	Total selling price	10^6 US$/year	1.4	19.1	191.0	
Cost	Personal cost	10^6 US$/year	1.0	2.0	4.0	(10/20/40 persons) × US$10 × 10^6/year
	Maintenance cost, etc.	10^6 US$/year	0.4	2.3	12.4	1% of construction cost/year
	Depreciation of initial cost	10^6 US$/year	2.2	11.5	61.8	Fixed depreciation: 20 years, Interest: 0
	Total initial construction cost	*10^6 US$*	*44.0*	*230.7*	*1,235.8*	
	Floating structure	*10^6 US$*	*25.0*	*116.0*	*538.6*	*2/3*
	OTEC plant	*10^6 US$*	*15.0*	*94.6*	*597.2*	*0.8*
	Desalination plant, etc.	*10^6 US$*	*4.0*	*20.0*	*100.0*	
	Total cost	10^6 US$/year	3.6	15.8	78.1	
Profit (selling price–cost)		10^6 US$/year	−2.2	3.3	112.9	

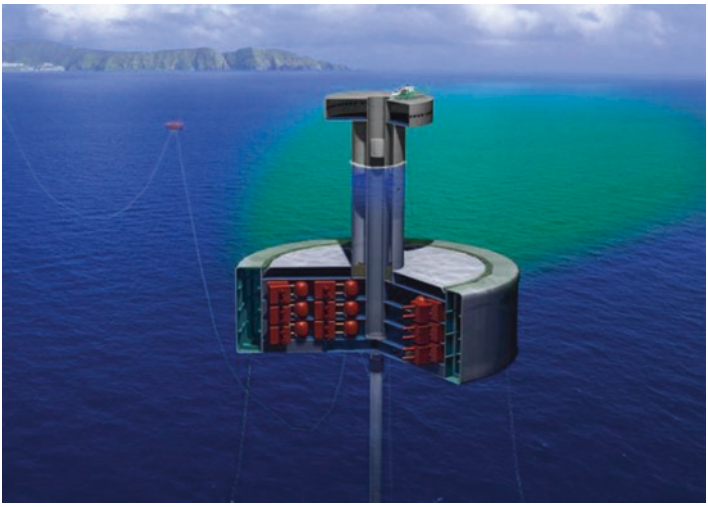

Fig. 11.11 Image of "Ekmene in the Sea"

References

Avery WH, Wu C (1994) Renewable energy from the ocean: a guide of OTEC. Oxford University Press, New York

Daniel TH (1992) An overview of ocean thermal energy conversion and its potential by-products. In: Proceedings of Pacific Congress on Marine Science and Tech, PACON-92, pp 263–272

Meadows D, Randers J, Meadows D (2004) Limits to growth—the 30-year update. Earthscan, New York

Ouchi K, Ogiwara S, Kobayashi E, Fukushima K, Yonezawa M, Kato K (2002) Ocean nutrient enhancer—creation of fishing ground using deep ocean water. In: Proceedings of OMAE'02, Oslo Norway

Ouchi K, Jitsuhara S, Watanabe T (2007) Concept design for offshore platform generating electric power, fresh water and nutrient sea (in Japanese). In Conference Proceedings of the Japan Society of Naval Architects and Ocean Engineers, vol 4, pp 205–208

Ouchi K, Otsuka K, Nakatani N, Yamatogi T, Awashima Y (2008) Effects of density current generator in semi-enclosed bay. In: Proceedings of OCEANS 2008

Roels OA, Laurence S, Van Hemelryck L (1979) The utilization of cold, nutrient-rich deep ocean water for energy and mariculture. Ocean Management 5:199–210

Stommel H, Arons AB (1960) On the abyssal circulation of the world ocean—II. An idealized model of the circulation pattern and amplitude in oceanic basins. Deep-Sea Res 6:217–233

Takano K (1984) Ocean energy (in Japanese). Kyoritsu Science Books Series 69, Kyoritsu Shuppan, Tokyo

U.S. Census Bureau (2016) U.S. and World Population Clock. http://www.census.gov/popclock/

Van Ryzin J, Leraand T (2000) Air conditioning with deep seawater: a cost-effective alternative. In: Ocean resource 2000, pp 37–40

Prof. Koji Otsuka graduated from Department of Naval Architecture, Osaka Prefecture University (OPU) in 1987. He took Masters and Doctoral Degrees in Engineering from OPU in 1989 and 1993, respectively. After taking Master Degree, he served as a research associate at the College of Engineering in OPU. Before he was assigned a professorship at College of Sustainable System Sciences in OPU in 2012, he was a visiting researcher at University of Hawaii for 1995–1996, an assistant professor at College of Engineering in OPU for 1997–1999, as an associate professor at College of Engineering in OPU for 1999–2007, and a professor at College of Engineering in OPU for 2007–2012. He is now a dean of College of Sustainable System Sciences in OPU.

Dr. Kazuyuki Ouchi graduated from The University of Tokyo, Department of Naval Architect in 1970, he Joined Mitsui OSK Lines Ltd. in 1971, he awarded prize from The Ministry of Trade Japan for the invention of "PBCF (Propeller Boss Cap Fins)" in 1991. After obtaining Ph.D degree from the University of Tokyo in 1994, he established Ouchi Ocean Consultant, Inc. In 2004, he awarded the prize from The Society of Naval Architects of Japan for the development of Ocean Nutrient Enhancer "TAKUMI" In 2008 he invited from the University of Tokyo as a professor, and now the leader of The Wind Challenger Project which is the next generation sailing vessel.

Part III
Metallurgical Processing and Their Sustainable Development

Chapter 12
Metallurgical Processing of Polymetallic Ocean Nodules

R.P. Das and S. Anand

Abstract During the last five decades metallurgical processing of polymetallic nodule is of global interest—as well as a challenge—for researchers, and industries. This has generated a vast knowledge base, but till now there is no commercial operation. Some of the main reasons are: (1) lack of a techno-economically feasible mining operation, (2) poor economics of metal extraction, in comparison with similar terrestrial resources, and (3) environmental impact of mining as well as metal extraction. For metallurgists, the processing of polymetallic nodules becomes more challenging with passage of time because the environmental and processing norms keep changing for lean resources like polymetallic nodules. Considering the processes developed for nodule, and the current trend, the authors feel (1) production of alloy pig iron for use in series 200 stainless steel, and (2) aqueous reduction processes based on sulphuric acid, HCl/Cl_2, or ammonia under atmospheric conditions hold good promise for a cost-effective, low capex, and environmentally accepted process.

12.1 Introduction

With the development of mankind, there is a growing need for resources, including the mineral resources. Considering the history of mankind, there is a very strong demand for mineral resources during the last two centuries, compared to any other time in the history. A part of the reason is rapid growth in population during the last two centuries. It is estimated that the population in the world has grown from 900 million in 1800 to the current level of six billion. Such sixfold increase in population has placed a high demand on all the resources and especially on energy and minerals. It is estimated that the earth will have a population of ten billion by the year 2050. In addition, this population will not be evenly distributed, creating heavy local demand for minerals. Thus there will be a scarcity of minerals, and the extent of scarcity will depend on the geographic location. In order to meet local demand for minerals, several countries are planning to exploit the sea as resource base.

R.P. Das (✉) • S. Anand
Regional Research Laboratory (Currently Institute of Minerals and Materials Technology), Bhubaneswar, Orissa, India
e-mail: drrpdas@yahoo.com

R. Sharma (ed.), *Deep-Sea Mining*, DOI 10.1007/978-3-319-52557-0_12

The seas have several types of minerals, which can be used for different human activities. These are classified as primary and secondary minerals. Some of the important primary minerals are: (1) Polymetallic nodules, (2) Massive sulphides, (3) Metalliferous mud (Red sea), (4) Calcium carbonates (from coral, bryozoan sands, and calcareous algae), (5) Phosphatic pellets, phosphatic concretions, massive beds of phosphates, (6) Silica of the diatom, and (7) Sea salts (chlorides, iodides, bromides, sulphates of Mg, Na, K). The nodules, massive sulphides, and metalliferous mud have drawn a lot of attention as potential sources of metals like Cu, Ni, Co, and Mn. The technology for mining the minerals from deep sea is on its way to be established. Though the estimated cost of mining is presently higher than that of land mining, in times to come it is projected to be competitive with that for land mining. Out of all the minerals, polymetallic nodules have emerged as the most likely candidate for exploitation, because it is spread over most of the oceans in the world, and it is abundantly available. This has led to a worldwide effort to develop metallurgical processes for treating polymetallic nodules. Attempts to process polymetallic nodules started almost 50 years back, as an aftermath of the oil crisis. Several oil companies visualized large-scale ocean mining, where their expertise on high-sea operations could be useful. This led to formation of several consortiums. This chapter will discuss the developments that have taken place in processing the nodules over last five decades with emphasis on more recent developments.

12.1.1 Polymetallic Nodule as an Ore

As a metallurgical ore, polymetallic nodule is very different from terrestrial deposits. A typical chemical composition of nodules from different locations in the world is shown in Table 12.1 (Kotlinski 1999). This may be compared with commercially used terrestrial deposits—~40% Mn in manganese ore, ~2.5% Ni in sulphidic nickel ore, ~1% Cu in sulphidic copper ore, and ~0.2% Co in ores—used for cobalt extraction. Besides the major elements, nodule also contains several minor elements which may

1. Interfere in the extraction of major elements as contaminants
2. Make the effluent from a processing plant environmentally unacceptable
3. Contribute to the revenue, if economically extracted

Most metallurgical processes, based on terrestrial deposits, would incorporate a beneficiation stage which upgrades the metal content of the ore. The nodule has a core which could be a rock, a shark tooth, or some other hard material containing little metal. It also contains as much as 30% seawater. The nodules are not amenable to conventional upgradation and hence need to be processed as mined.

Table 12.1 Chemical composition of polymetallic nodule from different locations (Kotlinski 1999)

Regions and fields	Mean metal content																					
	Mn (%)	Fe (%)	Ni (%)	Cu (%)	Co (%)	Mo (%)	Ti (%)	Zn (%)	Pb (%)	Zr (%)	V (%)	Au (ppm)	Pt (ppm)	Y (ppm)	La (ppm)	Ce (ppm)	S + P + As (%)	SiO_2 (%)	Al_2O_3 (%)	CaO (%)	MgO (%)	Ni_E [a]
North-East Pacific Basin																						
Clarion-Clipperton 2186 thou. km^2	27.24	6.29	1.216	1.022	0.214	0.057	0.374	0.152	0.053	0.054	0.042	0.0204	0.104	264.16	152.99	303.26	0.2971	15.15	5.04	2.66	3.20	6.3
Peru Basin																						
Peru 1018 thou. km^2	33.43	5.76	1.249	0.659	0.082	0.067	0.259	0.147	0.042	0.064	0.051	0.0025	–	3.07	35.33	72.18	0.3502	11.95	4.80	2.72	2.70	5.79
Central-Pacific Basin																						
Central-Pacific 1960 thou.km^2	21.49	9.63	0.763	0.696	0.237	0.042	0.695	0.092	0.050	0.086	0.042	0.0083	0.085	135.00	119.00	552.50	0.4635	13.62	4.58	2.75	3.10	5.2
South-West-Pacific-Basin																						
Menard 1244 thou. km^2	19.95	12.50	0.835	0.357	0.344	0.043	0.759	0.064	0.112	0.056	0.045	0.0022	–	138.33	100.00	–	0.072	16.09	6.03	2.18	2.46	5.1
Mid-Indian-Basin																						
Central-Indian 1470 thou. km^2	22.68	9.00	0.931	0.798	0.141	0.030	0.266	0.112	0.052	0.036	0.034	0.0070	0.120	–	–	–	0.208	17.36	4.14	2.80	2.68	5.7
South-Australian-Basin																						
Diamentina 867 thou. km^2	22.73	12.02	0.829	0.407	0.190	–	0.518	0.149	0.100	–	–	0.0300	0.047	–	–	–	0.468	17.12	5.41	2.62	2.79	4.96

[a]Ni_E nickel index, calculated as: $Ni_E = 1.0\ Ni + 0.13\ Mn + 0.25Cu + 5.0\ Co$. It indicates the value of the nodule in terms of its metal content

12.1.2 Considerations for Metallurgical Processing of Nodule

The nodules contain about 2.5% Cu, Ni, and Co, which are considered high value metals. Over the last decade, a strong demand for terrestrial manganese ore has made extraction of Mn from nodules a viable proposition. In addition to extraction of these four metals, other considerations for processing nodules include

1. High moisture content (~30%)
2. Operation of a process under ambient pressure and moderate temperature
3. Tolerance of the process to seawater
4. Selectivity for metals of concern
5. Low consumption of reagents
6. Low toxicity of reagents
7. Acceptable environmental impact
8. Competitive with processes for terrestrial deposit
9. Economical for three metals (Cu, Ni, and Co) and/or four (Cu, Ni, Co, and Mn) metals
10. No or safe disposal of effluents

12.2 The First Phase of Development of Metallurgical Processes for Nodules (1970–1985)

The first work on metallurgical process development was started during 1970s by four main investigating agencies for recovery of Cu, Ni, and Co or Cu, Ni, Co, and Mn. They were: The Kennecott Corporation, Deep Sea Ventures, The Métallurgie Hoboken-Overpelt, and The International Nickel Company (INCO). In addition, several individual researchers and laboratories also contributed to different aspects of metallurgy of nodules. These processes are briefly described in the following paragraphs.

12.2.1 The Cuprion Process

For aqueous processing of polymetallic nodules, it was recognized that the most important step is reduction of Mn(IV) to Mn(II). Such reduction helps in breaking the manganese matrix, and allows the metals of interest, namely Cu, Ni, and Co to react with a lixiviant like ammonia. Reductive leaching process was pioneered by Kennecott Copper by using CO as a reducing agent under ammoniacal condition (Agarwal and Wilder 1974, 1975; Agarwal et al. 1978, 1979; Sazbo 1976). Kennecott Copper operated a 250 kg/day pilot plant based on 'Cuprion' process. Carbon monoxide reduces Cu(II) to Cu(I) in solution. In turn, Cu(I) is used for the reduction of Mn(IV) as shown below. The name 'Cuprion' is derived from this important role of

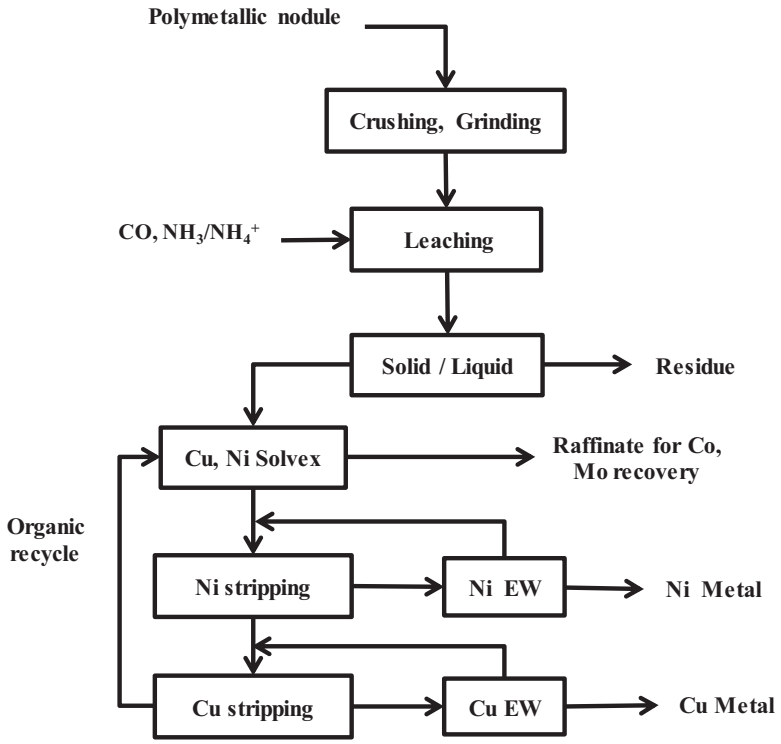

Fig. 12.1 Schematic flowsheet of Cuprion process. Developed by Kennecott

Cu(II)—Cu(I) couple. The metals of interest, namely Cu, Ni, and Co, form soluble complexes with ammonia while manganese and iron are rejected as residue. Schematically, the process is shown in Fig. 12.1. The main reactions taking place during leaching are:

$$MnO_2 + 2Cu\left(NH_3\right)_2 + 4NH_3 + CO_2 + \mathrm{H_2O} = \mathrm{MnCO_3} + 2Cu\left(NH_3\right)_4^{2+} + 2OH^- \quad (12.1)$$

$$2Cu\left(NH_3\right)_4^{2+} + CO + 2OH^- = 2Cu\left(NH_3\right)_2^{+} + 4NH_3 + CO_2 + \mathrm{H_2O} \quad (12.2)$$

After reduction, the metal ions, namely Cu, Ni, and Co, are present as soluble ammine complexes. The downstream process comprises solvent extraction–electrowinning for producing Cu and Ni cathodes. Co and Mo are recovered from the raffinate generated after Cu and Ni extractions. With the projections of better economics of process with Mn recovery, Kennecott produced Mn concentrate from leach residue. The main advantages of the process are: (1) its mild operating conditions and (2) its selectivity. Low Co recovery (~50%), low pulp density, and use of CO as a reductant are its main disadvantages.

12.2.2 Deep Sea Ventures (DSV) Process

The process developed is based on total dissolution of all the metals including manganese and iron in hydrochloric acid. This is an interesting process, using solvent extraction in chloride medium to separate and extract most of the common metals present in nodule. The process involves leaching of ground nodule in concentrated HCl, which is reducing enough to reduce Mn(IV) to Mn(II), according to reaction (12.3).

$$MnO_2 + 4HCl = \mathrm{MnCl_2} + Cl_2 + \mathrm{H_2O} \tag{12.3}$$

The leach liquor is then subjected to a series of solvent extraction and electrowinning operations. These are: (1) sequential extraction of Fe and Cu, (2) co-extraction of Ni and Co, and rejection of $MnCl_2$ in raffinate, (3) selective stripping of Ni from loaded organic, followed by stripping of Co, and (4) electrowinning of Cu, Ni, and Co from their respective chloride solutions. In the process, HCl/Cl_2 is regenerated through pyrohydrolysis for recycling during leaching. The process gave high recoveries of all the metals. However, the corrosive nature of chloride was the main disadvantage of this process (Monhemius 1980).

12.2.3 The Métallurgie Hoboken-Overpelt (MHO) Process

This process is quite similar to DSV process, but uses Cl_2 generated in reaction (12.3) to oxidize Mn(II) in solution to Mn(IV) and precipitate as MnO_2. Besides the 'four metals', MHO process also had provision to recover V, Mo, and Zn from chloride leach liquor. It may be mentioned that these elements occur in nodules as traces (Monhemius 1980).

12.2.4 International Nickel Company (INCO) Process

Smelting of nodules was pioneered by INCO. The salient features of the process (Sridhar 1974; Sridhar et al. 1976, 1977) are the reduction of the dried and ground nodules in a kiln, and then smelting in an electric furnace to produce (1) a manganese and iron rich slag and (2) an alloy containing Cu, Ni, Co, and residual Fe and Mn. The slag is later treated for the production of ferro-manganese. The alloy is sulphidized to produce a matte containing Cu, Ni, and Co. The matte so generated is then leached with H_2SO_4. The leach liquor is processed through a solvent extraction–electrowinning stage to produce Cu metal. The raffinate from this stage is again processed through another solvent extraction–electrowinning stage to produce Ni metal, and finally Co is reduced from solution with hydrogen to produce Co powder. The process is schematically shown in Fig. 12.2.

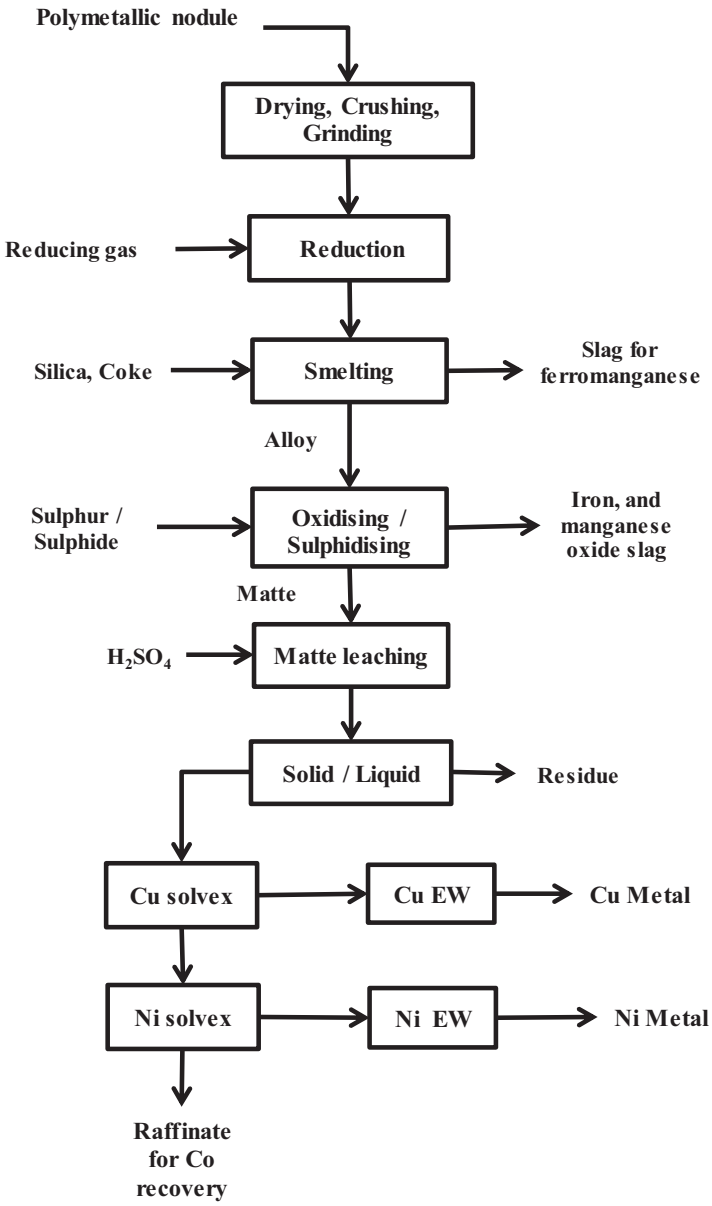

Fig. 12.2 Smelting—leaching process developed by INCO

Some of the typical reactions taking place during smelting are:

$$MnO_2 + \mathrm{C} = MnO + CO \tag{12.4}$$

$$MnO + CO = Mn^{o} + CO_2 \tag{12.5}$$

$$MnO + SiO_2 = \mathrm{MnSiO_3} \tag{12.6}$$

$$2MnO + SiO_2 = Mn_2SiO_4 \tag{12.7}$$

$$2Mn^{o} + \mathrm{O_2} = 2MnO \tag{12.8}$$

$$Fe_2\mathrm{O_3} + \mathrm{C} = 2FeO + CO \tag{12.9}$$

$$FeO + CO = Fe^{o} + CO_2 \tag{12.10}$$

$$NiO + \mathrm{C} = Ni^{o} + CO \tag{12.11}$$

$$CuO + \mathrm{C} = Cu^{o} + CO \tag{12.12}$$

$$CoO + \mathrm{C} = Co^{o} + CO \tag{12.13}$$

$$Co_2\mathrm{O_3} + 3\mathrm{C} = 2Co^{o} + 3CO \tag{12.14}$$

During reduction, slag generated in smelting furnace is reduced to ferromanganese alloy as shown by Eqs. (12.5) and (12.10), and Ca and Al are rejected as silicate slag.

$$Mn_2SiO_4 + 2CaO = 2MnO + Ca_2SiO_4 \tag{12.15}$$

$$\mathrm{MnSiO_3} + CaO = MnO + \mathrm{CaSiO_3} \tag{12.16}$$

$$SiO_2 + 2CaO + Al_2\mathrm{O_3} = Ca_2Al_2SiO_7 \tag{12.17}$$

$$SiO_2 + 2CaO = Ca_2SiO_4 \tag{12.18}$$

12.2.5 High Pressure Acid Leaching Process

Several researchers worked on developing high pressure acid leaching (HPAL) for processing of nodules. This was similar to processing of nickel laterite, operating in Canada and Cuba. Here also the emphasis was on recovery of Cu, Ni, and Co while leaving manganese in the leach residue (Hubred 1973; Hanieg and Meixner 1974; Han and Fuerstenau 1975; Junghanss and Roever 1976; Watanabe et al. 1982). The process comprised (1) HPAL at 200 °C, (2) solvent extraction of Cu, (3) precipitation of Ni-Co bulk sulphide, (4) HCl dissolution of sulphide, (5) solvent extraction for Co and Ni separation, (6) pyrohydrolysis of Co and Ni chlorides for producing respective oxides, and (7) reduction of oxides (Neuschutz et al. 1977).

In a variation of Cuprion process, Pahlman and Khalafalla (Pahlman and Khalafalla 1979; Khalafalla and Pahlman 1981) used SO_2 as a reducing agent in lieu of CO. Lee et al. (1978) carried out low temperature leaching studies on Pacific ferromanganese nodules with sulphur dioxide. In the subsequent years, processes were developed based on use of SO_2 in acid as well as in ammoniacal medium which are discussed in later sections.

While several processes were being developed, the fluctuating metal prices, the ease of oil crisis, and the lack of a viable mining technology resulted in slowing down developmental efforts and in many cases stoppage of metallurgical activities by the research institutions and contractors. A number of excellent reviews on extractive metallurgy of nodules were published outlining the progress till that point of time (Hubred 1980; Monhemius 1980; Fuerstenau and Han 1983; Haynes et al. 1985; Han and Fuerstenau 1986). The advantages and disadvantages of various process routes were highlighted in these publications.

12.3 Second Phase of R and D Efforts for Processing of Nodules (1985–2000)

The requirement of Cu, Ni, and Co by many resource-starved countries like Japan, India, China, and Korea encouraged the research organizations in these countries to develop processes for treating nodules which may prove to be economical, and environment friendly. Several alternative processes to treat nodules were developed based on three main routes namely: (1) aqueous reduction (hydrometallurgical), (2) moderate temperature reduction roasting-leaching (pyro-hydrometallurgical), and (3) high temperature smelting, matte formation, and leaching (pyro-hydrometallurgical).

12.3.1 Four Metal Recovery by Aqueous Reduction in Acidic Media

Most of the investigations pertaining to four metal recovery aimed at using common mineral acids, i.e. sulphuric or hydrochloric acid, in the absence/presence of a reducing agent. Various reductants used included hydrogen peroxide (Kawahara and Mitsuo 1992), charcoal (Anand et al. 1988a; Das et al. 1989), sulphur dioxide/sulphite in the presence/absence of sulphuric acid (Asai et al. 1986; Kanungo and Das 1988; Acharya et al. 1999; Das et al. 2000), pyrite/pyrrhotite (Kanungo and Jena 1988a, b; Paramaguru and Kanungo 1998; Kanungo 1999a, b), nickel matte (Hsiaohong et al. 1992; Chen et al. 1992), aliphatic alcohols (Jana et al. 1993, 1995), aromatic alcohols and ammines (Zhang et al. 2001a, b). In most of these cases, Cu, Ni, Co, and Mn extractions exceeded 90% while in some cases two stages of leaching were proposed for selective leaching of two/three metals at a time. Researchers also

continued investigations on chlorination/HCl leaching (Kim and Park 1997; Park and Kim 1999). Sodium sulphite in combination with ammonium chloride was also tried as a leachant for four metal recovery (Choi and Sohn 1995).

12.3.2 Three Metal Recovery by Aqueous Reduction in Ammoniacal Medium

The principle of aqueous reductive leaching is same as in the Cuprion process. Under ammoniacal conditions—depending on nature of reductant—5 to 30% manganese is leached, while the rest is rejected in the residue. Leaching studies have been reported using a variety of reductants such as glucose (Das et al. 1986; Acharya et al. 1989), manganous ion (Acharya and Das 1987), ferrous sulphate (Anand et al. 1988b; Bhattacharya et al. 1989), elemental sulphur (Mohanty et al. 1994), and sulphur dioxide (Das and Anand 1997). Most of these studies present the extractions of metal values during leaching and project that the downstream processing can be done by solvent extraction or precipitation to separate Cu, Ni, and Co. The basic aspects of Mn and Co behaviour in ammonia ammonium sulphite solutions have been reported (Das et al. 1997; Mohapatra et al. 2000). Various options for Mn recovery from residue generated after NH_3-SO_2 leaching process have been addressed by Sanjay et al. (1999).

12.3.2.1 The National Institute for Resources and Environment (NIRE) of Japan

NIRE, Tsukuba, Japan developed a novel process flowsheet which combined the strengths of NH_3-CO and NH_3-SO_2 systems (Rokukawa 1990, 1995). In this process leaching of polymetallic nodule, or Co-rich crust, is carried out in a solution of $(NH_4)_2CO_3$, and $(NH_4)_2SO_3$. During leaching, all the manganese is converted to $MnCO_3$, and rejected as residue along with iron. The iron and manganese free leach liquor is then processed through solvent extraction for co-extraction of Ni and Cu. The raffinate, containing Co, $(NH_4)_2SO_4$, and $(NH_4)_2CO_3$, is then handled in an innovative way. On addition of methanol to the raffinate, cobalt ammine carbonate sulphate is precipitated. The solution after cobalt precipitation is recycled. During leaching, the recoveries for Co, Ni, and Cu are 92.8%, 82%, and 80.5%, respectively. The flowsheet is schematically shown in Fig. 12.3.

12.3.2.2 Reduction Roasting Ammoniacal Leaching Process

This process is similar to the Caron's (Caron 1924) process for treating the nickel laterites. In this process nodules are reduced in the temperature range of 500–750 °C using oil or gas as the reductant. The reduced mass is leached with ammonia

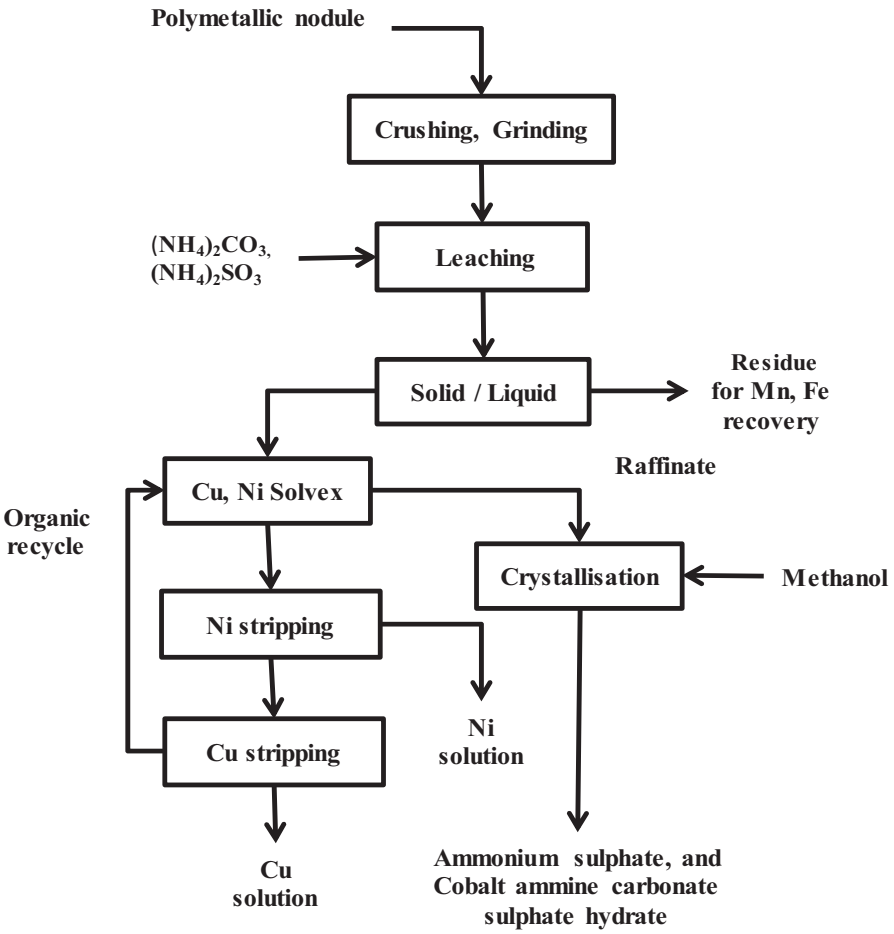

Fig. 12.3 The NIRE process developed by Japan

ammonium carbonate solution to dissolve Cu, Ni, and Co as their respective ammines. Metal separation is carried out through solvent extraction/precipitation. Manganese remains in the residue as $MnCO_3$. National Metallurgical Laboratory (NML), India has extensively innovated this basic process and incorporated several new steps to improve metal recoveries especially for cobalt (Jana and Akerkar 1989; Jana et al. 1990, 1999a; Srikanth et al. 1997).

The authors' laboratory (formerly Regional Research Laboratory, and now renamed as Institute of Materials and Mineral Technology—IMMT) at Bhubaneswar, India extensively worked on a number of process alternatives for manganese nodules. Some of these are listed in Table 12.2. As the new developments took place in processing metallurgy of manganese nodules, several authors reviewed numerous processes developed for the recovery of metal values from Mn nodules (Han 1997; Premchand and Jana 1999; Sen 1999).

Table 12.2 Leaching processes tested at IMMT (earlier Regional Research Laboratory) Bhubaneswar

Process	Recovery of, %					Main advantages	Main disadvantages
	Cu	Ni	Co	Mn	Fe		
Acid: HCl (1.5 M) (un-published data)	87	87	30	20	70	1. Higher recovery may be obtained by using stronger acid	1. Poor selectivity
						2. Process operates at room temperature	2. Corrosive condition
Acid: H_2SO_4, carbon (160 g/L acid, t 12 h) (Das et al. 1989)	100	100	100	91	100	1. Process uses easily available reagents	1. 12 h leaching time
							2. Poor selectivity
Acid: HPAL (T 170 °C, pO_2 5.5 MPa, pd. 5%, acid 20 g/L, t 4 h) (Anand et al. 1988a)	90	95	95	20	5	1. Selectivity with respect Fe and Mn is achieved	1. High pressure autoclaves require high pulp density for economic operation
						2. Low consumption acid during leaching	2. Presence of chloride ion and make the process corrosive
Acid: same conditions as above, but in presence of 5% carbon w/w nodule (Anand et al. 1988a)	do	do	do	100	do	1. Can be a very good alternative for four metal recovery	-Do-
Acid: H_2SO_3; SO_2 4.5%, t 10 min, T 30 °C (Kanungo and Das 1988; Das et al. 2000)	84	95	86	52	18	1. The process has very fast kinetics and can operate at room temperature	1. Certain degree of selectivity is possible, but at the cost of recovery
						2. It uses easily available reducing agent	
Ammonia: with glucose, (t 4 h, T 85 °C, 20% glucose wt/wt nodule, NH_3 2.5 M, NH_4Cl 0.37 M), (Das et al. 1986)	100	90	60	–	–	1. Leaching is possible under moderate condition	1. Process requires a large quantity of reducing agent which is expensive
Ammonia with $FeSO_4$ (t 60 min, T 70 °C, $FeSO_4$ 1.4 stoich, NH_3 5.4 M) (Anand et al. 1988b)	74	76	60	30	–	1. Uses one of the cheapest reagents for leaching	1. Requirement of $FeSO_4$ is very high
							2. disposal $Fe(OH)_3$ will be a problem
Ammonia-metal ions as reducing agents (Acharya and Das 1987, Acharya et al. 1989)	do	do	do	do	–	1. Metal ions are easily available reagents	1. Reagent requirement is high unless metal ions are regenerated
Ammonia-SO_2 (pH: 9.3–10.8, t 2 h, T 120 °C, $(NH_4)_2SO_3$/nodule: 30% wt/wt) (Das and Anand 1997, Das 2001)	99	98	96	33	–	1. Combines the advantages of acid-SO_2 route with iron rejection capacity of ammonia	1. $(NH_4)_2SO_4$ is generated

t time, *T* temperature

12.4 Recent Developments in Metallurgical Processing of Nodules by Some of the Contractors (2000 Onwards)

The major organizations/investors/contractors which are presently active in pilot scale testing of metallurgical processing of nodules are: Ministry of Earth Sciences (MoES, earlier Department of Ocean Development) India, Interoceanmetal Joint Organization (IOM—a consortium of east European countries), China Ocean Mineral Resource R&D Association (COMRA) China, and Korea Institute of Geology and Mining (KIGAM) Korea. The progress of metallurgical activities by various organizations was presented at the ISA workshop held at Chennai, India in 2008 (ISA 2008). The processes which have been tested in 100–500 kg/day are now being considered and evaluated. These processes are briefly discussed below:

12.4.1 Processes Developed by Various Organizations Sponsored by MOES India

12.4.1.1 NH_3-SO_2 Process

This process was developed by IMMT and Bhabha Atomic Research Centre (BARC). It is based on aqueous reduction using SO_2 as a reductant in ammoniacal medium (Das 2001; Mittal and Sen 2003). The schematic flowsheet, given in Fig. 12.4, shows that the process dissolves the metals of interest while totally rejecting iron and partially rejecting manganese. The process envisages (1) leaching of polymetallic nodule in presence of NH_4OH and SO_2, (2) copper SX-EW, (3) precipitation of mixed Ni-Co sulphide followed by its dissolution at elevated temperature, (4) separation of Ni-Co by solvent extraction, and (5) electrowinning for Ni and Co cathodes. In association with Hindustan Zinc Ltd. (HZL), a 500 kg/day processing plant was operated from 2002 to 2006.

The chemical reactions taking place during leaching are given below:

$$2CuO + 2\left(NH_4\right)_2 SO_3 + 2NH_3 = Cu_2\left(NH_3\right)_4 SO_4 + \mathrm{H_2O} \tag{12.19}$$

$$CuO + \left(NH_4\right)_2 SO_3 + 2NH_3 = Cu\left(NH_3\right)_4 SO_4 + \mathrm{H_2O} \tag{12.20}$$

$$NiO + \left(NH_4\right)_2 SO_3 + 2NH_3 = Ni\left(NH_3\right)_4 SO_4 + \mathrm{H_2O} \tag{12.21}$$

$$CoO + \left(NH_4\right)_2 SO_3 + 3NH_3 = Co\left(NH_3\right)_5 SO_4 + \mathrm{H_2O} \tag{12.22}$$

$$MnO_2 + \left(NH_4\right)_2 SO_3 = MnO + \left(NH_4\right)_2 SO_4 \tag{12.23}$$

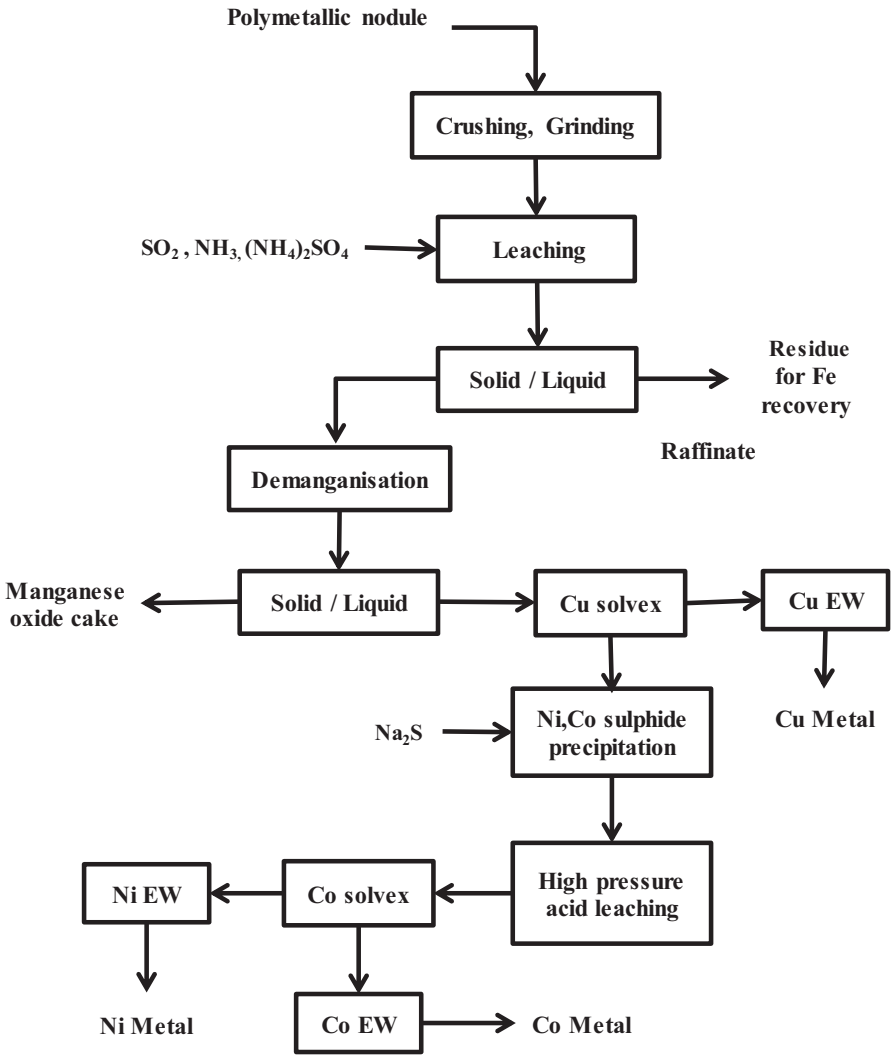

Fig. 12.4 Schematic flowsheet of NH_3-SO_2 process developed in India

$$MnO_2 + \left(NH_4\right)_2 SO_3 + 2NH_3 = Mn\left(NH_3\right)_4 SO_4 + \mathrm{H_2O} \tag{12.24}$$

$$2\mathrm{FeOOH} + \left(NH_4\right)_2 SO_3 + \mathrm{H_2O} = 2Fe\left(OH\right)_2 + \left(NH_4\right)_2 SO_4 \tag{12.25}$$

The process has the option to recover manganese from the residue as silico-manganese. This part of work was carried out by NML, India.

12.4.1.2 Reduction Roasting Ammoniacal Leaching Process

As mentioned earlier, NML, India has been working on reduction roasting ammonia leaching process since mid-1980s. The main drawback of the process was low cobalt recovery (~55%). Several modifications in the leaching step including pre-treatment of roasted nodules with a surfactant followed by leaching with ammonia ammonium carbonate could improve the recovery of cobalt to ~80% with >90% extractions of Ni and Cu (Mishra et al. 2011). The leach solution containing Cu, Ni, and Co is processed for metal separation by solvent extraction–electrowinning to obtain Cu, Ni, and Co as cathodes. In the process, Mn is recovered as standard silico-manganese (Si16Mn63), via carbothermic reduction smelting in electric arc furnace. The lower Mn/Fe ratio of residue was improved by blending it with Mn ore (Randhawa et al. 2013).The leaching process has been tested in 100 kg/day scale.

12.4.1.3 Aqueous Reduction in Sulphuric Acid

HZL, India developed a sulphuric acid leaching process. It was aimed at four metal recoveries in the leaching stage itself. A cellulosic novel reductant was used. Very high recoveries of Cu, Ni, Co, and Mn were achieved. The downstream processing comprised Cu separation by solvent extraction, Ni-Co sulphide by precipitation, dissolution of sulphide at elevated temperature, and Ni-Co separation by solvent extraction. Cu, Ni, and Co are recovered as cathodes. Manganese is recovered as $MnCO_3$. The leaching process was tested in 100 kg/day scale.

12.4.2 Processes Developed by IOM (an Intergovernmental Consortium of Bulgaria, Cuba, Czech Republic, Poland, Russian Federation, and Slovakia)

The IOM member countries have developed a number of processes based on pyrohydrometallurgical or hydrometallurgical leaching routes (Rodriguez et al. 2001; Vranka 2001; Vranka and Kotlinski 2005; Kotlinski et al. 2008). Two processing routes which have been tested in 100–150 kg/day scale are briefly described below.

12.4.2.1 Pyro-hydrometallurgical Process

This process is similar to INCO process with some modifications in alloy dissolution. Cu, Ni, and Co form a complex alloy while most of the Mn and part of Fe are rejected in slag. The novelty of this process is selective dissolution of Ni and Co with part of Mn and Fe in sulphuric and sulphurous acid. Copper is precipitated as CuS. Mn is recovered as Si-Mn alloy. High recoveries of metal values (Cu 92%, Ni 93%, Co 89%) in the alloy formation step have been reported (Kotlinski et al. 2008).

12.4.2.2 Hydrometallurgical Process

The hydrometallurgical nodule processing schemes were developed mainly at NIGRI Moscow, Russia (Kotlinski et al. 2008). This process is based on H_2SO_4-SO_2 leaching of the ground nodules for dissolution of Cu, Ni, Co, and Mn. Copper is first selectively precipitated as CuS and then Ni-Co are precipitated as sulphides. Cu, Ni, Co free solution containing $MnSO_4$ is processed for Mn recovery. A simplified flowsheet is given in Fig. 12.5. In view of detailed work carried out on this process, Solvek engineering company had prepared a pre-feasibility for 0.5 million ton/year nodule processing (Kotlinski et al. 2008) and it was projected to be profitable. The process was tested in 100–150 kg/day scale.

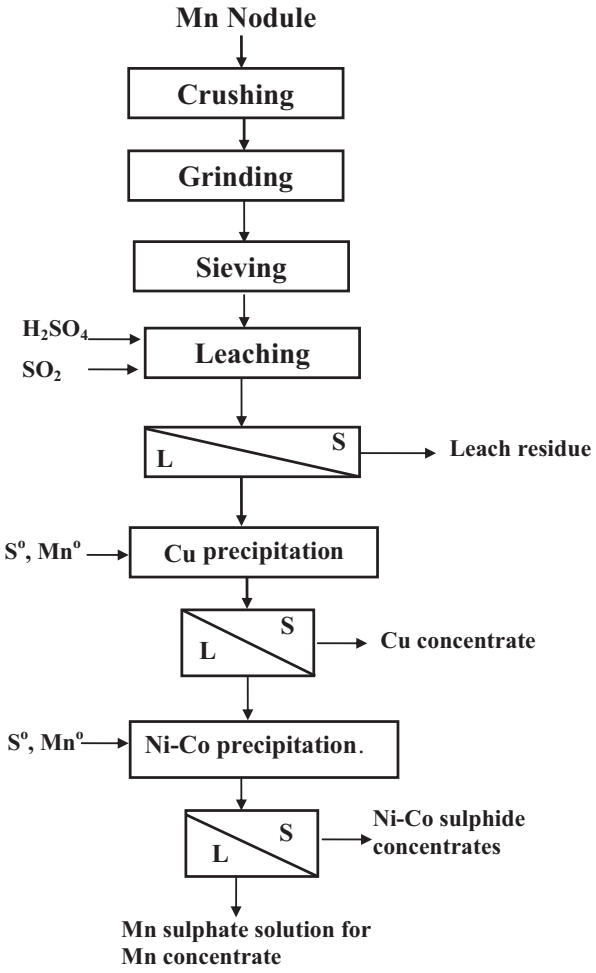

Fig. 12.5 A simplified hydrometallurgical flowsheet for IOM process

12.4.3 Processes Developed by COMRA

In China, several research groups are actively involved in processing of polymetallic nodules. Most of the results of their studies are not easily accessible through publications.

12.4.3.1 Pyro-hydrometallurgical Process (Improved INCO Process)

This process is based on INCO smelting technology with an improvement with respect to dissolution of alloys. It is 'smelting and rusting' process. Schematically, the process is presented in Fig. 12.6. The process envisages formation of an alloy containing Cu, Ni, Co, Mn, and Fe through smelting. Most of the manganese is transferred to a manganese-rich slag for subsequent recovery of manganese as ferro-manganese. During rusting of the above alloy in dilute HCl solution, most of the iron is precipitated while a solution of Cu, Ni, Co, and Mn is obtained. Purification of the solution is carried out through solvent extraction. The Chinese have reported high recoveries of Cu, Ni, and Co, approximately 95% for each individual metal (Xiang et al. 1999).

12.4.3.2 Improved Cuprion Process

The other process developed by COMRA is similar to the Cuprion process with modification of leaching step using an additive. The process has been tested in 100–150 kg/day scale. The downstream processing is carried out through solvent extraction–electrowinning to produce Cu and Ni as cathodes, Co as oxide, and Mn as $MnCO_3$.

12.4.4 Processes Developed by KIGAM

KIGAM, Korea is also actively involved in treating polymetallic nodule. The process being upscaled is smelting followed by acid leaching of matte at elevated temperature. Oxidative leaching of matte in ammonia ammonium sulphate media has also been tried (Park et al. 2007). The downstream processing is similar to other processes through solvent extraction–electrowinning. Mn is recovered as Si-Mn. The Korean process plans to bring in improvements to the basic 'smelting-leaching' process, so that the current environmental norms and the technologies can be incorporated to make the process more efficient (Table 12.3) shows some of the main processes wherein complete flow-sheets have been tested.

The efforts on improvement of various process steps, i.e. viz. leaching, solvent extraction, and precipitation, are still continuing. In later years, with a view to improve the INCO process several researchers have introduced alternative downstream

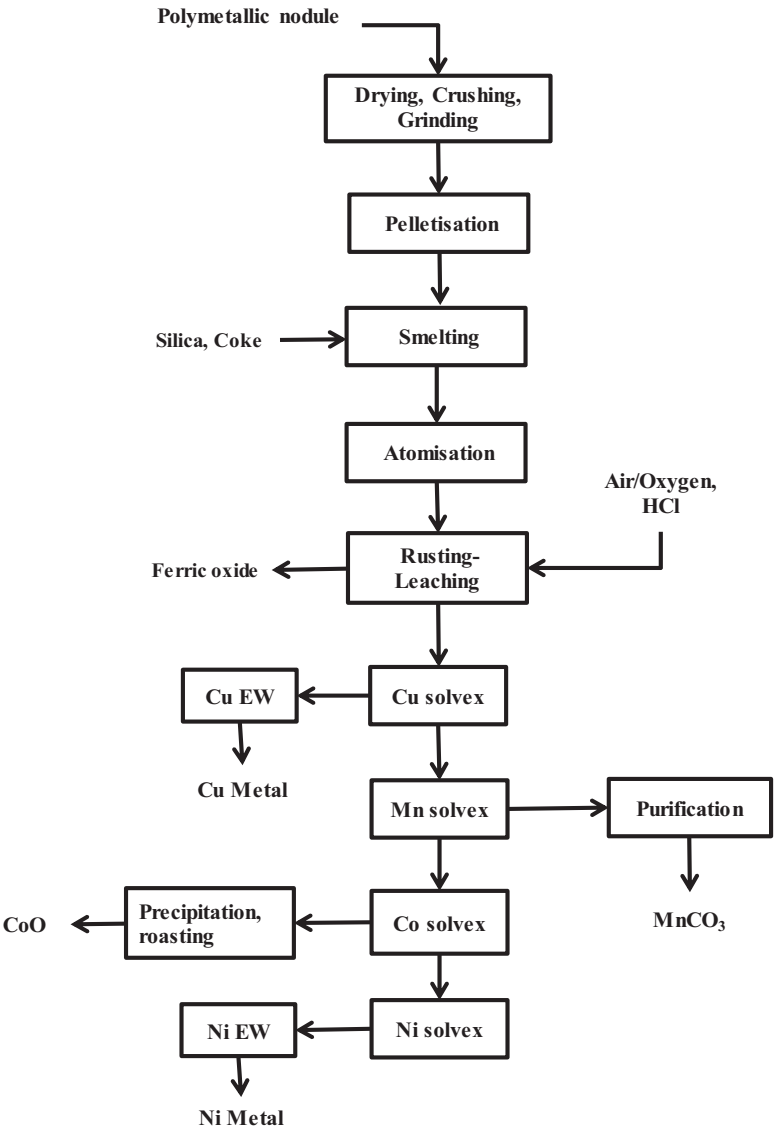

Fig. 12.6 Pyrohydrometallurgical process developed by COMRA, China

options like chloride leaching of matte and electro-leaching of alloy (Kim et al. 2005; Shen et al. 2008, Stefanova et al. 2009, 2013). Further modification in Caron's process has also been attempted (Jiang et al. 2013). New solvents are being tested for a better and more efficient Cu, Ni, Co separation from nodule leach liquors (Sridhar and Verma 2011). The recovery of Mo and or rare earths is another area where the R and D efforts are being made (Mohwinkel et al. 2014; Parhi et al. 2011, 2013, 2015).

Table 12.3 Some of the main processes developed wherein the complete flowsheets have been tested

Main process steps	Main advantages	Main disadvantages
HPAL at 200 °C, solvex for Cu, precipitation of Ni-Co bulk sulphide, HCl dissolution of sulphide, solvex for Co and Ni, pyrohydrolysis and oxide reduction (Neuschutz et al. 1977)	(1) High recovery, (2) rejection of iron during leaching	(1) Expensive pressure reactors, (2) based on several complicated operations like HPAL, HCl dissolution, and pyrohydrolysis
HCl leaching, solvex for Fe, Cu precipitation with H_2S, Ni and Co co-precipitation as sulphide, Mn precipitation as oxide, and pyrohydrolysis to regenerate HCl/Cl_2 (Monhemius 1980)	(1) High recovery, (2) almost complete recycling of HCL and Cl_2	(1) Lack of selectivity leads to high reagent consumption
Reductive roasting and leaching in presence of ammonia: Reduction with CO gas at 500–700 °C; Cu solvex-electrowinning, Ni solvex-electrowinning, Co recovery as sulphide; Ammonia recovery (Haynes et al. 1985)	(1) Based on well-tested Caron's process for nickel laterites, (2) less operating and design problems	(1) Based on high temperature roasting, (2) gives low recovery of Co
Reduction smelting for alloy preparation. Smelting of alloy for matte formation. Acid pressure leaching of matte followed by metal separation by SX-Precipitation (Sridhar 1974)	High recoveries	High temperature smelting and pressure leaching expensive
Improved Caron process by NML[a]. Use of additives and activation prior to leaching. Cu, Ni, and Co separation by SX-EW to recover as cathodes (Premchand and Jana 1999; Jana et al. 1999a, b; Mishra et al. 2011; Srikanth et al. 1997)	High Cu and Ni recoveries, Co ~75%	Low Co recovery
Improved INCO process by IOM[b] to produce Cu as concentrate, Ni-Co as concentrate, Mn as Si-Mn (Kotlinski et al. 2008)	High metal recoveries	(1) Alloy formation at high temperature expensive (2) metals as concentrates require further processing
IOM[b] hydro process SO_2 acid leach process. Precipitation and metal separation. Cu as sulphide, Ni-Co as sulphides, Mn as concentrate Kotlinski et al. (2008)	High recoveries of Cu, Ni, Co, and Mn > 92%	metals as sulphide/concentrates require further processing
COMRA[c] INCO improved process Patented novel dissolution process. Cu, Ni-cathode, Co oxide, Mn as Si-Mn (Xiang et al. 1999; ISA 2008)	High recoveries of Cu, Ni, and Co, >90%, Mn 82%	Smelting at high temperature for alloy formation expensive
Improved cuprion process by COMRA. Hydro process. Activation during leaching. Cu, Ni, Co recovered as cathodes. Mn as $MnCO_3$	Cu, Ni > 95%, Co 90, Mn > 88, Mo ~ 96%. Additive for activation during leaching	NH_3 recovery and recycle

(continued)

Table 12.3 (continued)

Main process steps	Main advantages	Main disadvantages
IMMT[d] NH_3-SO_2 process. Leaching, solvent extraction for separation of Cu. Ni-Co sulphide precipitation, elevated temperature dissolution. Separation by SX-EW and recovered as cathodes. Mn as Si-Mn. NH_3 recovery and recycle(Das 2001; Mittal and Sen 2003)	Complete hydro process for Cu, Ni, and Co. All unit operations are well tested. Moderate temperature operation. Cu, Ni >90%, Co >80%	(1) NH_3 recovery and recycle, (2) large quantities of ammonium sulphate production
HZL[e] H_2SO_4-reductant hydro process. Leaching, Cu separation by SX. Ni-Co sulphide precipitation, oxidative elevated temperature dissolution. Cu, Ni, and Co as cathodes. Mn as $MnCO_3$	Cu, Ni >95%, Co 92%, Mn 92%. A; unit operations are simple. No corrosive reagents are used	High consumption of reductant

HPAL high pressure sulphuric acid leaching, *SX* solvent extraction
[a]NML National Metallurgical Laboratory, India
[b]Interoceanmetal Joint Organization (IOM), a consortium formed by Bulgaria, Cuba, Czech Republic, Poland, Russian Federation and Slovakia, the Government of the Republic of Korea, and The Federal Institute for Geosciences and Natural Resources of the Federal Republic of Germany
[c]COMRA China Ocean Minerals Resources Research and Development Association
[d]IMMT Institute of Mineral and Material Technology, India
[e]HZL Hindustan Zinc Limited, India

The recovery of these metals can have a positive impact on economics of nodule processing. New low cost, environmentally compatible reductants are being explored for metal recovery from manganese nodules (Vu et al. 2005; Ghosh et al. 2008; Hariprasad et al. 2013). Some novel techniques for treatment of nodules have been reported (Wang et al. 2005, 2010). Bacterial leaching of manganese nodule as an alternative to chemical leaching has been studied by several authors (Mukherjee et al. 2003a, b, 2004; Mehta et al. 2008, 2010). IOM is developing an improved HPAL process by carrying out leaching in the presence of additives (Rodriguez et al. 2013).

A feasibility study for mining to metal recovery and marketing for Clarion-Clipperton Zone was carried out by Agarwal et al. (2012). Pophanken and Friedrich (2013) presented the challenges while processing manganese nodules. It was emphasized that the metal losses in each processing step need to be minimized so as to have a better economics of the process. Sen (2010) has mentioned that an efficient processing scheme for manganese is very important for considering nodules as a potential source of metals. Martino and Parson (2012) have projected that based on Ni and Co prices manganese nodule or co-crust mining can yield return on investment comparable to land mining for these metals.

12.5 A Few New Concepts

12.5.1 Direct Use of Nodule Alloy in Stainless Steel

In recent years, demand for 200 series stainless steel has led to the consumption of nickel as nickel pig iron. Currently, approximately about 20% nickel (~8 Mtpa) is produced as nickel pig iron. The technology for the production of nickel pig iron from nickel laterites (Kyle 2010; Rao et al. 2013) involves carbothermic reduction of nickel laterite in a blast furnace, or submerged electric arc furnace. Similar approach for manganese nodule has also been examined. Typical compositions of alloy 'pig iron' obtained from manganese nodule are given in Table 12.4. Similar to nickel laterite, the nodule can be reduced in a blast furnace, or a submerged arc furnace, to produce an alloy. This alloy will have a composition similar to the one reported (Stefanova et al. 2013), and the slag will be suitable for the recovery of manganese as silico-manganese. It may be noted that 200 grade stainless steel has Cu and Mn as its constituents. A typical composition of such steel is also shown in Table 12.4. As in the case of Co in lateritic nickel ore, Co from alloy 'pig iron' may not affect the basic properties of stainless steel. The technology of nickel pig iron is one of the lowest capital cost technologies for treating lateritic nickel ore and may prove so for the nodules as well. The major advantages of such an alternative are:

1. It will be a simple, one-step smelting operation using an established technique.
2. It will use small blast furnace for reduction smelting, or a submerged arc furnace.
3. The products alloy pig iron and manganese slag are directly marketable.

Alternatively, the alloy 'pig iron' may be a feed material to modified copper smelters, e.g. Umicore, Boliden, Xstrata, and LS Nikko, which accept electronic wastes. These smelters can accept alloy 'pig iron' from nodule and separate Cu, Ni, and Co. But the process will perhaps lose all the Fe, and Mn in alloy to slag. This may affect the overall economics of the process.

Table 12.4 Compositions of alloy from nodule, and series 200 stainless steel

Grade	Mn	Cr	Ni	N	Cu	Fe	Co	P	other
Nodule 'pig iron' I (Stefanova et al. 2013)	5.33	–	12.81	–	12.07	65.9	1.33	0.93	0.54
Nodule 'pigiron' II (Kim et al. 2005)	–	–	22.1	–	19.2	53.3	5.4	–	–
Nodule 'pig iron' III (Wilder and Galin 1976)	0.29	–	27.7	–	22.9	44.3	4.25	–	1.23 (Mo)
Nodule 'pigiron' IV (Sridhar et al. 1977)	2.5	–	14.5	–	9.3	70.2	2.3		
204 Cu Stainless steel Anon (2006)	7	16	2	0.15	2.5	Rest			
Anon (2006)	9	16	1.5	0.2 max	1.7	Rest			

12.5.2 Process Based on HCl-$MgCl_2$ Leaching

As mentioned in earlier sections, the basic processes for nodule are similar to treatment of nickel laterites. In chloride-based processes, the main concerns are material of construction. Many of these challenges have been overcome by some of the newer processes based on high chloride leaching for nickel laterite (Harris et al. 2004, 2006). Leaching of lateritic nickel ore with a mixture of $MgCl_2$ and HCl brings in all the metals into solution. Later, Fe is converted to Fe_2O_3 and Mn is converted to hydroxide, while the solution contains Ni, Cu, and Co. On neutralization with MgO, a mixed hydroxide of these metals will be produced. The process envisages recycling of Mg as MgO, and recovery of HCl through pyrohydrolysis. The process has several advantages, namely:

1. The only solid residue generated is leach residue.
2. Both Fe and Mn values are separated and recovered.
3. The reagents are almost totally recycled.
4. The recoveries are close to 100%.

The above process was developed using MgO-$MgCl_2$ system because of the presence of significant quantity of MgO in nickel ore. In case of manganese nodule, where CaO and entrained NaCl are more likely to be present, the process can be modified (Jennings et al. 1973) to use cheaper CaO as a neutralizing agent. INTEC process is based on such a modification (Kyle 2010). Similarly, the energy intensive pyrohydrolysis step can be replaced with a reaction for regenerating HCl from $CaCl_2$ as shown by Eq. (12.26) (Smit and Steyl 2005; Demopoulos et al. 2008), and producing crystalline $CaSO_4$ (Fig. 12.7).

$$CaCl_2 + H_2SO_4 + 0.5H_2O = CaSO_4.0.5H_2O + 2HCl \tag{12.26}$$

So far as processing of nodules is concerned, it is a green field process which needs to be tested for data generation and evaluation.

12.6 Conclusion

In recent years, several processes have been developed for recovery of metal values from nodules, and a number of these were scaled up. Some of these scaled up processes, like those developed by IOM, COMRA, and NML are improved INCO, Cuprion, and Caron processes. In addition, two new hydrometallurgical processes have been developed and scaled up by IOM, HZL, and IMMT. These are based on reductive acid and ammonia leaching. These processes are summarized in Fig. 12.8.

Most of these processes efficiently recover Cu, Ni, Co, and Mn. Manganese is converted to $MnCO_3$ in the hydrometallurgical processes, while in the pyrometallurgical process, it is recovered as Si-Mn after smelting. Polymetallic nodules contain a significant quantity of moisture, and therefore any process based on high temperature

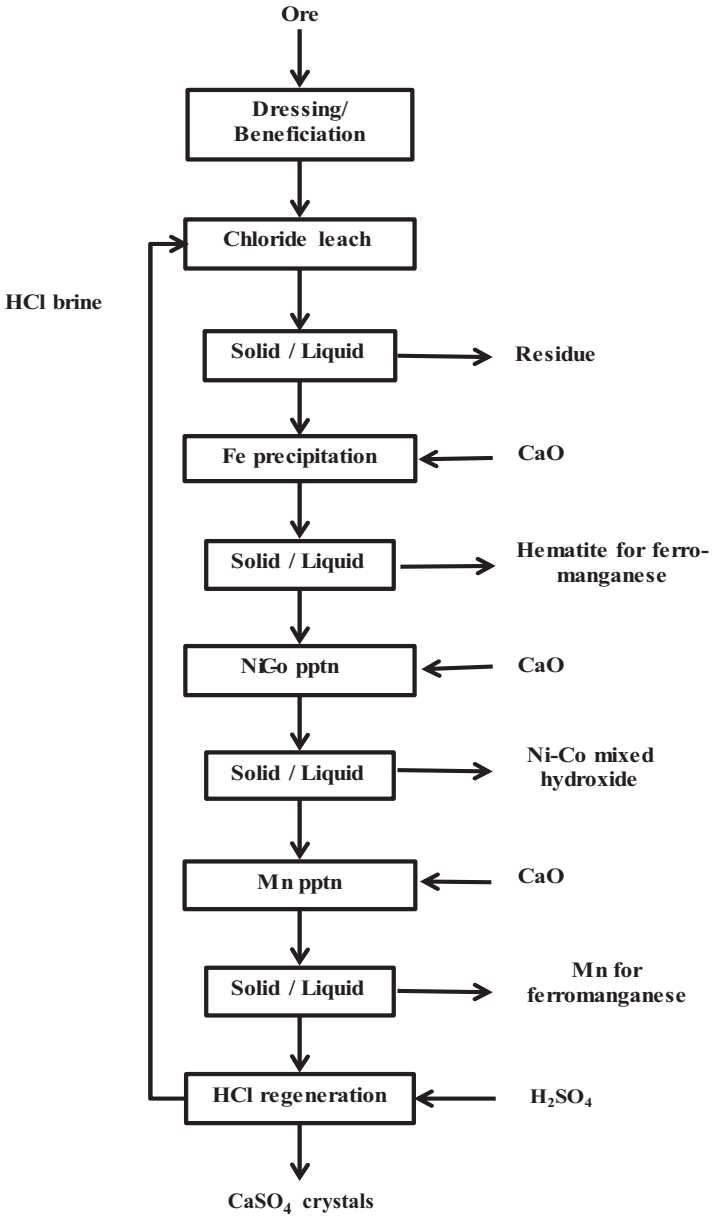

Fig. 12.7 A simplified INTEC flowsheet, with suggested modification for manganese

operation would appear to lead towards a high processing cost, which is often offset by ease of downstream processing. Pyro-hydrometallurgical route for nodule also offers several positive benefits, which include (a) production of almost all the manganese in the form of ferro-/silico-manganese, (b) generation of a compact residue in the form of slag and, (c) the slag so generated is usually environmentally stable.

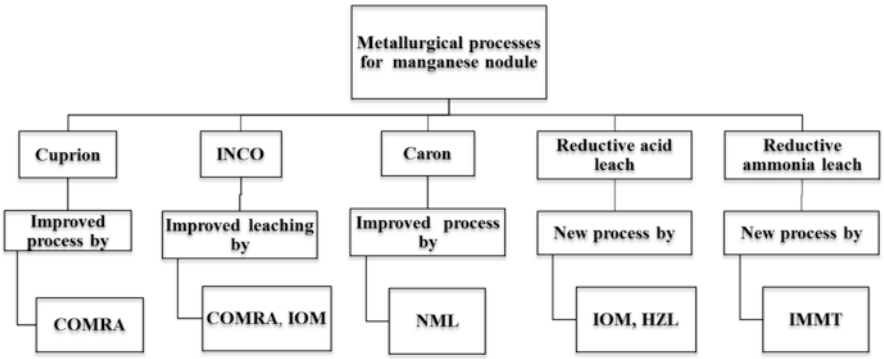

Fig. 12.8: Summary of the scaled up metallurgical processes for manganese nodule

The processes being developed by China and Korea consider the pyrometallurgical alternative and these are developed based on the initial work on smelting followed by leaching and metal separation. The modified processes consider different alternatives for the downstream, such as rusting, high pressure acid leaching for matte, and efficient solvent extraction technique for purification.

One of the IOM and one of Indian processes, on the other hand, are based on reductive acid leaching resulting in dissolution of all the four metals. The modified Cuprion process or Caron process has aimed at high recovery of metals including cobalt. The aqueous reduction in NH_3-SO_2 is a new process developed by IMMT. The ammonia-based processes need to take a great care to minimize ammonia loss so as to recycle as much ammonia as possible.

The commercial viability of any of the developed processes coupled with the mining cost still remains to be ascertained due to the following reasons:

1. Non-development of a mining site and mining technology
2. Estimated high cost of mining polymetallic nodule, compared to the cost of terrestrial mining
3. Fluctuating metal price
4. Emphasis on recycling of secondary metal resource
5. Stricter environmental regulations

The economics of processing polymetallic nodule is not easy to determine, due to the absence of reliable mining cost. However, it is possible to estimate the market price of nodule as a metallurgical raw material, by considering all the metals and the minerals contained in nodule, and fixing a market price for the same.

For any green field metallurgical process to treat polymetallic nodule, in present times, there are some essential requirements as mentioned below:

1. Zero or minimum discharge
2. Minimum carbon footprint by consuming least energy
3. Subsidization of the main products with by-products of the process
4. Capital (capex) and operating costs (opex) similar to existing commercial operations

The production of alloy ‘pig iron’ for 200 series stainless steel and recovery of silico-manganese may fulfil the above requirements. In hydrometallurgical processing of nodules, aqueous reduction under ammoniacal conditions or through a chloride route with reagent recycling schemes also offers viable alternatives.

References

Acharya S, Anand S, Das SC et al (1989) Ammonia leaching of ocean nodules using various reductants. Ertzmetall 42(2):66–73

Acharya S, Das RP (1987) Kinetics and mechanism of the reductive ammonia leaching of ocean nodules by manganous ion. Hydrometallurgy 19:169–186

Acharya R, Ghosh MK, Anand S et al (1999) Leaching of metals from Indian ocean nodules in SO_2-H_2O-H_2SO_4-$(NH_4)_2SO_4$ medium. Hydrometallurgy 53(2):169–175

Agarwal B, Hu P, Placidi M et al (2012) Feasibility study on manganese nodules recovery in the Clarion-Clipperton Zone. https://www.southampton.ac.uk/assetsimported/transforms/peripheral-block/UsefulDownloads_Download/8BC7B9645A8E4690A375D527F98DF7EC/LRET%20Collegium%202012%20Volume%202.pdf

Agarwal JC, Wilder TC (1974) Recovery of metal values from manganese nodules. U.S. Patent 3,788,841, 29 Jan 1974

Agarwal JC, Wilder TC (1975) Recovery of metal values from manganese nodules. Canadian Patent 980,130, 23 Dec 1975

Agarwal JC, Barner HE, Beecher N et al (1978) Kennecott process for recovery of copper, nickel, cobalt and molybdenum from ocean nodules. Paper presented at AIME Annual Meeting, Denver, CO, February, SME preprint, pp 788–789

Agarwal JC, Barner HE, Beecher N et al (1979) Kennecott process for recovery of copper, nickel, cobalt and molybdenum from ocean nodules. Min Eng 31(12):1704–1709

Anand S, Das SC, Das RP et al (1988a) Leaching of manganese nodules at elevated temperature and pressure in the presence of oxygen. Hydrometallurgy 20:155–168

Anand S, Das SC, Das RP et al (1988b) Leaching of manganese nodule in ammoniacal medium using ferrous sulphate as reductant. Metall Trans B 19B:331–335

Anon (2006) 200 series stainless—an overview. Stainless Steel Industry, p 6–8

Asai S, Negi H, Konishi Y (1986) Reductive dissolution of manganese dioxide in aqueous sulphur dioxide. Can J Chem Eng 64:237–242

Bhattacharya IN, Anand S, Das SC et al (1989) Ammonia leaching of manganese nodules in nodule test plant. Trans Indian Inst Metals 42(4):385–392

Caron MH (1924) Process of recovering values from nickel and cobalt-nickel ores. US Patent 1,487,145, 18 Mar 1924

Chen HH, Fu C, Zheng DJ (1992) Reduction leaching of manganese nodules by nickel matte in hydrochloric acid solution. Hydrometallurgy 28:269–275

Choi KS, Sohn JW (1995) Reduction leaching of manganese nodules with sodium sulfite in ammonium chloride solution. In: Proceedings of the ISOPE—ocean mining symposium, Tsukuba, Japan, 21–22 Nov, pp 193–200

Das GK, Anand S, Das RP et al (2000) Sulfur dioxide—a leachant for oxidic materials in aqueous and non-aqueous media. Miner Process Extr Metall Rev 20(4–6):377–407

Das PK, Anand S, Das RP (1997) Minimization of nickel precipitation from H_2O-NH_3 $(NH_4)_2SO_4$-SO_2-MnO_2 system. Int J Miner Process 50:77–86

Das RP (2001) India’s demonstration metallurgical plant to treat ocean nodule. In: Proceedings of the 4th ocean mining symposium, ISOPE, Szczecin, Poland, 23–27 Sept, pp 163–167

Das RP, Anand S (1997) Aqueous reduction of polymetallic nodule for metal extraction. In: Proceedings of the 2nd ocean mining symposium, ISOPE, Seoul, 24–26 Nov, pp 165–171

Das RP, Anand S, Das SC et al (1986) Leaching of manganese nodules in ammoniacal medium using glucose as a reductant. Hydrometallurgy 16:335–344
Das SC, Anand S, Das RP et al (1989) Sulphuric acid leaching of manganese nodules in the presence of charcoal. AusIMM Bull Proc 294(1):73–76
Demopoulos GP, Li Z, Becze MG et al (2008) New technologies for HCl regeneration in chloride hydrometallurgy. World Metallurgy Erzmetall 61(2):89–98
Fuerstenau DW, Han KN (1983) Metallurgy and processing of marine manganese nodules. Miner Process Technol Rev 1:1–83
Ghosh MK, Barik SP, Anand S (2008) Sulphuric acid leaching of polymetallic nodules using paper as a reductant. Trans Indian Inst Metals 61(6):477–481
Han KN, Fuerstenau DW (1975) Acid leaching of ocean nodules at elevated temperatures. Int J Miner Process 2(2):163–171
Han KN (1997) Strategies for processing of ocean floor manganese nodules. Trans Indian Inst Metals 51(1):41–54
Han KN, Fuerstenau DW (1986) Extraction behaviour of metallic elements from deep sea manganese nodules in reducing medium. Mar Min 2:155–169
Hanieg G, Meixner MJ (1974) Pressure leaching of manganese nodule with sulphuric acid. Erzmetall 27(7–8):335
Hariprasad D, Mohapatra M, Anand S (2013) Non-isothermal self-sustained one pot dissolution of metal values from manganese nodule using NH_3OHCl as a novel reductant in sulphuric acid medium. J Chem Technol Biotechnol 88(6):1114–1120
Harris BG, Lakshmanan VI, Sridhar R (2004) Process for the recovery of value metals from material containing base metal oxides. Patent WO/2004/101833, 25 Nov 2004
Harris B, White C, Jansen M et al (2006) A new approach to the high concentration chloride leaching of nickel laterites. In: ALTA Ni/Co, vol 11, Perth, Australia, 4–7 July 2006, pp 1–20
Haynes BW, Law SL, Barron DC, et al. (1985) Pacific manganese nodules: characterization and processing. Bulletin 679, U.S. Bureau of Mines
Hsiaohong C, Chongyue F, Di-Ji Z (1992) Reduction leaching of manganese nodules by nickel matte in hydrochloric acid solution. Hydrometallurgy 28:269–272
Hubred GL (1973) An extractive metallurgy study on deep sea manganese nodules with special emphasis on the sulphuric acid autoclave leach. Ph.D. thesis, University of California, Berkley, p 220
Hubred GL (1980) Manganese nodule extractive metallurgy: a review 1973–1978. Mar Min 2:191–212
ISA (2008) Workshop on polymetallic nodule mining technology, status and challenges ahead. NIOT, Chennai. http://www.isa.org.jm/files/documents/EN/Pubs/Chennai.pdf. Accessed 18–22 Feb 2008
Jana RK, Akerkar DD (1989) Studies of the metal–ammonia–carbon dioxide–water system in extraction metallurgy of poly metallic sea nodules. Hydrometallurgy 22:363–378
Jana RK, Murthy DSR, Nayak AK et al (1990) Leaching of roast-reduced poly metallic sea nodules to optimize the recoveries of copper, nickel and cobalt. Int J Miner Process 30:127–141
Jana RK, Singh DDN, Roy SK (1993) Hydrochloric acid leaching of sea nodules with methanol and ethanol addition. Mater Trans JIM (Japan) 34(70):593–598
Jana RK, Singh DDN, Roy SK (1995) Alcohol-modified hydrochloric acid leaching of sea nodules. Hydrometallurgy 38(3):289–298
Jana RK, Srikanth S, Pandey BD et al (1999a) Processing of deepsea manganese nodules at NML for recovery of copper, nickel and cobalt. Met Mater Process 11:133–144
Jana RK, Pandey BD, Premchand (1999b) Ammoniacal leaching of roast reduced deep-sea manganese nodules. Hydrometallurgy 53:45–56
Jennings PH, Stanley RW, Ames HL et al (1973) Development of a process for purifying molybdenite concentrates. In: Evans DJI (ed) Proceedings of second international symposium on hydrometallurgy, AIME, Chicago, New York, 25 Feb–1 Mar 1973, p 868
Jiang K, Jiang X, Feng L et al (2013) Study on self-catalysis reduction leaching of ocean Co-Mnpolymetallic ores in ammonia solution. In: Proceedings of the ISOPE ocean mining and gas hydrate symposium. Szczecin, Poland, 22–26 Sept

Junghanss H, Roever W (1976) Method for reprocessing of manganese nodules and extraction of valuable materials contained in them. German Patent 2,501,284, 1 Sept 1976
Kanungo SB (1999a) Rate process of the reduction leaching of manganese nodules in dilute HCl in the presence of pyrite Part-1: dissolution behavior of iron and sulphur species during leaching. Hydrometallurgy 52:313–330
Kanungo SB (1999b) Rate process of the reduction leaching of manganese nodules in dilute HCl in presence of pyrite Part-2: leaching behavior of manganese. Hydrometallurgy 52:331–347
Kanungo SB, Das RP (1988) Extraction of metals from manganese nodules of Indian ocean by leaching in aqueous solution of sulphur dioxide. Hydrometallurgy 20:135–146
Kanungo SB, Jena PK (1988a) Reduction leaching of manganese nodules of Indian Ocean origin in dilute hydrochloric acid. Hydrometallurgy 21(1):41–58
Kanungo SB, Jena PK (1988b) Studies on the dissolution of metal values in manganese nodules of Indian Ocean origin in dilute hydrochloric acid. Hydrometallurgy 21(1):23–39
Kawahara M, Mitsuo T (1992) Dilute sulphuric acid leaching of manganese nodules using hydrogen peroxide as a reductant. J Min Mater Process Inst Japan 108(5):396–401
Khalafalla S, Pahlman JE (1981) Selective extraction of metals from Pacific sea nodules. JOM 33(8):37–42
Kim DJ, Park KH (1997) Study on the leaching mechanism of Cu and Ni from deep sea manganese nodules with hydrochloric acid. In: Proceedings of the 2nd ocean mining symposium, ISOPE, Seoul, Korea, 24–26 Nov, pp 172–176
Kim I-S, Park K-H, Kim H-I (2005) Electroleaching of Fe-Ni-Cu-Co alloy. In: Proceedings of 6th ISOPE ocean mining symposium, Changsha, Hunan, China, 9–13 Oct, p 223
Kotlinski R (1999) Metallogenesis of the world's ocean against the background of oceanic crust evolution. Polish Geological Institute Special Papers, 4, 1999
Kotlinski R, Stoyanova HV, Avramov HA (2008) An overview of the interoceanmetal (IOM) deep sea technology development (mining and processing). http://www.isa.org.jm/files/documents/EN/Workshops/Feb2008/IOM-Abst.pdf
Kyle J (2010) Nickel laterite processing technologies—whereto next? In: ALTA 2010 Nickel/cobalt/copper conference, Perth, WA, Australia, 24–27 May
Lee JH, Gilje J, Zeitlin H (1978) Low temperature interaction of sulphur dioxide with Pacific ferromanganese nodules. Environ Sci Technol 12(13):1428–1431
Martino S, Parson LM (2012) A comparison between manganese nodules and cobalt crust economics in a scenario of mutual exclusivity. Mar Policy 36:790–800
Mehta KD, Das C, Pandey BD (2010) Leaching of copper, nickel and cobalt from Indian Ocean manganese nodules by *Aspergillus niger*. Hydrometallurgy 105:89–95
Mehta KD, Kumar R, Pandey BD et al (2008) Bio-dissolution of metals from activated nodules of Indian Ocean. Paper presented at International conference on Frontiers in Mechanochemistry and Mechanical Alloying held at CSIR-National Metallurgical Laboratory (CSIR-NML), Jamshedpur, India, 1–4 Dec 2008, under the aegis of International Mechanochemistry Association (IMA)
Mishra D, Srivastava RR, Sahu KK et al (2011) Leaching of roast-reduced manganese nodules in NH_3–$(NH4)_2CO_3$ medium. Hydrometallurgy 109:215–220
Mittal NK, Sen PK (2003) India's first medium scale demonstration plant for treating polymetallic nodules. Miner Eng 6:865–868
Mohanty PS, Ghosh MK, Anand S et al (1994) Leaching of manganese nodules in ammoniacal medium with elemental sulphur as reductant. Trans Inst Min Metall Sec C 103:C151–C155
Mohapatra M, Mishra D, Anand S et al (2000) Aqueous reduction of cobalto-cobaltic oxides in ammoniacal medium using ammonium sulphite as the reductant. Hydrometallurgy 58(3):193–202
Monhemius AJ (1980) The extractive metallurgy of deep sea manganese nodule. In: Burkin R (ed) Topics in non ferrous extractive metallurgy. Society of Chemical Industry, London, pp 42–69
Mukherjee A, Raichur AM, Modak JM et al (2003a) Bioprocessing of Indian Ocean nodules using marine isolate—effect of organics. Miner Eng 16:651–657
Mukherjee A, Raichur AM, Modak JM et al (2003b) Solubilisation of cobalt from ocean nodules at neutral pH—a novel bioprocess. J Ind Microbiol Biotechnol 30(10):606–612

Mukherjee A, Raichur AM, Modak JM et al (2004) Exploring process options to enhance metal dissolution in bioleaching of Indian Ocean nodules. J Chem Technol Biotechnol 79(5):512–517

Mohwinkel D, Kleint C, Koschinsky A (2014) Phase associations and potential selective extraction methods for selected high-tech metals from ferromanganese nodules and crusts with siderophores. Appl Geochem 43:13–21

Neuschutz D, Scheffler U, Junghans H (1977) Verfahren Zur Aufarbeitung von Manganknollen Durch Schwefelsaure Drucklaugung. (Method for the processing of manganese nodules by sulphuric acid pressure leaching). Erzmetall 30(2):61–67

Pahlman JE, Khalafalla SE (1979) Selective recovery of nickel, cobalt, manganese from sea nodules with sulfurous acid. US patent 4,138,465, 6 Feb 1979

Paramaguru RK, Kanungo SB (1998) Electrochemical phenomena in MnO_2-FeS_2 leaching in dilute HCl. Part-3: manganese dissolution from Indian Ocean nodules. Can Metall Q 37(5):405–417

Park KH, Kim DJ (1999) Kinetics of copper and nickel leaching of manganese nodules with hydrochloric acid. Met Mater Process 11(2):117–124

Park KH, Mohapatra D, Reddy BR et al (2007) A study on the oxidative ammonia-ammonium sulphate leaching of a complex (Cu-Ni-Co-Fe) matte. Hydrometallurgy 86:164–171

Parhi PK, Park KH, Nam CW, Park JT et al (2013) Extraction of rare earth metals from deep sea nodule using H_2SO_4 solution. Int J Miner Process 119:89

Parhi PK, Park KH, Kim HI et al (2011) Recovery of molybdenum from the sea nodule leach liquor by solvent extraction using Alamine 304-I. Hydrometallurgy 105:195–200

Parhi PK, Park KH, Nam CW et al (2015) Liquid-liquid extraction and separation of total rare earth (RE) metals from polymetallic manganese nodule leaching solution. J Rare Earths 3(2):207–213

Pophanken A, Friedrich B (2013) Challenges in the metallurgical processing of marine mineral resources. In: EMC 2013, University of Notre Dame, Indiana, 26–28 June 2013, p 681

Premchand P, Jana RK (1999) Processing of polymetallic sea nodules: an overview. In: Proceedings of the 3rd ocean mining symposium, ISOPE, Goa, India, 8–10 Nov, pp 237–245

Randhawa NS, Jana RK, Das NN (2013) Silicomanganese production utilising low grade manganese nodules leaching residue. Trans Inst Min Metall Sec C 122(1):6–14

Rodriguez MP, Mosqueda AM, Ariza SB (2001) Hydrometallurgical processing technology of the polymetallic nodules from Interoceanmetal mining site. In: Proceedings of the 4th ISOPE ocean mining symposium, Szczecin, Poland, 23–27 Sept, p 177

Rodriguez MP, Aja R, Miyares RC (2013) Optimization of the existing methods for recovery of basic metals from polymetallic nodules. In: Proceedings of the 10th ISOPE ocean mining and gas hydrates symposium, Szczecin, Poland, 22–26 Sept 2013, p 173

Rokukawa N (1990) Extraction of nickel, cobalt and copper from ocean manganese nodules with mixed solution of ammonium carbonate and ammonium sulphite. Shigen-to-Sozai 106(4):205–209

Rokukawa N (1995) Development for hydrometallurgical process of cobalt rich crusts. In: Proceedings of the ISOPE—ocean mining symposium, Tsukuba, Japan, 21–22 Nov, pp 217–221

Rao M, Li G, Jiang T, Luo J et al (2013) Carbothermic reduction of nickeliferous laterite ores for nickel pig iron production in China: a review. JOM 65(11):1573–1583

Sanjay K, Subbaiah T, Anand S et al. (1999) Manganese recovery from leach liquors/residues generated during hydrometallurgical processing of manganese nodules. In: Proceedings of the 3rd ocean mining symposium, ISOPE, Goa, India, 8–10 Nov 1999, p 246

Sazbo LJ (1976) Recovery of metal values from manganese deep sea nodules using ammoniacal cuprous leach solutions. US patent 3,983,017, 28 Sept 1976

Sen PK (1999) Processing of sea nodules: current status and future needs. Met Mater Process 11(2):85–100

Sen PK (2010) Metals and materials from deep sea nodules: an outlook for the future. Int Mater Rev 55(6):364–391

Shen YF, Xue WY, Niu WY (2008) Recovery of Co(II) and Ni(II) from hydrochloric acid solution of alloy scrap. Trans Nonferrous Metals Soc China 18(5):1262–1268

Smit JT, Steyl IDT (2005) Leaching process in the presence of hydrochloric acid for the recovery of a value metal from an ore. WIPO Patent Application PCT/IB2005/003136, 21 Oct 2005

Sridhar R (1974) Thermal upgrading of sea nodules. J Metals 26(12):18–22

Sridhar R, Jones WE, Warner JS (1976) Extraction of copper, nickel, cobalt from sea nodules. J Metals 28(4):32–37

Sridhar R, Warner JS, Bell MCE (1977) Non-ferrous metal recovery from deep sea nodules. US Patent 4,049,438, 20 Sept 1977

Sridhar V, Verma JK (2011) Extraction of copper, nickel and cobalt from the leach liquor of manganese-bearing sea nodules using LIX 984 N and ACORGA M5640. Miner Eng 24:959–962

Srikanth S, Alex TC, Agrawal A et al. (1997) Reduction roasting of deep-sea manganese nodules using liquid and gaseous reductants. In: Proceedings of the 2nd ocean mining symposium, Seoul, South Korea, 24–26 Nov 1997, pp 177–184

Stefanova VP, Iliev PK, Stefanov BS (2013) Copper, nickel and cobalt extraction from FeCuNiCoMn alloy obtained after pyrometallurgical processing of deep sea nodules. In: Proceedings of the 10th ISOPE ocean mining and gas hydrates symposium, Szczecin, Poland, 22–26 Sept 2013, p 180

Stefanova VP, Iliev PK, Stefanov BS et al (2009) Selective dissolution of FeCuNiCoMn alloy obtained after pyrometallurgical processing of polymetallic nodules. In: Proceedings of the 8th ISOPE ocean mining symposium, Chennai, India, Sept 2009, p 186

Vranka F (2001) Optimisation of technologies for processing of polymetallic nodules. In: Proceedings of the 4th ocean mining symposium, ISOPE, Szczecin, Poland, 23–27 Sept 2001, pp 172–175

Vranka F, Kotlinski R (2005) Polymetallic nodules processing in Interoceanmetal—the present and the future. In: Proceedings of the 15th International offshore and polar engineering conference, Seoul, Korea, 19–24 June, pp 392–397

Vu H, Jandova J, Lisa K et al (2005) Leaching of manganese deep ocean nodules in $FeSO_4$–H_2SO_4–H_2O solutions. Hydrometallurgy 77:147–153

Wang C-Y, Qiu D-F, Yin F et al (2010) Slurry electrolysis of ocean polymetallic nodule. Trans Nonferrous Metals Soc China 20:s60–s64

Wang Y, Li Z, Li H (2005) A new process for leaching metal values from ocean polymetallic nodules. Miner Eng 18:1093–1098

Watanabe A, Miwa S, Sakakibara S (1982) Sulphuric acid leaching of manganese nodules at elevated temperature. Nogoya Kogyo Gijutsu Shikensho Hokoku 31(6–7):190 (Japan), (CA 100: 107148)

Wilder TC, Galin WE (1976) Reduction smelting of manganese nodules with a liquid reductant. U.S. Patent 3,957,485, 18 May 1976

Xiang Z, Zequan H, Yujun S et al. (1999) The smelting–rusting-solvent extraction processes to recover valuable metals from polymetallic nodules. In: Proceedings of the 3rd ocean mining symposium, ISOPE, Goa, India, 8–10 Nov 1999, pp 227–231

Zhang Y, Liu Q, Sun C (2001a) Sulphuric acid leaching of ocean manganese nodules using phenols as reducing agents. Miner Eng 14(5):525–537

Zhang Y, Liu Q, Sun C (2001b) Sulphuric acid leaching of ocean manganese nodules using aromatic amines as reducing agents. Miner Eng 14(5):539–542

Dr. R. P. Das and his team at former Regional Research Laboratory, Bhubaneswar, pioneered hydrometallurgical processing of polymetallic nodule in India. They were associated with testing the first nodules collected from central Indian Ocean and upto pilot testing of India's first 500 kg/day nodule processing plant. Currently, Dr. Das freelances as a process metallurgist for treating complex metal bearing ores and industrial by-products.

Dr. S. Anand has been working on processing of Indian Ocean polymetallic nodules for almost three decades. Her main achievements include development of low temperature leaching of polymetallic nodule, and impurity control during leaching. Dr. Anand successfully led a team of researchers, who operated India's first 500 kg/day nodule processing plant. She has a number of publications on processing of polymetallic nodule. Currently, she is involved in precipitation and development of special materials.

Chapter 13
Sustainable Processing of Deep-Sea Polymetallic Nodules

P.K. Sen

Abstract The possibility of commercialization of processing technology for sea nodules has been linked with comparisons with similar terrestrial process operations. In addition to techno-economic viability, an added focus to commercialization is the sustainability of the process route. The general context of sustainability is discussed. The importance of material flow analysis, recycle rates of the metals produced as well as the possibility of a flow sheet being developed to supply short supply critical metals are brought out in this context. Environmental management for flow sheets under development is important for sustainable operations. Cradle-to-gate environmental burdens such as greenhouse gas emissions and solid waste burden both for common metals as well as for several other metals are provided as a basis of comparison. Polymetallic nodules (PMN) have been likened to low-grade manganese ores where three approaches have been reported for processing. Two of these approaches involve initial processing similar to laterite ore processing for recovery of Ni, Cu, and Co followed by manganese recovery similar to terrestrial ferroalloy production/manganese compound precipitation. The third approach attempts manganese recovery as ferroalloy followed by recovery of Cu, Ni, and Co as practiced for terrestrial sulfide ores. The relatively high values of gross energy requirements and emissions for terrestrial Ni and Co as compared to common metals point out that flow sheet development effort needs to focus on controlling these parameters for a nodules processing operation. On the other hand, these parameters have relatively low values for manganese ferroalloys produced from terrestrial resources. Production of ferroalloys from sea nodules needs to be comparable to their production from land resources. An approach for impact analysis is evolved where a system expansion strategy is followed for Cu, Ni, and Co with a subprocess of recovering manganese bearing ferroalloy. Regarding the later process step, both the Gross Energy Requirement (GER) and Emission (150 MJ and 10 t CO_2/t ferroalloy produced) far exceed the terrestrial processing values. For recovery of Ni, Cu, and Co, the results are process specific. For a roast reduction ammoniacal leach process, an energy input of 525 MJ and 40 kg CO_2/kg of Ni equivalent is estimated as compared to 200 MJ and 12 kg CO_2/kg of nickel equivalent for a complete hydrometallurgical process. Thus, the roast reduction ammoniacal leaching process

P.K. Sen (✉)
Indian Institute of Technology, Kharagpur 721302, West Bengal, India
e-mail: prodip.sen@gmail.com

R. Sharma (ed.), *Deep-Sea Mining*, DOI 10.1007/978-3-319-52557-0_13

is not sustainable for sea nodules processing for recovery of Ni, Cu, and Co because of high GER values and high specific CO_2 emissions. The high pressure acid leaching route has comparable values to similar laterite processing operations. For flow sheet concepts involving manganese dissolution, recovery of manganese as electrolytic manganese dioxide is less energy intensive compared to residue smelting operation with high gross energy requirements and emissions. For nodule processing flow sheets involving use of energy chemicals (NH_3, HCl, H_2),appropriate reagent recycle schemes for reagents need to be conceived; else process integration with external flow sheets needs to be contemplated for enhancing sustainability. Considering resource crunch of rare earth elements with respect to terrestrial resources, the recovery of rare earth from sea nodules will enhance the sustainability of the sea bed deposits.

13.1 Introduction

The fact that deep sea bed ferromanganese nodules can be regarded as a major economic potential of industrial metals like associated nickel, copper, cobalt in addition to manganese was recognized only within the past 40 years by Mero (1965). Halbach and Fellerer (1980) have cited that the ratio of metal reserves on land (approved, probable and possible reserves) and metal amounts held by the nodules is approximately 1 for nickel and manganese and 10 for copper; however for cobalt, it is 0.08, i.e., 12 times more than the continental cobalt. Although the above figures are subject to revision in absolute terms, the fact remains that sea nodules could behave as an exploitable manganese resource depending on the price ratios of the associated metals with respect to manganese. Thus, in addition to the existing thrust on utilization of low and medium grade of terrestrial manganese ores, utilization of additional manganese bearing resources from the sea resembling low-grade manganese ores but with added values has been critically examined in several countries. Several different approaches adopted for processing the deep-sea marine resources have been proposed.

Processing of sea nodules has been traditionally compared to nickel laterite ore processing and initial process flow sheets formulated bear a remarkable similarity to roast-reduction/leaching route and direct leaching of laterite ores (the ammoniacal leaching based Caron process and the Moa Bay type of direct acid leaching operations). Treatment processes include the approach of recovering only Cu, Ni, and Co while generating a manganese bearing residue for further treatment. Alternatively, the process of direct smelting of the nodules produces Fe-Cu-Ni-Co alloys and manganese bearing slag. The slag is however not suitable for direct production of high carbon ferromanganese. As much as the above processes have been subjected to detailed process analysis with a focus on comparison with laterite-based processing flow sheets, Metallurgie Hoboken-Overpelt (MHO) had experimented on flow sheet development with HCl as the lixiviant (Van Peteghem 1977); the important aspect of this work is that the cycle is almost closed, meaning thereby that all reagents used are virtually regenerated. The manganese is recovered in precipitated form.

Detailed process information is only available through patents, and mass/energy balances have not been reported in literature.

Several other processes (Zhang et al. 2001; Mukherjee et al. 2004) have been reported. However, little information is available on sustainability of the processing operations which is the subject of this chapter. The context of sustainability for land-based processing operations of deep-sea nodules becomes extremely important as comparisons drawn with similar land-based operations would have a bearing on commercialization possibilities of novel flow sheets.

At the onset, the general context of sustainable development will be briefly mentioned. This will lead to a focus on parameters which need to be monitored for sustainable process development. Typical values of such parameters for sustainable production of metals will be discussed. For a process based on metal production from sea nodules, it is important to deal with comparative values of the parameters chosen, both with respect to other metal production processes and terrestrial exploitation of metals relevant to sea nodules processing, since this will lead to an appreciation of monitoring sustainability parameters during processing.

13.2 Sustainability: General Outlook

It is indisputable that modern life is enabled by the use of materials in its technologies. Those technologies do many things very well, largely because each material is used for purposes to which it is exquisitely fitted. Metals and minerals are inputs to several product metals and materials; for example, the increased output of metals and the increased value of most metals have resulted in a rise in value of the global metal and industrial minerals mining industry from US$214 billion in 2000 to US$644 billion by 2010 (International council of Mining and Metals 2012). The phenomenal increase in the quantities of inputs available for production of materials has led scientists and technologists alike to experiment with the development of new materials using a variety of inputs. All such efforts are affected by the implications of sustainable development, because none of our material resources are infinite and only a few sources of energy (solar, wind, hydro, tidal, and geothermal) are sustainable. There are several other aspects of development which needs to be covered under one tent: sustainable development needs to capture the concepts of environmental stewardship, materials management, green manufacturing, renewable and clean energy technologies, and water and air management together. The challenges of sustainable development will require materials engineers and scientists to think beyond the current definition of what constitutes the “best” material for a given application.

Sustainable development also needs to include constraints imposed by economic and social goals as well in addition to environmental goals related to materials management and manufacturing (Fig. 13.1). These three goals must be met locally and globally for both present and future generations. While this concept is generally accepted and relatively easy to comprehend, difficulties would arise if there is a need to measure the “level of sustainability” of different sections of society, i.e., local and national governments, industry, local communities, and individuals, to

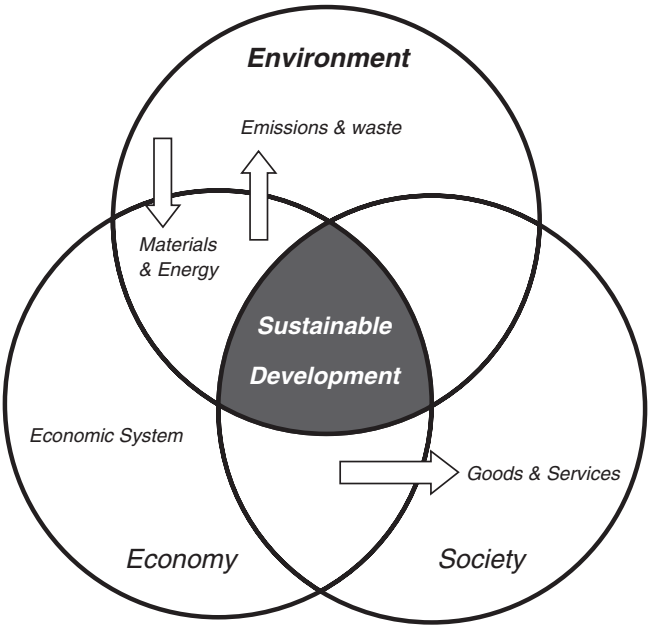

Fig. 13.1 Factors affecting sustainability

determine which directions of change are towards sustainability. Dealing with such aspects is indeed a task which would include wide-ranging aspects and a discussion of these is beyond the purview of this chapter.

Rather than attempting to discuss on quantitative measures of sustainability levels, in this chapter the principle focus is to review the basic issues which need to be looked at while carrying out process development work on flow sheet development in the context of deep-sea nodules directed towards attaining sustainability. The objective of this chapter is thus twofold: (a) to examine the possible platform to examine the issues related to sustainability of metals processing flow sheet development and (b) look at qualitative measures which can offer a basis of comparison of different alternative processes and products considering that future process routes and products marketed need to be sustainable (Azapagic and Perdan 2000).

13.3 Sustainability and Process Development: Material Flow, Reuse and Critical Metals

The immediate and direct connections between sustainable development and process development include efficient use of materials (conservation, substitution, reuse, repurposing, recycling), materials life cycle assessment (LCA), replacement materials (scarcity, resource availability, materials economics), energy (materials to support alternative energy technologies, to mitigate problems with fossil fuel technologies, and to increase energy efficiency), and mitigation of undesirable environmental

impacts from technology and economic growth. These considerations on sustainable developments of processing inputs have encompassed several applications and strategies. For example, (a) Light-weighting is strategy for all forms of transportation which follows from LCA including use phase, (b) Photovoltaic materials have the potential to be deployed on a large scale for the economical and sustainable generation of electrical power with a possible decrease of energy-related emissions, and (c) The recyclate stream from electronic waste, a component of "urban mining," can be richer in strategic elements than an actual mine: recycle streams increase the life span of resources. Certain issues where attention is required are discussed below.

1. Increasing material flows contribute to the world's environmental as well as social problems. As brought out by Fiksel (2006) the broader objective is to seek to reduce the material throughput required for sustainable growth and prosperity and to minimize the adverse impacts of material usage upon environmental and social well-being. Typically, a material flow analysis (MFA) needs to be performed. The importance of dematerialization and detoxification has been brought out in this context. More mass usually means more energy use, more waste, and more emissions. A direct quantification of material use viz-a-viz the environmental effects requires development of the option of life cycle analysis of material flows in which not only the materials themselves, but everything connected to them is part of the picture: energy use for extraction and production, transport, the use of auxiliary materials, land use, other emissions at the production or waste stage, etc. The importance of attaining higher process recoveries may be noted.
2. Van der Voet et al. (2004) point out that dematerialization is not just weight reduction, but refers to quantitative impacts based on per kg of the flow of the chosen material. Five categories of impacts have been reported. Data on impacts on materials flow in the Netherlands have been analyzed. Rhodium, palladium, and platinum have been reported with very high scores. Further, tables presented in the publication show that metals with large flows with moderate impacts per kg are at the top, as expected. Materials which did not make many of the top-twenties for the different categories chosen include ammonia, sulfur, and chlorine. The precious metals, having a very large contribution per kg, can be found at rankings 29, 32, and 41. Copper and zinc flows are relatively smaller but contribute relatively a lot per kg so they still appear in the top-20. Although the data presented is local, the approach is worth noting. Case studies on actual systems have been presented by Hekkert (2000) in his thesis on reduction of greenhouse gas (GHG) emissions through better materials management.
3. The reduction of material throughput in an economic system can be effected through a number approaches: increase of material efficiency in materials production flow sheet, thus reducing waste, eco-design of products to reduce mass, material substitution by reducing mass keeping in view the environmental effects, etc. If the material flow cannot be gainfully reduced, supplementary approaches for reduction of environmental effects for larger flows are examined, which include replacing toxic or hazardous materials with benign ones, use of cleaner technologies, reducing the toxic or hazardous properties of waste streams, reduction of greenhouse gas emissions associated with fossil fuel combustion through carbon sequestration, etc. (Fiksel 2006).

4. Subsequent to the analysis of material flows, a natural question in the present context is can robust supplies of all these materials be ensured for the required material flows? Doubts have been raised with respect to available metal and mineral supplies with escalating demands. In the context of deep-sea nodules, disruption of nodules supply would require adaptability of the flow sheet to alternative terrestrial supplies.
5. One way of ensuring steady supply of nonfuel inputs to the nodules processing operation is to ensure that the outputs being produced have acceptable recycle rates so that resource crunch on this account is not experienced. The higher is the recycle rate, lesser will the targeted reserve be used. Hence lesser inputs are expected to be used. Elemental life cycle analyses have increasingly been conducted to characterize rates of recycling and loss of materials in new systems based on operating information of flow sheets. The criticality of a resource base is hence linked to the recyclability of the target output metals from the point of view of sustainability of the evolved flow sheet.

   The recycle process for the products is schematically shown in Fig. 13.2. The life cycle of a metal is closed if end-of-life products enter appropriate recycle chains. On the other hand, open life cycle includes products discarded to landfills or application of inefficient technologies which recover the metals inefficiently leading to nonfunctional recycling. Several metals are not recirculated because of trade considerations: the discards are exported reducing the recycling rates as well as opening up the possibility of a resource crunch for the importing country if it is dependent of such resources in a major way. A recent report from UNEP (UNEP Report 2011) indicates that 18 out of 60 metals have a recycle rate of >50%. These include Al, Ti, Cr, Mn, Fe, Co, Ni, Cu, Zn, Nb, Rh, Pd, Ag, Pt, Pd,

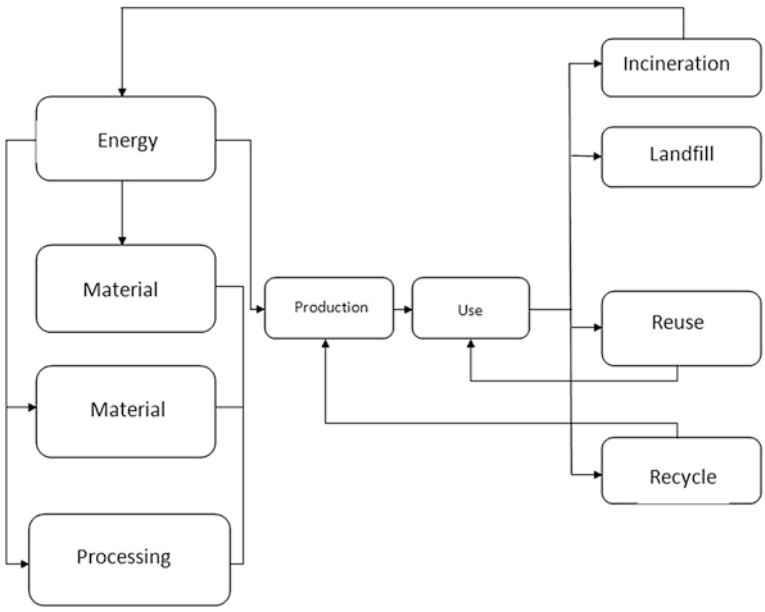

Fig. 13.2 The recycle chain (UNEP/SETAC Life Cycle Initiative 2011)

Au, Sn, and Pb. Metals such as Mo, Ir, and Mg have a recycle rate of 10–25%. The rare earths and a number of other metals have a recycle rate of <1%. It is not appropriate to deal with the details of this report in the present context. Since the recycle rates are very poor for the lanthanides and a host of other metals, some of these are deemed as critical metals.

In the context of the sea bed nodules resource final products, Mn, Ni, Co, and Cu have good recycle rates. Metals which have low recycle rates will prove to be valuable if these metals are present in the sea bed nodules resources. If rare earths are considered as recoverable metals from the deep-sea nodules, the deep sea bed resource base as metal supplier of such metals can have enhanced value. The flow sheet developed will be more sustainable.

6. Sustainability considerations also look at criticality of availability of the final metals derived from a resource base in addition to the considerations of recyclability. In 2006, the US National Research Council analyzed data on nonfuel minerals criticality as a function of use and availability (Graedel et al. 2015; Lorenz and Graedel 2011). Factors cited include supply risks, demand growth, and recycling restrictions.

   Of the metals surveyed, a number were identified as critical: rhodium, platinum, manganese, niobium, indium, and the rare earths. Copper was not considered critical, not because of lack of importance but because supply risk was judged to be low. A UNEP study categorized the critical metals under the heads of electrical and electronics equipment, (Ta, In, Ru, Ga, Ge, Pd), photovoltaic (Ga, Te, Ge, In, etc.), batteries (Co, Li, and rare earths), and catalysts (Pt, Pd, rare earths) (UNEP Report 2009) (Fig. 13.3).

   It may be noted that supply of Co, rare earths, and precious metals (once extraction technology is developed) from the sea nodule resource base will enhance the value of the resource base.

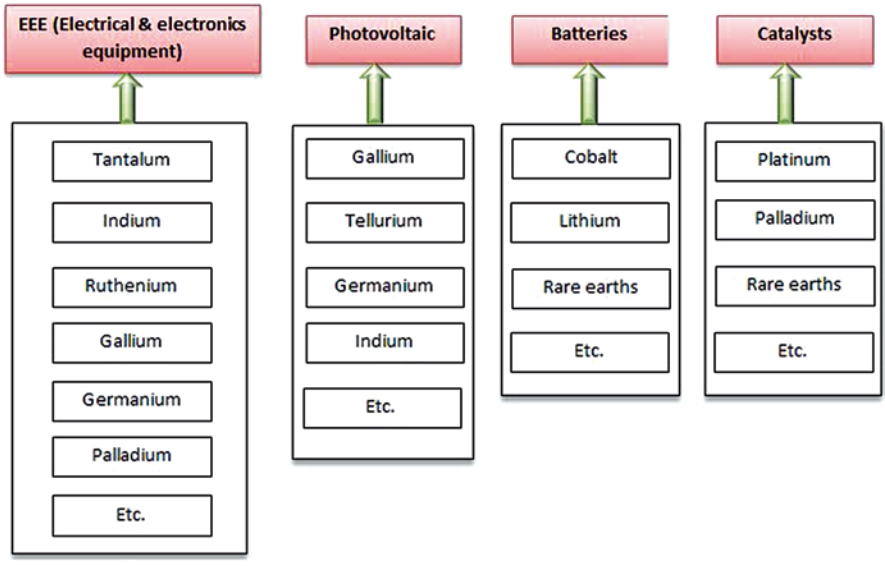

Fig. 13.3 Criticality clusters after UNEP (UNEP Report 2009)

7. It is not only resource constraint which is of concern; materials production will not be sustainable if they are too expensive to produce, the materials required for their manufacture are depletable, or they are environmentally unsafe. Typical externalities include potential climate change due to emissions and degradation of air, water, land, and wildlife habitats.

13.4 The Context of Environmental Management

The process of materials production involves a number of stages commencing with resource extraction, processing of resources which yields input to the product design and manufacturing stage. Subsequently there is a use phase of the products at the end of which the discarded product is either finally disposed or reused through appropriate processing stages. The steps are covered in an EPA report and are reproduced below (Fig. 13.4) (EPA Report 2009). Each of these steps involves use of energy and auxiliary resources. Emissions to air, water, and land are a direct consequence of the use of the varied inputs. The quantification of the environmental issues is dependent on reuse/recycling/remanufacturing/waste utilization steps and

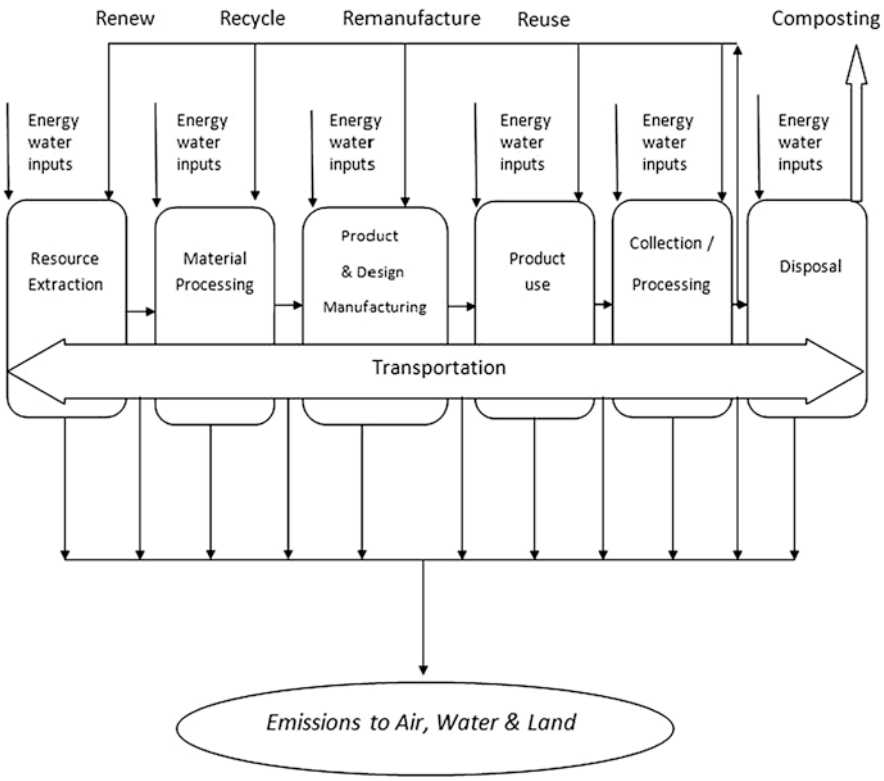

Fig. 13.4 The life cycle analysis chain

hence the life cycle chain (LCA). Whereas resource depletion needs to be evaluated in terms of the use of alternative resources, generally industrial production processes are linked to consequences of resource depletion and environmental degradation and constitute an evaluation point for sustainability.

It is of some importance to examine the response of the industry to the issue of environmental degradation and resource depletion. Initially, adoption of end-of-pipe solutions as cleanup measures (disposal) has been looked at irrespective of the production process. Soon it was realized that reduction of waste through efficient use of resources was more beneficial. At present, environmental performance reports are being integrated with business strategies. More responsible environment management processes such as zero emission and by-product synergy have evolved.

The concept of eco-efficiency is important for business translation (vide economic system, Fig. 13.1; Azapagic and Perdan 2000). It is concerned with creating more value with less impact. Environmental performances are normalized with respect to economic indicators. The interested reader may refer to Siemens Sustainability Report (2012) which describes the key performance indicators with respect to society, economic performance, and environment.

The report emphasizes the thrust on sustainability by a large group like Siemens as follows:

> "*At Siemens, we're preparing for this future with an overarching strategy that has sustainability as its guiding principle. Sustainability is more than just a buzzword: It derives from ways of thinking and acting which were developed 300 years ago and affect many areas of our life today. The concept of sustainability also had an impact on our company's founder. Werner von Siemens recognized early on that sustainability had great potential for an innovative company and that the principles of good business—that is, efficiency and growth on the one hand, and responsibility for society and the environment, on the other—were not mutually exclusive but mutually reinforcing. This understanding of sustainability as a business opportunity that drives economic, environmental and social progress has dominated our strategy and activities for 165 years*."

A critical look at environment performance reports of industries will offer process developers and engineers several opportunities to incorporate sustainable development into their work so that these can be tuned to the larger scenario of business applications.

It is necessary that the researcher and technologist be familiar with basic approaches of LCA so that the conceptualization of new processes/product is tuned to sustainable process thinking. We have already discussed a few consequences of LCA earlier during discussions on resource depletion.

The seeds of life cycle assessment for developing sustainable products were first grown in the late 1960s/early 1970s, during the oil crisis when energy costs were skyrocketing. Companies were looking for ways to cut down on energy costs and develop more energy efficient products. Subsequently, greater energy efficiency was followed by resource analysis and greenhouse gas assessment, all of which were encompassed within the broad framework of LCA. The different analyses which have been reported are:

- Cradle-to-gate: From raw material extraction to factory gate.
- Cradle-to-grave: From raw material extraction through product use and disposal.

Gate-to-Gate: From one defined point along the life cycle (e.g., where incoming raw materials cross the fence-line of a manufacturing site) to a second defined point further along the life cycle (e.g., where a finished product is delivered to an end user).

Sometimes the term 'cradle-to-cradle' is used to indicate a 'cradle-to-grave' approach where some of the products are recycled to the initial point.

Generally, an inventory analysis of resource use and emissions is made for each life cycle stage. Using impact category considering the various category indicators (briefly discussed below), characterization models and weighting values are used to translate the raw data into potential into potential impact on health and environment. The widely used category indicators comprise the following:

1. Cumulative energy demand (CED) over the entire life cycle of the product including waste management: This includes both the fossil energy demand and the renewable energy demand. It also includes feedstock energy. The gross energy requirement (GER) pertains to a flow sheet boundary in which feed stock energies may not feature. These terms have been used interchangeably.
2. Global warming potential (GWP), also known as carbon footprint: This category reflects the climate change impact over a fixed period of time in terms of the total emissions of greenhouse gases. Impact factors with respect to different gases with respect to the global warming potential are different and are available. The GWP value of a system incorporates these impact factors. The Green House Gas emission (GHG, measured as t CO_2/t functional unit) is a direct measure of impact of emissions from a flow sheet and is widely used.
3. Ozone Depletion Potential (ODP): A category that reflects the relative effect of total emissions of gases that deplete stratospheric ozone across the life cycle of a product.
4. Acidification Potential (AP): A category that reflects the relative effect of total emissions of acidic gases (e.g., sulfur oxides (SOx), nitrogen oxides (NOx), hydrochloric acid (HCl), etc.,) to air across the life cycle of a product.
5. Eutrophication Potential (EP), also called Nutrification Potential (NP): A category that reflects the overgrowth of algae caused by emissions of limiting nutrients (compounds containing phosphorus or nitrogen) directly or indirectly to water bodies (lakes, slow moving rivers, estuaries, etc.) and soil across the life cycle of a product.
6. Photochemical Ozone Creation Potential (POCP): A category that reflects the relative effect of total emissions of volatile organic compounds (VOCs) and oxides of nitrogen across the life cycle of a product.
7. Consumptive Water Footprint and Water Emissions Footprint: This describes the total life cycle requirement of water necessary for delivering the functional unit, including end-of-life waste management.
8. Eco- and Human Toxicity Assessment: Chemical-specific characterization factors that quantify the environmental fate of chemical emissions and their impact on human health and on ecosystems.
9. Direct/indirect land use change (LUC): Direct conversion of land refers to alteration from its original form (forest, grassland, cropland, etc.) to an altered state for the production of agricultural or forestry products (e.g., biofuel feedstock), with resulting changes in GHG emissions and carbon stocks on that land.

Often the impact categories can be related to a single impact category such as GWP, described later. The paragraphs below report how the impact categories have been generally related to sustainability for systems of our interest.

The discussions below refer to cradle-to-gate stages (primary metal production from raw material extraction) for which environmental burdens are worked out specifically for emissions and solid waste burden. Implications for cradle-to-grave stages (finished product from raw material extraction) are product specific. Sometimes gate-to-gate (chosen entry point to chosen exit point) analysis is made for specific contexts such as comparative energy analysis.

13.5 Impact Analysis of Processes

It is instructive to review briefly the impacts of process development for a number of metals from terrestrial ores so that one can draw comparisons with sea nodules processing. The impacts considered do not include sea mining operations since the focus is to examine the impact of land-based processing only.

13.5.1 Cradle-to-Gate Environmental Burdens: Common Metal Production and GHG Emissions

Metals constitute major inputs to various materials in use. Several studies have been conducted on life cycle analysis of metals on a gate-to-gate basis based on energy requirements of metal production (Norgate and Jahanshahi 2010). Higher energy requirements lead to greater environmental burden as GHG emissions. In the general methodology of estimation for impacts for LCA for metal production, in addition to the gross energy requirement leading to estimation of GHG, AP and SWB (solid waste burden) have been considered (Norgate et al. 2007). The gross energy requirement has also been referred to as embodied energy. The embodied energy is calculated based on waste rock to ore ratio, grade of the ore body, and the fraction of ore recovered during mining, beneficiation, and chemical processing stages. With knowledge of the unit energies for all the stages, the energy per ton of value in the products is calculated. Typical values are provided in Table 13.1.

Table 13.1 Gross energy requirements for common metals

Gross energy requirement (MJ/kg metal produced)	Al	Cu	Steel
Mining	0.2	13.9	0.15
Beneficiation	0.13	2.5	0.45
Chemical processing I	30	45.5	21.1
Chemical processing II	186		1.05
Embodied energy	216	61.9	22.7

Table 13.2 Gross energy requirement and environmental parameters

	Copper	Nickel	Lead	Zinc	Aluminum	Steel	Cement[a]
GER (GJ/tonne metal)	64.5	93.08	9.6	8.4	211.5	2.7	5.6
GHG(CO_2/tonne of metal)	6.16	6.08	2.07	4.61	22.7	2.19	0.9
Solid waste burden (kg/kg)[b]	125	51	4.8	29.3	4.5	2.4	–

[a]For reference purposes [b]Includes mining wastes

Rankin (2011) has provided example embodied energy calculation (E) based on EM (mining energy, MJ/t rock), waste ore:rock ratio (W), ore sent to beneficiation plant/tonne of ore mined (RM), energy required/t ore treated (EB), grade of the ore (G0), and recoveries in extraction stages (RC1 and RC2) as provided by the equation below:

$$E = \frac{1}{\mathrm{G0}.RM.RC1.RC2}\left(\frac{EM\left(1+W\right)}{RM}\right)+\frac{EC1}{RC2}+EC2$$

The embodied energy for nickel from terrestrial ores for pyrometallurgical route (sulfide ores) and hydrometallurgical route (laterite) have been reported by the same author as 113.5 MJ/t Ni and 193.7 MJ/t Ni, respectively. The smelting process energy includes energy for beneficiation. For purposes of comparison with energy requirements for processing of sea nodules, these figures will have important significance.

The gross energy requirement is correlated with the global warming potential of metals, as shown below in Table 13.2 (Rankin 2012).

Since metal production processes have been traditionally linked to the impact of greenhouse gases and waste production, at the exit gate of the crude metal production, the gross energy requirement and the associated GHG emissions are to be loaded to the manufacturing product cycle where the site is spatially separated, whereas waste management is within the purview of the metal producer.

13.5.2 Cradle-to-Gate Environmental Burdens: Several Metals

Cradle-to-gate burdens for several metals have been recently discussed (Nuss and Eckelman 2014). While a century ago, the diversity of metals employed was limited to perhaps a dozen in common uses such as infrastructure and durable goods, today's technologies utilizes virtually the entire periodic table. For example, the number of elements employed in integrated circuits used in most electronics products has increased from only 12 elements in 1980 to more than 60 elements today, while electronic products themselves are used in an increasing number of applications. Similarly, the elemental complexity of super alloys, which are a class of materials to allow the operation of turbines and jet engines at high temperatures

and under corrosive environments, has increased over time as new alloying elements (e.g., rhenium, tantalum, hafnium) are added. Metal refining when carried out to achieve sufficiently high purities requires intensive use of fossil fuel inputs directly or indirectly such as reductant, heat, and electricity. While the environmental implications of the major industrial metals (e.g., iron and copper) have been extensively studied, the environmental burdens of many of the minor metals (e.g., niobium, rhenium, hafnium) are essentially unknown, even though they are increasingly employed by industry. Several metal production routes are interlinked with each other and form an intricate network of industrial processes (Reference above, highlighted in red color in Fig. 13.1 of the reference). For metals obtained in multi-output processes (joint production), it is necessary to divide the environmental impacts from the process and all upstream processes among all metal coproduct(s). Assigning each metal coproduction an appropriate proportion of environmental impacts can be done in multiple, standardized ways, for example by applying mass allocation or economic allocation as specified in the ISO standards for LCA. This is discussed in brief subsequently.

Typical values of some elements in terms of correlation between GWP and CED are reported in Table 13.3 below. The rare earths (lanthanide group of elements) and the actinide elements have high values of cumulative energy demand. The CED values are equivalent to GER values once input energy is considered. The GWP value is also equivalent to GHG if only CO_2 is considered.

The CED values (MJ/kg) for products of interest to sea nodule processing have been reported as 23.5, 23.5, and 138 for Fe-Mn, Si-Mn, and Co with values of global warming potential (kg eq.CO_2/kg) as 1.2, 1.2, and 11.5, respectively. The author brings out interestingly that it is necessary to perform stage-wise environmental impacts to identify opportunities to reduce the impacts. Nuss and Eckelman (2014) additionally bring out that for elements in their metallic form (either metals or alloys) the environmental burden is largely due to the purification (i.e., smelting) and refining stages required to obtain the final metal product (see Li, Be, Al, ferrochromium (Fe-Cr), Cr, ferromanganese (Fe-Mn), Fe, Cu (combined metal production, SE), Zn, Ge, Se, Zr, ferroniobium (Fe-Nb), Ru, Ag (from Pb), Cd, In, Te, Pb (from Pb-Zn), and Bi). For Ge, In, and Ag, the purification stage contributes more to overall impacts than subsequent refining. This is because for metals the smelting process, producing intermediates such as anode slime or leaching residue, is included in the purification stage. For example, the purification stage of Ge and In includes the environmental burdens of Zn smelting, yielding a leaching residue from which both elements are recovered as coproducts (together with Bi, and Tl) (see section 20 of Supporting Information S1, Nuss and Eckelman 2014).

Table 13.3 Cumulative energy demand and global warming potential for rare earth metals

	La	Ce	Pr	Nd	Sm	Eu	Gd	Tb	Dy	Fe[a]
CED MJ-eq/kg	215.0	252.0	376.0	344.0	1160.0	7750	914.0	5820	1170.0	23.1
GWP (kg CO_2eq/kg)	11.0	12.9	19.2	17.6	59.1	395	46.6	297	59.6	1.5

13.5.3 GER/CED to Predict Environmental Burdens

One of the difficulties of carrying out complete LCA is that a relatively large amount of data is required. Although various software programs with inventory data are available, the data gathering for specific production processes is not without problems. This is due to the fact that process data are not (publicly) available or that they are not provided in a standardized format. The applicability of LCAs would greatly improve if less information with relatively high reliability could be used to compare or improve production processes. This is particularly the case for LCA studies focusing on early product development phase. The CED represents the energy demand, valued as primary energy during the complete life-cycle of a product. Particularly, from fossil energy demand it is well known that it is dominantly responsible for global warming and depletion of fossil resources.

A close examination of the data provided will bring out that there is a correlation between CED and GWP. Compared to complete LCA studies, the calculation of CEDs requires substantially less information in the inventory analysis (Huijbregts et al. 2010).

13.5.4 Recycle Rates and CED/GHG

It needs to be kept in view that the recycle rates of the input metals used in a new system development decide the indicative values of the GWP of the inputs. An example of this, information is cited below (International Aluminum Institute 2013) from a document published by the Aluminum Research Institute.

Aluminum produced has a GWP of 10.4 kg CO_2/kg of aluminum for a specific input energy mix for producing aluminum. The GWP (carbon footprint) of an aluminum window frame with a mass of 20 kg is calculated as cradle-to-gate, with no recycled content assumed, is 20*(1.6 + 10.4) kg CO_2e = 240 kg CO_2e, from which 20*10.4 kg CO_2e = 208 kg CO_2e is related to the production of primary aluminum from bauxite and 20*1.6 kg CO_2e = 32 kg CO_2e is related to the production or the window frame from the ingot. This value is significantly higher than the carbon footprint values of window frames made of alternative materials.

However, when the typical recycling rate of a window frame of 94% is considered, then 94% of the 208 kg CO_2e for the production of primary aluminum, i.e., 196 kg CO_2e, are substituted, but 11 kg CO_2e have to be added for the end-of-life operations. Taking all this into account, the real carbon footprint value of the aluminum window frame is 55 kg CO_2e, i.e., 32 kg CO_2e related to the production of the window frame from the ingot, 11 kg related to the recycling operations, and 12 kg CO_2e related to the substitution of the 6% recycling loss. This value compares positively with the carbon footprint values of window frames made of alternative materials.

Application of LCA procedures to recycling has been detailed out in literature (Ligthart and Toon 2012). Information pertaining to recycle rates of metals has been comprehensively presented in a UNEP report cited earlier in this chapter (UNEP Report 2011).

Sea nodules process development efforts presently do not consider incorporation of external recycle of the metal bearing solids with a view to lower GER/GHG values. Presumably this is because only cradle-to-gate processes are considered and external streams are readily incorporated at the manufacturing end, i.e., beyond gate. However, recycle of reagent streams which have high input energy is particularly important during process development. This may well lead to a more sustainable process with lower energy and emissions.

13.6 Sea Nodules Processing and Sustainability Issues

The general context of sustainability issues described in the previous paragraphs brings out the necessity of flow sheet development (conceptual/actual) with material flow analysis and its optimization. Also, maintaining recycle rate of different inputs and the possibility of enhancing the value of the resource base through extraction of critical metals from the deposit are important considerations. Once a process flow sheet is available, it is possible to estimate environmental burdens (GHG/CED and GHG emissions) and draw a comparison with land-based resources. The gross energy requirement (GER/CED) is a good guideline to estimate GHG emissions pertaining to a specific flow sheet, as has been brought out earlier. Additionally, of solids waste burden as well as liquid effluents can be estimated with respect to a process. Thus, flow sheet development is of prime importance for establishing the sustainability of a process considering the parameters for sustainability discussed earlier.

The following paragraphs briefly review the status of process development, subsequent to which attempts of estimating impact information are made using available data. A comparison with land-based operations can then be drawn.

13.7 Observations on Sea Nodules Processing Efforts

Ongoing efforts have been recently reviewed by the author (Sen, 2010). Salient aspects of processing are drawn from this publication. A scrutiny of a typical sea nodules composition leads us to conclude that this resembles a low-grade manganese ore with added metal contents Ni, Co, and Cu which are coproducts to the principal ore. The multi-metal deep-sea nodules as a resource has been compared to terrestrial nickel laterite ores which can be processed via pyrometallurgical or hydrometallurgical means. Although the process development strategies for sea nodules could be drawn from processing of similar terrestrial ores, the exploration, mining, and transportation costs are substantially greater than laterite ores. Thus, researchers who had embarked upon newer routes have been drawn into the manganese recovery option to work out a viable route for recovery of all metals. The manganese recovery option is not necessarily connected to the market situation; for recovery of three metals, stability of the manganese containing residue becomes an important consideration, specifically for environmental considerations. The polymetallic nodules

resources can thus be compared to low-grade manganese ores with higher investment risks where additional income from copper and nickel recovery is expected to balance the extra costs for exploration, mining, and transportation.

13.7.1 Process Research and Flow Sheet Development

Chemical composition of the nodules changes from location to location across the vast sea bed. Manganese, which is present as manganese dioxide, is the major metallic component, varying over a wide range of 17–30%. Other associated metals present in the nodule matrix are of lower proportions in comparison to manganese. The composition of medium grade sea nodules on average varies between Mn: 17–28%, Cu: 0.5–1.3%, Ni: 0.5–1.3%, and Co: 0.1–0.26%. Higher grade sea nodules, as is typically displayed for Pacific sea nodule, have the range of Mn: 24–30%, Cu: 0.8–1.4%, Ni: 0.8–1.4%, and Co: 0.16–0.26%.

As much as earlier research was conducted on recovery of Ni, Cu, and Co, subsequent efforts globally have realized the importance of manganese recovery, although these have scarcely been directed towards flow sheet development and subsequent testing for commercial viability. There has been a thrust on more towards finding alternative reagents which could enhance performance of conventional reagents. Zhang et al. (2001) have described use of specific aromatic reductants in sulfuric acid medium for which laboratory scale studies were conducted leading to solubilization of all metals including manganese. Other potentially novel reagents for manganese nodules have been reviewed by Mukherjee et al. (2004). Whereas these studies were directed at improving the performance of sulfuric acid leaching, the results cannot be analyzed from the point of view of flow sheet development and process sustainability in terms of GER/CED and emissions.

More information is available on flow sheets through consortia information dissemination (Sen and Das 2008). Earlier work by various consortia partners and companies had led to piloting of certain key steps in the processing operation. Pilot operations have been run for limited time periods and there are no references to suggest that these have been sustained. Only the processes studied by Kennecott Copper Corporation (KCC) and Deep Sea Ventures (DSV) were carried out till the end phase along with aspects such as reagents recycles. No pilot plants activities have been reported during 1980 other than the CEA plant (AFERNOD). Active research on nodules processing is being pursued presently by some Indian Laboratories, Chinese, Japanese, and Korean Firms/Laboratories. However, large-scale testing information has scarcely been reported.

13.7.2 Three Metal Option to Four Metal Option

The various approaches for process development treat nodules processing as a primary nickel producing operation with by-product recoveries of copper, cobalt, and manganese. The major advantage of doing this is to draw a direct comparison with

land-based nickel laterite operation and also highlight the importance of recovering other revenue bearing products namely copper, cobalt, and manganese. For example, processing of sea nodules has been traditionally compared to nickel laterite ore processing and initial process flow sheets formulated bear a remarkable similarity to roast-reduction/leaching route of the Caron process and the Moa Bay type of acid leaching operations. With a view to bring down the capital expenditure, increase the revenues, and reduce the amount of waste to be disposed off, four metal processes were developed. This included the manganese recovery option (Lenoble 1990) from the residue of the leaching operations; in this approach, the residue generated was further treated to obtain manganese through pyrometallurgical processing. This approach was developed as a corollary to the three metal processes, where the manganese-iron residue after leaching was subjected to smelting to obtain ferrosilicomanganese. Thus, all the reported processes bear resemblance to terrestrial processing of laterite ores as well as processing of manganese ores.

13.7.3 Upscaled Flow Sheet

It is difficult to assess process sustainability unless the process has been translated to a flow scheme with relevant material and energy flows. The flow schemes become more realistic when engineering flow diagrams are prepared, which allows us to assess process sustainability. The various options which have been tested at larger scale form the basis of engineering flow diagrams along with preliminary equipment specifications as have been detailed out in USBM reports (Haynes et al. 1982). It is interesting to note that various updated flow sheets presented by USBM reflect preferred versions of five processes as perceived by the authors (Gas reduction/ammoniacal leach, Cuprion, high temperature sulfuric acid leach, reduction/hydrochloric acid leach, smelting/sulfuric acid leach); these versions, however, may not represent the most optimized flow sheet alternatives based on present technological advances.

Such information does provide a basis of techno-economic evaluation as well as indicative estimates of GER/CED for sustainability assessment. Additionally, almost all the reported processes which have proceeded to the flow sheet upscaling stage bear resemblance to terrestrial similar operations, as detailed out below.

A review of upscaled flow sheets suggests that typically three approaches have been followed for metallurgical treatment. In the first approach, Ni, Cu, and Co metals are solubilized directly/after pretreatment and recovered. Manganese is recovered from the residue. Roast reduction ammoniacal leach process adapted for sea nodules is one of the earliest endeavors and is similar to Caron Process for laterites; alternatively direct hydrometallurgical treatment of nodules such as the one reported by Lenoble (1990) has been reported which also generates a manganese bearing residue. In the second approach, all the metals (including Mn) are solubilized and then the individual metals are recovered. In the third approach, manganese is recovered in the slag after smelting for further processing to ferroalloy and subsequently Cu-Ni-Co sulfide produced is treated hydrometallurgically, much like terrestrial processes. Except for the third approach which resembles two-stage smelting

process for terrestrial manganese ores followed by Cu-Ni-Co sulfide treatment resembling terrestrial operations for laterites, the other two approaches are similar to laterite processing. The first two approaches resemble treatments for laterite ores. These are described below.

13.7.3.1 Ni, Co, and Cu Recovery (Approach 1)

Both pyrometallurgical and hydrometallurgical processes for nodule treatment have been examined for recovery of copper, nickel, and cobalt. Pyrometallurgical processes have been used as a pretreatment step to enhance the solubilization of these metallic values without dissolving manganese. The uniqueness of PMN as a single source of four metals has also led to complexity of such treatment processes for PMN. The pretreatment options examined include reductive roasting followed by leaching, sulfuric acid leaching and reductive leaching without manganese dissolution. These are described below.

In the early 70s, Kennecott Copper Corporation had carried out detailed work at fairly large scale of operation for pretreatment of nodules by the reduction roasting option. The effects of different roasting variables utilizing synthesis gas mixture have been described in detail (Barner et al. 1977). The reduced nodules are solubilized through ammoniacal medium leach. Kennecott Copper Corporation claimed to have finished nodules research during early 70s.

13.7.3.2 Manganese Recovery from Residue (Approach 1)

A typical metallurgical grade manganese ore may contain 48.6% Mn, 3.8% Fe, 4% Al_2O_3, and 6.8% SiO_2 (Matricardi and Downing 1995) which is considered to possess a favorable Mn:Fe ratio for smelting. The sea nodule (rich, Pacific Grade) on the other hand contains only 30% Mn, 6% Fe, and 15% SiO_2 (Lenoble 1990). For making standard grade ferromanganese, the Mn:Fe ratio should be around 6:1. Also, the ores should be low in silica which is not the case with sea nodules. It is thus apparent that if one desires to produce ferromanganese from "rich" sea nodules, the silicon content would be high because of the rather high SiO_2 content of the nodules. In direct smelting processes, the objective is to produce a Ni-Cu-Co alloy and a slag for further smelting to silicomanganese. Recovery of Cu, Ni, and Co can be practiced from the alloys after producing a matte for maximizing revenues from the marine deposits. The matte smelting operations are again similar in nature to terrestrial production of crude ferronickel and producing shipping mattes.

Manganese-rich residues (generated after recovery of Ni, Cu, and Co from sea nodules), although poorer in manganese as compared to terrestrial ores, can be smelted similarly to the terrestrial ores; however, it is necessary to resort to the two-slag smelting practice. It is not possible to produce standard grade ferromanganese from nodule-related raw materials in a single stage by a process similar to the

discard slag practice for terrestrial ores. Such a practice is ruled out for producing ferromanganese of standard grade from the input nodule smelt slag/residue because of adverse Mn:Fe ratio (<6) and high silica content of the input materials as pointed out earlier. Rather, an offgrade Mn bearing alloy is produced after the first stage smelt. The slag produced after first stage has a more favorable Mn:Fe ratio for production of silicomanganese.

13.7.3.3 Ni, Co, and Cu Recovery with Manganese Dissolution (Approach 2)

This approach has been researched, but details of flow sheets are not readily available, since the target is to produce a value-added manganese compound after Cu/Ni/Co separation. The process resembles hydrometallurgical treatment of nickel laterite ores with the additional bonus of manganese dissolution.

Subsequent to Cu/Ni/Co recovery, manganese can be recovered at an energy consumption of 1.5–1.8 kWh/kg as electrolytic manganese dioxide at a lesser energy consumption than ferroalloy production. (Vide Sect. 13.8.2)

13.7.3.4 Smelting of Sea Nodules (Approach 3)

Direct smelting of manganese nodules results in removing bulk of the iron, an iron bearing nickel-copper-cobalt-manganese alloy being produced in addition to a manganese bearing slag; the alloy produced requires development of further recovery schemes to produce separate nickel, copper, and cobalt bearing products/metals subsequent to the first stage smelting procedure. The manganiferous slag produced after smelting will have to be treated in a subsequent smelting step to produce ferrosilicomanganese. This would thus involve two-stage smelting. It is extremely important to consider a high temperature pre-reduction stage earlier to the two-stage smelt process primarily to reduce electrical energy consumption and reduce environmental impact.

13.7.4 Flow Sheets and Techno-economic Evaluation

Majority of the earlier studies have reported indicative costs for the various flow sheet development works with a single focus on economic viability (Sen and Das 2008). The reported values of IRR provided in the Table 13.4 below (Biswas et al. 2009a) bring out that flow sheet development efforts similar to land-based existing operations may yield acceptable rates of return in future. The computed values closely match the reported values. These flow sheets provide guidelines of processing technology for sustainability analysis, and also demonstrate that the three metal recovery route is not preferred for such an analysis.

Table 13.4 Reported values of IRR for three metal/four metal processes

Reference	Hillman (1985)	Andrews et al. (1983)	Charles (1990)	Lenoble (1990)	Lenoble (1990)	Ham (1997)	Soreide (2001)
IRR (%)	7.4	6.4	12.0	15.4	15.7	11.93	9.6
Capacity (DMTPA)	3.0, three metal	1.5, four metal	1.5, four metal	1.5, four metal	1.5, four metal	3.0, four metal	0.7, three metal
Process route	Cuprion	Reduction smelting and Cuprion processes	Reduction HCl Leach	Sulfuric acid Leach	Smelt reduction	Reduction Roast Ammonia Leach	Sulfuric acid Pr. Leach

13.8 Approach for Flow Sheet Impact Analysis: Using Nickel Equivalent

Flow sheets taken up for techno-economic evaluation have a prime focus on nickel/copper/cobalt recovery and residue treatment for manganese recovery. We may consider that sea nodules are similar to laterite ores with added value addition from manganese in the residue. For techno-economic analysis, an approach which has been followed involves formulation of nickel equivalent concept (Biswas et al. 2009b); the capital and operating costs for proposed processing operations can be compared with land-based laterite ore processing because of similarities in processing approaches being followed. The focus of earlier global techno-economic studies had also been to draw up comparative estimates of metal processing from nodules vis-à-vis terrestrial resources of laterites.

A single and unique function called as Nickel Equivalent can be formulated to account for metal production and compare economic impacts. The function is direct measure of the sales revenue of processing scheme. The function Ni equivalent (Ni Eqv t/h) can be defined as:

$$\text{NiEqv,t}\Big/\text{h} = \sum_{i=1}^{4} \frac{P_i M_i}{P_{Ni}}$$

where

P_i denotes price of metals/kg for recovered metal from nodules.
M_i is metals recovered, ton/h.
P_{Ni} is price of the nickel/kg.
(Index "i" refers to the four metals considered in this study, namely Mn, Cu, Ni, and Co.)

However, the use of Ni equivalent is of relevance for economic returns since it is based on prevailing price ratios. Extension of this parameter to impact analysis requires some discussions.

13.8.1 Partitioning of Flow Scheme for Environmental Impact Using Nickel Equivalent

A careful review of all the three approaches shows that in one part of the flow sheet resembling terrestrial laterite ore processing, in addition to nickel, other associated metals are recovered during the dissolution phase. The associated metals are dissolved with the same input energy which would be approximately applicable to dissolution to only nickel in a laterite operation. Comparison with laterite operations can be invoked to determine the impact of the flow sheet. Thus for this part of the flow sheet, the use of the concept of nickel equivalent is relevant for normalizing CED/GER values. In another part of the flow sheet which deals with pyrometallurgical smelting operations involving nodules leach residue or direct sea nodules smelting, comparison needs to be drawn with CED/GER values of manganese ore smelting following different practices. In fact, the manganese recovery process can be separately compared with terrestrial flow sheet processing of terrestrial grade manganese ores with lesser GER values. Thus, in the case where manganese is recovered separately from residue/sea nodules, it is not appropriate to bring in the concept of nickel equivalent for the manganese recovery option which is useful for comparing techno-economic analysis.

In summary, for purposes of estimation of impacts, it is desirable to split up the impacts into laterite (Ni, Co, and Cu) processing followed by manganese recovery option. This would be different from IRR calculations where a composite value of Ni equivalent can be used.

In terms of life cycle assessment, total assessment requires establishing the system boundary of the study and is a key part of the LCA scoping phase. System boundaries should be drawn to effectively support the goal of the study, ensuring that the results comprehensively characterize the life cycle of the product. This is particularly important for comparative assertions, where proper system boundary and functional unit definitions enable fair comparisons between alternatives. The environmental impacts in a multi-output process are distributed between the coproducts in one of three ways: (1) dividing the process into subprocesses that are specific to individual outputs (i.e., subdivision); (2) subtracting the inventories of functionally equivalent products produced by monofunctional processes (i.e., system expansion by substitution); or (3) allocating the process inventory among all co-outputs using a shared relationship, such as mass or economic value. In the case of sea nodules processing, system expansion may not be appropriate since impacts of the products related to nickel (in our case Ni equivalent) and manganese are expected to be markedly different. Dividing the process into two subprocesses is more appropriate. As far as nickel, copper, and cobalt recoveries are concerned, this multiproduct system could be analyzed in terms of system expansion mode. The concept of nickel equivalent is really an economic allocation tool.

13.8.2 Impact of Manganese Recovery

The impact is dependent on whether a leach residue is being smelted or the sea nodules are directly smelted. Initially, we consider smelting of the residue. The GER values reported in literature (Haque and Norgate 2013) for ferromanganese and silicomanganese production lie between 50 and 80 GJ/t of alloy and are derived from 2.4 MWh/t and 4.0 MWh/t electricity usage for ferromanganese and silicomanganese, respectively. It needs to be appreciated that the net energy consumption of the two-stage smelting process is rather high if it is considered that a single product (silicomanganese) is produced. The power consumption values reported are scarce and the value may exceed 8000 kWh/ton of final alloy produced. For a two-stage smelting practice using a particular feedstock of sea nodules residue generated from nodules containing 30% Mn, this is likely to be around 10.0 MWh/t of alloy. The GER values are thus high and could be higher than FeSi75 production depending on the quantity of coke used (150 GJ/t alloy, including electricity). The CO_2 emissions for the manganese recovery option from sea nodules residue are likely to be high and could reach up to 10 tCO_2/t alloy considering electricity emissions. If the values are converted to per ton of dry nodules feed, for a 30% Mn content in the dry feed, 85% recovery, and 65% Mn in silicomanganese, the dry feed requirement works out to be 2.55 tons. Thus, around 3.92 CO_2/t nodules would be produced with specific energy of around 60 MJ/t nodules.

For a terrestrial ore containing 48% Mn with 90% recovery (77% Mn in ferroalloy), about 1.8 tonnes of ore are required to produce the alloy. Considering emission of 1.8 t CO_2/t alloy, about 3.24 t CO_2 is produced per ton of ore. For production of silicomanganese from discard slag, total feed of 1.7 t is reported to be used to produce 1 t of 67% Mn ferroalloy (silicomanganese). The reported CO_2 emission is 2.79 t for this step per ton of alloy. It is also reported that a total of 2.82 t of manganese ore is required to generate 1 ton each of ferromanganese and silicomanganese. Since total CO_2 emission is 4.59 t, the specific CO_2 emission/t ore is 1.62 t/t feed. The total energy requirement for these two steps is 117 MJ (58.5 MJ/t of total ferroalloy) leading to specific energy consumption/t ore as 41.48 MJ/t feed. Comparing these with values of 10 t CO_2/t alloy and 150 MJ/t of ferroalloy (1.62 t CO_2/t ferroalloy and 58.5 MJ/t ferroalloy for terrestrial processing), it is apparent that a reduction of energy and emission is mandatory to make the technology of residue processing sustainable.

On closer inspection of these values, it appears that residue processing generates a single value-added product as compared to two value-added products in terrestrial ferroalloy production. A possibility is to use terrestrial ore in the second smelting stage along with the residue. Else, the first stage smelt can be bypassed if larger quantities of terrestrial ores are available for blending. This would however lock up the manganese recovery option with terrestrial ore processing at comparatively larger capacities of production of ferroalloys. If a two-stage smelt procedure is to be followed, slag produced from the first smelting stage should be charged hot to the second smelt.

Although no specific estimates are available for direct smelting of sea nodules, the values are unlikely to be markedly different since again a two-stage smelting process is involved unless hot charging of the first stage smelt is practiced for the

second stage. The downstream processing for Ni, Cu, and Co recovery is separately discussed below.

13.8.3 Impact of Ni, Cu, and Co Recovery

Different variants of process options are available. The first variant is processes similar to Caron process (approach 1). Estimations of energy requirements are readily made, as summarized below.

Drying, Heating, de-hydroxylation, and selective reduction	5.6 GJ/t dry feed
Power and steam for leaching[a]	3.8 GJ/t dry feed
Other downstream miscellaneous	1.0 GJ/t dry feed

[a]Considering a base estimate of 7 T of steam requirement for recovering of 1 ton NH_3 from aqueous solution, the estimates of energy for steam production for 1:2 S/L ratios for nodules containing 1.3% Ni and leach solution containing 50 kg/m^3 ammonia work out to be 3.24 GJ/t of leach circuit feed. Additional steam requirement for preheating the leach solution as well as power is estimated as 0.6 GJ/t. The total power and steam requirement is thus approximately 3.8 GJ/t of leach feed

The gross energy requirement (10.5 GJ) is comparable to pyrometallurgical laterite process operation producing ferronickel (Roorda and Hermans 1981). If a nickel equivalent of 2.0 is attained considering a Pacific grade nodule and high recoveries of Ni, Cu, and Co with average prevailing price ratios, the energy input 525 MJ per kg of nickel equivalent is comparable to terrestrial operation. In terms of fuel oil equivalent, this works out to be around 12–13 kg of fuel oil/kg of Ni equivalent with a CO_2 emission of around 40 kg CO_2/kg of Ni equivalent. The high values may be noted.

The second variant of sulfuric acid high pressure leaching leads to different considerations of energy consumption since this involves direct treatment of the feed in aqueous solution. The practices followed for terrestrial laterite include Moa Bay/Amax flowsheet concepts as well as Australian flow sheet concepts (Murrin-Murrin, Bulong and Cawse) (Mayze 1999). The nodules treatment flow sheets propose to utilize Bulong and Cawse flow sheet concepts of solvent extraction/electrowinning for Ni and Co as contrasted to hydrogen reduction of the pregnant solution at Murrin Murrin. The steam requirements for high pressure acid leaching are readily worked out: for a leach temperature of 250 °C and an L:S ratio of 2:1, the thermal requirement is 500 Mcal/t feed. This leads to 0.67 t steam/t ore. For LCA concept implementation, a H_2SO_4 production plant from S is also integrated; this plant may generate about 20–30% of the steam requirement depending on the S input. The fuel oil requirement thus works out to be 35 kg/t feed for steam generation (about 2.1 kg/t Ni equivalent, 90% recovery). Considering fuel oil requirement for steam generation is about 70% of the fuel oil required for thermal heating, the oil requirement works out to be 50 kg/t feed. Norgate and Rankin (2000) provide a value of electrical energy requirement for heating as 3.58 kWh/kg of Ni equivalent; if electricity is generated from fuel oil, the fuel oil requirement goes up to 4.0 kg. This provides us a value of 160 MJ/kg of Ni equivalent. When electrowinning power requirement is considered, (4.0 kWh/kg of metals,

Rankin), 40 MJ/kg needs to be further added, leading to GER value of 200 MJ/kg Ni equivalent. The CO_2 emission works out to be 15 kg/kg of Ni equivalent if a fuel oil based operation is planned.

Considering the estimated nickel equivalents for a sea nodule process, it appears that the first variant is energy intensive and may not be sustainable.

13.9 Reagents, Recycles, and Effect on GER

Several reagents have been used for processing of sea nodules through hydrometallurgical/pyrometallurgical routes. The paragraphs above have attempted to evaluate metal recovery routes similar to terrestrial Ni laterite/manganese ore processing. Life cycle analysis studies and GER estimates require input energy estimates for reagents which need to be separately made. Inputs which have predominantly featured include H_2, NH_3, HCl, etc. The input energy associated with H2 has been described earlier. Production of NH_3 from methane will require feed and fuel energy of 28.8 GJ/t NH_3. The IKARUS database (IKARUS 1998) provides GER for HCl and Cl_2 as 17 and 18 GJ/t, respectively. The input energies lead to upstream CO_2 emissions ascribed to the processing route. In the absence of flow sheet information, it is difficult to obtain reliable values of GER and emissions using such inputs.

For minimizing the net usage of these inputs, it is important to conceive of recycle processes. The recycling process described for solid stream recycle is also applicable to liquid stream recycles. Associated GHG emissions need to be obtained both for input stream and recycle streams. Generally recycle stream energy emissions are expected to be lower than input fresh stream. Thus the energy required for a specific recycle process needs to be evaluated to obtain the net reduction of emissions as compared to a no recycle case. The Metallurgie Hoboken-Overpelt process proposing to use HCl as the preferred input (Van Peteghem 1977) has proposed flow sheet design involving a pyrohydrolysis step for recycling HCl, thus attempting to arrive at a sustainable flow sheet.

Additionally, the use of non-carbon bearing reagents needs to be analyzed from the point of view of liquid/gaseous effluent disposal issues arising out of the use of the specific reagent combination used. For example, excess Cl2 generated from use of HCl may be used by an adjoining industry and energy credit claims are possible. Also, excess ammonium sulfate produced in some processes needs to be bled out to an adjoining user industry.

13.10 Beyond Four Metal Recovery Route

World demand for rare earth elements and the metal yttrium—which are crucial for novel electronic equipment and green-energy technologies—is increasing rapidly. Several types of seafloor sediment harbor high concentrations of these elements

(Yasuhiro et al. 2011). New considerations for the augmentation of REE supplies come from the REEs in the very large tonnage deep-ocean mineral deposits, specifically polymetallic nodules and cobalt-rich crusts. Both deposit types have a significant potential to supply REEs to the marketplace as a by-product of the extraction of copper, nickel, cobalt, and manganese. Even though the grades (concentration of REEs) of the marine deposits are generally lower than for the land-based deposits, the tonnages are much greater than the land-based deposits (Hein 2012).

As pointed out earlier, sustainability considerations also look at criticality of availability of the final metals derived from a resource base in addition to the considerations of recyclability. Considering resource crunch of REE with respect to terrestrial resources, the recovery of rare earth from sea nodules will enhance the sustainability of the sea bed deposits. It would be interesting to know if the CED/GER values pertaining to rare earth elements for terrestrial resources can be maintained.

13.11 Conclusions

1. The general context of sustainability of metal extraction processes shows that material flow analysis for a flow sheet is an important consideration along with reuse of inputs as well as the possibility of extraction of critical metals. Environmental management for impact analysis and enhanced sustainability requires estimation of gross energy requirement and greenhouse gas emissions for a process flow sheet under consideration. Cradle-to-gate environmental burdens have been presented for several metal extraction processes so that a basis of comparison with processing approaches of sea nodules is obtained.
2. The roast reduction ammoniacal leaching process is not sustainable for sea nodules processing for recovery of Ni, Cu, and Co because of high GER values along with high specific CO_2 emissions.
3. The high pressure acid leaching route has comparable values to similar laterite processing operations.
4. In terms of nickel equivalent, a lesser value of GER and CO_2 emission is expected with a higher nickel equivalent; this assumes that a higher nickel equivalent advantage is not offset by additional electricity consumption because of copper extraction for high pressure acid leach systems.
5. The acid consumption values are likely to be of the same order if manganese is not dissolved. For manganese dissolution, the value can be higher, implying that a higher capacity S plant will be envisaged. Additional steam availability from this plant is to be foreseen, leading to some reduction in fuel oil requirement.
6. The GER values depend on the leach L:S ratio. It is always advantageous to operate at higher pulp densities for a sustainable operation.
7. The processing a mixed sulfide concentrate/matte generated from direct smelting of sea nodules is expected to operate with lesser specific acid consumption and lesser steam consumption during leaching. However, electrowinning energy

for Ni and copper/cobalt needs to be added to the steam generation energy. Because of concentrated sulfide feed, the overall specific energy consumption is likely to be lesser than 200 MJ/kg Ni + Co.

8. For flow sheet concepts involving manganese dissolution, comparison needs to be drawn with residue smelting operation for manganese producing ferrosilicomanganese. The power consumption will be markedly lesser when EMD is produced; however, a bulk discard residue will be generated as compared to benign slag after ferroalloy production. The residue needs to be evaluated for process sustainability.
9. For flow sheet attempting recovery of manganese as ferroalloy, comparison with terrestrial processing of manganese ores for ferroalloy production is useful. The estimated GER for terrestrial processing is 58.5 MJ/t of total ferroalloy with CO_2 emission of 1.62 t/t ferroalloy. Comparing these with estimated values of 10 t CO_2 and 150 MJ/t of ferroalloy, it is apparent that a reduction of energy and emission is mandatory to make the technology of ferroalloy production from manganese bearing input from sea nodule processing sustainable. Hot charging of the slag from the first stage smelting process and integration with terrestrial silicomanganese production are possible options.
10. Care needs to be exercised for selecting various inputs at different stages of the flow sheet so that CED/GER values are optimized. For example, use of hydrogen for metal powder production needs to consider that an input energy term comprising of the fossil fuel resource used to generate hydrogen is included in GER calculation. The specific energy consumption for hydrogen production based on steam methane reforming translates approximately into 13,628–15,204 kJ/Nm^3 based on the high heating value basis of hydrogen produced (Peng 2012). High specific energies for certain other inputs (NH_3, HCl, and Cl_2, 28.8, 17, and 18 MJ/t, respectively) need to be minimized by employing recycling/process integration strategies so that the CED/GER values are not unduly affected.

Acknowledgement Parts of this write-up are based on an invited lecture by the author on "Metals, Materials and Sustainability" delivered in 2015.

References

Andrews BV, Flipse JE, Brown FC (1983) The economic viability of a four metal pioneer deep ocean mining venture. Texas A&M University, College Station, TX, pp 84–201

Azapagic A, Perdan S (2000) Indicators of sustainable development for industry: a general framework. Process Saf Environ Prot 78(4):243–259

Barner HE, Davies DS, Szabo LJ (1977) Two-stage fluid bed reduction of manganese nodules. US Patent No. 4044094, 1977

Biswas A, Chakraborti N, Sen PK (2009a) Use of process optimization and cost model for metal recovery from manganese nodules: the role of manganese recovery. In: Proceedings of the 8th (2009) ISOPE ocean mining, pp 124–130

Biswas A, Chakraborti N, Sen PK (2009b) A genetic algorithm based multiobjective optimisation applied to a hydrometallurgical circuit for process optimisation. Miner Process Extr Metall Rev 30:163–189

Charles C (1990) Views on future nodules technologies based on IFREMER-GEOMONOD Studies. Mater Soc 14:299–326
EPA Report (2009) Sustainable materials management. June 2009.
Erdmann L, Graedel TE (2011) Criticality of non-fuel minerals: a review of major approaches and analyses. Environ Sci Technol 45:7620–7630
Fiksel J (2006) A framework for sustainable materials management. JOM 58(8):15–22
Graedel TE, Harper EM, Nassar NT, Reck Barbara K (2015) On the materials basis of modern society. PNAS 112(20):6295–6300
Halbach P, Fellerer R (1980) The metallic minerals of the Pacific Sea floor. GeoJournal 4(5):413–414
Ham K-S (1997) A study on economics of development of deep sea bed manganese nodules. In: Proceedings of the 2nd ocean mining symposium, pp 105–111
Haque N, Norgate T (2013) Estimation of green gas emissions from ferroalloy production with life cycle assessment with particular reference to Australia. J Clean Prod 39:220–230
Haynes BW, Law SL, Maeda R (1982) Updated process flow sheets for manganese nodule processing. IC 8924, p 99
Hein J (2012) Prospects of rare earth elements from marine minerals. Briefing paper 02/12, International Seabed Authority, New York seminar Feb 2012, pp 1–4
Hekkert MP (2000) Materials management to reduce Green House Gas Emissions. Thesis, Ultrecht University. ISBN: 90-393-2450-6
Hillman CT, Gosling BB (1985) Mining deep ocean manganese nodules: description and analysis of a potential venture. USBM IC9015. United States Department of the Interior, Bureau of Mines, Washington, DC, 19p
Huijbregts MJ, Hellweg S, Frischnecht R, Hendriks HWM, Hungerbuhler K, Hendriks AJ (2010) Cumulative energy demand as predictor of the environmental burden for commodity production. Environ Sci Technol 44:2189–2196
IKARUS (1998) Datenbase Industry. Fraunhofer Institute for system and innovation research, Karlshruhe
International Aluminum Institute (2013) Carbon Foot print guidance document. www.world-aluminium.org/media/filer_public/2013/…/fl0000169.pdf. Accessed 8 Aug 2015
International Council of Mining and Metals (2012) Trends in the Mining and Metals industry, Mining's contribution to sustainable development. https://www.icmm.com/document/3716. Accessed 19 Aug 2015
Lenoble JP (1990) Future deep sea bed mining of poymetallic nodules. IFFREMER, Issy-les-Moulineaux Cedex, France
Ligthart TN, Toon A (2012) Modeling of recycle in LCA. www.intechopen.com. Accessed 12 Nov 2015
Lorenz E, Graedel TE (2011) Criticality of non-fuel minerals: a review of major approaches and analyses. Environ Sci Technol 45:7620–7630
Matricardi LR, Downing J (1995) Manganese and manganese alloys. In: Kirk-Othmer encyclopedia of chemical technology, vol 15, 4th edn. Wiley, New York, pp 963–990
Mayze R (1999) An engineering comparison of the three treatment flow sheets in WA nickel laterite projects. ALTA hydrometallurgy forum
Mero JL (1965) The mineral resources of the sea. Elsevier, Amsterdam, p 312
Mukherjee A, Raichur AM, Natarajan KA (2004) Recent developments in processing ocean nodules-a critical review. Miner Process Ext Metall 25:91–127
Norgate TE, Jahanshahi S (2010) Low grade ores—smelt, leach or concentrate. Miner Eng 23:65–73
Norgate TE, Rankin WJ (2000) Life cycle assessment of copper and nickel production. In: Proceedings, Minprex 2000, international conference of mineral processing and extractive metallurgy, Sept 2000, pp 133–138
Norgate TE, Jahanshahi S, Rankin WJ (2007) Assessing the environmental impact of metal production processes. J Clean Prod 15(8–9):838–848
Nuss P, Eckelman MJ (2014) Life cycle assessment of metals: a scientific synthesis. PLoS One 9(7):e101298. doi:10.1371/journal.pone.0101298

Peng XD (2012) Analysis of the thermal efficiency limits for steam methane reforming of methane. Ind Eng Chem Res 51:16385–16392
Van Peteghem (1977) Extracting metal values from manganiferous ocean nodules. US Patent 4026773, 31 May 1977
Rankin WJ (2011) Minerals metals and sustainability: meeting future material needs. CRC Press, Boca Raton, FL, pp 226–230
Rankin J (2012) Energy use in metal production. In: High temperature processing symposium, Swinburne University of Technology: Presentation 1
Roorda HJ, Hermans JMA (1981) Energy constraints in the extraction of nickel from oxide ores (II). Erzmetall 34(4):186–190
Sen PK (2010) Metals and materials from the deep sea: an outlook for the future. Int Mater Rev 55(6):364–391
Sen PK, Das SK (2008) Sea bed processing status review for commercialization. In: Polymetallic nodule mining technology, proceedings of the workshop, International Sea bed Authority, Chennai, 18–22 Feb 2008, pp 153–167
Siemens Sustainability Report (2012) Driving sustainability. www.siemens.com/about/sustainability. Accessed 25 Aug 2015
Soreide F, Lund T, Markussen JM (2001) Deep ocean mining reconsidered: a study of the manganese nodules deposits in cook island. In: Proceedings of the 4th ocean mining symposium, Szezecin, Poland, pp 88–93
UNEP Report (2009), Critical metals for future sustainable technologies and their recycling potential. Öko-Institut e.V., July 2009
UNEP Report (2011) Recycle rates of metals. Panel, International Resource
UNEP/SETAC Life Cycle Initiative (2011) Towards life cycle sustainability assessment. ISBN: 978-92-807-3175-0
Van der Voet E, van Oers L, Nikolic I (2004) Dematerialization: not just a matter of weight. J Ind Ecol 8(4):121–137
Yasuhiro K, Koichiro F, Kentaro N, Yutaro T, Kenichi K, Junichiro O, Ryuichi T, Takuya N, Hikaru I (2011) Deep sea mud in the Pacific Ocean as a potential resource for rare earth elements. Nat Geosci 4:535–539
Zhang Y, Liu Q, Sun C (2001) Sulphuric acid leaching of Ocean Manganese nodules using phenols as reducing agents. Miner Eng 14:525–537

Professor P. K. Sen graduated from the Indian Institute of Technology, Kharagpur. He commenced his professional career at Hindustan Steel Limited. Subsequently, he joined Jadavpur University, Kolkata, as a Professor. He then proceeded to France as a CNRS fellow. Subsequently, he joined Engineers India Limited, New Delhi, where he had worked for more than 25 years. He has spearheaded the development of several technologies which were scaled up as well as commercialized. His major interests include New Process Development and Design, scale-up of metallurgical processes, process optimization, and sustainability engineering. He is presently holding the position of Ministry of Steel Chair Professor at IIT Kharagpur.

Chapter 14
Sustainable Development and Its Application to Mine Tailings of Deep Sea Minerals

John C. Wiltshire

Abstract Sustainable development is a commitment being demanded of industry. It will almost certainly be required for a new deep-sea enterprise mining manganese nodules or crusts. One of the areas where sustainable development can most easily be introduced is in the management of tailings from the mineral processing plant. These tailings can be used beneficially. Given the need to use large tonnages of tailings, several large tonnage applications have been studied. These include first and foremost agricultural applications. The second rung of applications includes highway fill, reclamation fill, drilling mud and asphalt and concrete. The third rung of applications would be more specialty applications relying on valuable properties of the tailings themselves. These include plastic and rubber fillers, coatings, and ceramics. All of these applications were successfully tested with manganese tailings. Collectively, they can utilize all of the processing tailings of a deep-sea mining operation, reducing the tailings waste needing land-based disposal to zero.

14.1 Introduction

The idea of sustainable development will soon be applied to a vast array of new projects. It is a coming trend. After years of struggling against this, the mining industry is slowly coming into compliance. However, for a new ocean mining industry, like deep-sea manganese nodule mining, a higher standard will be applied. This is because the industry is unproven, potentially large, and there is great concern about the lack of full quantitative measurement of processes in the deep sea.

As the planet reels to a greater and greater extent under the pangs of climate change and public environmental consciousness grows, it becomes ever more obvious that new development must be increasingly sensitive to environmental constraints. The recent demise of the coal industry in the United States has shown the futility of resistance to this trend and documented that new mining projects may expect to be held to a higher standard than hitherto considered (Mining Engineering 2015). Even the Vatican has recently demanded a higher sense of social responsibility for the mining industry (Mining Engineering 2015). For ocean mining, an industry

J.C. Wiltshire (✉)
University of Hawaii, Honolulu, HI, USA
e-mail: johnw@soest.hawaii.edu

R. Sharma (ed.), *Deep-Sea Mining*, DOI 10.1007/978-3-319-52557-0_14

moving into a highly sensitive environment and an environment that many scientists note is understudied (Muslow 2015), it would seem certain that environmental regulation will be high, if not extreme. One of the areas of high regulation will be tailings disposal. Given the sad history of the terrestrial mining industry and the countless number of tailings dam and pond failures (Williams 2015; Jacobs 2015), one cannot help but think that this will be a major area of scrutiny. However, recent research has shown that there are viable alternatives to dumping processing tailings back into the ocean or putting them into a tailings dump on land. Once processed, manganese tailings in particular have some very beneficial properties.

In the deep sea, mining for manganese nodules and crusts is projected to begin within the decade (Muslow 2015). In terms of sustainability, little can be done about bottom impacts including the stirring up of sediment. These impacts are likely to be relatively small and restricted in area in any case (Muslow 2015). Of greater concern are the impacts of processing (Williams 2015). The largest of these is what to do with the tailings. For the process to be sustainable, something constructive must be done with these tailings. For the manganese nodule and crust mining projects studied in this work, these tailings are a large volume, low value commodity. Their nature must be investigated carefully to determine which of a number of potential applications may be appropriate. Over a period of 10 years, a range of investigations has been carried out on several kinds of manganese tailings. Tailings tested included those of a small-scale sulfuric acid leach manganese nodule processing test, a manganese crust acid leach process, and the heavy media beneficiated tailings of the Groote Eylandt manganese mine in Northern Australia. All of the tailings of manganese operations had similarities in terms of their fine-grained nature and residual manganese contents. Further discussion of the exact nature of these tailings may be found in Troy and Wiltshire (1998). As the precise applicability of different beneficial uses will depend on the precise chemistry of given tailings, the results of this study should be used as a guideline. Although in general many of the same applications will be relevant, each application must be thoroughly validated with each new tailings type.

Ultimately, the economy as a whole and every industry in it must operate in a sustainable manner. This means that all processes must be cyclical, as they are in natural systems. Nature depends on cycles in the maintenance of life. Nature does not have linear flow-through. There are no situations in which raw materials go in one end and waste material (tailings in this case) comes out the other end to be unused by something else. In nature, nutrients and materials are continuously cycled. The sustenance of one organism is the waste from another. It is this natural system that the mining industry of the future must emulate.

The history of tailings management is anything but sustainable (Jacobs 2015). Mineral beneficiation or processing plants dispose tailings in large tailings ponds near the plant often with little treatment. The tailings are left to leach into aquifers after the mine is closed. There is no maintenance to assure that the structure of the tailings dam remains intact after minerals processing ceases. Often over time the walls of the tailings dam collapse spewing the contents over the land or into the natural drainage system. Particularly in the developing world, there are

well-documented cases of environmental catastrophe associated with tailings neglect (Williams 2015). Given rising global consciousness on environmental issues, it is safe to say that great scrutiny will be paid to the plans for tailings disposal from a deep ocean mining industry.

To obtain the goal of sustainability, manganese mine tailings need to be used beneficially rather than disposed. A 10-year project at the University of Hawaii has attempted to explore a variety of ways to do this. There are several problems with a project of this nature. First, as no tailings of a full-scale commercial deep-sea mining operation currently exist, their precise physical and chemical properties must be postulated. There are more than a dozen published methodologies (Haynes et al. 1985; Lay et al. 2009) for the processing of manganese nodules and crusts. To be meaningful, a study must look at common features of this range of tailings and determine the sensitivity of the proposed uses to these properties. Second, a supply of tailings must be either made or obtained sufficient to do a reasonable range of experiments including agricultural experiments needing relatively large volumes of tailings.

A study was made of a range of the tailings of different processes (Troy and Wiltshire 1998). It was determined that there is a great commonality among the tailings of acid leach processes once the tailings are neutralized. Smelted tailings and tailings of sulfide operations, such as seafloor polymetallic sulfides, tend to be inert glassy masses and may not pose the same environmental threat, although if needed, can be ground and have most of the properties of the acid leach manganese tailings.

In order to get sufficient tailings for a range of large volume experiments, we went to an active mine mining a manganese crust deposit on land. The Groote Eylandt mine in Northern Australia provided tailings to the project after high-grade manganese had been extracted but lower grade finer grain manganese remained. These tailings proved very analogous to acid leach manganese nodule and crust tailings both of which were tested (Troy and Wiltshire 1998). With a sufficient source of tailings, a range of applications could be tested. These are considered in the rest of the study.

A manganese nodule or crust operation would require 1–3 million tons a year of production in order to be economically viable (Muslow 2015; Wiltshire and Loudat 1998). As relatively minor amounts of metals may be extracted and some processing materials are added, we may expect 1–3 million tons a year of tailings would have to be managed. This means that whatever technique or combination of techniques we choose, we would need to handle large tonnages of tailings (Verlaan and Wiltshire 2000). As tailings are inevitably a low value commodity, this also means that the uses to which the tailings are being applied should be relatively near the mineral processing plant or very good, cheap, shipborne transport needs to be available (Loudat et al 1994, 1995). Given the need to use large tonnages of tailings, several large tonnage applications come to mind. These include first and foremost agricultural applications (El Swaify and Chromec 1985). The second rung of applications would include highway fill, reclamation fill, drilling mud and asphalt and concrete. The third rung of applications would be more specialty applications relying on valuable properties of the tailings themselves (Bai et al 2008). These are inevitably more select applications and would use lower tonnages. The various applications and their success will be reviewed in turn.

14.2 Applications in Agriculture

The use of tailings in agriculture is the best single use of tailings. In addition to the use of tailings as a soil additive to grow crops or graze animals on grass, there are a range of other agricultural applications that may be more applicable. These include orchards, vineyards, ornamental plant nurseries, sod farms, Christmas tree farms or agro-forestry for pulpwood, lumber or woody crops to be burned/converted in a biogas operation. The advantage of all of the latter applications listed is that there is no way heavy metals from the mine tailings can be passed up the food chain, as the final products are not eaten. Even eating the fruit or nuts, rather than leaves, seeds, or stems of a tree grown in a tailings rich soil is usually sufficiently removed from the tailings to limit any undesirable element in the tailings from passing to humans. When selecting a crop to match a given area and given type of tailings, much thought must be given to soil engineering. It is unlikely that the tailings in their raw form will support an efficient agricultural operation so tailings and soil mixes will have to be engineered.

The engineering of a soil mix using tailings is a complex process. Factors to be considered include maintaining soil mineral levels, microstructure including porosity and water drainage as well as available nutrient levels at various pH levels. According to Wild (1993), the following requirements of commercial plant species must be met by the soil: (1) anchorage for roots allowing for penetration, (2) supply of water, (3) supply of air and particularly oxygen, (4) supply of nutrients, and (5) buffering against adverse changes in pH and temperature. Most species need the following macronutrients from the soil: nitrogen, phosphorus, potassium, calcium, magnesium, and sulfur. Micronutrients are also needed but are required in much lower amounts. These include iron, copper, manganese, zinc, boron, molybdenum, chlorine, and nickel. Epstein (1972) provides actual average minimum nutrient requirements needed in plants as measured by amounts in dried plant tissues. The key metal nutrients are absorbed as cations. The key nutrients are listed in Table 14.1. For comparison, there are no established minimum manganese daily requirements

Table 14.1 Concentration in dried plant tissue of key nutrient elements absorbed from the soil that are considered adequate for plant growth (after Epstein 1972)

Cu	6 ppm
Zn	20 ppm
Mn	50 ppm
Fe	100 ppm
B	20 ppm
C	1100 ppm
S	0.1%
P	0.2%
Mg	0.2%
Ca	0.5%
K	1.0%
N	1.5%

for humans. Usual human intake is 2–5 mg/day, with a maximum recommended dose of 10 mg/day and an OHSA maximum air limit of 5 mg/cubic meter (Wiltshire and Moore 2000). Mn tailings are most beneficial in their provision of micronutrients and soil stability, fine granularity, and binding of toxic metals and least helpful in their tendency to "hard-pan" drying and absorbing water, as well as toxicity at high manganese, copper or nickel levels, and the potential to lower pH. In a fully optimized tailings/soil mix, other additives would be provided to neutralize some of the negative tendencies of the manganese tailings. Addition of Ca, lime, and organic matter would be typical of material possibly required for optimization. Hue et al. (1998) have demonstrated that management of the problem caused by excess metals absorption (for example manganese toxicity) can be completely controlled by raising the pH of the mix (i.e., moving from 4.5 or 5.0 to 5.5 or 6.0). Manganese addition to the soil seems to prevent root rot as noted in an experiment using orchid cuttings in which the manganese orchid roots were relatively disease free, whereas 100% of those in the control soil suffered severe root rot. A similar effect has been noted with respect to manganese grown plants which exhibited a higher resistance to insect predation.

In our experimental work, 17 plant species were selected to represent a wide range of commercially important tropical plants. They were chosen with the guidance of a local agricultural cooperative. Initial work included ten species. These were red ginger, avocado, coffee, hibiscus, citron, papaya, night jasmine, Koa, Bermuda grass, and onions. Later, ongoing experiments for which full data is not yet available included macadamia nuts, limes, lemons, tangerines (sunkist and honey varieties), flax, bell peppers, and mango. Seeds or cuttings were planted at the recommended depth in pots. The pots contained a 20% tailings/soil mix for the experimental plants and soil alone for the controls. Standard planting procedures were followed (Epstein 1972). Experiments were designed to provide careful controls on as many variables as possible. All growth was in pots and grown in outside conditions exposed to pests of all sorts. No insecticides were used. Both controls and tailings pots were watered when natural rainfall was insufficient. Measurements of the plants were taken at 2–4 month intervals to provide sufficient time for the plants to mature. Plants were grown from seeds, seedlings, or cuttings as appropriate to the species being tested. Tests were initially run for 18 months and in most cases are ongoing.

Plants were photographed and measured using a tape and calipers at regular intervals and the number of plants sprouted from seeds or surviving from cuttings was recorded. The general health of the plants was noted and given a numerical value (one—minor disease, three—moderate disease, and five—severe disease). Only the avocados (both Mn and controls) displayed significant blight during part of their growth history. Equal numbers of controls and manganese plants in equal health were always started. Equal volumes of growing medium were present. Watering was equal. The number of plants was counted at each stage of development. The average height was calculated. To account for the differences in productivity in some pots, a growth factor was calculated (Wild 1993; Epstein 1972). In its simplest form, this was the number of plants times the average height (or total

Table 14.2 Red ginger: Group 1

Soil	Plants (N)	Height (H in inches)	Growth factor (N times H)	Growth ratio (NH Mn/ NH control)
Trial 1				
Tailings	25	7 (max)	175	1.60
Control	18	6.1 (max)	110	
Trial 2				
Tailings	25	8.3 (max)	208	.94
Control	24	8.9 (max)	222	
Trial 3				
Tailings	30	10.8 (max)	323	1.08
Control	25	12.0 (max)	299	
Tailings	30	6.9	207	1.04
Control	25	7.9	199	
Trial 4				
Tailings	37	14.8 (max)	548	1.21
Control	30	15.0 (max)	452	
Tailings	37	10.0	369	1.16
Control	30	10.6	318	
Average				1.19

plant growth). This partially corrects for anomalies such as a single very tall plant versus many average size plants, both grown from an equal set of seeds in an equal growing volume. The growth factor suggests that a pot producing one 20 cm plant is only half as productive as a pot producing four 10 cm plants. The relative effects of the growth factors for different plant species in both tailings and soil control can be compared by calculating a growth ratio (the tailings growth factor divided by the control growth factor). Equal growth gives a growth ratio of one. A tailings mix that is twice as productive gives a growth ratio of two.

The results are presented in Tables 14.2, 14.3, 14.4, 14.5, 14.6, 14.7, and 14.8. These results represent 5 years of work growing a range of tropical plant species in a mix of 20% manganese tailings and soil, grown in pots. Table 14.2 presents the results for red ginger, a semicommercial species grown in the flower industry. The growth ratios for red ginger grown in tailings show that initially there was a very high growth rate among these plants which decreased with time. This likely indicates that the tailings were supplying needed micronutrients in early growth stages which were less necessary later. Overall, the manganese tailings/soil mix stimulated growth moderately in comparison to the controls.

Table 14.3 presents results for avocados, an important commercial food crop. Avocados are highly subject to disease in Hawaii because of heavy in breeding. Not only did the tailings mix heavily stimulate avocado growth resulting in almost double growth rates but the level of disease experienced in these avocados was much lower.

Table 14.3 Avocado: Group 2

Soil	Plants (N)	Height (H in inches)	Growth factor (N times H)	Growth ratio (NH Mn/ NH control)
Trial 1				
Tailings	10	22.2	222	2.10
Control	6	18.0	108	
Trial 2				
Tailings	10	24.5	245	1.90
Control	6	21.3	128	
Trial 3				
Tailings	10	27.6	276	1.80
Control	6	25.1	151	
Trial 4				
Tailings	15	32.2	483	1.80
Control	10	27.3	273	
Average				1.90

Table 14.4 Coffee seedlings: Group 3

Soil	Plants (N)	Height (H in inches)	Growth factor (N times H)	Growth ratio (NH Mn/ NH control)
Trial 1				
Tailings	13	6.71	87.1	1.00
Control	13	6.69	86.9	
Trial 2				
Tailings	14	7.04	98.5	1.34
Control	13	5.62	73.0	
Trial 3				
Tailings	14	7.86	110	1.90
Control	7	8.28	58	
Average				1.41

Table 14.4 gives the results for coffee, one of the most important commercial crops in Hawaii. The tailings grown coffee plants survived much better than the controls, although actual growth of the surviving plants was similar. Tailings seem to have a marked effect in both protecting roots from predators and reducing insect and pest damage.

Table 14.5 gives the results for hibiscus, a semicommercial flower crop in the same family as cotton. This was a small study, as several of the controls died shortly after planting. For this reason, the results while showing greater than double growth rates in the tailings compared to the controls cannot be considered numerically significant.

Table 14.6 gives the results for citrons, a coarse-skinned lemon and a commercial crop of increasing importance in Hawaii. Growth of citrons in both the control soil and tailings was essentially equal. This is a very hardy fruit and the added nutrients provided by the tailings appear unnecessary.

Table 14.5 Hibiscus: Group 4

Soil	Plants (N)	Height (H in inches)	Growth factor (N times H)	Growth ratio (NH Mn/ NH control)
Trial 1				
Tailings	3	11.6	35	3.60
Control	1	9.75	9.8	
Trial 2				
Tailings	3	19.0	57	2.28
Control	1	25	25	
Trial 3				
Tailings	3	21.7	65	1.97
Control	1	33	33	
Average				2.61

Table 14.6 Citron from seeds: Group 5

Soil	Plants (N)	Height (H in inches)	Growth factor (N times H)	Growth ratio (NH Mn/ NH control)
Trial 1				
Tailings	8	0.5	4.0	1.00
Control	8	0.5	4.0	
Trial 2				
Tailings	6	3.0	18.0	1.22
Control	6	2.46	14.8	
Trial 3				
Tailings	6	3.8	23	0.88
Control	8	3.25	26	
Average				1.03

Table 14.7 Papaya from seeds: Group 6

Soil	Plants (N)	Height (H in inches)	Growth factor (N times H)	Growth ratio (NH Mn/ NH control)
Trial 1				
Tailings	8	9.6	77	1.18
Control	5	13	65	
Trial 2				
Tailings	4	18.5	74	0.78
Control	5	18.8	94	
Average				0.98

Table 14.7 gives the results for papayas, a cornerstone commercial crop on the east side of the Island of Hawaii. Papayas, like avocados, are subject to significant disease. This is the only crop for which control growth was greater than growth in the tailings/soil mix. In the case of the papayas, although the tailings plants started off better, over time, more of them became diseased and died. It is unclear whether this had anything to do with the tailings. This experiment is being repeated.

Table 14.8 Night jasmine from cuttings: Group 7

Soil	Plants (N)	Height (H in inches)	Growth factor (N times H)	Growth ratio (NH Mn/ NH control)
Trial 1				
Tailings	3	1–3		n/a
Control	2	1–3		
Trial 2				
Tailings	2	9.5	19	1.36
Control	1	14	14	
Trial 3				
Tailings	3	16	48	2.18
Control	1	22	22	
Average				1.77

Table 14.9 Koa trees from seedlings: Group 8

Soil	Plants (N)	Height (H in inches)	Growth factor (N times H)	Growth ratio (NH Mn/ NH control)
Trial 1				
Tailings	4	14.0	56	1.04
Control	4	13.5	54	
Trial 2				
Tailings	4	15.75	63	1.01
Control	4	15.5	62	
Trial 3				
Tailings				
(10%)	4	21.0	84	1.40
Control	4	15.0	60	
Trial 4				
Tailings (10%)	4	24.0	96	1.50
Control	4	16.0	64	
Average				1.03

Table 14.8 gives the results of a small trial on night jasmine, a semicommercial flower species. The night jasmine showed a significant positive effect from the tailings. Part of this effect was due to the very poor survival of the controls in a small study.

Table 14.9 gives the results for Koa trees grown from seedlings. Koa is a commercial hardwood prized for furniture and woodworking. Results in Table 14.9 are given for the standard 20% manganese to soil mix and also for a 10% manganese to soil mix. Growth results for the 20% mix are about the same as for the control soil. Results are a little better for the 10% mix but are not used in the average growth ratio calculation, as they are not comparable with the other data in this chapter (which used a 20% mix).

Table 14.10 Summary of growth ratios for tested plant species (Mn tailings/controls)

Red ginger	1.19
Avocado	1.90
Coffee	1.41
Hibiscus	2.61
Citron	1.03
Papaya	0.98
Koa	1.03
Jasmine	1.77
Average	1.49

Table 14.10 summarizes the growth ratios for eight species. A growth rate of one means the controls and experimental plants grew equally well. In only one case is the number below one. In 7 of 8 species listed, and also in the case of the vast majority of the other species in ongoing experiments, the 20% manganese tailings mix produced significantly superior growth results compared to plants grown in the control soil. These are dramatic results from well-controlled, long-term experiments.

The preceding data clearly indicate that the hypothesis underlying the experiments is correct. A wide variety of commercial species grow at least equally, and almost uniformly better, on a soil mix engineered to contain 20% manganese tailings. A 20% mix would be sufficient to dispose the tailings generated by a 3 million metric ton per year manganese nodule mining operation. At this mining rate and using a 10 m disposal thickness at 20% tailings, a land area of 1 km^2 would be covered each year. This is typical of large mine tailings disposal. However, in the case proposed here, this land would be agriculturally productive. Nonetheless, the situation is not altogether rosy. One of the reasons that manganese soil protects the roots of certain crops and appears to decrease the range of pests eating the plants, as noted earlier, is its inherent toxicity. Manganese is toxic both to people and plants at elevated concentrations. A review of the literature (Wiltshire and Moore 2000) shows considerable risks to manganese workers particularly those in mines, smelters, battery plants, and ceramic facilities dealing with airborne manganese dust or metal fume. Similarly manganese, although a required element for plant nutrition, is also toxic to most plants at elevated concentration. The initial effects of manganese toxicity appear to begin at a soil concentration around 5% (Hue et al. 1998). The tailings used in this study contain 23% manganese, which at a fivefold dilution gives manganese content in the final test mix of 4.6%, just below the manganese toxicity limit. This is certainly another factor in support of the 20% selection as the mix ratio for the manganese tailings/soil growing media.

Soils may be engineered using Mn tailings and other components. Our research has indicated that about 20% tailings is ideal (Wiltshire 2000). Other components need to include a coarse grained fraction perhaps sand; a high organic, nitrogen-rich fraction which could include leaf and twig mulch, compost, manure, sewer sludge, or plant cuttings; and a calcium and phosphate rich fraction which could include coral rubble, shell, or ash. This last fraction would also serve to raise the pH. Low-grade soil could also form the bulk of the mix. Presumably, tailings would not be

mixed into an area that already had rich, high-grade, productive, agricultural soils. A typical engineered tailings soil might be by volume: 20% manganese tailings; 30% sand; 40% organics; and 10% shell, ground rubble, and ash. This could represent the initial mix spread on barren rocky land or lava. More likely tailings would be mixed into existing poor or gravely soil. A future area of work will involve mixing various kinds of tailings to try to offset the negative features of one and balance out the useful features of another, for example, mixing manganese tailings (which often have the useful property of binding heavy metals from other waste streams), power plant fly ash, sewer sludge, and wood chips. An engineered tailings soil may also be used to cap a tailings pond. In order to fully stabilize the pond, a tree crop with deep roots needs to be planted on top at a moderate to high tree spacing density. To prevent the tree crop from being killed by manganese toxicity as it matures and the root system deepens, the engineered soil cap needs to be 3–4 m deep over the tailings. A typical tailings pond capped in this manner could contain 10–20 m of tailings below the cap and extend over many hectares.

14.3 Application in Concrete

The American Concrete Institute (1990) has done a considerable amount of work on admixtures to concrete. This includes the successful incorporation of super plasticizers to increase concrete durability and blast furnace slag to increase strength and weight, fly ash from power plants and a very fine grained industrial waste, known as silica fume, to increase strength. Specialty concretes for the marine environment have been given a lot of study. Another area of major ongoing research is in the texturing of concrete pavements particularly to provide tough skid-resistant roadways. This is done both by sculpturing the concrete with grooves and also by adding hard gritty material, such as tailings, to the concrete. Considerable electron microscopy work has recently been undertaken to document the advantages of new nontraditional additives to concrete mixes (Kosmatka and Parnesse 1988). The successful incorporation of very fine grained fly ash and silica fume has made the concrete industry more open to the benefits of incorporating manganese tailings.

Wiltshire (1997a) tested varying mixtures of Portland cement, coarse sand, and tailings. Mixtures were made with 0–60% tailings in the concrete. Two sets of experiments were conducted. The first involved nodule tailings which were not fully neutralized after acid leach processing. These tailings had been washed and had a pH of approximately 4. They were made into standard 8-in. long, 4-in. diameter, concrete testing cores and tested for compressive strength by a commercial concrete testing company after curing for 33 days. The sample containing no tailings had a strength of 3460 psi effectively the same as the standard value given for concrete of 3500 psi. The other samples decreased considerably in strength with increasing amount of tailings. To determine whether the decrease in strength was solely due to the tailings content, the experiment was repeated with tailings which had been fully neutralized. The results were very different. Compressive strengths above 4000 psi

were achieved in concrete containing 20–25% tailings. The strength decreased fairly rapidly to 1000 psi for concrete containing 50% tailings. Although 1000 psi concrete could not be used in buildings, it would still be applicable for driveways and many other paving applications.

In addition to increased strength, the tailings appear to give the concrete several other interesting properties. The fine-grained nature of the tailings appears to make the concrete more moldable and bubble-free.

This was demonstrated in two ways. First, a moldability test was performed using a 12-in. by 4-in. latex rubber mold of an ornamental Japanese fish. The mold was made with considerable attention to fine detail. This fine detail was picked up in a casting using concrete containing 30% tailings but not by the standard concrete. Further, the ferromanganese concrete gave a much smoother bubble-free surface. The surface textures were compared in another test by examining cut surfaces of the ferromanganese tailings concrete and a standard precast concrete brick. The ferromanganese surface had bubble pits over less than 2% of its surface. These pits ranged in size from pinholes to 2 mm in diameter averaging about 500 μm. By contrast, the precast brick had pits covering over 20% of its surface ranging to 8 mm in diameter and averaging about 2 mm in diameter. The difference was very marked. The precast brick had a rough surface, the ferromanganese concrete a very smooth surface. In addition, the tailings give the ferromanganese concrete a considerably greater density than regular concrete in that iron and manganese are being substituted for the less dense silica and aluminum of sand and the ferromanganese concrete has less than one tenth the bubbles found in regular concrete.

Greater density and bubble reduction are two particularly important properties for concrete to be used in the marine environment. In the marine environment, wave action compresses air into the pores and pits of the concrete which over time breaks the concrete down. The same action results from water freezing and expanding in these pores. The lower number of pores subjected to this action the longer the concrete will endure. There is evidence to indicate that ferromanganese surfaces repel the growth of organisms. If this can be confirmed, it may be that ferromanganese concrete would not be covered as quickly as other types of concrete with algae or encrusting organisms which would offer advantages for outfall pipes as well as many other marine structures.

When the physical properties of the tailings are related to the characteristics of the resulting concrete, it becomes clear what is happening. The tailings have a specific gravity of 3.46, much higher than normal silica sand. They are making the concrete denser. The tailings have a very high surface area which rapidly absorbs water. This makes the concrete dry faster. It also causes the fine clay grains in the tailings to expand to fill voids in the concrete causing the concrete to have lower pore space and better moldability. The greater density, reduced pore space and better grain linking, caused by this void filling, in turn translate into higher compressive strength. Evidently this advantage begins to be lost above an addition of about 20% tailings to the concrete mix, presumably after all the small voids have already been filled by the tailings.

Concrete theory suggests that manganese tailings below 300 μm in size should not be desirable for aggregate. Testing indicates this not to be the case (Wiltshire 1997a). The tailings make the concrete denser, darker in color, more moldable, of lower porosity and somewhat stronger. While it is too early in the testing phase to tell exactly what is happening, the chemical scavenging properties of manganese may in some way be creating a bonding effect in addition to the normal hydration of the concrete. If this is the case, the concrete should strengthen over time beyond what would normally be anticipated.

A recent round of experiments tried to determine the optimum mix components for a manganese tailings concrete. Specifically, the nature of this test was to try to quantify the optimum size and percentage of the coarse aggregate fraction. Work by Kosmatka and Parnesse (1988) has shown that as a general rule the fine aggregate portion of a concrete mix should be 30–35%. Using manganese tailings at 33% and 15% and four different coarse aggregate mixes, it was determined that with a 40 mm maximum size aggregate over the 15–33% range tested produced a stronger than standard concrete (standard type I Portland cement mixed in standard proportions with a standard aggregate has a nominal compression strength of 3500 psi).

The results give manganese tailings a definite role to play in commercial concrete production. These results also suggest the possibility of looking for other coarse grain natural aggregate deposits which are not ideal for concrete at the moment because of grain size, but could be successfully mixed with the fine grain manganese tailings to achieve a very attractive result. This could be particularly beneficial in the South Pacific Island economies, some of which have in excess of $50/ton aggregate costs.

Clearly, there are considerable avenues for further research on the properties of ferromanganese tailings concrete. Initial indications of increased compressive strength, superior moldability, higher density, and lower porosity give reason to believe that, particularly for specialty concretes, the addition of the ferromanganese waste is imparting very economically desirable characteristics. Ongoing work is looking at the characteristics of manganese concrete with respect to anti-biofouling properties and ferrocement applications for marine structures.

14.4 Application as Construction Fill

A possible use of mine tailings is as fill for a variety of construction projects. Unless a smelting process is involved, these tailings are typically fine grained. There are a number of issues involved in using tailings as fill. These included toxicity of the tailings and their likelihood of leaching into the ground water aquifers. This situation must be avoided at all cost. One way of doing this is to enclose the tailings in geotextile membranes. These membranes are widely available at relatively low cost. They may even permit the tailings to be used as sand bag fill or as bag constructed breakwaters in the marine environment. Another major issue in the use of fine-grained tailings material is dust control. If the tailings are potentially toxic, as is the

case with manganese tailings, such control, particularly of micron size dust, gets to be very important. Keeping the tailings wet and or using membrane bags can handle dust control. The third major issue in tailings use as construction fill is cost of transport. Essentially in the role of fill, the tailings would be replacing sand and gravel. The tailings provide no beneficial properties beyond sand or gravel fill hence command the same price or less. This probably limits the effective distance to which tailings can be used to 100 km or less from the processing site.

Cemented or bagged tailings may be very useful in the construction of walls of ponds to be used in aquaculture. Part of the idea of a sustainable mine site is to use the waste in a useful way. It therefore may be that several other industries need to be founded in the same location as a mining development. These include small-scale agroforestry particularly something like a Christmas tree farm and aquaculture ponds. The tree farm can be constructed to serve as a windbreak between the mineral operation and the tailings built aquaculture ponds. It is important that the economic viability of these secondary operations be calculated as a tailings disposal operation (hence a cost or tax on the mineral processing industry) rather than assessed as to their independent viability as revenue generators.

14.5 Applications as Industrial Fillers

14.5.1 Resin Casting-Solid Surface

A major use of fillers is in countertops and fixtures. These are referred to as solid surface and cultured marble applications. The filler is mixed with specialty resins usually in proportions of about one-third resin, two-thirds filler. The resin–filler mix is activated by the addition of a catalyst and the mix is poured into a mold to cure as a casting. Sink and shower fixtures were professionally cast using manganese tailings by a small Hawaii synthetic marble producer. They were very attractive and considered commercially equivalent to white synthetic marble (only black or gray). There is major casting industry interest in the tailings. Tailings samples and information packages were sent to 20 manufacturers at their request.

14.5.2 Tiles

Tailings tiles were also manufactured in a similar manner to the fixtures. They were laid in a warehouse on the Island of Hawaii. They are attractive and can be easily installed with a little practice. The tiles were sent to the Ceramic Tile Institute of America for commercial testing. The manganese tiles tested within the range of certifiable floor tiles for some but not all of the required standard properties. The tests showed the tiles to have undesirably high thermal expansion and to have only

60% of the bonding strength to the floor required for certified tiles. Part of the problem here is that the bonding agent used in the test was designed for ceramic tile not resin cast tile. While attractive and testing in the general range of commercial products, it is clear that more work will have to be done before tailings could be made into tiles for wide commercial application.

14.5.3 Rubber

Fillers are also extensively used in the rubber industry. Two rubber corporations conducted commercial testing using the tailings as filler. The tailings mix well in rubber mixes, show increased abrasion resistance and tear strength over standard fillers, and had a high index of dispersion. However, the range of grain size of the tailings is too large for the rubber industry. In general, rubber applications require 100% of the filler grains to be less than 10 μm. In the case of the manganese tailings only 80% of grains are less than 10 μm. This is an easily resolvable problem, but one that would incur some sizing costs. Without this size correction the tailings performed poorly on rubber tests where the particle size distribution was a major factor. This was particularly true for overall strength and modulus of elongation.

14.5.4 Plastic

A variety of minerals, particularly calcium carbonate, is used as inert filler with many different polymers to achieve plastics of a wide variety of characteristics. Normally carbon black is added to the plastic to get dark, gray, or black colors for electronic housings, computers, and automobile parts. Generally, plastic properties are determined by the polymer and not the filler. Black plastics tend to fade rapidly under UV light. Plastics made with manganese tailings do not fade. This is very significant for external applications. Manganese tailings tested successfully in a range of plastics. However, as in the case of rubber, the tailings would be better if the fraction above 10 μm in size were removed. A few applications can tolerate grains size to 200 μm but this is a small portion of the plastic filler market.

14.5.5 Coatings

Two sets of long-term coating experiments have been undertaken (Wiltshire 1997b; Bai et al. 2016). The first examined the tailings as a rust preventative. This was done in three phases. The first was a yearlong experiment coating rusty steel beams with five different carriers, to three of which tailings were added. After 1 year of exposure the tailings based coatings showed superior results even to commercial

products such as rustoleum. The experiment was repeated on eight strips of aluminum flashing (five tailings mixes and three controls) and on three large segments of roof on a warehouse. In both of these experiments, the results were the same. When tailings are added to commercial carriers, the results were often better than those obtained directly with commercial rust preparations. This result, having been duplicated three times, is very significant.

The second group of tailings coating experiments was a yearlong effort aimed at developing a termite-resistant coating. Various pieces of wood were coated with tailings based mixtures and put with controls in a termite-infested area. In the first round of experiments, the controls were completely eaten away and the tailings coated boards almost unaffected. In a second larger experiment, in which untreated boards were set in pots of tailings as well as left completely exposed, neither the controls nor the tailings coated wood were affected. This may be because of the large amount of tailings in the experiment site, which repelled the termites, or it may be an inconclusive result because there were insufficient termites in the known nesting area when the experiment took place.

14.5.6 Drilling Mud

Several Russian operations have successfully used fine-grained manganese tailings as a weighting agent in drilling mud in the Baku fields. Research on drilling mud indicates that any clay must be taken out of the tailings to raise specific gravity and to prevent swelling. Recent work has focused on removing clay. After detailed SEM and XRD characterization of the tailings, clay removal studies focused on two routes, froth flotation and magnetic separation. Froth flotation proved difficult, as a significant fraction of the tailings is 5 μm or less in size. It proved tricky to keep flow rates optimally adjusted. One run out of four successfully separated the manganese and clay. By contrast, wet high intensity magnetic separation proved easy to use and very effective at separating the manganese and clay fractions. The separated manganese has a specific gravity over four and appears well suited for drilling mud.

14.5.7 Ceramics

A breakthrough has occurred with the help of several ceramics specialists. Lay and Wiltshire (1997) and Lay et al. (2009) developed a very hard manganese glaze which is honey brown to jet-black in color depending on the mix. Mixes vary from 50–70% tailings, the remainder being one of several silica frits or borates (especially borax). After limited testing, a ceramics industry evaluator felt that the combination of color and hardness was unique. About one hundred melts were made in an effort to construct a phase diagram for the system (Troy and Wiltshire 1998). It is important to design a melt that is a single phase. This occurs only over a narrow compositional range which appears to be about 40–70% tailings. Major work in this

area is ongoing (Bai et al. 2016). Manganese tailings make a superior ceramic that has major potential structural and decorative applications and the possibility of enclosing nuclear or toxic waste.

14.6 Conclusions

Sustainable development is a goal that can be achieved in the handling of processing tailings of deep-sea manganese nodules and crusts. What is required is the clever utilization of as much of the tailings material as possible in beneficial applications. A range of applications has been studied for these tailings (Wiltshire 1993, 2001). As a generalization, the potential for tailings utilization in the area of agriculture is the largest potential utilization by tonnage. This potential is, in fact, enormous (Wiltshire and Loudat 1999). Many areas of the world have mineral-poor or mineral-depleted soil. In Hawaii, there are thousands of hectares of land covered with barren lava flows. Manganese tailings are mineral rich; Hawaiian soil is mineral poor. Project work has characterized tailings from several potential processing routes and developed a tailings/soil mix that has displayed good growing characteristics. In the past, the standard mining company approach has been to try to plant directly on a tailings pile after heavy fertilization. This usually has not worked or worked initially until the plants received a toxic dose of one of the contained metals and then everything suddenly died. The results of our experiments with 17 different plant species and manganese tailings/soil mixes suggest that about 20% tailings to soil mix is optimal. At this level, plant growth for most of the 17 test species was stimulated, in one case achieving double growth rates in comparison with the controls. Management of the problem caused by excess metals pickup (for example manganese toxicity) was undertaken by raising the pH of the mix (moving from 4.5 or 5.0 to 5.5 or 6.0). Addition of Ca and organic matter also helped. A future area of work will involve mixing various kinds of tailings to try to get the negative features of one to balance out the useful features of another; for example, mixing manganese tailings (which often have the useful property of binding heavy metals from other waste streams) with power plant fly ash, sewer sludge, and wood chips.

The key to a sustainable tailings development is a wide use of applications for tailings. In this study we have looked at successful applications in agriculture, concrete, highway fill, drilling mud, ceramics, industrial fillers for coatings, plastics, and asphalt. Care must be taken to not cause additional problems with the tailings through contamination, toxicity or the manufacture of substandard products. This is a delicate balance and will be heavily influenced by the location of the processing plant. As a generalization our work suggests that although there is a wide range of potential beneficial applications, agricultural applications relying on a mixed soil using tailings engineered with other soil components and growing a nonedible crop will likely give the most universally satisfactory result. While our initial agricultural work has been with a limited range of crust and nodule products and specific results presented in this chapter will not be universally applicable, we suspect the general approach of engineering a tailings based soil has wide merit.

References

American Concrete Institute (1990) Manual of concrete practice. ACI, Detroit

Bai Z, Wen Z, Wiltshire JC (2008) Marine mineral tailings use in anticorrosive coatings. In: Proceedings of the OCEANS 2008 MTS/IEEE QUEBEC conference, QC, Canada, 15–18 Sept 2008

Bai Z, Wen Z, Wiltshire JC (2016) Anticorrosive coatings prepared using the tailings of cobalt-rich manganese crusts: preparation and properties. Mar Georesour Geotechnol (in press)

El Swaify S, Chromec W (1985) The agricultural potential of manganese nodule waste material. In: Humphrey P (ed) Marine mining: a new beginning. Department of Planning and Economic Development, State of Hawaii, Honolulu, pp 208–227

Epstein E (1972) Mineral nutrition of plants: principles and perspectives. Wiley, New York

Haynes B, Barron D, Kramer G, Maeda R, Magyar M (1985) Laboratory processing and characterization of waste materials from manganese nodules. Bureau of Mines Report of Investigations, RI, p 893

Hue N, Silva J, Uehara G, Hamasaki R, Uchida R, Bunn P (1998) Managing manganese toxicity in former sugarcane soils on Oahu. Soil and Crop Management Reports, SCM-1, College of Tropical Agriculture and Human Resources, University of Hawaii, Honolulu, p 7

Jacobs M (2015) Tailings: effective stewardship. Mining, Nov 2015, pp 50–51

Kosmatka S, Parnesse W (1988) Design and control of concrete mixtures. Portland Cement Association, Skokie, IL

Lay GF, Wiltshire J (1997) Formulation of specialty glasses and glazes employing marine mineral tailings. In: Recent advances in marine science and technology'96, Pacon International, Honolulu, pp 347–361

Lay GF, Rockwell MC, Wiltshire JC (2009) Investigation of the properties of a borosilicate glass from recycled manganese crust tailings. J Charact Dev Novel Mater 1(3):225–240

Loudat T, Wiltshire J, Zaiger K, Allen J, Hirt W (1994) An economic analysis of the feasibility of manganese crust mining and processing. State of Hawaii Department of Business, Economic Development and Tourism Technical Report, p 105

Loudat T, Zaiger K, Wiltshire J (1995) Solution mining of johnston island manganese crusts: an economic evaluation. In: Proceedings of the Oceans'95 conference, Marine Technology Society, Washington, p 10

Mining Engineering (2015) Editorial: vatican hosts mining executives. Mining Engineering, Nov 2015, pp 12–20

Muslow S (2015) Update on the status of deep sea mining beyond national jurisdictions. J Ocean Technol 10(1):1–12

Troy PJ, Wiltshire J (1998) Manganese tailings: useful properties suggest a potential for gas absorbent and ceramic materials. Mar Georesour Geotechnol 16:273–281

Verlaan P, Wiltshire J (2000) Manganese tailings—a potential resource? Min Environ Manage 8(4):21–22

Wild A (1993) Soils and the environment. Cambridge University Press, Cambridge, 287

Williams M (2015) Tailings: differentiating between 'alarm 'and 'harm'. Mining, Nov 2015, pp 46–49

Wiltshire J (1993) Beneficial uses of ferromanganese marine mineral tailings. In: Saxena N (ed) Recent advances in marine science and technology, PACON International, Hawaii, pp 405–412

Wiltshire J (1997a) Use of marine mineral tailings for aggregate and agricultural applications. In: Proceedings of the international offshore and polar engineering conference, 25–30 May, Honolulu, Hawaii, ISOPE, Golden, CO, pp 468–474

Wiltshire J (1997b) The use of marine manganese tailings in industrial coatings applications. In: Proceedings of oceans 97, Marine Technology Society, Washington, DC, pp 1314–1319

Wiltshire J (2000) Innovations in marine ferromanganese oxide tailings disposal. In: Cronan D (ed) Handbook of marine mineral deposits. CRC Press, Boca Raton, FL, pp 281–305
Wiltshire J (2001) Future prospects for the marine minerals industry. Underwater, May/June 2001, pp 40–44
Wiltshire J, Loudat T (1998) The economic value of manganese tailings to marine mining development. In: Proceedings of the offshore technology conference, American Association of Petroleum Geologists, Houston, pp 735–742
Wiltshire J, Loudat T (1999) The uses of fine grained manganese as an industrial filler. In: Saxena N (ed) Recent advances in marine science and technology, vol 98. Pacon International, Honolulu, pp 279–289
Wiltshire J, Moore K (2000) Manganese tailings concrete: antibiofouling properties and manganese toxicity. In: PACON'99 proceedings, Pacon International, Honolulu, pp 400–409

Dr. John C. Wiltshire has a B.Sc. in geology from Carleton University, Canada, and a Ph.D. in oceanography from the University of Hawaii. After working in the oil and mining industries, he became Ocean Resources Manager for the State of Hawaii. He is currently Director of the Hawaii Undersea Research Lab and Associate Chairman of the University of Hawaii's Department of Ocean and Resources Engineering. He is the Editor-in-Chief of the peer-reviewed journal *Marine Georesources and Geotechnology*. He is a fellow of the Marine Technology Society (MTS) and has authored over 100 papers on ocean resources, marine technology, energy and sustainable development. He serves as President of the international consulting group TCI-Hawaii.

Part IV
Environmental Concerns of Impact of Deep-Sea Mining

Chapter 15
Recent Developments in Environmental Impact Assessment with Regard to Mining of Deep-Sea Mineral Resources

Y. Shirayama, H. Itoh, and T. Fukushima

Abstract Growing attention to seabed mineral resources is being paid, private enterprises as well as governmental organizations are beginning to develop them. Along with this, more applications for development of new areas beyond national jurisdiction have been submitted to the International Seabed Authority. In addition, some development licenses in the sea areas under jurisdiction of coastal countries have been also issued. Furthermore, some of the countries and enterprises working towards development of mining technologies have announced model mining systems that they had contrived. In response to these developments, increased accuracy and efficiency are required in the field of environmental impact assessment. Besides, the United Nations and related organizations, as well as the Convention of Biological Diversity Conference of the Parties, have discussed how marine environment should be conserved from coastal areas to the deep seabed. Thus far, plans for environmental conservation have not been considered as a primary issue in the development of deep-sea mineral resources. With this background, this chapter will introduce how Japan has considered developing methodologies for environmental impact assessment, followed by the advanced environmental conservation measures with international trends taken into account.

15.1 Current Status of Deep-Sea Mineral Resources Development

Expectations for seabed mineral resources have been growing. In this section, this trend is briefly explained from the angle of applications and grants of mining license in areas beyond national jurisdiction (ABNJ) and those within it, as well as from that of development by private enterprises and advancement of mining technologies.

Y. Shirayama (✉) • H. Itoh • T. Fukushima
Japan Agency for Marine-Earth Science and Technology, Yokosuka, Japan
e-mail: yshira@jamstec.go.jp

R. Sharma (ed.), *Deep-Sea Mining*, DOI 10.1007/978-3-319-52557-0_15

15.1.1 Applications for Exploration/Exploitation Licenses

First, we will discuss licenses for exploration area in ABNJ. Since 2011, there have been more than ten of applications for exploration areas to the International Seabed Authority (ISA) (ISA 2014). This is the second peak followed by the first peak of the application by the pioneer investor in 2001/2002 (see Chap. 16, Fig. 16.1). Compared to the first peak, the second one shows its characteristics such as partaking of private capital with sponsoring states, exemplified by Tonga Offshore Mining Ltd. (TOML) (ISA 2008), and some applications such as the Marawa Research Exploration Ltd. of Kiribati (Marawa) (ISA 2015a, b, c) targeting reserved areas relinquished by pioneer investors. However, even in sea areas under the jurisdiction of coastal countries, there are an increasing number of cases where private enterprises, such as Nautilus Minerals Inc. (Nautilus) and Neptune Minerals Inc. (Neptune), entered into contracts with these coastal countries (see Chap. 16, Table 16.2) and obtained exclusive licenses. These include exploitation licenses obtained by Neptune for Papua New Guinea and by Diamond Fields International Ltd. for the Red Sea (Nautilus Minerals Nuigini Ltd 2012; Diamond Field International Ltd 2010). Although applications for exploration/exploitation licenses, regardless of whether or not it is under national jurisdiction, can be costly, the number of applications has increased in recent years. This suggests that developers are becoming increasingly confident of benefits from mining in future.

15.1.2 Participation of Private Enterprises

Private enterprises initiated work in the development of seabed mineral resources in the 1970s. At that time, four international consortia were formed; Kennecott Consortium, OMA (Ocean Mining Association/US Steel Group), OMI (Ocean Management Incorporated/Inco Group), and OMCO (Ocean Minerals Company/Lockheed Group). These were composed of private companies from the USA, Canada, the UK, West Germany, Belgium, Holland, Italy, and Japan (Table 15.1) (Theil et al. 1992; Kaufman et al. 1985; IFREMER 2013). However, all of these consortia became dormant in the 1980s due to the low price of metal, and the United Nations Convention on the Law of the Sea (UNCLOS) brought into effect. Since then, with the exception of Nautilus and Neptune, the participation of private enterprises was inconspicuous for some time. However, in 2010, the number of mining applications to ISA from private enterprises increased because applicants such as UK Seabed Resources Ltd. (UK), Global Sea Mineral Resources (Belgium), Nauru Ocean Resources Inc. (Nauru), and Ocean Mineral Singapore Holding Pte Ltd. (Singapore), in addition to the aforementioned TOML and MARAWA, started to apply (ISA 2011a, 2013a, b, 2016). While the maintenance of mining areas would generally be carried out as part of a mid- to long-term plan based on the resource policies of the country concerned, private parties would expect short-term profits. Taking this into consideration, we can expect the commencement of resource development in

Table 15.1 Consortiums in 1970s (Theil et al. 1992; Kaufman et al. 1985; IFREMER 2013)

Consortium	KCON (Kennecott Consortium)	OMA (Ocean Mining Association)	OMI (Ocean Management Incorporated)	OMCO (Ocean Mineral Company)
Established	1974	1974	1975	1977
Joint corporations	Kennecott (USA)	Essex Minerals Company (USA)	Inco Limited (US-Canada)	Lockheed Billititon (USA)
	Noranda Mine (Ca)	Union Seas Inc. (Belgium)	AMR (RFA)[a]	Amco (Standard Oil)
	CGF (UK)[b]	Sum Ocean Ventures Inc. (USA)	Deep Ocean Mining Co., Ltd. (Japan)	Shell Billiton
	Mitsubishi Cop (Japan)	Japan Manganese Nodules		Bos Kalis
	Rio Tinto Zinc (UK)	Development (Japan)	SEDCO (USA)	
	BP (UK)[c]	Samin Ocean Inc. (Italy)		
Exploration	1962 start		1975 start	1978 start
	1984 exploration license (US Domestic Law)	1984 exploration license (US Domestic Law)	1984 exploration license (US Domestic Law)	1984 exploration license (US Domestic Law)
Mining	1975–1976: collector model test at depth of 5000 m	1970; mining system test at the depth of 800 m	1976: collector test in deep sea	1978: mining system test in shallower water
	1978: lift up test on-land	1978; pre-mining pilot test in the DOMES site C (4400 m) and lift up 500 t nodules	1978; pilot miner test in the DOMES A(5000–5200 m) and lift up 500 t nodules	1979; mining system test in deep sea
Refining	1974 start basic study	1974 pilot plant test	1962–1963 basic study	Small plant test
	1976 start technical development	target; Ni, Cu, Co, and Mn	target; Ni, Cu, Co	
	target; Ni, Co, Cu			

[a]Arbeitsgemeinschaft Meerestechnisch Gewinnbare Gewinnbare Rohstoff
[b]*CGF* consolidated gold fields
[c]BP Petroleum Development Ltd

near future. Especially, the participation of UK Seabed Resources Ltd. and Ocean Mineral Singapore Holding Pte Ltd. is notable. Both have received capital from Lockheed Martin, one of the four groups of the former international consortium, indicating that Lockheed Martin is undertaking the challenge once again.

15.1.3 Current Technical Progress

Through various initiatives including ocean experiments, the aforementioned international consortia worked towards the development of the airlift mining system (Table 15.1). For example, Kennecott Consortium succeeded a lifting tube experiment on land in 1978, OMA was successful in lifting 500 t of manganese nodules in an offshore experiment in 1977, OMI succeeded in lifting 800 t of them in 1978, and OMCO carried out a deep-sea testing of mining systems successfully in 1979. If we consider the 1970s to be the first peak of mining system development, then the second peak would be the initiatives taken since 2000, relating to the demonstration of various mining systems. One example includes three types of mining subsystems developed by Nautilus, such as Seafloor Production Tools (SPTs), the Bulk Cutter, and the Auxiliary Machine. Nautilus also unveiled the plan to lift the collected minerals onto production support vessels (PSV) using the Subsea Slurry Lift Pump (SSLP) and Rising and Lifting System (RALS) (Nautilus Minerals 2015). In addition, Neptune focuses on lifting using mining devices made up from drilling rigs and crushers, and airlifting with flexible risers (Neptune 2015). India examined simultaneous multiple operating systems of small self-propelled mining machines and resulted in the success in lifting sand on two occasions: from the seabed at 410 m using imported testing equipment in 2004, and from 450 m using domestic testing equipment in 2007. Furthermore, pilot mining experiments are expected to be scheduled for 2016 (Atmanand 2011; Schwarz 2001). In 2013, South Korea was successful in its driving test of a 6000 m crawler machine, and it plans a pilot mining experiment combined with a lifting system in 2016 (Hong 2013; Yamazaki 2015). In the case of Japan, Japan Oil, Gas and Metals National Corporation (JOGMEC) has also developed test mining equipment, which targets seafloor massive sulfide, and is preparing for verification tests in future (JOGMEC 2015; Kawano et al. 2015). Out of all the examples introduced above, each mining system is different from previous systems developed during the first peak of 1970s.

15.2 Environmental Impact Evaluation

This section will discuss the environmental impact for which evaluation is essential, and the development of new environmental impact assessment methods.

15.2.1 Impact Identification Thus Far

Environmental impact investigations done alongside the development of seabed mineral resources started as a desk study in 1972 by the Columbia University Lamont–Doherty Earth Observatory (Ozturgut et al. 1997). After this, the USA carried out a large-scale environmental basics investigation known as the Deep Ocean Mining Environmental Study (DOMES: 1975–1980) (Ozturgut et al. 1978), and potential environmental impacts were listed within the Programmatic Environmental Impact Study (PEIS: 1981) (NOAA 1981). The following year, the Marine Environmental Research Plan 1981–1985 was published, which narrowed the serious concerns about environmental impact down to the following two points: (1) the destruction of benthic organisms in and near the collector track and (2) the blanketing of the benthos and dilution of their food supply away from the mining site (NOAA 1982; Ozturgut et al. 1997). In relation to (2) in particular, the USA, Japan, the Interoceanmetal Joint Organization (IOM), and India have verified the environmental impact through marine examinations (Tables 15.2 and 15.3) (Kaneko et al. 1997; Sharma et al. 2003; Trueblood et al. 1997; Shirayama and Fukushima 1997; Radziejewska et al. 2001, 2003; Radziejewska 1997; Fukushima and Imajima 1997; Fukushima et al. 2000; Rodrigues et al. 2001; Fukushima 2004). Furthermore, Japan, IOM, and India all carried out long-term monitoring investigations 17 years, 5 years, and 44 months after the impact, respectively (Ingole et al. 2005; Stoyanova 2014; Deep Ocean Resources Development Co Ltd 2015). According to a report from Japan, the difference in abundances of benthic organisms between pre- and post- (17 years) disturbance could not observed (Deep Ocean Resources Development Co Ltd 2015). The mining systems assumed in these environmental studies are similar to those which were considered in the 1970s for evaluating the relationship between the cause and effect of deep-sea mining and based on the results certain conclusions can be thought to have been reached on the potential impacts.

Table 15.2 Summary of benthic disturbances in the BIE-type experiences (Fukushima 2004)

	BIE II (1)	JET (2)	IOM (3)	INDEX (5)
Disturbed area	150 × 3000 m	200 × 2000 m	120–230 m × 2500 m	3000 × 200 m
Number of tows	49 times	20 times	14 times	26 times
Towing duration (days)	19 days	16 days		9 days
Towing duration (time)	88 h 11 min	20 h 27 min		42 h 14 min
Towing distance		32 km		88 km
Total volume of sediment discharged	4694 m^3	2475 m^3	1800 m^3(4)	6023 m^3
Total mass of dried sediment discharged		352 tones		580 tones

Table 15.3 Comparisons of abundance of benthic organisms between their original levels (control levels) and levels after benthic disturbance, as seen in the monitoring results (Fukushima 2004)

Experiment	Study item	First monitoring	Second monitoring	Third monitoring	Results/prediction
Sedimentary bacteria					
JET (1)	Total cells number	Lower (NS)	Not published	Not published	
INDEX (2)	Total cells number	Lower	Lower	Lower	Fourth monitoring
Meiobenthos					
BIE II(3)	Namatoda	Higher (NS)	Lower*	–	It is not clear the cause of the decrease
	Harpacticoida	NS	NS	–	
JET(4)	Nematoda	Lower**	Lower (NS)	Higher (NS)	Monitoring results after 2 years the disturbance exceed the original level
	Harpacticoida	Lower (NS)	Higher (NS)	Higher (NS)	Monitoring results after 1 year the disturbance exceed the original level
IOM (5) (6)	Total	Lower (NS)	Lower*	Higher (NS)	In second and third monitoring: control was split into control (C) and resedimentation (R) area; in second monitoring, impacted area abundance lower than in control (C + R) because of a significant increase in R, presumably due to phytodetritus input
	Nematoda	Lower (NS)	Lower*	Higher (NS)	In second monitoring: marked increase in abundance of Desmoscolecidae in part of control (R)
	Harpacticoida (ab)	Lower (NS)	Lower*	Higher (NS)	In second monitoring: marked increase in abundance of Argestidae in part of control (R)

INDEX (2)	Total abundance	Lower (<50%)	Lower (<41%)	Lower (<13%)	
	NO of Group	Unchanged	Decrease	Decrease	Increase percentages of opportunistic species
Macrobenthos					
BIE II(3)	Majority of macrofaunal taxa	NS	–		
	Sabellidae (Polychaeta)	Higher**	–	ANOVA	
	Macrostylidae (Isopoda)	Higher**	–	ANOVA	
	Glyceridae (Polychaeta)	Higher**	–	PCA-H	
JET(7)	Polychaeta	–	–	Lower*	Comparing with the control area using *T-test*
	Crustacea	–	–	Higher (NS)	
INDEX (2)		Lower (<33%)	Higher (NS)	–	*t-test*
Megabenthos					
JET (8)	Total abundance	–	–	Lower*	Comparing with the control area using *T-test*
	Deposit feeder	–	–	Lower*	
	Suspension feeder (ab)	–	–	NS	
IOM (9)	Total number (ab)	Lower*	Higher*		Two-way ANOVA (difference between impacted and control area significant; however, significant temporal differences both in impacted and in control detected)
INDEX (10)		Lower (32%)	–	–	

NS not significant, *$p < 0.05$, **$p < 0.01$

Fukushima (2004), Kaneko et al. (1997), Sharma et al. (2003), Trueblood et al. (1997), Shirayama and Fukushima (1997), Radziejewska et al. (2001, 2003), Fukushima and Imajima (1997), Fukushima et al. (2000), Rodrigues et al. (2001)

15.2.2 Recent Developments in Environmental Impact Assessment

With the development of marine science, certain environmental impacts that could be caused due to deep-sea mining require a new kind of investigation. One such, example is underwater sound (IFAW 2016), which is given as one of the evaluation parameters in Nautilus' environmental impact assessment report. However, in 'Recommendations for the guidance of contractors for the assessment of the possible environmental impacts arising from exploration for marine minerals in the Area ISBA/19/LTC/8′(ISA 2013c) (hereafter, "Environmental Guidelines") published by ISA, both seismic and sonic explorations causing underwater sound are classified as "activities not requiring environmental impact assessment" (Environmental Guidelines, see Chap. 16) under the conditions of being "of a frequency which will have no significant impact on marine life." Even so, there are no tangible numeric references in relation to "frequencies which will have no significant impact on marine life." On the other hand, there are already several examples of studies on the impact of underwater sound on living creatures. With fish, about which there is continuously progressive research, there are the following results: an attracted response level of 110–130 dB, a startle response level of 140–160 dB, and a lethal level of 220 dB (Hatakeyama 1995). Observation in the natural environment also reported that marine mammals showed evasive behavior at 110–120 dB (Richardson et al. 1995), and sea turtles at 170 dB (LGL Ltd, Environmental Research Associates, and JASCO Research Ltd 2005). Backed with such scientific knowledge, environmental impact assessment for seismic and sonic exploration is mandatory in the USA and Australia (Safety and Environment Center for Petroleum Development 2015). In addition, environmental impact assessment of underwater noise is listed within "guidelines in relation to environmental consideration" which were developed by financial institutions for loan agreements, for example, the IFC (International Finance Corporation) Environment, Health and Safety Guidelines (IFC 2016). Furthermore, with regard to the impact of anthropogenic underwater noise on habitats and the marine biodiversity, the SBSTTA (Subsidiary Bodies for Scientific, Technical and Technological Advice), which was set up under the Convention on Biological Diversity, reported at least 55 types of animal impacts, including crustaceans, osteichthyes, and mollusks as well as other invertebrates (CBD 2012). Underwater sound is given as an example here, but there are other issues which have not been considered in EIA towards development of ocean mineral resources. For example, it is possible that the environmental impact assessment will be required to look at the greenhouse gases generated by vessels, caused by ore transportation and the impact of metal toxicity such as arsenic (As) on the marine environment.

15.2.3 Impact Evaluation Process

The connection between each activity and the related environmental risk is basic information which should be shared between those parties concerned. However, the environmental guidelines issued by ISA describe only the contents and methods of

		Magnitude of Effect				
		5	4	3	2	1
Likelihood of Occurrence	5	High	High	High	Moderate	Moderate
	4	High	High	Moderate	Moderate	Moderate
	3	High	Moderate	Moderate	Moderate	Low
	2	Moderate	Moderate	Moderate	Low	Low
	1	Moderate	Moderate	Low	Low	Low

Fig. 15.1 A hypothetical environmental risk classification matrix

environmental surveys for the contractors, whereas the relation between "activities and risk" is not clear. As in case of the petroleum industry, there is a process known as ENVID (Environmental Aspects Identification), in which each activity and the associated environmental risks are identified with the parties concerned in the early stages of development, which comprise engineers, environmental officers, and environmental consultants (Safety and Environment Center for Petroleum Development 2015). This process makes it possible to consider all potential environmental risks during the initial stage of the plan and provides all parties concerned with shared recognition ensuring that the technical side can design a system which takes environmental risks into account, while the environmental side can carry out the assessment of environmental impacts efficiently. Furthermore, while ENVID is a workshop for those who are engaged in development to share information, ToR (Terms of Reference) is also used as a process whereby advance rules are set involving the stakeholders, such as local authorities and NGO, as well as the supervisory authorities and business operators (Safety and Environment Center for Petroleum Development 2015). ToR is a process through which the condition settings of environmental impact assessments are decided between the stakeholders, and can become a tool for consensus building. It is thought that the importance of ToR will increase in the future, if stakeholders continue to increase. In addition, in case of petroleum industry, a risk matrix can be developed which quantifies the magnitude and likelihood of the environmental impacts. Magnitude is judged from scarcity, importance, vulnerability, and time to recover, and likelihood is judged from scale and occurrence frequency (Fig. 15.1) (INPEX Browse Ltd 2010; PETROBRAS 2007). Considering such examples, from fields in which commercialization has already taken place, the development of suitable environmental guidelines for deep seabed mineral resources is possible.

15.3 Environmental Conservation Measures

The environmental impact assessment detailed above is the first step in the processes to maintain harmony between the marine environment and the development of mineral resources. This section will outline the proposed initiatives for developing environmental conservation plans.

15.3.1 Initiatives in United Nations

The United Nations Informal Consultative Process on Ocean Affairs and the Law of the Sea (UNICPOLOS), which was established by the 1999 UN resolution, deliberated in 2003 in relation to marine protected areas (MPA) in ABNJ, and in 2004 in relation to sustainable use and maintenance of biodiversity beyond national jurisdiction (BBNJ) (DOALOS 2003, 2004). As a result, during the 2005 general assembly, the UN secretary general pointed out that "there was little knowledge obtained from the research carried out on BBNJ" and "knowledge of biodiversity in the deep sea is particularly limited (UN 2004)." In 2006 the "Ad Hoc Open-ended Informal Working Group to study issues relating to the conservation and sustainable use of marine biological diversity beyond areas of national jurisdiction" (BBNJ Group), which was established under UNICPOLOS in 2004, reported that research into marine biodiversity—with a focus on seamounts, hydrothermal vent, and cold-water corals—was of particular importance (UN 2006). As a result, during the 2006 UN General Assembly, the BBNJ group was urged to look at problems including "the influence of artificial actions on biodiversity outside of national jurisdiction (UN 2007a)." Following this, at the 65th UN General Assembly in 2010, the Secretary General was asked to report on "the capacity building (CB) and environmental impact assessment (EIA) of oceans which had been changed by human activity, such as the development of mineral resources in deep seabed outside national jurisdiction (UN 2007b)." The above enumerated the deliberation of biodiversity conservation plans in the UN and UNICPOLOS, but there were references to the impact of the development of deep-sea mineral resources, and ocean environment conservation plans such as MPA everywhere. Furthermore, at the 69th U.N. General Assembly in 2015, the creation of international documentations including MPA and EIA was adopted under UNCLOS, and this work is scheduled to begin in 2016 (UN 2015). These series of developments show that the examination of ocean environment conservation plans, including ocean development of deep seabed mineral resources, the protection of ocean biodiversity, as well as establishment of MPAs, has begun to work concurrently within international communities.

15.3.2 Ocean Governance in Relation to CBD

At the Convention on Biodiversity 9th Conference of the Parties (CBD COP9), held in Bonn in 2009, the seven scientific criteria relating to the selection of Ecologically or Biologically Significant Marine Areas (EBSA), which became the proposed sites of MPA, were decided (CBD 2009). The seven scientific criteria were as follows: (1) uniqueness or rarity, (2) special importance for life history stages of species, (3) importance for threatened, endangered, or declining species and/or habitats, (4) vulnerability, fragility, sensitivity, or slow recovery, (5) biological productivity, (6) biological diversity, and (7) naturalness. During the COP10 held in Japan the following year, the "Aichi Targets"—which are made up from five strategic objectives and 20

goals—were adopted, in order to take "effective urgent action" between 2011 and 2020 (CBD 2010). The following is an excerpt (partial) from goal 11 of strategic objective C (improving biodiversity to protect the diversity of ecosystems, species, and genetics) of the Aichi Targets; "By 2020, at least 17% of terrestrial and inland water, and 10% of coastal and marine areas, especially areas of particular importance for biodiversity and ecosystem services, are conserved through effectively and equitably managed, ecologically representative and well connected systems of protected areas and other effective area-based conservation measures, and integrated into the wider landscapes and seascapes." In other words, the Aichi Targets look to make 10% of ocean area MPA. Considering the proposed sites for development of deep seabed mineral resources, in many cases, there is insufficient information to judge whether the aforementioned standards are met, meaning it is not possible to select EBSA. However, because the initiatives taken by CBD mentioned above are "effective urgent action," they cannot be reversed once progressed. The speed of EBSA selection work for the MPA set target of 10% is thought to be moving faster. This shows that scientific knowledge about the deep sea is necessary for EBSA selection, and moreover, depending on the knowledge accumulated, high precision is a must for the environmental impact assessments of deep-sea development.

15.3.3 Environmental Conservation in Relation to Deep-Sea Mineral Resources Development

As already discussed, the UN and CBD have become actively linked with the development of the ocean environment conservation measures, and as such, various stakeholders have come to have a strong interest in the environmental impact of seabed mineral resources. The declaration "We call on the International Seabed Authority to continue, with early involvement of all relevant stakeholders, its work on a clear, effective and transparent code for sustainable deep sea mining, taking into account the interests of developing states," which was made during the G7 Summit held in Elmau, Germany in 2015, backed by the surge of interest in "Deep-Sea Mining beyond the limits of National Jurisdiction," is one such example(G7 GERMANY 2015 Schloss Elmau 2015). In addition, the fact that projects on environmental impact assessment/conservation measures in relation to deep-sea mining—such as Blue Mining, MIDAS, INDEEP, JPI Oceans, and DOSI—are being carried out, is not unrelated to the aforementioned surge in interest towards the deep-sea mining industry and the series of movements around environmental conservation measures (see Chap. 16). Furthermore, some NGOs say that "there should be a moratorium on conditions in which the impact on the environment of deep-sea mining is not clear" and "the development of deep-sea mineral resources is not at all sustainable (Steiner 2015)." Under such circumstances, and in order to understand the stakeholders in the development of deep-sea mineral resources, ISA carried out a survey in 2015, which was split into four sections: economy, environmental conservation, safety, and general (ISA 2015a). Also, nine controlled sea areas were established (Areas of

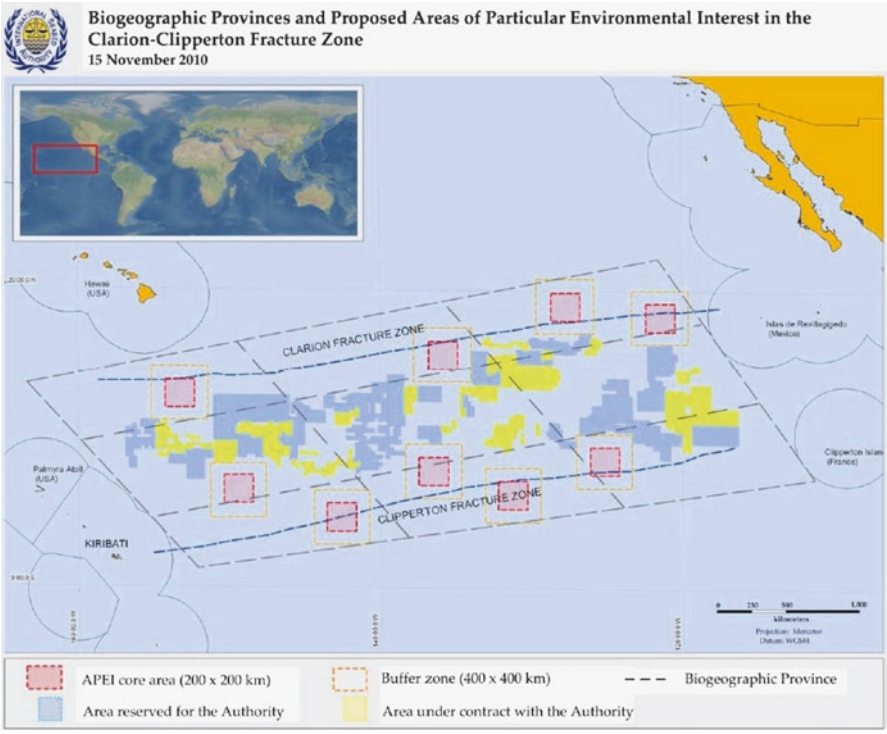

Fig. 15.2 Location of the areas of particular environmental interest (ISA 2016)

Particular Environmental Interest: APEI) (Fig. 15.2) (ISA 2011b) east, west, south, and north around the Clarion-Clipperton Fracture Zone (CCFZ), in order for the UN to take EIA and MPA into the new documentation, and to match the examination and pace of EBSA and MPA which were being examined by CBD and SBSTTA. APEI is a biodiversity conservation measure which assumes that the biodiversity of the CCFZ as a whole can be maintained, even if mining activity is carried out in part of CCFZ. In Japan, JOGMEC, which aims to develop seabed hydrothermal deposits within the area under its jurisdiction, examined genetic level environmental conservation measures, selecting numerous sites with gene flows for digging, and establishing locations where development would and wouldn't be carried out within these sites (Narita et al. 2015). In this way, within the field of development of deep-sea mineral resources, efforts are repeatedly made to catch up with environmental conservation plans pursued by international communities including the UN.

Stakeholders with an interest in the ocean/deep sea are increasing; deep-sea mining is not just an issue limited to the mining industry, and it is important to progress while maintaining alignment with world opinion. This means "we cannot avoid examining conservation measures without limiting impact assessments for environ-

ments." With regard to environmental conservative measures for deep-sea mining at the present time, these are limited to the implementation of APEI by ISA, and there has not yet been sufficient discussion; however, the initiatives of CBD and UNICPOLOS can be taken into account.

15.4 Japan's Initiatives

In this section, new initiatives for environmental impact assessment developed in Japan will be discussed. With regard to the manganese nodules of the CCFZ, the Deep Ocean Resource Development Co. Ltd. (DORD) is carrying out an investigation and associated environmental evaluation, under contract of ISA (Tsune and Okazaki 2015). After acquiring a mining area for cobalt-rich ferromanganese crusts in 2014, JOGMEC also started work on an environmental impact assessment in the West Pacific Ocean (ISA 2015b). In addition, JOGMEC is in the process of implementing an environmental impact evaluation and a technical feasibility study as a part of its development project for deep-sea hydrothermal deposits in sea areas under its national jurisdiction (Ishida et al. 2012; Maeda et al. 2012). Thus far, DORD and JOGMEC have been leading the development of marine mineral resources and associated environmental examinations in Japan; however, since 2014, the Japanese government have appointed the Japan Agency for Marine-Earth Science and Technology (JAMSTEC) to start work on a "Cross-ministerial Strategic Innovation Promotion Program (SIP)" (JAMSTEC 2013), to establish a new method for the development of seabed mineral resources, using a novel approach as compared to those adopted by DORD and JOGMEC. Attempts to establish a new technique for environmental impact assessment are also being carried out as part of such efforts. In particular, the method with feasibility, which enables environmental impact assessment matched with the progress of mining techniques and the participation of private enterprises, and the evaluation method which matches pace with international trends are under examination. This project which has been started recently is introduced below followed by the next section that describes the research approach which the authors wished to highlight.

15.4.1 Ascertaining the Relationship Between Mining Methods and Environmental Impacts

As already discussed, new mining methods have been suggested by various organizations. Naturally, when mining methods change, so does the impact they cause. As a result, if considering the economics of seabed resource development, it is required that unnecessary evaluations should be omitted (or only those required may be added, if necessary), in light of each individual mining method. With SIP, a list of impacts which are cause for concern is created, aiming to

establish a project which creates environmental research plans that can be selected by different organizations as per the design of their mining method.

15.4.2 Development of Effective Taxonomic Technologies

While stakeholders in the development of marine mineral resources are increasing, environmental impact assessments examinations and their results have the implication of joint ownership documentation, for the creation of an agreement within stakeholders. To create this agreement, the transparency and scientific objectivity of the process from examination to evaluation is essential. With regard to scientific objectivity in particular, if we consider that the developer is also a stakeholder, the formation of an agreement will be difficult if the technique does not take economic rationality into account. This project aims to develop an analysis technique which takes this variety of conditions into consideration (see Chap. 16).

15.4.3 Development of Practical Environmental Monitoring System

Scientific objectivity and economic rationality are not only necessary for analysis techniques, but also for marine observation techniques. In SIP environmental impact monitoring, as automation and mechanization are the objectives, downsizing is pursued for economic rationality. Due to the fact that automation also saves manpower, it can be expected within economic rationality. Furthermore, if we hypothesize the connection between the various stakeholders, selection of versatile machinery is important. Taking this into consideration, the devices being worked on are those such as a monitoring device that is set up on the seabed (JAMSTEC 2013), and a marine observation device with automatic lifting.

15.4.4 Harmonizing with International Trends

Environmental impact assessment and environmental conservation measures, particularly with regard to the deep sea, are in the process of evolution, and changes to system and structure are expected as we move forward. Thus whether inside or outside of national jurisdiction, it is important to match pace with international trends and have the flexibility to work under any conditions. In the environmental field of SIP, a subproject was built named EcoDEEP, in cooperation with the French Research Institute for Exploitation of the Sea (IFREMER: France) (Menot 2015). Aside from this, development of a globally versatile environmental impact assessment technique is being attempted, in the form of arranging a collaboration system with overseas research organizations, and matching with the approach of ISA.

15.5 Conclusion

Diverse initiatives towards utilization of the oceans have been initiated amongst these, the global movement for the development of deep-sea mineral resources is especially dynamic. Furthermore, environmental impact assessment, which is one of the cornerstones of the development of deep-sea mineral resources, needs to be approached with a new direction, including the suggestion of conservation measures as suggested in this chapter. It is essential to examine this new approach while allowing for the input of scientific knowledge, international cooperation, and the establishment of economic activities.

Acknowledgement This study was conducted as a part of next-generation technology for ocean resources exploration, which is one of cross-ministerial strategic innovation promotion program (SIP), organized by Cabinet Office, Government of Japan. Authors would like to express our gratitude to members of "Research and Development Center for Submarine Resources" of "Japan Agency for Marine-Earth Science and Technology (JAMSTEC)" for their valuable advice.

References

Atmanand MA (2011) Status of India's polymetallic nodules mining programme. In: ISOPE 2011 Maui Conference

CBD (2009) Decision adopted by the conference of the parties to the diversity at its ninth meeting. UNEP/CBD/COP/DEC/IX/20, 9 Oct 2008

CBD (2010) Decision adopted by the conference of the parties to the diversity at its ninth meeting. UNEP/CBD/COP/DEC/X/2, 29 Oct 2010

CBD (2012) Scientific synthesis on the impacts of underwater noise on marine and coastal biodiversity and habitats. UNEP/CBD/SBSTTA/16/1/INF/12

Deep Ocean Resources Development Co Ltd (2015) Status of Japanese activities on biological survey of macrofauna in CCFZ. Document for ISA workshop on taxonomic methods and standardization of macrofauna in the Clarion-Clipperton Fracture zone, Uljin-gun, South Korea, 23–30 Nov 2014

Diamond Field International Ltd (2010) Atlantis II Red Sea Deeps. http://www.diamondfields.com/s/AtlantisII.asp. Accessed 15 Jan 2016

DOALOS (2003) Discussion panel B on protecting vulnerable marine ecosystems. http://www.un.org/depts/los/consultative_process/4thMeetingPanels.htm. Accessed 19 Jan 2016

DOALOS (2004) New sustainable uses of the oceans, including the conservation and management of the biological diversity of the seabed in areas beyond national jurisdiction. http://www.un.org/depts/los/consultative_process/5thmeetingpanel.htm. Accessed 19 Jan 2016

Fukushima T (2004) Ecological characteristics of deep-sea benthic organisms in relation to manganese nodules development practices. Thesis, Kyoto University

Fukushima T, Imajima M (1997) A study of a macrobenthos community in a deep sea resedimentation area. In: Proceedings of the international symposium on environmental studies for deep sea mining, MMAJ, Tokyo, Japan, pp 331–336

Fukushima T et al (2000) The characteristics of deep-sea epifaunal megabenthos two years after an artificial rapid deposition event. Publ Seto Mar Biol Lab 39:17–27

G7 GERMANY 2015 Schloss Elmau (2015) G7 Leaders' Declaration G7 Summit 7–8 June 2015. http://www.mofa.go.jp/mofaj/files/000084020.pdf. Accessed 19 Jan 2016

Hatakeyama Y (1995) Research on hearing abilities and responses of fish to underwater sounds in Japan. IEICE technical report. Ultrasonics 95(219):19–26

Hong S (2013) Pilot mining robot for polymetallic nodules (oral presentation). In: 42th UMI, Rio de Janeiro, 21–29 Oct
IFAW (2016). International Fund for Animal Welfare H.P. http://www.ifaw.org/united-kingdom/frontpage. Accessed 19 Jan 2016
IFC (2016) Environmental, health, and safety guidelines. http://www.ifc.org/wps/wcm/connect/topics_ext_content/ifc_external_corporate_site/ifc+sustainability/our+approach/risk+management/ehsguidelines. Accessed 19 Jan 2016
IFREMER (2013) Marine geoscience/consortia nodules. http://wwz.ifremer.fr/drogm_eng/Activities/Mineral-resources/Ressources-minerales-grand-fond/Polymetallic-nodules/Nodule-consortia. Accessed 19 Jan 2016
Ingole BS, Pavithran S, Ansari A (2005) Restoration of deep-sea macrofauna after simulated benthic disturbance in the Central Indian Basin. Mar Georesour Geotechnol 23:267–288
INPEX Browse Ltd (2010) Ichthys gas field development project draft environmental impact assessment. INPEX, p 728
ISA (2008) Tonga becomes second developing state to sign contract with ISA. https://www.isa.org.jm/news/tonga-becomes-second-developing-state-sign-contract-isa. Accessed 15 Jan 2016
ISA (2011a) Seabed Authority and Nauru Ocean Resources Inc. sign contract for exploration. https://www.isa.org.jm/news/seabed-authority-and-nauru-ocean-resources-inc-sign-contract-exploration. Accessed 19 Jan 2016
ISA (2011b) Environmental management plan for clarion-clipperton fracture zone. ISBA/17/LTC/7
ISA (2013a) UK Seabed Resources Ltd. applies for approval of second plan of work for exploration for polymetallic nodules. https://www.isa.org.jm/news/uk-seabed-resources-ltd-applies--approval-second-plan-work-exploration-polymetallic-nodules. Accessed 19 Jan 2016
ISA (2013b) G-TEC Sea Mineral Resources NV (GSR) of Belgium signs exploration contract. https://www.isa.org.jm/news/g-tec-sea-mineral-resources-nv-gsr-belgium-signs-exploration-contract. Accessed 19 Jan 2016
ISA (2013c) Recommendations for the guidance of contractors and sponsoring States relating to training programmes under plans of work for exploration. ISBA/19/LTC/8
ISA (2014) Deep seabed minerals contractors. https://www.isa.org.jm/deep-seabed-minerals-contractors. Accessed 5 Jan 2016
ISA (2015a) ISA and MARAWA Research Exploration Ltd. sign exploration contract for polymetallic nodules in reserved areas in the Clarion-Clipperton Zone. https://www.isa.org.jm/news/isa-and-marawa-research-exploration-ltd-sign-exploration-contract-polymetallic-nodules--reserved. Accessed 15 Jan 2016
ISA (2015b) Seabed authority launchers “Stakeholder Survey” on Mineral Exploitation Code. https://www.isa.org.jm/news/seabed-authority-launchers-stakeholder-survey-mineral-exploitation-code. Accessed 19 Jan 2016
ISA (2015c) Japan Oil, Gas and Metals National Corporation (JOGMEC) and ISA sign exploration contract. https://www.isa.org.jm/news/japan-oil-gas-and-metals-national-corporation-jogmec-and-isa-sign-exploration-contract. Accessed 19 Jan 2016
ISA (2016) ISA and Ocean Mineral Singapore Pte Ltd. sign exploration contract for polymetallic nodules in reserved areas in the Clarion-Clipperton zone. https://www.isa.org.jm/news/isa-and-ocean-mineral-singapore-pte-ltd-sign-exploration-contract-polymetallic-nodules-reserved. Accessed 19 Jan 2016
Ishida H et al (2012) Environmental baseline survey for mining of the sea-floor massive sulfide (SMS) areas around Japanese Islands. In: Proceedings of the ASME 2012 31th OMAE, Rio de Janeiro, Brazil, 1–6 July 2012
JAMSTEC (2013) R/V KAIYO Cruise Report KY13-13 KY13-E05, JAMSTEC, p 23
JOGMEC (2015) National resources challenge to development: seafloor massive sulfide. JOGMEC News, p 16 (in Japanese)
Kaneko T et al (1997) The abundance and vertical distribution of abyssal benthic fauna in the Japan Deep-sea Impact Experiment. In: Proceedings of the 2nd ISOPE ocean mining symposium, ISOPE, vol 1, Honolulu, pp 475–480

Kaufman R, Latimer JP, Tolefson DC (1985) The design and operation of a Pacific Ocean deep-ocean mining test ship: R/V Deepsea Miner II. In: Proceedings of the 17th offshore technology conferences, Paper No. 4,901

Kawano S et al (2015) Study on mining system for seafloor massive sulfide mound and results of on-site excavation test in Okinawa Trough. J MMIJ 131:614–618

LGL Ltd, Environmental Research Associates, and JASCO Research Ltd (2005) Assessment of the effects of underwater noise from the proposed Neptune LNG project. LGL Report No. TA4200-3, p 12

Maeda N et al (2012) Dynamics of the setting and suspended particle around a seafloor massive sulfide in Japan. In: Proceedings of the ASME 2012 31th OMAE, Rio de Janeiro, Brazil, 1–6 July 2012

Menot L (2015) EcoDEEP workshop: the crafting of seabed mining ecosystem-based management. MIDAS Newsletter issue 5 summer 2015, p 17

Narita T et al (2015) Summary of environmental impact assessment for mining seafloor massive sulfides in Japan. J Shipp Ocean Eng 5:103–114

Nautilus Minerals (2015) Status of the equipment. http://www.nautilusminerals.com/irm/content/status-of-the-equipment.aspx?RID=424. Accessed 19 Jan 2016

Nautilus Minerals Nuigini Ltd (2012) Mineral Resource Estimate Solwara Project, Bismark Sea, PNG. Technical Report compiled under NI43-101, p 240

Neptune HP (2015) Minerals extraction. http://www.neptuneminerals.com/our-business/minerals-extraction/. Accessed 19 Jan 2016

NOAA (1981) Deep seabed mining final programmatic environmental impact statement 1 (NOAA, 1981)

NOAA (1982) Marine Environmental Research Plan 1981–1985

Ozturgut E et al (1978) Deep ocean mining of manganese nodules in the North Pacific: pre-mining environmental conditions and anticipated mining effects. NAA Technical Memorandum ERL MESA-33, p 133

Ozturgut E, Trueblood DD, Lawless J (1997) An overview of the United States' benthic impact experiment. In: Proceedings of the International Symposium on Environmental Studies for Deep Sea Mining, MMAJ, Tokyo, Japan, pp 23–32

PETROBRAS (2007) Desenvolvimento Integrado da Produção e Escoamento na Área Denominada Parque das Baleias e no Campo de Catuá. Petrobras, p 80

Radziejewska T (1997) Immediate responses of benthic meio- and megafauna to disturbance caused by polymetallic nodules miner simulator, deep-sea meiobenthic communities to sediment disturbance simulating effects of polymetallic nodule mining. In: Proceedings of the international symposium on environmental impact of deep sea mining, MMAJ, Tokyo, Japan, pp 223–235

Radziejewska T et al (2001) IOM BIE revisited: meiobenthos at the IOM BIE site 5 years after the experimental disturbance. In: Proceedings of the 4th ISOPE ocean mining symposium, Szczecin, Poland, pp 63–68

Radziejewska T et al (2003) Marine environment in the IOM Area (Clarion-Clipperton Region, Subtropical Pacific): current knowledge and future needs. In: Proceedings of the 5th ISOPE ocean mining symposium, ISOPE, Tsukuba, Japan, pp 188–193

Richardson WJ et al (1995) Marine mammals and noise. Academic Press, London, p 594

Rodrigues N et al (2001) Impact of benthic disturbance on megafauna in Central Indian Basin. Deep Sea Res Part II 48:3411–3426

Safety and Environment Center for Petroleum Development (2015) Report for Research on Environmental Measures for Oil and Gas Exploration and Development in Deepwater (Environmental Impact Assessment). METI. http://www.meti.go.jp/meti_lib/report/2015fy/000154.pdf. Accessed 19 Jan 2016 (in Japanese)

Schwarz W (2001) Advanced nodule mining system. In: Proceedings of the proposed technologies for deep seabed mining of polymetallic nodules, Kingston, Jamaica, ISA, pp 39–54

Sharma R et al (2003) Monitoring effects of simulated disturbance at INDEX site: current status and future activities. In: Proceedings of the 5th ISOPE ocean mining symposium, ISOPE, Tsukuba, Japan, pp 208–215

Shirayama Y, Fukushima T (1997). Responses of meiobenthos community to the rapid re-sedimentation. In: Proceedings of the international symposium on environmental impact of deep sea mining, MMAJ, Tokyo, Japan, pp 187–196
Steiner R (2015) Deep sea mining a new ocean threat. The Huffington Post, 20 Oct
Stoyanova V (2014) Status of macrofaunal studies carried out by the Interoceanmetal Joint Organization (IOM). Document for workshop on taxonomic methods and standardization of macrofauna in the Clarion-Clipperton Fracture zone, Uljin-gun, South Korea, 23–30 Nov 2014
Theil H, Foell E, Schriever G (1992) Potential environmental effects of deep seabed mining. In: Preparatory Commission for the International Seabed Authority and for the international Tribunal for the Law of the Sea, New York, 10–21 Aug, p 214
Trueblood DD et al (1997) The ecological impacts the joint US-Russian Benthic Impact Experiment. In: Proceedings of the international symposium environmental studies for deep sea mining, MMAJ, Tokyo, Japan, pp 237–243
Tsune A, Okazaki M (2015) Current situation of manganese nodule exploration in Japanese License Area. J MMIJ 131:602–609
UN (2004) Resolution adopted by the General Assembly on 17 November 2004 (A/Res/59/24)
UN (2006) Report of the Ad Hoc Open-ended Informal Working Group to study issues relating to the conservation and sustainable use of marine biological diversity beyond areas of national Jurisdiction (A/61/65)
UN (2007a) Resolution adopted by the General Assembly on 22 December 2007 (A/Res/62/215)
UN (2007b) Letter dated 17 March 2010 from the Co-Chairpersons of the Ad Hoc Open-ended Informal Working Group to the President of the General Assembly (A/65/68)
UN (2015) Resolution adopted by the General Assembly on 19 June 2015 (A/RES/69/292)
Yamazaki T (2015) Past, present, and future of deep-sea mining. J MMIJ 131:592–696

Dr. Yoshihisa Shirayama born in 1955 in Tokyo, Japan, obtained D. Sc. Degree from Graduate School of Science, The University of Tokyo (UT), in 1982. He then served as Assistant Professor and then as Associate Professor at Ocean Research Institute, University of Tokyo. In 1997, he became a professor of Seto Marine Biological Laboratory, Faculty of Science, Kyoto University. In 2003, the laboratory moved to Field Science Education and Research Center where he served as Director from 2007. In April 2011, he became Executive Director of Research, Japan Agency for Marine-Earth Science and Technology. His major research field is marine biology, especially taxonomy and ecology of deep-sea meiobenthos. He is also working on the marine biodiversity and the impact of ocean acidification on it. He was awarded "Okada Prize" from Oceanographic Society of Japan in 1988, and Ministry of Environment Japan Recognition in 2011. He also was awarded Cosmos International Prize as a member of Scientific Steering Committee of Census of Marine Life in 2011.

Mr. H. Ito is an engineer belonging to the Ecosystem Observation and Evaluation Methodology Research Unit, Project Team for Development of New-generation Research Protocol for Submarine Resources in Japan Agency for Marine-Earth Science and Technology (JAMSTEC). In 1991, he completed a graduate school of agriculture in University of Kagawa and joined Japan NUS Co., Ltd. (JANUS). He is in charge of projects related to environmental impact assessment for marine developments in JANUS. He has been on loan to JAMSTEC since 2015.

Dr. Tomohiko Fukushima is working for Research and Development (R&D) Center of Submarine Resources, Japan Agency for Marine-Earth Science and Technology (JAMSTEC). He graduated from the Faculty of Fisheries, Tokyo University of Fisheries in 1984 (bachelor degree) and obtained postgraduate degree from Faculty of Fisheries, Tokyo University of Fisheries in 1986 (master degree). In 2004, he obtained Doctor of Science Degree from Kyoto University. The title of doctoral thesis is "Ecological Characteristics of Deep-Sea Benthic Organisms in Relation to Manganese Nodules Development Practices." After being awarded the doctoral degree, he continued his research activities in the Ocean Policy Research Foundation (as Research Fellow), The University of Tokyo (as Associate Professor), and then joined JAMSTEC.

Chapter 16
Taxonomic Problems in Environmental Impact Assessment (EIA) Linked to Ocean Mining and Possibility of New Technology Developments

Tomohiko Fukushima and Miyuki Nishijima

Abstract The expectation for the development of deep-sea mineral resources has grown as global metal resources have continued to run short. At the same time, there is also a demand for rigorous environmental impact assessments. However, unlike risk assessments for human health, there are no clear standards or indicators for impact assessments for the natural environment. For this reason, although the importance of environmental impact assessments has been stressed at the conceptual level, it is not easy to suggest specific methods. In the case of shallow water, for which knowledge of the taxonomy and ecosystem is relatively rich, the impact is generally evaluated based on biomass, abundance, species richness, rare species, endemic species, dominant species, or keystone species. In contrast, for deep waters, there is a deficiency in highly specialized taxonomists and identification technicians, making it difficult to obtain such indicators as for shallow waters. On the other hand, opportunities for deep-sea mineral resources development are increasing. Therefore it is difficult to imagine that the development will be interrupted by EIA issues. These facts suggest that there is an urgent need for environmental impact evaluators to resolve the issues in indexing the impacts of mining of deep-sea minerals. In this chapter, the current problems of environmental assessment in relation to development of deep-sea mineral resources are explained, and the possibility of impact assessment through molecular biological approach is discussed.

16.1 The Potential of Deep-Sea Mineral Resource Development

There have been growing expectations for deep-sea mineral resource development in both Areas Beyond National Jurisdiction (ABNJ) and waters within jurisdiction. The growing expectations for deep-sea mineral resource development in ABNJ can be seen from the recent number of applications for exploration areas to the International Seabed Authority (ISA 2014). The Regulations on Prospecting and

T. Fukushima (✉) • M. Nishijima
Japan Agency for Marine-Earth Science and Technology, Yokosuka, Japan
e-mail: fukushimat@jamstec.go.jp

R. Sharma (ed.), *Deep-Sea Mining*, DOI 10.1007/978-3-319-52557-0_16

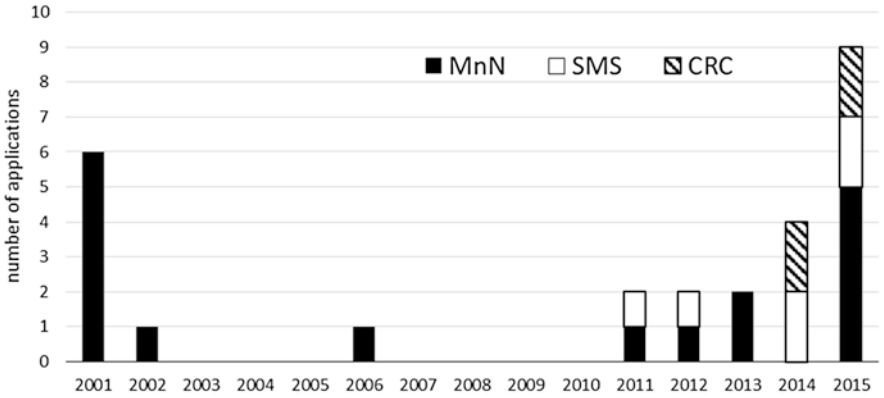

Fig. 16.1 Changes in the application number of exploration area to International Seabed Authority

Exploration for Manganese Nodules in the Area (ISA 2013a) were published in 2000, and seven Pioneer Investors received approvals for exploration areas from the ISA by 2002. There was a period with no new applications until 2010; since 2011, 17 new exploration areas have been approved. In addition, the Regulations on Prospecting and Exploration for Seafloor Massive Sulfide (SMS) (ISA 2010) and for Cobalt-rich Ferromanganese Crust (CRC) (ISA 2012) in the Area were published in 2010 and 2011, for which six and four applications for exploration areas were approved, respectively (Fig. 16.1).

Many of the recent applications were made by private companies and sponsored by certifying states. Such companies include: G-TEC Sea Mineral Resources NV (GSR) in contract with Cook Islands Investment in the Cook Islands, UK Seabed Resources Ltd. (the British branch of Lockheed Martin from the USA) and Ocean Mineral Singapore Pte. Ltd. (branch of Keppel Corporation from Singapore) in Singapore, Marawa Research and Exploration Ltd. in Kiribati, Nauru Ocean Resources Inc. (affiliated with Nautilus Minerals) in Nauru, Tonga Offshore Mining Ltd. (affiliated with Nautilus) in Tonga, and Companhia Pesquisa de Recursos Minerais S.A in Brazil (ISA 2015).

As for areas within the jurisdiction of coastal states, exploitation licenses were obtained by Diamond Fields International (for Red Sea) in 2010 and by Nautilus Minerals (for Solwara 1, Papua New Guinea (PNG)) in 2011 (Diamond Fields 2015; The Guardian 2012). The targets are seabed hydrothermal deposits in both cases. In regard to exploratory licenses, Nautilus Minerals applied for Tonga, Fiji, Solomon, Vanuatu, PNG, and New Zealand, and some of them were approved. Similarly, Neptune Minerals and its affiliated companies obtained exploration areas for seabed hydrothermal deposits in PNG, Solomon, Tonga, Fiji, Vanuatu, Micronesia, and Palau (Neptune Minerals 2015). The Korea Institute of Ocean Science and Technology (KIOST) (KIOST 2012) also obtained the same license in Tonga and Fiji (Table 16.1). In 2015, the Seabed Mineral Authority of Cook Islands held an international bid on exploration licenses for manganese nodules present within the waters of its jurisdiction (Seabed Minerals Authority 2005).

Table 16.1 List of international collaborative projects

Project	Supported by	Members	Terms
Blue Mining	EP7	19 Research organization from across Europe (11 countries)	2014–2018
MIDAS	EP7	32 Organizations from across Europe (11 countries)	2013–2015
JPI Oceans	Each member country	20 Member countries	2011–
INDEEP	Total foundation	More than 500 members from 38 countries	2011–2016
DOSI	INDEEP, etc.	185 Members in mailing lists	2013–
EcoDEEP	Each organization	Ifremer and Jamstec	2015–

EP7 European Commission's Framework 7 programme

Following this trend of obtaining licenses for mining areas both within and outside national jurisdictions, there are also moves towards international collaborations for developing the mining technologies. One such effort is that of Blue Mining (2014–2018), a technological development project for deep-sea mineral resource that is part of the European Union's Seventh Framework Programme for research, technological development, and demonstration (FP7). Blue Mining consists of 11 EU countries and 19 research institutes and companies. In particular, there are considerations for exploratory production technologies such as deep-sea tailing technology (Blue Mining 2015).

The cases discussed above are examples of an increasing trend of deep-sea mineral resource development.

16.2 Regularization of Environmental Impact Assessments

As the expectations for deep-sea mineral resource development continue to increase, further efforts in environmental impact assessments have also been made. Environmental issues pertaining to deep-sea mining beyond the limits of national jurisdictions were discussed in the declarative statement at the Summit Conference (G7), held in Elmau, Germany, on June 7–8, 2015. The declarative statement at the Summit read "We call on the international Seabed Authority to continue, with early involvement of all relevant stakeholders, its work on a clear, effective and transparent code for sustainable deep-sea mining, taking into account the interests of developing states." With this background, a number of environmental projects are born in the EU. Similar to Blue Mining, the EU is also implementing "Managing Impacts of Deep-sea Resource Exploitation" (MIDAS) as part of FP7 (MIDAS 2012). This is a 3-year program, initiated in 2013, to reduce the environmental impacts made by deep-sea mineral resource developments. The program involves 11 European countries and 32 organizations involved in science, industry, social science, law, and NGOs. The targets of this project are manganese nodules, seabed hydrothermal deposits, cobalt-rich crusts, and rare-earth mud. Its focus is on environmental impact assessment, and the project has been joined by various stakeholders.

Though not funded by the EU headquarters, the Joint Programming Initiative Healthy and Productive Seas and Oceans (JPI Oceans) is jointly funded by EU countries. One of the 13 current research projects of JPI Oceans is on exploring deep-sea resources, and its objectives include the establishment of habitat maps for deep-sea mining areas (JPI Oceans 2015). In addition, one of the environmental projects funded by Total Foundation (France) is the International Network for Scientific Investigation of Deep-sea Ecosystems (INDEEP) (INDEEP 2015). This is a project to fill the gap between science and society by supporting sustainable environmental management for deep seas. The planned project period is from 2011 to 2016, and currently 38 countries and 500 individuals are involved. Another project derived from INDEEP is the Deep Ocean Stewardship Initiative (DOSI 2015). This project aims at a holistic approach through science, technology, policy, and economy for advancing the ecosystem management of deep seabed to be developed in the future.

The efforts described above share common elements such as a multi-stakeholder, multinational approach, integrated environmental protection, and the cooperation of society and science (Table 16.2). In addition to multinational projects such as these, there also many cases involving individual countries or organizations. Countries that have exploration contracts with the ISA are required to conduct environmental impact assessments. For developments within national jurisdictions, environmental impact assessments are carried out pursuant to the regulations of the respective countries. As for Japan, Deep Ocean Resources Development Co., Ltd. (DORD) and the Japan Oil, Gas and Metals National Corporation (JOGMEC) are conducting environmental impact assessments in a manganese nodule exploratory mining region near the central Pacific equator and a cobalt-rich crust exploration area region in the Western Pacific Ocean, respectively (DORD 2015; JOGMEC 2015). Within national jurisdiction areas, JOGMEC is examining the environmental protection for SMS developments in the Okinawa and Ogasawara sites (Narita et al. 2015). Moreover, the Japan Agency for Marine-Earth Science and Technology (JAMSTEC) is investigating the prediction and monitoring technology for ecosystem change associated with deep-sea mineral resource development, as part of the Cross-ministerial Strategic Innovation Promotion Program (SIP) organized by the Cabinet Office (SIP 2015).

These projects reflect recent trends, in which both deep-sea mineral resource development and environmental impact assessments are underway in response to the societal demand for dwindling resources. However, there are problems in both efforts. The following sections will discuss the issues presented by environmental impact assessments.

16.3 Issues with Environmental Impact Assessments

While deep-sea mineral resource development has a clear goal of economic profit, the goal in regard to environmental protection is still conceptual. For example, in the United Nations Convention on the Law of the Sea (UNCLOS), economy is

Table 16.2 Activities list of deep-sea mineral resources development in the areas of national jurisdiction

No	Country	Project	Location 1	Core company	License	Granted by/ apply to	Ore
1	Saudi Arabia	Atlantis II Deep project	Red Sea	Core: Diamond Fields International (Ca) Joint:Manafa International (Saudi)	2010–2040 (EpL)	Red Sea Commission (G)	SMS
2	PNG	Solwara 1 project	Bismark Sea	Nautilus Minerals (Ca)	2010–2030 (EpL)	PNG (G)	SMS
3	PNG	Solwara 2–19	Bismark Sea	Nautilus Minerals (Ca)	1997– (EL)	PNG (G)	SMS
4	PNG	Woodlark Area	Solmon Sea	Nautilus Minerals (Ca)	2012, 2014 (EL)	PNG (G)	SMS
5	PNG	New Ireland Arc	Off the coast of New Ireland	Nautilus Minerals (Ca)	2012, 2014 (EL)	PNG (AP)	SMS
6	PNG			Neptune Minerals(USA)	2012–2014 (EL)	PNG (G)	SMS & epithermal Gold
7	Solmon Islands		Solmon Sea	Nautilus Minerals (Ca)	2011–2014 (PL)	Solmon Islands Gov. (G)	SMS
8	Solmon Islands		Solmon Sea	Blue Water Metals (Aus)/ Subsidiary of Neptune	2007–2014 (PL)	Solmon Islands Gov. (G)	SMS
9	Kingdom of Tonga		Tonga	Nautilus Minerals (Ca)	2006–2007 (PL)	Tonga (G?)	SMS
10	Kingdom of Tonga		Tonga	Neptune Minerals(USA)	2008–2014 (PL)	Tonga (G)	SMS
11	Kingdom of Tonga		Tonga	KIOST	2008–2014 (EL)	Tonga (G)	SMS
12	Fiji		Fiji	Nautilus Minerals (Ca)	2014–2016 (EL)	Fiji (G)	SMS
13	Fiji		Fiji	Blue Water Metals (Aus)/ Subsidiary of Neptune	2012–2014 (EL)	Fiji (G)	SMS
14	Fiji		Fiji	KIOST	2011– (EL)	Fiji (G)	SMS
15	Vanuatu		Vanuatu	Nautilus Minerals (Ca)	2014– (PL)	Vanuatu (G)	SMS
16	Vanuatu		Vanuatu	Bismarck Mining Corporation/ part of Bluewater Mining	2011–2014 (EL), 2012–2015 (EL)	Vanuatu (G)	SMS
17	F.S. of Micronesia		Micronesia	Neptune Minerals(USA)	?		?
18	Palau		Palau	Neptune Minerals(USA)	?		?
19	New Zealand		Bay of Plenty	Nautilus Minerals (Ca)	2007 (PL)	New Zealand (AP)	SMS
20	New Zealand		Gisborne	Neptune Minerals(USA)	2002 (PL)	New Zealand (AP)	SMS
21	Portugal		Azores	Nautilus Minerals (Ca)	2012 (EL)	Portugal (AP)	SMS
22	Italy		Tyrrhenian Sea	Neptune Minerals (USA)	2007 (EL)	Italy (AP)	SMS
23	Norway		Mid-Atlantic ridge	Nordic Ocean Resources(NORA)/Subsidy of Nordic Mining ASA and Ocean Miners AS			SMS
24	Commonwealth of the Northern Mariana Islands				2006 (EL)	Northern Mariana Islands Gov. (AP)	SMS

PL prospecting license, *EL* exploration license, *EpL* exploitation license

referred to as "the promotion of just and stable prices remunerative to producers and fair to consumers … (Article 150)." On the other hand, environmental protection is mentioned as follows: "Necessary measures shall be taken in accordance with this Convention with respect to activities in the Area to ensure effective protection for the marine environment from harmful effects which may arise from such activities (Article 145)." Similarly, in the ISA's Mining Code, while specific commercial values were estimated based on physiochemical investigations (Appendix II, no. 18), comments on the environment only amount to "… to ensure effective protection for the marine environment from harmful effects which may arise from activities in the Area… (Mining Code 31)." As the aforementioned suggests, there is ambiguity in regard to what needs to be done for environmental impact assessments.

To specify goals of environmental assessment, clarification of end points[1] and the establishment of methods are necessary. However, there are no general standards for setting the end points for "environmental impacts." This is in contrast to the case of human health risk assessment,[2] for which the cancerous criteria have been established. This issue indicates the difficulty in specifying the goals of environmental policies on the global and national levels.

In order to make assessments without clear end points, assumptions, preconditions, and reinterpretations need to be made. For example, when a water quality standard for zinc was set, as per the advice from the OECD in 2002 (OECD 2002), for protection of Japanese fresh waters, the goal of "protecting natural environments" was interpreted as "prevention of species extinction" based on some assumptions. Moreover, since it is difficult to study all species when setting the standards, the toxicity test results for specific species (fresh water species of *Salvelinus leucomaenis* and aquatic insect *Epeorus latifolium*) were used as representative examples. The water quality standard thus established for zinc is 3 mg/L.

The more the assumptions, preconditions, and reinterpretations are made, the more discrepancy arises between the original and actual policy goals. However, despite regulations and conditions, environmental policies cannot be free from specifications. Therefore, in actual investigations, the effect of the development on the biological groups in the target areas is evaluated based on population, number of species, rare species, endemic species, typical species, dominant species, and keystone species. However, this is the case for environmental impact assessments in coastal areas, and the results of applying such standards to the deep seas are quite limited.

[1] End point: Nakanishi (1995) described end points as "consequences to be avoided at all costs" (Nakanishi 1995). Sharing the end points can lead to common measures in regard to various risks. In human health, for example, if the end point is the death caused by a certain action, it is possible to compare risks based on their death score (=loss of life expectancy). Today, however, the definition of end points for protection of natural environments has not been generalized. Nakanishi proposed end points to be the extinction of a species, but this has not been generalized.

[2] Human health risk assessment: In the water quality guidelines for drinking water, the WHO sets the lifetime carcinogenic rate to be less than 10^{-5}. In Japan, the value of 10^{-5} is set to be the lifetime risk level for air and water.

16.4 Lack of Human Resources in Taxonomy and Identification for Indexing the Impacts (Issues with Indexing)

One of the reasons for which the use of biological indicators of coastal areas for environmental impact assessments for the deep seas is limited is the lack of human resources in taxonomy and identification of deep-sea organisms, which are the basis of indexing. Advancement in indexing thus requires either filling the deficiency in human resources or establishing other indicators. Therefore, this chapter outlines the situation involving the development of human resources for the taxonomy and identification of organisms. Here taxonomy refers to morphological taxonomy, in which organisms are classified based on their gross morphologies.

16.4.1 Taxonomy and Identification

Taxonomy is the study of naming and sorting a variety of species and organizing them into theoretical frameworks. The researchers in this field are called taxonomist. Identification involves determining the species of organisms based on taxonomic knowledge, and technicians who apply identification to the field of environmental assessment are referred to as identification technicians. Though similar, taxonomy and identification have differences. In general, taxonomists' research subjects are specific taxa or taxonomic characters, whereas identification technicians handle a variety of taxa. In many companies that carry out environmental assessments for overall aquatic life, the responsibility is divided into, for example, marine and freshwater organisms, or planktonic and benthic organisms. There are also cases in which benthos is divided into megabenthos, macrobenthos, and meiobenthos, or the responsibility for fish eggs and larva is separated from that for plankton. In either case, all organisms in the aforementioned biological groups are the subjects, and the number of species to be handled is by no means small. For example, it is normal to identify more than 200 species from one sample of sessile organisms (classified as benthos) from enclosed bays.

Even if the sample condition is not satisfactory, or the specimen is damaged, identification technicians need to find observable parts and reflect these in the analysis results. It is a specialized skill of identification technicians to make comprehensive judgments, even with insufficient taxonomic characters, based on other characters (needless to say, samples might be "unidentifiable" if they are in poor condition).

Since identified data can be compared to past or future results, the taxonomic precision needs to be of an equivalent level.[3] The ability to make lists of the organisms

[3] For example, if in a certain year A and B are classified as two separate species but classified as one species in the following year, the numbers of biological groups discovered becomes different. This could happen if the taxonomic system changes. Identification technicians would have to explain and handle such changes.

present while adjusting the taxonomic precision for comparison purposes might not be part of the taxonomy, but it is a common method used in ecological study, which examines changes over time.

Since identification done by environmental assessment companies is an economic activity, efficiency is also required. In other words, it is difficult to spend an excessive amount of time on one sample, and there exists know-how in regard to efficient works.

16.4.2 Development of Human Resources

One of the possible reasons for the difficulty in developing taxonomists is that the allocation of research budgets is limited due to the fact that it does not directly lead to profit, and the investment result is not obvious. Other explanations include the long time required for human development due to the large dependence on experience. In other words, both taxonomists and identification technicians must go through the processes of not only surveying the literature but also observing target organisms with their own eyes as well as through microscopes. It is no exaggeration to say that the latter processes are of higher importance. These processes cultivate the ability to observe target organisms as well as the "intuition" for detecting different and common features within a species, which cannot be obtained from manuals. The development of taxonomists and identification technicians will likely follow experience-based approaches. It is no easy task to develop fully qualified taxonomists in a short time. In the long run, this fact suggests that large costs are needed for the development of human resources.

To provide an example of the difficult situation in regard to taxonomy, an organism called *kinorhyncha* is one of the meiofauna widely distributed from shallow to deep seas, and its abundance is sometimes reported to be comparable to that of nematoda and harpacticoida (Shirayama 2000). This organism was once considered to be a potential pollution index species due to its early disappearance from poor-oxygen environments (Murakami 2005). Today, about 150 of its species are said to exist in the world, and eight of these are in Japan. However, in each case, the sampling sites for type specimen are limited to locations near specific research facilities. For example, many reports come from the US east coast, where the Smithsonian Institution is located, and near the Mediterranean. The localization is more prominent in Japan, where the type specimens for five of the species are produced in Wakayama prefecture, home to the Seto Marine Biological Laboratory at Kyoto University. The strong correlation between the sampling sites of type specimen and the locations of research facilities indicate that the study of *kinorhyncha* is limited to specific researchers. To extend the argument, an increase in the number of kinorhyncha researchers should lead to significant changes in the reported species richness and areas of distribution. This is one of the examples that symbolizes the current situation and challenges in taxonomy.

16.4.3 Issues Related to the Lack of Human Resources in Taxonomy and Identification

Due to the lack of human resources in deep-sea taxonomy and identification, it is difficult to evaluate the environmental impact of deep-sea mining. If the environmental protection agencies do not resolve this issue, inexperienced taxonomists may be involved in environmental impact assessment projects. This can, in turn, lead to a spread of incorrect data and to inconsistency between the data before and after developments, confusing the environmental evaluation itself. In cases of ABNJ, it is unfair that certain countries fill in the gap with hasty human resource development while other countries and companies make efforts under the ISA's instructions. For this reason, the subject interested countries must continue their efforts to maintain data accuracy to avoid such a situation. Furthermore, the ISA should provide rigorous supervision. In reality, however, while it is possible to cast doubt in regard to the precision of data, it is difficult to come to the conclusion that mistakes were made, except in extreme cases. Cross-checking is sometimes practiced for environmental assessments for land and shallow water areas, for which there is abundant data; however, there is not enough data accumulated for deep seas to make cross-checking possible. To stress the point, standardization of taxonomy and identification techniques needs to be established in order to ensure correct environmental impact assessments. The next section discusses the potential of the molecular biological approach, which has attracted attention as a new technology.

16.5 Molecular Biological Approach in Environmental Impact Assessment

Owing to the advances in molecular biology, differences in the genetic level have come to be applied in a part of environmental impact assessments. In the field of deep-sea mineral resource development, too, there are movements for introducing the new technology, such as the mentions of the molecular biological approach in the ISA's recommendation (ISA 2013b) and guidance on the technology in workshops for taxonomy and identification (Dahlgren 2014). Currently, this technology is mainly used as an impact assessment method for prokaryotes, but its application to relatively large organisms is expected depending on advancements in the technology.

The advantages of using a molecular biological technique, as compared with the conventional classification and identification methods, are as follows: it has relatively low dependence on the analyst's experience, objective data acquisition can be expected, and its standardization can be promoted with relative ease. In addition, DNA information allows for the identification of samples at an early stage of development (larva and immature specimen) and of damaged samples. Even though the name of the species is unknown, the nucleotide sequence can be recorded and later compared to the database for identification. This is why ISA has requested the contracting

parties to submit the collected nucleotide sequences to the database (ISA's recommendation, Annex I. 40 (ISA 2013b)).

The following sections outline the molecular biological approach in three parts: (1) application to species identification, (2) metagenomic analysis, and (3) metatranscriptomic analysis. However, it is not an aim of this chapter to describe the technological details, so the discussions will be confined to the outline of each topic.

16.5.1 Application to Species Identification

For species identification, it is a general practice to use ribosomal RNA (rRNA) gene sequences, and such rRNA genes include prokaryotes' 16S rRNA gene sequence and eukaryotes' 18S rRNA gene sequence. In rRNA gene sequences, conserved regions exist that are common to many organisms, and variable regions exist that are unique to each species (Fig. 16.2) (Neefs et al. 1993). Species identification using rRNA gene sequence is performed as follows: (1) the target region sequence is amplified using the rRNA gene sequence of conserved regions as the primer[4] (Hadziavdic et al. 2014) for PCR,[5] (2) the obtained PCR amplicon DNA fragments are analyzed by a DNA sequencer, and (3) the determined sequence is used to identify species with similar sequences in the DNA database (Fig. 16.3).

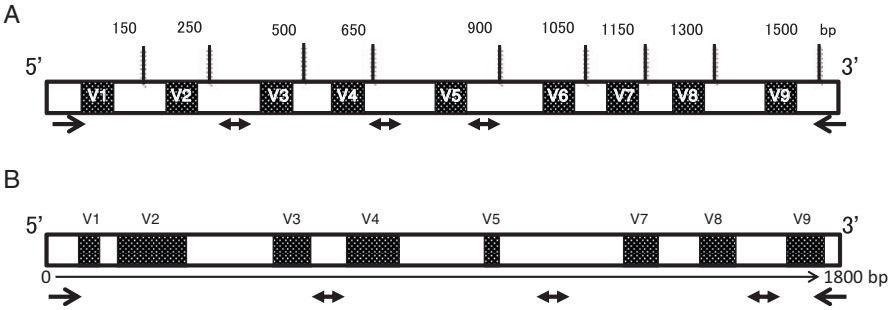

Fig. 16.2 The schematic diagram of the variable region and conserved region in the small subunit (SSU) rRNA gene sequence. (**A**) Prokaryotes SSU rRNA; (**B**) Eukaryotes SSU rRNA. V1–V9 are variable regions. In Eukaryotic SSU rRNA gene sequence, the V6 region which is corresponding to the prokaryotic SSU rRNAs is more conserved (Neefs et al. 1993). *Arrows* mean example of universal primer position for PCR amplification

[4] Primers are DNA fragments on both sides of the target gene nucleotide sequence region to be amplified by PCR.

[5] PCR stands for polymerase chain reaction, which is a method for multiplying a DNA fragment of the nucleotide sequences of interest by some hundreds of thousand times by repeating DNA synthesis reaction of template DNA, DNA polymerase, and two primers, which are short DNA fragments. This method is called the PCR method.

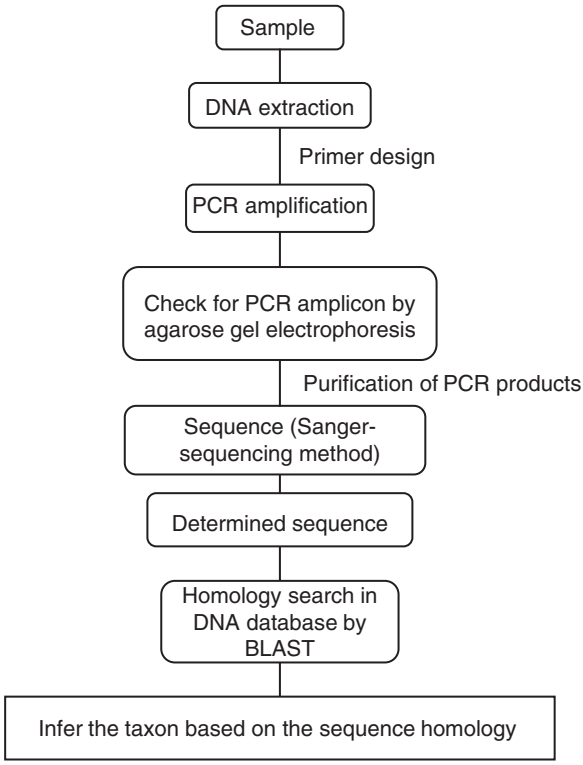

Fig. 16.3 Procedure for DNA sequence analysis for species identification

This technology replaces microscopic observations with molecular biological methods but gives the same resulting information for the species. This method can also be applied to indexing for coastal regions. On the other hand, repeating microscopic observation for all the organisms present in a sample would require a tremendous amount of manual work, time, and cost. Moreover, estimation of taxa based on the nucleotide sequence requires a record of that sequence in the database. Though the nucleotide sequence database[6] is improving, there are differences in the number of sequences registered for certain taxa, and as such, the database is still incomplete (Table 16.3).

[6] There are three public DNA databases in the world (The DNA data bank of Japan (DDBJ; http://www.ddbj.nig.ac.jp/), the NIH genetic sequence database (GenBank; http://www.ncbi.nlm.nih.gov/genbank/), and the European Molecular Biology Laboratory (EMBL; http://www.ebi.ac.uk/)). These institutes form a collaboration known as the Nucleotide Sequence Database Collaboration (INSDC) and share their data. Registered information is updated daily, and the registration numbers of whole genome sequences and a large number of sequences derived from such as metagenomic analysis have been increasing in recent years.

Table 16.3 Number of registered nucleotide sequences for each taxon in the NCBI database

Taxonomic hierarchy	Taxon	Number of sequence[a]
Phylum	Loricifera	5
Phylum	Nematoda	1,956,229
Phylum	Foraminifera	35,113
Phylum	Tardigrada	20,153
Subclass	Copepoda	765,549
Ordar	Harpacticoida	76,476

[a]As of 13 Nov 2015

16.5.2 Metagenomic Analysis

Cloning and DGGE[7] are methods for estimating the biota by extracting DNA from all organisms present in the sample (as mixed DNA of each organism) and comprehensively analyzing the nucleotide sequences. However, due to their complicated procedure, high cost, and low detection limit, they have mainly been used for understanding the dominant species in a sample (Fig. 16.4). However, the recent spread of next generation sequencers, which can analyze hundreds of millions of units of base sequence at a time, has enabled high-resolution analysis of biological communities (Pawlowski et al. 2014). Analytical methods using next generation sequencers include an amplicon sequence,[8] which analyzes the PCR amplicon of a specific gene sequence, and a shotgun sequence, which directly analyzes extracted DNA without PCR. The merit of an amplicon sequence is that it can analyze samples with low DNA concentration through PCR amplification. On the other hand, the technological challenge presented by this method[9] is the difficulty of designing a universal primer for one-step PCR amplification from biological communities with multiple taxa, especially for eukaryotes, which have introns[10] in their base sequences.

[7] DGGE stands for denaturing gradient gel electrophoresis, which is a method for separating amplified (by PCR) sequences such as 16S rRNA gene sequence from a mixed extraction DNA in an environment and analyzing them. Muyzer et al. introduced a case of analysis on bacteria (Muyzer et al. 1993). By changing the target genes, this method can be applied to fungi and nematoda (Möhlenhoff et al. 2001; Waite et al. 2003).

[8] In analyses using next generation sequencers, the analysis method using PCR amplicons is called an amplicon sequence to distinguish it from methods without PCR.

[9] When using PCR with primers designed from conserved regions for 16S rRNA gene sequence, amplicons produced are sometimes longer than expected if the PCR target regions contain organisms with introns. For example, an 16S rRNA gene sequence of foraminifera contains many introns, and this should be taken into consideration when treating them as meiofauna and applying amplicon sequence analysis in the presence of nematoda and harpacticoida.

[10] Introns are the parts of a DNA sequence that are not transcribed into an amino acid sequence. Splicing is a process for eliminating introns during transcription. In contrast, regions of nucleotide sequences that are translated to amino acids are called exons. Though introns are often found in eukaryotes, they are also found in prokaryotes and viruses (Belfort et al. 1995; Berget et al. 1977).

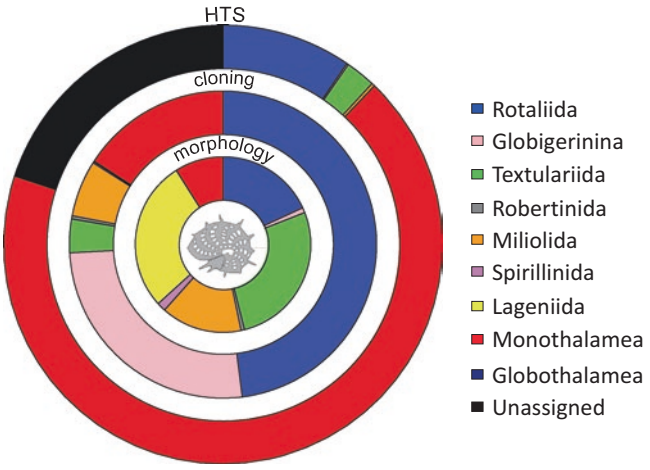

Fig. 16.4 Comparison of the relative proportions of the major foraminiferal taxa found using morphospecies number (*inner circle*), cloning and Sanger-sequencing (*middle circle*), and high-throughput sequencing (*outer circle*). The morphospecies counts are based on the foraminiferal entries to the World Register of MarineSpecies (WoRMS) database. The Sanger data are based on single-cell sequences available in the GenBank and their own database. The HTS data correspond to a concatenation of 8 Illumina sequencing runs gathering 26,135,707 sequences. (After Pawlowski et al. 2014)

Considering the bias induced by PCR, a shotgun sequence can produce results that better reflect the actual biota of the sample.[11]

Both techniques can analyze biological diversity based on rRNA gene sequences or analyze metabolic systems based on functional genes such as enzymes, which are used to estimate metabolism in an ecosystem, although the estimation of relation to the original species and functional genes is difficult.[12]

To infer the taxon based on the nucleotide sequence, a homology search is performed for DNA sequences registered in the database. The sequences with a certain homology are defined as members of the same biological group (species) for convenience, and the diversity evaluation of a sample is conducted by using such groups as operational taxonomic units (OTU). In general, it can be regarded as the same OTU by 97% or more homology value of SSU rRNA gene sequences (Ong et al. 2013; Creer et al. 2010).[13]

[11] A shotgun sequence with a next generation sequencer can produce large amounts of nucleotide sequence, but the ribosomal RNA gene, mainly used for estimating biota, makes up a small portion (less than 1% of an entire sequence) (Kawai et al. 2014; Shi et al. 2011). For this reason, shotgun sequencing for the analysis of biological diversity requires a large number of handled sequences.

[12] If the genome information of the species is registered in a database, the origin of functional genes can be estimated.

[13] This definition is for convenience, and it is possible that a 97% homology of a 16S rRNA gene sequence does not conclude the identity of the two species. In such cases, species richness in an environment might be underestimated.

The results from metagenomic analysis can provide insights on the biodiversity analysis by OTU and metabolic system by functional genes, which could be used as new indicators to the field. Yet, challenges remain in understanding what the changes in such indicators signify and in comparing the magnitudes of other human-induced impacts and effects.

16.5.3 Metatranscriptomic Analysis

DNA is more difficult to degrade than RNA. For this reason, metagenomic analysis with DNA may also detect nucleotide sequences of remains and residues of organisms. Moreover, although metagenomic analysis can comprehensively obtain genetic information, it cannot tell whether those genes are functioning. On the other hand, metatranscriptomic analysis, which handles messenger RNA (mRNA), the primary transcriptome transcribed from DNA, can detect actual functional genes in an environment (or in cells). For example, there exists a study that detected functional genes related to the metabolic pathways such as photosynthesis, carbon fixation, and nitrogen uptake based on metatranscriptomic analysis of microbial community in the northern Pacific surface seawater (Frias-Lopez et al. 2008). In an environmental impact assessment of deep-sea mineral resource developments such as SMS, if it is made possible to measure the expression amounts of genes related to sulfate reduction and sulfur oxidization, this could be applied to understanding temporal changes in the ecosystem of the target mining area or the habitat distribution. Moreover, as introns and exons (see Footnote 10) coexist in the DNA of eukaryotes, estimation of introns is possible by comparing the RNA and DNA. Expression analysis can also be performed by introducing the obtained sequences in other organisms, which can efficiently search for new functional genes. Analysis of rRNA in extracted RNA can produce information of gene sequences of 16S rRNA and 16S rRNA, which can reveal biological groups present in the environment.

As mentioned above, by performing the analysis using the RNA, it is possible to know the dynamic change in the active biota and material cycle in the ecosystem, and also to obtain more detailed environmental data.

However, RNA, especially mRNA, is unstable and has a short half-life (Selinger et al. 2003), and its amount is a few percent smaller than that of rRNA (Stewart et al. 2010).[14] This poses many technological challenges. Particularly for sample collection from deep seabed, challenges include methods of sampling and preservation.

Simultaneous use of metagenomic and metatranscriptomic analyses could enable not only the study of biological diversity and functional genes but also the introduction of indicators for environmental impact assessments on the genetic level based on the functions of an ecosystem.

[14] Experiments with mouse cultivation cells reported that mRNA, compared to rRNA, is about 1–2% (Johnson et al. 1977).

16.6 Conclusion

In order to effectively carry out the environmental impact assessment of any human activity, it is important to create an index of all living species of organisms in an area which could be used as the reference for comparison after the activity. For this, identification technicians as well as taxonomists are required. Whereas, the main task of identification technicians is matching organisms with existing taxonomic records, the basic information for this is provided by the taxonomists. There is particularly insufficient knowledge of deep-sea organisms, so the dependence on taxonomists for their specialty in recoding species is high. Thus, in the near future, when deep-sea mineral resource development will begin, there will be an increasing demand for taxonomists and identification technicians who can handle deep-sea organisms. However, the development of taxonomists takes time and is a costly endeavor. This problem is even more serious in developing countries, which might have difficulty in independently participating in the development of deep-sea mineral resources.

In order to develop indicators similar to those used for coastal areas, such as species present, dominant species, rare species, population, typical species and keystone species for deep seas, of which there is insufficient data available, one must invest time and funds on developing taxonomists and identification technicians. In this case, there are two important considerations. One is a time required for human resource development vis-a-vis seabed mineral resources development. Whereas, seabed mining is expected to be initiated in the near future, human resource development for training of identification technicians also requires time. Another issue is of equal opportunity between developed and developing countries. The former can afford to develop human resource for the purpose of taxonomic identification; it could be relatively difficult for the latter. Consequently, given the fact that few taxonomists and identification technicians are available, divergence from the conventional evaluation techniques should be considered, and technologies based on the molecular biological approach should be adopted despite the associated technological challenges.

Acknowledgement This study was conducted as a part of next-generation technology for ocean resources exploration, which is one of cross-ministerial strategic innovation promotion program (SIP), organized by Cabinet Office, Government of Japanese. Authors would like to express our gratitude to members of “Research and Development Center for Submarine Resources” of “Japan Agency for Marine-Earth Science and Technology (JAMSTEC)” for their valuable advice.

References

Belfort M, Reaban ME, Coetzee T et al (1995) Prokaryotic introns and inteins: a panoply of form and function. J Bacteriol 177:3897–3903

Berget SM, Moore C, Sharp PA (1977) Spliced segments at the 5′ terminus of adenovirus 2 late mRNA* (adenovirus 2 mRNA processing/5′ tails on mRNAs/electron microscopy of mRNA-DNA hybrids). Proc Natl Acad Sci U S A 74:3171–3175

Blue Mining (2015) Welcome to the Blue Mining project. http://www.bluemining.eu/. Accessed 5 Oct 2015

Creer S, Fonseca VG, Porazinska DL et al (2010) Ultrasequencing of the meiofaunal biosphere: practice, pitfalls and promises. Mol Ecol 19(Suppl. 1):4–20

Dahlgren T (2014) Advances in molecular methodologies and the application and Interpretation of molecular methodologies for macrofauna classification—their relevance to environment assessment and monitoring. International Seabed Authority. https://www.isa.org.jm/files/documents/EN/Workshops/2014b/Abs/Dahlgren.pdf. Accessed 13 Nov 2015

Diamond Fields (2015) Projects Atlantis II. http://www.diamondfields.com/s/AtlantisII.asp. Accessed 5 Oct 2015

DORD (2015) Our business. http://www.dord.co.jp/english/business/index.html. Accessed 5 Oct 2015

DOSI (2015) Home. http://dosi-project.org/. Accessed 5 Oct 2015

Frias-Lopez J, Shi Y, Tyson GW et al (2008) Microbial community gene expression in ocean surface waters. Proc Natl Acad Sci U S A 105:3805–3810

Hadziavdic K, Lekang K, Lanzen A et al (2014) Characterization of the 16S rRNA gene for designing universal eukaryote specific primers. PLoS One 9(2):e87624. doi:10.1371/journal.pone.0087624

INDEEP (2015) Welcome to INDEEP. http://www.indeep-project.org/. Accessed 5 Oct 2015

International Seabed Authority (2010) Regulations on prospecting and exploration for polymetallic sulphides in the area. https://www.isa.org.jm/sites/default/files/files/documents/isba-16a-12rev1_0.pdf. Accessed 5 Oct 2015

International Seabed Authority (2012) Regulations on prospecting and exploration for cobalt-rich ferromanganese crusts in the area. https://www.isa.org.jm/sites/default/files/files/documents/isba-16a-11_0.pdf. Accessed 5 Oct 2015

International Seabed Authority (2013a) Regulations on prospecting and exploration for polymetallic nodules in the area. https://www.isa.org.jm/sites/default/files/files/documents/isba-19c-17_0.pdf. Accessed 5 Oct 2015

International Seabed Authority (2013b) Recommendations for the guidance of contractors for the assessment of the possible environmental impacts arising from exploration for marine minerals in the area. https://www.isa.org.jm/sites/default/files/files/documents/isba-19ltc-8_0.pdf. Accessed 11 Nov 2015

International Seabed Authority (2014) Deep seabed minerals contractors. https://www.isa.org.jm/contractors/exploration-areas. Accessed 5 Oct 2015

International Seabed Authority (2015) International Seabed Authority. https://www.isa.org.jm/. Accessed 5 Oct 2015

JOGMEC (2015) News releases. http://www.jogmec.go.jp/english/news/release/news_10_000014.html. Accessed 5 Oct 2015

Johnson LF, Abelson HT, Penman S et al (1977) The relative amounts of the cytoplasmic RNA species in normal, transformed and senescent cultured cell lines. J Cell Physiol 90:465–470

JPI Oceans (2015) About. http://www.jpi-oceans.eu/. Accessed 5 Oct 2015

Kawai M, Futagami T, Toyoda A et al (2014) High frequency of phylogenetically diverse reductive dehalogenase-homologous genes in deep subsea floor sedimentary metagenomes. Front Microbiol 5:80. doi:10.3389/fmicb.2014.00080

Korea Institute of Ocean Science & Technology (KIOST) (2012) http://eng.kiost.ac/kordi_eng/main.jsp?sub_num=354&state=view&idx=161&ord=0. Accessed 5 Oct 2015

MIDAS (2012) Welcome to MIDAS. http://www.eu-midas.net/. Accessed 5 Oct 2015

Möhlenhoff P, Müller L, Gorbushina AA et al (2001) Molecular approach to the characterisation of fungal communities: methods for DNA extraction, PCR amplication and DGGE analysis of painted art objects. FEMS Microbiol Lett 195:169–173

Murakami C (2005) A brief review of general biology of Kinorhyncha, with proposed new standard Japanese names for the species from Japan. Taxa Proc Jpn Soc Syst Zool 19:34–41 (in Japanese)

Muyzer G, de Waal EC, Uitierlinden AG (1993) Profiling of complex microbial populations by denaturing gradient gel electrophoresis analysis of polymerase chain reaction-amplified genes coding for 16S rRNA. Appl Environ Microbiol 59:695–700

Nakanishi J (1995) Environmental risk theory. Iwanami Shoten Publisher, Tokyo (in Japanese)
Narita T, Oshika J, Okamoto N et al (2015) Summary of environmental impact assessment for mining seafloor massive sulfides in Japan. J Shipping Ocean Eng 5:103–114
Neefs J-M, Van de Peer Y, De Rijk P et al (1993) Compilation of small ribosomal subunit RNA structures. Nucleic Acids Res 21:3025–3049
Neptune Minerals (2015) Our business. http://www.neptuneminerals.com/our-business/tenements/. Accessed 5 Oct 2015
OECD (2002) Environmental performance reviews Japan. Conclusions and recommendations, OECD, 12p
Ong SH, Kukkillaya VU, Wilm A et al (2013) Species identification and profiling of complex microbial communities using shotgun illumina sequencing of 16S rRNA amplicon sequences. PLoS One 8(4):e60811. doi:10.1371/journal.pone.0060811
Pawlowski J, Lejzerowicz F, Esling P (2014) Next-generation environmental diversity surveys of foraminifera: preparing the future. Biol Bull 227:93–106
Seabed Minerals Authority (2005) Exploration the deep for minerals. Newsletter 1, issue Apr 2015
Selinger DW, Saxena RM, Cheung KJ et al (2003) Global RNA half-life analysis in *Escherichia coli* reveals positional patterns of transcript degradation. Genome Res 13:216–223
Shi Y, Tyson GW, Eppley JM et al (2011) Integrated metatranscriptomic and metagenomics analyses of stratified microbial assemblages in the open ocean. ISME J 5:999–1013
Shirayama Y (2000) Phylum Kinorhyncha. In: Shirayama Y (ed) Diversity and evolution of invertebrates. Shokabo, Tokyo, pp 148–150 (in Japanese)
SIP (2015) https://www.jamstec.go.jp/sip/ (in Japanese). Accessed 5 Oct 2015
Stewart FJ, Ottesen EA, DeLong EF (2010) Development and quantitative analyses of a universal rRNA-subtraction protocol for microbial metatranscriptomics. ISME J 4:896–907
The Guardian (2012) Papua New Guinea's seabed to be mined for gold and copper. http://www.theguardian.com/environment/2012/aug/06/papua-new-guinea-deep-sea-mining. Accessed 5 Oct 2015
Waite IS, O'Donnell AG, Harrison A et al (2003) Design and evaluation of nematode 16S rDNA primers for PCR and denaturing gradient gel electrophoresis (DGGE) of soil community DNA. Soil Biol Biochem 35:1165–1173

Dr. Tomohiko Fukushima is working for Research and Development (R&D) Center of Submarine Resources, Japan Agency for Marine-Earth Science and Technology (JAMSTEC). He graduated from the Faculty of Fisheries, Tokyo University of Fisheries in 1984 (bachelor degree) and obtained post-graduate degree from Faculty of Fisheries, Tokyo University of Fisheries in 1986 (master degree). In 2004, he obtained Doctor of Science Degree from Kyoto University. The title of doctoral thesis is "Ecological Characteristics of Deep-Sea Benthic Organisms in Relation to Manganese Nodules Development Practices." After being awarded the doctoral degree, he continued his research activities in the Ocean Policy Research Foundation (as Research Fellow), The University of Tokyo (as Associate Professor), and then joined JAMSTEC.

Dr. Miyuki Nishijima is a microbiologist belonging to the Ecosystem Observation and Evaluation Methodology Research Unit, Project Team for Development of New-generation Research Protocol for Submarine Resources, in Japan Agency for Marine-Earth Science and Technology (JAMSTEC). She graduated from **Agricultural Science** Department, **Graduate School of Agriculture**, Tokyo University of Agriculture in 1987. She worked at Marine Biotechnology Institute in 1990–2002. From 2002, she jointed Techno Suruga Laboratory Co., Ltd. She is in charge of microbial diversity in the deep-sea sediment. She has been on loan to JAMSTEC since 2015.

Chapter 17
Development of Environmental Management Plan for Deep-Sea Mining

Rahul Sharma

Abstract Deep-sea mining is currently at a stage when several mine sites have been identified, mining technologies are under development, processing technologies are being tested, studies for assessing potential environmental impacts have been conducted by different contractors, and guidelines for monitoring the impacts have been issued by the International Seabed Authority. At this stage, it is essential to review the information acquired so far in relation to environmental impacts so as to enable development of an environmental management plan for deep-sea mining which will include analyses of the background resource and environmental data, prediction of potential environmental impacts of commercial mining, identification of mitigation measures, and ensure compliance with regulatory authority's stipulations.

17.1 Introduction

Deep-sea mining has generated significant interest around the world for over five decades, due to the potential of deep-sea minerals such as polymetallic nodules, ferromanganese crusts, and hydrothermal sulphides that occur on the deep seafloor and are considered as alternative source of strategic metals as the terrestrial reserves of some of these metals (e.g. Cu, Ni, Co) are depleting fast (Table 17.1). This chapter looks at the information available on potential impacts, mitigation measures, and regulations and suggests an outline for developing an environmental management plan for deep-sea mining.

R. Sharma (✉)
CSIR-National Institute of Oceanography, Council of Scientific and Industrial Research, Dona Paula, Goa 403004, India
e-mail: rsharma@nio.org; rsharmagoa@gmail.com

R. Sharma (ed.), *Deep-Sea Mining*, DOI 10.1007/978-3-319-52557-0_17

Table 17.1 Uses and status of selected metals found in deep-sea minerals

Metal	Uses[a]	World reserves on land[b]
Nickel	Making steel (46%), nonferrous alloys and superalloys (34%); electroplating (11%), coins, ceramics, batteries, hard discs	71 million tonnes
Cobalt	Alloys, magnets, batteries, catalysts, pigments and coloring, radio-isotopes, electroplating	6.6 million tonnes (52% in Congo)
Copper	Electrical, telecom and electronic applications such as generators, transformers, motors, PCs, TVs, mobile phones (65%), automobile (7%), anti-bacterial agent, and consumer products (coins, musical instruments, cookware)	140 million tonnes (low grade)
Manganese	Steel production (>85% of ore used for this), corrosion-resistant alloys (cans), additive in unleaded gasoline, paint, dry cell and alkaline batteries, pigments, ceramic and glass industry	540 million tonnes (metal)
Iron	Pig iron/sponge iron/steel (>90%), alloys, automobiles, ships, trains, machines, buildings, glass	160 billion tonnes (ore) and 77 billion tonnes (metal)

[a]www.wikipedia.com
[b]IBM (2010)

17.2 Potential Environmental Effects of Deep-Sea Mining

The probable causes for environmental impact from deep-sea mining could be broadly attributed to:

1. Quantity of substrate mined, methods of separation, and mechanism of discharge of effluents
2. Suspension of solids due to movement of the miner, crusher, lift mechanism, and discharge
3. Sub-system losses such as pipes, chains, tools, or any other hardware
4. Oil spills and leakages from mining and transport vessels
5. Ballast water discharge from transport vessels
6. At-sea processing waste including chemicals, debris, water
7. Human waste such as garbage including plastics, metals, glass, and other non-biodegradable items

The impact of deep-sea mining is expected to be at various levels in the water column that includes generation of plume at the seafloor, turbidity in the water column, and addition of bottom sediments to the surface waters resulting in change in the marine ecosystem (Fig. 17.1), as well as on land owing to collection, separation, lifting, transportation, processing, and discharge of effluents (Fig. 17.2). According to an estimate, for the cut off nodule abundance of 5 kg/m^2, an area of 300–600 km^2 will be disturbed every year for mining of 1.5–3 million metric tonnes of nodules per year (Sharma 2011), and with every tonne of manganese nodules mined from seabed, 2.5–5.5 tonnes of sediment will be resuspended (Amos and Roels 1977).

A summary of the probable impacts at various levels in the water column has been given in the following section (ISA 1999):

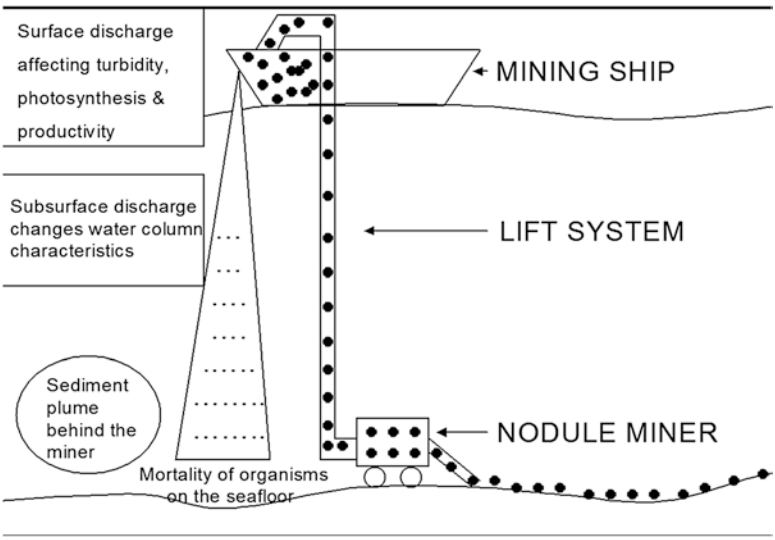

Fig. 17.1 Schematic for environmental impact of deep-sea mining

Activity	Seafloor	Water Column	Surface	Land
Collection				
Separation				
Lifting				
Washing				
At-sea processing				
Transport				
Extraction				
Tailing discharge				

Fig. 17.2 Areas likely to be affected due to different activities of deep-sea mining

17.2.1 Potential Seafloor Impacts

It is anticipated that the primary benthic impacts caused by mining will be (Fig. 17.3):

- Direct impacts along the track of the nodule collector, where the sediments and associated fauna will be crushed or dispersed in a plume and the nodules removed;

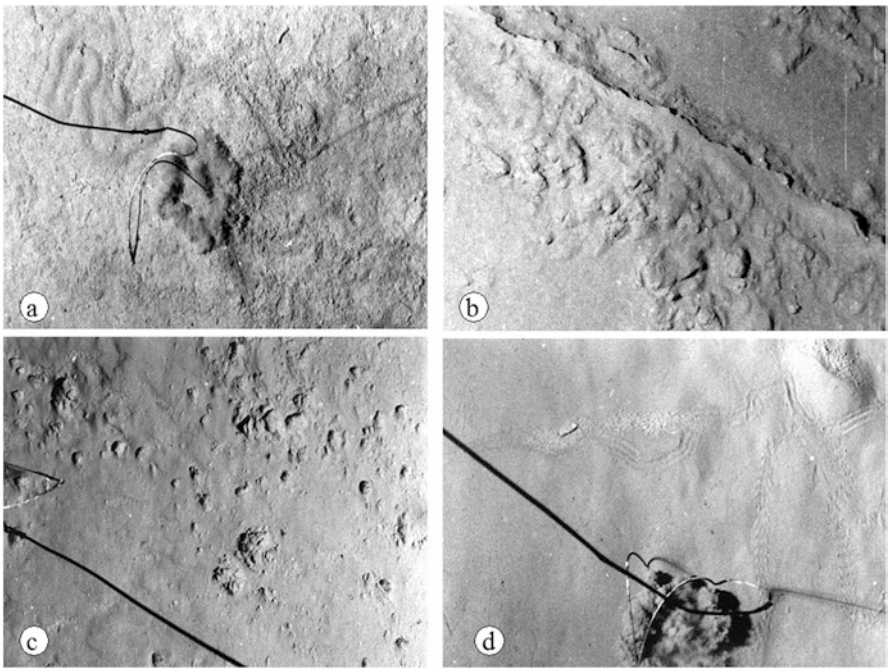

Fig. 17.3 (**a**) Seafloor with animal tracks before the disturbance, (**b**) 'disturber' track on the seafloor, (**c**) sediment lumps close to the disturber track, (**d**) resedimented surface after disturbance experiment

- Smothering or entombment of the benthic fauna away from the site of nodule removal, where the sediment plume settles; and
- Clogging of suspension feeders and dilution of deposit-feeders food resources.

17.2.2 Potential Water-Column Impacts

Discharge of tailings and effluent below the oxygen-minimum zone may cause some environmental harm to the pelagic fauna, such as:

- Mortality of zooplankton species at mid-water depths or that migrate to these depths
- Effects on meso-and bathypelagic fishes and other nekton caused directly by the sediment plume or associated metallic species or indirectly through impact on their prey
- Impacts on deep-diving marine mammals
- Impacts on bacterioplankton through addition of fine sediment in meso- and bathypelagic zones
- Depletion of oxygen by bacterial growth on suspended particles
- Effects on fish behaviour and mortality caused by the sediments or trace metals
- Mortality of and changes in zooplankton species composition caused by discharges

- Dissolution of heavy metals (e.g. copper and lead) within the oxygen-minimum zone and their potential incorporation into the food chain
- The possible clogging of zooplankton by filtering particles in the plume.

17.2.3 Potential Upper-Water Column Impacts

If tailings consisting of sediment and effluent are discharged in near-surface waters (and above the thermocline), then there are additional impacts to those listed above, as follows:

- The potential for trace-metal bioaccumulation in surface waters due to discharges from the test mining
- Reduction in primary productivity due to shading of phytoplankton by the surface discharge
- Effects on phytoplankton from trace metals in the surface discharge
- Effects on behaviour of marine mammals by the mining operation.

17.3 Global Efforts to Understand the Environmental Impacts

Several studies to assess the potential impacts of deep-sea mining have been carried out, most of them in the Pacific Ocean and one in the Indian Ocean. These are briefly described as under:

17.3.1 Deep Ocean Mining Environment Study by OMI and OMA, USA

The **D**eep **O**cean **M**ining **E**nvironment **S**tudy (DOMES, 1972–1981) conducted by National Oceanic and Atmospheric Administration (USA) monitored environmental impacts during two of the pilot scale mining tests conducted by the Ocean Mining Inc. and the Ocean Mining Associates (OMA) in 1978 in the Pacific Ocean. During the study, the concentration of particulates was measured in the discharge and the biological impacts in the surface as well as benthic plumes were assessed (Ozturgut et al. 1980).

17.3.2 Disturbance and Re-colonisation Experiment by Germany

The **DIS**turbance and Re-**COL**onisation (DISCOL) experiment was conducted by the scientists of the Hamburg University, Germany, in the Peru Basin in the Pacific Ocean from 1988 to 1998. Collection of pre-disturbance baseline environmental data was

followed by the disturbance caused by a plough harrow in a circular area of 10.8 km^2 (Foell et al. 1990). Post-disturbance studies were carried out to monitor the impact and recolonisation after 6 months, 3, and 7 years. The results have shown that over a period of time, although certain groups of benthic organisms may show a quantitative recovery, the faunal composition is not the same as the undisturbed one (Schriever et al. 1997).

17.3.3 Benthic Impact Experiment by NOAA, USA

The **B**enthic **I**mpact **E**xperiment (NOAA-BIE) by the National Oceanic and Atmospheric Administration (NOAA, USA) was conducted in the Clarion Clipperton Fracture Zone (CCFZ) of the Pacific Ocean (1991–1993). After baseline studies in a pre-selected area, the Deep-Sea Sediment Resuspension System (DSSRS) (Brockett and Richards 1994) was used for 49 times in an area of 150 × 3000 m. The post-disturbance sampling indicated changes in the faunal distribution in the area (Trueblood 1993) and monitoring observations after 9 months indicated that, whereas some of the meiobenthos showed a decrease in abundance, the macrobenthos showed an increase in their numbers probably due to increased food availability (Trueblood et al. 1997).

17.3.4 Japan Deep-Sea Impact Experiment by MMAJ, Japan

The **J**apan deep-sea impact **E**xperimen**T** (JET, 1994–1997) was conducted by MMAJ (Metal Mining Agency of Japan) in the CCFZ of the Pacific Ocean in 1994 with the DSSRS. Disturbance was created during 19 transects over two parallel tracks of 1600 m length (Fukushima 1995). The impact was assessed from sediment samples, deep-sea camera operations, sediment traps, and current meters and the results show that the abundance of meiobenthos decreased in deposition areas immediately after the experiment and returned to originals levels 2 years later, but the species composition was not the same; whereas the abundance of certain groups of mega and macro-benthos was still lower than the undisturbed area (Shirayama 1999).

17.3.5 Interoceanmetal: Benthic Impact Experiment by East European Consortium

A **B**enthic **I**mpact **E**xperiment was conducted by Interoceanmetal (IOM-BIE) Joint Organisation, in CCFZ in Pacific Ocean in 1995, using DSSRS. In all, 14 tows were carried out on a site of 200 × 2500 m and the impact was observed from deep-sea camera tows and sediment samples (Tkatchenko et al. 1996). The results have shown that whereas no significant change was observed in meiobenthos abundance and community structure in the re-sedimented area, alteration in meiobenthos assemblages within the disturbed zone was observed (Radziejewska 1997).

17.3.6 Indian Deep-Sea Environment Experiment by NIO, India

The **In**dian **D**eep-sea **E**nvironment E**x**periment (INDEX) was conducted by National Institute of Oceanography (CSIR-NIO, Goa, India) in 1997 under the polymetallic nodules program of the Ministry of Earth Sciences in the Central Indian Ocean Basin. The DSSRS was used 26 times in an area of 200 × 3000 m, during which about 6000 m^3 of sediment was resuspended. The post-disturbance impact assessment studies have indicated lateral migration and vertical mixing of sediment leading to changes in physico-chemical conditions (Sharma et al. 2001) and reduction in biomass around the disturbance area (Ingole et al. 2001). Subsequent monitoring of the conditions showed that restoration and recolonisation process had started and the natural variations had taken over in the impacted areas.

17.4 Evaluating the Results of the Benthic Impact Experiments (BIEs)

17.4.1 Mechanism of the Experiments

The DISCOL experiment was conducted from multi-directions, in contrast to the other BIEs, which were conducted in single direction, thereby disturbing an elongated stretch of the seafloor. During the DISCOL, the emphasis was on scraping the seabed, as against the BIEs, which concentrated on sediment re-suspension. Both of these operations, being complimentary to each other in the actual mining scenario, contributed in different ways to study the potential impacts on the seafloor environment.

Whereas the device used in DISCOL (plough harrow) led to mixing up the seafloor sediments due to its ploughing action from different directions, the device used by other BIEs (DSSRS, also called as the 'disturber') not only compacted the sediment along its towing track, but also resuspended and redistributed the sediment to adjacent areas. The outcomes of these studies (other than DOMES) are given n Table 17.2. These experiments not only provided an opportunity for evaluation of baseline seafloor conditions associated with the mineral deposits not well known previously, but also produced results that initiated the understanding of the potential impacts that can now be extrapolated through suitable models.

17.4.2 Scale of the Experiments

A comparison of BIEs to commercial mining (Table 17.3) shows that whereas the operation time of the BIEs lasted for 18–88 h, a large-scale mining operation is expected to continue for about 300 days per year (UNOET 1987). The distance

Table 17.2 Sediment properties and outcomes of different Benthic Impact Experiments

Experiment name	No. of tows	Duration of disturbance (min)	Distance covered (km)	Average speed (km/h)	Water content (%)	Density (g/cm^3)	Sediment content (g/l)	Weight of sediment		Volume of sediment		Depth of excavation (mm)
								Dry (t)	Wet (t)	Recovered (m^3)	Discharged (m^3)	
(a) NOAA-BIE	49	5290	141+	1.6+	73.0+	2.7+	33.30	1500 (1332+)	4888	4000 (4049+)	4328 (6951+)	29+
(b) JET	19	1227	32.7	1.6+	78.5+	2.7+	38.30	355+	1651+	1427+	2495+	44+
(c) IOM-BIE	14	1130	35.0	1.8+	80.0	2.7+	42.10+	360+	1800	1573+	1300	45+
(d) INDEX	26	2534	88.3	2.1+	84.5	2.6+	30.23	580+	3737+	3380+	6015+ (2693+)	38+

Yamazaki and Sharma (2001)

Numbers given in the table with (+) are estimated by authors, the others are taken from

(a) Trueblood (1993), Nakata et al. (1997), and Gloumov et al. (1997)

(b) Fukushima (1995)

(c) Tkatchenko et al. (1996) and Kotlinski (personal communication)

(d) Sharma and Nath (1997), Sharma et al. (1997), and Khadge (1999)

Table 17.3 Scale of benthic impact experiments vis-à-vis commercial mining

Parameter	BIEs data	Commercial mining data
Duration	18–88 h	300 days/year
Distance/area	33–141 km	300–600 km^2/years
Recovery	0.77–1.4 m^3/min	37.5 m^3/min

Yamazaki and Sharma (2001)

(and area) covered during these experiments ranged between 33 and 141 km (or 10.8 km^2) as compared to that of commercial mining (300–600 km^2). Similarly, the volume of sediment recovered during different experiments (1.16 m^3/min for JET, 0.77 m^3/min for NOAA-BIE, 1.39 m^3/min for IOM-BIE, and 1.33 m^3/min for INDEX) ranges between 2 and 3.7% of the estimated volume of sediment (i.e. 54,000 m^3/day, i.e. 37.5 m^3/min) expected to be recovered during a commercial mining operation (Yamazaki et al. 1991). Hence, all these experiments can be considered as micro-scale experiments in terms of duration, area coverage as well as sediment re-suspension. In future, it may be advisable to conduct similar experiments on relatively larger scale in order to study the impacts of such a disturbance on the benthic ecosystem, because the scale directly affects the area and thickness of re-sedimentation.

The thickness of deep-sea sediment layer expected to be excavated by a commercial scale collector was calculated as 57 mm on the basis of 10,000 t/day nodule production rate in wet condition and other assumptions (Yamazaki et al. 1991). The estimated average depth of sediment excavated during different experiments is 29–45 mm (Table 17.2). Since most nodules range in size between 2–4 cm and many of them are half exposed on the seafloor, this depth of excavation appears to be adequate to simulate the depth of excavation for recovery of nodules.

17.4.3 Estimation of Weight and Volume of Sediment Discharge

Sediment properties such as water content and density play a key role estimation of weight and volume of sediments discharged during a mining operation as these sediments are responsible for the environmental impact on the seafloor. Whereas water content determines the weight of water and sediment discharged, the density helps determine the volume. The total weight divided by the total estimated volume also gives the bulk density of the sediment layer recovered from the seafloor, which is an important factor for the design of a mining system. The estimation of dry weight and wet volume of sediment at the discharge point are also important for calculating the weight and volume of sediment discharged during an operation. Whereas the dry weight of sediment is estimated in terms of weight per volume, the volume of sediment is the volume concentration ratio of the discharged sediment with respect to the total volume (Yamazaki and Sharma 2001).

17.4.4 Extrapolation to Commercial Mining

In spite of the data from different experiments and estimations based on these for evaluating the possible effects of future mining activities, many questions remain unanswered, due to the limited scope of these studies. One of the major questions is 'What will be a likely mining system or systems in next 20 years that can be a basis of environmental tests? It is difficult to specify 'commercial-scale' now, because commercial system size and type are likely different depending upon the use of nodule elements and production target, and can vary with metal market situation' (Chung et al. 2001). It has also been suggested earlier that for arriving at a proper design of a mining system to minimize the environmental impact, it is important that the scale of 'experimental' mining should be representative of commercial mining venture which should preferably be the pilot mining system (Markussen 1994).

17.5 Environmental Considerations for Deep-Sea Mining

As early as the 1970s, several studies had indicated the potential impacts of different mining systems such as Continuous Line Bucket, Air-Lift, Hydraulic-Lift (e.g. Amos et al. 1977) and some others also suggested procedures for safe deep-sea mining (e.g. Pearson 1975). This section summarises different measures that need to be taken into design considerations of the deep-sea mining system so as to minimise environmental impacts:

17.5.1 Collector Device

- There should be minimum interaction of the collector system with the seafloor environment, to keep it disturbance free.
- The separation of minerals from sediments (or other debris) should be as close as possible to the seabed, so that minimum water column is affected.
- Strip-wise (or 'patch') mining to be carried out, leaving alternate strips of undisturbed seafloor, to allow re-population by organisms from adjoining areas.

17.5.2 Surface Discharge

- Sediment discharge should be the least at the surface, to allow sufficient sunlight to penetrate for photosynthetic activity.

- Any surface water discharge can be sprayed over a large area so that it can get diluted without much delay.
- Discharge of bottom waters and debris should be at different levels of water column preferably below the oxygen minimum zone where the faunal density is relatively lower than in the levels above

17.5.3 At-Sea Processing, Ore Transfer, and Transport

- Proper treatment of waste disposal to be carried out before discharging. Biodegradable methods should be used for treatment of discharge.
- Proper care to be taken during transfer of ore from the collector to the mining platform as well as the transport vessels to avoid spilling.
- Oil spills from these ships also should be monitored.

Few other considerations to predict the severity of deep-sea mining could be as follows:

- The proportion of area that will be affected, with respect to total area
- Influence of surface and subsurface currents in different seasons
- Distance of coastal areas and inhabited areas from the area of influence
- Existence of fishing potential or any other commercial activity in the area of influence

17.6 Environmental Management Plan for Deep-Sea Mining

An Environmental Management Plan can be defined as 'The synthesis of all proposed mitigation and monitoring actions, set to a timeline with specific responsibility assigned and follow-up actions defined. The EMP is one of the most important outputs of the environmental assessment process' (World Bank 1999). It can also be defined as '..... a tool used to ensure that undue or reasonably avoidable adverse impacts of the construction, operation and decommissioning of a project are prevented; and that the positive benefits of the project are enhanced' (Lochner 2005).

Very often Environmental Management Plan (EMP) and Environment Impact Assessment (EIA) are used interchangeably. An EIA is a process of assessing and analysing the potential or actual environmental impacts (positive or negative) of a project. The output of this process is an EIA report which normally should culminate into an EMP. Hence, an EMP is essentially an action plan based on the results of the EIA study that would spell-out specific strategies to minimize the negative impacts. Environmental management plans are thus an outcome of a thorough environmental assessment process of any development activity.

There is a need, therefore, for environmental management actions to be properly addressed in EMPs and thereby improve the effectiveness of EIA (University of Manchester 2003).

The objectives of an EMP should include (World Bank 1999; Hill 2000):

- Ensuring compliance with regulatory authority stipulations and guidelines which may be local, provincial, national, and/or international;
- Ensuring that there is sufficient allocation of resources on the project budget so that the scale of EMP-related activities is consistent with the significance of project impacts;
- Outlining the mitigation measures for the anticipated negative impacts of the proposed activity
- Verifying environmental performance by monitoring the information on impacts as they occur;
- Responding to changes in project implementation not considered in the EIA;
- Responding to unforeseen events; and
- Providing feedback for continual improvement in environmental performance

Hence, an EMP would flow from the EIA and should continue throughout the life of the project. The format for an EMP and its contents would vary with the purpose for which it is being designed and the scale of the project. Another important feature of the EMP is that it should be dynamic. As the project gets into the operational stage, major impacts occur and as the processes keep changing, the impacts vary. Thus, a periodic review of the management plan is required. The extent to which EMPs should be reviewed and updated varies between and within sectors (World Bank 1999). Institutional arrangements should be made such that the implementation and review of the plan is built into the functioning of the system.

17.7 International Regulating Agencies for Deep-Sea Mining

17.7.1 United Nations Convention on the Law of the Sea

United Nations Convention on the Law of the Sea (UNCLOS), also known as the Law of the Sea Convention, defines the rights and responsibilities of nations in their use of the world's oceans, establishing guidelines for businesses, the environment, and the management of marine natural resources. The members who ratify the Convention have the general obligation to prevent, reduce, and control pollution of the marine environment from any source, to monitor the risks or effects of pollution, and to assess the potential effects of activities under the States parties jurisdiction and control that may cause substantial pollution of or significant and harmful changes to the marine environment (UNCLOS 1982).

17.7.2 International Seabed Authority

The International Seabed Authority (ISA) is responsible for administering the mineral resources of the Area (i.e. areas beyond the Exclusive Economic Zones or national jurisdictions of any country), including prospecting, exploration, and exploitation activities for the resources (UNCLOS 1982). As part of its responsibility, the Authority is charged with taking the measures necessary to ensure effective protection of the marine environment from the harmful effects that may arise from such activities.

Thus, the ISA has laid down appropriate rules, regulations, and procedures that govern the actions of the Pioneer Investors (ISA 2011) with an aim to:

- Prevent, reduce, and control pollution and other hazards to the marine environment, including the coastline, that have the potential to interfere with the ecological balance of the marine environment. It states that attention is required to protect the environment from the harmful effects of all the activities such as drilling, dredging, excavating, disposing of waste, and constructing and operating or maintaining installations, pipelines and other devices;
- Protect and conserve the natural resources of the Area, preventing damage to the flora and fauna of the marine environment. (UNCLOS 1982).

In order to provide a guideline to the Contractors, ISA has developed preliminary requirements for EMP for the Clarion–Clipperton Zone of the Pacific Ocean (ISA 2011). Also, ISA has issued guidelines to Contractors for environmental monitoring due to exploration of polymetallic nodules (ISA 2013).

17.7.3 International Maritime Organization

International Maritime Organization (IMO) regulates the international shipping industry. Its main task is to develop and maintain a comprehensive regulatory framework for shipping (www.imo.org). As many of the proposed mine sites for the deep-sea minerals are in the international waters and might be falling in the way of some shipping routes, IMO must be informed and involved while planning the mining operations. International Convention on Preservation of Pollution from Ships (MARPOL) and International Convention on Safety of Life at Sea (SOLAS) are conventions under IMO which provide guidelines for prevention of pollution at seas and safety of life at sea, respectively. These govern all the merchant ships and could be applicable to the mining as well as transport ships as well.

17.7.4 World Meteorological Organization

World Meteorological Organization (WMO) provides framework for international cooperation in meteorology (weather and climate), operational hydrology, and related geophysical sciences (www.wmo.int). WMO can be helpful in providing real or near-real time data about the weather, environment, and natural disasters.

In addition to these, there would be several national agencies such as those dealing with mining, environment, and pollution that would also have a role in regulating activities within the EEZ as well as the territorial waters and on land once the ore is brought to shore for further processing.

17.8 Mitigation of Impacts Due to Different Activities

17.8.1 Components of Marine Mining and Their Mitigation Measures

The entire activity can be divided into four broad components such as exploration, environmental studies, mining, and processing (Fig. 17.4), which could further be divided into several sub-activities. It is expected that the place, type, and magnitude of environmental impact due to mining will vary depending upon the type and intensity of these sub-activities that will have to be compliant with guidelines laid down in international conventions (Table 17.4).

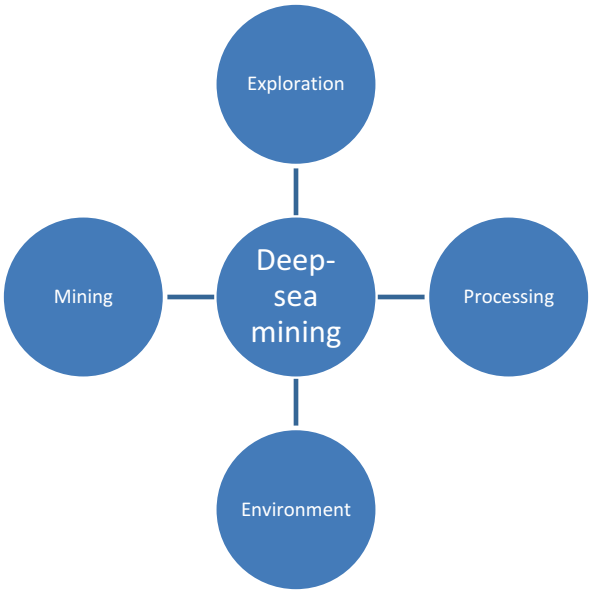

Fig. 17.4 Major components of deep-sea mining

Table 17.4 Activity-wise impacts and mitigation guidelines

Activity	Place of impact	Type of impact	Magnitude of impact	Mitigation guidelines
1. Exploration				
Cruising	Atmosphere, sea surface, water column, seafloor	Emissions, noise, heated water, oil, garbage (plastics, metal, glass, chemicals), human waste	Minor	As per SOLAS and MARPOL guidelines
On-board data collection (including radio communication and echo sounding)	Atmosphere, sea surface	Impacts on humans and marine animals due to propagation of waves through air and water	Minor	As per SOLAS guidelines (Chap. 4)
Sample collection	Water column, seafloor	Physical disturbance, chemical reactions, changes in faunal abundance and diversity, alteration in seafloor micro topography	Minor	As per MARPOL and ISA guidelines
2. Environment assessment				
Cruising	Atmosphere, sea surface, water column, seafloor	Emissions, noise, heated water, garbage (plastics, metal, glass, chemicals), human waste	Minor	As per SOLAS and MARPOL guidelines
Experimental EIA	Water column, seafloor	Turbidity, mixing of sediments, alteration in faunal assemblage	Medium	As per MARPOL and ISA guidelines
Baseline data collection and environmental monitoring	Water column, seafloor	Physical disturbance, chemical reactions, changes in faunal abundance and diversity, alteration in seafloor micro topography	Minor	As per MARPOL and ISA guidelines
3. Mining				
Cruising	Atmosphere, sea surface, water column, seafloor	Emissions, noise, heated water, oil, garbage (plastics, metal, glass, chemicals), human waste	Medium	As per SOLAS and MARPOL guidelines
Deployment and operation of equipment	Surface, water column, seafloor	Physical disturbance, chemical reactions, changes in faunal abundance and diversity, alteration in seafloor micro topography	Major	Minimum sediment penetration, avoid leakage/spillage, discharge below oxygen minimum zone, treat tailings before discharge

(continued)

Table 17.4 (continued)

Activity	Place of impact	Type of impact	Magnitude of impact	Mitigation guidelines
Ore transfer	Surface, Water column, Seafloor	Turbidity, mixing of sediments, alteration in faunal assemblage	Medium	As per SOLAS and MARPOL guidelines
Transport	Atmosphere, sea surface, water column, seafloor	Emissions, noise, heated water, oil, garbage (plastics, metal, glass, chemicals), human waste	Medium	As per SOLAS and MARPOL guidelines
At-sea pre processing	Surface, water column, seafloor	Turbidity, mixing of sediments, alteration in faunal assemblage	Medium to Major	As per SOLAS and MARPOL guidelines
Power generation (nuclear, solar or ocean thermal)	Surface, water column, seafloor	Alteration in the physico-chemical conditions, waste disposal	Medium to Major	As per SOLAS and MARPOL guidelines
4. Processing				
Transportation	Land, air	Emissions, noise, dust	Minor to Medium	As per national guidelines
Storage	Land, air, water	Growth of microbes and chemical alteration		As per national guidelines
Washing/pre-processing	Land, air, water	Leaching of clay particles, nodule fragments and massive microbes	Minor	As per national guidelines
Extraction	Land, air, water	Addition of chemicals and reagents to the environmental resources	Medium to Major	As per national guidelines
Waste disposal	Land, air, water, sea	Addition of slag to the environment	Major	As per national guidelines

17.8.2 Measures for Developing environmentally 'Safe' Mining System

Deep-sea mining is still in its developmental stages; hence the best environment management practices can be incorporated into the design, technology, scheduling, and monitoring of the activity. Some of the fundamental considerations to keep the impacts to a minimum level have been enlisted by ISA (2001) and are as under:

1. Minimize sediment penetration of collector and mining vehicle
2. Avoid disturbance of the more consolidated suboxic sediment layer
3. Reduce mass of sediment swirled up into the bottom near-water layer
4. Induce high rate of re-sedimentation from the plume behind the miner
5. Minimise the transport of sediment and abraded nodule fines to the ocean surface
6. Reduce the discharge of tailings into the bathyal or abyssal depth
7. Reduce the drift of tailings by increasing their sedimentation

17.8.3 Identification of Preservation Reference Zone (PRZ)

ISA defines Preservation Reference Zone as 'Areas in which no mining will occur to ensure representative and stable biota of the seabed in order to assess any changes in the flora and fauna of the marine environment.' The preservation reference zone(s) should be carefully located and large enough so as not to be affected by the natural variations of local environmental conditions. The zone(s) should have species composition comparable to that of the test mining area(s). The preservation reference zone(s) should be located upstream of the test mining area(s). The preservation zone(s) should be outside of the test mining area(s) and areas influenced by the plume (ISA 1999).

Further, ISA has also proposed certain guidelines for identifying/proposing preservation zone(s) (ISA 2008) as follows:

- The design and implementation should fit into the existing legal framework of the International Seabed Authority.
- The interest of all stakeholders should be incorporated into the design process. Stakeholders include ISA, signatories of UNCLOS, mining claim holders, non-governmental organization, and the scientific community.
- The conservation goals to be followed should consider preservation of marine biodiversity, unique marine habitats, and the ecosystem structure and function along with management of mining activity in a sustainable manner.
- The zones should be identified taking into consideration the productivity gradients in the ecosystem structure of the area.
- The boundaries of the preservation zones must be straight lines in order to facilitate rapid recognition.
- The core area of the preservation zone should be at least 200 km in length and width. This size of the area is required to maintain minimum viable population of the species.

- The preservation zone should contain full range of habitat types found within the region
- The preservation zone should be surrounded by a buffer zone of 100 km.

17.8.4 Hazard Management

Hazard management is an important part of the EMP. At the mine site, the hazards can be categorised as human-induced and natural. A brief description about these is as under:

17.8.4.1 Human-Induced Hazards

Safety of Life: The International Convention for the Safety of Life at Sea (SOLAS) specifies minimum standards for the construction, equipment, and operation of ships, compatible with their safety (www.imo.org). All mining activities along with its personnel will be required to abide by the convention which has provisions for the following:

- General Provisions regarding survey and documentation
- Stability of the vessel, machinery, and electrical installations
- Fire protection, detection, and extinction
- Life-saving appliances and arrangements
- Radio-communications
- Safety of navigation
- Carriage of cargoes and dangerous goods
- Nuclear ships
- Management of Safe Operations of ships
- Special measures to enhance maritime safety

Pollution hazards: The International Convention for the Prevention of Pollution from Ships (MARPOL) deals with prevention of pollution of the marine environment by ships from operational or accidental causes (www.imo.org). As marine mining will comprise of a stationed ship as its base as well as several ore carriers and supply vessels, these will be governed by MARPOL as per the following regulations:

- Regulations for the Prevention of Pollution by Oil
- Regulations for the Control of Pollution by Noxious Liquid Substances in Bulk
- Prevention of Pollution by Harmful Substances Carried by Sea in Packaged Form
- Prevention of Pollution by Sewage from Ships
- Prevention of Pollution by Garbage from Ships
- Prevention of Air Pollution from Ships

Pirate attacks and role of defence agencies: Piracy and marine robbery are threats to the safety of the personnel and the mining equipment deployed at the mine site. International Maritime Bureau (IMB) deals with all types of maritime crimes and malpractices (www.icc-ccs.org). As incidents of piracy at high seas are reported frequently, adequate measures may have to be taken by the concerned national and international agencies to ensure safety of their personnel and machinery.

17.8.4.2 Natural Hazards

Hazards related to natural conditions such as cyclones, winds, waves, and currents will also have to be monitored either based on meteorological data provided by World Meteorology Organisation (www.wmo.int), local weather forecasting stations, or by deploying weather data stations in and around the mining areas and contingency plans for evacuation, maintenance, repairing as well as meeting with any emergency situation will have to be put in place in the EMP by each Contractor.

17.9 Institutional Set-Up and EMP Framework

17.9.1 Establishment of Environmental Monitoring Office

For the effective implementation of the proposed plan, institutional mechanisms need to be in place right from the beginning and the monitoring activities scheduled appropriately. Thus, a dedicated Environmental Management Office (EMO) must be set up by the Contractor with clear roles, responsibilities, and authorities. A probable structure of the EMO along with other departments/offices under the Contractor is given in Fig. 17.5.

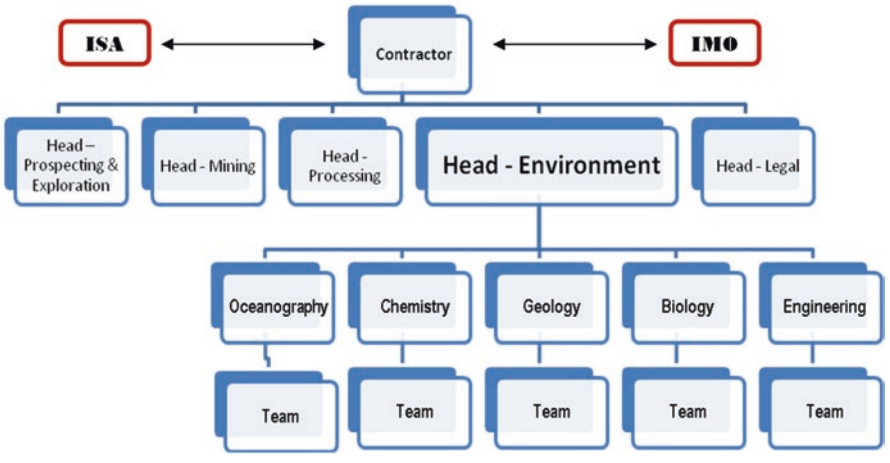

Fig. 17.5 Proposed structure of the Environmental Management Office

The structure proposes that the EMO and its Head, Environment be given equal status and importance as that of the other major departments. This would grant them authority to implement the EMP properly. The EMO should be advised by an Environmental Consultant, who keeps the office abreast with the latest developments on the subject, including assessment, monitoring, and mitigation techniques and ensures compliance with international regulations. Environment being a multidisciplinary field, the composition of EMO should have scientists and technicians from oceanography, chemistry, biology, geology, and engineering who would be involved in data collection in the field as well as analyses and report preparation in the office as per the guidelines and requirements of the regulating agencies.

Roles and Responsibilities of the EMO will include the following:

- Monitor all environmental parameters for assessment of effects of all activities related to mining
- Develop mitigation techniques in consultation with other departments
- Review and adopt new technologies for environmental monitoring and management
- Organise awareness and training programmes
- Coordinate with ISA and other agencies
- Continuously improvise the EMP
- Prepare a mine closure plan and ensure its implementation

17.9.2 Proposed Framework for EMP

A broad framework of the EMP is proposed as follows:

Section	Chapter	Contents
Section 1	Project description	Contractor brief
		Geographical area
		Economic feasibility
		Mining area delineation and estimation of area to be mined
		Concepts of proposed mining activity
Section 2	Environmental assessment	Results of experimental mining (or based on other studies)
		Potential impacts of commercial mining
Section 3	Mitigation of impacts due to various activities	Major components of marine mining
		Detailed sub-activities with mitigation measures
		Measures for developing environmentally safe mining system
		Identification of Preservation Reference Zone
		Hazard management
Section 4	Institutional set-up and monitoring	Institutional set-up
		Monitoring method and schedule
		Review

The EMP thus prepared for deep-sea mining should be reviewed from time to time for updating and to bring about necessary modifications depending upon the changes in technology or operating methods.

The review may be conducted at following intervals:

- Before commencement of the mining operation—once every 2 years
- During mining operation—every year
- After mining operation—every year until closure is filed

17.10 Conclusions

The world is on a path of rapid growth and development which are propelled extensively by non-renewable sources of energy. Minerals and metals play a vital role in the growth-driven economy. Man has been excavating the minerals mostly from the land. However, as the land resources are depleting at a fast rate and the demand of metals for industrial growth is increasing, man has discovered marine minerals which are a potential source of strategically important metals for industrial growth.

As marine mining evolved, it has passed through various stages of exploration, development of technology, as well as setting up of international regulating agencies for developing framework for eventual mining. Deep-sea mining system will consist of a surface platform, a miner device, and a riser which connects the two as well as several transport and supply vessels. The operations are expected to have certain environmental impacts not only at the seafloor where the minerals will be mined, but also the sea surface from where most of the activities will be conducted and the water column through which the ores will be lifted and unwanted material be discharged. The miner will crush the benthic organisms and lead to dispersion of the sediments associated with the minerals. Discharge of tailings, sediments, and effluent in the near surface waters will have adverse effects on the water quality and in turn affect the biota of the region and spillage will impact the water column.

Different Contractors have carried out baseline studies and experimental mining in order to understand the marine environment and the possible effects mining could have on it. With the entire world becoming increasingly aware about the conservation of environment, adopting sustainable practices from the developmental stages has given rise to the need for developing an environmental management plan for marine mining.

An environmental management plan is an outcome of the environmental impact assessment process which contains mitigation and monitoring plans to ensure undue and reasonably avoidable adverse impacts of various activities involved in the project. It would also ensure compliance to the guidelines laid down by the regulating authorities and allocation of resources for its strict adherence. This chapter reviews the likely impacts of deep-sea mining, evaluates the results of benthic impact experiments, discusses measures for reducing environmental impacts, highlights the role of various regulating agencies as well as proposes a framework for preparation of an environmental management plan that could be adopted for conservation of marine ecosystem.

Acknowledgment The author acknowledges the contribution of Ms. Pooja Kamat in compiling information for certain sections of this chapter during her internship at the Institute.

References

Amos AF, Roels OA (1977) Environmental aspects of manganese nodule mining. Mar Pol Int Bull 1:160–162

Amos AF, Roels OA, Garside C, Malone TC, Paul AZ (1977) Environmental aspects of nodule mining. In: Glasby GP (ed) Marine manganese deposits, Elsevier Oceanographic series 15. Elsevier Scientific, Amsterdam, pp 391–438

Brockett T, Richards CZ (1994) Deep-sea mining simulator for environmental impact studies. Sea Technology, August, pp 77–82

Chung JS et al (2001) Deep seabed mining environment: preliminary engineering and environment assessment. Special report OMS-EN-1, International Society of Offshore and Polar Engineers. ISBN: 1-880653-57-5, pp 1–19

Foell EJ, Thiel H, Schriever G (1990) DISCOL: a longterm largescale disturbance—recolonisation experiment in the abyssal eastern tropical Pacific Ocean. In: Proc of offshore technology conference, Houston, USA, Paper No. 6328, pp 497–503

Fukushima T (1995) Overview "Japan Deep-sea Impact Experiment = JET". In: Proc. of 1st ISOPE ocean mining symp, Tsukuba, Japan, ISOPE, pp 47–53

Gloumov I, Ozturgut E, Pilipchuk M (1997) BIE in the Pacific: concept, methodology and basic results. In: Proc. of Int. Symp. Environmental Studies for Deep-sea Mining, Metal Mining Agency of Japan, Tokyo (Japan), pp 45–47

Hill RC (2000) Integrated environmental management systems in the implementation of projects. S Afr J Sci 96:50–54

IBM (2010) Indian Bureau of Mines Year book 2010

Ingole BS, Ansari ZA, Rathod V, Rodrigues N (2001) Response of deep-sea macrobenthos to a small-scale environmental disturbance. Deep Sea Res II 48(16):3401–3410

ISA (1999) Deep seabed polymetallic nodule exploration: development of environmental guidelines. In: Proc ISA workshop, Sanya, China, 1–5 June 1998, The International Seabed Authority, Pub No ISA/99/02, pp 222–223

ISA (2001) Recommendations for guidance of contractors for the assessment of the possible environmental impacts arising from exploration for polymetallic nodules in the Area. International Seabed Authority, Jamaica. ISBA/7/LTC/1/Rev.1

ISA (2008) Rationale and recommendations for the establishment of the preservation reference areas for nodule mining in the Clarion-Clipperton Zone. International Seabed Authority, Jamaica. ISBA/14/LTC/2

ISA (2011) Environmental Management Plan for the Clarion Clipperton Zone. International Seabed Authority, Jamaica. ISBA/17/LTC/7

ISA (2013). Recommendations for the guidance of contractors for the assessment of the possible environmental impacts rising from exploration for marine minerals in the area. International Seabed Authority, Jamaica, ISBA/19/LTC/8, pp 32

Khadge NH (1999) Effects of benthic disturbance on geotechnical characteristics of sediment from nodule mining area in the Central Indian Basin. In: Proc. of the third ISOPE—ocean mining symp., Goa (India), pp 138–144

Lochner P (2005) Guideline for environmental management plans. CSIR report no ENV-S-C. 2005-053 H. Republic of South Africa, Provincial Government of the Western Cape, Department of Environmental Affairs & Development Planning, Cape Town

Markussen JM (1994) Deep seabed mining and the environment: consequences, perception and regulations. In: Bergesen H, Parmann G (eds) Green Globe Yearbook of international cooperation on environment and development. Oxford Univ. Press, London, pp 31–39

Nakata K, Kubota M, Aoki S, Taguchi K (1997) Dispersion of resuspended sediments by ocean mining activity—modeling study. In: Proc. of int. symp. environmental studies for deep-sea mining, Metal Mining Agency of Japan, Tokyo (Japan), pp 169–186

Ozturgut E, Lavelle JW, Steffin O, Swift SA (1980) Environmental investigation during manganese nodule mining tests in the North Equatorial Pacific, in November 1978. NOAA Tech. Memorandum ERL MESA-48, National Oceanic and Atmospheric Administration, USA, 50
Pearson JS (1975) Ocean floor mining. Noyes Data Corporation, Park Ridge, 201pp
Radziejewska T (1997) Immediate responses of benthic meio- and megafauna to disturbance caused by polymetallic nodule miner simulator. In: Proc int symp environmental studies for deep-sea mining, Metal Mining Agency of Japan, Tokyo, Japan, pp 223–236
Schriever G, Ahnert A, Borowski C, Thiel H (1997) Results of the large scale deep-sea impact study DISCOL during eight years of investigation. In: Proc int symp environmental studies for deep-sea mining, Metal Mining Agency of Japan, Tokyo, Japan, pp 197–208
Sharma R (2011) Deep-sea mining: economic, technical, technological and environmental considerations for sustainable development. Mar Technol Soc J 45:28–41
Sharma R, Nath BN (1997) Benthic disturbance and monitoring experiment in Central Indian Ocean Basin. In: Proc 2nd ISOPE ocean mining symp, Seoul, Korea, ISOPE, pp 146–153
Sharma R, Parthiban G, Sivakholundu KM, Valsangkar AB, Sardar A (1997) Performance of benthic disturber in Central Indian Ocean. National Institute of Oceanography, Goa (India), Tech. Report NIO/TR-4/97, 22
Sharma R, Nath BN, Parthiban G, Sankar SJ (2001) Sediment redistribution during simulated benthic disturbance and its implications on deep seabed mining. Deep Sea Res II 48:3363–3380
Shirayama Y (1999) Biological results of JET project: an overview. In: Proc 3rd ISOPE ocean mining symp, Goa, India, ISOPE, pp 185–190
Tkatchenko G, Radziejewska T, Stoyanova V, Modlitba I, Parizek A(1996) Benthic impact experiment in the IOM pioneer area: testing for effects of deep-sea disturbance. In: Int seminar on deep sea-bed mining tech, China Ocean Mineral Resources R&D Assoc., Beijing, China, pp C55–C68
Trueblood DD (1993) US Cruise Report for BIE—II Cruise. NOAA Technical Memo OCRS 4, National Oceanic and Atmospheric Administration, Colorado, USA, pp 51
Trueblood DD, Ozturgut E, Pilipchuk M, Gloumov IF (1997) The echological impacts of the joint U.S.-Russian benthic impact experiment. In: Proc. int. symp. environmental studies for deep-sea mining, Metal Mining Agency of Japan, Japan, pp 237–243
UNCLOS (1982) United Nations Convention on the Law of the Sea. pp 7–202
University of Manchester (2003) EIA Centre. EIA Newsletter 12. www.art.man.ac.uk/EIA/publications/newsletters
UNOET (1987) Delineation of mine sites and potential in different sea areas. UN Ocean Economics and Technology Branch and Graham & Trotman Limited, London, 27pp
World Bank (1999) Environment management plans. Environ Assess Sourcebook Update 25:1–8
Yamazaki T, Sharma R (2001) Estimation of sediment properties during benthic impact experiments. Marine Georesour Geotechnol 19:269–289
Yamazaki T, Tsurusaki K, Handa K (1991) Discharge from manganese nodule mining system. In: Proc. of the first int. offshore and polar eng. conf., Edinburgh, UK, vol 1, pp 440–446

Websites (Accessed Between 10 June 2012 and 20 July 2012)

International Seabed Authority. www.isa.org.jm
International Maritime Organization. www.imo.org
International Maritime Bureau. www.icc-ccs.org/icc/imb
Wikipedia. www.wikipedia.org
World Meteorological Organization. www.wmo.int

Dr. Rahul Sharma (rsharma@nio.org, rsharma-goa@gmail.com) has been working as a Scientist at the CSIR-National Institute of Oceanography in Goa, India, and has led a multi-disciplinary group on 'Environmental studies for marine mining'. He has a master's degree in Geology and a doctorate in Marine Science. His professional interests include application of exploration and environmental data to deep-sea mining. He has edited 3 special issues of scientific journals and 1 symposium proceeding, published scientific 35 papers and 20 articles, and presented 50 papers at international symposia.

His international assignments include Visiting Scientist to Japan, Visiting Professor to Saudi Arabia, member of the UNIDO mission 'to assess the status of Deep-sea mining technologies' in Europe, USA, and Japan, invited speaker and consultant for the International Seabed Authority, Jamaica, and has contributed to the 'World Ocean Assessment report I' of the United Nations.

Chapter 18
The Crafting of Seabed Mining Ecosystem-Based Management

Yves Henocque

Abstract Deep-sea environments are faced with cumulative effects of many human activities, e.g. waste deposition, oil exploitation, fishing, maritime transport, and potential seabed mining. The ecosystem approach requires that we look at the cumulate impacts of all these pressures on each specific habitat and living community. Therefore, deep seabed ecosystem-based management should be considered in relation with the varied governance and management regimes from the coast to international waters, in a regional context. Many frameworks and instruments already exist, but they are fragmented, while the ocean and its resources is a totally interconnected system without borders. Within EEZ as well as international waters, new thinking is required about the way governance and management should be applied through a polycentric-like approach articulating existing agreements and their implementation framework from local to global level. Along Aichi Target 11, ecologically and biologically significant areas (EBSAs), coastal, and very large marine protected areas (MPAs) might be used as the first elements of a comprehensive 3D-dimension regional network of area-based managed units with a 100% coverage including varied levels of biodiversity conservation and sustained supply of ecosystem services on which people and maritime activities development depend.

18.1 Introduction: 2025, the Optimistic

Deep-sea environments are faced with cumulative effects of many human activities, e.g. waste deposition, oil exploitation, fishing, maritime transport, and potential seabed mining. Recently, growing interest in deep-sea mining, within States' Exclusive Economic Zones or in areas beyond the limits of national jurisdiction, has increased exploration and the development of early environmental impact assessments and scientific research. The issues on seabed mining raised recently, such as the potential environmental impacts, have given rise to many workshops, meetings, and conferences, since the initial discovery of polymetallic nodules at 5000–6000 m depth on the seafloor of Pacific Ocean was raised in the latter decades of the 1900s.

Y. Henocque (✉)
IFREMER (JAMSTEC), Hongo 4-5-17-105, Bunkyo-ku, Tokyo 113-0033, Japan
e-mail: yves.henocque@ifremer.fr

R. Sharma (ed.), *Deep-Sea Mining*, DOI 10.1007/978-3-319-52557-0_18

In the Pacific region, the first site likely to be commercially exploited is located in Papua New Guinea, where seafloor massive sulfide (SMS) deposits at 1600 m water depth occur in the Bismarck Sea, and this has received the appropriate approvals. The mining company, Nautilus Minerals Ltd., expects a first production in 2018. Another operation with strong potential is Atlantis II Deep in the Red Sea which has also been granted an exploitation license (EU DG MARE 2013)

Seabed mining industry will probably know a slow start, but that could quickly accelerate with metals' international market fluctuations, technological development, and of course the pro-active policy of countries enjoying rich seabed mineral resources within their EEZ. Ten years from now may look a bit short, but whatever the time Bolman et al. (2014) have proposed a foresight vision for seabed mining up to 2025 while recommending 'to work towards Good Environmental Practices':

> "Seabed mining in 2025 is internationally accepted; it is a worldwide common practice, both inside EEZs and in areas beyond national jurisdictions. It is a crucial activity to guarantee a secure supply of minerals including rare earth metals to the global economy. Seabed mining in 2025 has a proven capacity to utilize a set of tools by which environmental impacts can be identified, scoped (which are the relevant ecosystem components and ecological pressures) and prioritized (which pressures have the largest consequences for ecosystem) and management plans developed before operations have started. The industry is capable of an early phase assessment of ecological risks, mitigation of impacts and identification of monitoring objectives that are legally and socially accepted and to install adaptive management strategies that respond to monitoring results. Companies in seabed mining are transparent and fully open to scrutiny, have a continuous dialogue with all stakeholders including governments, NGOs, research institutes, and the public and are open in terms of explaining its activities and all issues surrounding its operations. In 2025, the seabed mining industry actively implements principles, such as Building with Nature, to enhance ecological values during its operations to the extent possible. In a decade from now, seabed mining supports a diversified minerals processing industry that represents investment, training and employment opportunities in nations whose EEZ hosts mineral deposits."

Even being optimistic, we know that such an ideal situation will certainly not be in 10 years from now. Like most of the scenarios, reality will probably be a mix of situations, weak in certain aspects and stronger in others. Nevertheless, it is worth looking at some of the above predicates, put them into context, and see how much they are feasible given the current political, legal, and institutional situations we have at different scales, from local to global and vice-versa.

18.2 From Global to Local: An Imperfect But Forward-Thinking International Impetus

After Rio+20, where the seas and oceans were high on the agenda, the recent UNFCCC[1] COP21 organized in Paris (December 2015) recognized the crucial role of the ocean in keeping our planet safe. Actually, since immemorial times, seas and

[1] United Nations Framework Convention on Climate Change.

oceans have been central actors in international relations between states and between populations. They have also been the place of conflicts progressively leading to the necessity of better organizing activities at sea and delimitating areas where they could exercise their power.

Today, about 50% of the world's population lives in coastal areas, leading to huge pressures on coastal habitats and resources. In addition, most of the world's ever-increasing population depends on oceans for food, sewage or waste disposal, energy production, or for maritime transport which is more than ever crucial to the world economy. These people see the coast as their life-place, their provider of food, inspiration, and recreation. Managing all of these uses, and the expectations of an ever-increasing coastal population, is a huge challenge for all developed and developing countries.

Further offshore, the 1982 Convention on the Law of the Sea, endorsed in 1994, recognizes the freedom to use waters located beyond nation's economic exclusive economic zones. Marine areas beyond national jurisdiction represent around half of the Planet's surface and a significant amount of its biodiversity, but there are significant gaps in their governance which prevent their effective conservation and sustainable use. For example, no global and detailed legally binding frameworks exist for the establishment of marine-protected areas or the conduct of environmental impact assessments in these areas and, though a UN process is engaged, a legal uncertainty still surrounds the status of marine genetic resources found in the deep seabed and in the water column of areas beyond national jurisdiction (ABNJ) (Druel et al. 2013).

Although a consensus has been reached at the UN General Assembly (UNGA) of September 2014 about the necessity of a specific agreement on conservation and sustainable use of marine biodiversity in ABNJ by the end of 2018, there is no coherent global system to ensure the protection of vulnerable marine ecosystems from actual and potential threats. There are only agreements and separate organizations for, among others, vessels' discharges, hydrocarbon pollution, and land-based pollution. Different organizations exist for the fishing of tuna and other species, and there are different organizations depending on regions. At the end, there is little or no coordination between international conventions (development and protection) and their institutions. In these conditions, the policing of the commitments made is very uncertain and coordination between organizations receives little incentives. One of the current and lasting consequences is, for example, the persistent issues of illegal, unregulated, and unreported fishing, especially in international waters. Such practices are estimated to represent roughly 30% of the global catch, and they remain unabated if not increasing in certain regions. A recent EU-funded 2-year study concluded 276,000–380,000 tonnes of Pacific tuna were taken illegally every year, i.e. a 'staggering' value of up to US$ 740 m a year.[2]

[2] http://www.dailymail.co.uk/wires/afp/article-3492749/Illegal-tuna-fishing-costs-Pacific-US-740m-report.html.

The Convention on the Law of the Sea provides for environmental impact studies for activities which could cause significant or damaging changes on the marine environment. However, there is no procedure for international monitoring to ensure that these studies are carried out before the start of the activities. Such procedures would have significantly helped to check the rapid increase in trawling deeper and deeper, and thus to avoid the loss of rare and very vulnerable deep-water ecosystems like those on seamounts.

The then Secretary General of the United Nations' attempt to launch a new deal for oceans in 2012 was certainly commendable, but, unfortunately, it did not last long due to poor dealings with the developing countries mainly represented within the G77. In order to move towards greater coherence for "healthy oceans in a prosperous world", we must give ourselves the means for true coordination between the agencies of the United Nations. At the same time, progress must be made with international negotiations for further adapting the Law of the sea as an original legal framework for making the entire ocean our "common heritage of mankind".

This last concept of "common heritage of mankind", highlighted by the globalization move, involves common places ("common pool resources" (Ostrom 2010)) without borders and not dependent on states' direct sovereignty. Such is the case for the outer atmosphere and maritime spaces (including the ocean floor), but it applies as well to the Internet or other kind of space 'without borders' like finance, media, NGOs or, more generally, knowledge. These spaces have in common, like maritime transport, a non-hierarchic organization around groups of networks. They connect nodal points made up by different areas of settlement, exploitation, transformation of resources or immaterial data, concentration of knowledge (databank), or policy centres. Freedom of circulation, interconnection, continuity, fluidity, reconfiguration, plasticity, circumvention, capillarity, diffusion, or concentration: these are all characteristics that bring these networks closer to maritime practices established since time immemorial.

The building of a shared world requires us to reconsider our modern world-view, which is based on dualisms between subject and object (e.g., human and nature), science and politics, experts and laypeople, facts and values, modern and traditional, etc. In this respect, knowledge should be totally connected to man's plans and hopes to learn how to live together, to achieve personal fulfillment and communities' moral development. From that perspective, environmental and maritime policies should aim the fulfillment and development of individuals within each community in achieving a 'good environmental status'.[3] There is no recipe to achieve such an ambitious goal, but the necessity to keep avenues open with creativity and imagination, trusting man's ability to adapt with success to changes and uncertainties in an increasingly complex and connected world. The ideal of conservation would have no meaning without an ambition for individual's democracy and autonomy against

[3] An allusion to the EU Marine Strategy Framework Directive aiming by 2020 the 'Good Environmental Status' of European waters following 11 descriptors operated through the ecosystem-based management approach.

institutional hierarchies and barriers. It means encouraging polycentric modes of governance, integrating different levels—from the individual to the global level, structured around physical locations—from the coast to international waters.

18.3 The Ecosystem Approach: The Dynamics of Societies and Ecosystems

The Millennium Ecosystem Assessment (MEA 2005) offered a description of the interactions between society and nature, using the concept of ecosystem services and making somewhat the link between the four categories of 'capital' (physical, natural, human, and social), sources of human development, and well-being. Actually, the main challenge related to the ecosystem approach is found in the social system and its complex interactions with the former. As Holling (1986) showed that ecological surprises are more likely to occur where large-scale systems become highly interconnected, it is the same for social systems, which get more prone to instability the bigger and more interconnected they become. It is therefore not surprising that, when dealing with two unstable and highly interconnected systems, their overall stability remains very uncertain. This is why the coasts, seas and oceans management require an integrated approach, in the adaptive and pragmatic meaning of the term, while a certain number of constants emerge from the dynamics of interactions between society and nature:

- Generally speaking, a specific sector of society will be the main beneficiary of developed activities. They inevitably will cause a certain stress onto the ecosystem, the cost of which will have to be borne by other groups or by the whole society ('Share the costs, privatize the benefits'). Since there are many interacting users, the goal is to get them to minimize their activities' ecological footprint, while making them contributing to the tracking (monitoring) and possible restoration of the ecosystem concerned;
- The key to better sharing out the benefits is in understanding what actually directs society's dynamics in the use of the ecosystems on which it depends;
- Management and social research have shown the dynamic nature of groups of people involved in problems and the crucial role played by social networks for conflict resolution. Usually, the first hint of ecosystem degradation is revealed by well-informed people or "whistleblowers" (Chateauraynaud 1999). These are sometimes scientists, affected people, and more and more NGO representatives, potentially trying to stop or reverse the degradation, using social networks and media to share their cause with the largest possible number of people and decision-makers. If their message is clear and convincing, and if their outreach capacity permits it, they have a good chance to mobilize action. However, almost at the same time, other interest groups might mobilize as a reaction. If the social links between the two opposing groups are too weak, or do not exist, the polarization of ideas could stick for a long time. Only links between groups, and to higher hierarchical levels, can help in finding a solution which might lead to proper decision;

- Certain political and social processes can lead to a compromise, but, in fact, it has often been shown that compromise adds little, or can, in the end, be harmful for the entire community because it leads to un-satisfaction and frustration.

When looking at the 12 principles of the ecosystem approach as agreed in the Convention of Biodiversity (Box 18.1), it is worth noticing that the first four principles are about society choices, decentralization, collateral damages, and economy. The term of 'ecosystem structure and functioning' is to be found only as the fifth principle, making clear that we definitely don't manage nature but people and societies.

Box 18.1 The Twelve Principles of the Ecosystem Approach from the Biodiversity Convention (1992)

1. The objectives of management of land, water, and living resources are a matter of societal choices.
2. Management should be decentralized to the lowest appropriate level.
3. Ecosystem managers should consider the effects (actual or potential) of their activities on adjacent and other ecosystems.
4. Recognizing potential gains from management, there is usually a need to understand and manage the ecosystem in an economic context. Any such ecosystem-management programme should: reduce those market distortions that adversely affect biological diversity; align incentives to promote biodiversity conservation and sustainable use; internalize costs and benefits in the given ecosystem to the extent feasible.
5. Conservation of ecosystem structure and functioning, in order to maintain ecosystem services, should be a priority target of the ecosystem approach.
6. Ecosystems must be managed within the limits of their functioning.
7. The ecosystem approach should be undertaken at the appropriate spatial and temporal scales.
8. Recognizing the varying temporal scales and lag-effects that characterize ecosystem processes, objectives for ecosystem management should be set for the long term.
9. Management must recognize the change is inevitable.
10. The ecosystem approach should seek the appropriate balance between, and integration of, conservation and use of biological diversity.
11. The ecosystem approach should consider all forms of relevant information, including scientific and indigenous and local knowledge, innovations, and practices.
12. The ecosystem approach should involve all relevant sectors of society and scientific disciplines.

18.4 The Ecosystem Approach in the Deep Sea

The case of the deep sea is particularly interesting because we are addressing could-be genuine ecosystems that have been left unaffected (or relatively so) by human impacts. More specifically, these areas include the abyssal deeps and the most southerly Antarctic waters (Halpern et al. 2008). In these areas, very specific deep-water habitats, such as seamounts or hydrothermal vents, are still poorly known, making difficult to predict what impact certain uses might have on the structure, function, and properties of these ecosystems. The ecosystem approach is not only concerned with the direct and indirect value of uses, but also with the intrinsic (related to the history of our planet) value of ecosystems that might be immediately threatened by exploration, bio-prospection, and soon mining activities.

We are not yet talking of implementing strategic maritime planning in these international regions. However, large oceanic marine protected areas have attracted increasing attention and may be regarded as instruments serving the ecosystem approach. For example, negotiations in the North East Atlantic have led to the protection of a part of the Charlie Gibbs fracture zone (deformation zone in the mid-Atlantic ridge). This involves the OSPAR regional convention and the Regional Commission for Fisheries covering the North East Atlantic. Similarly, the International Seabed Authority (ISA) works with its "contractors" and the international community to develop environmental action plans for granting mining exploration permits in international zones. The only one currently in place is in the polymetallic nodules-rich zone of Clarion-Clipperton in the Pacific, and another one is in preparation along the mid-Atlantic ridge (Morato et al. 2015). We will come back later to the possible role MPAs (all kinds of MPA) and very large MPAs could play in regard to planning and management.

According to articles 204–206 of the UN Convention on the Law of the Sea, states are required to assess the potential effects of activities within their jurisdiction or control that may cause pollution or significant damage to the marine environment. The results of this work must be communicated to international organizations and made available to all states. The same applies for the Convention on Biodiversity (articles 4 and 14), which requires that signatories carry out environmental impact studies when their activities might affect biodiversity in areas under national jurisdiction, but also in international waters. Nevertheless, progress remains to be made to better specify how these studies should be carried out in these waters. Other activities that are subject to international resolutions include deep-sea trawling and the discharge of waste into the sea.

These examples show that a complex set of international and regional legal instruments already exists for the conservation and management of international waters. However, as already stated above, there is no coherent governance system which might ensure the assessment and regulation of new activities that might endanger marine ecosystems. For this reason, organizations, such as the IUCN (International Union for Conservation of Nature), demand that the UN General Assembly adopts, as a matter of urgency, a resolution urging states to: (1) develop

assessment procedures, including for the cumulative impacts of human activities on marine biodiversity; and (2) to ensure that the activities under assessment, which may affect the environment, are subject to prior authorization for the nationals and vessels for which the states are responsible, while ensuring that they are managed in such a way as not to cause damage to the environment (Gjerde 2008).

18.5 Building with Nature

Although the ecological engineering concept of 'Building with Nature' has first been applied in the creation of new land, more particularly in the Netherlands (Waterman 2016), it has since been expanded and applied on a variety of coastal ecosystems including seabed landscaping. Rather than just minimizing the negative impacts of envisaged infrastructure projects (building *in* nature) and compensating for any residual negative effects (building *of* nature), building *with* nature aims to be proactive, utilizing natural processes and providing opportunities for nature as part of the infrastructure development process (EcoShape 2012). Contributing to the ecosystem-based management approach, associating engineers, ecologists, and social scientists, it deals with, (1) the knowledge of the type of ecosystem at stake, its characteristics, related ecosystem services, and associated opportunities; (2) the project cycle and management; and (3) the governance context (networks, regulatory context, knowledge context, implementation framework).

The approach 'building with nature' is therefore operating at the interface between ecosystems and infrastructure, between research and industry. It is coming from coastal engineering but ecological engineers' interest is and will be, in relation with the development of maritime activities (e.g. offshore oil and gas extraction), turn towards deeper waters. But its development will much depend on the acquired knowledge and characterization of the main environment impact sources, i.e. the type of physical removal of substrate, the 'cutting' and 'return' plumes, the extraction machines, and riser noise, not only to minimize them (reactive) but also to try to conceive more innovative and less intruding tool design.

Within the ecosystem approach, the 'building with nature' concept might help to better link scientific research and technological development in between scientists, engineers, and the industry.

18.6 New Challenges, New Forms of Governance

As said before, the ocean is highly interconnected, but our governance and management regimes are very fragmented. National jurisdictions and boundaries are not recognized by marine populations or natural changes, and additional stressors of anthropogenic impacts can cause cumulate effects onto the same ecosystem. The very special features of the deep sea require new thinking

(within EEZ and in international waters) about the way governance and management should be applied, provided (Levin 2015):

- We are addressing huge, remote, and far from shore areas inferring high exploration (and future exploitation) costs dealing with high heterogeneity of living communities and where it will be impossible to catalogue all biodiversity;
- In such particular habitats, recovery of long-lived species may be impossible with probably a great time lag between biodiversity response and ecosystem services recovery;
- We have a lack of scientific knowledge and are still technology-limited to deal with well-targeted indicators that we can measure in situ with the help of multiplatform censors;
- We are dealing with different governance regimes, mainly between EEZ and international waters, and it will be a great challenge to align policy and legislation which is coherent, adaptive, and protective whilst ensuring the balanced development of maritime activities;
- There is a lack of public awareness (and more particularly coastal stakeholders) regarding the role and richness/vulnerability of the ocean.

18.7 A Nested and Progressive Governance Approach Building on Existing Frameworks and Instruments

As pointed out in the "Call for Deep-Ocean Stewardship" (Deep Ocean Stewardship Initiative (DOSI) 2015), "overcoming fragmented governance requires improved collaboration…. through interdisciplinary, transboundary, and multisector management to ensure that cumulative effects are minimized and explicit trade-offs made". Although this call concerns the deep sea, the same approach should apply in a continuum from the watershed to the international waters (Fig. 18.1). Looking at the principles of each of the applying concept, they look very similar but they apply in different environmental, institutional, and social contexts. The approach should then be progressive, departing from what exists already and see how it can be articulated with the next bigger scale.

For example, the European Union is promoting a progressive approach to ecosystem-based management through the environmental pillar of its Integrated Maritime Policy, the Marine Strategy Framework Directive (MSFD). This directive applies to the EU member states' EEZ, but we are still far from common standards and harmonized methodologies. Understanding and quantifying drivers, pressures, and impacts in the deep sea, together with cumulative impacts, is a crucial step towards developing a comprehensive set of environmental targets and associated indicators that can be used to extend the concept of Good Environmental Status (GES) to the deep sea and to inform conservation and management, including the identification of Special Areas of Conservation and the design of Marine-Protected Area networks (European Marine Board 2015).

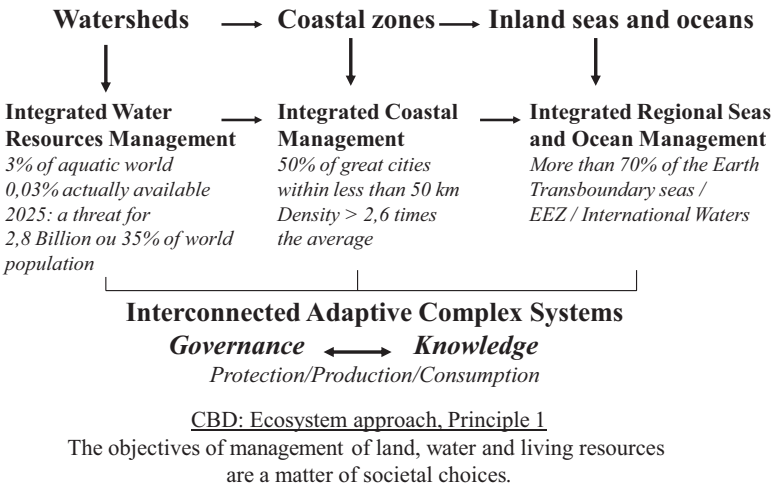

Fig. 18.1 Integrated coast and ocean management

Besides the construction of the environmental pillar, there are a whole set of other indispensable pillars (economical, legal, political, institutional, capacity-building) to build a coast and ocean coherent governance framework, but realistically this cannot be done in once, as a whole, so complex is the functioning of the socio-ecosystems we want to address.

In spite of a fragmented system, one interesting entry point towards a nested governance approach is the concept and current development of marine-protected areas at local, national, regional, and global level, not taken into isolation but as networks of marine managed areas along the Convention of Biological Diversity Aichi Target 11 (Box 18.2).

Therefore, Aichi Target 11 calls for a great deal more than mere MPA coverage. As we will see below, there is a variety of area-based management tools that, put together, could better achieve the preservation of ecosystem services, thus maximizing human benefits (Spalding et al. 2013). Among them, the process of identifying and prioritizing the CBD Ecologically and Biologically Significant Areas (EBSAs) is exemplary and could become the 'common currency' of them all.

Box 18.2 Aichi Target 11

By 2020, at least 17% of terrestrial and inland water areas,
and 10% of coastal and marine areas,
especially areas of particular importance for biodiversity and ecosystem services,
are conserved through effectively and equitably managed,
ecologically representative, and well-connected systems of protected areas
and other effective area-based conservation measures
and integrated into the wider landscapes and seascapes

18.8 Ecologically or Biologically Significant Areas: An Inter-Institutional Process

After several years of intense debates, the Parties to the Convention on Biological Diversity (CBD) decided in 2010 (COP10) "to cooperate, on a regional or subregional basis, to identify and adopt, according to their competence, appropriate measures for conservation and sustainable use in relation to Ecologically or Biologically Significant Areas (EBSAs)", and for that purpose, "to organize a series of regional workshops, … with a primary objective to facilitate the description of ecologically or biologically significant marine areas through application of agreed scientific criteria as well as other relevant compatible and complementary nationally and inter governmentally agreed scientific criteria**".**

Then, from 2011 to 2014, the Secretariat of the CBD held 9 regional workshops involving experts from 92 countries and 79 regional and international bodies (Bax et al. 2015). Two-thirds of the world ocean have been thus covered with identification of 204 areas in national and international waters along the internationally agreed criteria (Table 18.1).

Table 18.1 EBSAs criteria, definition, and example (adapted from Bax et al. 2015)

CBD Scientific criteria	Definition	Example
1. Uniqueness or rarity	"Area contains either (1) unique, rare or endemic species, populations or communities, and/or (2) unique, rare or distinct habitats or ecosystems, and/or (3) unique or unusual geomorphological or oceanographic features"	Sargasso Sea, hydrothermal vents, endemic communities around submerged atolls or seamounts
2. Special importance for life-history stages of species	"area that is required for a population to survive and thrive"	Breeding grounds, nursery, feeding, wintering, resting areas
3. Importance for threatened, endangered, or declining species and/or habitats	"area containing habitat for the survival and recovery of endangered, threatened, declining species, or area with significant assemblages of such species"	The same as above but regarding threatened, endangered, or declining species
4. Vulnerability, fragility, sensitivity, or slow recovery	"area that contains a relatively high proportion of sensitive habitats, biotopes or species that are functionally fragile or with slow recovery"	Habitat forming species (e.g. corals, sponges); long-lived species with low reproductive rates (e.g. sharks), area vulnerable to pollution (e.g. ice covered)
5. Biological productivity	"area containing species, populations, or communities with comparatively higher natural biological productivity"	Frontal areas, upwellings, hydrothermal vents, seamounts

Table 18.1 (continued)

CBD Scientific criteria	Definition	Example
6. Biological diversity	"area contains relatively higher diversity of ecosystems, habitats, communities, or species, or has higher genetic diversity"	Fronts, convergence zones, seamounts, cold coral communities, deep-water sponge communities
7. Naturalness	"area with a comparatively higher degree of naturalness as a result of the lack of or low level of human-induced disturbance or degradation"	Mostly deep sea habitats when not yet damaged by deep sea fishing trawls

The intense identification work and gathering of data (though with a lot of gaps) have led, and for the first time, to an inter-institutional collaboration, more particularly between regional convention organizations and regional fisheries organizations where they exist. The coverage of identified EBSAs concerns national, transboundary, as well as areas beyond national jurisdiction, and as such is informing future ecosystem-based management, including marine spatial planning, in these regions.

It is important to recall that EBSAs are not marine-protected areas (MPAs), but areas that may require specific management measures (e.g. through environmental impact assessment procedures) including enhanced conservation and possible establishment of MPAs. Some Parties like Japan (Yamakita et al. 2015) have already used the EBSAs criteria to inform national MPA processes, although the EBSA programme was initiated to support area-based management in areas beyond national jurisdiction.

As an example of future integration for management, the Central Pacific Equatorial Productivity Zone, identified as an EBSA, is a huge area that spread across the entire Pacific, from West to East, which corresponds to tuna ocean route hence important for the South Pacific tuna longline fleet, and overlaying the Clipperton-Clarion Fracture Zone (CCZ), the well-established International Seabed Authority (ISA) managed 'Area' for polymetallic nodules. This is a typical and most concrete example of the big challenge ahead of us: ISA did develop an "Environmental Management Plan" based on an MPA network to safeguard biodiversity and ecosystem function at depth (Wedding et al. 2013), but the upper ocean used by fishers and identified as an EBSA is not included, despite the inevitable surface activities that would occur in case of polymetallic nodules industrial exploitation. Based on this information, gained by international consensus, ISA will have now to complement the existing 'Environmental Management Plan' considering the pelagic system so that future environmental impact assessments (including baselines) cover the bottom and the whole water column up to the surface.

The above criteria (Table 18.1) used to identify EBSAs are not unique to the CBD. As we said before, there are many other area-based management tools depending on international conservation and sectoral agreements and their management bodies (Fig. 18.2).

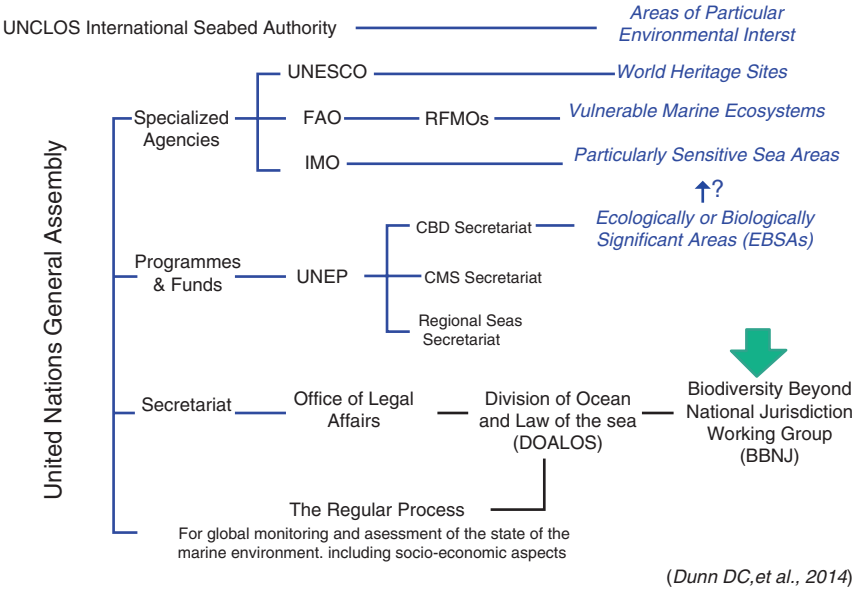

Fig. 18.2 EBSAs criteria, a common currency across international conservation agreements, sectoral management bodies, and States?

These conservation-oriented area-based management tools have a number of common criteria, cross-cutting those of the EBSAs which then could be used as a rational framework for regional, ecosystem-based, marine spatial planning (MSP) processes, where a variety of management tools, spatial and dynamic, can be applied by competent authorities (Dunn et al. 2014).

The question becomes then the implementing bodies which, realistically, under the varied international agreements, are the existing regional organizations like for example in the North-East Atlantic under OSPAR (regional sea convention) and NEAFC (regional fisheries organization), which, on a 'collective arrangement', set up the first network of MPAs and fisheries closures including EEZ and areas beyond national jurisdictions (ABNJ).

While the formal negotiation for a new international legally binding instrument under the UNCLOS Framework is ongoing (Wright et al. 2016), the EBSA process could be part of a global mechanism for the future implementing agreement to UNCLOS on marine biodiversity in ABNJ where the international organizations like FAO (and its RFMOs), IMO, ISA, regional seas conventions, together with states, could contribute to a coherent set of action plans to prevent significant adverse impacts due to human activities in international waters and within the EEZ of each country within a same region.

18.9 Very Large Marine-Protected Areas: Experimenting Large-Scale Integrated Management

This move could first be experimented in specific but sufficiently large areas, which are the multiplying large-scale marine-protected areas (LSMPA) as it is the case in the Pacific.

Thanks to the 1982 UN Convention on the Law of the Sea (UNCLOS), the new 200 miles EEZs dramatically increased the territory of Pacific Island nations, particularly archipelagic ones. For example, Fiji's 18,272 km^2 of land provided an EEZ of 1,290,000 km^2, Kiribati's 690 km^2 of islands translated into an EEZ of 3,550,000 km^2, while Federated States of Micronesia's 701 km^2 of land equated to an EEZ of 2,978,000 km^2. Till now, the main revenues generated from these huge new 'territories' are derived from fishing and fishing license fees (Bambridge and D'Arcy 2014), but with the development of new activities like deep sea mining, they should become more diversified in the future.

Beyond their official basic function of marine conservation, LSMPA like the Great Barrier Reef Marine Park, the oldest and most experienced one, has shown that they are totally in agreement with the Aichi Target 11's spirit by applying the concept of ecosystem-based management in a multi-use context and multi-tier scheme, combining local community near-shore management with national and regional frameworks. Because of their expansion from the coast to offshore waters (for the moment, till the EEZ outer boundaries), LSMPA might facilitate this kind of integration in the different governance and management regimes, from the coast to the deep sea. In the case of the West Pacific, the regional 'cement' could be the 'Framework for a Pacific Oceanscape', its principles, scope, and vision.[4]

Till now, there is no legal framework for the creation of LSMPA in areas beyond national jurisdiction (ABNJ), and it will be one of the challenges in the starting negotiating process under the UN General Assembly (UNGA). Practically, the ground for their identification is already well-prepared with the EBSAs' identification process covering most of the seas and oceans, though EBSAs are not MPAs or any marine-managed area yet. Good example of states using efforts underway at regional level is given by the OSPAR Commission and the Sargasso Sea Commission, though it remains to be seen if existing institutional agreements and structures are sufficient to meet global commitments to reconcile, at a regional scale including the deep sea in international waters, biodiversity conservation and maritime development (co-benefit) (Jonas et al. 2014), or if additional mechanisms may be required besides the necessary but insufficient role (as regards the water column) played by the International Seabed Authority (ISA) in the 'Area' (the bottom of the sea in ABNJ).

[4] Framework for a Pacific Oceanscape: a catalyst for implementation of ocean policy. Our Sea of Islands—Our Livelihoods—Our Oceania. http://www.forumsec.org/pages.cfm/strategic-partnerships-coordination/pacific-oceanscape/pacific-oceanscape-framework.html.

18.10 The Primacy of a Regional Approach

In many instances mentioned earlier, we have seen how much the regional approach was a constant in terms of ocean governance hence "bypassing existing regional oceans governance mechanisms with internationally funded projects is not a solution,…. Not only does it fail to strengthen governance mechanisms, but it also weakens those which are not supported, making them ever more difficult partners to work with" (Rochette et al. 2015). If they are shortcomings in regional oceans governance, rather than ignoring them, it is better to look at them and see how synergies and complementarities in the international oceans governance regime can be promoted to strengthen the various regional oceans governance mechanisms, regarding both conservation and maritime sector agreements. Often, such a strengthening will require expanding mandates like in the case of the OSPAR Commission, in order to allow new and emerging issues to be addressed or, more generally speaking, regarding the regional marine fisheries organizations (RFMOs) beyond the management of target species to more and more take into consideration the whole ecosystem.

Among the other types (and there are many) of regional arrangement, figure the Large Marine Ecosystems (LMEs), based on a concept developed from within the US National Oceanic and Atmospheric Administration (NOAA). So far, with mainly the funding and assistance of the Global Environment Facility (GEF),[5] 66 LMEs have been identified.[6] Each LME boundaries are based on ecological criteria which are bathymetry, hydrography, productivity, and trophic relationships. Typically, an LME project has a 5-module strategy covering (1) productivity, (2) fish and fisheries, (3) pollution and ecosystem health, (4) socio-economics, and (5) governance. Some of them have given birth to a specific governance mechanism, as in the case of the Benguela Current Commission (BCC) or the Partnerships in Environmental Management for the Seas of East Asia (PEMSEA). Nevertheless, as suggested by Rochette et al. (2015), LME mechanism may form a useful platform for environmental and fisheries assessments, capacity building, and on-the-ground interventions, "but these should be operated under existing regional oceans governance networks wherever possible" as in the case of the Mediterranean LME and the Barcelona Convention mechanism.

18.11 Knowledge and Expertise

As we have seen, the creation and evolution of all of these policies and programmes depend on a network of international and regional organizations including the large international NGOs, but also multiple public and private agencies, formal or informal institutions, and so-called "global" experts (Henocque and Kalaora 2015).

[5] As of 2013, the total GEF funding for 21 LME projects involving 110 countries amounted to USD 3.1 billion.

[6] http://www.cbd.int/ecosystems/newsletters/ea-2009-10.htm.

These experts build the regulatory instruments and devise the norms of this "empire" of "environmental knowledge" (Goldman 2004). Experts and expert knowledge (published by the experts) are unquestionably the core features of the emergence of globalization. This is through the dissemination of global means of conceptualization, the transformation of the populations' experiences and the behaviours, the spreading of "environmental know-how" and of the sustainable development paradigm. These can be communicated through governmental, private, or group networks, from a global to a local level (but not in the opposite direction). Scientific knowledge and expertise are important factors for the emergence of globalization, via the creation and dissemination of conceptual models and of a global system.

These models have created an ontological link in between overarching environmental and social issues. The power of these scientific authorities is expressed through the development of databases and monitoring networks, which provide sophisticated systemic models of the evolution of global processes and remodel local places through given categorizations. In this regard, local knowledge is not ignored, but exploited for the purpose of globalization and abstract modelling. Keeping in mind the necessity of a regional approach and of local populations' involvement, the expert should remain cautious with standardization of models and solutions that may hamper the expression of situations and practices in the field, which, like biodiversity conservation, ensure the resilience of our planet.

18.12 Ocean Literacy

How can one care about something he/she doesn't know? How local populations and the public in general can feel concerned and positively get involved into the development of maritime activities, especially in the deep sea? As the global ocean has a crucial role for our planet survival, but at the same time is changing rapidly and bear the pressure of ever-increasing maritime activities, public engagement in understanding the vital connections between people and the ocean becomes important because sooner or later informed and responsible decisions will need to be taken regarding the oceans and the exploitation of their resources like in the case of deep sea mineral resources. Ocean literacy is, therefore, an urgent imperative to face the societal challenge of a more-oriented 'blue growth' or rather 'blue society' engaged in the sustainable development of maritime activities.

For centuries, the fascination of the unknown and the mystery of the deep sea have inspired arts and literature, entertainment, and all kind of media, but still outreach projects and informal education efforts are essential tools for more public involvement. As an example, a network of scientists and educators decided to work out the "Ocean literacy framework"[7] defined as an understanding of the ocean's influence on each of us and, in return, our influence on the ocean, so that a so-called "ocean-literate" person understands the essential principles and fundamental con-

[7] http://oceanliteracy.wp2.coexploration.org/ocean-literacy-framework/.

cepts, can communicate about the ocean in a meaningful way, and is able to make informed and responsible decisions regarding the ocean and its resources.

Cabled ocean observatories like Ocean Networks Canada[8] offer a whole package of learning resources and events for students and educators and 'citizen science' projects. But, in the case of deep sea minerals exploration and future exploitation, the outreach effort is also to be carried out directly towards concerned local citizens to allow them to understand any deep sea minerals (DSM) development proposal and to have their view incorporated in decision-making processes. The South Pacific Commission (SPC) EU-funded project on DSM emphasizes that "it is in the interest of the people of the country, Government officials, and marine developers that a project has the requisite "social licence" to proceed". The project then recommends that mechanisms for public participation in DSM decisions (including environmental impact assessment processes) be incorporated within national DSM legislation, "for example by establishing a National Offshore Minerals Committee that includes civil society representatives".[9]

18.13 Conclusion: The Way Forward

Although a compromise between the principles of freedom, sovereignty, and common heritage of mankind, the United Nations Convention on the Law of the Sea (UNCLOS), together with accompanying agreements, functions as a kind of 'constitution of the seas and oceans' since its adoption in 1982 and its enforcement in 1994. However, ocean governance remains highly fragmented pursuant to a sectoral (including conservation) and geographical approach, and more recent insights are either absent (e.g. marine genetic resources in the water column) or given insufficient attention (e.g., climate change and transnational organized crime including illegal, unregulated, and unreported fishing).

In order to consider the problems of ocean space and resources 'as a whole', there is a need of better enforcement and integration of international agreements for their effective implementation. To do that, we are in need of a global 'social contract for the seas' (German Advisory Council on Global Change (WBGU) 2013), hence a common vision for the sustainable stewardship of the oceans. The still-born Oceans Compact of 2012 should be reconsidered to at last develop an overall strategic vision of the United Nations on the conservation and sustainable use of the oceans. This has to be considered in close connection with the Sustainable Development Goal related to the ocean (SDG14) to 'Conserve and sustainably use the oceans, seas and marine resources for sustainable development'. This SDG contains ten targets, ranging from reducing marine pollution of all kinds and minimizing the impacts of acidification to increase the scientific knowledge, develop research capacity, and transfer marine technology. But, the ocean SDG looks for the

[8] http://www.oceanetworks.ca/learning.

[9] http://gsd.spc.int/dsm/images/pdf_files/dsm_brochures/DSM_Brochure14.pdf.

moment like an ‘orphan’ as no UN organization has been specifically tasked with promoting the achievement of its targets (European Marine Board 2015).

The global ocean governance is indeed in need of a well-identified and efficient coordinating body, but we cannot wait for such a change and, among others, should strengthen and extend the existing regional seas agreements and organizations. Where they exist, cooperation should be deepened between adjacent marine conservation and sector agreements, more particularly in the case of fisheries, with and between Regional Fisheries Management organizations (RFMOs). The existing inter-regional collaborations should be based on the common heritage of mankind principle, the ecosystemic approach, and the precautionary principle.

Governance needs to be based on knowledge of complex social-ecological systems involving many interacting elements at multiple spatial, temporal, and administrative scales. Studying them requires an ecosystem approach thus interdisciplinary by nature, ensuring that scientific knowledge is processed in an integrated way to give to the decision-makers and industry operators a reliable overview of the current state of knowledge and possibilities for action where needed (e.g., main indicators to be taken into account in EIA and long-term monitoring of deep sea mining).

Simultaneously, there is a need for greater cooperation between global governance research, mainly focusing on social and political sciences, and the natural and engineering sciences, in order to develop suitable, multi-level (or ‘nested’) governance processes in between the ecological, socio-economic, and technical systems.

This chapter has been trying to make clear that the governance and management of deep ocean resources cannot be considered in isolation of the whole system which is the ocean, from coast to coast and from the surface to the bottom. Any marine-managed area like marine-protected areas (MPAs) should be considered as part of a wider management strategy of seascapes (not to be considered neither managed as landscapes). Therefore, successful and sustainable marine spatial management depends on a multi-track approach of marine-managed areas (including MPAs) couched within broader management settings for maintaining biodiversity and enabling socio-economic development. The challenge ahead of us is, therefore, not about protecting 10% or 30% of our seas and oceans, but to manage, under varied legal forms and governance regimes, 100% of them and in their three dimensions, from shallow waters to the deep sea.

To achieve such an ambitious goal, we have to avoid standardizing problems and solutions; we have to rethink how knowledge is gained. Beyond the simplistic vision that knowledge and expertise will solve everything, we have to become more “situational”, contextualizing knowledge, using existing meeting places or creating them for collective learning. This requires new approaches to scientific knowledge production that transcend the formalism of a single discipline altogether and operationalize integrative collaborations between academics and non-academics, such as local communities, industry, policy-makers, as a core part of the scientific work (Stenghers 2013), a much more open view of science which sees the population and its representatives, including whistleblowers, as sources of information, involving them in building knowledge for adaptive management.

References

Bambridge T, D'Arcy P (2014) Large-scale marine protected areas in the Pacific: cultural and social perspectives. In: Féral F, Salvat B (dirs) Gouvernance, enjeux et mondialisation des grandes aires marines protégées: recherché sur les politiques environnementales de zonage maritime, le challenge maritime de la France de Méditerranée et d'Outre-mer. L'Harmattan, Collection Maritimes, Paris,. 218 pages

Bax NJ, Cleary J, Donnelly B, Dunn DC, Dunstan PK, Fuller M, Halpin PN (2015) Results of efforts by the convention on biological diversity to describe ecologically or biologically significant marine areas. Conserv Biol 30(3):571–581

Bolman B, Steenbrink S, Oppermann J (2014) Working towards good environmental practice for seabed mining. In: Harvesting seabed minerals resources in harmony with nature, UMI 2014, Lisbon, Portugal

Chateauraynaud F (1999) Les sombres precurseurs: une sociologie pragmatique de l'alerte des risques. EHESS

Deep Ocean Stewardship Initiative (DOSI) (2015) A call for Deep-Ocean Stewardship (DOSI). http://www.indeep-project.org/deep-ocean-stewardship-initiative

Druel E, Rochette J, Bille R, Chiarolla C (2013) A long and winding road. International discussions on the governance of marine biodiversity in areas beyond national jurisdiction. IDDRI studies no 07/2013. 42p

Dunn DC et al (2014) The convention on biological diversity's ecologically or biologically significant areas: origins, development, and current status. Mar Policy 49:137–145

EcoShape (2012) Building with nature. Thinking, acting and interacting differently. www.EcoShape.nl

EU DG MARE (2013) Study to investigate the state of knowledge of deep-sea mining. Final report under FWC MARE/2012/06–SC E1/2013/04

European Marine Board (2015) Delving deeper. How can we achieve sustainable management of our deep sea through integrated research? EMB Policy Brief No 2, November 2015. www.marineboard.eu

German Advisory Council on Global Change (WBGU) (2013) World in transition. Governing the marine heritage. Summary. www.wbgu.de

Gjerde J (2008) Regulatory and governance gaps in the international regime for the conservation and sustainable use of marine biodiversity in Areas Beyond National Jurisdiction. IUCN Marine series 1

Goldman M., Imperial science, imperial nature: environmental knowledge for the World (Bank), dansJasanoff S., Martello M.L. (dir.) Earthly politics: local and global in environmental governance, MIT Press, Cambridge, 2004.

Halpern BS, Wallbridge S, Selkoe KA, Kappel CV, Micheli F et al (2008) A global map of human impacts on marine ecosystems. Science 319:948–952

Henocque Y, Kalaora B (2015) Integrated management of seas and coastal areas in the age of globalization. In Governance of Seas and Oceans. A. Monaco & P. Prouzet (Ed.), ISTE Ltd and John Wiley & Sons, Inc. pp 235–279

Jonas HD et al (2014) New steps of change: looking beyond protected areas to consider other effective area-based conservation measures. Parks 20(2):111–128

Levin L (2015) Needs of interdisciplinary multi-sectoral stewardship for deep-sea ecosystem management. EcoDeep-SIP workshop on "The crafting of seabed mining ecosystem-based management—assessing deep-sea ecosystems in the Pacific Ocean". Final Report, Tokyo

MEA (2005) Ecosystem and human well-being: synthesis. Millennium ecosystem assessment. Island Press, Washington

Morato T, Cleary J, Taranto GH, Vandeperre F, Pham CK, Dunn D, Colaca A, Halpin PN (2015) Data report: towards development of a strategic Environmental Management Plan for deep seabed mineral exploitation in the Atlantic basin. IMAR & MGEL, Horta, Portugal, 103pp

Ostrom E (2010) The challenge of common-pool resources. Environ Sci Policy Sustain Dev 50(4):8–21

Rochette J, Bille R, Molenaar EJ, Drankier P, Chabason L (2015) Regional oceans governance mechanisms; a review. Mar Policy 60:9–19
Spalding MD, Meliane I, Milam A, Fitsgerald C, Hale LZ (2013) Protecting marine spaces: global targets and changing approaches. In: Ocean Yearbook 27, IOI, Martinus Nijhoff Pub
Stenghers I (2013) Une autre science est possible! Les Empêcheurs de penser en rond, La Découverte, Paris
Waterman RE (2016) 'Building with nature': principles and examples. www.ronaldwaterman.com
Wedding LM, Friedlander AM, Kittinger JN, Watling L, Gaines SD, Bennett M, Hardy SM, Smith CR (2013) From principles to practice: a spatial approach to systematic conservation planning in the deep sea. Proc R Soc B Biol Sci 280:20131684
Wright G, Rochette J, Druel E, Gjerde K (2016) The long and winding road continues: towards a new agreement on high seas governance. IDDRI study no 01/16 March 2016
Yamakita T et al (2015) Identification of important marine areas around the Japanese Archipelago: establishment of a protocol for evaluating a broad area using ecologically and biologically significant areas selection criteria. Mar Policy 51(2015):136–147

Yves Henocque started his career in the field of aquaculture and sea ranching to the benefit of small-scale fishermen, after getting his Ph.D. in marine ecology. He then acquired environmental management and international cooperation skills through technical training in the United States and professional practice in Japan, to start a new coastal environment laboratory in Toulon (IFREMER) where he developed integrated coastal management and strategic planning practices in collaboration with a number of Mediterranean organizations including PAP/RAC within the Mediterranean Action Plan. Since then, he has led several ICM projects in the Mediterranean, West Indian ocean, and South-East Asia regions. He is now Senior Adviser for Maritime Policy and Ocean Governance at the French Research Institute for the Sustainable Development of the Sea (IFREMER), keeping working on Mediterranean issues and initiatives (Chair of CIESM Committee 6 on Coastal Ecosystem and Marine Policy) and with the Asia-Pacific region and more specifically Japan where he is currently based as JAMSTEC (Japan Agency for Marine-Earth Science and Technology) guest researcher.

Correction to: Composition, Formation, and Occurrence of Polymetallic Nodules

T. Kuhn, A. Wegorzewski, C. Rühlemann, and A. Vink

Correction to:
Chapter 2 in: R. Sharma (ed.), *Deep-Sea Mining*, https://doi.org/10.1007/978-3-319-52557-0_2

This chapter was inadvertently published with error.

On pages 44-45 in Equations 2.1 – 2.4 the formula for ammonia is wrong. It must read NH_3 instead of HN_3. In Table 2.1 the data for the Ce anomaly got lost somehow (last line of the table). The original chapter has been updated with these corrections.

The updated online version of this chapter can be found at
https://doi.org/10.1007/978-3-319-52557-0_2

R. Sharma (ed.), *Deep-Sea Mining*, https://doi.org/10.1007/978-3-319-52557-0_19

Index

R. Sharma (ed.), *Deep-Sea Mining*, DOI 10.1007/978-3-319-52557-0